Pathogen manipulation of intracellular membrane traffic

Adam Peter Rofe

PhD

University of York

Biology

September 2015

Abstract

The use of *in vitro* assays to study membrane fusion events has been instrumental in discovering the molecular requirements of membrane fusion. The processes involved in phagosome-lysosome fusion are not clear. Some intracellular pathogens, such as *Rhodococcus equi,* are able to prevent phagosome-lysosome fusion. Thus, this study aimed to develop an *in vitro* phagosome-lysosome fusion assay to better understand the fusion of these two organelles and to understand the molecular mechanisms behind *R. equi* pathogenesis.

Transfer of biotin-conjugated horseradish peroxidase (biotin-HRP) from lysosomes to streptavidin-bead containing phagosomes (sBCPs) was used to measure organelle fusion. A protocol for the purification of lysosomes from J774.2 mouse macrophages was developed using superparamagnetic iron oxide nanoparticles (SPIONs). Lysosomes were enriched with LAMP1 and devoid of EEA1. Biotin-HRP from lysosomes could be detected and was able to bind to sBCPs in a binding assay. A protocol for the purification of sBCPs from J774.2 cells was also developed. Phagosomes were enriched with LAMP1 and contained Rab5, Rab7 and EEA1. Fusion between organelles, in cytosol and in the presence of an ATP regenerating system, was not detected and may have been disrupted by factors present in pig brain cytosol used to support the vesicle fusion.

R. equi virulence depends a 90 Kb plasmid harbouring several virulence-associated proteins (Vaps). Only one of these, VapA, is essential for virulence but *R. equi* may have additional virulence factors. To identify these potential additional *R. equi* genes, a *R. equi* gene library was expressed in yeast which were then screened for membrane trafficking defects. The screen failed to yield any potential *R. equi* virulence factors that disrupted membrane trafficking in yeast. In a targeted approach, recombinant VapA when fed to cells, induced swelling of mammalian cell lysosomes and late endosomes. This activity was conferred by the C-terminal core of VapA. VapA induced LAMP1 expression suggesting lysosome dysfunction. The effects of VapA were not seen with other *R. equi* Vap proteins.

This thesis presents the framework for further developing an *in vitro* phagosome-lysosome fusion assay. Secondly, this work builds on our understanding of how *R. equi* uses VapA to survive intracellularly.

Table of Contents

List of Figures

List of Tables

Acknowledgements

Firstly I would like to thank my supervisor Paul Pryor for teaching me an enormous amount over the course of my PhD. I have gained a great deal of technical expertise while at York but also have gained the skills necessary to critically evaluate my own work and that of others – you can never have enough controls. Thank you for reminding of how much I have learnt and progressed when my experiments were not going to plan – it was definitely welcome. I am grateful for you always being approachable and for finding the time to help me despite how busy you are. I would also like to thank him for his patience during the painful process of proof-reading this thesis and apologise for my overuse of commas and lack of full stops!

I would like to acknowledge the members of my Thesis Advisory Panel, Adrian Mountford and Dimitris Lagos, for their guidance and constructive advice during my PhD. I also extend my gratitude to the members of the Imaging and Cytometry team at York for training me in the use of the confocal microscopes. I would like to thank Nathalie Signoret for her suggestions and feedback during lab meetings. I would also like to thank Marjan van der Woude and Debbie Smith for allowing me to participate in their lab meetings and expand my knowledge of microbiology and parasitology, respectively.

Finally, I would like to thank anyone who has given me help or guidance with any aspect of my work over the last four years. Thank you to the past and present members of the Pryor, Signoret and Lagos groups for making this a great place to be.

Author's Declaration

This work as not been previously presented for an award at this, or any other University. All sources are acknowledged as References. All work and data presented in this thesis are original and were performed by Adam Peter Rofe with the exception of mass spectrometry analysis of VapA-interacting proteins (Appendix 1.0 & 1.1) which was performed by the Proteomics Department of the Technology Facility (University of York, York).

The lysosome purification protocol described in section 3.2.2 has been published in: *Subcellular Fractionation*. *A laboratory manual*. Cold Spring Harbour Protocols 2015 (Purification of lysosomes using supraparamagentic iron oxide nanoparticles (SPIONS). A.P.Rofe and P.R. Pryor)

The phagosome isolation protocol described in section 3.7.1 has been published in: *Subcellular Fractionation*. *A laboratory manual*. Cold Spring Harbour Protocols 2015 (Isolating Phagosomes from Tissue Culture Cells). P.R. Pryor and A.P.Rofe)

Chapter 1: Introduction

1.1 The endocytic pathway

Intracellular membranes allow the partitioning of cellular components into membrane-bound compartments allows for their specialisation for different cell functions. Differences in the protein and lipid compositions of such intracellular compartments are key for their interaction and function. The plasma membrane is the surface at which the cell senses and communicates with its environment. Thus, the composition of the plasma membrane is highly regulated. Endocytosis is a general term used to described the internalisation of extracellular fluid, particles, plasma membrane receptors and solutes through the invagination of the plasma membrane. Conversely, exocytosis is the process by which vesicles fuse with the plasma membrane and expel their contents into the extracellular environment. In endocytosis, part of the plasma membrane is deformed inwards forming a vesicle which pinches off and seals through the active process of membrane fission. This nascent organelle is termed the early endosome (EE) and will contain a vast range of material, including nutrients, signalling receptors, receptor-ligand complexes, solutes, fluid, lipids, membrane proteins, bacteria, viruses, cell debris and extracellular matrix components. Early endosomes are key sorting stations of the cell. It is here that these different cargo are either recycled back to the plasma membrane or further trafficked along the endocytic pathway for degradation in the lysosome. Typically, 0.5 - 1.8 fold of the plasma membrane is internalised and returned to the cell surface per hour (Steinman et al., 1983) and in macrophages, the volume of incoming vesicles is 10 times larger than the volume of lysosomal compartments (Steinman et al., 1976). Clearly, there must be extensive regulation of endocytosis and return of material to back to the plasma membrane if the cell is to maintain the correct size and composition.

The early endosome undergoes extensive remodelling within minutes of its formation. This includes the acquisition and removal of membrane proteins, lipids and cytoplasmically associated proteins such as Rab GTPases and tethering factors such as the class C core endosome vacuole tethering (CORVET) complex (Balderhaar et al., 2013). This confers specific functions onto the maturing endosome allowing cargo recycling to be kept spatially and temporally separate from degradation of macromolecules. A schematic representation of endosome

maturation is shown in figure 1.0. Key regulators of early endosome maturation include the GTPase RAB5 and other factors such as its effector protein VPS34. During the transition to a late endosomal configuration the EE membrane begins to bud inwards forming intraluminal vesicles (ILVs) that contain ubiquitinated membrane proteins that have been targeted for degradation (Scott et al., 2014). This function is performed by a series of oligomeric protein complexes known as endosomal sorting complexes required for transport (ESCRT) proteins (Schuh and Audhya, 2014). Concomitantly, Rab5 and its effectors are exchanged for Rab7 and a different set of effector proteins and lipids such as Rab-interacting lysosomal protein (RILP), Rubicon and the HOPS complex (Cantalupo et al., 2001, Sun et al., 2010, Balderhaar and Ungermann, 2013). This allows the progression of the EE to a late endosome also known as a multivesicluar body (MVB). Early endosomes maintain a peripheral location within the cell (dependent on cell type) whereas late endosomes begin to move along microtubules towards the perinuclear region of the cell where they encounter lysosomes (Loubery et al., 2008). LEs transiently interact with lysosomes in a series of rapid “kiss and run” fusion events and eventually fully fuse with lysosomes to form hybrid organelles or endolysosomes (Storrie and Desjardins, 1996). Endolysosomes are thought to be distinct from dense core/primary lysosomes, as they do not appear in the same fractions as primary lysosomes in isopycnic centrifugation gradients (Bright et al., 1997). Finally, lysosomes are reformed from hybrid organelles in a process of membrane retrieval and the removal and recycling of mannose 6-phosphate receptors (M6PRs) back to the Golgi (Luzio et al., 2003).

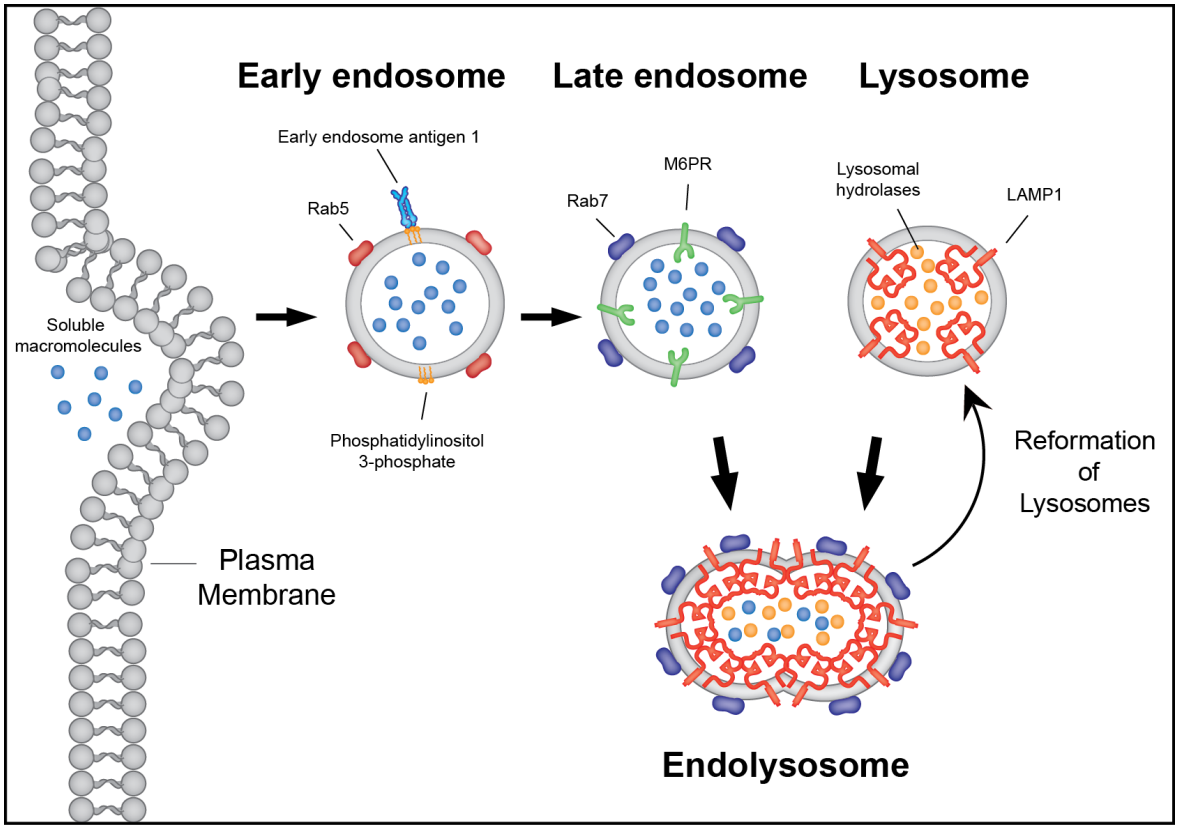

Fig. 1.0 Schematic representation of endosome maturation. The formation of early endosomes begins with the invagination of the plasma membrane to partition part of the extracellular milieu into a membrane-bound compartment called the early endosome (EE). The EE undergoes rapid membrane remodelling and acquires proteins and lipids that regulate this process, such as the GTPase RAB5, the lipid phosphatidylinositol 3-phosphate (PtdIns[3]P) and tethering factors such as early endosomal antigen 1 (EEA1). As the EE matures it loses its association with early effectors and acquires proteins such as RAB7 and mannose-6-phosphate receptors (M6PRs) that confer a late endosomal identity. The late endosome (LE) then fuses with the lysosome to form an endolysosome, where it acquires lysosomal hydrolases and membrane proteins such as LAMP1. Finally, membrane is retrieved from the endolysosome to reform primary lysosomes.

Clearly there must be extensive regulation of these processes. However, this regulation is susceptible to manipulation by intracellular pathogens (Gruenberg and van der Goot, 2006) and genetic deficiencies in genes controlling endocytic process can result in a wide range of pathologies (Maxfield, 2014). The stages of endosome maturation and pathogen manipulation of intracellular membrane trafficking are discussed in greater detail below.

1.1.1 Formation of the early endosome

The invagination and subsequent fission of the plasma membrane to form an early endosome is an active process that is highly regulated. Membrane fission is an energetically unfavourable reaction, as the removal of one membrane into two is counteracted by strong hydrophobic forces that try and maintain the lipid membrane structure (Frolov and Zimmerberg, 2010). This is achieved by range of fission machinery that acts to overcome this energy barrier and facilitate membrane fission. These include clathrin-mediated and clathrin-independent mechanisms (Mayor and Pagano, 2007, Doherty and McMahon, 2009).

Within minutes of early endosome formation proteins associate with the cytoplasmic face of the endosome membrane. These proteins are necessary for recycling of the endosome contents and remodelling of the endosome membrane which define its identity and function. One of these proteins that is associated with the early endosome is RAB5. Rabaptin-5, a RAB5 effector protein that that promotes the GEF activity of Rabex-5 (Horiuchi et al., 1997), is essential for endosome fusion (Stenmark et al., 1995). Rabaptin-5 forms a complex with another Rab5 effector, Rabex-5, which acts to catalyse Rab5 nucleotide exchange (Horiuchi et al., 1997). After it is activated by Rab5, the Rabaptin-5-Rabex-5 complex drives its own recruitment to the endosomal membrane and establishes a feedback loop whereby GTP associated Rab5 promotes further Rab5 recruitment (Lippe et al., 2001) which may help to promote clusters of active Rab5 forming on the endosome. Active Rab5 recruits effector proteins such as VPS34/p150 to the endosomal membrane (Murray et al., 2002). VPS34 is a phosphatidylinositol 3-kinase (PI[3]K) that generates phosphoinositide 3-phosphate (PtdIns[3]P) (Christoforidis et al., 1999), a key lipid of early endosomal membranes. The importance of this lipid is shown in Vps34 knockout mice that display a range of defects including disrupted endocytic and autophagic degradation, as well as heart and lung problems (Jaber et al., 2012). EEA1 is a large (170 kDa) tethering factor that contains two Rab5 binding sites (Callaghan et al., 1999, Simonsen et al., 1998, Lawe et al., 2000) and a Fab1, YOTB, Vac1 and EEA1 (FYVE) domain (Stenmark et al., 1996) that is critical for Rab5 binding (Lawe et al., 2000). EEA1 binds to PtdIns[3]P lipids on the endosomal membrane and forms a molecular complex with Rabaptin-5, Rabex-5 and *N*-ethylmaleimide-sensitive factor (NSF).

This complex then interacts with the soluble-NSF attachment protein receptor (SNARE) protein, Syntaxin 13, which may help to drive vesicle fusion (McBride et al., 1999). Thus, the generation of different lipids and the recruitment of fusion proteins allows the early endosome to interact with other endocytic compartments. This is essential for the retrieval of membrane proteins and receptors that need to be redistributed to the plasma membrane.

1.1.2 Sorting of early endosomal cargo

Early endosomes fuse with each other and pre-existing sorting endosomes. The EE contents are either destined for degradation (via lysosomes), rapid retrieval to the plasma membrane, or delivery to the endocytic recycling compartment (ERC). The mildly acidic pH of the early endosome causes the dissociation of some receptor-ligand complexes, allowing receptors to be reused (Mukherjee et al., 1997). There are two main routes for the sorting of endosomal cargo back to the cell surface, a fast and a slow route. Using fluorescent lipid analogues, Hao and Maxfield (2000) showed approximately 50 % is returned to the plasma membrane within 1-2 minutes suggesting a rapid recycling mechanism. The remaining 50 % is returned to the cell surface after 12 min and is trafficked via the ERC. The ERC is a tubular compartment that often resides near the Golgi and is associated with microtubules (Yamashiro et al., 1984). It is hypothesised that the majority of early endosomes mature to form the late endosomes, whereas endosomal tubules form ERCs. Transport between the early endosome and ERC may prevent the degradation of cargo and most proteins trafficked to the ERC normally return to the plasma membrane (Maxfield and McGraw, 2004). Sorting in the ERC is also controlled by Rab GTPases, in particular, Rab11. Overexpression of Rab11 in HeLa cells disrupted the localisation of the transferrin receptor, which accumulates in the ERC (Wilcke et al., 2000) and altered the location of the ERC in the cell (Grant and Donaldson, 2009). The exact mechanisms behind Rab11 regulation of the ERC are not clear (Horiuchi et al., 1997).

1.1.3 Late endosome formation

Following sorting of the contents of the early endosome, the EE begins to mature to a late endosome. This is characterised by a series of changes that alters the

identity and function of the early endosome and results in a more degradative organelle. Soluble cargo that remains at this stage is destined for degradation, although retrograde trafficking from the LE to the Golgi has been described. The most well characterised examples of retrograde transport are the trafficking of the vps10 receptor in yeast (Valls et al., 1987, Cooper and Stevens, 1996, Seaman et al., 1997) and mannose 6-phosphate receptors in mammalian cells (Geuze et al., 1985, Hirst et al., 1998, Diaz and Pfeffer, 1998). This is mediated by the retromer complex which is essential for the retrieval of these receptors (Seaman et al., 1997(Arighi et al., 2004). Retrograde trafficking is also regulated by Rab9, which is able to stimulate the transport of MPRs from late endosomes to the *trans* Golgi network (TGN) in a cell free system (Lombardi et al., 1993) and is required for late endosome stability (Ganley et al., 2004).

1.1.4 The Rab5-Rab7 conversion

Although Rab5 is associated with the EE it must be removed if endosomal maturation is to progress, since expression of a constitutively active form of Rab5 prevents the maturation of the early endosome (Rink et al., 2005) and results in the formation of giant organelles that take on characteristics of both early and late endosomes (Hirota et al., 2007). GTP-locked Rab5 expression also affects lysosome biogenesis and reduces the amount of lysosomes found in dense fractions on Percoll gradients (Rosenfeld et al., 2001). For endosomes to mature Rab5 must be replaced with Rab7, a dynamic process referred to as the Rab conversion or Rab switch (Rink et al., 2005). This is essential to redefine the composition of the early endosome to a late endosome by the removal of Rab5 effectors and the acquisition of Rab7 effectors and other late endosome/lysosome associated proteins. As previously described, a Rab5 feedback promotes the generation of Rab5 domains on endosomal membranes. Rab5 must be displaced and its GTP hydrolysis activity enhanced to promote its own inactivation. One model proposes that Rab5 recruits Rab7, which inactivates and supresses Rab5 activity through a “cut off switch” whereby accumulation of Rab7 reaches a critical threshold upon which Rab5 is replaced. Thus, Rab5 is able to facilitate its own removal to allow endosomal progression (Del Conte-Zerial et al., 2008). The Rab conversion is necessary for the Rab7-mediated recruitment of fusion machinery so

that late endosomes can only fuse homotypically with other late endosomes or heterotypically with lysosomes.

1.1.5 Intraluminal vesicle formation

As the EE matures the surface invaginates to form intraluminal vesicles (ILVs). This results in the extracellular domain of membrane proteins being exposed to hydrolytic enzymes within the endolysosome and allows for their degradation. This process is essential for the sequestering and degradation of signalling receptors and is an important mechanism of downregulating cell signalling (Dobrowolski and De Robertis, 2012). Late endosomes containing ILVs are also known as a multi-vesicular bodies (MVBs). This membrane invagination is achieved through the actions of a series of protein complexes termed the endosomal sorting complexes required for transport (ESCRT) complexes. There are 5 main ESCRT complexes, (ESCRT 0, I, II, III and the VPS4 ATPase complex) that each have distinct roles in ILV formation (Schmidt and Teis, 2012b). ESCRT 0 is a heterodimer composed of two subunits; HRS and STAM1 (Vps27 and Hse1p in yeast). Proteins that are ubiquitinated are recognised by this complex and are targeted to ILVs for degradation. The ESCRT 0 complex recognises ubiquitin motifs through VHS (Vps27p/Hrs/STAM) domains and is recruited to the endosome membrane through binding of its FYVE to PtdIns[3]P (Bilodeau et al., 2002). Interaction of the ESCRT 0 FYVE domain and PtdIns[3]P is essential for recruitment of ESCRT 0 which accumulates in the cytoplasm if this domain is mutated (Urbe et al., 2000). ESCRT I is a hetero-tetramer composed of TSG101 (vps23), VPS28, VPS37A-C (vps37) and MBV12A/MVB12B (Mvb12), known as Vps23, Vps28, Vps37 and Mvb12 in yeast, respectively (Kostelansky et al., 2007, Katzmann et al., 2001, Morita et al., 2007). ESCRT I is recruited from the cytoplasm to the endosomal membrane by ESCRT 0 (Ren and Hurley, 2011). ESCRT I also recognises ubiquitinated cargo and forms a rigid stalk-like structure that may act to regulate the spacing of other ESCRT components and participate in the mechanical aspects of membrane remodelling (Kostelansky et al., 2007). ESCRT II is composed of VPS36/EAP45, VPS22 (also known as SNF8) and two VPS25/EAP20 proteins, know as Vps36, Vps22 and Vps25 in yeast respectively (Babst et al., 2002b). One VPS25 protein associates with either VPS36 or VPS22, resulting in a characteristic Y-shaped complex (Hierro et al., 2004). VPS36 contains a GRAM-like ubiquitin-binding in

EAP45 (GLUE) domain that simultaneously binds ubiquitin, PtdIns[3]P (Slagsvold et al., 2005) and ESCRT I via VPS28 (Gill et al., 2007). ESCRT II is required to recruit ESCRT III machinery to the endosome membrane. The VPS25 subunit of ESCRT II induces a conformational change in the ESCRT III subunit VPS20, which then serves as a nucleation point for the assembly of the full ESCRT III complex (Teis et al., 2010). ESCRT III is also a hetero-oligomeric complex formed from a core of CHMP4 (Snf7 in yeast), along with CHMP6 (Vps20), CHMP2 (Vps2) and CHMP3 (Vps24). These four subunits are joined by three accessory proteins, CHMP1 (Did2), CHMP5 (Vps60) and Ist1 (Schmidt and Teis, 2012a). ESCRT complexes 0, I and II form stable cytoplasmic complexes, whereas ESCRT III polymerises from cytoplasmic monomers and only transiently associates with endosomes (Henne et al., 2011). ESCRT III has two distinct subcomplexes; CHMP4 and CHMP6 bind to the endosomal membrane via a myristoyl group on CHMP6. The VPS4 subcomplex then associates with the endosome and allows the recruitment of additional proteins (Babst et al., 2002a). CHMP4 is present in the highest concentrations in the cytoplasm and the other subunits of the complex act to polymerise CHMP4 (Teis et al., 2008). ESCRT III is widely accepted as being the main complex responsible for the actual formation of ILVs from membrane invaginations and their eventual release into the lumen of the MVB. The mechanisms behind this have yet to be elucidated (Schuh and Audhya, 2014). The VPS4 complex is the fifth complex of the ESCRTs. VPS4 is a type I AAA-ATPase and forms a complex with its co-factor LIP5 (VtA1 in yeast). The ESCRT III protein VPS2 is needed along with CHMP1A (Did2 in yeast) to recruit VPS4 to the ESCRT III complex (Nickerson et al., 2006). The Vps4 complex is assembled as two hexameric rings with a central pore. CHMP1A binding to VPS4 activates this complex and enhances the ATPase activity of VPS4 (Azmi et al., 2006). Vps4 then uses the energy from ATP hydrolysis to drive the disassembly and recycling of ESCRT III components, pulling each subunit through the Vps4 ring (Odorizzi, 2015). Vps4 also participates in membrane neck constriction during ILV budding (Adell et al., 2014). This is hypothesised to shorten the membrane neck of the forming ILV and be a possible mechanism to facilitate membrane scission (Saksena et al., 2009). Alternatively, Vps4 may alter the conformational state of the ESCRT III proteins to induce membrane scission (Hanson et al., 2008). Thus, the ESCRT proteins act in a highly regulated manner target membrane proteins for degradation. This process is also interestingly, independent of other endosomal

maturation events. Over expression of constitutively active Rab5 does not block ILV formation (Wegner et al., 2010) and the vacuolar ATPase (vATPase) is not required for ILV biogenesis (Vaccari et al., 2010). Rab7 is not essential for ILV formation (Vanlandingham and Ceresa, 2009) but the Rab7 effector Rab-interacting lysosomal protein (RILP) may facilitate ILV formation as in the absence of RILP, ILV numbers are reduced (Progida et al., 2007). Figure 1.2 depicts the activity of ESCRTs 0, I, II and III and figure 1.3 shows the activity of the Vps4-Vta1 complex.

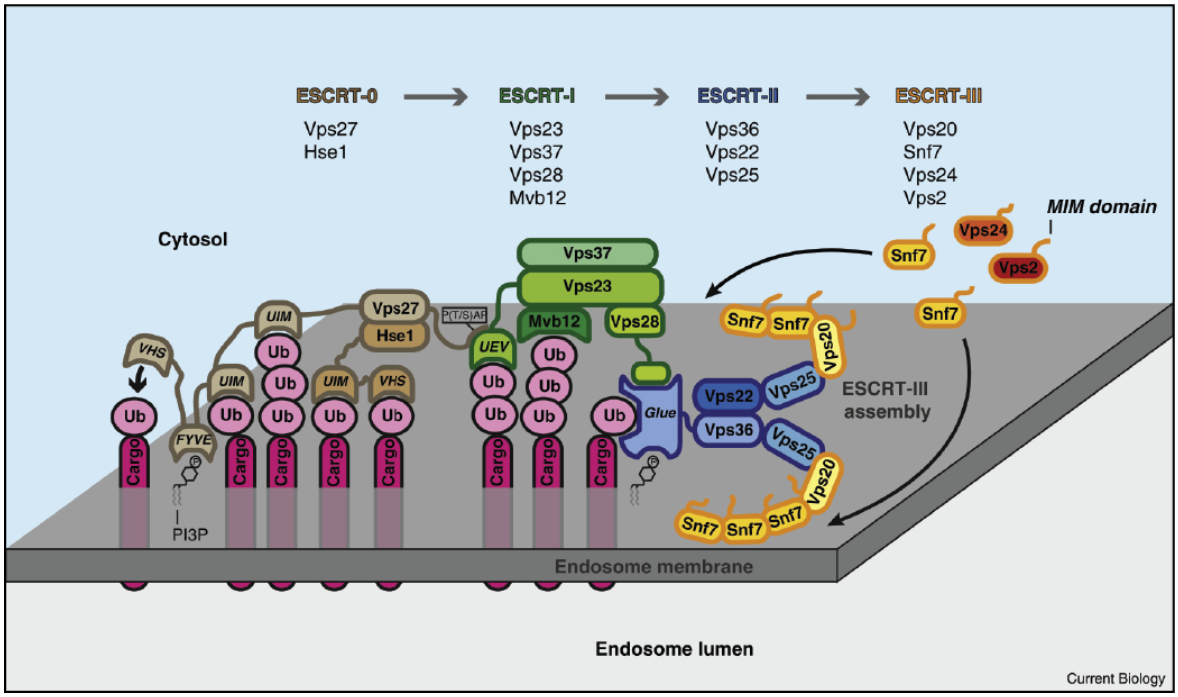

Fig. 1.1. Schematic representation of the ESCRT machinery in intraluminal vesicle formation in yeast. ESCRT 0 (brown) initiates the formation of intraluminal vesicles (ILVs) by binding to ubiquitinated membrane proteins. ESCRT I (green) associates with ESCRT 0 (via the Vps27 subunit) and also binds to ubiquitinated cargo. ESCRT II (blue) subunit Vps36 interacts via a GLUE domain with ESCRT II Vps28, ubiquitinated cargo and phosphatidylinositol 3-phosphates (PtdIns[3P). Vps25 then serves as a nucleation point for the formation of ESCRT III (yellow/orange) which drives inward vesiculation of the endosomal membrane. Figure reproduced with permission from (Schmidt and Teis, 2012b).

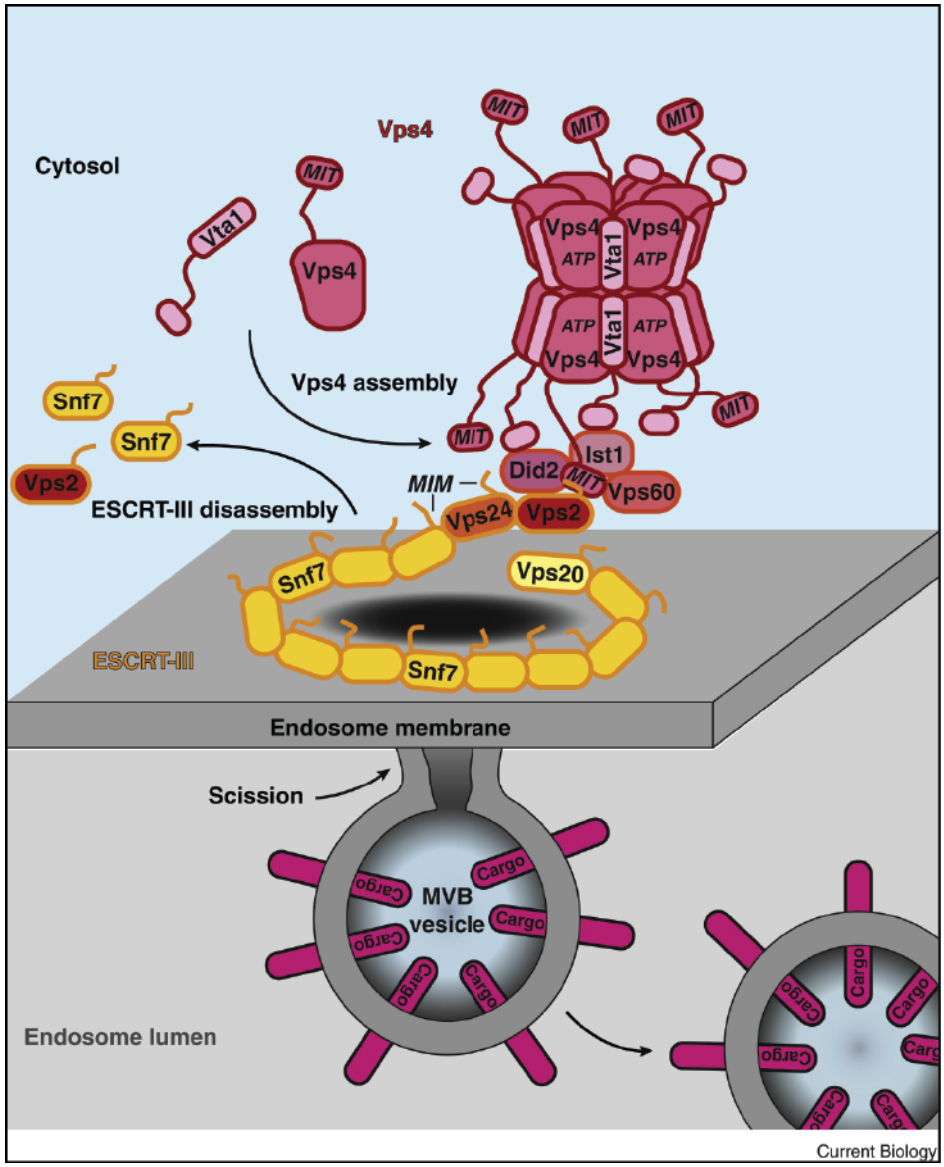

Fig. 1.2. Schematic representation of the Vps4-Vta1 complex in ESCRT III disassembly and ILV formation in yeast. The ESCRT-III subunits Vps24 and Vps2 terminate assembly of the ESCRT-III filaments (orange) on the endosome surface. Vps2 together with Did2, Ist1 and Vps60 build a recruitment complex for the AAA-ATPase Vps4 and its cofactor Vta1. Once assembled, the Vps4 complex (pink) catalyses disassembly of the ESCRT-III filament in an ATP-driven reaction. ESCRT-III disassembly terminates each round of the MVB pathway, which results in the generation of a cargo-laden 25 nm MVB vesicle (50 nm in human cells). Figure and figure legend reproduced with permission from (Schmidt and Teis, 2012b).

1.1.6 Late endosome acidification

As the late endosome matures the endosome lumen becomes more acidic. The pH of the early endosome is between 6.8 and 6.1 but this drops to 6.0-4.8 as the endosome matures (Maxfield and Yamashiro, 1987). This pH drop is essential for the proper function of lysosomal enzymes which only operate within a narrow range of pH values. The progressive acidification also allows the dissociation of receptors and their soluble cargoes.

This acidification is also manipulated by some bacterial toxins and viral proteins which only become active when they are trafficked to EEs, LEs or lysosomes. For example, the anthrax toxin protective antigen (PA) is only able to form pores in membranes at < pH 6.0 (Koehler and Collier, 1991, Mercer et al., 2010). Similarly, endocytosed influenza viral particles require a drop in pH to induce a conformational change in the hemagglutinin fusion peptide to facilitate fusion with the endosome membrane (Bullough et al., 1994, Durrer et al., 1996). The task of acidifying endocytic vesicles is performed by the vacuolar ATPase (vATPase). This is a large protein complex that is separated into two domains. The ~650 kDa V_1 domain is located on the cytoplasmic face of the vesicle membrane and the ~260 kDa V_0 domain is embedded in the membrane. V_1 is composed of eight subunits (A-H) and is responsible for the ATPase activity of the pump (Forgac, 2007). V_0 in yeast contains 6 subunits (a, b, c, c' and c''), whereas c'' is substituted for Ac45 in higher eukaryotes (Supek et al., 1994). The V_0 domain is responsible for the using the energy of ATP hydrolysis to translocate protons across the endosomal membrane to generate a proton gradient. Acidification is regulated by the association and dissociation of the vATPase subunits with membrane lipids, as well as the different in abundances of the V_1 on early and late endosomal membranes (Lafourcade et al., 2008). Alternatively, differential expression of vATPase isoforms with different proton translocation efficiencies can determine the extent to which a membrane-bound compartment acidifies (Kawasaki-Nishi et al., 2001).

Currently, there is some controversy regarding the requirement of the vATPase for vesicle fusion. It was hypothesised that vacuole acidification is essential for vacuole fusion (Ungermann et al., 1999) and *in vitro* studies of yeast vacuole

fusion suggested that that the V_0 subunit is essential for vacuole fusion (Baars et al., 2007). The V_0 was also suggested to participate in membrane fusion by generating a fusion pore (Strasser et al., 2011). However, it is difficult to separate requirement for the acidification of the vacuole or the physical presence of the V_0 subunit, as vacuoles of yeast lacking V_0 do not acidify. More recently, it was demonstrated that it is actually the acidification of the vacuole that is needed for membrane fusion, rather than the vATPase *per se* (Coonrod et al., 2013*)*. Yeast vacuoles with a mutant vATPase that lacked a proton translocation function could not fuse and vacuole fusion could be rescued through vacuole acidification by an exogenous H^+ translocating inorganic pyrophosphatase (Coonrod et al., 2013). Similarly, in macrophages the vATPase was shown not to be essential for late endosome/lysosome fusion, but interestingly, pharmacological disruption leading to an increase in lysosome pH did not prevent lysosome fusion (Kissing et al., 2015). Thus the exact relationship between endosome/vacuole acidification and membrane fusion has yet to be fully understood.

1.1.7 The role of lipids in endosome maturation

As previously discussed, integral membrane proteins and cytoplasmic effector proteins must be removed and exchanged for those that confirm a late endosomal identity. The same is true for membrane lipids. Phosphatidylinositides are lipids present in low levels in endocytic membranes (Di Paolo and De Camilli, 2006) The main lipids that contribute to endosomal identity are PtdIns[3]P and phosphatidylinositol 3,5-bisphosphate (PtdIns[3,5]P_2), which are associated with early and late endosomes/lysosomes respectively (Li et al., 2013). The synthesis of these lipids is performed in their subcellular location allowing strict regulation of compartment identity (De Matteis and Godi, 2004). The division of different lipid species between endocytic vesicles allows the recruitment of vesicle-specific effector proteins.

VPS34 forms a protein complex with other proteins that regulate its kinase activity. These include p150 (Vps15 in yeast) and Beclin-1 (Vps30 in yeast), which form a core complex that associates with another protein, UVRAG (Funderburk et al., 2010, Itakura et al., 2008, Thoresen et al., 2010). UVRAG is an activator of the HOPS complex, but is sequestered by the RAB7 effector, Rubicon. Thus, upon the

switch from RAB5 to RAB7, RAB7 competes with UVRAG for binding to Rubicon, causing UVRAG to become released and free to interact with the HOPS complex (Sun et al., 2010). Moreover, VPS34 and p150 also bind to inactive RAB7, suggesting that RAB7 is able to inhibit VPS34 activity and stop the production of PtdIns[3]P (Stein et al., 2003). This intimately links the activation of RAB7 with the generation of lipids of the late endosomal membrane. PtdIns[3,5]P_2 is synthesised by phosphatidylinositol 3-phosphate 5-kinase (PIKfyve, Fab1p in yeast) which uses PtdIns[3]P as a substrate to generate PtdIns[3,5]P_2 (Sbrissa et al., 1999). PIKfyve knockouts are embryonically lethal (Ikonomov et al., 2011) demonstrating that this kinase is essential. PtdIns[3]P must first be dephosphorylated to be used as a substrate by PIkfyve. This is performed by a family of 3-phosphatases, the myotubularins (Robinson and Dixon, 2006), mutations in which are linked to X-linked neuromuscular disorders and Charcot-Marie-Tooth disease type 4B (Begley and Dixon, 2005). Overexpression of myotubularins results in disrupted late endosome to lysosome trafficking suggesting that these proteins are also important in endosomal maturation events (Tsujita et al., 2004). The production of PtdIns[3,5]P_2 is a prerequisite for LE/lysosome acidification in lower eukaryotes but the situation in yeast and mammals is not so clear (Ho et al., 2015, de Lartigue et al., 2009). PIKfyve inhibition in macrophages has recently been shown to disrupt phagosome acquisition of lysosomal proteins LAMP1 and cathepsin D but acidification appeared unaffected (Kim et al., 2014). PIKfyve also actives ion channels on late endosomal membranes. For example, the calcium channel TRPML1 is activated by PtdIns[3,5]P_2 (Dong et al., 2010) and the lysosomal two pore channel TPC-2 (also a calcium channel) is activated by PtdIns[3,5]P_2. As calcium is known to regulate lysosome fusion (Pryor et al., 2000, Hay, 2007) this may be a mechanism by which PIKfyve regulates LE fusion. Some PtdIns[3,5]P_2 binding proteins have been identified including sorting nexin (SNX) 1 (Carlton et al., 2004), which is part of the retromer complex and VPS24 (Whitley et al., 2003), which is part of the ESCRT machinery. It is likely that other PtdIns[3,5]P_2 binding proteins will be found that may be involved in endosome maturation. Other lipids are also important in endosome maturation. Bis-(monoacylglycero) phosphate, also known as lysobisphosphatidic acid (BMP/LBPA, hereon referred to as LBPA), is also found on late endosome/lysosomes (Piper and Katzmann, 2007), but in greater abundance than phosphaditylinositides. The presence of LBPA in membranes promotes inward budding of acidic liposomes *in vitro* and this

invagination process is controlled *in vivo* by ALIX (bro1 in yeast), a cytosolic protein involved in MVB biogenesis (Matsuo et al., 2004)

1.2 Lysosomes

1.2.1 Characteristics of lysosomes

Lysosomes are the terminal compartment in the endocytic pathway and are the degradative organelles of the cell. Lysosomes have key roles in membrane trafficking, including endocytosis, exocytosis, autophagy and phagocytosis but also have other roles such as membrane repair (Reddy et al. 2001). The primary role of lysosomes is to degrade the soluble cargo that they receive via fusion with late endosomes. Lysosomes contain around 60 acid hydrolyses which degrade a diverse range of molecules, including lipids, proteins and carbohydrates (Schulze et al. 2009). These enzymes operate within the low pH of the lysosome (4.5-5.0) which is maintained the vATPase proton pump (Mellman et al., 1986). By sequestering these degradative hydrolases into the lysosome the cell is able to regulate the digestion of macromolecules and provide an optimal environment for their degradation. This also prevents degradation of the cell itself. If lysosome membrane integrity is disrupted the enzymes become inactive in the more alkaline cytoplasm.

Lysosomes appear as dense bodies and are often seen in close apposition to the cell nucleus. The size and shape of lysosomes varies between cell types but they are generally spherical and 0.5-1 μm in diameter (Mellman et al., 1986). The membrane of the lysosome is around 7-10 nm thick (Saftig et al., 2010) and is characterised by the presence membrane proteins such as LAMP1 and LAMP2, as well as lipids such as LBPA, which is also found in late endosome membranes (Kobayashi et al., 1998). There are at least 100 known lysosomal membrane proteins (Schroder et al., 2010) with LAMPs, CD-63 and lysosomal integral membrane protein (LIMP)-2, amongst the most abundant (Eskelinen et al., 2003). Lysosomal membrane proteins are also heavily glycosylated on their lumenal domains which is hypothesised to prevent degradation of the lysosome membrane by resident hydrolases (Schwake et al., 2013).

1.2.2 Lysosomal storage disorders

Deficiencies in lysosomal hydrolases and lysosomal associated proteins can cause a lysosomal storage disease (LSD) either through accumulation of a substrate, or perturbation in a related biochemical pathway (Dierks et al. 2009). This ultimately disrupts lysosomal function resulting in a wide variety of clinical manifestations that includes, but is not limited to; neurological problems, kidney damage, blindness and premature death (Ballabio & Gieselmann 2009). Individual LSDs are themselves quite rare, but together they are estimated to occur in 1 in every 5,000 live births, with the true figure probably higher due to misdiagnosed or undiagnosed cases (Fuller et al., 2006). LSDs are almost all due to deficiencies in lysosomal hydrolases but there are a few that are caused by deficiencies in non-enzymatic lysosomal membrane proteins. Thus, the study of LSDs can offer insights into lysosome physiology (Platt et al., 2012). As lysosomes play a key role in degrading macromolecules, disruption of enzyme activity can result in the accumulation of substrates within lysosomes. When lysosomes accumulate high levels of substrates this can have a secondary effect and result in the inhibition of an further enzymes that are not mutated or genetically deficient. For example, the protein degradative capacity of lysosomes in fibroblasts from mucopolysaccharidoses I and VI and GM-1 gangliosidosis is disrupted despite these cells not suffering from a protease deficiency (Kopitz et al., 1993). Lysosomes are an integral part of the autophagy process, of which there are three distinct mechanisms of autophagy; macroautophagy, microautophagy and chaperone-mediated autophagy (CMA), all of which require lysosomes (Boya et al., 2013). The rate of lysosome-autophagosome fusion is reduced in most LSDs (Ballabio and Gieselmann, 2009). For example, autophagosome-lysosome fusion is perturbed in mucolipidosis type III A and multiple sulfatase deficient mouse embryonic fibroblasts (Fraldi et al., 2010). The impact of LSDs on microautophagy are not clear, despite a recent report that a mouse model of Pompe disease had impaired microautophagy (Takikita et al., 2009). CMA is also affected in some lysosomal storage disorders. CMA is the direct targeting of cytoplasmic proteins to the lysosome for degradation. Substrates are recognised and bound by heat shock cognate protein of 70 kDa (hsc70) which delivers proteins to the lysosome surface. The hsc70-substrate complex then binds to LAMP-2A and the substrate is unfolded and translocated across the lysosome membrane, assisted by a

lysosomal form of hsc70 (lys-hsc70) that is present in the lysosome lumen (Kaushik and Cuervo, 2008). Danon disease is caused by mutations in LAMP-2A and results in defective CMA (Fidzianska et al., 2007). CMA is also affected in mucolipidosis type IV. The transient receptor potential mucolipin (TRPML1) associates with hsc70 and hsc40 on the lysosomal membrane and might be a regulator of CMA. TRPML1 is mutated in mucolipidosis type IV and patients with this disease have decreased CMA (Venugopal et al., 2009). Given the role of lysosomes in pathogen destruction, it is not surprising that some LSD patients have defective clearance of infections. Gaucher disease is caused by a deficiency in glucocerebrosidase leading to an accumulation of glucosylceramide in macrophages, also called “Gaucher cells” (Platt et al., 2012). Gaucher cells have impaired bactericidal activity (Marodi et al., 1995) and non-pathogenic bacteria can cause infections in Gaucher patients (Castaneda et al., 2008). These examples demonstrate the importance of correct lysosomal function in a variety of different cellular processes and cell types.

1.2.3 Lysosome-endosome fusion

The final step in endosome maturation is fusion between late endosomes and lysosomes, forming a hybrid organelle/endolysosome. This is critical for the delivery of lysosomal hydrolases into the acidic lumen of the late endosome. Fusion between LEs and lysosomes (and between any two membranes) can be described in three stages; vesicle docking, *trans*-SNARE formation and finally full fusion.

As described previously, the exchange of Rab5 for Rab7 and its effector proteins is necessary for late endosome maturation and for LE-lysosome fusion. A complex consisting of SAND-1 (Mon1 in yeast) and CCZ-1 has been suggested to act as a switch in this process The SAND-1/CCZ-1 complex is able to bind to active Rab5, PtdIns[3]P, bind Rab7, remove Rabex-5 from endosomal membranes and interact with the HOPS complex (Poteryaev et al., 2010). This allows SAND-1/CCZ-1 to couple the removal of Rab5 and the recruitment of Rab7, along with the HOPS complex to initiate vesicle tethering and promote vesicle fusion. Additionally, it has been shown in yeast that Mon1-Ccz1 functions as a GEF for Rab, promoting the exchange of GDP for GTP and thereby activating Rab7 (Nordmann et al., 2010).

In mammalian cells SAND1/CCZ-1 has also been shown to be a RAB7 GEF (Kinchen and Ravichandran, 2010) and this role has been confirmed in *Arabidopsis thaliana* (Cui et al., 2014).

The HOPS complex is a oligomeric protein tethering complex consisting of 6 subunits, Vps41, Vps18, Vps39, Vps11, Vps16 and Vps33. Consistent with a role in mediating membrane fusion between Rab7 positive compartments, the HOPS complex is able to bind Rab7 through Vps39 and Vps41 at either ends of the complex with a SNARE binding domain (Vps39) between the two (Brocker et al., 2012). The HOPS complex has been shown to have affinity for different phosphatidylinositide lipids including PtdIns[3]P and PtdIns[3,5]P_2 (Stroupe et al., 2006). It is interesting that SAND-1/Ccz1 can bind both PtdIns[3]P and the HOPS complex (Poteryaev et al., 2010). Moreover, the interplay between the Rab7 effector Rubicon and UVRAG, an activator of the HOPS complex (Sun et al., 2010) may be a mechanism that links Rab conversion with tethering between LEs and lysosomes.

Once LEs-lysosomes have been brought together in close proximity there must be correct SNARE pairing if membrane fusion is to proceed. SNAREs (soluble NSF-attachment protein receptor, where NSF stands for *N*-ethylmaleimide-sensitive factor) are a group of proteins that act as docking and fusion machinery between lipid membranes and drive fusion between them. SNAREs are identified by a 60-70 amino acid heptad repeat called a SNARE motif (Fasshauer et al., 1998a). Most SNAREs have a C-terminal transmembrane domain that is connected to the SNARE motif by a short flexible linker (Jahn and Scheller, 2006). Monomeric SNARE proteins are unstructured but when present in the correct combination, four SNARE proteins assemble into a intertwined coiled-coil structure that is extremely stable (Fasshauer, 2003). Within the central hydrophobic core of the complex there are conserved residues – three glutamines and one arginine. These are used to divide the SNARE proteins into two groups, Q-SNAREs containing glutamine and R-SNARES containing arginine (Fasshauer et al., 1998b). SNAREs on opposing membranes then interact to form the helical bundle that brings vesicle membranes in close apposition. Although it has not been proven, it is widely accepted that this is most likely the driving force behind membrane fusion (Chen and Scheller, 2001). The SNARES are thought to “zip” together from their N-

terminal ends and that the formation of this extremely stable complex pulls the membranes together, excluding water molecules and allowing mixing of the hydrophobic lipid layers (Sutton et al., 1998). However, there are also reports that suggest SNAREs are not the final step in membrane fusion. Disruption of SNARE formation with a blocking antibody has been reported not to affect vacuole content mixing in a cell-free yeast vacuole system (Ungermann et al., 1998). An alternative hypothesis is that SNAREs may be involved in vesicle docking which may cause lysosomal calcium release. This is sensed by the calcium binding protein calmodulin, which binds tightly to vacuole membranes and could trigger mixing of the lipid bilayers (Peters and Mayer, 1998, Schekman, 1998). Finally, *cis* SNARE complexes must be dissociated if SNARES are to be reused in additional rounds of vesicle fusion. This process requires the ATPase NSF and α-SNAP (soluble NSF attachment protein) to disassemble SNARE bundles back into individual monomers (May et al., 2001). In the mammalian endosomal system, evidence for the identity of the SNAREs necessary for LE-Lysosome or lysosome-lysosome fusion has come from an *in vitro* fusion study (Pryor et al., 2004). This determined that Syntaxin 7, Vti1b and Syntaxin 8 form the Q a/b/c SNAREs and that Vamp7 and Vamp8 are the R-SNAREs that mediate heterotypic fusion (between late endosomes and lysosomes) or homotypic fusion (between two lysosomes), respectively (Pryor et al., 2004).

Interestingly, *in vitro* studies of yeast vacuole fusion have also demonstrated a proof reading ability of the HOPS complex which recognises incorrect SNARE pairings and inhibits vacuole fusion (Starai et al., 2008). Sec1/Munc18 (SM) proteins are essential for vesicle fusion and interact with cognate SNARE proteins to accelerate vesicle fusion (Yu et al., 2013). The HOPS subunit Vps33 itself is an SM protein that binds to SNARE bundles (Lobingier and Merz, 2012). However, the proof reading ability of the HOPS complex is conferred by the complex as a whole, not via Vps33 alone (Starai et al., 2008). HOPS itself does not promote *trans* SNARE formation but ensures that SNARE assemble in the proper 3Q:1R configuration (Solinger and Spang, 2013). This provides an additional layer of regulation in ensuring fusion only occurs between correctly paired vesicles and suggests the HOPS complex participates in the fusion reaction.

1.2.4 Lysosome biogenesis

Clearly lysosome homeostasis is essential for proper cell function. While there is still some debate as so whether newly formed lysosomes are synthesized *de novo* or made by retrieving membrane from other organelles, studies in recent years have shed light on the mechanisms behind lysosome biogenesis.

In a study of the promoter region of lysosomal genes, it was found that many shared a 10 bp palindromic repeat (GTCACGTGAC) that was present either as a single or in tandem repeats. This motif was named the coordinated lysosomal expression and regulation (CLEAR) element. It was subsequently shown that the transcription factor EB (TFEB) binds to this element and regulates lysosomal gene expression. TFEB belongs to the MiT/TFE subfamily of basic helix-loop-helix (bHLH) transcription factors (Steingrimsson et al., 2004). Over expression of this protein in HeLa cells led to an upregulation of mRNA of lysosomal genes as well as an increase in the number of lysosomes (Sardiello et al., 2009). TFEB directly regulates the expression of 471 genes encoding lysosomal hydrolases, membrane proteins, autophagy genes and non-enzymatic proteins associated with lysosome biogenesis (Palmieri et al., 2011). TFEB also regulates the expression of some non-lysosomal genes. These include *N*-acetylglucosamine-1-phosphotransferase (GlcNAc-P) and members of the biogenesis of lysosome related organelles complex (BLOC) family, BLOC1-3 and Hermansky-Pudlak syndrome genes (HPS) HPS1, HPS3 and HPS5 (Palmieri et al., 2011). GlcNAc-P is responsible for adding mannose 6-phosophate residues to lysosomal hydrolases in the Golgi. Mutations in this enzyme which prevent it from recognising lysosomal enzymes cause the lysosomal storage disorder mucolipidosis IIIC (pseudo-Hurler polydystrophy (Raas-Rothschild et al., 2000). Similarly, mutations in HPS genes causes Hermansky-Pudlak syndrome in which patients are deficient in lysosome-related organelles such as melanocytes and platelet granules (Nazarian et al., 2003). Some of these TFEB regulated genes, such as UVRAG, are involved in autophagy and lysosome biogenesis (Liang et al., 2006). TFEB has also shown to be a regulator of autophagy, providing a link between autophagy and lysosome biogenesis (Settembre et al., 2011). Recently, it has been demonstrated that TFEB is a master regulator of proteostasis and that its upregulation in Gaucher disease fibroblasts helped to increase folding and activity of a mutated lysosomal

hydrolase suggesting TFEB could be used as a therapeutic target in lysosomal diseases (Song et al., 2013). It has also been reported that some lysosomal genes implicated in lysosomal storage disorders are also under the control of circadian rhythms which may have important implications in enzyme replacement therapy (ERT) used to treat these conditions (Mazzoccoli et al., 2015).

1.3 Phagocytosis

Macrophages and other immune cells eliminate foreign particles and invading microorganisms by internalising them into a membrane bound organelle called the phagosome (Vieira et al., 2002). The phagosome matures through a series of sequential interactions with endocytic organelles and eventually fuses with the lysosome. This process is highly analogous to endosome maturation and involves many of the same regulatory and effector proteins (Fig. 1.4).

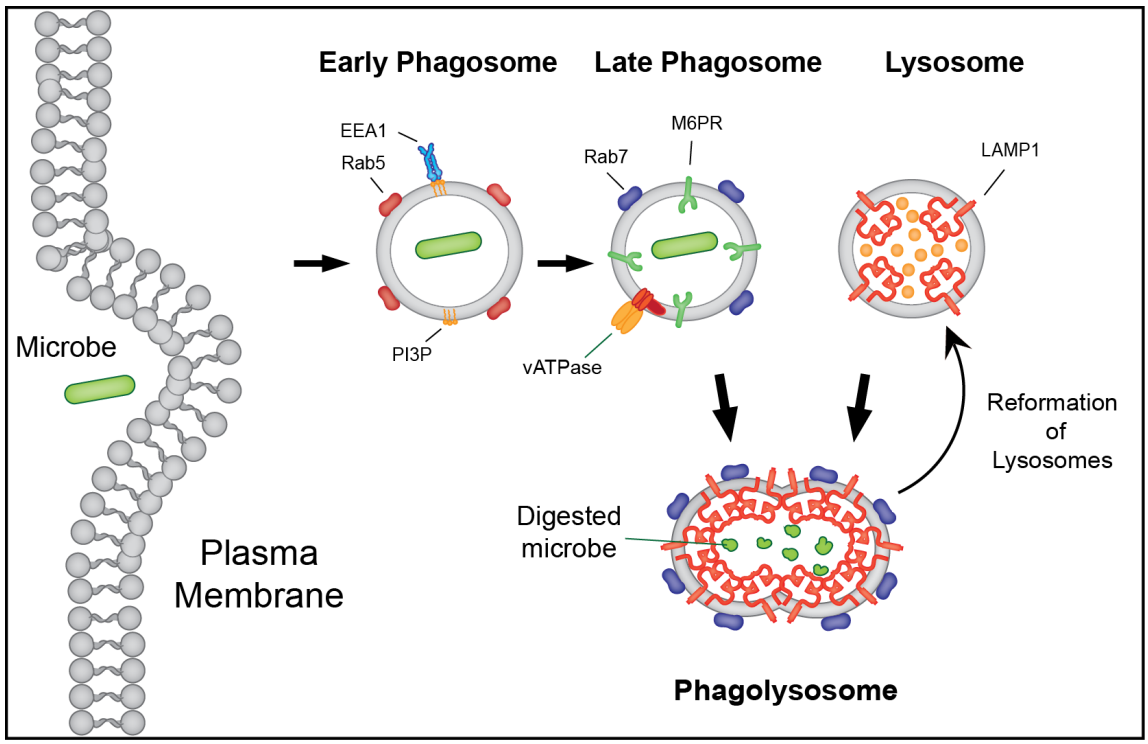

Fig. 1.3 Schematic representation of phagosome maturation. Phagocytic cells internalise microbes or foreign particles into membrane bound compartments called phagosomes (early phagosome). The early phagosome undergoes extensive membrane remodelling and acquires proteins and lipids that regulate this process, such as the GTPase Rab5 the lipid phosphatidylinositol 3-phosphate (PI3P) and tethering factors such as early endosomal antigen 1 (EEA1). As the early phagosome matures to a late phagosome, it loses its association with early effectors and acquires proteins such as Rab7, mannose 6-phosphate receptors (M6PRs) and the vATPase proton pump. The late phagosome then fuses with the lysosome to form a phagolysosome, where it acquires lysosomal hydrolases and membrane proteins such as LAMP1. Finally, membrane is retrieved from the phagolysosome in a process of lysosome reformation.

1.3.1 Initiation of phagocytosis

Phagocytic cells can be loosely classified as being professional, paraprofessional, or non-professional phagocytes, based upon their high, medium or low phagocytic capacity, respectively (Rabinovitch, 1995). For simplicity, only professional phagocytic cells of the immune system (such as macrophages) will be discussed further. The initiation of phagocytosis is very much dependent upon the particle or microbe being internalised but begins with the interaction of a ligand and cognate receptor present on the cell surface. These ligands are present on the surface of the bacteria or particle being internalised or on cells of the body that need to be cleared, such as phosphatidylserine present on the surface of apoptotic cells (Wu et al., 2006). Given the vast array of particles or microbes that cells could encounter there are a wide range of receptors that recognise different ligands. In the case of bacteria or other microbes, pattern-recognition receptors (PPRs) interact with pathogen-associated molecular patterns (PAMPs) which are present on the surface of the phagocytic particle (Janeway, 1992). These can include molecules such as mannans present in the yeast cell wall which are recognised by mannose receptors (Ezekowitz et al., 1990). Other ligands include the lipopolysaccharides (LPS) of Gram negative bacteria, that is recognised by the CD14 receptor (Schiff et al., 1997) or lipoteichoic acids of Gram-positive bacteria recognised by the CD204 receptor (Thomas et al., 2000). These are known as non-opsonic phagocytic ligands as they are present on the surface of the phagocytic particle. Alternatively, host-derived proteins may coat the pathogen or particle being internalised which is termed opsonic phagocytosis (Aderem and Underhill, 1999). The most well studied opsonic ligands are immunoglobulin G (IgG) and complement factor C3bi. IgG antibodies display specificity towards particular surface epitopes and are recognised by Fcγ receptors of which there are 6 in humans; FcγRI, FcγRIIA, FcγRIIB, FcγRIIC, FcγRIIIA and FcγRIIIB (Freeman and Grinstein, 2014). In contrast, C3bi binds non-discriminately to the surface of foreign particles and is recognised by the complement receptor CR3 (Wright et al., 1987). Crosstalk and synergy between different phagocytic receptors that recognise the same ligand further complicates the understanding of phagocytic processes (Aderem and Underhill, 1999). Upon ligand binding, signalling cascades are initiated that result in the recruitment of the cytoskeleton and other components such as GTPases, protein kinases, phospholipases and motor

proteins to the site of phagocytosis (Freeman and Grinstein, 2014). This results in the internalisation of the phagocytic particle.

1.3.2 Parallels to endosome maturation

Phagocytic maturation has many parallels to endosome maturation but it is important to remember that the receptors used to initiate phagocytosis may influence the progression and maturation of phagosomes differently. Immediately after the sealing of the phagosome its membrane composition is much like that of the plasma membrane. The phagosome at this stage posses no microbiocidal activity and must be modified to achieve this. This maturation depends on interactions with early endosomes and eventually late endosomes and lysosomes, resulting in the formation of the phagolysosome which has the degradative capacity needed to digest the contents of the phagosome (Vieira et al., 2002). Interactions between phagosomes and endocytic organelles becomes apparent immediately after phagosome formation (Pitt et al., 1992, Mayorga et al., 1991) and has been recapitulated *in vitro* (Jahraus et al., 1998, Desjardins et al., 1994, Desjardins et al., 1997). The selective nature of phagosome interactions with early endosomes mirrors *in vitro* homotypic endosome fusion (Mills et al., 1998). Although a lot is understood about endosome maturation the molecular mechanisms behind phagosome maturation are not as well characterised. Despite this, the molecular events behind phagosome maturation are likely to mirror those in endosome maturation. Early phagosomes acquire early endosomal markers such as Rab5 (Duclos et al., 2000) and EEA1 (Pitt et al., 1992, Fratti et al., 2001). These are important in phagosome maturation as persistence of Rab5 on the phagosomes of *Mycobacterium tuberculosis* (*M. t*u*berculosis*) and loss of Rab5 on the phagosomes of *Legionella pneumophila* (*L. pneumophila*) prevents their maturation (Clemens et al., 2000).

1.3.3 The Rab conversion in phagosome maturation

The RAB5-RAB7 conversion is likely to play a key role in phagosome maturation but this has not yet been proven. In mammalian cells, RAB5 has been shown to be recruited to phagosomes in a manner that requires active PI[3]PK, but the recruitment of RAB5 was not essential for the appearance of RAB7 on phagosome

membranes (Vieira et al., 2003). RAB7 itself however is not sufficient for fusion between phagosomes and lysosomes (Vieira et al., 2003). RAB7 is likely to play a role in linking phagosomes to the actin cytoskeleton and trafficking them towards lysosomes, a process mediated by its effector protein RILP (Harrison et al., 2003). However, Rab7 has been shown to be important in both early and late phagosome maturation in *Dictyostelium* (Rupper et al., 2001), suggesting that these mechanisms may differ slightly in higher and lower eukaryotes. The HOPS complex, a Rab7 effector, is another likely candidate in phagosome maturation. In *C. elegans*, the HOPS subunit Vps41 is thought to have a role in removing Rab5 from phagosomes and functions before Rab7 acquisition by phagosomes. In the same study it was shown that RNAi knockdown of the HOPS complex subunits prevented phagosome maturation (Kinchen et al., 2008).

1.3.4 The role of protein sorting in maturing phagosomes

Akin to recycling in early endosomes, components of the plasma membrane have been shown to be recycled from phagosomes. Rab coupling protein (RCP) interacts with both Rab11 and Rab4 to regulate membrane recycling from phagosomes (Damiani et al., 2004). Furthermore, the loss of plasma membrane components (such as Fcγ receptors) from late phagosomes has been suggested to be due to recycling from phagosomes (Pitt et al., 1992).

The role of intraluminal vesicle formation in phagosome maturation is not clear but may be of importance. ILV formation is regulated by the ESCRT proteins. The *M. tubercuolosis* effector proteins EsxH, binds to the ESCRT protein Hrs. Furthermore, EsxH forms a complex with another effector protein, EsxG, to disrupt ESCRT function and prevent bacterial delivery to the lysosome (Mehra et al., 2013). In yeast, expression of the *L. pneumophila* effector protein VipA, disrupts ILV formation by binding to Bro1 (Franco et al., 2012). Bro1 is the yeast orthologue of ALIX, a protein involved in MVB formation (Odorizzi, 2006). LBPA is thought to have a role in ILV formation. LBPA is present in phagosomal membranes (Vieira et al., 2003) and is able to promote inward budding of pure liposomes *in vitro* (Matsuo et al., 2004). LBPA also has a role in cholesterol transport from late endosomes (Kobayashi et al., 1999). Moreover, in macrophages where cholesterol

transport was pharmacologically inhibited, phagosome-lysosome fusion was impaired (Huynh et al., 2008).

1.3.5 The involvement of SNARES in phagosome maturation

As with late endosome-lysosome fusion, the fusion between phagosomes and lysosomes is likely to be mediated by SNAREs. *In vitro* LE/lysosome fusion involves the Q-SNAREs Syntaxin7, Vti1b and Syntaxin 8 and the R-SNARE Vamp7 or Vamp8 (LE-lysosome and lysosome-lysosome fusion respectively) (Pryor et al., 2004). It is likely that these proteins are involved in phagolysosome formation and Vti1 and Vamp7 have been found on *Dictyostelium* phagosomes (Gotthardt et al., 2002). Syntaxins 2, 3 and 4 have also been found on macrophage phagosomes (Hackam et al., 1996) and SNAP-23 (also a SNARE protein) has been found in phagosome membranes and is implicated in phagosome maturation (Sakurai et al., 2012). Syntaxin 7 and 13 have been found on phagosomes, although Syntaxin 13 is associated more with recycling compartments and is rapidly removed from phagosome membranes (Collins et al., 2002). Recombinantly produced SNARE proteins lacking transmembrane domains (solSNARES) cannot support vesicle fusion reactions but inhibit them by binding to SNAREs present on vesicle membranes. In an *in vitro* phagosome-lysosome fusion assay, a combination of solSNARES Syntaxin 7, Vti1b and Syntaxin 8 were able to inhibit fusion reactions suggesting these SNARES are involved in phagosome-lysosome fusion (Becken et al., 2010).

1.3.6 Phagosome acidification

As with endosome maturation, the pH of the phagosome decreases as it matures. The most commonly used marker of a functional phagosome is this drop in pH as it allows lysosomal hydrolases to become active, facilitating the digestion of phagocytosed particles (Kinchen and Ravichandran, 2008). This is performed by the vATPase which is rapidly recruited to phagosomes after their formation (Pitt et al., 1992). The acidic pH of the phagolysosome also supports the generation of reactive oxygen species (ROS), such as nitric oxide, which is particularly damaging to pathogens and is a key part of innate immunity (Kotsias et al., 2013).

In *Dictyostelium* the vATPase appears to be delivered to the phagosome through fusion with vATPase containing endosomes (Clarke et al., 2002). In mammalian cells this is not so clear, as the vATPase is synthesised in the Golgi and is delivered to the phagosome along with cathepsins (Fratti et al., 2003). The vATPase has also been shown to be retrieved from phagosome membranes during exocytosis (Clarke et al., 2010).

1.2.7 LAMP proteins and phagosome maturation

LAMP1 and LAMP2 are heavily glycosylated integral membrane proteins with currently undefined functions, but LAMP2 has recently been shown to be involved in chaperone mediated autophagy (Eskelinen et al., 2003). Loss of both LAMP1 and LAMP2 results in embryonic lethality in mice. In $LAMP1^{-/-}$ and $LAMP2^{-/-}$ mouse embryonic fibroblast model, it was shown that these proteins were required for phagosome maturation. While phagocytic uptake in these cells proceeded as normal, phagosomes failed to acquire Rab7 and accumulated the early phagosomal lipid PtdIns[3]P (Huynh et al., 2007).

Clearly there is much overlap between the molecular mechanisms governing phagosome and endosome maturation events. Phagosome maturation is highly regulated and disruption of this regulation can prevent the interaction between phagosomes and lysosomes. The proteins that regulate these processes are often targetted by the effector proteins produced by intracellular pathogens.

1.4 Pathogen manipulation of intracellular membrane traffic

Intracellular pathogens by their definition must be able to modulate or disrupt host cell defences if they are to survive intracellularly. Once phagocytosed, a bacteria is destined for destruction in the lysosome unless it escapes into the host cell cytoplasm or is able to disrupt events in membrane trafficking that arrest phagosome maturation. For a pathogen to be successful, it must be able to avoid the immune system of its host. It is striking however, that some bacteria actually seek out host immune cells and actively encourage their uptake into the host cell. This may seem counterintuitive, but the intracellular lifestyle has several advantages. Firstly, by being intracellular a pathogen is afforded protection from the rest of the immune system and avoids circulating antibodies and humoral factors. Secondly, the phagosome provides a replicative niche with a supply of nutrients for bacterial growth. Thirdly, it may allow dissemination of the pathogen throughout the rest of the host and in some cases can facilitate transmission between hosts. The intracellular niche is one that is intriguing, but can also shed light on the mechanisms that underlie host cell biology. By studying intracellular pathogens and understanding how they manipulate host cells it is possible to unravel novel mechanisms in membrane trafficking and other cellular functions.

To prevent delivery to the lysosome a pathogen could opt to escape the phagosome and reside in the host cell cytoplasm. This would also prevent the host cell from presenting foreign bacterial or viral peptides from the endosomal system on the cell surface via MHC class II molecules (Roche and Furuta, 2015), leading to the T-Cell activation and induction of host cell apoptosis (Mogensen, 2009). However, immune surveillance of the cytoplasm is carried out by specialised cytosolic PPPs such as retinoid acid-inducible gene I-like receptors (RLRs) (Loo and Gale, 2011) which recognise viral RNA and nucleotide-binding oligomerization domain-like receptors (NLRs) which recognise bacterial ligands (Franchi et al., 2009). Activation of these receptors induces a cascade of proinflammatory cytokines and chemokines which can activate the inflammasome and induce host cell death (Latz et al., 2013). Furthermore, host cell autophagic machinery can induce autophagosome formation around cytosolic bacteria, leading to their sequestration and eventual delivery to the lysosome, a process which has recently been termed xenophagy (Bauckman et al., 2015). Some intracellular bacteria such

as *Shigella* have adapted to a cytoplasmic lifestyle and actively downregulate autophagy to avoid this (Ogawa et al., 2005).

A prerequisite of being an intracellular pathogen is the production of proteins or lipids that interfere with host cell function. If a pathogen is within a phagosomal compartment then effector proteins or lipids must either exert their effect from within the phagosome or they must be actively translocated across the phagosome membrane where they become active in the cytoplasm. The latter is achieved by secretion systems. These are specialised bacterial protein complexes that are responsible for exporting a variety of virulence proteins outside of the bacterial cell. Two of these secretion systems, the type III secretion system (T3SS) and type IV secretion system (T4SS) are unique in that they span both the bacterial cell envelope and host cell membranes (Costa et al., 2015). Many intracellular bacterial use these systems to deliver many different effector proteins into the host cell cytoplasm. For example, *Legionella pneumophila* is thought to have over 300 different effector proteins that it uses to disrupt host cell function (Segal, 2013). Bacterial effector proteins effect phagosome maturation by interacting with many different regulators of membrane trafficking, including Rab and Rho GTPases, phosphoinositide lipids, multisubunit tethering complexes and the actin cytoskeleton (Ham et al., 2011). While there are many intracellular bacteria, the classical and most well studied include *Salmonella, Legionella, Yersinia, Leishmania, Shigella, Chlamydia* and *Mycobacterium* species (Hueck, 1998).

1.4.1 Salmonella

Salmonella enterica is a Gram-negative facultative intracellular pathogen that has over 2500 different serovars and causes a variety of pathologies ranging from gastroenteritis to systemic typhoid fever (Coburn et al., 2007). *Salmonella* is phagocytosed and resides within the *Salmonella* containing vacuole (SCV). *Salmonella* uses a variety of T3SS substrates to regulate the fusion of this compartment with early and late endosomes, but it remains unclear whether or not the SCV also fuses with lysosomes (Knodler and Steele-Mortimer, 2003). The SCV has been shown to acidify (Rathman et al., 1996), acquire lysosomal proteins such as LAMPs (Steele-Mortimer et al., 1999) but does not acquire mannose 6-

phosphate receptors and cathepsin delivery to the SCV is delayed (Garcia-del Portillo and Finlay, 1995).

The effector protein SopB is a phosphatidylinositol phosphatase (PI-P) that has multiple roles in host cell invasion and maturation of the SCV. SopB catalyses the hydrolysis of PtdIns(4,5)P_2 present on the cell surface. This promotes bacterial uptake at the site of SCV formation by promoting membrane fission through reorganisation of the actin cytoskeleton (Hernandez et al., 2004, Terebiznik et al., 2002). By hydrolysing PtdIns[4,5]P_2 SopB indirectly recruits RAB5 to the SCV surface by maintaining high levels of PtdIns[3]P. This in turn recruits the Rab5 effector VPS34 which increases PtdIns[3]P levels further. Low levels of PtdIns(4,5)P_2 reduces the negative charge on the SCV membrane preventing the recruitment of RAB35 and RAB23 to the SCV and inhibiting SCV-lysosome fusion (Mallo et al., 2008). A schematic of this is depicted in figure 1.5.

A characteristic of SCVs is the formation of Salmonella induced filaments (Sifs). These are tubular protrusions of the SCV that contain LAMP1, the vATPase and LBPA and so are thought to be of late endocytic origin (Srikanth et al., 2011). The effector protein SifA is essential for tubulation of the SCV. SifA binds to the kinesin binding protein SKIP (Diacovich et al., 2009). The correct position of the SCV and the formation of SifA filaments/tubules is essential for bacterial replication and maintaining the integrity of the SCV (Ham et al., 2011). The SCV also moves along microtubules towards the microtubule organising centre (MTOC). This process requires the recruitment of the RAB7 effector RILP and the dynein motor complex by the effector SseF, which acts with SifA and SseG to regulate the juxtanuclear positioning of the SCV (Abrahams et al., 2006).

Interestingly, *Salmonella* may also modulate host cell-gene expression. The effectors SptP and SspH1 are involved in the downregulation of interleukin-8. Moreover, SspH1 enters the nucleus and disrupts NF-κB-dependent gene expression. This suggests that the suppression of inflammation is crucial for *Salmonella* infections (Haraga and Miller, 2003).

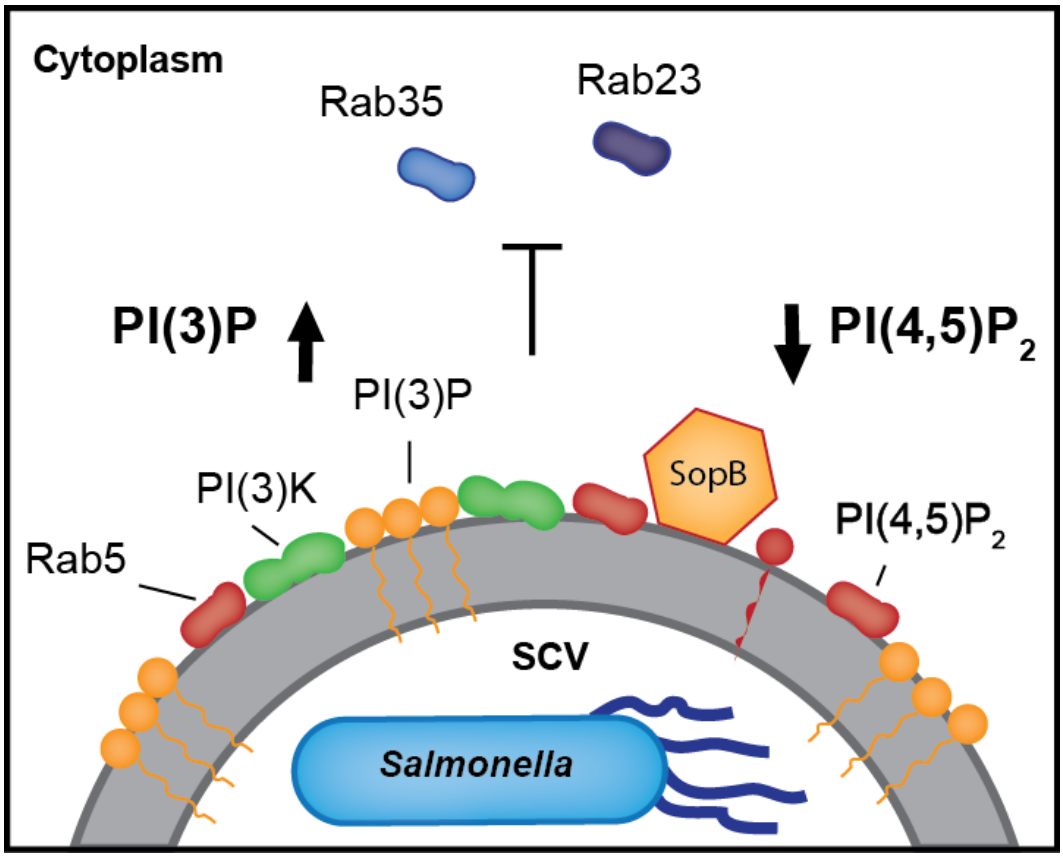

Fig. 1.4 Modulation of the SCV by SopB. *Salmonella* actively translocates the type III secretion substrate SopB, from the *Salmonella*-containing vacuole (SCV) into the host cell cytoplasm. SopB is a phosphatidylinositol phosphatase (PI-P) that hydrolyses phosphatidylinositiol 4,5,bis-phosphate (PI(4,5,)P_2) to phosphatidylinositol 3-phosphate (PI(3)P). This has the effect of recruiting RAB5 which in turn recruits its effector protein phosphatidylinositol 3-phosphate- kinase (PI(3)PK). This generates more PI(3)P. The decrease in PI(4,5,)P_2 levels on the SCV membrane reduces the negative charge on the membrane surface, preventing the association of RAB35 and RAB23 on the SCV and inhibiting SCV-lysosome fusion.

1.2.5 Mycobacterium tuberculosis

Mycobacterium tuberculosis (*M. tuberculosis*) is a Gram-positive bacterium that resides inside alveolar macrophages and causes tuberculosis. *M. tuberculosis* arrests phagosome maturation at an early endosomal stage and is positive for RAB5 and does not fuse with the lysosome (Kumar and Valdivia, 2009). The mycobacterial cell wall is composed of unique lipids such as mannose-capped lipoarabinomannan (ManLAM) and trehalose dimycolate (Meena and Rajni, 2010).

ManLam is of particular interest due to the fact that it mimics host cell phosphatidylinositol and is a potent inhibitor of phagosome maturation. The SNARE Syntaxin 6 interacts with EEA1, which is recruited to phagosome membranes by the binding of its FYVE domain to PtdIns[3]P (Simonsen et al., 1999). ManLam insertion into the phagosome membrane prevents association of Syntaxin 6. This subsequently blocks membrane trafficking between the Golgi and the *Mycobacterium* phagosome which prevents delivery of LAMPs, lysosomal hydrolases and the vATPase (Fratti et al., 2003).

The secreted effector protein SapM is also involved in intracellular survival of *M. tuberculosis* (Fig. 1.6). SapM is an acid phosphatase that converts PtdIns[3]P to PtdIns. The phagosomes of live *Mycobacterium* continuously remove PtdIns[3]P whereas phagosomes of dead *Mycobacterium* do not (Vergne et al., 2005). This prevents the association of PtdIns[3]P-interacting proteins necessary for phagosome maturation such as EEA1. When added to an *in vitro* fusion assay, SapM was shown to inhibit late endosome-phagosome fusion (Vergne et al., 2005). Another *M. tuberculosis* effector protein, Protein tyrosine phosphatase A (PtpA) has been shown to be involved in preventing phagosome-lysosome fusion. The HOPS complex is a key regulator of SNARE formation and is necessary for fusion with the lysosome. When PtpA binds to the HOPS subunit VPS33, resulting it its dephosphorylation and inactivation, subsequently preventing phagosome-lysosome fusion (Bach et al., 2008). Interestingly, PtpA has also been shown to have a second function in arresting phagosome acidification. PtpA binds to subunit H of the vATPase. The HOPS complex is recruited to the vATPase where PtpA is then able to dephosphorylate VPS33 and disrupt the interaction between HOPS and the proton pump (Wong et al., 2011). Intriguingly, *M. tuberculosis* has no known means of translocating effector proteins across the phagosomal membrane into the host cell cytoplasm. Despite this, effectors such as SapM and PtpA clearly have their targets in the cytoplasm. While PtpA has been detected in immuno-electron microscopy and western blot analysis of macrophages (Bach et al., 2008), the mechanisms behind which *M. tuberculosis* effector proteins reach the cytosol remains elusive (Wong et al., 2013). A similar Gram-positive pathogen *Rhodococcus equi* (*R. equi*) also resides intracellularly in alveolar macrophages. *R. equi* arrests phagosome maturation at the early endosomal stage but the mechanisms by which it does so are unclear (Fernandez-Mora et al., 2005).

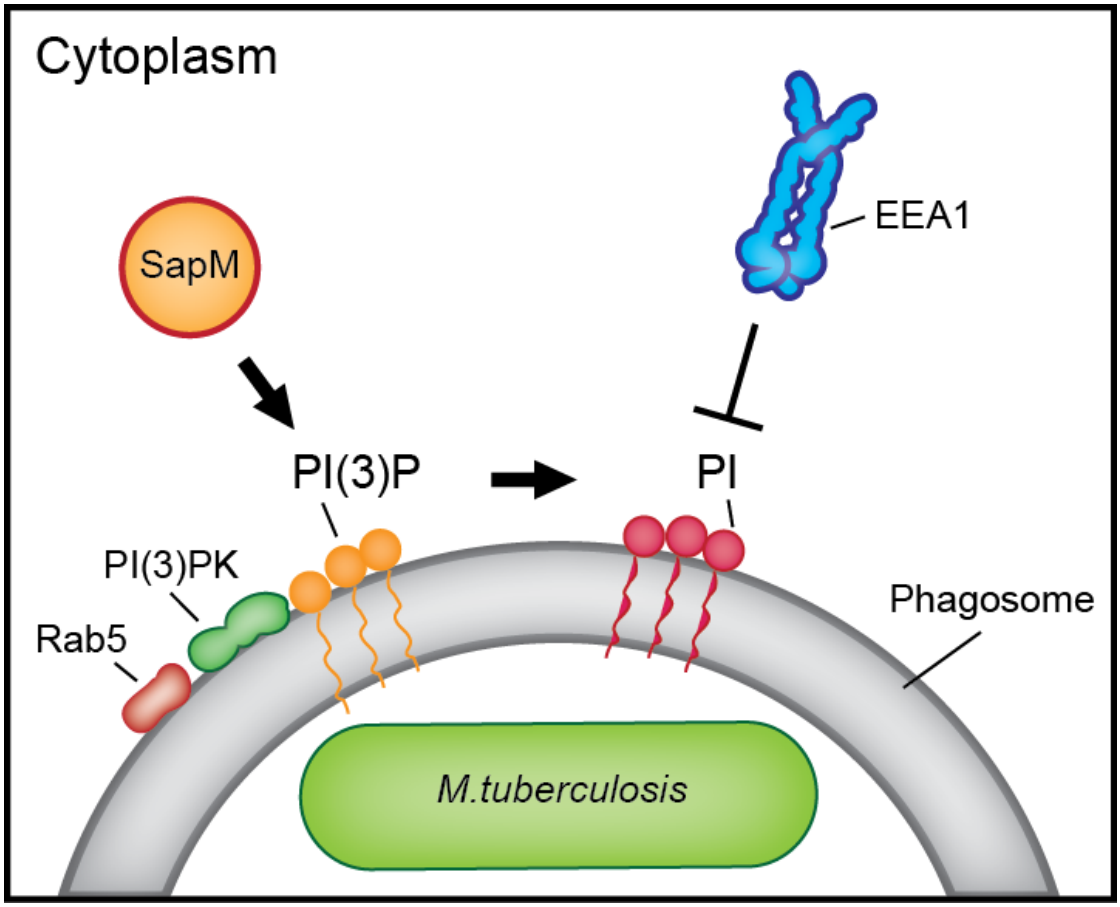

Fig. 1.5 SapM disruption of phagosome maturation. SapM is an acid phosphatase secreted by *Mycobacterium tuberculosis* that crosses the phagosomal membrane (through a currently unknown mechanism) and is active in the host cell cytoplasm. *M. tuberculosis* phagosome acquire RAB5 and its effector VPS34, a phosphatidylinositol 3-phosphate kinase (PI(3)PK). Production of PI(3)P is essential for phagosome maturation and fusion with the lysosome. SapM converts phosphatidylinositol 3-phosphate (PI(3)P) to phosphatidylinositol (PI) which prevents the acquisition of the PI(3)P binding protein EEA1 which is needed for maturation of the phagosome.

1.5 Rhodococcus equi

1.5.1 *Rhodococcus equi*

Rhodococcus equi, first identified almost 90 years ago (Magnusson, 1923), is a Gram-positive mycobacterium found in the soil. *Rhodococcus equi* grows on a variety of substrates forming mucoid salmon-pink colonies after several days of growth. The genus is comprised of more than 40 species which are used in a range of biotechnological applications such as the biodegradation of hydrophobic and organic compounds (Larkin et al., 2005). *R. equi* is the only pathogenic *Rhodococcus* species and is a cause of pneumonia in new born foals up to 6 months of age but also causes a similar disease in humans (Prescott, 1991). Transmission of infection is thought to occur through inhalation of contaminated dust or soil particles (Muscatello et al., 2006). *R. equi* shares some similarities with *M. tuberculosis* such as production of mycolic acid cell wall components (Sutcliffe, 1998) and causes a similar disease pathology (Yamshchikov et al., 2010). Incidence of *R. equi* disease has been increasingly reported in the literature and *R. equi* may be becoming an emerging pathogen (Weinstock and Brown, 2002). *R. equi* is a substantial economic impact to the equine industry (Muscatello, 2012) and is estimated to cost around $2-4 million annually in Australia (Muscatello et al., 2006). However, the precise worldwide economic cost to the equine industry and the healthcare industry is not known.

1.5.2 Taxonomic status of *R. equi*

Currently, there is some controversy regarding the naming of *R. equi*. Although almost every research publication uses the term *R. equi*, the original description of the bacteria was termed *Corynebacterium equi* (Magnusson, 1923). However, it was reported that *R. equi* should be reclassified as *Corynebacterium hoagii* (Goodfellow and Alderson, 1977). This should take precedence over the name *Rhodococcus equi* as the naming of *Corynebacterium hoagii* occurred before that of *Rhodococcus equi* (Tindall, 2014). The situation is further complicated by the proposed renaming of *Rhodococcus equi* to *Prescottia equi* (in honor of the substantial contribution to the *R. equi* field by John Prescott) and subsequent revision of *Prescottia* to *Prescottella* (Jones et al., 2013, Goodfellow et al., 2015).

Subsequently, there has been much confusion regarding the appropriate naming of this bacterium.

1.5.3 Infection of horses

Foals aged up to 6 months appear to be susceptible to *R. equi* infections and the mortality rate if left untreated can be as high as 80 %. This is reduced to around 12 % with antibiotic therapy (von Bargen and Haas, 2009). In horses, *R. equi* causes severe lung abscesses with the formation of granulomas and an influx of immune cells into the lungs. More rarely, the infection can also spread to the intestines (Prescott, 1991).

1.5.4 Human infections of *R. equi*

The first reported case of *R. equi* infection in humans was of a man receiving immunosuppressive therapy (Golub et al., 1967) and it is thought that transmission in humans may be due to exposure to *R. equi* through contact with infected animals (Weinstock and Brown, 2002). *R. equi* is an increasingly reported zoonosis of immunocompromised patients, such as AIDS patients (Samies et al., 1986, Shin et al., 1999, De Nardi et al., 2011, Topino et al., 2010) and organ transplant patients (Guerrero et al., 2011, Hayes et al., 2011, Munoz et al., 2008). Infection in healthy individuals is rare (Hondalus, 1997) but the outcome can be fatal in the immunocompetent, even with adequate treatment (Gabriels et al., 2006). Mortality rates among the immunocompromised varies from 25%-55%, compared to 11 % in the immunocompetent (Kedlaya et al., 2001). Compromised cellular immunity is associated with an increase in morbidity in *R. equi* infections, as shown by experiments with T-cell deficient and severe combined immunodeficient (SCID) mice which are particularly susceptible to *R. equi* infection (Nordmann et al., 1992, Yager et al., 1991). Treatment of *R. equi* is with antibiotic therapy, but this is difficult due to the low *in vivo* uptake of these drugs (Berghaus et al., 2013) Antibiotic resistance in *R. equi* has also been reported (Cisek et al., 2014).

1.5.5 Virulence of *Rhodococcus equi*

R. equi has been shown to survive and replicate *in vitro*, within mouse macrophages (Hondalus and Mosser, 1994) and human alveolar epithelial cells (Ramos-Vivas et al., 2011). Maturation of the *Rhodococcus* containing phagosome (RCV) is arrested after the early endosome stage and RCVs do not fuse with lysosomes (Fernandez-Mora et al., 2005). However, it has been reported that while *R. equi* was unable to prevent phagosome-lysosome fusion, the resulting hybrid organelle was not as acidic as that of phagolysosomes containing avirulent *R. equi* strains (Toyooka et al., 2005). As such, is it currently not clear how *R. equi* is able to survive intracelluarly. *R. equi* shares many similarities to *M. tuberculosis* as demonstrated by the similarities in their disease pathologies. Both have mycolic acids in the cell wall and sequencing analysis of 1417 *R. equi* sequences showed that 799 (47%) shared homology with genes in *M. tuberculosis*. These included genes for metabolism, lipid biosynthesis, iron acquisition and virulence (Rahman et al., 2003). It may be possible to understand *M. tuberculosis* infection by studying the mechanisms by which *R. equi* survives inside cells.

The susceptibility of new-born foals to *R. equi* infection is likely to be due a variety of factors, such as the immaturity of their immune system and the decline of maternal antibodies. However, *R. equi* clearly must have virulence factors that allow its persistence in the immunocompetent human host. The main focus of current research is on the 90Kb virulence plasmid that virulent *R. equi* strains possess, which allows the expression of Virulence associated proteins (Vaps). The virulence plasmid contains 64 open reading frames (ORFs). 22 have homology to genes of a known function and 3 have homology to genes of unknown function in other species. The plasmid also contains a 27.5kb pathogenicity island (PI) containing 7 *Vap* genes all of which have a high degree of homology in their C-terminus regions to VapA (Takai et al., 2000). Expression of the Vaps is induced when *R. equi* is exposed to low pH (pH 5.0) (Benoit et al., 2001), H_2O_2 (Benoit et al., 2002) and when cultured at 37 ºC (Byrne et al., 2001). These conditions mimic the acidic pH, reactive oxygen species (ROSs) and the higher temperature of the macrophage phagosome. These genes are indeed upregulated when *R. equi* is grown inside macrophages (Rahman et al., 2005). Strains which do not posses the plasmid are avirulent in a mouse model of virulence (Takai et al., 1996), but

addition of constitutively expressed *VapA* to an plasmid cured strain is not sufficient to rescue the full virulent phenotype (Giguere et al., 1999). This suggests *VapA* is not the only virulence factor that *R. equi* utilises for intracellular survival and potential there are chromosomal genes that facilitate persistence.

1.5.6 Putative virulence factors

R. equi has several mycobacterial gene families that may have roles in virulence. These include three mammalian cell entry (mce) gene clusters and an ESX gene cluster, which may have role in mycobacterial pathogenesis (Letek et al., 2010). In *Mycobacterium,* the ESX gene clusters are type VII secretion systems (T7SS) that secrete virulence factors (Feltcher et al., 2010). Whether these factors are important in *R. equi* pathogenesis is not clear. *R. equi* also possess membrane damaging toxins such as cholesterol oxidase and a potential phospholipase. However, it was recently shown that cholesterol oxidase (ChoE) was not essential for intracellular survival of *R. equi* (Pei et al., 2006). *R. equi* also has genes with homology to *M. tuberculosis* effector proteins PtpA and PtpB. Similarly, *R. equi* has a gene with homology to *M. tuberculosis* nucleoside-diphosphate kinase (Ndk) which interferes with GTPase function to prevent phagosome maturation (Sun et al., 2013). It is not known if these proteins are produced by *R. equi* or have a role in virulence. Other putative virulence factors include the lipids produced by *R. equi*. In a study of *R. equi* mutants that could not stop their delivery to the lysosome, it was found that the length of mycolic acid chains on the bacterial cell surface is particularly important for virulence (Sydor et al., 2013).

1.6 Research Aims

Lysosomes have multiple roles in cell functions and in particular in the clearance and degradation of pathogenic bacteria. The molecular mechanisms behind phagosome-lysosome fusion are not clear and currently there is no suitable means of assaying phagosome-lysosome fusion *in vitro*. The use of *in vitro* assays in understanding fusion events has several advantages. Firstly, the specific conditions of vesicle fusion can be easily altered to examine the effect on membrane fusion e.g. temperature, salt concentration, etc. Secondly, cell-free assays allow membrane fusion to be studied in isolation from the other processes of the cell which could influence the results or make their interpretation difficult. Finally, specific inhibitors can be used to disrupt the activity of a single protein e.g the production of PtdIns[3]P by PtdIns[3]P-kinase can be disrupted by wortmannin. The use of *in* vitro assays of vesicle fusion have been invaluable in the dissection of the molecular requirements these events. Examples of these include fusion at the Golgi (Balch and Rothman, 1985, Balch et al., 1987) and fusion of liposomes to understand SNARE function (Schuette et al., 2004). *In vitro* fusion of lysosomes and late endosomes resulting in hybrid organelle formation has also been studied and shown to require NSF, ATP, physiological temperature, cell cytosol and the activity of a Rab GTPase (Mullock et al., 1998). However, there is only one report of *in vitro* phagosome-lysosome fusion (Becken et al., 2010). Thus, the first aim of this research is:

i) develop an *in vitro* phagosome-lysosome fusion assay to determine the molecular requirements behind phagosome-lysosome fusion.

Some intracellular pathogens manipulate their trafficking to the lysosome to reside within a modified phagosomal compartment. In the case of *R. equi*, the molecular mechanisms behind intracellular persistence and disruption of membrane trafficking are not known. Thus, the second aim of this research is:

ii) Unravel the molecular mechanisms that *R. equi* uses to survive intracellularly.

Chapter 2: General Materials and Methods

2.1 Chemicals

All chemicals unless otherwise stated, were of analytical grade and were purchased from Sigma or Fisher.

2.2 Antibiotics

Stocks of antibiotics were made by dissolving the required amount antibiotic in water unless otherwise stated. All stocks were stored at -20 ºC unless otherwise stated. Ampicillin was made at 100 mg/ml in H_2O and used at 100 µg/ml. Chloramphenicol was made as a 25 mg/ml stock in absolute ethanol and used at 25 µg/ml. Kanamycin was made at 40 mg/m in H_2O and used at 40 µg/ml. Gentamycin was made at 20 mg/ml in H_2O and used at 150 µg/ml or 10 µg/ml. Hygromycin B was stored at 4 ºC as a 50 mg/ml stock (Roche) and used at 100 µg/ml.

2.3 Bacterial and yeast culture and media

All bacterial media was purchased from Oxoid or Formedium, and all yeast media was purchased from Formedium, UK, unless otherwise stated.

All autoclaving was performed at 121 ^{o}C at 38.4 psi for 28 min. Bacterial media was made as follows: Lysogeny broth (LB), was made by dissolving 10 g of NaCl, 10 g of tryptone, and 5 g of yeast extract in 1 L of ddH_2O and autoclaved. For LB agar, 15 g of agar was added per litre. Brain heart infusion (BHI, Sigma, UK) broth was prepared by dissolving 37 g of premade media in 1 L of ddH_2O. BHI agar (Sigma, UK) was prepared by dissolving 52 g in 1 l ddH_2O. SOC media was prepared by dissolving 20 g of tryptone, 5 g of yeast extract, 5 ml of 2 M $MgCl_2$ and 0.5 g of NaCl in 1 l of ddH_2O and autoclaving. After autoclaving the media, 20 ml of 1 M glucose (sterile filtered) was added. 2TY broth was made by dissolving 16 g of tryptone, 5 g of NaCl, and 10 g of yeast extract in 900 ml of ddH_2O. The pH was adjusted to 7.0 with 5 M NaOH, volume made to 1 L, and the media autoclaved.

All yeast media were made as per the manufacturer's instructions: For YEP broth, 30 g of premade YEP (Formedium, Cat # CCM0402) was dissolved in 1l ddH_2O. For YPD broth, 50 g of premade YDP (Formedium, Cat # CCM0202) was dissolved in 1 L ddH_2O and then autoclaved. For Synthetic depleted (SD) - ura media, 6.9 g of yeast nitrogen base, and 1926 mg of Kaisers dropout mix (– uracil) was dissolved in 1 L of ddH_2O and autoclaved. Synthetic complete (SC) media was made by dissolving 6.9 g nitrogen base and 2002 mg of Kaisers' complete dropout mix in 1 L ddH_2O and autoclaved. Agar plates were made by adding agar to 1.5 % (w/v) to the required media where appropriate. Sterile glucose or fructose (from a 40 % w/v stock) was added to all yeast media after autoclaving, to a final concentration of 2 % (v/v) . All bacterial cultures were grown at 37 ^{o}C in LB (with antibiotics where appropriate) with shaking, unless otherwise stated. *R. equi* was grown in BHI at 30 ^{o}C with shaking unless otherwise stated. All yeast were grown in non selective media (YEP or YPD, with glucose as the carbon source or fructose as the carbon source where CPY-invertase secretion was to be assayed) or selective media (SD-Ura) at 30 ºC with shaking, unless otherwise stated.

2.4 Mammalian cell culture

All mammalian cell culture (for J774.2, Raw 264.7, NRK, and HeLa cells) was performed as following unless otherwise stated. Cells were cultured in Dulbecco's modified Eagle's medium (DMEM) supplemented with 10 % (v/v) FBS, 2 mM glutamine and 1 % (v/v) penicillin-streptomycin (10 U/ml and 10 µg/ml respectively) in a humidified 5 % CO_2 atmosphere at 37 ºC. Where antibiotic selection was required, media was supplemented with Hygromycin B (Roche, 50 µg/ml from a 50 mg/ml stock).

2.5 DNA extractions

2.5.1 Plasmid DNA Minipreps from bacteria

DNA plasmids were routinely extracted from 7.5 ml overnight cultures using the Qiagen mini prep kit as per the manufacturers' instructions. For low copy plasmids, the volumes of buffers P1, P2, and P3 were doubled. Where the volume of bacterial lysate exceeded the capacity of the column, the remainder was passed through the same column.

2.5.2 Plasmid DNA Midipreps from bacteria

DNA plasmids were routinely extracted from 50 ml overnight cultures using the Qiagen Midi prep kit as per the manufacturers' instructions with the following modifications. At the final elution step, 500 µl of TE was used to elute DNA, and the eluate was passed through the filter disc a second time.

2.6 DNA electrophoresis

Agarose gels were prepared by dissolving 0.5- 2.0 % (w/v) agarose in 75 ml in TAE buffer (40 mM Tris, 20 mM Acetic acid, 0.5 mM EDTA, pH 8) by heating in a microwave until dissolved. Either ethidium bromide (diluted 1:1000 from a 10 mg/ml stock) or Sybr Safe, used at 1:10,000 (Invitrogen) was added to the melted agarose and gently mixed. DNA was electrophoresed at 60 V for approximately 1 h. DNA was visualised using UV light (ethidium bromide) or a blue light box (Sybr Safe), and images captured using a Syngene gel imager and Genesnap software.

2.7 Purification of PCR products

PCR products were electrophoresed using an appropriate percentage agarose gel containing Sybr Safe DNA stain (1:10,000). DNA bands were visualised on a blue light box, and excised from the gel using a sterile scalpel blade. DNA was purified from gel slices using the Qiagen gel purification kit, as per the manufacturer's instructions, with the following modifications: 600 µl of buffer QC was used regardless of gel slice size, and 200 µl of isopropanol was added to the dissolved agarose gel slice.

2.8 DNA restriction digests.

All restriction digests were performed in a total volume of 40 µl unless otherwise stated. All digests were carried out in 0.5,1, 1.5 or 2 X KGB buffer (10 X KGB, 1 M glutamic acid (monopotassium salt), 250 mM Tris acetate, pH 7.6, 100 mM magnesium acetate, 0.5 mg/ml bovine serum albumin, 5 mM β-mercaptoethanol), depending on the dilution of KGB that gave the highest activity for a particular restriction enzyme (McClelland et al., 1988). For plasmid digests, 1 µg of plasmid DNA was incubated with 1 µl of the appropriate restriction enzyme for a minimum

of 45 min at the appropriate temperature. For overnight digests, a further 1 µl of restriction enzyme was added after a 2 h incubation. Digested DNA was analysed by gel electrophoresis (section 2.6) and DNA was gel-purified where appropriate using a Qiagen gel extraction kit (section 2.7) as per the manufacturer's instructions.

2.9 Polymerase chain reaction (PCR)

All PCRs was performed in a Biorad PTC-200 DNA engine cycler unless otherwise stated.

2.9.1 Generation of PCR products for cloning

For the generation of high-fidelity PCR products for cloning, reactions were set up as follows: PCR reactions were performed in a total volume of 50 µl, containing 37.5 µl of ultrapure 18 Ω H_2O, 5 µl of 10X *pfu* polymerase buffer, 0.5 µl of dNTPs (final concentration of 100 µM each of dATP, dTTP, dCTP and dGTP from a 10 mM stock), 2.5 µl each of forward and reverse primers (final concentration of 0.5 µM from a 10 µM stock), and 1.0 µl of *pfu* polymerase (2.5 units). The mixture was vortexed, and approximately 10 ng of template DNA was added to the tube, which was vortexed again. The PCR programme used for *pfu* polymerase was as follows: template denaturation was performed for 45 seconds at 94 ºC followed by primer binding for 45 seconds at 50 ºC (unless otherwise stated). Extension was performed for 72 ºC for 1 min per Kb of template length. These steps were repeated for a further 29 cycles, with a final extension at 72 ºC for 10 min.

2.9.2 General PCR

For general PCR reactions where high-fidelity amplification of the PCR product was not required, reactions were set up as follows: All reactions were performed in a final volume of 20 µl and contained 11.2 µl of 18 Ω ddH_2O, 4 µl of 5X Go *Taq* Flexi polymerase buffer, 0.4 µl of dNTPs (final concentration of 100 µM each from a 10 mM stock), 1 µl each of forward and reverse primers (final concentration of 0.5 µM from a 10 µM stock), 1.2 µl of 25 mM MgCl, and 1.0 µl of Go *Taq* polymerase (1.0 unit). The mixture was vortexed, and approximately 10 ng of template DNA was added to the tube, which was vortexed again. The PCR

programme used for *Taq* polymerase was as follows: DNA was denatured at 95 ºC for 1 min followed by primer annealing at 50 ºC for 1 min. This was followed by extension at 74 ºC for 1 min (per 1 Kb of product). This was performed for 29 cycles followed by a final extension at 72 ºC for 10 min.

2.9.3 Colony PCR screening of transformed bacteria

Colony PCR screening of transformed *E.coli* colonies was performed as follows: bacteria were lifted from an agar plate and spotted onto a fresh plate using a sterile pipette tip. The remainder of the colony was added to a PCR reaction as section 2.9.2 instead of template DNA.

2.9.4 Colony PCR screening of *R. equi*

For colony PCR of *R. equi* colonies, template DNA was generated as follows. Single colonies of *R. equi* were resuspended in 20-30 µl of sterile ddH_2O and heated to 95 ºC for 15 min. The sample was then briefly centrifuged to pellet cell debris and 1 µl was taken for use as template DNA.

2.9.5 Colony PCR screening of transformed yeast

For colony PCR of yeast, template DNA was generated as follows. Single colonies were resuspended in sterile 0.2 % (w/v) SDS and heated to 95 ºC for 15 min. The sample was then briefly centrifuged to pellet cell debris and 1 µl was taken for use as template DNA.

2.10 Ethanol precipitation of DNA

DNA solutions were concentrated by ethanol precipitation. A volume of 3 M sodium acetate, pH 5.5, equal to that of $1/10^{th}$ of the DNA solution was added and mixed by inverting the tube several times. 2-3 volumes of 100 % ice-cold ethanol was added and mixed gently by inversion to precipitate the DNA. DNA was pelleted at *16,000 x g* in a microcentrifuge at 4 ºC for 15 min. The supernatant was discarded and the pelleted washed with 500 µl of 70 % ethanol (prechilled to -20 ºC). The solution was centrifuged again for 2 min, and the supernatant carefully discarded. The pellet was air dried at room temperature for 10 min, and

resuspended in an appropriate volume of TE (10 mM Tris, pH 8.0, 1 mM EDTA). DNA was then stored at – 20 ºC until further use.

2.11 PCR product insertion into vectors

PCR products were recombined into linearised vectors using In-Fusion HD cloning kits (Clontech) as per the manufactuerer's instructions.

2.12 Generation of detergent soluble lysates

Tissue culture cells were rinsed once with phosphate buffered saline (PBS) and then cells were scraped into in ice-cold cell lysis buffer (0.15 M NaCl, 20 mM Tris-HCl, pH 8.0, 2 mM EDTA, 1 % (v/v) NP-40) with EDTA-free protease inhibitors (Roche). The lysate was incubated at 4 ºC for 15 min and then centrifuged at *16,000 x g* for 10 min at 4 ºC. Detergent-soluble lysates were retained for experiments.

2.13 Bicinchoninic acid (BCA) protein assay

Estimation of protein concentrations was carried out using the Pierce Bicinchoninic acid assay kit, in a 96 well microplate (Corning NY) as per manufacturer's instructions. 5 µl of 0.2 M NaOH was added to 5 µl of the protein sample. Where the concentration of protein was measured, dilutions of protein samples were performed with ddH_2O where appropriate. A standard curve of 0 - 10 µg was prepared using a stock of 1 mg/ml BSA in 0.1 M NaOH. 200 µl of BCA working reagent was added to each well and incubated at 37 ^{o}C for approximately 30 min. The absorbance was read at 570nm on a plate reader.

2.14 SDS PAGE

Protein samples to be resolved by gel electrophoresis were prepared by adding Laemmli sample buffer (3 X stock 188 mM Tris pH 6.8, 6 % (w/v) SDS, 30 % (v/v) glycerol, and 0.03 % (w/v) Bromophenol blue) and heating at 95 ^{o}C for 5 min. Samples were resolved using discontinuous polyacrylamide gels (lower resolving gel and upper stacking gel) using the Bio-Rad minigel apparatus (Mini-PROTEAN Tetra cell). Resolving gels were made with acrylamide (Protogel, National Diagnostics) at concentrations between 7.5 % (v/v) and 15 % (v/v) using resolving

gel buffer (final concentration 0.375 M Tris-HCl, pH 8.8, 0.2 % (w/v) SDS), plus ammonium persulfate (APS) at a final concentration of 0.05 % (v/v) and TEMED at a final concentration of 0.05 % (v/v). Stacking gels were made with acrylamide at a final concentration of 7.5 % (v/v) plus stacking gel buffer (final concentration 0.125 M Tris-HCl, pH 6.8, 0.2 % (w/v) SDS). Ammonium persulfate (APS) was added to a final concentration of 0.05 % (v/v) and TEMED was added to a final concentration of 0.05 % (v/v). Protein samples were resolved at 200 V until the bromophenol blue dye front had eluted from the bottom of the gel, or as appropriate. A protein ladder (Precision Plus Kaleidoscope ladder, Biorad), was used to estimate the molecular mass of proteins. Both the anode and cathode running buffer was 25 mM Tris, 0.1 % (w/v) SDS, 192 mM glycine. For the visualisation of proteins using Coomassie staining, gels were rinsed once with ddH_2O and incubated with Coomassie stain in destain (0.2 % (w/v) Coomassie Blue in 10 % glacial acetic acid (v/v), 30 % (v/v) methanol) for 5 min on a shaking platform. Gels were rinsed once with destain (30 % methanol, 10 % acetic acid) to removed excess stain, and left in destain for 30 min or until protein bands were visible.

2.15 Western blotting

Proteins were transferred to nitrocellulose membranes using the iBlot system (Invitrogen) as per the manufacturer's instructions. Alternatively proteins were transferred to nitrocellulose membranes equilibrated in transfer buffer (48 mM Tris, pH 8.8, 39 mM glycine, 20 % (v/v) methanol, 0.0375 % (w/v) SDS) using a Pharmacia Biotech Nova blot semi-dry transfer apparatus at 1 mA/cm^2 for 1.5 h. Transferred proteins were visualised by incubating membranes with Ponceau S (0.2 % Ponceau S in 3% (w/v) trichloroacetic acid) for 10 seconds and removing excess stain with copious amounts of ddH_2O. Membranes were then blocked in either 5 % (w/v) semi-skimmed milk or 5 % (w/v) BSA in TBS (100 mM NaCl, 10 mM Tris-HCl, pH 7.4) + 0.1 % (v/v) Tween-20 (TBST) for 30 min at room temperature or overnight at 4 ^oC. Membranes were probed with primary antibodies in 5 % (w/v) milk or 5 % (w/v) BSA TBST for 1 h at room temperature or 4 ^oC overnight. Membranes were then washed with TBST (3 x 5 minute washes) and incubated with horseradish peroxidase conjugated secondary antibodies in milk or

BSA at room temperature for 30 min. Membranes were washed a further 3 times with TBST and then proteins were visualised using ECL reagent (Amersham).

2.16 Immunofluorescence

Cells were rinsed once with Dulbecco's PBS (Sigma) and fixed as follows. For methanol fixation, cells were incubated at -20 ºC for 5 min with methanol that was prechilled to -20 ºC. Methanol was then removed and coverslips left to air dry and stored at 4 ºC overnight, or processed immediately. For formaldehyde fixation, cells were rinsed with PBS and fixed for 20 min in 4 % formaldehyde in PBS. The formaldehyde was removed and coverslips incubated in 50 mM NH_4Cl in PBS for 10 min. Coverslips were stored in this solution for up to a week at 4 ºC, or processed immediately. After fixation, cells were permeabilised (where appropriate) in 0.2 % (w/v) BSA, 0.05 % (v/v) Saponin, in PBS, for 10 min. All further washes and antibody dilutions were carried out in BSA/Saponin/PBS (BSP) solution, unless otherwise stated. For permeabilisation and cytosol extraction of cells before fixation, coverslips were treated as follows: coverslips were rinsed once with cytosol extraction buffer (CEB, 25 mM HEPES-KOH, pH 7.4, 25 mM KCl, 2.5 mM magnesium acetate, 5 mM EGTA (sodium free), 150 mM potassium glutamate (monopotassium L- glutamic acid)) and then incubated in CEB containing 0.05 % (w/v) saponin for 30-60 seconds. Cells were then immediately fixed with 4% formaldehyde solution. In all cases, coverslips were incubated in primary antibody diluted in BSP for 1 h at room temperature, by inverting the coverslips into drops of antibody solution on a strip of parafilm (25-30 µl for 10 mm round coverslips, 70-80 µl for 22 mm coverslips). Coverslips were washed 3 x 5 min (minimum) with approximately 1 ml of BSP. Coverslips were then incubated with Alexa fluorophore-conjugated secondary antibodies (diluted 1:300 in BSP) for 30 min, followed by a further 3 x 5 min washes with 1 ml of BSP. For visualisation of DNA, 4',6-diamidino-2-phenylindole (DAPI), was included in the final wash (used at 1 µg/ml from a 10 mg/ml stock). Coverslips were rinsed once in distilled water, blotted dry, and mounted onto slides with MOVIOL 4-88 containing 2.5 % (w/v) DABCO (1,4-diazobicyclo [2,2,2]-octane). MOVIOL was prepared as follows: 2.4 g of MOVIOL 4-88 (Calibiochem) was added to 6 g of glycerol and 6 ml of ddH_2O and was mixed on a rotating wheel at room temperature for several hours. 12 ml of 0.2 M Tris (pH 8.5) was added, and the solution heated to 50 ºC for 10

min with occasional mixing. After the MOVIOL had dissolved, the solution was clarified by centrifugation at *5,000 x g* for 15 min, then DABCO was added to 2.5 % (w/v). The solution was then aliquoted into air tight tubes and stored at – 20 ºC for long term storage.

2.17 Image acquisition

Slides were viewed on a Zeiss LSM 880 Axio Observer.Z1 inverted confocal laser microscope running Zen software (2015) or a Zeiss LSM 510 meta Axioplan 2M upright confocal laser microscope running Zen software (2009, Carl Zeiss Ltd, Germany). Live-cell imaging was performed on a Andor Revolution XD spinning disk Axiovert 200M confocal microscope running Andor IQ software (2009), with the microscope stage contained within a sealed chamber preheated to 37 ºC. Gain and laser powers were set accordingly. All images are single slices or maximum-intensity Z projections unless otherwise stated. Post-acquisition image processing was performed using ImageJ software (Schneider et al., 2012)

2.18 Fusion protein production

2.18.1 Fusion protein test production

Recombinant GST-Myc-VapA and Myc-VapA-His_6 fusion proteins were expressed in *E.coli* expression strain BL21 (DE3) pLysS as follows. For initial test production, 10 ml of LB (plus the appropriate selective antibiotics) was inoculated with a single bacterial colony and grown overnight at 37 ºC with shaking at 450 rpm. The overnight starter culture was diluted 1:500 into 10 ml of LB and grown at 37 ºC with shaking until OD_{600} 0.6-2.0. 5 ml of this culture was then transferred to a new tube. Isopropyl β-D-1-thiogalactopyranoside (IPTG) was added to the remaining 5 ml, to a final concentration of 0.2 mM. Both cultures were incubated for 4 h. 40 µl was taken from each culture for -/+ IPTG samples to be analysed by SDS-PAGE. The induced culture was pelleted at *2,465 x g* for 10 min at 4 º C. The pellet was resuspended in 1 ml bacterial lysis buffer (1 % (v/v) Triton X-100, 1 mg/ml lysozyme, 2 mM $MgCl_2$, 1 U/ml DNAse, in PBS) with protease inhibitors (Roche). The resuspended bacteria were frozen at -20 ºC. The lysate was defrosted and then centrifuged at *16,000 x g* for 20 min at 4 ºC in a microcentrifuge. 8 µl of the supernatant was taken to represent a detergent-soluble protein sample. The pellet

was resuspended in 100 µl of Laemmli sample buffer and 1 µl used to represent an insoluble protein sample.

2.18.2 Large scale fusion protein production

For large scale production, fusion proteins were grown in 2 x 600 ml of LB or 2TY broth as follows: 7.5 ml of LB (plus the appropriate selective antibiotics) was inoculated with a single bacterial colony and grown overnight at 37 ºC with shaking. The next day, starter cultures were diluted 1:500 into a total volume of 600 ml LB or 2TY broth, and grown at 37 ºC until an OD_{600} of 0.6 - 2.0 was obtained. Protein production was induced with IPTG to a final concentration of 0.2 mM, and cultures grown for a further 4 h. The bacteria were pelleted at *2,645 x g* for 15 min at 4 ºC. The cell pellet was resuspended in 10 ml of bacterial lysis buffer (1 % (v/v) Triton X-100, 1 mg/ml lysozyme, 2 mM $MgCl_2$, 1 U/ml DNAse, in PBS) with protease inhibitors (Roche), and frozen at -20 ºC overnight. The cell pellet was defrosted on ice and centrifuged at *47,800 x g* in a Sorvall SS34 rotor for 20 min at 4 ºC. For GST fusion proteins, the supernatant was incubated with 1 ml (packed volume) of glutathione sepharose (GE healthcare) for 1 h at 4 ºC with gentle rotation. The sepharose beads were then collected and washed with 3 x 20 ml of wash buffer (1 % (v/v) Triton X-100 in PBS). GST/GST-fusion proteins were eluted with 20 ml elution buffer (50 mM Tris, pH 8.0, 10 mM reduced glutathione), and 1 ml fractions collected to determine which fractions the proteins were in. Fractions were analysed by spotting 1 µl of each fraction onto 3M chromatography paper, which was dried, and then stained with Coomassie stain to see which fractions the protein was in. These fractions were then analysed by SDS-PAGE. The eluted proteins were then pooled and dialysed extensively into PBS at 4 ºC for 2 days and stored at -20 ºC until needed. For the purification of His_6-tagged proteins, cell pellets were processed as above. The soluble supernatant was incubated with 134 µl (packed volume) of His-Select resin (Sigma) for 1-2 h at 4 ºC with gentle rotation. The beads were washed with 3 x 20 ml wash buffer (10 mM imidazole, 0.3 M NaCl, 50 mM Na_2HPO_4, pH 8.0). Proteins were eluted with 20 ml elution buffer (250 mM imidazole, 0.3 M NaCl, 50 mM Na_2HPO_4, pH 8.0) and 1 ml fractions collected. Fractions were analysed by spotting 1 µl of each fraction onto 3M chromatography paper and analysed by SDS-PAGE as previously described.

The eluted proteins were then pooled and dialysed extensively into PBS at 4 ºC for 2 days and stored at -20 ºC until needed.

2.19 Immunoprecipitation of proteins

2.19.1 Antibody purification

Antibodies raised against a myc epitope were purified from 9E10 mouse Hybridoma (Developmental studies Hybridoma bank, University of Iowa, USA) cell culture supernatants as follows: cells were brought up from liquid nitrogen stocks and cultured in Iscove's modified Dulbecco's medium (IMDM, Sigma UK) containing 1 % (v/v) penicillin-streptomycin (10 U/ml and 10 µg/ml respectively), and 10 % (v/v) Ultra-Low IgG FCS (Thermo). After several days of growth, the cells were resuspended in 12 ml of IMDM and 3 ml of Ultra-low IgG FCS. The cells were seeded into the lower chamber of a 1 L CELLine disposable bio-reactor (Integra, Switzerland). 1 L of serum-free Hyclone ADCF-MAb media (GE healthcare, USA) containing 5 % regular FCS was added to the top chamber of the bioreactor. After approximately 16 days of continuous culture the cells were removed from the bottom chamber and pelleted. The supernatant (containing secreted α-myc antibodies) was collected and sterile filtered. ¼ of the cells were then used to reseed the flask.

2.19.2 Antibody coupling

The IgG-containing supernatants were dialysed extensively against PBS at 4 ºC for 2 days Antibodies were covalently coupled to Amino-link beads using the Pierce Direct Co-IP kit as per the manufacturer's instructions. Amino-link beads were first washed extensively with PBS. 1 µg of antibody was covalently coupled to 1 µl (packed volume) of Amino-link beads, by the addition of 3 µl of 5 M $NaCNBH_4$, per 200 µl volume (sepharose and antibody). The suspension was rotated gently at 4 ºC for 1-2 h. The beads were gently pelleted at *3,300 x g*, and washed 3 times with 1 M Tris-HCl, pH 8.0. 0.5 ml of the Tris solution was added per 500 µl of packed resin, and then 3 µl of 5 M $NaCNBH_4$ was added per 200 µl total volume (sepharose and Tris). The beads were further rotated for 15 min at room temperature and then washed 3 times with PBS. The beads were then

washed 6 times with 1 M NaCl, followed by 3 washes with PBS. An equal volume of mammalian cell lysis buffer (0.15 M NaCl 20 mM Tris-HCl, pH 8.0, 2 mM EDTA, 1 % (v/v) NP-40) was added to create a 50 % slurry, and the resin was stored at 4 ºC until further use.

2.19.2 Immunoprecipitation

Immunopreciptation experiments were performed as follows: Flp In HeLa cells expressing Myc-VapA (under the control of an inducible promoter) were induced by the addition of 1 µg/ml doxycycline for 16 h. Flp In HeLa cells (not expressing any exogenous proteins) were used as a control for non-specific protein interactions. Cells were washed once with ice cold PBS and resuspended in mammalian cell lysis buffer (0.15 M NaCl, 20 mM Tris-HCl, pH 8.0, 2 mM EDTA, 1 % (v/v) NP-40) with protease inhibitors. The lysate was incubated on ice for 15 min, and then centrifuged at 13,200 *x g* at 4 ºC for 15 min. The pellet was discarded and BCA assay used to estimate the protein concentration of the supernatant. The lysate was precleared (to reduce non specific protein binding), by incubation (for 1-2 h at 4 ºC with gentle rotation) with a volume of inert control sepharose resin equal to that of α-Myc resin. The beads were pelleted and the precleared lysate incubated with α-Myc resin at a ratio of 1 mg of lysate per 20 µl (packed volume) of α-Myc resin (40 mg lysate, 1600 µl of packed resin). This was incubated at 4 ºC for 1-2 h with gentle rotation. The supernatant was removed and the beads washed 5 times with 20 ml of lysis buffer. Proteins were eluted by the addition of 1 ml of 10 mM Na_2HPO_4, pH. 7.4, followed by 1 ml of Pierce low pH IgG elution buffer. Beads were then incubated with 3 ml of IgG elution buffer for 10 min at room temp, and then with a further 5 ml for 10 min. 10 ml of eluate was then concentrated to 160-200 µl by placing the eluate into a Slide-A-Lyzer cassette (3,500 MWCO, Pierce) and then placing the cassette onto Aquacide (a hygroscopic powder) for ~ 10 h. 3X Laemmli sample buffer (with 10 % (v/v) β-mercaptoethanol) was added and protein samples resolved on a 8-15 % SDS PAGE gel run at 12 mA for 16 h (using a BioRad Protean II XL cell). Gels were then silver stained using a Pierce silver stain kit as per the manufacturer's instructions.

2.20 β-Hexosaminidase Assay

3-25 µl of sample was incubated with 100 µl of substrate solution (100 mM Citrate buffer pH. 5.0 (74 mM Sodium citrate, 37 mM citric acid), 0.5 mM 4-methylumbelliferyl-2-acetamido-2-deoxy-**β**-D-glucopyranoside, 0.27 M sucrose) for exactly 3 min (samples were added at regular timed intervals). The reaction was stopped with 1 ml of 1 M Na2CO3. The estimation of lysosomal latency was calculated by assaying the activity of the lysosomal enzyme β-Hexosaminidase, in the presence and absence of 0.1 % (v/v) Triton X-100 detergent. Samples were measured in a Lumina fluorescence spectrophotometer (Thermo Scientific) at 360 nm excitation and 443 nm emission. The % latency/intactness of lysosomes was calculated as follows:

$$\frac{\beta\text{-hex (AU) with Triton X-100} - \beta\text{-hex (AU) without Triton X-100}}{\beta\text{-hex (AU) with Triton X-100}} \times 100$$

2.1 Antibodies

The primary and secondary antibodies used in this study are listed in table 2.0

Primary Antibodies					
Cat. No.	Source	Target	Target Species	Dilution	
				W.B.	IF
N/a	Dr Ashley Toyne	LAMP1	Hu		1:1000
1D4B	DSHB	LAMP1	Mu	1:500-1:5000	1:500-1:1000
C45B10	Cell signalling Tech.	EEA1	Mu/Rat/Hu	1:1000	
C8B1	Cell signalling Tech.	Rab5	Mu/Rat/Hu	1:1000	
D95F2	Cell signalling Tech.	Rab7	Mu/Rat/Hu	1:1000	
DM1A	Sigma-Aldrich	α-tubulin	n/a	1:1000	
610978	BD Transduction Labs	GRP78	Hu/Rat/Mu	1:250	
C10456	BD Transduction Labs	EEA1	Hu	1:5000	
EPR7691	Santa Cruz	cdM6PR	Mu/Hu/Rat	1:1000	
EPR6599	Santa Cruz	ciM6PR	Mu/Hu/Rat	1:1000	
9E10	DSHB	myc	Myc epitope	1:200	1:200
VapA	Dr.Albert Haas	VapA	*R. equi*	1:1000	1:500
1001	Prof. J.P. Luzio	ciM6PR	Rat		1:1000
6217	Prof. J.P. Luzio	Syntaxin 7	Rab	1:200	
N/a	Dr Katherine Bowers	PHO8/ALP	*S. cerevisiae*	1:50	
580	Cambridge	Lgp110	Rat	1:1000	
MA1-21315	ThermoFisher	6x His	n/a	1:1000	1:1000
8738	Cambridge	ciM6PR	Rat	1:1000 - 1:200	1:1000 - 1:200
MA1-164	ThermoFisher	Lgp120	Hu/Mu/Rat	1:500	
Secondary Antibodies/other					
Cat. No.	Source	Antigen	Label	Dilution	
				W.B.	IF
405210	BioLegend	Biotin	Streptavidin HRP	1:10,000-1:40,000	
A9169	Sigma Aldrich	α-Rab IgG	HRP	1:8000	
A9044	Sigma Aldrich	α-Mu IgG	HRP	1:8000	
A9542	Sigma Aldrich	α-Rat IgG	HRP	1:8000	
A21424	ThermoFisher	α-Mu IgG	AF 555		1:300
A11029	ThermoFisher	α-Mu IgG	AF 488		1:300
A21429	ThermoFisher	α-Rab IgG	AF 555		1:300
A11034	ThermoFisher	α-Rab IgG	AF 488		1:300
A21434	ThermoFisher	α-Rat IgG	AF 555		1:300

Table 2.0 Source and details of antibodies used in this study. Hu; human, Mu; mouse, Rab; rabbit, W.B; western blot, IF; immunofluorescence, AF; Alexa fluor, IgG; immunoglobulin G.

Chapter 3: Development of an *in vitro* phagosome-lysosome fusion assay

3.1. Lysosome purification

3.1.1 Introduction

To set up an *in vitro* phagosome-lysosome fusion assay, it is necessary to purify both phagosome and lysosomes from cells The purification of these lysosomes requires a protocol that isolates functional lysosomes, and with a marker that can be used to asses fusion. The challenge in purifying endocytic organelles has led to the development of a wide range of novel strategies, each with their own advantages and disadvantages, which are discussed below. Obtaining fractions with a high degree of purity can be cumbersome and time consuming. Lysosomes were traditionally isolated by isopycnic centrifugation on sucrose gradients (Novikoff et al., 1956, De Duve et al., 1955), but these typically produced lysosomal fractions containing contamination from the endoplasmic reticulum (ER), peroxisomes and mitochondria, which have overlapping densities in sucrose gradients (Beaufay, 1969, Graham, 2001). Furthermore, the density of the lysosomes are altered on a sucrose gradient by the efflux of water from the lysosomes, since they are subjected to the osmotic stress of the hyperosmotic sucrose centrifugation medium. This may render the lysosomes abnormal or non-functional. Purification by centrifugation is further complicated by the heterogeneity of the lysosomal population resulting in subpopulations of lysosomes which display different densities (Pertoft et al., 1978). Alternative purification methods include altering the density of lysosomes by loading them with a substrate such as Triton WR 1339 (Wattiaux et al., 1963), iron (Glaumann et al., 1975), or gold (Henning and Plattner, 1974). However, these methods involve the pre-treatment of animals, and significantly alter the lysosome rendering it abnormal (Wattiaux et al., 1978). For example, Triton WR 1339 loading results in different enzyme activities (Plattner et al., 1975) membrane characteristics compared to normal lysosomes (Weglicki et al., 1973). A centrifugation technique using Metrizamide (a medical contrast agent used in imaging) allowed better separation of lysosomes from mitochondria (Wattiaux et al., 1978). However, the development of newer contrast

agents halted the production of Metrizamide, rendering it impractical for long term use in lysosome isolation. While better than sucrose, Metrizamide still exerts osmotic effects on organelles at densities above 1.2 g/ml (Castle, 2004).

Lysosomes can also be purified magnetically using superparamagnetic iron oxide nanoparticles (SPIONS, Walker, 2015). These are small (<100 nm) iron oxide (Fe_2O_3 or Fe_2O_4) particles coated in inert and biocompatible polymers, such as dextran, which have wide ranging biomedical applications (Wahajuddin and Arora, 2012). Unlike ferromagnetic materials (those which retain magnetic properties in the absence of a magnetic field), SPIONS display magnetic properties, but only when in the presence of an externally applied magnetic field (Dave and Gao, 2009). Colloidal-iron dextran (FeDex) has previously been used to isolate lysosomes and other endocytic organelles from a variety of cell types (Rodriguez-Paris et al., 1993, Diettrich et al., 1998, Becich and Baenziger, 1991, Cardoso et al., 2009, Duvvuri et al., 2004). This method can also be used to purify lysosomes from the cells of patients with lysosomal storage diseases (LSDs), where the abnormal composition of the lysosomes makes purification by density gradient centrifugation impractical (Diettrich et al., 1998). Furthermore, the pH of isolated lysosomes has been reported to be between 4-6, indicating pH gradients of isolated organelles can be retained and that they remain functional (Satori et al., 2011). FeDex purified organelles are less likely to be contaminated with mitochondria or peroxisomes as these organelles would not be labelled during the purification protocol. The study of lysosomes in different pathologies is a wide ranging field that encompasses many different cell and tissue types. Because of this there are numerous publications describing protocols for purification of lysosomes that have been heavily optimised for a particular purpose. Subsequently, different protocols accept differing levels of contamination from other subcellular organelles, or do not require the lysosomes to be intact.

For an *in vitro* fusion assay utilising lysosomes from macrophages, there is a requirement for an optimised method of isolating lysosomes that is rapid, simple, and yields lysosomes that have a high degree of latency. To purify lysosomes, cells must first be fractionated in order to separate out the different organelles. This must be conducted carefully and optimised depending on the organelle being purified, the cell type, and the final use of the organelles. For example, a

purification method that yields 90 % of a cell's lysosomes, but renders them broken and non-functional, is of no use if the final application requires intact lysosomes capable of fusing with other membranes. Such a protocol would be more suited for applications not requiring intact lysosomes, e.g. proteomic analysis. Many techniques have been used to disrupt cells, including physical disruption (ball-bearing homogenisation, (Balch and Rothman, 1985), passage through high-gauge needles, nitrogen cavitation (Kelly et al., 1989), a French press, chemical lysis, sonication etc. These all have advantages and disadvantages. For example, passage through a needle is widely used to disrupt cells, but some cell types remain refractory to this method of fractionations (such as J774.2 macrophages, data not shown). Nitrogen cavitation is a rapid, gentle, fractionation method that uses nitrogen gas pressure to lyse cells. Unlikely other physical disruption methods (such as ball bearing homogenisation), nitrogen cavitation does not generate localised friction or heat, which can lead to sample degradation. Nitrogen cavitation has been used for lysosome purification (Gottlieb and Adachi, 2000, Graves et al., 2008, Sparrow et al., 2008, Ghislat et al., 2012).

This chapter describes development of a lysosome purification protocol for J774.2 mouse macrophages, based upon the isolation of colloidal iron dextran-containing *Dictyostelium* lysosomes (Rodriguez-Paris et al., 1993). In brief, J774.2 cells are pulse chased with colloidal iron dextran (FeDex), before a gently lysis by nitrogen cavitation. A post-nuclear supernatant (PNS) is generated from the lysate, which is then applied to a iron column held within a magnetic field. The magnetic field retains the iron-containing lysosomes, which are then washed of label-free organelles and cell debris. The column is then removed from the magnetic field to allow the elution of the lysosomes. In order to use these organelles in an *in vitro* fusion assay, it was important to optimise the protocol to give a high yield of intact organelles. Thus, the following experiments were performed with the aim of optimising the isolation of a sufficient quantity of intact lysosomes.

3.1.2 Lysosome purification specific methods

3.1.2.1 Colloidal Iron Dextran (FeDex)

Colloidal iron dextran was made as previously described (Rodriguez-Paris et al., 1993). Briefly, 5 ml of 1.2M $FeCl_2$ and 5 ml 1.8 M Fe_2Cl_3 were mixed in a beaker and 5 ml of 30 % (v/v) NH_4OH was added drop wise, whilst stirring. The precipitate was collected on a large permanent magnet and washed once with 5 % (v/v) NH_4OH and twice with ddH_20. Washing was performed by removing the magnet, thoroughly resuspending the precipitate, then re-gathering the precipitate using the magnet and disposing of the supernatant. The precipitate was resuspended in 40 ml of 0.3M HCl and stirred. After 30 min, 2 g of dextran (Mr ~ 40,000) was added and quickly dissolved, followed by stirring for 40 min. The colloidal solution was then dialysed extensively against ddH2O for 2 days at 4 ºC. Large aggregates were removed by centrifugation at *26,800 x g* for 15 min at 4 ºC in a Sorvall SS-34 rotor. The supernatant was sterile filtered through a 0.22 µm filter and stored at 4 ºC for up to 2 months.

3.1.2.2 Lysosome purification using superparamagnetic iron particles (SPIONS)

This is the final protocol used to isolate lysosomes. Section 3.3 describes how this method was developed. This protocol has been published in: Subcellular Fractionation. A laboratory manual. Cold Spring Harbour Protocols 2015 (Purification of lysosomes using supraparamagentic iron oxide nanoparticles (SPIONS). A.P.Rofe and P.R. Pryor)

J774.2 macrophages were seeded at 6 - 8 $x10^6$ cells per 10 cm tissue culture dish (Starstedt) in DMEM and cultured overnight. The next day the tissue culture media was replaced with FeDex diluted 1:20 in DMEM for a 1 h pulse. FeDex containing media was removed and the cells were washed carefully 3 times with warm DMEM to remove any remaining extracellular FeDex. Cells were then incubated in DMEM for a 2 h chase. The cells were then scraped and pelleted at 1000 *x g* for 3 min, washed once in PBS, and resuspended in 1 ml of STM fractionation buffer (250 mM sucrose, 10 mM TES (2-[[1,3-dihydroxy-2-(hydroxymethyl) propan-2-yl] amino] ethanesulfonic acid), pH 7.4, 1 mM $MgCl_2$). Routinely, between 20 and 40 x 10^6 cells were resuspended in 1 ml of STM. Cells were fractionated in a nitrogen

cavitation vessel (Parr Instrument Company, IL USA, model number Q913534). The pressure vessel was prechilled to 4 ºC on ice, and cells were placed under pressure for 5 min at 250 psi. The lysate was then eluted into a 50 ml tube with a parafilm splash guard. A post-nuclear supernatant (PNS) was generated by centrifugation of the lysate at 800 *x g* for 5 min at 4 ºC. The PNS was then applied to a MACS cell column (Miltenyi Biotech, Cat # 130-042-202) held within a magnetic MiniMACS separator (Miltenyi Biotech) that had been previously equilibrated with 3 ml of ice cold STM buffer. A 23G needle was used to reduce the flow rate of the PNS. The PNS was reapplied to the column twice more. The column was washed with 3 ml of STM and then removed from the MiniMACS separator. FeDex containing lysosomes were then eluted from the column directly into an ultracentrifuge tube using 3 ml of STM. The lysosome-containing solution was then centrifuged at 37,500 *x g* for 15 min at 4 ºC in a Beckman TLA-110 rotor. The supernatant was discarded and the lysosomal pellet resuspended in appropriate volume of STM for subsequent experiments.

3.1.2.3 Purification of lysosomes by isopycnic centrifugation

A 4 ml cushion of 45 % (w/v) Nycodenz was loaded into a Beckman Quick-seal centrifuge tube at 1 ml/min. 30ml of a 1-22 % (w/v) Ficoll gradient was layered on top and left at 4 ºC overnight to settle. The next day, 20 x 10^6 J774.2 cells were fractionated at 250 psi for 5 min on ice in 1 ml of homogenisation buffer (HB, 10 mM sucrose, 10 mM TES, pH 7.4, 1 mM $MgCl_2$). Three separate lysates were pooled to give a total of 60 x10^6 cells. 900 µl of restoration buffer (RB, 500 mM sucrose, 10 mM TES, pH 7.4, 1 mM $MgCl_2$) was added to the lysate and gently mixed. The lysate was made to a final volume of 6 ml with STM, and loaded on top of the gradient. The centrifuge tube was heat sealed and centrifuged at *241,830 x g* in a VTi50 rotor, for 1 h at 4 ºC with slow acceleration and deceleration (3 min). 1 ml fractions were collected from the bottom of the gradient at 1 ml/min at 4 ºC using a fraction collector. 25 µl of each fraction was assayed for β-hexosaminidase activity, and the refractive index of each fraction was measured on a refractometer. Equal volumes (180 µl) of each fraction were analysed by western blotting.

3.1.3 Results

3.1.3.1 Purification of lysosomes using superparamagnetic iron oxide nanoparticles (SPIONS)

The purification of lysosomes using colloidal iron dextran (FeDex) had previously been used in the Pryor lab. However, it required extensive modification and optimisation to purify lysosomes for use in a fusion assay. The variables that were investigated will be discussed further, but included:

- the use of ball bearing homogenisation or nitrogen cavitation to disrupt cells.

- varying the concentration and the pulse/chase times of FeDex used in lysosome purification.

- changing the osmolarity of the fractionation buffer.

- changing the number of cells fractionated and the confluency of cells.

- biochemical characterisation of purified lysosomes.

This method was used as the starting point for lysosome purification. Lysosomes were purified from J774.2 macrophages and samples taken at each stage of the purification protocol. Samples were biochemically analysed by western blot for lysosomal (Lysosome-associated membrane protein 1, LAMP1) and cytoskeletal (α-tubulin) markers (Fig. 3.0 A), and assayed for the activity of the lysosomal enzyme β–hexosaminidase (Fig. 3.0 B) in order to monitor the enrichment of lysosomal material. The final lysosome fraction showed increased levels of LAMP1, and decreased levels of α-tubulin compared to the other fractions. The final fraction was enriched with lysosomal material as shown by the average 12.4-fold increase in the activity of β-hexosaminidase (β-hex) relative to the starting fraction. However, this was highly variable, with the fold increase ranging from 3.3 to 36.7. The average latency of these final lysosomal fractions was 42.8 % and the average recovery was 5.58 % (data not shown). Thus, the purification protocol was further optimised to improve the latency and recovery of lysosomes.

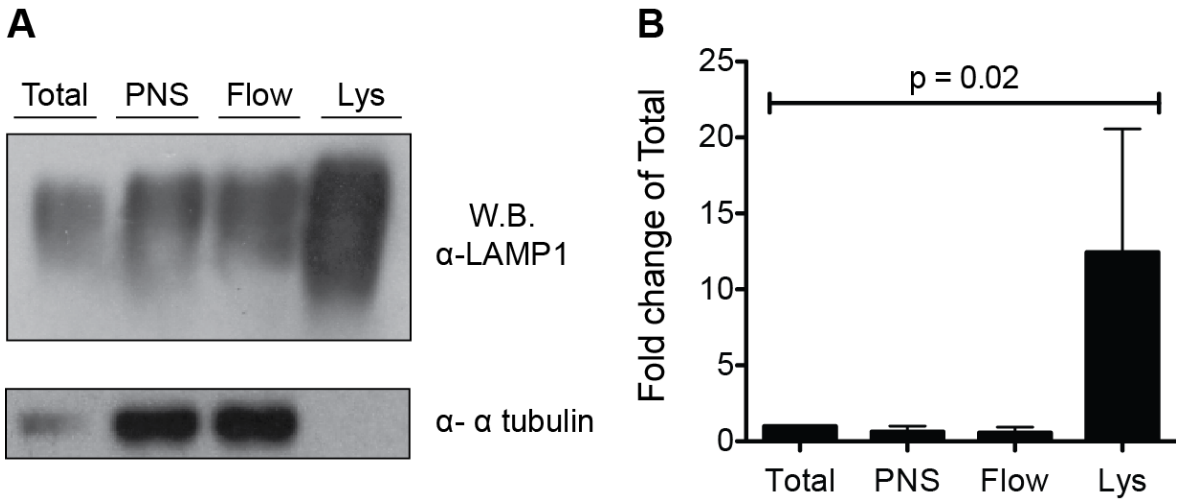

Fig. 3.0 Analysis of lysosomes purified using FeDex. A. J774.2 cells were incubated with colloidal-iron dextran (FeDex) diluted 1:20 in DMEM for 6 h followed by a chase with DMEM for 18 h. The cells were then scraped and resuspended in 1 ml of ice cold HB buffer (10 mM sucrose, 10 mM TES, pH 7.4, 1 mM $MgCl_2$) for 10 min on ice. Cells were then homogenised by 40 passes of a ball bearing homogeniser with a clearance of 6 µm. The lysate was restored to 250 mM sucrose by the addition of an equal volume of restoration buffer (490 mM sucrose, 10 mM TES, pH 7.4, 1 mM $MgCl_2$) and then centrifuged at *1,500 x g* for 10 min at 4 ºC to generate a post-nuclear supernatant (PNS). The PNS was applied to a cell column held within a magnetic field. The flow through was collected, and the column washed with 3 ml of STM buffer (250 mM sucrose, 10 mM TES, pH 7.4, 1 mM $MgCl_2$). The column was removed from the magnetic field, and lysosomes eluted with 3 ml of STM. Lysosomes were pelleted by centrifugation at *104,000 x g* for 15 min at 4 ºC, and resuspended in 100 µl of STM using a 1 ml dounce homogeniser. Samples were taken of the starting material (Total), PNS, column flow through (Flow), and the final lysosome eluate (Lys). Samples were analysed by western blotting using α-LAMP1 (lysosome-associated membrane protein 1) and α-α tubulin antibodies. 5 µg of protein was loaded per lane. Western blotting is representative of 4 separate experiments. **B**. 5 µl of each of the fractions in A. were assayed for the activity of the lysosomal enzyme β-hexosaminidase (β-hex) as previously described in section 2.20. The amount of (β-hex) activity (AU) per µg of protein of each fraction was determined and normalised to the activity of the total fraction. Data are means ± SEM and were analysed by one-way ANOVA (n=4).

3.1.3.2 Optimisation of FeDex purification protocol

The conditions used to fractionate cells can vary greatly depending upon the downstream application of the subcellular fractions. Previous studies in the Pryor lab had demonstrated that smaller ball bearing sizes gave better lysosomal latency values. As intact lysosomes were required, the size of the ball bearing used to homogenise cells was changed to see if it would improve the latency and recovery of lysosomes (Fig. 3.1). Cells were fractionated with 40 passes of an 8.012 mm or 8.014 mm ball bearing (8 μm and 6 μm clearance, respectively) and FeDex-labelled lysosomes purified from the post-nuclear supernatant. Changing ball bearing size did not significantly affect lysosome latency ($p = 0.721$) or recovery ($p = 0.444$), and the latency and recovery was poor for both ball bearing sizes (latency ≤ 50 %, recovery ≤ 10 %).

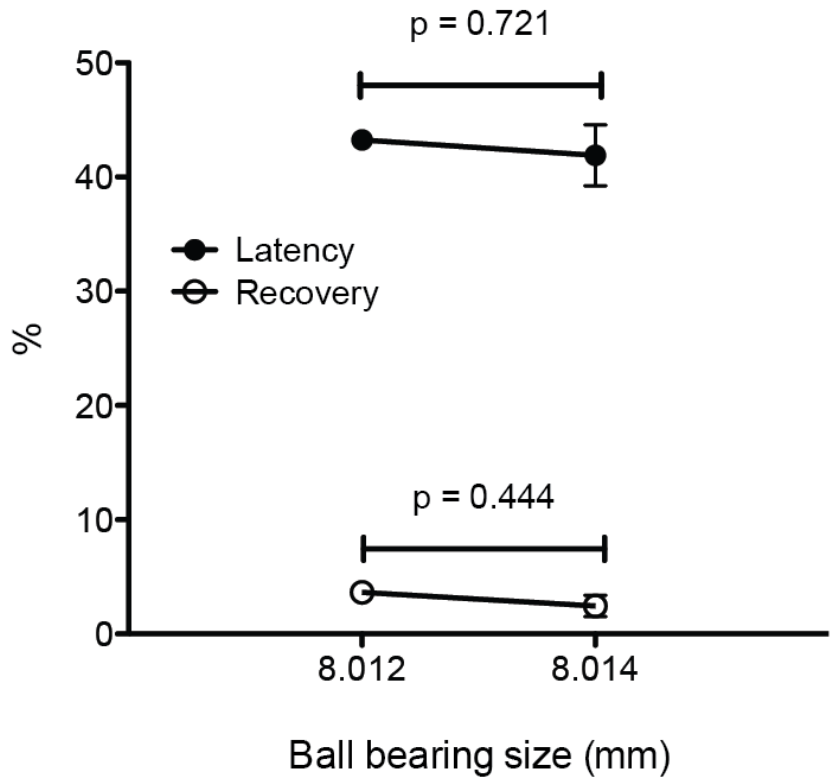

Fig. 3.1. Homogenisation of J774.2 cells using two different sized ball bearings. J774.2 macrophages were pulsed for 6 h with FeDex diluted 1:20 followed by a FeDex-free chase for 16 h in order to label lysosomes. The cells were then scraped and resuspended in 1 ml of ice cold HB buffer (10 mM sucrose, 10 mM TES, pH 7.4, 1 mM $MgCl_2$) for 10 min on ice. Cells were then homogenised by 40 passes of a ball bearing homogeniser with a clearance of 6 µm (8.014 mm ball bearing) or 8 µm (8.012 mm ball bearing). The lysate was restored to 250 mM sucrose by the addition of an equal volume of restoration buffer (490 mM sucrose, 10 mM TES, pH 7.4, 1 mM $MgCl_2$) and was centrifuged at *1,500 x g* for 10 min at 4 ºC to generate a post-nuclear supernatant (PNS). The PNS was applied to a cell column held within a magnetic field. The flow through was collected, and the column washed with 3 ml of STM buffer (250 mM sucrose, 10 mM TES, pH 7.4, 1 mM $MgCl_2$). The column was removed from the magnetic field, and lysosomes eluted with 3 ml of STM. Lysosomes were pelleted by centrifugation at *104,000 x g* for 15 min at 4 ºC, and resuspended in 100 µl of STM using a 1 ml dounce homogeniser. Lysosomal latency was calculated by calculating the activity of the lysosomal enzyme β-hexosaminidase (β-hex) in the presence and absence of detergent (as described in section 2.20). The same assay was used to determine the recovery of lysosomal material from the starting material. Data are means ± the range and were analysed by an unpaired t-test (n=2).

To determine if the poor latency and recovery was due to the protocol, or a particular trait of J774.2 cells, an alternative cell line, RAW 246.7 were fractionated using the same protocol. RAW 246.7 cells are a macrophage-like cell line used in studies of phagocytosis (Anand et al., 2008, Rogers and Foster, 2007, Nakanishi-Matsui et al., 2012), signal transduction (Zhu et al., 2006), and cell migration (Murray et al., 2013). These cells are used partly because they have a flattened morphology and have a less extensive cytoskeleton (N. Signoret, personal communication, Oct 2011). This may mean that there is less association between lysosomes and the cytoskeleton in these cells, making it easier to recover lysosomes. For optimisation experiments, the latency and recovery of lysosomes in the PNS was first determined to quickly assess whether or not a particular variable had made a significant change to lysosome latency or recover. The lysosome purification protocol was performed on RAW 264.7 cells, but with additional FeDex concentrations. This was done to determine if RAW 264.7 cells were suited to this method, and secondly, to determine if altering FeDex concentration had an effect on lysosome purification (Fig. 3.2 A). FeDex was diluted 1:20. 1:50 or 1:100, and the latency of lysosomes in the PNS ranged from 68 % - 82 %. However, no clear trend in the latency of lysosomes in the PNS was seen as the FeDex concentration was varied. The recovery of lysosomes in the PNS ranged from 17 % - 58 % and appeared to follow a downward trend as the amount of FeDex was increased. This was most likely due to the increased density of FeDex-filled lysosomes, when FeDex was incubated with cells at a higher concentration. As these latency and recovery values in the PNS were high, lysosomes were then purified fully from RAW 264.7 cells with FeDex diluted 1:20 or 1:100 to see if the same would be true for purified lysosomes. These values were chosen as they were the highest and lowest concentrations of FeDex used previously. The latency and recovery of lysosomes purified from these cells was then determined (Fig. 3.2 B&C). The latency of lysosomes purified using FeDex at 1:20 was 43.6 % compared to 48.1 %. The recovery of purified lysosomes was 4.46 % (FeDex 1:20) compared to 22.5 % (FeDex 1:100). The low latency was mostly likely due to damage to the lysosomes when resuspending them using the dounce homogeniser. Alternatively, this may have been due to the FeDex damaging the lysosomes, as iron oxidation products can be particularly damaging to lysosomes (Kurz et al., 2011) Some FeDex-containing lysosomes were probably lost during the centrifugation step used generate the post-nuclear

supernatant, as the FeDex would increase the density of the lysosomes. The PNS would also contain FeDex-free lysosomes that would not be pelleted out during the PNS spin. This may account for the high latency seen in the PNS compared to the lower latency seen in the final fraction, as unlabelled, intact lysosomes, would be present in the PNS but not in the final fraction.

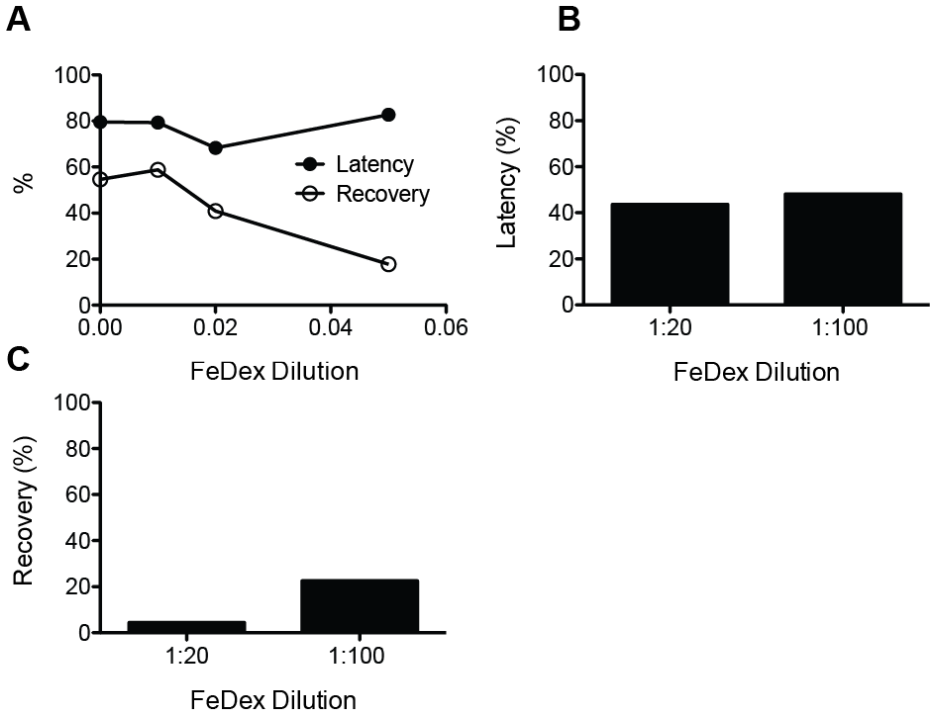

Fig. 3.2. Purification of lysosomes from RAW 264.7 macrophages. A. RAW 264.7 cells were incubated with colloidal-iron dextran (FeDex) (at the concentrations indicated) in DMEM for 6 h followed by a chase with DMEM for 18 h. The cells were then scraped and resuspended in 1 ml of ice cold HB buffer (10 mM sucrose, 10 mM TES, pH 7.4, 1 mM $MgCl_2$) and incubated on ice for 10 min. The cells were then homogenised by 40 passes of a ball bearing homogeniser with a clearance of 6 µm. The lysate was restored to 250 mM sucrose by the addition of an equal volume of restoration buffer (490 mM sucrose, 10 mM TES, pH 7.4, 1 mM $MgCl_2$) and centrifuged at *1,500 x g* for 10 min at 4 ºC to generate a post-nuclear supernatant (PNS). 5 µl of the PNS was assayed for the activity of the lysosomal enzyme β-hexosaminidase (β-hex) as previously described in section 2.20. The amount of (β-hex) activity was used to determine the latency and recovery of lysosomes in the PNS. **B&C.** Lysosomes were purified from RAW 264.7 cells as per the method described in the figure legend of Fig. 3.1, but with FeDex dilutions of 1:20 and 1:100. The purified lysosomes were then subjected to β-hexosaminidase (β-hex) assay to calculate the latency (**B**) and recovery (**C**) of lysosomes (n=1).

Given that lysosome recovery from RAW cells dropped when FeDex concentration was increased it was decided to see if the same trend would be true for J774.2 cells (Fig. 3.3 A). Indeed, the latency of lysosomes in the PNS did not vary greatly between the FeDex concentrations used (87.3 % 1:100 FeDex compared to 80.1 % 1:20 FeDex). However, as seen previously with the RAW cells, there was downward trend in the recovery of lysosomes in the PNS (46 % 1:100 FeDex compared to 8.5 % 1:20 FeDex).

The latency and recovery of lysosomes did not differ greatly between J774.2 cells or RAW 264.7 cells but there was the potential for improvement. As such, it was decided to investigate if alternative fractionation methods would leave more lysosomes intact. Ball bearing homogenisation places cells under high shear forces, resulting in the release of the cytoplasm and organelles. However, the amount of force applied during each stroke can vary due to its manual operation. This can result in high variation between experiments and between users. Furthermore, the mechanical stress and friction placed on the sample generates localised increases in temperature, which can result in sample degradation. In contrast, nitrogen cavitation places the sample under high pressure with nitrogen gas, which dissolves in the cell. When the pressure is released, the gas expands and gently stretches the cell membrane, causing it to rupture and release the cellular contents. This method has several advantages that make it particularly attractive. As the cell lysate is saturated with inert nitrogen gas, it provides excellent protection against oxidative damage, and also does not change the pH of the fractionation media. This property also prevents the sample being damaged by increases in temperature, as the adiabatic expansion of the gas cools the sample (Simpson, 2010). Furthermore, as there are no limitations to the fractionation buffer that can be used, this reduces the manipulation of the sample, and does not require additional reagents to be added during the protocol. The fractionation is also uniform, as the nitrogen gas is applied evenly across the sample. Nitrogen cavitation has been used to isolate polyribosomes (Dowben et al., 1968), microsomal fractions, (Short et al., 1972), mitochondria (Gottlieb and Adachi, 2000), and endosomal vesicles (Lamb et al., 2012). Consequently, it was investigated if nitrogen cavitation could be used to optimise lysosome purification. J774.2 cells were pulse-chased with varying dilutions of FeDex and were fractionated at 500 psi for 5 min (Fig. 3.3 B).

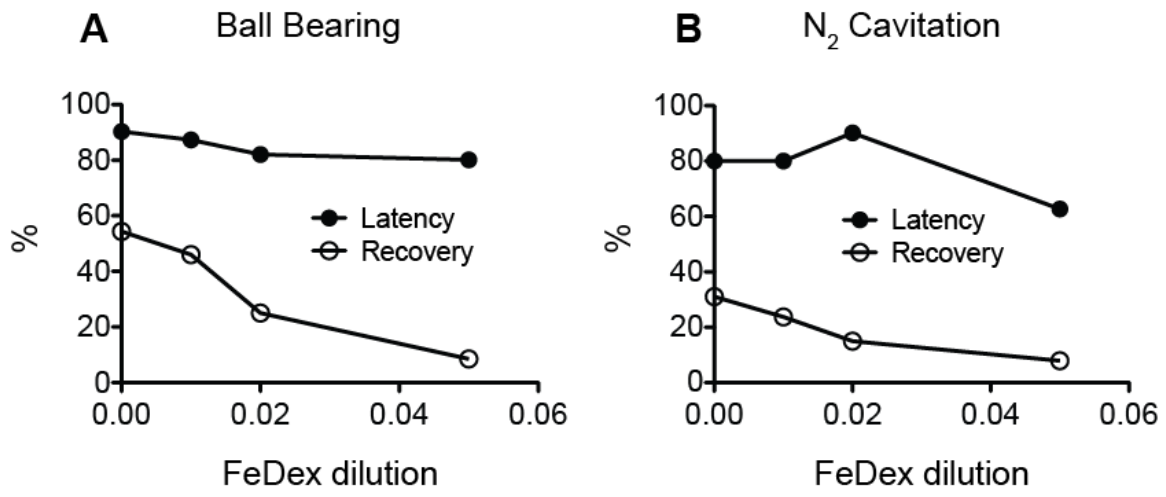

Fig. 3.3 The effect of FeDex concentration on latency and recovery of FeDex-labelled lysosomes in J774.2 cells. J774.2 macrophages were pulsed for 6 h with FeDex at varying concentrations, followed by a FeDex-free chase for 16 h in order to label lysosomes. The cells were then scraped and resuspended in 1 ml of ice cold HB buffer (10 mM sucrose, 10 mM TES, pH 7.4, 1 mM $MgCl_2$) for 10 min on ice. Cells were then homogenised by 40 passes of a ball bearing homogeniser (**A**) with a clearance of 6 µm (8.014 mm ball bearing) or lysed by nitrogen cavitation (**B**) at 500 psi for 5 min at 4 ºC. In both cases, the lysate was restored to 250 mM sucrose by the addition of an equal volume of restoration buffer (490 mM sucrose, 10 mM TES, pH 7.4, 1 mM $MgCl_2$) and was centrifuged at *1,500 x g* for 10 min at 4 ºC to generate a post-nuclear supernatant (PNS). The PNS was subjected to β-hexosaminidase (β-hex) assay in the presence and absence of detergent (as described in section 2.20) to calculate the latency and the recovery of lysosomes in the PNS (n=1).

Unlike ball bearing homogenisation, when nitrogen cavitation was used to lyse the cells, there was a slight downward trend in lysosomes latency in the PNS as FeDex concentration was increased. Latency using FeDex at 1:100 was 80 % FeDex 1:100 compared to 62.7 % when the FeDex was used at 1:20. As with previous experiments, as the FeDex concentration was increased there was a downward trend in lysosome recovery in the PNS. Latency was 23.7 % when the FeDex was used at 1:100, compared to 7.9 % when the FeDex was used at 1:20. Despite this experiment only being performed once and the latency and recovery values of lysosomes in the PNS of cells broken by nitrogen cavitation appearing to be slightly less compared to ball bearing homogenisation, the use of the nitrogen bomb was further optimised. The justification for this decision was that it was

hypothesised that (along with the previously discussed advantages), nitrogen cavitation would be a more consistent and reproducible method of cell disruption compared to ball-bearing homogenisation. Secondly, J774.2 cells were incubated in a hypotonic buffer (HB) to facilitate cell disruption with the ball-bearing homogeniser. With nitrogen cavitation, this step was not necessary, thus cutting the protocol time down further. The nitrogen pressure vessel also could accommodate sample volumes of > 30 ml, without changing the parameters of cell disruption (i.e. cell breakage remains constant regardless of the volume of the sample used). With the ball bearing homogeniser, using larger sample volumes required the use of larger syringes that needed more force to pass the sample through the chamber. This would in turn increase the pressure within the homogenisation chamber. Using larger samples with the ball bearing homogeniser would alter the parameters previously optimised. As such, the nitrogen cavitation protocol might have been easier to optimise and improve upon, and so was taken forward.

The next variables investigated were the pressure used to lyse cells and the time under pressure (Fig. 3.4). J774.2 cells were lysed by nitrogen cavitation at 500 psi, 1000 psi, 1500 psi or 2000 psi, and the lysosomal latency and recovery in the PNS was determined by β-hexosaminidase assay (Fig. 3.4 A). The latency of lysosomes in the PNS did not vary significantly between the different pressures tested ($p=0.841$). There appeared to be a slight upward trend in the recovery of lysosomes in the PNS, but this was only measured once. In contrast, there was a clear downward trend in both the latency and recovery of lysosomes in the PNS of cells as the time under pressure was increased (Fig. 3.4 B). After 5 min under pressure (500 psi) the latency and recovery of lysosomes in the PNS was 51.2 % and 47.7 % respectively. After 30 min, this had decreased to 25.3 % and 21.4 % respectively. It was observed that using pressure above 1000 psi resulted in violent elution of the sample and resulted in excessive frothing of the sample. Therefore, the pressure was kept below 500 psi for further experiments. Increasing the time under pressure resulted in a decrease in both the latency and recovery of lysosomes in the PNS. As such, cells were subjected to high pressure for only 5 min in further experiments to improve lysosome recovery.

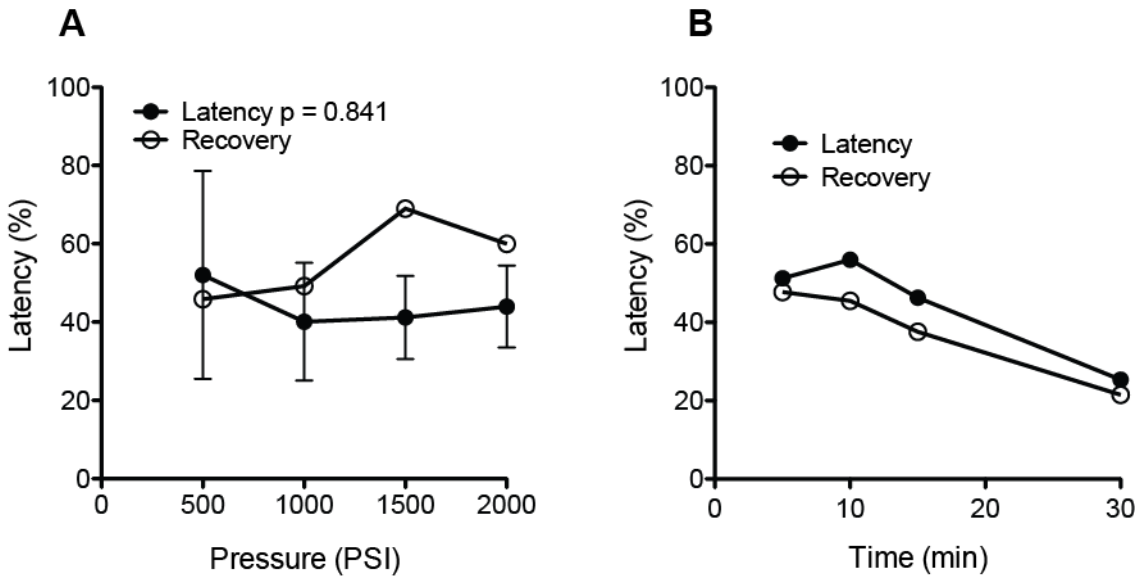

Fig. 3.4. Optimisation of cell disruption using nitrogen cavitation. A. J774.2 macrophages were scraped into 1 ml of ice cold HB buffer (10 mM sucrose, 10 mM TES, pH 7.4, 1 mM $MgCl_2$) and placed under nitrogen gas pressure at different pressures for 5 min at 4 ºC. The lysate was restored to 250 mM sucrose by the addition of an equal volume of restoration buffer (490 mM sucrose, 10 mM TES, pH 7.4, 1 mM $MgCl_2$). A post-nuclear supernatant (PNS) was generated from the lysate by centrifugation at *1,500 x g* for 10 min at 4 ºC. **B.** As in A, except cells were placed under pressure at 500 psi for the times indicated, at 4 ºC. The PNS from both A&B was subjected to β-hexosaminidase (β-hex) assay in the presence and absence of detergent (as described in section 2.20) to calculate the latency and the recovery of lysosomes in the PNS (A - latency data are means ± the range of two experiments, and were analysed by one-way ANOVA. Recovery values in A are from a single experiment. B - n=1).

For the previous experiments, J774.2 cells were incubated on ice in a hypotonic homogenisation buffer (HB) for 10 min to allow the cells to swell and become easier to homogenise. As such, it was decided to investigate whether it was necessary to incubate cells in HB for longer periods of time when using nitrogen cavitation at two different pressures (Fig. 3.5). Cells were incubated on ice for increasing lengths of time (5 min to 30 min) and disrupted at 500 psi (Fig. 3.5 A) or 250 psi (Fig. 3.5 B) for 5 min. The latency of lysosomes in the PNS of cells incubated on ice for increasing lengths of time did not vary greatly whether cells were fractionated at 500 psi (61.2 % to 67 %) or at 250 psi (71.9 % to 73.4 %). When cells were disrupted at 500 psi, the incubation on ice did not appear to change recovery of lysosomes in the PNS (53% to 62 %). When cells were

disrupted at 250 psi, there appeared to be a slight downward trend in recovery, with recovery dropping from 68.1 % (0 min on ice) to 42.9 % (20 min on ice). Although there was no clear trend in these results, it was decided to disrupt cells at 250 psi for further experiments as this made the elution of the sample from the nitrogen bomb much gentler with less frothing of the lysate and loss of the sample. Elution from the pressure vessel was also difficult to safely control at higher pressures, and disruption of subcellular organelles has been reported to occur at 1000 psi (Gottlieb and Adachi, 2000).

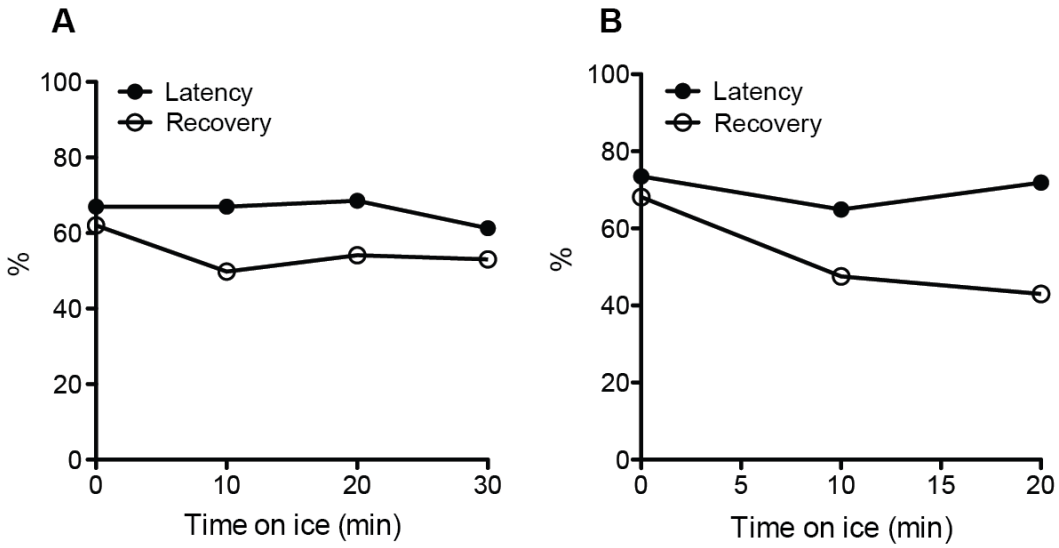

Fig. 3.5. The effect of incubating cells in a low osmolarity before nitrogen cavitation at 500 or 250 psi. J774.2 cells were incubated in a hypotonic buffer (10 mM sucrose, 10 mM TES, pH 7.4, 1 mM $MgCl_2$) and incubated on ice for increasing lengths of time. Cells were then placed under nitrogen gas pressure at 500 psi (**A**) or 250 psi (**B**) for 5 min at 4 ºC. The lysate was restored to 250 mM sucrose by the addition of an equal volume of restoration buffer (490 mM sucrose, 10 mM TES, pH 7.4, 1 mM $MgCl_2$) A post-nuclear supernatant (PNS) was generated from the lysate by centrifugation at *1,500 x g* for 10 min at 4 ºC. The PNS was subjected to β-hexosaminidase (β-hex) assay (as described in section 2.20) to calculate the latency and the recovery of lysosomes in the PNS (n=1).

The number of cells fractionated in an experiment was also an important consideration. For ball bearing homogenisation, changing the cell number would have altered the viscosity of the cell suspension and changed the shear forces placed upon the sample. Changing the cell number would have changed the ratio of buffer : cell. This would have resulted in a different osmolarity for each sample and would likely influence the outcome of the homogenisation. In contrast, nitrogen cavitation places each cell under the exact same gas pressure, so the fractionation should be equal across the entire sample. As such, the nitrogen cavitation should give similar results regardless of the number of cells fractionated. To investigate this, cells were fractionated in HB buffer at 250 psi for 5 min at 3, 6,12, or 24 x 10^6 cells/ml (Fig. 3.6) and the latency and recovery of lysosomes in the PNS calculated using β-hexosaminidase assay. There was no significant difference in lysosome latency or recovery in the PNS when cells were lysed at different cell densities ($p = 0.783$ and $p = 0.496$, respectively). Despite the previous optimisations to the protocol, both the lysosome latency and recovery were poor, with latency ranging from 45 % to 54 % and recovery ranging from 56.7 % to 70.6 %.

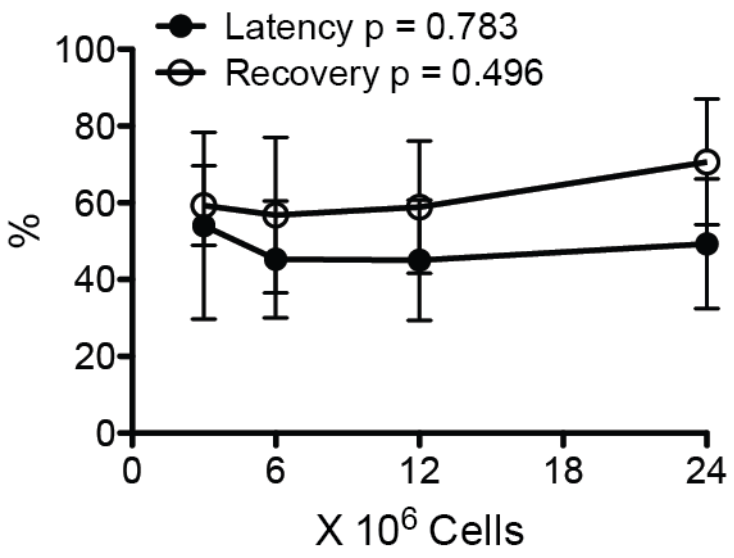

Fig. 3.6. The effect of cell number on lysosome latency and recovery in the PNS of cells fractionated by nitrogen cavitation. J774.2 macrophages were resuspended at 3,6,12, or 24 x 10^6 cells in 1 ml of HB buffer (10 mM sucrose, 10 mM TES, pH 7.4, 1 mM $MgCl_2$) and lysed by nitrogen gas at 250 psi for 5 min at 4 ºC. The lysate was restored to 250 mM sucrose by the addition of an equal volume of restoration buffer (490 mM sucrose, 10 mM TES, pH 7.4, 1 mM $MgCl_2$) and a post-nuclear supernatant (PNS) was generated from the lysate by centrifugation at *1,500 x g* for 10 min at 4 ºC. The PNS was subjected to β-hexosaminidase (β-hex) assay in the presence and absence of detergent (as described in section 2.20) to calculate the latency and the recovery of lysosomes in the PNS. Data are means ± SEM and were analysed by one-way ANOVA (n=6).

As cell number had no significant effect on latency or recovery, 20 x10^6 cells /ml were used as experimentally, this number of cells was easier to deal with. As a large degree of variability in the latency and recovery of lysosomes was seen in all previous experiments, the experimental protocol as it stood was repeated several more times to determine whether the variability was an inherent property of the cells used, or whether experimental variance was the cause of variability. 20 x 10^6 cells were incubated in 1 ml of HB for 10 min at 4 ºC. The cells were then disrupted at 250 psi for 5 min at 4 ºC, and a PNS generated. The latency and recovery of lysosomes in the PNS was calculated in 6 independent experiments (Fig. 3.7 A). The recovery and latency of lysosomes further purified from the PNS of two of these experiments was also calculated (Fig. 3.7 B). Encouragingly, the average latency and recovery of lysosomes in the PNS of cells fractionated using

nitrogen cavitation in HB was much higher than previous experiments (81.2 % and 73.7 % respectively). However, the average latency and recovery of the final lysosomal fraction was 34.3 % and 4.3 % respectively (Fig. 3.7 B). The drop in latency and recovery from the PNS to the final lysosome fraction most likely was a result of damage to the lysosomes while pelleting and resuspending them. These values were also lower than the latency and recovery values seen for lysosomes purified using ball-bearing homogenisation, from J774.2 and RAW 264.7 cells (Fig. 3.1; J774.2 ~50 % latency and ~10 % recovery & Fig. 1.2; 48 % latency, 22 % recovery). Despite this, further optimisation experiments were performed using the nitrogen cavitation, as the latency and recovery values of lysosomes from the original protocol had room for improvement, and use of the nitrogen bomb was simpler than the ball bearing homogeniser.

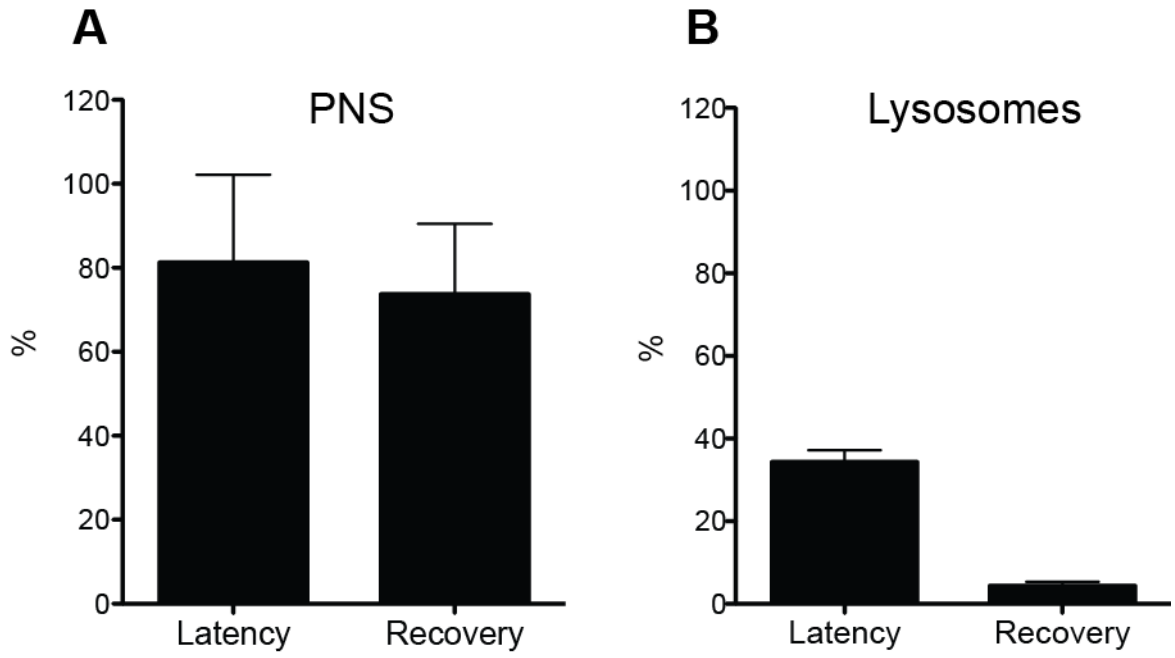

Fig. 3.7 Latency and recovery of lysosomes in the PNS and final lysosome fractions of cells fractionated by nitrogen cavitation. 20 x 10^6 J774.2 cells were pulse chased with FeDex diluted 1:20 for 6 h followed by a 16 h chase in FeDex-free media. The cells were then scraped and resuspended in 1 ml of ice cold HB buffer (10 mM sucrose, 10 mM TES, pH 7.4, 1 mM $MgCl_2$) for 10 min on ice. Cells were then lysed by nitrogen cavitation at 250 psi for 5 min at 4 ºC. The lysate was restored to 250 mM sucrose by the addition of an equal volume of restoration buffer (490 mM sucrose, 10 mM TES, pH 7.4, 1 mM $MgCl_2$) and was centrifuged at *1,500 x g* for 10 min at 4 ºC to generate a post-nuclear supernatant (PNS). The PNS was applied to a cell column held within a magnetic field. The flow through was collected, and the column washed with 3 ml of STM. The column was removed from the magnetic field, and lysosomes eluted with 3 ml of STM. Lysosomes were pelleted by centrifugation at *104,000 x g* for 15 min at 4 ºC, and resuspended in 100 µl of STM. Lysosomal latency and recovery of lysosomes in the PNS (**A** n=6) and final lysosome fraction (**B** n=2) was determined by calculating the activity of the lysosomal enzyme β-hexosaminidase (β-hex) in the presence and absence of detergent (as described in section 2.20). All data are means ± SEM.

One possibility for the variation seen could have been due to the homogenisation buffer used. Restoration buffer was added to the lysates to restore them to 250 mM sucrose (300 mOsm) in order to return the buffer to an osmolarity close to that of mammalian cells (280 mOsm). Lysosome integrity may have been affected by incomplete mixing of the two buffers. As such, it was investigated whether lysing cells directly into an osmotically balanced buffer (STM), could improve lysosome

latency and recovery. 20 x10^6 cells were fractionated at 250 psi for 5 min in either 1 ml of HB or STM buffers (Fig. 3.8), and the latency and recovery of lysosomes in the PNS was determined. There was no statistically significant difference between latency (Fig. 1.8 A p = 0.187) and recovery (Fig. 1.8 B p = 0.136) when using HB or STM. The average latency in the PNS was 61.7 % (HB) and 71.5 % (STM), and the average recovery in the PNS was 53.8 % (HB) and 37.4 % (STM). As there was no significant difference between the two buffers, it was decided to use STM for further experiments in order to reduce the need to manipulate the sample through adding additional buffers and mixing. Removing this step also removed another possible source of variability between experiments.

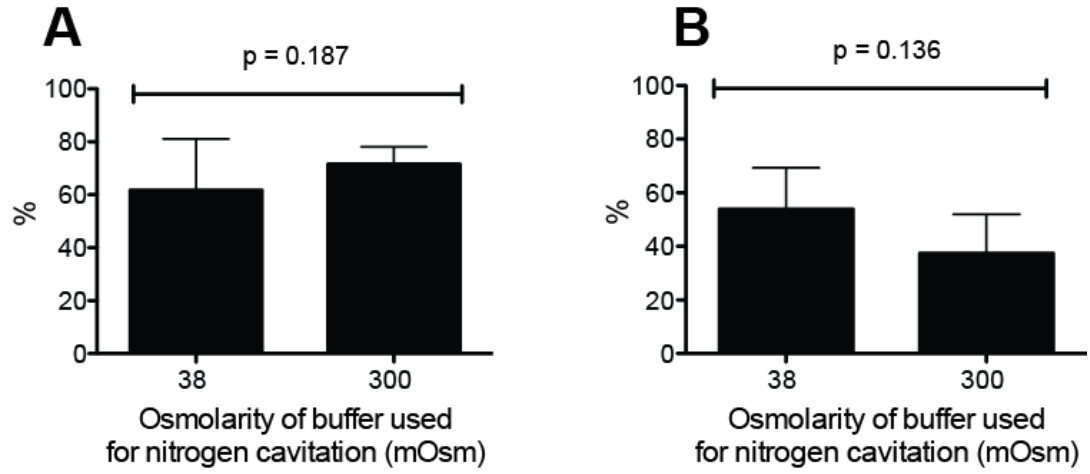

Fig. 3.8. Lysosome latency and recovery in the PNS of cells fractionated in HB and STM buffers. 20x10^6 J774.2 macrophages were resuspended in either 1 ml of hypotonic HB buffer (10 mM sucrose, 10 mM TES, pH 7.4, 1 mM $MgCl_2$, 38 mOsm) or osmotically balanced STM (250 mM sucrose, 10 mM TES, pH 7.4, 1 mM $MgCl_2$, 300 mOsm). Cells were then lysed by nitrogen cavitation at 250 psi for 5 min at 4 ºC (cells lysed in HB were restored to 300 mOsm by the addition of an equal volume of restoration buffer). A post-nuclear supernatant (PNS) was generated from the lysate by centrifugation at *1,500 x g* for 10 min at 4 ºC The PNS was assayed for the activity of the lysosomal enzyme β-hexosaminidase in order to calculate the lysosomal latency (**A**) and recovery (**B**) of lysosomes in the PNS. Data are means ± SEM. Data were analysed by two-tailed t-test (n=6).

To ensure that the previous results seen were consistent and would not be dramatically different when STM buffer was used instead of HB, it would have been necessary to repeat these experiments using STM. However, due to time

constraints, cell number was considered to be the variable that most likely could have affected lysosome integrity when using STM instead of HB. To test this, J774.2 cells were lysed at different cell numbers (Fig. 3.9 A). It has previously found that some cell types stiffen with passage number (Berdyyeva et al., 2005), or may produce more cytoskeletal proteins such as α-actin (Kato et al., 2008). Lysosome number may also increase with cell age and confluency (Thoene, 1992). As the growth state of the cells may have affected the efficiency of lysosome purification, the number of days the cells seeded for before fractionation was also investigated (Fig. 3.9 B). Changing cell number had no effect of lysosome latency ($p = 0.501$) or recovery ($p = 0.831$). Similarly, seeding cells for increasing lengths of time before cell lysis had no effect on latency ($p = 0.101$) or recovery ($p = 0.963$).

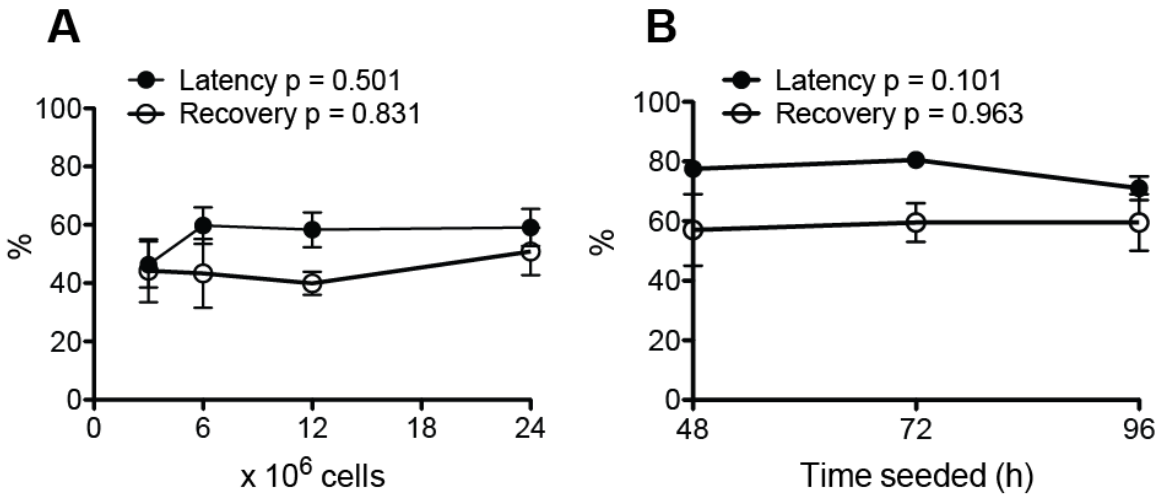

Fig. 3.9 The effect of cell number and cell age on lysosome latency and recovery. **A.** Increasing numbers of J774.2 macrophages were fractionated in 1 ml of STM at 250 psi for 5 min at 4 ºC in a nitrogen pressure vessel. A post-nuclear supernatant (PNS) was generated from the lysate by centrifugation at *1,500 x g* for 10 min at 4 ºC. The PNS was assayed for the activity of the lysosomal enzyme β-hexosaminidase in order to calculate the lysosomal latency and recovery (n=6). **B.** Cells were cultured for different lengths of time before they were resuspended at 20 x 10^6 cells in 1 ml of STM and were subjected to the same experimental protocol as in A. The latency and recovery of lysosomes was calculated by β-hexosaminidase assay (n=2). Data are means ± SEM and were analysed by one-way ANOVA.

The centrifugation speed and duration used to generate a PNS from the cell lysate was also considered. Lysosomal density increases with iron accumulation and can be correlated with the degree and duration of iron exposure (Dimitriou et al., 2000). It was hypothesised that once lysosomes reach a particular density through the accumulation of FeDex, they can be pelleted at relatively low centrifugation speeds. Secondly, FeDex-containing organelles may be denser than non-labelled lysosomes, and a slower centrifugation speed may have resulted in less FeDex-labelled lysosomes being pelleted along with cellular debris during the PNS spin (Fig. 3.10). To investigate this cells were fractionated in STM for 5 min at 250 psi and the lysates centrifuged at *800 x g* for 5 min or *1500 x g* for 10 min at 4 ºC. The latency (Fig. 3.10 A) and recovery (Fig. 3.10 B) in the PNS was then measured by β-hexosaminidase assay. There was no significant difference between centrifugation conditions on lysosome latency ($p = 0.325$). While it appeared that there was a slight drop in recovery at *1,500 x g* compared to *800 x g* this was no statistically significant ($p = 0.402$). Subsequently, post-nuclear supernatants were generated at *800 x g* for 5 min to reduce the protocol length further.

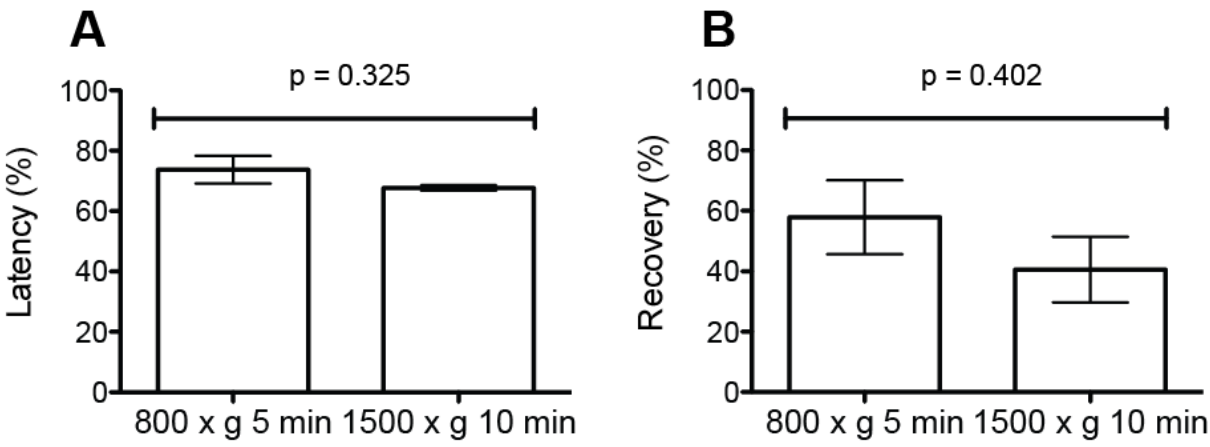

Fig. 3.10. The effect of different centrifugation conditions upon lysosome latency and recovery in a post-nuclear supernatant. 20 x10^6 J774.2 cells were fractionated in 1 ml of STM buffer at 250 psi for 5 min at 4 ºC. The lysate was then centrifuged at *800 x g* for 5 min or *1500 x g* for 10 min at 4 ºC to generate a post-nuclear supernatant (PNS). The latency (**A**) and recovery (**B**) in these PNS samples was then calculated by β-hexosaminidase assay. Data are means ± SEM and were analysed by un-paired t-test (n=2).

3.1.3.3 Determining the minimum pulse and chase time needed to purify lysosomes

It was previously seen that increasing the concentration of FeDex used to magnetically label lysosomes, resulted in a drop in recovery when using HB buffer (Fig. 3.2 & 3.3). The effect of FeDex using STM buffer was also investigated (Fig. 3.11 A). J774.2 cells were pulsed with increasing amounts of FeDex diluted 1:20, 1:50, 1:100 and 1:200 and the FeDex labelled lysosomes were isolated. FeDex concentration did not significantly affect lysosome latency ($p=0.986$) or recovery ($p=0.933$) in the final lysosome fraction, and FeDex was used at 1:20 for further experiments. Next, in order to improve lysosome purification and reduce the protocol length as much as possible, the length of the FeDex pulse required to label lysosomes was determined (Fig. 3.11 B) J774.2 cells were pulsed with FeDex (1:20) for 1 h, 2 h, 4 h, or 6 h followed by a 16 h chase period with FeDex-free media. FeDex-labelled lysosomes were isolated magnetically and the latency and recovery was determined by β-hexosaminidase assay. The latency of lysosomes followed a significant downward trend as the length of the FeDex pulse was increased ($p = 0.032$). The recovery also followed a downward trend, but this was not significant ($p = 0.423$). Encouragingly, the latency for 1 h pulse was 79 %, with a recovery of 7.2 %, indicating that a shorter pulse time may result in more intact lysosomes with a reasonable recovery. Thus, a 1 h pulse of FeDex diluted 1:20 was sufficient to purify lysosomes and gave the highest latency and recovery.

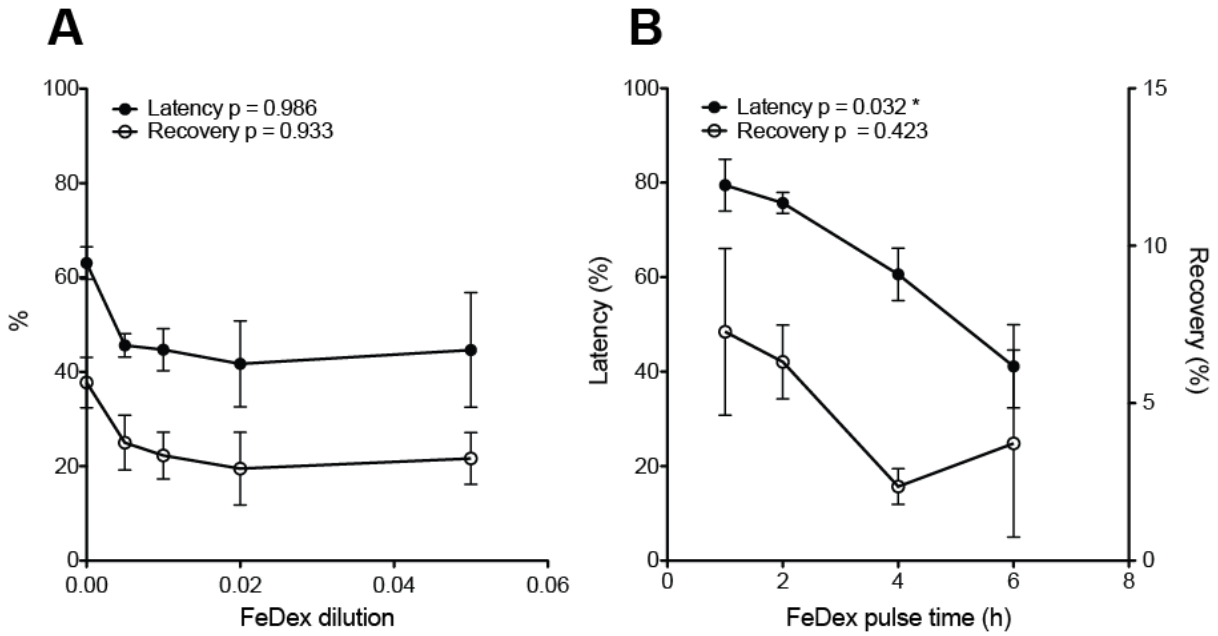

Fig. 3.11. The effect of FeDex concentration and pulse length on latency and recovery of FeDex-purified lysosomes. A. J774.2 macrophages were given a 6 h pulse of FeDex at increasing concentrations, followed by a 16 h chase in FeDex free media. The cells were then resuspended in 1 ml of STM buffer and lysed by nitrogen cavitation at 250 psi for 5 min at 4 ºC. The lysate was centrifuged at *800 x g* for 5 min at 4 ºC to generate a post-nuclear supernatant (PNS). The PNS was applied to a cell column held within a magnetic field. The flow through was discarded, and the column washed with 3 ml of STM. The column was removed from the magnetic field, and lysosomes eluted with 3 ml of STM. Lysosomes were pelleted by centrifugation at *104,000 x g* for 15 min at 4 ºC, and resuspended in 100 µl of STM. FeDex-labelled lysosomes were assayed for the activity β-hexosaminidase in order to calculate the lysosomal latency and recovery. Data are means ± SEM and were analysed by one-way ANOVA (n=3). **B.** J774.2 macrophages were pulsed with FeDex (1:20) for increasing amounts of time**,** followed by a 16 h chase in FeDex free media. FeDex labelled organelles were then magnetically isolated as described in (A) and the latency and recovery determined by β-hexosaminidase assay. Data are means ± SEM and were analysed by one-way ANOVA (n=2).

To reduce the protocol length further still, we sought to determine the minimum time required for all endocytosed FeDex to reach the terminal lysosomal compartment. J774.2 cells were given a 1 h pulse of FeDex and chased with FeDex-free media for 0, 30, 60, or 120 min (Fig. 3.12). Lysosomes were then magnetically isolated and probed for different markers of the endocytic pathway. Early endosomal antigen 1 (EEA1) and Rab5 were used as early endosomal

markers, Rab7 as a marker of late endosomes, and Lysosome associated membrane protein 1 (LAMP1) as a marker of lysosomes. The level of contamination with the cytoskeleton was determined by blotting for α-tubulin. In order to compare the levels of early and late endocytic markers, samples were first normalised to the activity levels of the lysosomal enzyme β-hexosaminidase. Levels of early endosomal antigen 1 (EEA1) dropped rapidly between 0 and 30 min chase and were almost absent after 120 min. The levels of LAMP1 were equivalent between all samples within an experiment, indicating that the loading of samples normalised to β-hexosaminidase activity can be used to normalise amounts of lysosomal material between samples. The levels of α-tubulin were similar between all chase times. The late endosomal marker Rab7 dropped steadily from 0 min to 120 min. Similarly, levels of the early marker endosomal marker Rab5 dropped from 60 min. After 120 min, endocytic compartments had high levels of LAMP1 and negligible levels of EEA1, Rab5 and Rab7. This was similar between three separate experiments. Therefore, a 1 h pulse and 2 h chase was deemed sufficient to purify terminal lysosomal compartments.

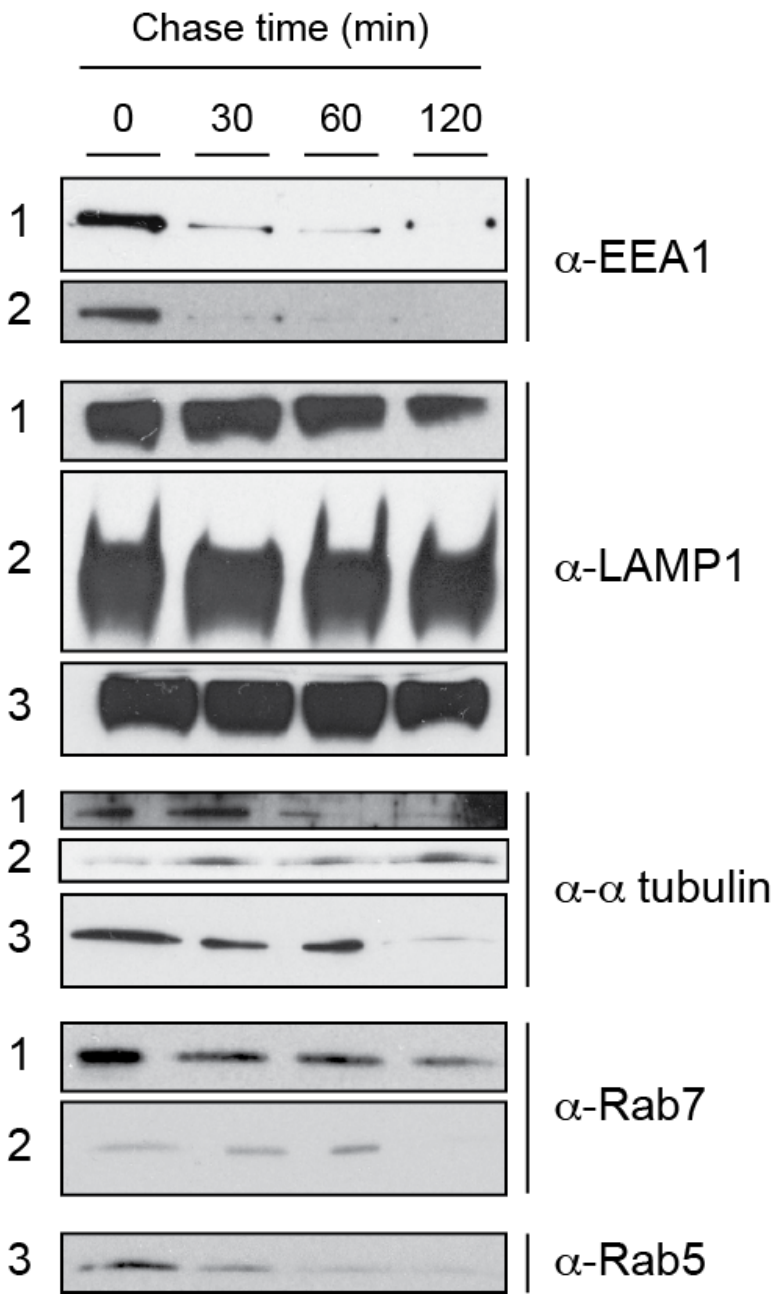

Fig. 3.12. Western blot analysis of magnetically purified endocytic compartments. J774.2 macrophages were given a 1 h pulse of FeDex diluted 1:20 followed by a chase with FeDex free media of 0,30,60,or 120 min. FeDex-labelled endocytic compartments were then magnetically isolated as described in Fig. 3.11. Purified organelles were subjected to western blotting for EEA1 (early endosomal antigen 1), LAMP1 (Lysosome associated membrane protein 1), α-tubulin, Rab7 and Rab5. Samples were normalised to levels of the lysosomal enzyme β-hexosaminidase in order to compare the levels of early and late endocytic markers relative for an arbitrary amount of lysosomal material. Data are results of three individual experiments (1,2,3), with blotting for EEA1 performed twice, Rab7 twice, and Rab5 once.

3.1.3.4 Purification of lysosomes using density centrifugation.

A major disadvantage of purifying lysosomes by density centrifugation is the amount of time the purification takes, as well as the inherent disadvantages of the centrifugation media used. As a more rapid lysosome purification protocol had been optimised, that was much quicker than centrifugation, it was decided to compare the purity of lysosomes isolated by both protocols (Fig. 3.13 & 3.14). Lysosomes were purified from J774.2 mouse macrophages on a 1-22% Ficoll density gradient (Fig. 3.13), in order to compare the level of contamination (of other subcellular fractions), relative to lysosome fractions purified using the FeDex protocol. J774.2 cells were lysed in STM by nitrogen cavitation at 250 psi for 5 min at 4 ºC and the lysate centrifuged to generate a post-nuclear supernatant (PNS). The PNS was loaded onto a 1-22 % Ficoll gradient, and centrifuged for 1 h in a vertical rotor to reduce the centrifugation time. 1 ml fractions were collected using a fraction collector and analysed by both enzymatic assay (Fig. 3.13 A) and western blotting (Fig. 3.13 B) to determine where lysosomes were on the gradient. There was a peak of β-hexosaminidase starting at fraction 3 and finishing at fraction 11. This peak was only visible when detergent was used to lyse lysosomal membranes, indicating intact lysosomes had been purified, and that the enzymatic activity was not due to the presence of free enzyme. Indeed, a second peak of β-hexosaminidase activity was seen from fractions 17-21, which did not increase when detergent was used in the β-hexosaminidase assay. This is indicative of free enzyme present in the soluble fraction. The average latency of lysosomes in fractions 7-15 was 78 %. The western blotting also corresponded to the results of the enzymatic assay. LAMP1 was detected most strongly in fractions 7-13, and was largely absent from lighter fractions on the gradient. Contamination of the endoplasmic reticulum (ER) was determined by the levels of glucose-regulated protein,78 kDa (GRP78). A small amount of GRP78 was detected in fraction 7, but the majority was found at the lighter end of the gradient in fractions 21-29. Similarly, no α-tubulin was detected in the lysosomal fractions, but was detected in fractions 23-29. Syntaxin 7 was detected as soon as fraction 7, but the highest amounts were detected in fractions 13-19. This is not surprising, as Syntaxin 7 is required for late endosome-lysosome fusion and would be present on some lysosomal membranes (Mullock et al., 2000).

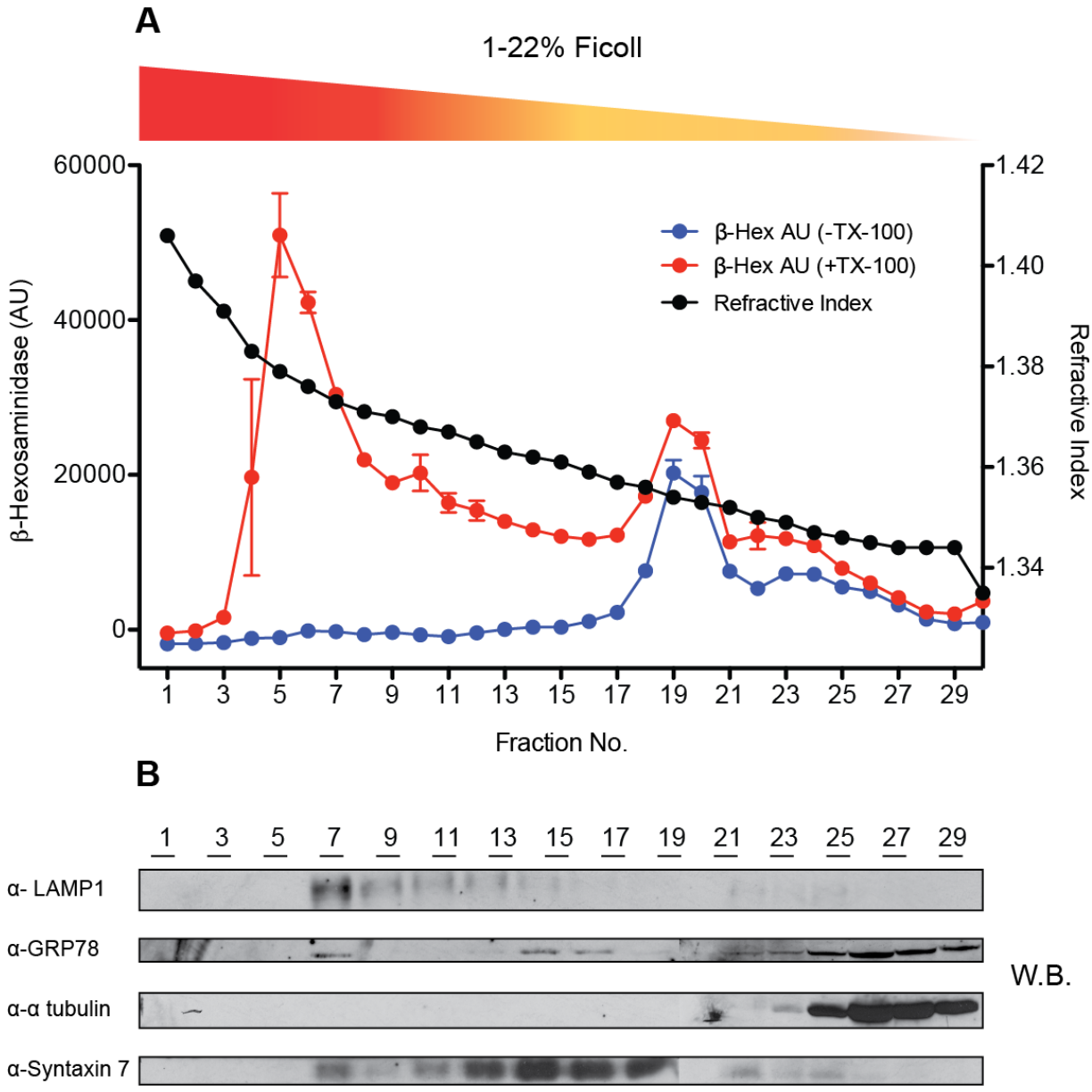

Fig. 3.13. Purification of lysosomes by isopycnic centrifugation. A. 60 x10^6J774.2 cells were lysed in 3 ml of STM by nitrogen cavitation at 250 psi for 5 min at 4 ºC. The lysate was centrifuged at *800 x g* for 5 min at 4 ºC to generate a post-nuclear supernatant (PNS). The PNS was then loaded onto a 1-22% Ficoll gradient and centrifuged in a Beckman Vti50 vertical rotor for 1 h at 50,000 rpm. 1 ml fractions were collected and subjected to β-hexosaminidase assay in the presence or absence of detergent. The refractive index of each fraction was also measured. **B.** Equal volumes of the fractions of the gradient in A were western blotted for markers of lysosomes (LAMP1), endoplasmic reticulum (GRP78), cytoskeleton (α-tubulin), and late endosomes/lysosomes (Syntaxin 7) (n=1).

Lysosomes were purified using isopycnic centrifugation (fractions 5-9) or magnetic isolation, and were then analysed for contamination of other subcellular fractions (Fig. 3.14). Lysosomes were purified on a 1-22 % Ficoll gradient, or by the FeDex protocol (using either nitrogen cavitation or ball bearing homogenisation to generate a PNS). Lysosomes were subjected to western blotting using antibodies against LAMP1, GRP78 and α-tubulin All lysosome fractions were positive for LAMP1, with lysosomes purified by ball bearing homogenisation having the highest amounts, followed by purification by density centrifugation. All fractions were contaminated with similar levels of endoplasmic reticulum, as judged by the levels of GRP78. However, lysosomes purified by ball bearing homogenisation had no contamination of α-tubulin. Small amounts of α-tubulin were present in lysosomes purified by density centrifugation and nitrogen cavitation.

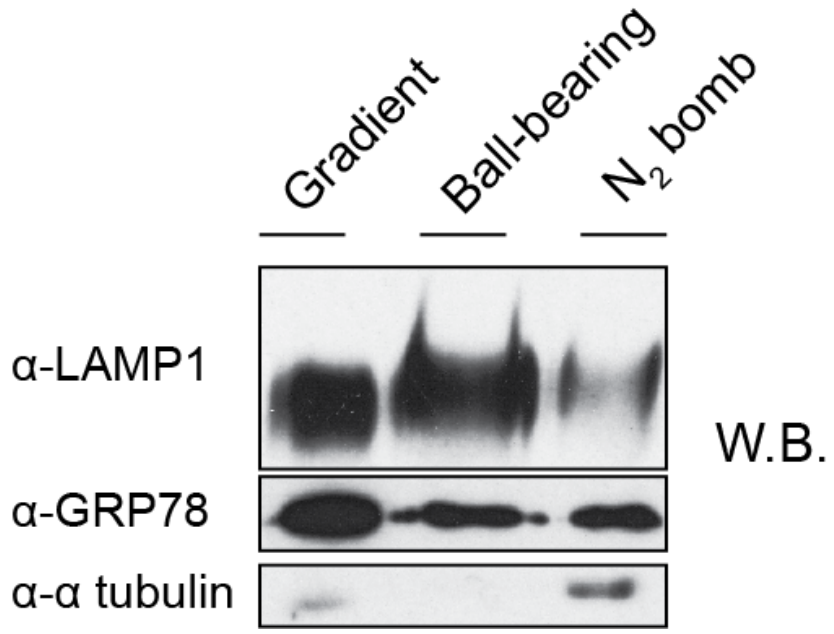

Fig. 3.14. Western blot analysis of lysosomes purified using three different purification protocols. J774.2 cells were pulse-chased with FeDex and were fractionated by nitrogen cavitation (N_2) or with a ball bearing homogeniser (Ball bearing). FeDex labelled endocytic compartments were then magnetically isolated as previously described. Alternatively, J774.2 cells were fractionated by nitrogen cavitation and lysosomes purified using isopycnic centrifugation on a 1-22 % Ficoll gradient (gradient) as per Fig. 1.13. Purified lysosomes were subjected to western blotting for lysosomal (LAMP1), ER (GRP78), and cytoskeletal (α-tubulin) markers. 5 μg of protein was loaded protein per lane of an SDS PAGE minigel (n=1).

While the lysosomes purified using nitrogen cavitation had less LAMP1 and more α-tubulin, the final protocol was quicker than isopycnic centrifugation, and simpler than ball bearing homogenisation. Thus the final protocol for purifying lysosomes was a 1h pulse of FeDex (1:20) followed by a 2 h chase. The total length of time from fractionation to a final eluate was approximately 3h 40 min – 4 h. The length of time to generate a lysosomal fraction using centrifugation was approximately 3-4 h, but required the setting up of the gradient the day before the experiment, and would result in a lysosome fraction containing Ficoll, which would require additional steps to remove it.

3.1.4 Lysosome purification - Discussion

Lysosome purification can be difficult and time consuming, and often requires the use of high speed centrifuges to separate lysosomes from other subcellular fractions by isopycnic centrifugation. Obtaining lysosome fractions free from impurities and in enough quantity for downstream applications is challenging. Monitoring the purification itself routinely requires enzymatic assays to determine levels of contamination and enrichment of lysosomes, which again are time consuming and results in less of the sample available for further experiments. Importantly, these methods are not necessarily optimised to ensure lysosomes remain intact. As we wished to use lysosomes in an *in vitro* fusion assay, they need to be intact to ensure the assay would be efficient as possible. Therefore a quicker, simpler method, that was optimised to purify intact lysosomes would be extremely beneficial. As such, we sought to investigate the variables that may improve upon established methods to magnetically isolate lysosomes.

While there are many published protocols for lysosome purification, they can require extensive optimisation for a particular cell or tissue type. For a fusion assay in particular, the purification protocol must be gentle enough to result in a final lysosome fraction that contains a large proportion of intact lysosomes. These lysosomes must also remain fusogenic and behave similarly *in vitro* to those *in vivo*. Thus, ligands or compounds introduced into lysosomes to aid in there purification must not interfere with lysosome function. The isolation of lysosomes from *Dictyostelium discoideum* (Rodriguez-Paris et al., 1993), was adapted to J774.2 cells, a mouse macrophage cell line. This method was chosen over other

lysosome purification protocols, as it allowed rapid isolation of lysosomes and was already an established method in the laboratory.

To begin with, cells were pulsed for 6 h with colloidal-iron dextran (FeDex), which was chased to the lysosome by a 16 h chase in FeDex-free media. Lysosome purification was monitored by western blot (Fig. 3.0 A) and β-hexosaminidase (β-hex) assay (Fig. 3.0 B). The final lysosomal fraction showed an enrichment of the lysosomal marker LAMP1, relative to the starting material. This was confirmed by the result of the enzymatic assay, which showed an average 12.4 fold increase in β-hex activity per µg of protein in the lysosome fraction compared to the total. The drop in β-hex activity in the post-nuclear supernatant compared to the total, suggests that a proportion of lysosomes are pelleted with nuclei and other cell debris during the PNS spin. This was supported by the western blot data, which showed that the level of α-tubulin was significantly lower in the lysosomal fraction compared to the total and PNS fractions. As lysosomes are linked to microtubule filaments (Wubbolts et al., 1999), and lysosome trafficking within the cell is dependant on microtubules (Matteoni and Kreis, 1987), this suggests that purified lysosomes were released from their contacts with the microtubule cytoskeleton, whereas pelleted lysosomes were not. While, these experiments demonstrated that the protocol was able to purify lysosomes from J774.2 cells effectively, the average latency of lysosomes over 5 experiments was only 44.5 %. Therefore, alternative cell disruption methods, and a wide range of variables were investigated to try and improve lysosome latency and recovery.

3.1.4.1 Cell line used

Initially, cells were broken open to release lysosomes by ball-bearing homogenisation. It was reasoned that using a smaller ball bearing to homogenise cells may have reduced the shear forces placed upon the sample and thus improved the latency and recovery of lysosomes (Fig. 3.1). However, when this was tested, the latency and recovery of final lysosome fractions was not significantly affected, and the latency and recovery of lysosomes was still poor. To determine whether this was due to the cell line or due to the experimental protocol, an alternative mouse macrophage cell line (RAW 264.7) was also investigated. Secondly, testing this cell line before optimising the protocol further would prevent

a lengthy repeat of optimisation experiments should the cell line have been changed at a later time. The suitability of RAW 264.7 cells was investigated, and additionally, the concentrations of FeDex used were also tested (Fig. 3. 2 A-C). While the latency and recovery of lysosomes in the PNS of RAW 264.7 cells looked promising, the latency and recovery values of lysosomes in the final fractions were no better than those obtained from J774.2 cells. It was observed that the recovery was 5-fold higher for lysosome purified using FeDex at 1:100 compared to 1:20 (22.5 % compared to 4.4 % respectively).

As the lysosome latency and recovery in the PNS of RAW 264.7 looked promising, lysosomes were then purified fully from these cells to determine whether the final lysosomal fraction would also have high latency and recovery values. However, the latency and recovery of lysosomes purified from RAW 264.7 cells did not differ greatly from the latency and recovery of lysosomes purified from J774.2 cells (Fig. 3.1). RAW 264.7 cells were investigated, as they reportedly have less cytoskeleton which may have made lysosome purification easier. However, no evidence was found that lysosomes purified from these cells had less α-tubulin associated with them, than those from J774.2 cells (data not shown). J774.2 cells also did not require an additional trypsin digest step to remove the cells from the tissue culture dishes, and such using them would make the protocol simpler.

3.1.4.2 FeDex concentration

When FeDex concentration in RAW 264.7 cells was increased, a downward trend was seen in lysosome latency and recovery (Fig. 3.2). This was not specific to this cell line or cell lysis method, as the same trend was seen in J774.2 cells whether they were broken open using ball-bearing homogenisation or nitrogen cavitation (Fig. 3.3). When this experiment was repeated multiple times (n=3) however, there was no significant change in lysosome latency ($p = 0.986$) or recovery (0.933) in the PNS of J774.2 cells (Fig. 3.11).

3.1.4.3 Different buffers and incubation on ice

It was previously found in the Pryor lab that J774.2 cells are particularly refractory to homogenisation by passage through low gauge needles, and ball bearing

homogenisation (data not shown). To homogenise cells using ball bearing homogenisation, requires that cells are incubated in a hypotonic buffer (HB, 10 mOsm) on ice for 10 minutes to allow the cells to swell and become easier to disrupt. It was hypothesised that incubating the cells in HB buffer for increasing amounts of time may increase the amount of osmotic swelling and could increase the recovery of lysosomes. However, no clear trend was seen for lysosomal latency or recovery in post nuclear supernatants of cells disrupted at 500 psi or 250 psi (Fig. 3.5). Moreover, lysates from cells lysed in HB needed to be restored to mammalian osmolarity (approximately 280 mOsms, (Waymouth, 1970) with restoration buffer. It was possible that lysosomes were partially protected from osmotic shock within the cell. Upon fractionation and release into the buffer, lysosomes would have been placed under osmotic stress until the osmolarity was restored. This would not be an issue if cells were lysed directly into an iso-osmotic buffer (STM, 300 mOsm). However, there was no significant difference in lysosome latency ($p = 0.187$) or recovery ($p = 0.136$) in the PNS when cells were fractionated in HB or STM (Fig. 3.8). Taken together, these data suggest that the buffer composition does not directly affect the efficiency of nitrogen cavitation *per se*. Despite these results, further optimisations were performed in STM in order to reduce the manipulation of the sample and reduce another potential source of variation.

3.1.4.4 FeDex pulse and chase times

The aim of optimising the protocol was not only to obtain intact lysosomes suitable for the fusion assay, but also to make the protocol as short as possible. This would also help to minimise any potential effects on lysosome integrity from iron accumulation. Therefore we aimed to determine the minimum amount of time needed for cells to endocytose enough FeDex to purify endocytic compartments. Cells were pulsed with FeDex at 1:20 for varying lengths of time followed by a 16 h chase in FeDex-free media (Fig. 3.12 B), the minimum length of the FeDex pulse needed to purify lysosomes was determined experimentally. A 1 h pulse was sufficient to purify FeDex-labelled organelles, and decreasing the length of the pulse improved the viability and integrity of the lysosomes (Fig. 3.11). Next, the shortest time necessary to chase FeDex from earlier endocytic compartments to the lysosome was determined. Cells were pulsed for 1 h with FeDex before a

label-free chase of 0, 30, 60, or 120 min (Fig. 3.12). Purified lysosomes were then subjected to western blot for the cytoskeletal, early endosome, late endosome and lysosomal markers. One problem with loading samples normalised to the same protein concentration, is that it is not clear how much early, late and lysosomal compartments contribute to the total protein. For example, if early endosomes are relatively devoid of protein compared to lysosomes, then loading equal amounts of protein of the two samples may result in large amounts of contaminating proteins being detected. This would be an artefact of loading large amounts of protein, rather than the actual content of those fractions. Furthermore, endosomes are very heterogeneous, and not all endocytic vesicles will mature at the same rate. As such, loading samples normalised to protein gives an average representation of the population of vesicles in the cell. Therefore, samples were normalised to the activity of the lysosomal hydrolase β-hexosaminidase, in order to load equal amounts of lysosomal material and compare the relative amounts of early and late endocytic material. This was confirmed by western blotting, which showed that LAMP1 levels remained constant between samples. When cells were pulsed with FeDex without a label-free chase, the entire endocytic pathway was purified as shown by the presence of EEA1, Rab5, Rab7 and LAMP1. After 30 min chase, levels of EEA1 significantly dropped and remained constant at 60 min and 120 min chase. Rab5 dropped slightly, and Rab7 was still present, indicating FeDex reaches late endosomes after 30 min. Levels of Rab7 and Rab5 continued to drop and were at their lowest levels at 120 min. This is consistent with the transition from a late endocytic compartment to a terminal lysosome, which is devoid of M6PR, Rab5 and Rab7 (Chavrier et al., 1990, Rabinowitz et al., 1992). However, J774.2 cells do not express high levels of cation-independent mannose-6-phosphate (ciM6PR) receptor (Gabel et al., 1983). The absence of blots for ciM6PR represents the low expression and the lack of a suitable antibody. Purifying a truly lysosomal fraction with no earlier endocytic organelles is particularly challenging, due to the highly dynamic and asynchronous nature of the endocytic pathway. Although a 120 min chase is sufficient to purify a pool consisting largely of terminal lysosomes, the detection of Rab5 and Rab7 indicates co-purification of some Rab5 positive early vesicles, as well as Rab7 positive vesicles such as endolysosomes (Humphries et al., 2011). As expected, α-tubulin was associated with purified vesicles at all time points. Endocytic vesicles interact with microtubules via specific motor proteins which are involved in intracellular

trafficking (Bananis et al., 2004, Loubery et al., 2008, Hunt et al., 2013), and the positioning of early endosomes, late endosomes and lysosomes is dependant on proper microtubule function (Matteoni and Kreis, 1987).

These results are in agreement with previous data, where magnetic endocytic vesicles isolated from HeLa cells showed an enrichment for EEA1 and Rab5 after 30-45 min internalisation, and maximum enrichment of Rab7 and LAMP1 at 90 - 180 min. Interestingly, EEA1 was absent after 180 min while Rab5 was not, suggesting Rab5 may associate with a small population of late endocytic compartments (Loubery et al., 2008). Furthermore, western blots of endocytic vesicles isolated using paramagnetic iron particles showed an increase in LAMP1, and decrease in Rab5 and Rab7 after a 120 min label-free chase. This was accompanied by an increase in lysosomal enzyme activity, which was also observed when lysosomes were isolated using FeDex (Becken et al., 2010). Rab5 was also found to be associated with lysosomes purified from J774A.1 cells (Jahraus et al., 1998), and was detected by western blot on isolated late endosomes and lysosomes (Tjelle et al., 1996). Thus, while thought to be enriched on early endosomal membranes, Rab5 may also be associated with late endocytic organelles. The difference in the rate at which endocytic markers are acquired and lost is likely due to differences in experimental methods and the fact that the dynamics of endosome maturation differs between professional phagocytic cells and other cell types. Despite these minor differences, it is clear that lysosomes and other endocytic organelles can be magnetically purified from cells. By characterising the fractions isolated using a panel of organelle markers and monitoring the acquisition of lysosomal enzymes, it is possible to determine the pulse/chase times needed to isolated an specific population of organelles from a particular cell type.

3.1.4.5 General considerations using FeDex

For many variables, lysosome latency and recovery in the PNS was measured rather than the final lysosome fraction. If a particular variable greatly reduced latency and recovery in the PNS, there would be little use in determining the latency and recovery of the final lysosomal fraction. A caveat to this approach could be that if FeDex labelled organelles are pelleted during the PNS spin due to

and increase in their density, then the PNS values for latency and recovery do not represent all FeDex-labelled organelles. For example, if when using FeDex at 1:100, the lysosomes do not become dense enough to pellet during the PNS generation whereas those labelled with 1:20 FeDex do, the PNS values for the latter would only represent unlabelled lysosomes. However, the latency and recovery values for final lysosomal fractions are most likely accurate, as unlabelled organelles are not retained on the magnetic column.

Lysosomal membranes are damaged by lipid peroxidation by OH • radicals, a product of Haber-Weiss reactions catalysed by iron (Mak and Weglicki, 1985). Indeed, iron accumulation renders the lysosome extremely fragile (Peters and Seymour, 1976), and isolating iron-containing lysosomes can be particularly difficult due to their fragility (Selden et al., 1980). However, iron-containing lysosomes are more normal in size than those purified using other ligands such as Triton WR-1339 (Glaumann et al., 1975), and have been purified with a recovery of 15-20 % and 60 fold enrichment of lysosomal enzyme activity relative to the starting material. Furthermore, some cell types are likely to be more susceptible to iron-induced damage than others. In one report, lysosomes isolated from rat hepatocytes using iron had a latency of 46 % compared to the control (78 %) (Myers et al., 1991). Lysosomal pH was increased and membrane fluidity was found to be decreased, which may have had serious consequences for vesicle fusion. Indeed, yeast mutants defective for membrane fusion at the vacuole can be pharmacologically rescued by the addition of chlorpromazine, which increases membrane curvature and fluidity (Karunakaran and Fratti, 2013). This suggests iron-containing lysosomes may not function as normal. Moreover, these lysosomes were abnormally shaped, larger, and increased in number. Indeed, the latter may be a response to lysosomal dysfunction, as lysosome biogenesis is upregulated when lysosomal function is impaired (Sardiello et al., 2009). Further work could include analysing FeDex-treated cells to determine if the levels of LAMP proteins increases, which may indicate if FeDex impairs lysosome function. This may not be necessary however, as FeDex-containing vesicles have been successfully used in an *in vitro* vesicle fusion assay indicating they remain fusogenic (Becken et al., 2010), but is something that should be considered.

3.1.4.6 Density centrifugation

The purification of lysosomes using FeDex was compared to those isolated using density centrifugation. A PNS was generated from J774.2 cells, which was fractionated on a continuous 1-22% Ficoll gradient (Fig. 3.15). There were two peaks of β-hexosaminidase activity detected throughout the gradient, one at the dense end of the gradient (50,960 β-Hex AU), and the other at the lighter end (27,000 β-Hex AU). The first peak was only detectable upon the release of membrane bound enzyme from detergent-lysed organelles, indicating the purification of intact compartments. The addition of detergent to the fractions corresponding to the second peak only slightly increased enzyme activity, indicating that the peak to corresponded to free enzyme and broken organelles. The membrane bound activity was associated with lysosomal and late endosomal markers (LAMP1 and Syntaxin 7 respectively), indicating this to be a lysosomal/late endosomal fraction. However, the bulk of Syntaxin 7 was detected in lighter fractions. The lysosomal fraction was also devoid of α-tubulin and had a low amount of the ER marker glucose-regulated protein of 78 kDa (GRP78). While in this instance, the lysosomal fraction was relatively pure, the setup and centrifugation is still lengthy and cumbersome. The removal of the Ficoll centrifugation media also adds and additional step needed to purify lysosomes for use in an *in vitro* assay. As such, gradients may be an attractive option for obtaining fractions for use in proteomic and biochemical studies, but for a fusion assay where degradation of a marker is a potential problem, speed is preferable. Peripheral membrane proteins that are transiently associated with the cytoplasmic face of endocytic vesicles may also be lost from lysosomal fractions during high speed centrifugation.

Lysosomes purified on a gradient or by magnetic isolation, were compared by western blotting (Fig. 3.16) Magnetically isolated organelles were first fractionated by nitrogen cavitation or ball bearing homogenisation. All lysosome samples were LAMP1 positive, with those purified using the ball bearing having the most LAMP1. Nitrogen cavitation had the least amount of LAMP1. All samples were positive for GRP78 and α-tubulin was detected in lysosomal fractions purified by on a gradient and using nitrogen cavitation, but not by ball-bearing homogenisation. These differences most likely reflect the different isolation methods used. The lysosomes

purified from the gradient and by ball-bearing homogenisation appeared to be more enriched for LAMP1 and have less α-tubulin associated with them than those purified using nitrogen cavitation. However, for the purposes of the fusion assay one of the aims of optimisation was to reduce the protocol length in order to reduce any potential degradation of ligands by lysosomal proteases. While gradient purification can produce high quality, latent lysosomes, there are some disadvantages. Firstly, the gradients may require large numbers of cells. The purification of lysosomes using FeDex could be performed on a single tissue culture dish of cells. Secondly, gradients are time consuming. Although the centrifugation time can be reduced by using a vertical rotor, the set up of the gradient and removal and analysis of fractions is itself time consuming. Thirdly, the centrifugation media necessary to purify lysosomes may result in irreversible damage to organelles through osmotic effects, which may in turn reduce organelle densities and alter the resolution of the gradient. Although more modern centrifugation mediums such as Nycodenz, Ficoll or Metrizamide do not exert osmotic pressure on lysosomes to the extent that traditional sucrose gradients do, they may still exert significant osmolarity at densities used to purify organelles. For example, Nycodenz and Metrizamide are only at mammalian cell osmolarity at densities below 1.2 mg/ml which is below that of many organelles (Castle, 2004). With FeDex purification the lysosomes can be kept in an isoosmotic buffer for the entire protocol. Moreover, FeDex purified lysosomes can easily be transferred to a different buffer, whereas those purified on a gradient must be extensively dialysed if the centrifugation medium needs to be removed.

3.1.4.7 Homogenisation methods

Others have reported that nitrogen cavitation is a preferred method of cell disruption when trying to obtain intact lysosomes (Kaushik and Cuervo, 2009, Koga et al., 2011). Mechanical rupture was found to damage lysosomes and release lysosomal enzymes, which was minimal when cells were fractionated by nitrogen cavitation (Klempner et al., 1980). Similarly, Gottlieb and Adachi, (2000), found that nitrogen cavitation resulted in little outer membrane damage to purified mitochondria, whereas homogenisation resulted in significant damage. Ball-bearing homogenisation may also be a suitable method for releasing lysosomes from cells. However, nitrogen cavitation was chosen as a preferred method with

J774.2 cells, as it did not require the use of different buffers, or a 10 minute pre-incubation of the sample on ice before cells were broken open. The nitrogen bomb could handle much larger sample sizes (30 ml compared to 1 ml for the ball-bearing homogeniser), meaning the protocol could be more easily adapted should a large number of cells be required.

3.1.4.8 Final Conclusions

These experiments have resulted in the development of a robust and rapid method to purify lysosomes from J774.2 cells, which remain intact and suitable for use in a fusion assay. In summary, the final protocol gave lysosomes with an average latency of ~80 % and a recovery of ~7 %. The time take to purify lysosomes using SPIONs (including a 3 h pulse- chase with FeDex), was around 3 h 40 min – 4 h in total. This protocol could also be easily altered to purify endocytic compartments of different ages, For example, a shorter pulse period and no chase would result in the purification of early endosomes rather than late endosomes and lysosomes. This method could also be used to purify lysosomes for other uses, such as proteomic analysis or purification of pathogen-containing compartments.

3.2 Phagosome purification

3.2.1 Introduction

To analyse phagosome-lysosome fusion, or understand how intracellular pathogens are able manipulate the phagosomal compartment, it necessary to isolate phagosomes from cells. For an *in vitro* phagosome-lysosome fusion assay, phagosomes also need to be purified. Phagosomes can be purified using similar techniques to lysosome purification. Purification of phagosomes is often carried out by allowing cells to internalise synthetic particles such as latex beads. This allows easy purification following cell fractionation, since latex beads will float on top of density gradients, allowing a simple one-step gradient to be performed (Weisman and Korn, 1967). Magnetic particles are even easier to purify and can simply be pulled out of a cell lysate using a strong magnet. Furthermore, other compounds or markers can be introduced to the cells at different time points to the study the kinetics of phagosome maturation. These methods are not without some disadvantages. Changing the properties of the phagosome to aid in its purification, will likely change the very properties of the phagosomes which one is trying to study. For example, latex bead phagosomes are often used as they allow for easy purification on one-step sucrose gradients (Desjardins and Griffiths, 2003, Desjardins et al., 1994b). However, latex beads have a particularly hydrophobic surface chemistry, which is likely to influence the maturation of these phagosomes (Oh and Swanson, 1996). Bacterial surface chemistry also effects phagosome maturation. For example, the cell wall of *Mycobacterium* species is particularly hydrophobic due to its high lipid content. This results in the phagosome membrane surrounding the bacterium very tightly, which has been hypothesised to prevent it from effectively maturing and fusing with lysosomes (Rhoades and Ullrich, 2000). Indeed, particle surface chemistry can influence the interaction of phagosomes with lysosomes (Thiele et al., 2003). So, while they are an attractive model system to study phagosome maturation, the data acquired through their use likely describes latex bead-phagosome maturation, but not necessarily that of phagosomes in general or those containing bacteria with a different surface chemistry (Luhrmann and Haas, 2000). Despite these limitations, latex beads are a very popular method of purifying phagosomes (Garin et al., 2001, Desjardins and Griffiths, 2003, Rabinowitz et al., 1992, Reiner, 2009).

Phagosomes containing bacteria have been isolated using density gradient centrifugation (Luhrmann and Haas, 2000, Kühnel et al., 2006). However, these methods are time consuming and laborious, due to the gradients that need to be set up and multiple centrifugation steps. These methods have some of the same problems associated with lysosome purification, such as the detrimental osmotic effects of the centrifugation media used. Isolation of phagosomes containing magnetic bacteria is an alternative method of phagosome purification (Lonnbro et al., 2008, Steinhauser et al., 2013). Alternatively, magnetic bead containing phagosomes have been successfully purified from cells in multiple studies (Manoury, 2013, Arora et al., 2000, Thi et al., 2012, Ramachandra and Harding, 2000). Isolation of magnetic bead phagosomes is rapid, as they can be removed quickly from a lysate and washed thoroughly on a strong magnet. Furthermore, cells that do not contain any beads are not co-purified. However, one disadvantage is that unbroken cells containing magnetic beads are also isolated, which is not desirable for some applications, e.g. western blotting. Furthermore, the fractionation method used to generate a cell lysate can damage the phagosomes, resulting in organelles that are not intact. As such, we sought to optimise this system for J774.2 cells, in order to purify streptavidin-bead containing phagosomes that were intact, for use in the *in vitro* fusion assay.

3.2.2 Phagosome-specific methods

3.2.2.1 Phagosome purification

This is the final protocol used to purify phagosomes. Section 3.7 describes how this method was developed. This protocol has been published in: Subcellular Fractionation. A laboratory manual. Cold Spring Harbour Protocols 2015 (Isolating Phagosomes from Tissue Culture Cells. P.R. Pryor and A.P.Rofe).

J774.2 cells were seeded at 1 x 10^6 cells per well in 6 well plates. An additional well was seeded to perform cell number counts. The next day, cells were counted and prechilled to 4 ºC for 15 min in binding media (RPMI pH 7.4, 0.2 % (w/v) BSA, 10 mM HEPES). Binding media was replaced with binding media containing streptavidin-coated magnetic microspheres (ProMag 3 series, Bangs Labs IN, USA) to a multiplicity of infection (MOI) of 3. Cells were incubated at 4 ºC for 1 h to allow the beads to bind, and then washed gently 3 times with ice cold PBS to remove unbound beads. Cells were incubated with DMEM (prewarmed to 37 ºC) to allow beads to be internalised. After an appropriate amount of time (25 min for fusion assay phagosomes), cells were scraped and rapidly cooled to 4 ºC by pelleting the cells at 1000 *x g* for 5 min at 4 ºC, and resuspending in PBS prechilled to 4 ºC. The cell pellet was resuspended in 1 ml of STM and incubated on ice for 10 min. The cells were then homogenised by 20 passages through a ball bearing homogeniser with an 8 µm clearance, at 4 º C. The homogenate was incubated on a DynaMag-2 magnet (Invitrogen) for 5 min on ice and the supernatant discarded. The phagosome pellet was gently resuspended in 1 ml of ice-cold STM. The washes were repeated twice more and the phagosomes were resuspended in STM. For characterisation of phagosomes by western blotting, phagosomes were normalised to OD_{600}, β-Hexosaminidase activity or protein levels. For the latter, phagosomes beads were resuspended in an appropriate volume of modified RIPA buffer (150 mM NaCl, 50 mM Tris-HCl, pH 7.5, 1 % (w/v) deoxycholate, 1 % (v/v) Triton X-100, 0.2 % (v/v) NP-40). Beads were vortexed vigorously, pelleted in a microcentrifuge, and the supernatant transferred to a fresh tube. A BCA protein assay was then performed on the supernatants.

3.2.3 Results

3.8.1 J774.2 cells internalise more beads as MOI is increased

Firstly, the uptake of 3 μm beads by J774.2 cells was investigated, as 1- 3 μm particles had been proposed as the optimal particle size for phagocytosis, (Paul et al., 2013), which is the average size of many water and airborne pathogens and may represent a conserved mechanism for phagocytosis of particles of this size (Champion et al., 2008). J774.2 cells were seeded onto glass coverslips and an appropriate number of beads added to give a multiplicity of infection (MOI) of 3 or 10, as this is a commonly used number for infection assays and phagosome studies. Where appropriate, beads were centrifuged onto cells at *50 x g* for 5 min to determine whether centrifugation increased the efficiency of bead uptake. Cells were incubated for a further 45 min to allow uptake and internalisation, and then washed with PBS (to remove extracellular beads) and chased for 1 h in bead free media. Cells were fixed and immunolabelled with α-LAMP1 antibodies followed by α-mouse Alexa Fluor 555 IgG, to distinguish between internal and external beads (Fig. 3.15 A). Internal beads were found to be surrounded by a LAMP1 positive membrane, indicating that the beads were most likely in a late phagocytic compartment. The corresponding Brightfield image showed that external beads could be found on top of cells or in close association with them, but were not surrounded by a LAMP positive membrane (white asterisks). A bead was scored as internal only if it was surrounded by a LAMP positive membrane. The average percentage of internalised beads was 43 % and 62 % for an MOI of 3 (not centrifuged and centrifuged respectively), and 61 % and 54 % for an MOI of 10 (not centrifuged and centrifuged respectively). Overall, there was a significant difference in the number of internalised beads between conditions (Fig. 3.15 B $p = 0.0003$). Centrifugation significantly increased the number of internalised beads when an MOI of 3 was used ($p = <0.05$) but not when an MOI of 10 was used. This may have been because at an MOI of 10 without centrifugation, enough beads make contact with the cells to be internalised and reach the capacity of that cell, whereas at an MOI 3, centrifugation increases the number of beads a cell makes contact with and subsequently internalised. There was a significant difference ($p = <0.05$) between the number of internalised beads using an MOI of 3 and an MOI of 10 when beads were allowed to settle onto cells. When beads were centrifuged

onto cells at an MOI of 3 or 10, there was no significant difference between the numbers of internalised beads ($p = >0.05$). At an MOI of 3, centrifuging beads onto cells increases the amount of uptake, but at an MOI of 10, centrifugation makes no difference to bead uptake. The average number of beads per cell was 2.29 and 1.75 for an MOI of 3 (not centrifuged and centrifuged respectively), and 3.77 and 3.59 for an MOI of 10 (not centrifuged and centrifuged respectively Fig. 3.15 C). There was a significant increase in the number of beads per cell when using an MOI of 10 compared to an MOI of 3 ($p = <0.0001$). Centrifuging beads onto cells did not increase the average number of beads per cell at either MOI. Cells were also scored for the numbers of internal beads (Fig. 3.15 D). The number of cells with 1 to 3 internalised beads was 94.3 % and 89.8 % (MOI:3, not centrifuged, and centrifuged respectively) and 55.3 % and 65.4 % (MOI:10 not centrifuged, and centrifuged respectively). The percentage of cells with between 4 and 6 beads was 10.2 % and 5.7 % for an MOI of 3 (not centrifuged and centrifuged respectively). No cells with an MOI of 3 had more than 6 internalised beads, regardless of centrifugation conditions. At an MOI of 10, 34 % and 27.5 % of cells had between 4 and 6 internalised beads (not centrifuged and centrifuged respectively). 8 % and 6.4 % of cells had between 7 and 10 internalised beads (not centrifuged and centrifuged respectively), and 2.7 % and 0.7 % of cells had more than 11 internalised beads (not centrifuged and centrifuged respectively). The highest number of beads seen inside a single cell was 16 beads (data not shown).

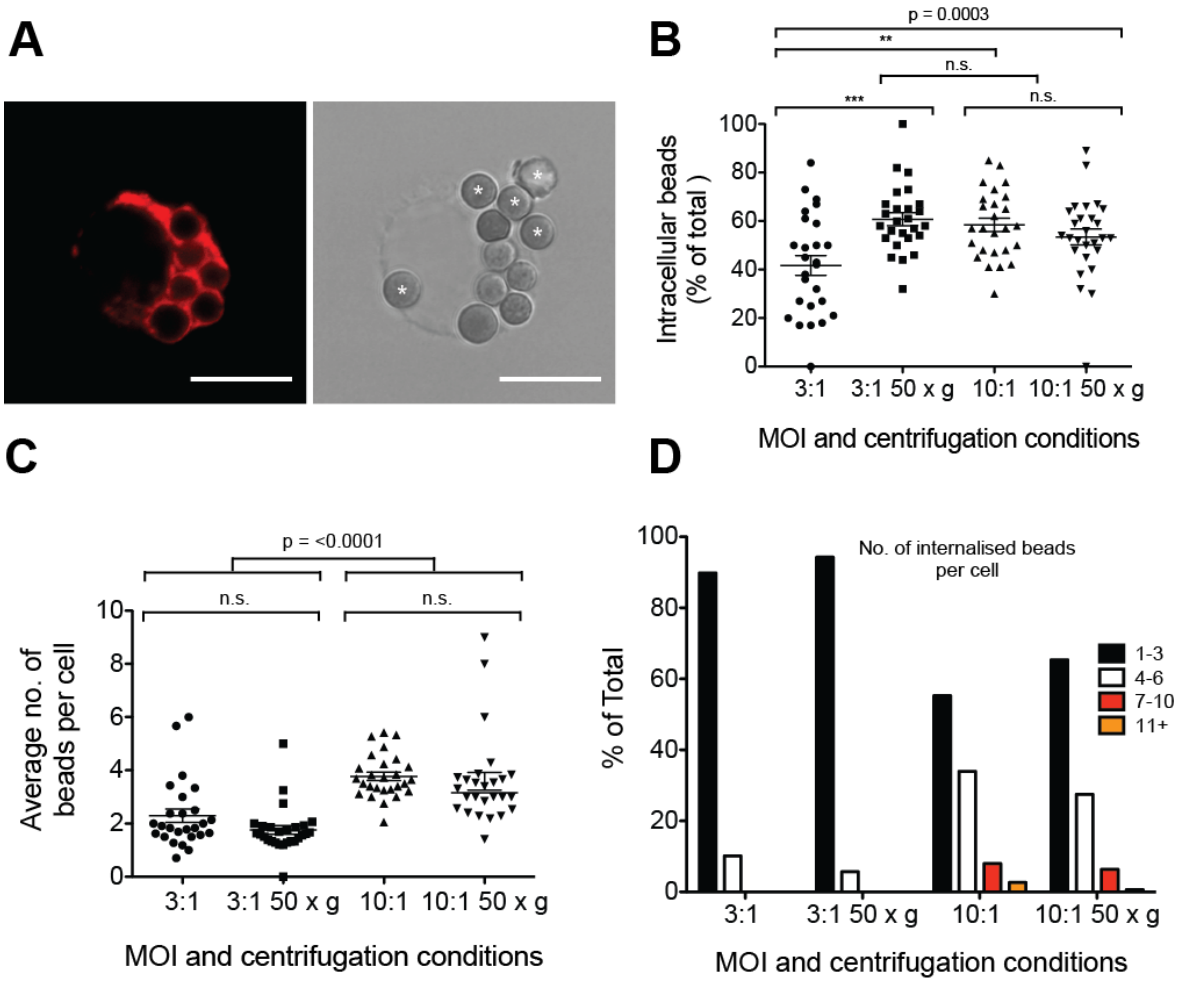

Fig. 3.15 Internalisation of magnetic beads by J774.2 cells. J774.2 cells were seeded onto glass coverslips. 3 µm magnetic beads were added to the cells at an MOI of 3 or 10. Beads were left to settle onto cells, or were centrifuged at *50 x g* for 5 min. The cells were incubated for a further 45 min and then washed 3 x with PBS. After a further 1 h chase at 37 ºC, cells were fixed and processed for confocal microscopy using α-LAMP1 antibodies to visualise phagosomal membranes. **A**. Representative confocal image of J774.2 cells immunolabelled with α-LAMP1 antibodies. Scale bar 10 µm. Asterisks show external beads associated with cells. **B** For each condition, beads were scored as being internal (surrounded by a LAMP1 positive membrane) or external, as judged by the corresponding Brightfield image. Data were analysed by one-way ANOVA**. C.** Average number of beads per cell for each condition. Data are means ± the range and were analysed by One-Way ANOVA**. D**. Histogram showing the distribution of numbers of internalised beads (as a percentage of the total number of internalised beads) for each condition tested. 300-600 cells were counted per condition, with an average of 1500 beads counted per condition (n=1).

3.2.3.2 Purification of latent phagosomes from J774.2 cells.

It was clear from these data that J774.2 cells would readily phagocytose magnetic beads and that at an MOI of 10, centrifugation was not necessary. Next, the purification of these phagosomes was optimised to try and yield intact phagosomes. While an MOI of 10 resulted in greater bead uptake, an MOI of 3 was used for the optimisation experiments to reduce the amount of beads used in each experiment. Given that characterising the phagosomes by western blotting would also have required large amounts of sample, using an MOI of 10 for the experiments would have been prohibitively expensive. Secondly, beads were centrifuged onto cells (where appropriate) to try and synchronise bead uptake. Cells were pulse-chased with beads which were then released from cells by nitrogen cavitation (Fig. 3.16). The latency of phagosomes purified using nitrogen cavitation at 250 psi for 5 min was low, at only 24.8 %. When the time under pressure was dropped to 1 minute, this increased phagosome latency slightly to 34.9 %, but this was not significant ($p = 0.391$). As nitrogen cavitation did not appear to be an appropriate method for phagosome purification, phagosomes were released from cells using a ball-bearing homogeniser to see if this would improve latency (Fig. 3.17). Both different ball-bearing sizes, and the number of passes used, was investigated. When cells were broken open using 40 passes the latency was slightly higher than nitrogen cavitation over the range of ball bearing sizes tested (30 % - 42 %). This was significantly ($p = 0.0008$) improved by reducing the number of passes from 40 to 20, which gave a much better latency over a range of ball bearing sizes (73 % to 85 %). The size of the ball bearing used did not significantly affect phagosome latency ($p = 0.477$). Phagosomes continued to be purified from cells using 20 passes and a 8.008 mm ball bearing. When the homogenisation was monitored under a light microscope, it became apparent that not all of the cells were broken open. While this would not interfere with the fusion assay, it was necessary to determine if these unbroken cells skewed the results of the β-Hexosaminidase assay and over estimated phagosome latency. The contribution of unbroken cells to the β-hexosaminidase assay was calculated by determining the AU of activity from a known number of cells (Table 3.1). This resulted in a slight (10 %) overestimation of phagosome latency. Despite this, phagosome latency was for the most part high (> 70 %).

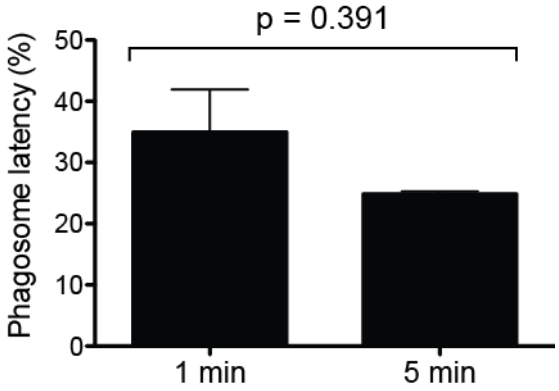

Fig. 3.16 Latency of phagosomes purified from J774.2 cells using a nitrogen bomb. J774.2 cells were pulsed with 3 µm magnetic beads at an MOI of 3 for 45 min, washed three times with PBS to remove extracellular beads and incubated for 1 h at 37 ºC. Cells were scraped and resuspended in 1 ml of STM and phagosomes released from cells by nitrogen cavitation at 250 psi for 1 min (n=4) or 5 min (n=2) at 4 ºC. The latency of the purified phagosomes was then measured by β-hexosaminidase assay. Data are means ± SEM and were analysed by t-test.

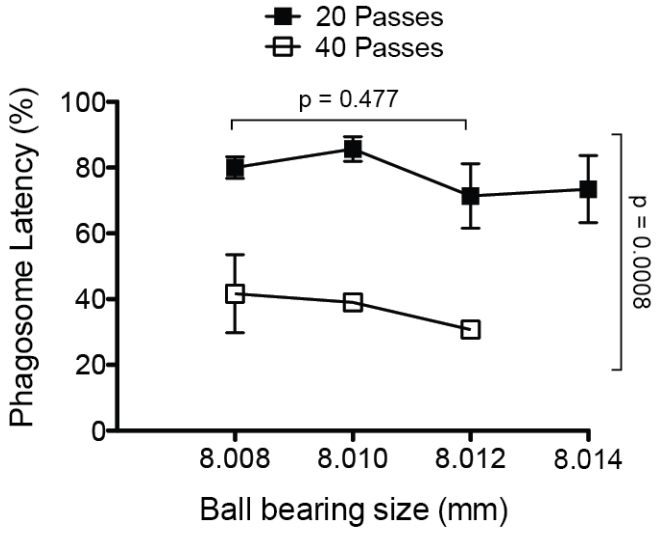

Fig. 3.17 Latency of phagosomes purified from J774.2 cells using ball-bearing homogenisation. J774.2 cells were incubated with 3 µm magnetic beads as per the figure legend of Fig. 3.16. Phagosomes were released from cells by 20 (n=3) or 40 (n=2) passes of a ball bearing homogeniser with different sized ball bearings. Phagosomes were then isolated on a magnet and washed three times with STM. The latency of the purified phagosomes were then measured by β-hexosaminidase assay. Data are means ± SEM and were analysed by two-way ANOVA.

β-Hexosaminidase activity (AU)		Ball bearing size (mm)			
		8.008	8.010	8.012	8.014
	- Triton	489	562	719	312
	+ Triton	3591	3354	2707	1599
	Latency (%)	86	83	73	80
	Unbroken Cells per µl of phagosomes	474.00	396.00	380.00	88.00
	No. of cells per assayed β-Hex sample	2370	1980	1900	440
	β–Hex AU overestimation per sample	1635	1366	1311	304
	Adjusted + Triton value	1956	1988	1396	1295
	Adjusted Latency (%)	75	72	48	76
	Difference (%)	11	11	25	4
	Average difference (%)	12.75			

Table 3.0 Contribution of unbroken cells to the results of phagosome β-Hexosaminidase assay. Phagosomes were purified as previously described at the latency determined by β-Hexosaminidase assay. To determine the contribution that unbroken cells made to the + Triton sample, the indicated number of cells were subjected to β-Hexosaminidase assay to determine the amount of fluorescence (AU) from unbroken cells. The number of unbroken cells was then estimated by placing some of the phagosome sample on a haemocytometer and counting the unbroken cells. The number of unbroken cells per sample was multiplied by the AU per cell to give the contribution (AU) that unbroken cells made to the assay. These values were then subtracted from the + TX sample and the adjusted phagosome latency was determined.

3.2.3.2 Characterisation of magnetic bead-phagosomes

Next, phagosomes were biochemically analysed in order to be sure of purifying late phagosomes, rather than early phagosomes or fully mature phagolysosomes. J774.2 cells were equilibrated in binding media for 15 min at 4 ºC to cool the cells and stop phagocytosis in order to try and synchronise bead uptake. 3 µm beads were centrifuged onto cells for 5 min at an MOI of 3, and left to bind for 1 h at 4 ºC. Unbound beads were then removed by three washes with ice cold PBS. The PBS was replaced with DMEM preheated to 37 ºC to warm the cells and the cells were cultured at 37 ºC and bead internalisation allowed to proceed for varying amounts of time. This resulted in phagosomes of different ages, which were then purified and characterised. Initially, phagosomes were allowed to mature for 1 h before isolation and analysis by western blotting (Fig. 3.18 A). EEA1 and Rab5 were used as markers of early phagosomes, and LAMP1 and Rab7 as markers of late phagosomes. The level of cytoskeletal contamination was monitored by blotting for α-tubulin. All markers probed (except Rab7) were detected on phagosomes from 10 min. The levels of EEA1, LAMP1, Rab5 and Rab7 remained low until 45 min where a large increase was seen. EEA1 and Rab7 then showed a slight drop from 45-60 min. Except for 0 min, the level of α-tubulin was approximately the same for all time points. There was a sharp increase in the level of β-hexosaminidase activity between 30 min and 45 min, which remained high at 60 min (Fig. 3.18 B). The experiment was then repeated twice more with increasing time points in order to determine the reproducibility of the protocol. Phagosomes were purified as before, but at times ranging from 0 h to 4 h (Fig. 3.19). EEA1 was detected on phagosomes from 20 min and was present on phagosomes up to 4 h (Fig. 3.19 A&B), where a large drop was observed (Fig. 3.19 B). LAMP1 increased to its highest levels between 80 min and 180 min. The levels of Rab5 and Rab7 were not significantly different between the different time points in either experiment. As seen previously, α-tubulin was associated with phagosomes at all time points. In contrast to the first experiment there was no lag in the increase of hex activity, which steadily increased as the maturation time increased. Based upon previously published data (Pitt et al., 1992, Mayorga et al., 1991, Desjardins et al., 1994b) and as a result of our data, we concluded that 25 min - 30 min phagosomes are likely to beginning to interact with lysosomes (as judged by the presence of Rab7 and LAMP1), but had not formed mature phagolysosomes, as there was no sharp

increases in β-hexosaminidase activity. However, from 60 min – 120 min, the increase in LAMP1 and β-hexosaminidase appeared to mirror each other, suggesting that phagosomes of these ages may indeed be reaching lysosomes.

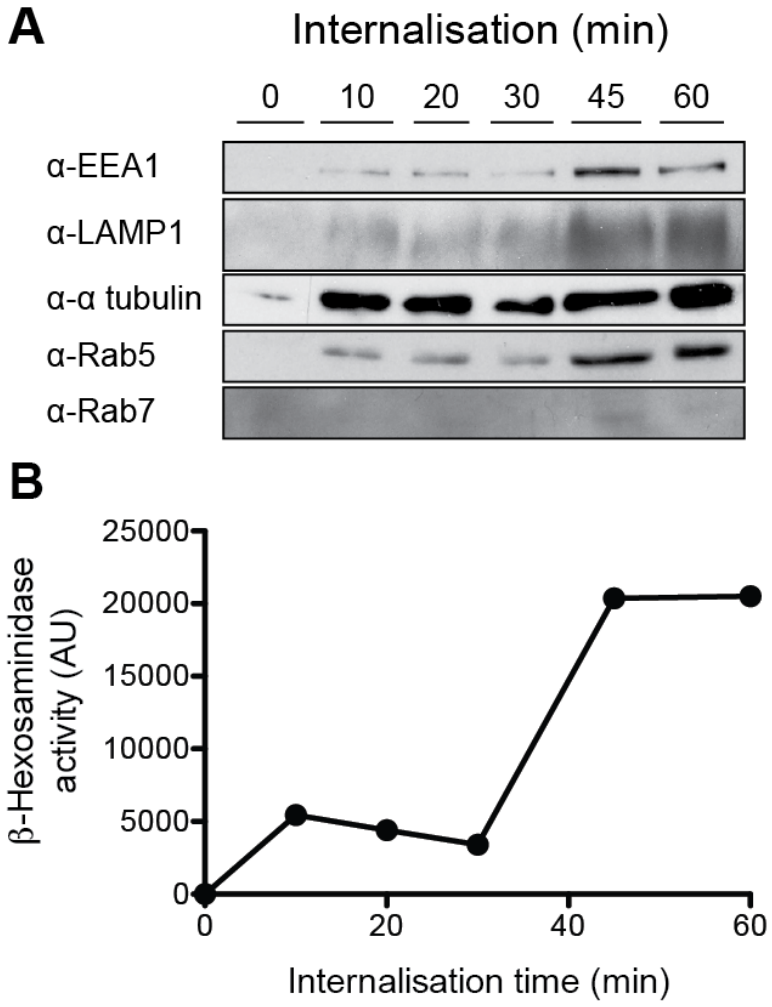

Fig. 3.18 Characterisation of magnetic bead-phagosomes purified from J774.2 macrophages. A. J774.2 cells were equilibrated in binding media (RPMI containing 10 mM HEPES, pH 7.5, 0.2 % (w/v) BSA) for 15 min at 4 ºC to cool the cells and stop endocytosis in order to try and synchronise bead uptake. 3 µm beads were centrifuged onto cells for 5 min at an MOI of 3, and left to bind for 1 h at 4 ºC. Unbound beads were then removed by three washes with ice cold PBS. The PBS was replaced with DMEM preheated to 37 ºC to warm the cells and the cells were cultured at 37 ºC and bead internalisation allowed to proceed for the times indicated. The cells were immediately placed on ice for 15 min, and then scraped into 1 ml of ice cold STM. Phagosomes were released from cells by 20 passes of a ball-bearing homogeniser with a clearance of 12 µm. Phagosomes were collected on a magnet, washed three times with STM, and then resuspended in 100 µl of STM. Phagosomes were then probed by western blotting for different endocytic and cytoskeletal markers. Samples were normalised to bead OD_{600}. **B.** The activity of the lysosomal enzyme β-hexosaminidase was determined for each sample and normalised to bead OD_{600} (n=1).

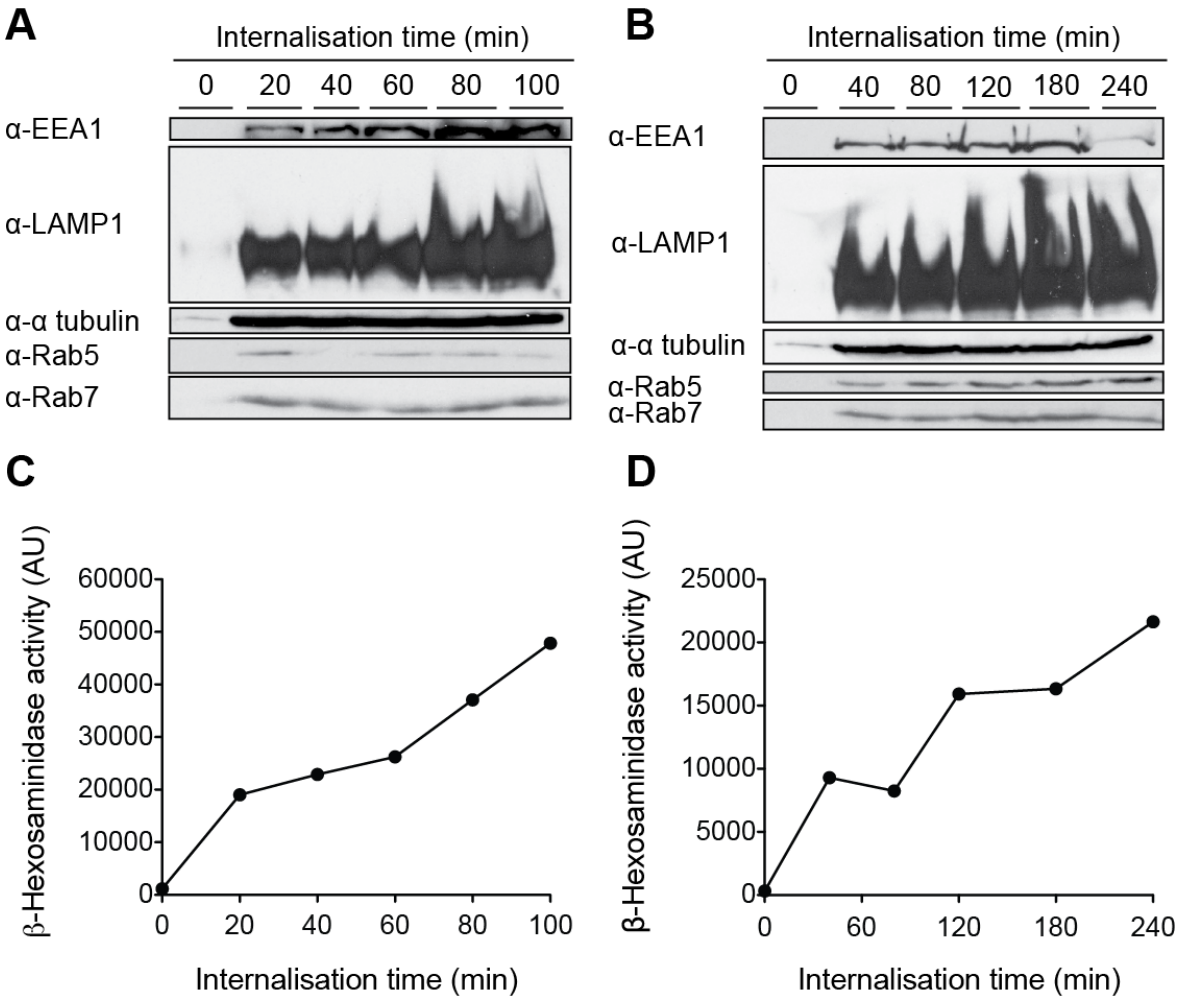

Fig. 3.19 Characterisation of magnetic bead-phagosomes of 0 - 4 h purified from J774.2 macrophages. Magnetic bead-phagosomes of varying ages (0-100 min **A.**, 0-240 min **B**.) were purified from J774.2 cells as per the figure legend of Fig. 3.18. Purified phagosomes were then probed by western blotting for different endocytic and cytoskeletal markers. Samples were normalised to bead OD_{600}.**C & D.** The activity of the lysosomal enzyme β-hexosaminidase was determined for each sample in A & B, respectively, and normalised to bead OD_{600}.

Due to the variability seen between phagosome isolations, and the possibility that not all phagosomes had matured after 4 h chase, the experiment was repeated a final time with phagosomes matured for 25 min, 4 h or 24 h. Samples were also normalised to OD_{600}, protein concentration, or the activity of the lysosomal enzyme β-hexosaminidase (Fig. 3.20). The levels of EEA1 were highest between 4 h and 24 h, regardless of normalisation method. Similarly, the highest amounts of LAMP1 detected on phagosomes were at 4 h and 24 h in all normalisations. Rab7

was detected at highest levels at 24 h when samples were normalised to β-hexosaminidase, but there was no significant difference between time points in the remaining samples. A similar pattern was seen for Rab5, but a slight peak was seen at 4 h when samples were normalised to protein levels. Levels of α-tubulin were the same between all time points and normalisations. The β-hexosaminidase activity of phagosomes normalised to protein, revealed that there was no significant difference between samples. However, when normalised to OD_{600}, β-hexosaminidase activity increased from 25 min to 4 h, with a sharp increase from 4 h to 24 h. As a result of these data, 25 min phagosomes were chosen as the ideal age for the fusion assay, as these most likely represent phagosomes that were capable of interacting with lysosomes, but the majority had not undergone full maturation to a phagolysosomal state.

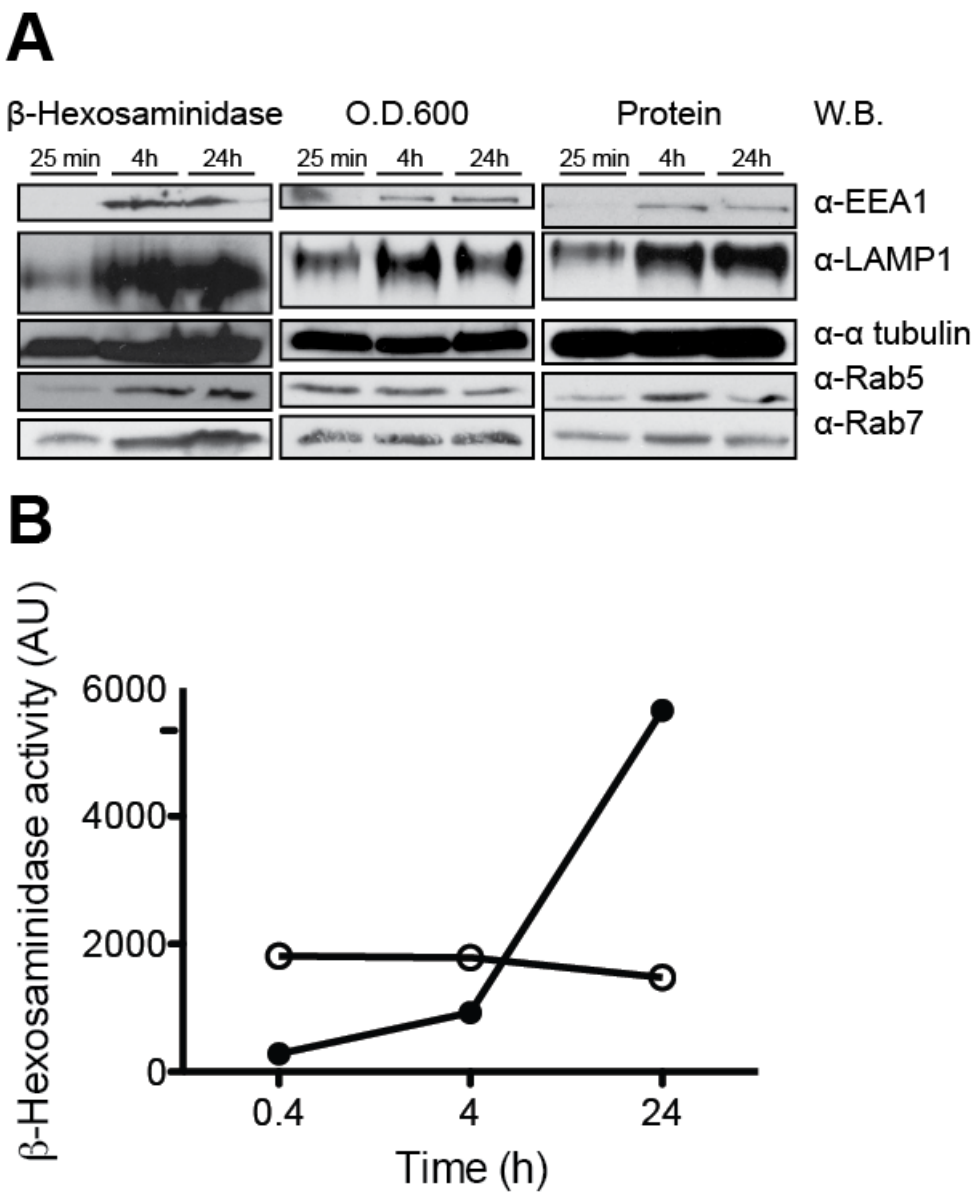

Fig. 3.20. Characterisation of magnetic bead containing-phagosomes normalised to β-Hexosaminidase activity, optical density, or protein concentration. Phagosomes of different ages were purified from J774.2 cells as per the figure legend of Fig. 3.18. **A**. Samples were normalised to OD_{600}, protein concentration, or the activity of the lysosomal enzyme β-hexosaminidase, and probed by western blotting (W.B.) for markers of the endocytic pathway. **B**. The levels of β-hexosaminidase of the samples in A, normalised to OD_{600} (closed circles) or protein concentration (open circles) (n=1).

In summary, the final phagosome purification protocol was as follows: cells were chilled to 4 ºC for 15 min in binding media. Beads were centrifuged onto cells at an MOI of 3 at 4 ºC, and left for 1 h to bind to cells. Unbound beads were then washed with ice-cold binding media, and the media replaced with DMEM pre-warmed to 37 ºC. The phagosomes were then allowed to mature for 25 min, before cells were scraped into cold PBS and pelleted. The cells were resuspended in 1 ml of STM and homogenised with 20 strokes of a ball bearing homogeniser with a clearance of 12 µm. The homogenate was then placed into a rack attached to a strong magnet to collect the phagosomes. The supernatant was discarded, and the phagosomes resuspended again in 1 ml of STM. This process was repeated three times to wash the phagosomes, which were then typically resuspended in 100 µl of STM. Phagosomes were typically around 70 % intact, with some unbroken cells (containing beads). Phagosomes were typically enriched for LAMP1, but other endocytic markers could also be detected. The recovery of phagosomes was not calculated.

3.2.4 Phagosome purification - Discussion

3.2.4.1 J774.2 cells internalise more beads as MOI is increased

Immunofluorescence analysis revealed that the bead-containing phagosomes appeared to be surrounded by a LAMP1 positive membrane, indicating that LAMP1 may have started to be incorporated into the phagosomal membrane. The caveat to this however, is that the volume of the cytoplasm of J774.2 cells is small. As such, was difficult to resolve a LAMP1 compartment from lysosomes in close apposition to internalised beads. The Z-stack images showed that the beads did appear to be completely surrounded by a LAMP1 membrane, and most likely were internalised (Fig. 3.15 A)

The percentage of internalised beads increased as more beads were used at an MOI of 3 but not 10. Centrifugation also increased the uptake of beads, but only at an MOI of 3. This may indicate that enough beads settle onto cells at an MOI of 10, and that the limit to uptake was the capacity of the cell to take up beads, rather than the availability of beads (3.15 B). For an MOI of 3 or 10, it would be likely that the percentage of internalised beads could be improved by ensuring cells were 90-100 % confluent, thus reducing the number of beads that land on non-confluent cells. The average number of beads per cell did not differ when beads were centrifuged onto cells, but a significant increase was seen when a higher MOI was used (Fig. 3.15 C). This suggests that centrifugation increases the number of cells that phagocytose beads, but does not increase the number of beads that become internalised. Increasing the MOI also had the effect of increasing the number of cells containing more than 1-3 beads (Fig. 3.15 D). At an MOI of 3, only ~ 10 % of cells containing beads only had more than 3 beads per cell, but at an MOI of 10, this increased to ~ 35 %. Thus, increasing the MOI increases the numbers of cells containing beads, and the numbers of cells containing more than 3 beads.

The maximum number of beads seen within a single cell was 16, which may not be surprising give the propensity of this cell line to engulf particles more than 5.5 X their resting surface area (Lam et al., 2009). These data indicate significant heterogeneity in a macrophage population, with regards the extent to which they phagocytose particles. Although this experiment was only performed once, it was

clear that J774.2 cells would be suitable for phagosome purification. A higher MOI was hypothesised to result in a heterogeneous phagosome population than a lower MOI. A group of cells that have only one particle to internalise and delivery to the lysosome would most likely have enough free membrane to do so. A group of cells with some having one particle to phagocytose, but the rest having 3 or 4, would most likely result in the delay of phagocytosis for some of the particles, while membrane has to be synthesised *de novo* or recovered from other organelles, resulting in a mixed population of phagosomes of different states.

Other phagosome purification protocols either do not take into account the importance of MOI when trying to synchronise cells, or they do not mention that they have done so. Clearly, the number of particles an individual cell has to internalise can have a great effect on the rate at which the phagosomes mature and is something that may need to be studied in greater detail.

3.2.4.2 Purification of latent phagosomes

Next, phagosome purification was optimised to yield intact phagosomes for use in the fusion assay. Cells were allowed to phagocytose beads, and were disrupted by nitrogen cavitation (Fig. 3.16) at 250 psi for 1 min or 5 min. The mean latency of the phagosomes was 35 % and 25 % respectively. This is in stark contrast to the latency of lysosomes purified by nitrogen cavitation. The poor latency may be due to increased fragility of phagosomes containing large solid particles. Both the membrane and lumenal contents of vesicles containing soluble cargo would be compressed under pressure. The membrane of phagosomes with insoluble contents (that do not compress easily) may be placed under increased pressure. For example, if the surface of the magnetic beads is not uniform and contains sharp or rough edges, this may provide a weak point in the membrane causing it to rupture. Phagosomes have previously been purified from cells using nitrogen cavitation (Lonnbro et al., 2008). However, the study used magnetically labelled-bacteria rather than an inorganic non-aqueous particle. Furthermore, the latency of the phagosomes purified was only 35 %. This may indicate that nitrogen cavitation in general is not an ideal method for purifying phagosomes. Next, cells were fractionated using 40 passes of a ball bearing homogeniser with different sized ball bearings (Fig. 3.17). Phagosome latency was low (42 %), and, there was a slight

downward trend when ball bearing size was increased. However, phagosome latency was significantly improved when only 20 passes was used to homogenise cells. There was no clear trend in phagosome latency when the ball bearing size was increased regardless of the number of passes. The range of latency for 20 passes was 71 % - 85 %, compared to 30 % - 41 % for 40 passes. Therefore, phagosomes continued to be purified from cells using an 8.008 mm ball bearing with 20 passes of the homogeniser. While the sample contained unbroken cells (as judged by monitoring the homogenate under a light microscope), these were deemed not to be a significant problem (Table 3.0). The number of unbroken cells counted did not alter the results of the β-hexosaminidase assay by more than an average of ~12.75 %. Unbroken cells would most likely not be an issue for the fusion assay, as they would not be able to participate in any fusion events.

3.2.4.3 Characterisation of magnetic bead-phagosomes

With regards to western blotting, one must assume that the same level of unbroken cells was present in all samples. Therefore, any contamination is present in all samples, and when analysed by western blot all samples should be the same. The fact that the levels of the markers analysed differed between phagosomes of different ages, indicates the changes are real and not due to sample contamination. Levels of contaminating proteins should not change, as they are present throughout each sample and do not participate in phagosome maturation (Rogers and Foster, 2007). Phagosome characterisation is not a trivial task. While the synchronisation of a cell population can be achieved, it is not possible to synchronise the process of phagocytosis. Within a cell population, and even within a single cell, phagosomes will mature at different rates due to the highly dynamic and heterogeneous nature of the endocytic and phagocytic pathway (Griffiths, 2004). The situation is further complicated by the nature of the particle(s) being phagocytosed, and the differing rates of phagocytosis between cells types. Much of the data obtained on phagosome maturation has been collected from many different lines of enquiry involving many cells types and different methods (Pitt et al., 1992, Duclos et al., 2000, Zimmerli et al., 1996, Manoury, 2013, Desjardins et al., 1994b, Garin et al., 2001). Therefore, proposed rates of phagosome maturation can only be taken as rough estimates. The fusion assay required phagosomes which remain fusogenic with lysosomes, but which

had not undergone fusion with the lysosome and reached a phagolysosomal endpoint. With that in mind, it was important to characterise the composition of phagosomes isolated from J774.2 cells.

Phagosomes were characterised using a panel of markers, including early phagosomal (EEA1, Rab5), late phagosomal (Rab7) phagolysosomal (LAMP1), and cytoskeletal (α-tubulin) components. In all experiments, cells were incubated with beads at 4 ºC in order to synchronise binding to the cells. A chase period began with the addition of media warmed to 37 ºC, and phagosomes were isolated at varying time points. The kinetics of phagosome maturation were examined from 0-60 min (Fig. 3.18), 0-100 min/0- 4h (Fig. 3.19) and 25 min to 24 h (Fig. 3.20). EEA1 was detected on phagosomes on all phagosomes regardless of age. Rab5 was detected at 10 min, but was also present on phagosomes from all time points and experiments. Rab5 is found on early endosomes and is involved in regulating homotypic endosome fusion (Hutagalung and Novick, 2011, Gorvel et al., 1991) EEA1 is a Rab5 effector, that binds activated Rab5 via two spatially separated domains (Simonsen et al., 1998, Callaghan et al., 1999), and is thought to act as a tether to bring endosomal membranes in close apposition in order for fusion to occur (Christoforidis et al., 1999). Despite the huge volume of information regarding the role of Rabs in endosome fusion and maturation, comparatively little is known about the roles of these proteins in phagosome maturation. Phagosome maturation is often thought to be analogous to endosome maturation, but many questions remained unanswered. Despite this, both Rab5 and EEA1 have been shown to be important in early phagosome maturation events. Rab5 is present on phagosomal membranes (Gutierrez, 2013) and regulates transient fusion events between phagosomes and endosomes (Duclos et al., 2000). The fact that many intracellular pathogens manipulate the function and distribution of Rab5 on phagosomal membranes, underlines its importance in phagosome maturation. *Legionella penumophilia* specifically excludes Rab5 from the phagosome membrane to prevent maturation. In contrast, Rab5 persists on the *Mycobacterium tuberculosis* containing-phagosome membrane, delaying the acquisition of proteins required for the maturation of the phagosome (Clemens et al., 2000). Moreover, *M.tuberculosis* phagosomes do not acquire EEA1 and microinjection of anti-EEA1 antibodies into macrophages delayed the acquisition of late endocytic markers onto latex bead phagosomes (Fratti et al., 2001). This can be in part,

attributed to the *M.tuberculosis* toxin lipoarabinomannan (LAM), that disrupts the production phosphatidylinositol-3-phosphate (PI3P) on phagosomal membranes, (Vergne et al., 2003). EEA1 to binds to PI3P on membranes via its FYVE domain (Lawe et al., 2000), and the inhibition of PI3P production by the PI3-kinase inhibitor wortmannin, reduces the recruitment of EEA1 to phagosome membranes (Vieira et al., 2001). Thus, any disruption to the localisation of Rab5 or EEA1 on phagosome membranes will result in retarded phagosome maturation.Rab7 and LAMP1 were found on almost all phagosomes. However, the changes in LAMP1 levels between time points were more substantial. This was the same for the levels of β-hexosaminidase, which increased over time in all experiments and were always at their highest points at the longest time points in each experiment.

A prerequisite of progression from an early endosome to a late endosome, is the removal of Rab5 the recruitment of Rab7 (Rink et al., 2005, Poteryaev et al., 2010) and its effector proteins (Zhang et al., 2009). The same Rab conversion may be necessary for phagosome maturation. The recruitment of Rab7 is required for phagosome maturation in *Dictyostelium* (Rupper et al., 2001), but its presence alone is insufficient to allow phagosome progression (Vieira et al., 2001). Rab7 effector proteins such as Rab-interacting lysosomal protein (RILP) (Jordens et al., 2001), and the HOPS complex (Balderhaar and Ungermann, 2013) are conceivably involved in phagosome maturation, but this has yet to be confirmed. Furthermore, it has been suggested that the Rab5 to Rab7 switch is regulated on *M.tuberculosis* phagosomes by Rab22a (Roberts et al., 2006). Interestingly, the gram-positive bacterium *Tropheryma whipplei* (the causative agent of Whipple's disease) has been reported to survive in a Rab5 and Rab7 positive compartment. This demonstrates that it is possible to find both these GTPases residing concomitantly on the same intermediate compartment (Mottola et al., 2014). Clearly, Rab7 is central to phagosome maturation but the exact mechanisms by which it functions remain to be elucidated.

Rab7 was detected on phagosomes as early as 20 min (Fig. 3.18), which may be indicative of an early to late phagosome transition. However, Rab7 has also been shown to accumulate on the phagosome membrane in as little as ten minutes, and this recruitment preludes any drop in phagosome pH and subsequent maturation (Harrison et al., 2003). Thus the presence or absence of Rab7 on its own is not a

sufficient criterion by which to class an organelle as a late phagosome. LAMP1 was detected on phagosomes as early as 10 min, with the largest increase seen at 45 min. This is in agreement with Pitt *et al*., (1992) who found that when using J774.2 E cells, formaldehyde fixed *Staphylococcus aureus* containing phagosomes acquired late endocytic markers (Cathepsin D, the mannonse-6-phosphate receptor (M6PR), β-glucuronidase and the vATPase proton pump), within 7 minutes of phagosome creation. This indicates that some phagosomes rapidly begin to acquire components of the late endocytic pathway. However, the authors reported that the absence of a drop of M6PR at the latest time point indicated that phagosomes either cannot recycle the receptor, or do not progress to a phagolysosomal state within the maximum time point observed (18 min). Interestingly, the presence of LAMP1 and detectable levels of β-hex activity at early time points may indicate some phagosomes rapidly interact with late endocytic compartments. Indeed, in vivo, 5 nm gold particles were observed to be transferred from late endosome/lysosomes to *S.aureus* containing-phagosomes within 10 min of phagosome formation (Mayorga et al., 1991), demonstrating that some but not all phagosomes follow the same rate of maturation. As with Rab7, the caveat to this is that the transfer of a single membrane marker cannot be used to define the formation of the phagolysosome.

Finally, we decided to compare 25 min phagosomes, with those isolated at extended time points (4 h & 24 h, Fig. 3.20). Samples were normalised to β-hexosaminidase activity (AU), bead OD_{600}, and protein concentration in order to characterise phagosomes. Normalising to β-hex shows the relative contribution of early endocytic markers when an equal amount of "phagolysosomal" material is loaded. Bead OD_{600} shows the "average profile" of all the phagosomes isolated from cells at a particular time point, while loading by protein normalises all the samples to the protein content in a phagosome sample. When loaded by β-hex, EEA1 was present to a greater extent in 4 h phagosomes, compared to 25 min and 24 h. 25 min phagosomes overall had less LAMP1, Rab5 and Rab7. This data was mirrored by the β-hex assay (Fig. 3.20 B), which showed that 25 min phagosomes had low levels of β-hex activity compared to those at 4 h and 24 h, indicating 25 min phagosome had not yet acquired large amounts lysosomal enzymes. Rab5 was found on 25 min phagosomes, with higher levels on 4 h and 24 h phagosomes. The presence of LAMP1 and Rab7 at 25 min indicates some

interactions with late endocytic compartments. These interactions increase as the phagosomes were matured for longer periods of time, as levels of both these markers increased.

While the presence of Rab5 on late phagosomes is unexpected, it has also been found to be present on latex bead phagosomes even after 25 h maturation (Jahraus et al., 1998). Therefore, this marker may never fully be lost from purified phagosome preparations. Alternatively, the levels of EEA1 and Rab5 proteins may be a reflection of contamination of the phagosomes with unbroken cells containing magnetic beads. However, this is unlikely, as the levels of the markers analysed change at different time points, rather than remaining constant. Similarly, EEA1 and Rab5 may be present due to contamination by other endocytic organelles. It is reasonable to assume that some fragments of other organelles co-purify with phagosomes, e.g. trapped in the actin cytoskeleton surrounding the phagosomes (Rogers and Foster, 2007). Although the ability of phagosomes to fuse with early endosomes rapidly declines as they age (Desjardins et al., 1997, Jahraus et al., 1998), this does not rule out the possibility that a small proportion of phagosomes may interact with early endosomes. Alternatively, early markers found in late phagosome samples may be due the creation of nascent phagosomes after the start of the chase period. The ability of a cell to internalise particles is limited by the amount of membrane it has available to facilitate phagocytosis. A cell with beads attached to the cell surface may internalise one or two, but cannot internalise the remaining beads until more membrane becomes available, either through remodelling of existing membrane or membrane biogenesis. Thus, within an individual cell there may be phagosomes of different ages with different membrane proteins (Griffiths, 2004).

Unsurprisingly, it was found that α-tubulin was associated with phagosomes at all time points in all experiments (Figs. 3.18 - 3.20). Early phagosomes display a preference for the plus end of microtubules and are trafficked to from the cell periphery to the perinuclear region, a movement which is disrupted by microtubule disrupting drugs nocodazole and taxol (Blocker et al., 1998). Phagosomes have been shown *in vitro* to move along microtubules via kinesin and dynein motor proteins (Blocker et al., 1997), and the transfer of membrane or fluid phase markers from lysosomes to phagosomes is inhibited by microtubule

depolymerisation (Desjardins et al., 1994b, Blocker et al., 1996). Rab-interacting lysosomal protein (RILP), is able to interact with active Rab7, the HOPS complex, and (indirectly) with microtubules (van der Kant et al., 2013), thus linking lysosomes to microtubules. A requirement for both Rab7 and RILP has been shown for phagosome maturation through tubules that extend along microtubules and allow interactions between phagosomes and lysosomes (Harrison et al., 2003) Transport of both organelles along microtubules is necessary for phagolysosome formation, as they must be brought in close proximity to allow membrane fusion to occur. The interaction between phagosomes and the cytoskeleton is one that has been exploited by intracellular pathogens. *Listeria monocytogenes* effector ActA activates the actin related protein complex Arp2/3 in order to promote the polymerisation of actin comet tails on the bacteria, in order to propel it throughout the cytoplasm and invade neighbouring cells (Radhakrishnan and Splitter, 2012). Actin is also the target of several pathogens. The lipophosphoglycan (LPG) present on the surface of the intracellular parasite *Leishmania donovani*, is thought to recruit F-actin to the phagosome, physically preventing it from interacting with endosomes/lysosomes (Holm et al., 2001). *Legionella penumophilia* effector protein VipA has been demonstrated to nucleate actin without any additional host factors. This results in disrupted host actin dynamics and may help prevent fusion of the *Legionella*-containing vacuole (LCV) with the lysosome. Finally, *Salmonella* has a unique way of manipulating the host cell cytoskeleton, to gain entry into the cell and then prevent its delivery to the lysosome. Firstly, SopE promotes membrane ruffling and actin rearrangement to gain accelerated entry into the host cell. Subsequently, SptP then promotes the disassembly of actin, thus disrupting the trafficking of the *Salmonella* vacuole to the lysosome (Kubori and Galan, 2003). Other cytoskeletal proteins have been found on phagosomes. Actin binding proteins annexin I (Kaufman et al., 1996), annexin II, IV, α-actinin and α-tubulin were found to be enriched on phagosomes (Desjardins et al., 1994a). As these binding proteins can interact with the actin cytoskeleton, this suggests that these could be possible mechanisms by which phagosome movement, (and subsequent maturation), is coupled to the movement of these organelles within the cell. Phagosome maturation is also highly dependant on interactions with the cytoskeleton. The movement of phagosomes away from the cell periphery may be analogous to the movement of lysosomes towards the nucleus, and may involve similar molecular mechanisms. Lysosomes typically display a perinuclear

distribution which is dependent upon microtubules (Swanson et al., 1987, Matteoni and Kreis, 1987) and their coupling to microtubules by motor proteins (Burkhardt et al., 1997) and cargo adaptors such as RILP (Cantalupo et al., 2001) and HSP6 (Li et al., 2014). Actin filaments and microtubules have also been shown to act together to transport lysosomes within the cell (Cordonnier et al., 2001).

Taken together, these data indicate that the purified phagosomes display a large degree of heterogeneity. This is due to the inability to synchronise the rate of uptake of the phagocytic probe by the cells. While it is possible to initiate phagocytosis at the same time, it is not possible to control how many beads, or how quickly individual cells internalise them. This is further complicated by the dynamic nature of phagosome maturation, and within an individual cell, phagosomes are likely to mature at different rates. Emans *et al*., (1996) showed that latex bead phagosomes (LBPs) displayed a cyclical nature of phosphorylation. LBPs isolated at 12 h displayed a significant decrease in *in vitro* phosphorylation compared to 2 h or 24 h phagosomes. A large number of lysosomal genes have recently been shown to display circadian rhythmicity (Mazzoccoli et al., 2015) and organelle remodelling may be under the control of circadian rhythms. Thus, it is possible that phagosomes may also oscillate, and phagosomes may be in different signalling states when isolated at different times. Furthermore, phagosomes isolated from RAW 264.7 cells were shown to have several markers that displayed a biphasic profile of abundance on phagosomes that was shown not to be due to nonsynchronous phagosome maturation (Rogers and Foster, 2007). Indeed, the pH of phagosomes can vary greatly (5.5-7.5), even within individual cells (Bouvier et al., 1994). As such, it must be accepted that the purified sample represents this entire range of phagosomes, and can only be enriched for a certain state (e.g. late phagosomes), rather than be a homogeneous preparation. Phagosomes are extremely complex organelles. In J774.2 cells alone, phagosomes most likely have over 1000 proteins, with roughly half of these remaining unidentified (Garin et al., 2001). The composition while similar, differs between phagosomes containing different cargo and even between similar cells types. For example, the phagosome proteome of the macrophage-like cell line RAW 264.7, and bone marrow-derived macrophages (BMDM) has been shown to be significantly different. Furthermore, the phagosomes of BMDMs mature considerably faster than that of the RAW cell line (Guo et al., 2014). Pathogen manipulation of membrane trafficking further

complicates what is already a difficult pathway to study. Therefore, the characterisation of phagosomes based upon the detection of a handful of membrane markers (that have other roles not limited to phagosome maturation), must be taken lightly. This paradigm must be accepted when working with these organelles.

3.3 Phagosome-lysosome fusion *in vitro*

3.3.1 Introduction

An advantage of studying vesicle fusion *in vitro* is that it is possible to specifically study the interaction of donor and acceptor organelles and the conditions that facilitate fusion between them. In *in vivo* systems, the overall complexity of the cell, the possibility of off-target effects, and compensatory mechanisms may allow vesicle fusion to continue when a particular condition is altered. This means it can be difficult to interpret results of such experiments. A cell-free assay allows the study of the interactions between specific vesicles under specific conditions, at a molecular level.

Previous vesicle fusion assays have been invaluable in addressing the requirements of vesicle fusion *in vitro*. These include transport between Golgi stacks (Balch et al., 1987, Rothman, 1987), transport between the endoplasmic reticulum and the Golgi (Barlowe, 1997), endosome fusion (Gorvel et al., 1991), endosome-lysosome fusion (Mullock et al., 1989), and SNARE-mediated liposome fusion (Schuette et al., 2004). These include factors such as cytosol, physiological temperature, and the presence of ATP/GTP, (Mullock et al., 1989, Becken et al., 2010, Mullock et al., 1998, Ward et al., 1997) which have been shown to be essential for vesicle fusion. However, only one such study to date, has attempted to dissect the fusion of phagosomes and lysosomes *in vitro* (Becken et al., 2010). However, this study is not without some caveats. Firstly, it measures the colocalisation of fluorescently labelled lysosomes and phagosomes. However, colocalisation cannot distinguish between vesicle tether and true fusion. The study uses FRET to demonstrate that vesicle fusion occurs, but does not use this measurement for every experiment. Secondly, it does not measure the intactness of the compartments being used and cannot rule out that the FRET signal seen was due to content mixing of leaky organelles rather than true fusion.

3.3.1.1 Phagosome-lysosome membrane fusion

The fusion of phagosomes with other endocytic organelles is crucial for their maturation. Nascent phagosomes mature through the addition and removal of

membrane proteins and other components by fusion with early and late endosomes, and finally, with lysosomes to form phagolysosomes (Vieira et al., 2002). Thus, membrane fusion must be tightly regulated in order for the correct vesicles to be targetted to the maturating phagosome. The fusion of intracellular vesicles is driven by several molecular complexes, which provide the energy required to overcome the energy barrier of lipid membrane fusion, but also confer specificity to interactions. SNARE (soluble NSF [*N*-ethyl-maleimide-sensitive fusion protein] attachment receptor protein) proteins have been demonstrated to be involved in almost all cellular membrane trafficking events so far. SNAREs are designated as being (arginine containing) R-SNAREs, or (glutamine-containing) Q-SNAREs, based upon the presence of these highly conserved residues (Fasshauer et al., 1998). SNAREs have been shown to be the minimal proteins required for membrane fusion (Weber et al., 1998), and may also help to provide a layer of specificity to the pairing of donor and acceptor vesicles (Sollner et al., 1993), along with Rab GTPases and other tethering factors.

3.3.1.2 Principle of the *in vitro* phagosome-lysosome fusion assay

In order to study the fusion of the phagosome and lysosome *in vitro,* two protocols were developed for the purification of these two organelles. A schematic representation of the fusion assay is shown in figure 3.21. Briefly, FeDex and biotin-HRP filled lysosomes are mixed *in vitro* with magnetic streptavidin bead-containing phagosomes. Fusion is enhanced by the addition of cytosol and an ATP regenerating system. To prevent binding of biotin-HRP to streptavidin phagosomes where the membrane integrity is compromised, the assay is performed in the presence of saturating amounts of biotinylated lysine (biocytin), to mop up any biotin binding sites on the beads. After fusion has proceeded, the bead containing phagolysosomes are collected on a magnet, lysed with detergent and washed thoroughly. The amount of HRP activity is then assayed using Amplex Red (AR) reagent to quantify the amount of fusion.

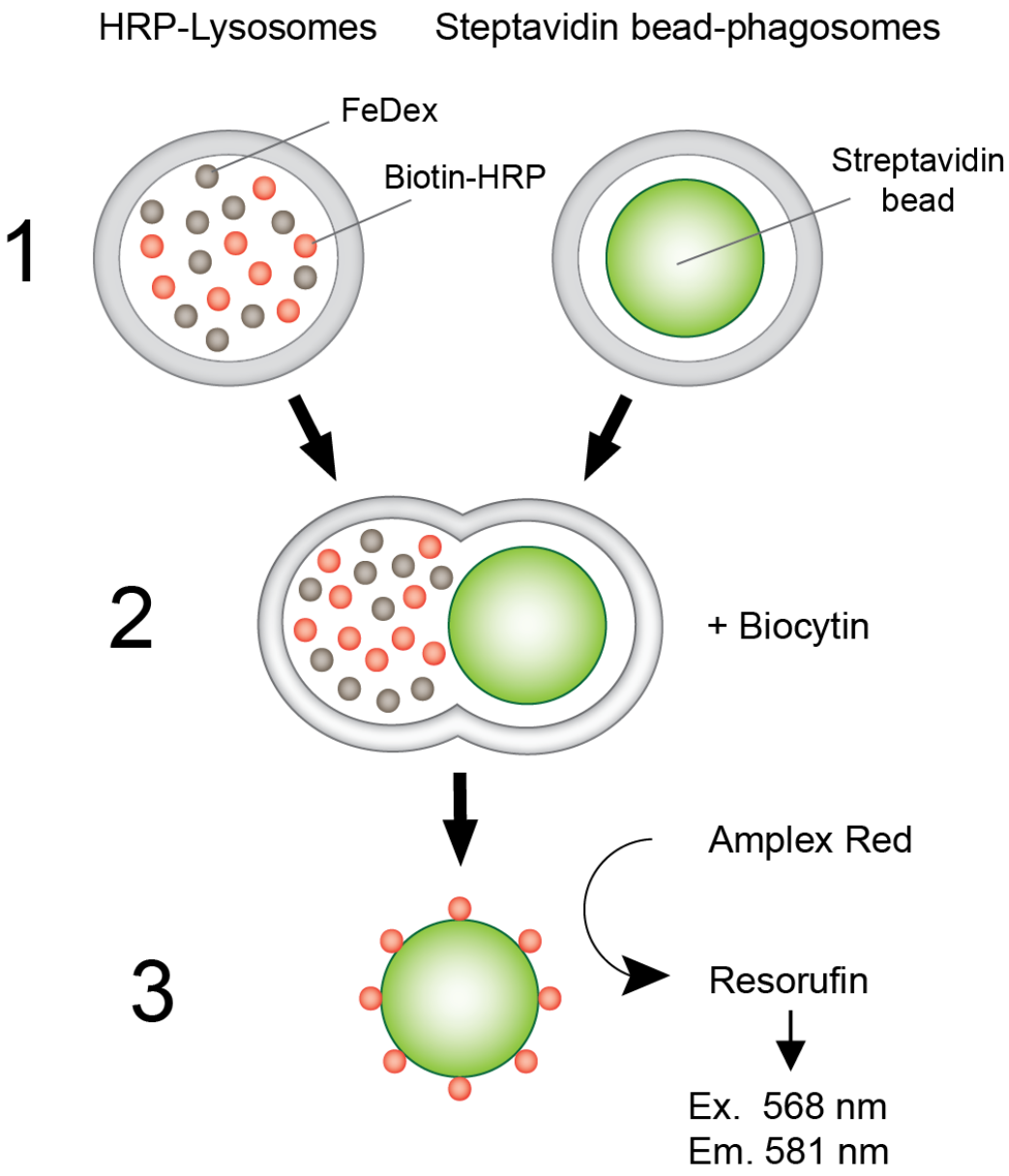

Fig. 3.21. Schematic representation of *in vitro* phagosome-lysosome fusion. 1. Biotin-HRP filled lysosomes are magnetically isolated using FeDex as previously described. Streptavidin bead containing phagosomes are also purified magnetically as previously described. The two organelles are then mixed *in vitro*. Fusion is enhanced by the addition of cytosol and an ATP regenerating system. To prevent binding of biotin-HRP to streptavidin phagosomes where the membrane integrity is compromised, the assay is performed in the presence of saturating amounts of biotinylated lysine (biocytin), to mop up and biotin binding sites on the beads. **2.** Fusion is allowed to proceed, and the bead containing phagolysosomes are collected on a magnet, lysed with detergent and washed thoroughly. **3.**The amount of HRP activity is then assayed using Amplex Red (AR) reagent to quantify the amount of fusion.

3.3.1.3 Amplex Red reaction

Amplex Red is a non-fluorescent and colourless compound that is used as a reagent for the measurement of H_2O_2. Amplex Red reacts with H_2O_2 in a 1:1 stoichiometry (Fig. 3.22). The reaction is catalysed by horseradish peroxidase (HRP), to form the highly fluorescent oxidation product, Resorufin, which is excited at 568 nm and emits at 581 nm (Zhou et al., 1997). Amplex Red is highly sensitive and can detect concentrations of H_2O_2 as low as 50 nM, or HRP concentrations as low as 1 x 1^{-5} U/ml (Thermo fisher product data sheet). Amplex Red has been used in a variety of different assays to measure HRP activity (Bulina et al., 2006, Nakanaga et al., 2007, Castello et al., 2007)

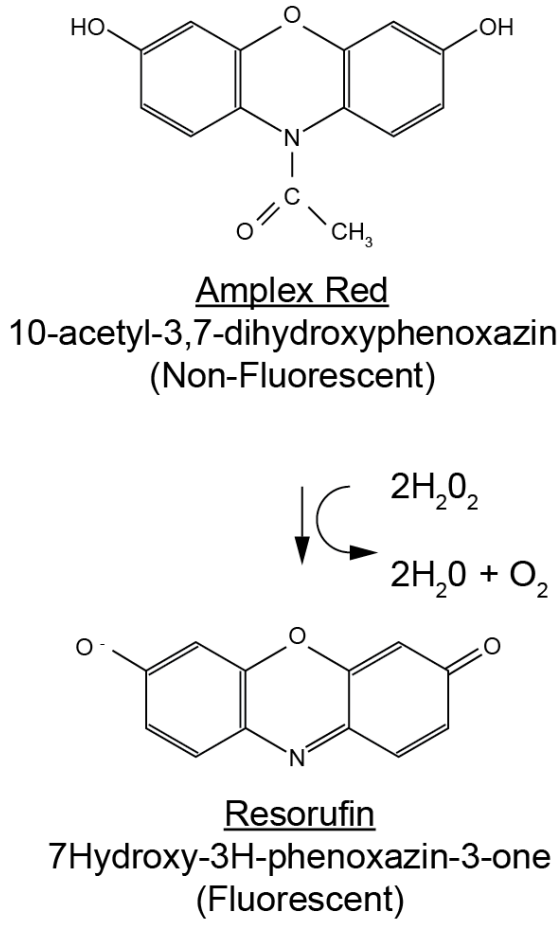

Fig. 3.22. Oxidation of Amplex Red to form Resorufin. Horseradish peroxidase (HRP) catalyses de-N-acetylation and oxidation of Amplex Red (Non-fluorescent) to Resorufin (Highly fluorescent) in a 1:1 stoichiometry.

3.3.2 Fusion assay specific methods

3.3.2.1 Detection of biotin-HRP using Amplex Ultra Red

To detect lysosomal biotin-HRP, lysosomes were purified from J774.2 cells as per the FeDex protocol (section 3.2.2) but with the following changes. Biotin-HRP (Invitrogen, catalogue number P-917) was added to the FeDex-containing tissue culture media to a final concentration of 0.5 mg/ml. Lysosomes were then purified as previously described. HRP-containing lysosomes were then assayed for HRP using Amplex Ultra Red (AR) reagent (Invitrogen, catalogue number A36006). In the presence of HRP, Amplex Red reacts (in a 1:1 stoichiometry) to produce a red oxidation product, Resorufin (excitation and emission maxima of 571 nm and 585 nm respectively, (Zhou et al., 1997). Lysosomes or phagosome beads were resuspended in RIPA buffer or STM containing 0.1 % (v/v) Triton X-100 and plated in duplicate into the wells of a black flat-bottomed microplate (Nunc). 50 µl - 150 µl of AR working reagent was then added immediately to each sample using a multichannel pipette.

Amplex red working reagent was prepared as follows: One vial of Amplex Ultra Red (1 mg) was dissolved in 389 µl of DMSO (dimethyl sulfoxide) to give a final concentration of 8.6 mM. 20 mM H_2O_2 was prepared fresh by adding 3 µl of 30 % (w/w) H_2O_2 in 977 µl of ice-cold STM or RIPA buffer. 50 µl of 8.6 mM Amplex Red, and 500 µl of 20 mM H_2O_2 were added to 4.45 ml of STM or RIPA buffer (giving a final concentration of 86 µM Amplex Red and 2 mM H_2O_2). Samples were measured in a BMG Polarstar plate reader preheated to 37 ºC with an excitation wavelength of 541 nm and emission read at 590 nm. Fluorescence measurements were taken every minute for 30 min, with the gain set appropriately between experiments (for the majority of experiments, this was 1800). Where appropriate, blank values were subtracted from data, and data were plotted at a point when the production of fluorescent resorufin was still occurring.

3.3.2.2 Isolation of pig brain cytosol

Fresh pig brains were finely minced and snap frozen in liquid nitrogen and stored at -80 ºC until required. Approximately 4 g of pig brain was partially defrosted and resuspended in 3 ml of ice-cold STKM (250 mM sucrose, 10 mM TES, pH 7.4, 1

mM $MgCl_2$, 25 mM KCl). Brain tissue was homogenised on ice with three strokes of a Potter-Elvehjem homogeniser (with the pestle attached to a household drill rotating at 1000 rpm). The homogenate was then centrifuged at *104,300 x g* , for 15 min at 4 ºC. The supernatant was adjusted to approximately 3 ml with STKM and passed through an Econo-Pac 10DG disposable chromatography column (BioRad). The cytosol was eluted from the column with 4 ml of STKM, snap frozen in liquid nitrogen, and stored at -80 ºC. The protein concentration was typically 5-10 mg/ml. Pig brain cytosol for use in the fusion assay was prepared a maximum of one day before the assay.

3.3.2.3 In vitro phagosome-lysosome fusion assay

This is the protocol as it currently stands. Section 3.13 shows the development of this assay protocol.

Lysosomes were purified from four 10 cm tissue cultures dishes of J774.2 cells as previously described with the following changes. Cells were pulse-chased with FeDex diluted 1:20 in DMEM, with the addition of 0.5 mg/ml biotin conjugated – HRP. Lysosomes were eluted from the iron column with 1 ml of pig brain cytosol. Streptavidin-bead phagosomes were prepared as previously described, except phagosomes were resuspended in 200 µl of pig brain cytosol. All samples were set up on ice in prechilled tubes. 25 µl of lysosomes and 25 µl of phagosomes were added to each tube. To reduce the background signal from damaged organelles, 25 µl of biocytin (25 µg/ml biotinylated lysine in STKM) or 25 µl STKM was added. Where appropriate, 25 µl of an ATP regenerating system (10 µl of 4 mg/ml creatine kinase in PBS, 10 µl of 261.2 mg/ml creatine phosphate in PBS, 2.5 µl of 50 mM ATP, and 2.5 µl of 50 mM GTP) or 25 µl of PBS was added to each tube. Fusion was allowed to proceed for 30 min on ice or in a 37 ºC water bath. After 30 min, tubes were plunged into ice-cold water.100 µl of 2 X RIPA buffer was added to each tube, which was vortexed and incubated on ice for 15 min. The streptavidin beads were collected on a magnet, washed three times with 1 X RIPA, and resuspended in 50 µl of RIPA buffer. Biotin-HRP bound to the beads was detected using Amplex Ultra Red, as previously described.

3.3.3 Results

3.3.3.1 Biotin-HRP can be detected in lysosomes

An inherent problem with studying lysosomes is that the hydrolytic enzymes they contain are able to degrade ligands or markers that are delivered to the lysosome. For the fusion assay, biotin-HRP needed to be detectable in FeDex-purified lysosomes. To test this, lysosomes were purified from cells incubated with biotin-HRP and were assayed with Amplex Red to determine if an HRP signal could be detected. 4x10 cm tissue culture dishes of J774.2 cells were incubated with 0.5 mg/ml biotin-HRP in DMEM containing FeDex (1:20) for 1 h followed by a HRP/FeDex-free chase for 2 h (Fig. 3.23). As a control, the same number of cells were subjected to the same protocol without biotin-HRP. Lysosomes were magnetically isolated, and assayed for the presence of HRP using Amplex Ultra Red reagent (AR).

A fluorescent signal (above that of the highest volume of control lysosomes), was detectable when AR was incubated with biotin-HRP containing lysosomes for all of the volumes of lysosomes tested (25 µl to 0.19 µl). Control lysosomes did not produce a fluorescent signal when incubated with AR, indicating that they do not react with Amplex Red. For lysosomes containing biotin-HRP, the rate of resorufin production increased over time and was dependent on the volume of HRP-lysosomes. After 10 min (Fig. 3.22) the highest amount of fluorescence seen in the samples with the highest amounts of lysosomes. 25 µl (2650 AU) was lower than 12.5 µl (3040 AU) but this was most likely experimental error. After 30 min the signal from 25 and 12.5 µl of biotin-HRP lysosomes decreased negligibly (2553 AU and 2915 AU). However, the signal from lower volumes of lysosomes increased. For example, at 10 min 1.56 µl gave a signal of 906 AU, which increased to 1832 AU after 30 min. Control lysosomes (containing no biotin HRP) did not give a signal at either 10 min or 30 min, indicating they did not react with Amplex Red. These data indicate that give enough time, small amounts of biotin-HRP can react with Amplex Red to give a much larger signal. Thus, 30 min endpoints were not suitable for the fusion assay, and it was decided that all data needed to be collected when the rate of resorufin production was linear and before the Amplex Red became a limiting factor in the samples with higher amounts of

HRP. The plateau of fluorescence seen with the highest volume of lysosomes (12.5 µl) was probably due to the depletion of AR substrate. If this was the case then all samples, given enough time, would eventually reach the same endpoint. Although, at 37 ºC, this would accelerate the rate at which H_2O_2 decomposes to water and singlet O_2. It is also possible that the production of resorufin from Amplex Red is self-quenching at high concentrations. Thus, large amounts of HRP give lower fluorescence signals than samples that have lower amounts of HRP.

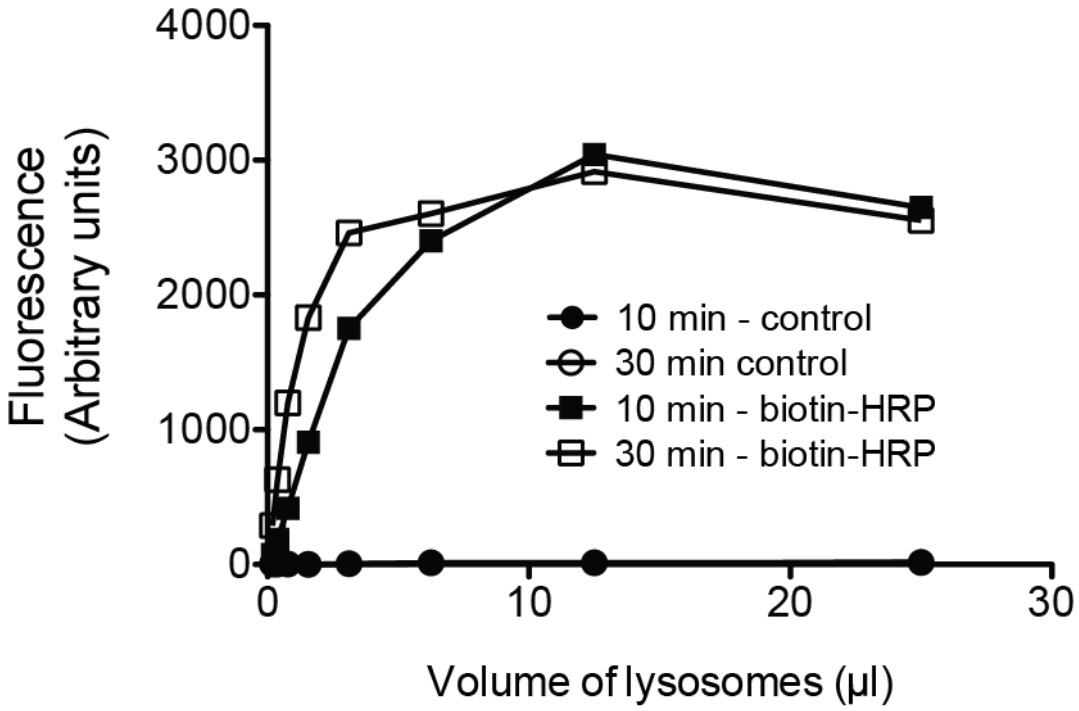

Fig. 3.23. Detection of biotin-HRP from FeDex-purified lysosomes. 4x10 cm tissue culture dishes of J774.2 cells were incubated with 0.5 mg/ml biotin-HRP in DMEM containing FeDex (1:20) for 1 h followed by a HRP/FeDex-free chase for 2 h As a control, the same number of cells were subjected to the same protocol without biotin-HRP. Lysosomes were isolated from cells as previously described lysosomes, and resuspended in a final volume of 100 µl of STM containing 0.2 % (v/v) Triton X-100. Serial dilutions of control or HRP lysosomes were performed in a 96 well plate (in duplicate), and 50 µl of Amplex Red (AR) reagent was used to assay for HRP. The fluorescence signal was read every minute for 30 min at 37 ºC. Data are means ± range of fluorescence values after 10 min or 30 min (Excitation wavelength 541 nm, emission wavelength 590 nm). Data are the results of one experiment, with the same trend seen in two separate experiments.

3.3.3.2 Transfer of biotin-HRP from lysosomes to phagosomes can be detected in a mixing assay

The previous experiment showed that biotin-HRP was detectable within lysosomes from cells incubated with biotin-HRP but not control cells. However, it was possible that the biotin could have been degraded in the lysosome and be unable to bind to the beads. Similarly, the streptavidin on beads could be degraded in the phagosomes, rendering the beads unable to bind biotin-HRP. To ensure that this was not the case a mixing assay was performed. This would also demonstrate that the mixing of the two organelles would give a detectable signal that could be blocked by the addition of biotinylated-lysine (biocytin) and finally, determine the lowest volume of phagosomes that could be used for an assay (Fig. 3.24). Briefly, HRP lysosomes were purified from 4x10 cm dishes of J774.2 cells and resuspended in 120 µl of STM containing Triton-X 100 at 0.2 % (v/v) to lyse lysosomal and phagosomal membranes. Phagosomes were purified from a second batch of cells, and again lysed in Triton X-100. Briefly, phagosomes were isolated from one 6-well plate of cells at an MOI of 3 (approximately 100 µl of beads). One half of the purified phagosomes were incubated in STM (unblocked) and the other half in STM containing 5 µg/ml biocytin for 30 min on ice. Biocytin will compete with biotin-HRP for streptavidin binding sites on the bead phagosomes, thus blocking the signal. 3 µl of lysosomes were then incubated with doubling dilutions of phagosomes for 15 min at room temperature with rotation, to allow the HRP to bind to the beads. Beads were then isolated, washed, and assayed for HRP activity using AR. The fluorescence signal after 10 min from 3 µl of lysosomes was 25563 AU (data omitted from the graph for brevity). At 10 min, the largest fluorescence signal was seen with unblocked phagosomes was 5410 A.U and the highest HRP signal obtained from blocked phagosomes was 610 A.U. The percentage of the total fluorescence signal (from 3 µl of lysosomes) for blocked phagosomes was 2.4 %, 3 %, 0.54 %, 0.68 %, 0.94 %, 0.23 %, 0.36 %, and 0.16 % (dilution 1-8 respectively). The percentage of the total fluorescence signal for unblocked phagosomes was 23 %, 16.6 %, 7.2 %, 5.6 %, 0.8 %, 0.4 %, 0.6 %, and 0.31 % (dilution 1-8 respectively). In general, the HRP signal dropped with each subsequent dilution of phagosomes (both blocked and unblocked). This experiment showed that the limiting factor in the fusion assay would most likely be the phagosomes. Only 2.5 % of the total volume of lysosomes were used for each

phagosome sample, yet over 75 % of the total HRP signal remained unbound. However, this may have been due to the fact that mixing of phagosomes and lysosomes was only performed for 15 min. If this incubation time was increased, it would be likely that the total percentage of HRP recovered would increase, giving a better estimation of the number of phagosomes needed to bind all of the available HRP. Approximately 100 µl of stock beads were used to purify phagosomes in this experiment. As this sample was split in half (blocked and unblocked) and then diluted, the lowest amount of beads where an HRP signal was detectable in this experiment was approximately 12.5 µl.

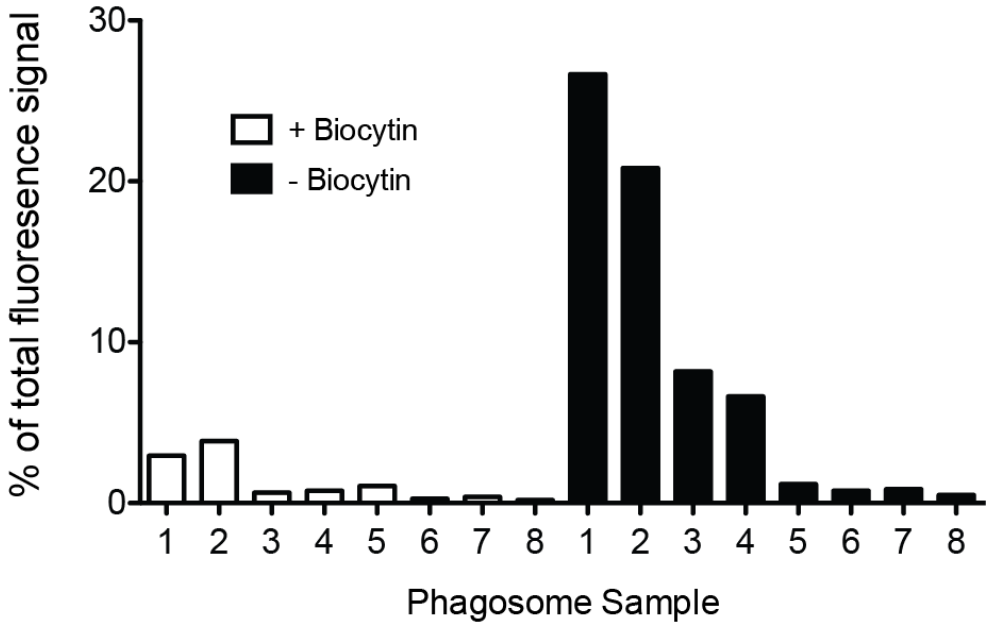

Fig. 3.24 *In vitro* phagosome-lysosome mixing A. Biotin-HRP containing lysosomes were purified from 4x10 cm tissue culture dishes of J774.2 cells and resuspended in 120 µl of STM + 0.2 % (v/v) T X-100. Streptavidin bead phagosomes were purified from a different batch of J774.2 cells as described in previously (approximately 100 µl of beads). Phagosomes were then incubated with (open bars) or without 5 µg/ml biocytin (closed bars) to block biotin binding sites on damaged phagosomes. Doubling dilutions of phagosome samples (1-8) were incubated with 3 µl of HRP-lysosomes for 15 min at room temperature with rotation. The beads were retrieved on a magnet, washed three times with STM and the amount of bound HRP assayed using 50 µl of Amplex Red. The fluorescence signal was read every minute for 30 min at 37 ºC. Data are means ± range of fluorescence (AU) after 10 min when the fluorescence signals were still increasing (n=1).

3.3.3.3 HRP binding to streptavidin beads can be blocked by biocytin

Previous data indicated that biotin-HRP was not degraded sufficiently in lysosomes to be undetectable and that binding to beads could still occur after the beads had been passed through cells. To be sure that the HRP signal was *bona fide* binding of biotin-HRP to biotin binding sites, rather than a non-specific interaction, the binding of HRP was blocked by titrating increasing amounts of biocytin. The streptavidin beads were capable of binding 0.44 µg of FITC-biotin per mg of beads (6.824×10^{-10} moles of FITC-biotin per mg of spheres). 20 µl of beads was roughly 200 µg in mass, which gave a binding capacity of 1.36×10^{-10} moles of FITC-biotin. Substituting in the estimated molecular weight of biotin-HRP (476.31 g/mole), this gave a bead binding capacity of 6.47×10^{-8} g (65 ng) of biotin-HRP per 20 µl of beads. Substituting in the molecular weight of biocytin (372.48 g/mole), 1.36×10^{-10} moles of biocytin, 50.65 ng of biocytin can bind to 20 µl of beads. Thus, 20 µl of beads (not incubated with cells) were added to 0.5 ml of STM containing a saturating amount of biotin-HRP (65 ng) plus biocytin at 0, 6.25, 12.5, 25, 50, 100, or 500 ng/ml (Fig. 3.25). Samples were incubated for 30 min, washed with RIPA buffer and then assayed for HRP activity using Amplex Red.

The signal decreased as the amount of biocytin was increased. The total fluorescence signal from 65 ng of biotin-HRP alone (no beads) was 31453 AU. The highest bead signal was seen with 0 ng/ml biocytin (21528 AU, 68.4 % of the total) and the lowest signal was detected at 100 ng/ml (2548 (8.1 % of the total). When the data was normalised so that 0 ng/ml = 100 % binding, and 500 ng/ml = 0 % binding), then the percentage of biotin-HRP bound to the beads was as follows; 87.3 % (6.25 ng/ml), 81.6 % (12.5 ng/ml), 61.5 % (25 ng/ml), 44 %, (50 ng/ml), and 1.8 % (100 ng/ml). 500 ng/ml gave no increase in signal for the duration of the time course (30 min). Therefore, for further experiments, 500 ng/ml (250 ng absolute amount) was deemed sufficient to block the binding of biotin-HRP to 20 µl of beads.

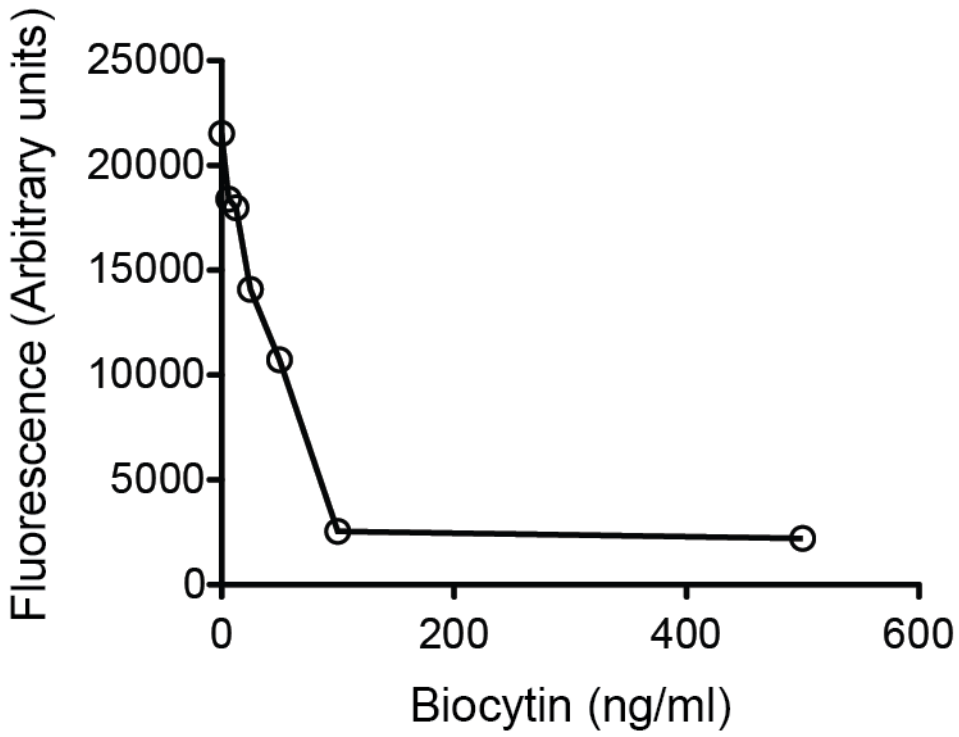

Fig. 3.25. Biotin-HRP binding can be blocked by biocytin. 20 µl of streptavidin beads were incubated with 0.5 ml STM containing biocytin at the indicated concentrations and 65 ng of biotin-HRP, for 30 min at room temperature. The beads were then isolated, washed three times with RIPA buffer, and resuspended in 50 µl of RIPA buffer. HRP activity was then detected using 50 µl of Amplex Red reagent using a plate reader heated to 37 ºC. The graph shows fluorescence after 10 min while the fluorescent signal was still increasing. Data is representative of a single experiment that was repeated twice.

3.3.3.4 J774.2 cell lysate does not interfere with HRP binding

As HRP-containing lysosomes and bead-containing phagosomes for the fusion assay were purified from J774.2 cells, it was important to ensure that any cellular debris carried over from washing the organelles did not react with the Amplex Red reagent to give a fluorescence signal. To test this, 20 µl of beads were incubated with a J774.2 cell lysate equivalent to that of the number of cells 20 µl of phagosomes would be purified from, i.e., for the phagosome purification, 20 µl of beads were incubated with approximately $4x10^6$ cells. Cells were lysed in cell lysis buffer and a detergent soluble lysate was made (as previously described). 20 µl of beads were incubated with or without 500 ng/ml biocytin, and then washed. Unblocked and blocked beads were then incubated with biotin-HRP or J774.2 cell

lysate (Fig. 3.26). The beads were then washed, and assayed for HRP activity. To demonstrate that any fluorescence seen was due to the binding of biotin-HRP, beads were incubated with or without biocytin to show that binding could be blocked. Indeed, there was no change in fluorescence (over 30 min) when beads were pre-incubated with biocytin and then incubated with biotin-HRP (919 AU) When blocked and unblocked beads were incubated with J774.2 cell lysate, the fluorescence signal remained constant, (J774 blocked 717 AU, J774.2 unblocked 756 AU), and below that of beads incubated with biocytin (HRP blocked). Similarly, a J774.2 cell lysate gave no fluorescence signal above that of the blocked beads (159 AU). The fluorescence signal after 10 min from the HRP control was 13150 AU. The fluorescence signal of the unblocked beads after 10 min was 51 % of this (6750 AU). This dropped to 6.9 % when beads were blocked with biocytin beforehand, but given that this signal did not change over the course of the assay (30 min), it is likely to be background noise. Overall, these data indicate that the J774.2 cell lysate does not react with Amplex Red to give a fluorescence signal, or it does not stick to the beads/is sufficiently removed when the beads are washed. Therefore, any fluorescence signal seen when assaying beads using Amplex Red is due to the presence of bound biotin-HRP alone.

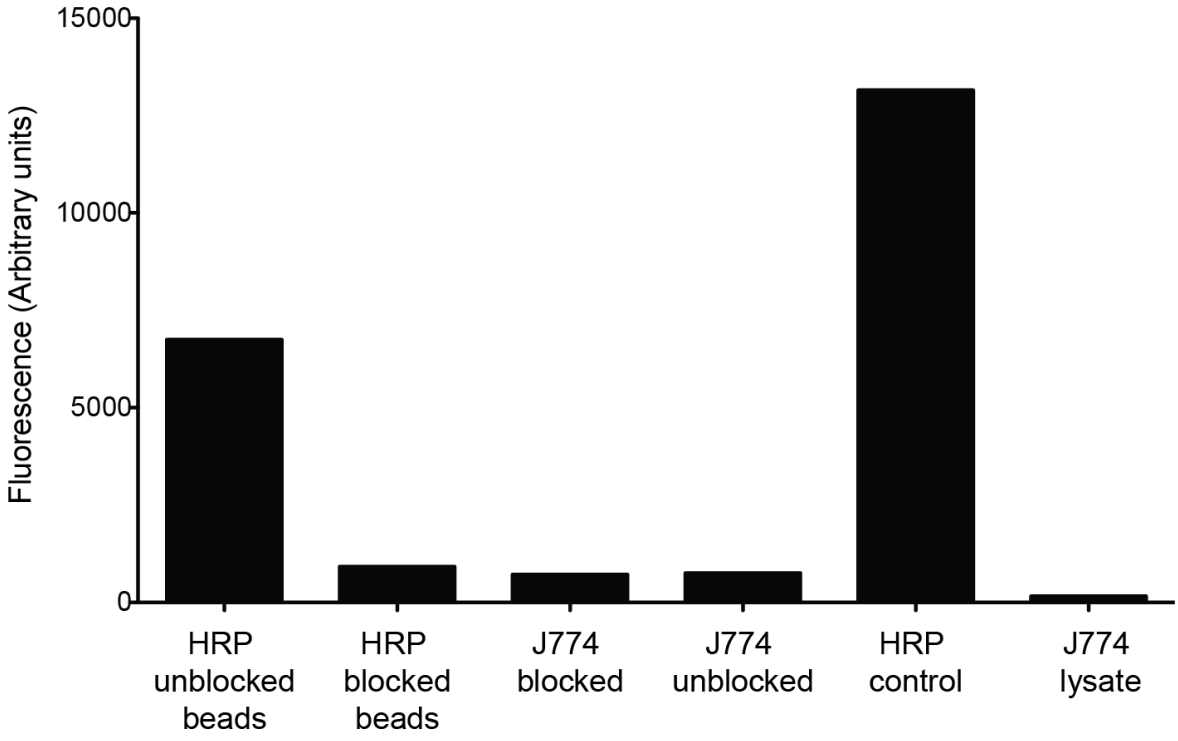

Fig. 3.26. J774.2 cell lysate does not produce a fluorescent signal when assayed with Amplex Red. 20 µl of streptavidin beads were either incubated with 0.5 ml STM (unblocked) or STM containing 500 ng/ml biocytin (blocked) for 15 min at room temperature. Beads were then washed 3 times with STM, and incubated with 65 µl of biotin-HRP in STM (1 µg/ml), plus 225 µl of STM, or 290 µl of a J774.2 cell lysate for 30 min at room temperature. Beads were then washed three times with RIPA buffer, and bound HRP activity assayed using Amplex Red. As a control, 65 µl of 1 µg/ml biotin-HRP, and 50 µl of J774.2 cell lysate were also assayed Data are fluorescent signals after 10 min while the fluorescence signal was still increasing (n=1).

3.3.3.5 Determining the maximum signal obtainable from streptavidin beads

Based upon previous fusion assays (Becken et al., 2010, Mullock et al., 1998, Mullock et al., 1989, Ward et al., 1997, Jahraus et al., 1998) the amount of vesicle fusion was likely to only be 5-10 % of the total obtainable signal. To maximise the sensitivity of the assay and see such low rates of fusion, it was necessary to determine the amount of biotin-HRP needed to saturate 20 µl of streptavidin beads (arbitrary volume of beads). This was previously calculated to be 65 ng. However, the binding of biotin-HRP to the beads was routinely performed for 30 min in 0.5 ml volumes. When using biotin-HRP at 130 ng/ml (65 ng per 0.5 ml), 30 min was

not long enough to saturate beads. To try and saturate the beads within this time frame, 20 µl of beads were incubated with increasing amounts of biotin-HRP in STM for 30 min at room temperature, washed, and then assayed for bound HRP with AR (Fig. 3.27 A&B). The fluorescence signal continued to increase as the concentration of biotin-HRP was increased, up to 1000 ng/ml (Fig. 3.27 A). The highest amount of fluorescence was seen at 1000 ng/ml (9540 AU), followed by 500 ng/ml (7340 AU), 125 ng/ml, (6000 AU), 250 ng/ml (5460), 62.5 ng/ml (2890 AU), 31.25 ng/ml (1990 AU), 15.6 ng/ml (1150 AU) and 7.8 ng/ml (446 AU). As no plateau in fluorescence was observed, the experiment was repeated using higher concentrations of biotin-HRP (1000-5000 ng/ml, Fig. 3.27 B). The highest amount of fluorescence was seen at 2000 ng/ml (12,500 AU), followed by 1000 ng/ml (11,700 AU), 500 ng/ ml (10,760), 3000 ng/ml, (10,400 AU), 5000 ng/ml (9740), 4000 ng/ml (9730), 250 ng/ml (8190 AU) and 125 ng/ml (4,800 AU). Given that the fluorescence did not differ greatly from 500-5000 ng/ml, it was concluded that 0.5 ml of 500 ng/ml biotin-HRP was probably sufficient to saturate 20 µl of beads in 30 min, but it was not clear if the beads were saturated or if the Amplex Red substrate itself was limiting. It was important to test this to ensure that the assay reagent was not limiting in the fusion assay. To test this, 20 µl of beads were saturated with biotin-HRP (0.5 ml of 500 ng/ml) for 30 min at room temperature. The beads were then washed and assayed with 50, 100, 150, 200, or 250 µl of Amplex Red (Fig. 3.28). Increasing the volume of Amplex Red by 5-fold did not result in a 5-fold increase in fluorescence. After 10 min, the fluorescence of samples incubated with 50 µl of Amplex Red was 55 % of the signal from 250 µl of Amplex red. 150 µl of AR gave 85 % of the signal seen from 250 µl. Doubling the volume of Amplex Red substrate did not result in a doubling of fluorescence, indicating resorufin production was not limited by the availability of the substrate, but possibly by the rate at which HRP could catalyse the production of resorufin. Alternatively, the rate of production may have altered as the amount of H_2O_2 was depleted. For further experiments, 150 µl of assay reagent was used as it was thought that this would be a sufficient volume to not be a limiting factor. However, as long as the fluorescence signals were measured at a point when the signal was still increases (i.e. before all of the substrate was used up) then the volume of assay reagent would not matter as long as it was the same for all samples used.

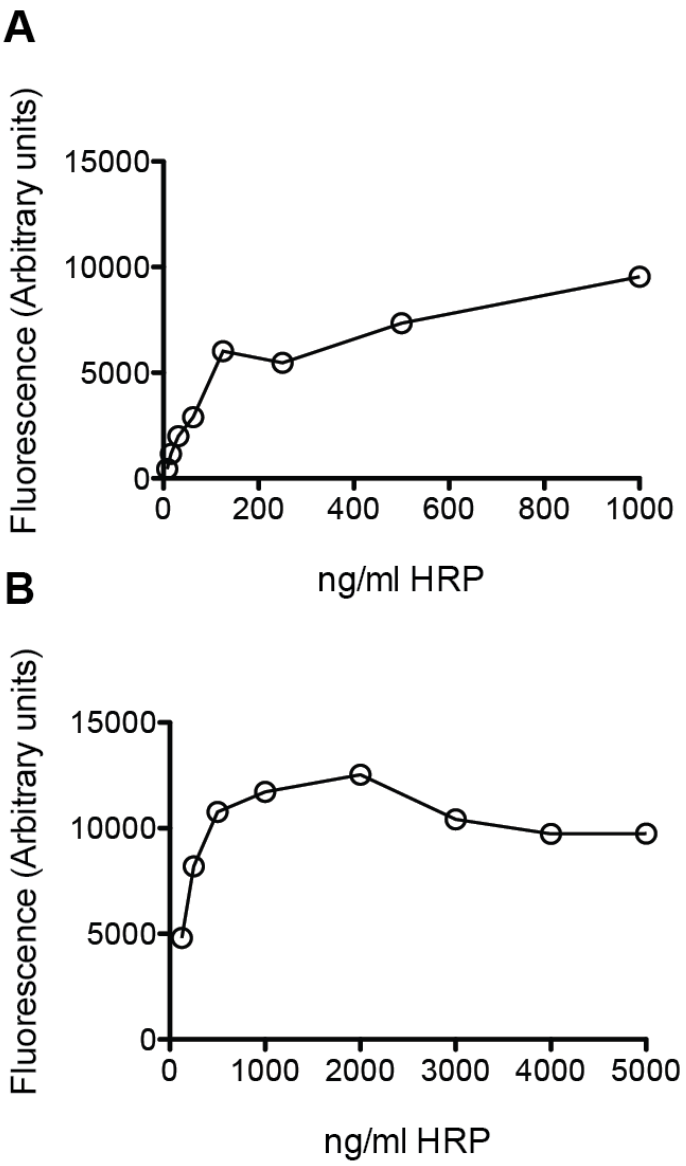

Fig. 3.26 Saturation of streptavidin beads with biotin-HRP. 20 µl of streptavidin beads were incubated with 0.5 ml of STM containing biotin-HRP at the concentrations shown (ng/ml) for 30 min at room temperature. The beads were washed three times with RIPA buffer, and the level of biotin-HRP bound to the beads determined by Amplex Red assay using a plate reader preheated to 37 ºC. **A&B** show the results of independent experiments over two different ranges of biotin-HRP concentrations. Data are fluorescence taken at 5 min when the fluorescence of the samples was still increasing.

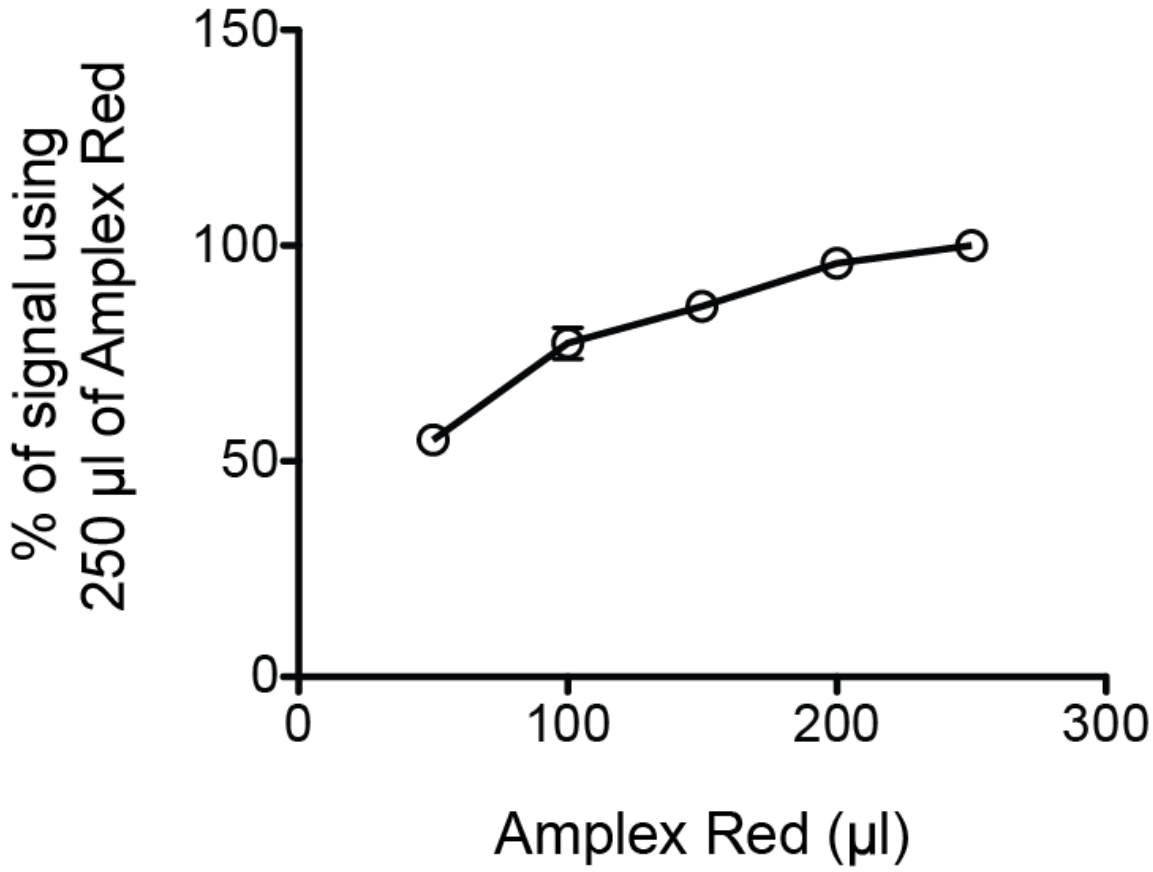

Fig. 3.28. Increasing the volume of Amplex Red increases the fluorescence signal. 20 µl of streptavidin beads were saturated with 0.5 ml of STM containing 500 ng/ml biotin-HRP. Beads were then washed three times and assayed with the indicated volumes of Amplex Red. Samples were adjusted to 250 µl by the addition of RIPA buffer. As a control, 20 µl of beads were incubated in STM alone (Beads only). Data are means ± the range, with each data point plotted as a % of the signal seen from 250 µl of Amplex Red in that experiment.

3.3.3.6 Determining the volume of lysosomes needed to saturate streptavidin beads

To ensure the conditions for the fusion assay produce the maximum chance of detecting a fusion signal, it was necessary to determine the volume of biotin-HRP containing lysosomes that were needed to saturate 20 µl of streptavidin beads (having determined the maximum single from 20 µl of beads incubated with biotin-HRP directly). This was necessary to ensure that the volume of lysosomes used in the fusion assay would not be a limiting factor. J774.2 cells were seeded at $8x10^6$

per dish (2 dishes) and cultured for 48 h. Cells were then incubated with 0.5 mg/ml biotin-HRP in FeDex (1:20) containing DMEM for 1 h, rinsed three times with PBS, then incubated with DMEM for a further 2 h. Control cells were incubated with FeDex containing DMEM only. The cells were lysed and lysosomes purified using the previously described method. Lysosomes were eluted in 1 ml of STM and Triton X-100 added to a final concentration of 0.1 % to lyse lysosomal membranes. 20 µl of beads were then incubated with 2.5, 5, 10, 25, 50, or 100 µl of HRP-containing or control lysosomes for 30 min. Beads were then washed and assayed for HRP activity using Amplex Red (Fig. 5.29).

The maximum fluorescence from the control and lysosomes containing HRP was also determined. As seen previously, control lysosomes did not give a fluorescence signal above that of the background (and as such have been omitted from the graphs for brevity). The maximum signal obtainable from 20 µl of beads saturated with HRP after 10 min was 16,700 AU. The lowest volume of HRP-containing lysosomes where a fluorescence signal could be detected was 10 µl. 100 µl of biotin-HRP lysosomes gave a fluorescence signal of 14,200, suggesting that 100 µl of lysosomes almost contained enough HRP to saturate the bead control (at 30 min, the 100 µl of lysosomes gave a fluorescence signal above that of the bead control). However, the fluorescence from beads incubated with 100 µl of lysosomes was only 13 % of the total signal (1940 AU). Similarly, beads incubated with 10, 25, and 50 µl of lysosomes only gave 33.8 %, 34.7 % and 14.2 % of the total fluorescence signal from 10, 25, and 50 µl of lysosomes, respectively. The fact that the beads did not bind all of the biotin-HRP that was present in the lysosome samples may have been due to degradation of the biotin part of the biotin-HRP molecule.

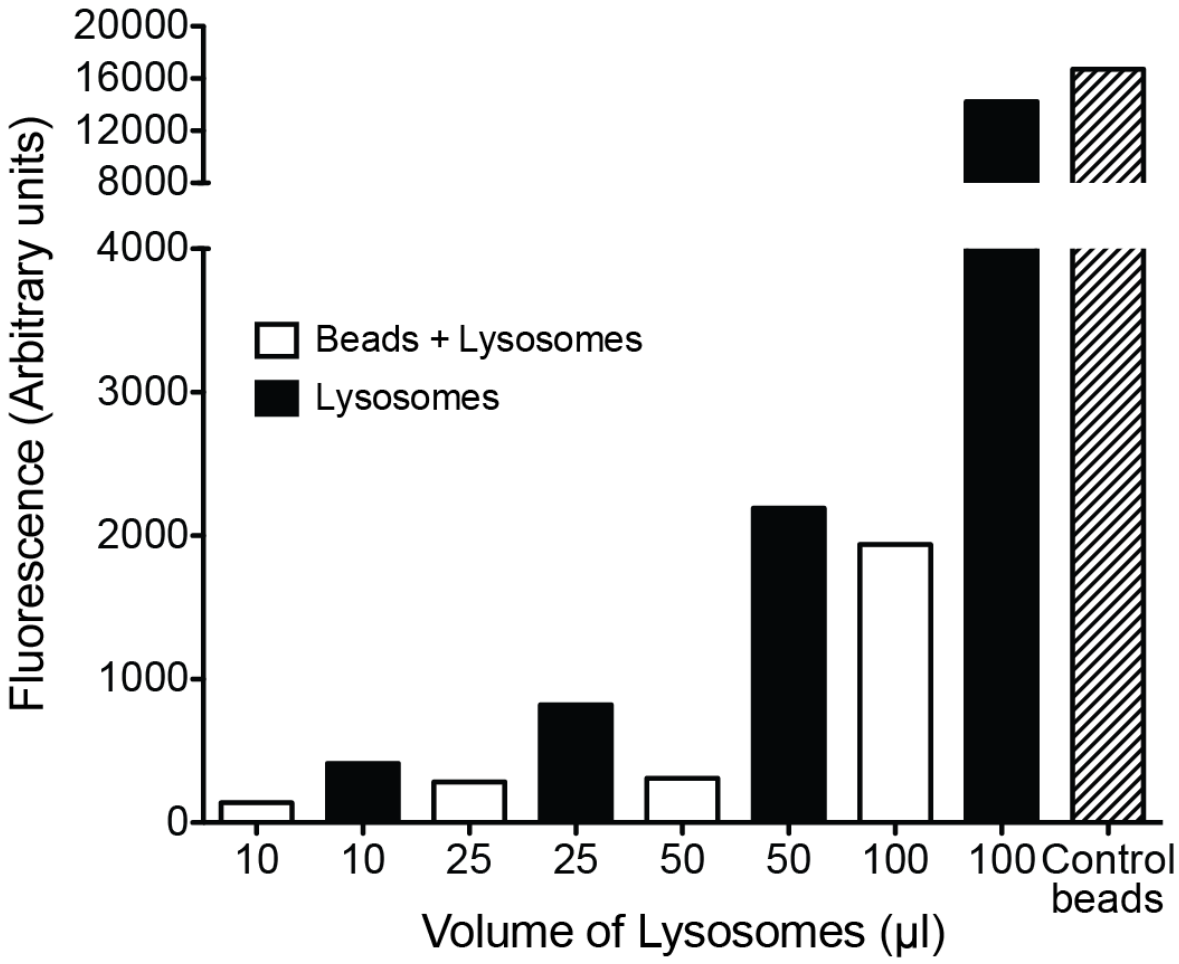

Fig. 3.29. Determining the volume of biotin-HRP lysosomes needed to saturate 20 µl of streptavidin beads. Biotin-HRP containing lysosomes were purified from 2x10 cm dishes of J774.2 cells and resuspended in 1 ml of STM containing 0.1 % (v/v) Triton X-100. 20 µl of streptavidin beads were incubated for 30 min at 4 ºC with 2.5, 5, 10, 25, 50, or 100 µl of HRP-containing lysosomes. The beads were then washed, and assayed for HRP activity using 150 µl of Amplex Red (Open bars). The same volume of lysosomes were also measured to give a total obtainable signal (Closed bars) For brevity, the signals from 2.5 µl and 5 µl of HRP-lysosomes are omitted. As a control, 20 µl of beads saturated with biotin-HRP (by incubation with 500 ng/ml biotin-HRP in STM for 30 min) were also assayed (hatched bar). Data are fluorescence values after 10 min of incubation with Amplex Red, while the fluorescence signal was still increasing (n=1).

This experiment was then repeated in order to try and reach a point where HRP-lysosomes were able to saturate the 20 µl control. This time, 4 dishes of cells were used and incubated with FeDex-HRP (or FeDex alone) to increase the amount of HRP available to the beads. Lysosomes were eluted in 1 ml of STM. 20 µl of beads were then incubated with 5, 10, 20, 25, 100, or 200 µl of FeDex-HRP or FeDex lysosomes. To try and increase the amount of HRP binding to the beads, the incubation was performed overnight (Fig. 5.30). The previous experiment had shown that 100 µl of HRP-lysosomes contained enough HRP to give a signal that was close to the saturated bead control. When repeated, 100 µl of lysosomes only gave 45.5 % of the control signal, whereas 200 µl of lysosomes gave 96.6 % of the saturated bead control. This discrepancy may be due to depletion of the HRP from the media after repeated uses (HRP-containing media was filter sterilised and reused for further experiments). Incubating the beads with 10 µl of lysosomes resulted in a 1.8-fold increase in fluorescence compared to 10 µl of assayed lysosomes (600 AU compared to 334 AU). Similarly, 25 µl of lysosomes gave a lower signal than beads incubated with the same volume of lysosomes (493 AU compared to 1813 AU), and 50 µl of lysosomes gave a slightly smaller fluorescence signal compared to 50 µl of beads incubated with lysosomes (3057 AU compared to 3341 AU). These differences could be due to biological variation between experiments in the fluorescence that the control lysosome blank gave. Beads incubated with 100 µl of lysosomes gave 66.2 % of the fluorescence from 100 µl of HRP lysosomes, and beads incubated with 200 µl of lysosomes gave 31.5 % of the fluorescence from 200 µl of HRP lysosomes. Despite increasing the incubation time from 30 min to overnight, the binding of HRP to the beads remained roughly 30 % of the total available HRP, which as in previous experiments, may be due to degradation of biotin from the HRP conjugate. This experiment also differed slightly to the previous experiment, where 100 µl of lysosomes was sufficient to saturate 20 µl of beads. Here, 200 µl of HRP-lysosomes were needed to almost saturate the control beads. This discrepancy was probably due to depletion of biotin-HRP from the FeDex media (biotin-HRP media was filtered and reused between experiments). Therefore, the reuse of media was kept to a minimum where possible.

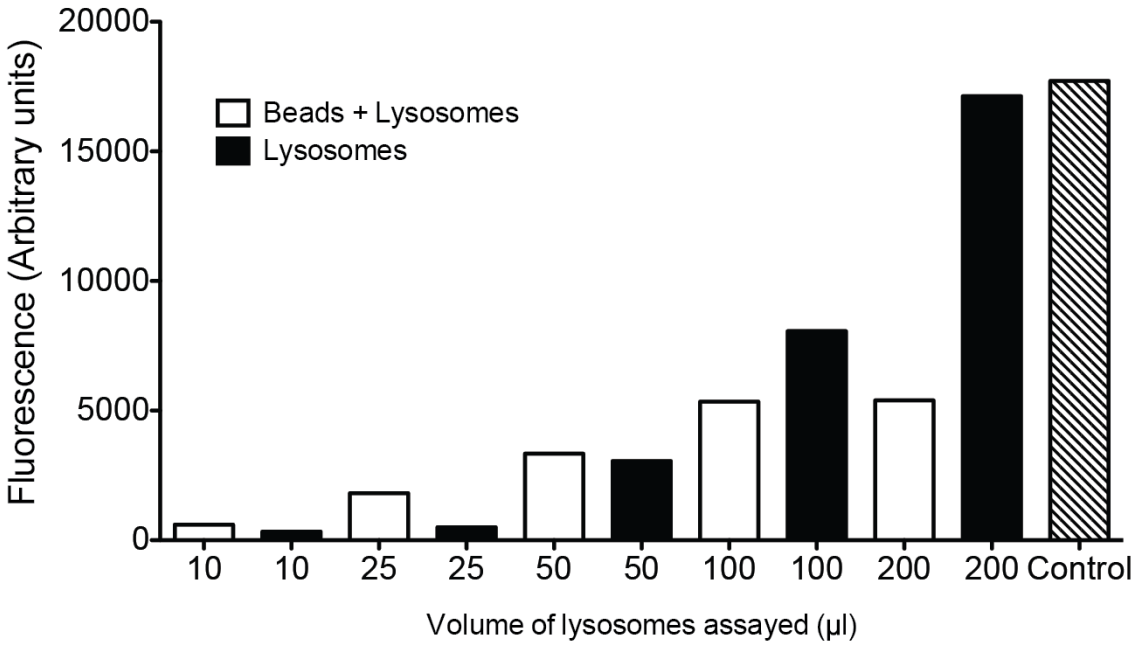

Fig. 3.30. Binding of biotin-HRP from lysosomes to beads overnight. Lysosomes were purified from J774.2 cells that were incubated with or without biotin-HRP. 20 µl of streptavidin beads were incubated overnight at 4ºC with, 10, 25, 50, 100 or 200 µl of control or HRP-containing lysosomes. The beads were then washed, and assayed for HRP activity using Amplex Red. For clarity, the fluorescence from non-HRP control lysosomes are omitted. 20 µl of beads saturated with biotin-HRP by incubation with 500 ng/ml HRP is shown (control; hatched bar). Data are fluorescence values after 10 min, taken while the fluorescence signal for all samples was still increasing (n=1).

This experiment was repeated a final time, with beads incubated with 100, 150, or 250 µl of HRP or control lysosomes overnight (Fig. 3.31). Similar to the previous two experiments, only 31.7 % (100 µl) and 34.3 % (150 µl) of the fluorescence signal was seen with beads incubated with lysosomes (250 µl of lysosomes were not assayed as this exceeded the volume of the 96 well plate). 150 µl of HRP lysosomes gave a fluorescence signal of 81.3 % of the saturated bead control. It is likely that 250 µl would have exceeded this. Taken together, these data suggest that some of the biotin-HRP may be degraded, or unable to bind to streptavidin beads after passing through lysosomes.

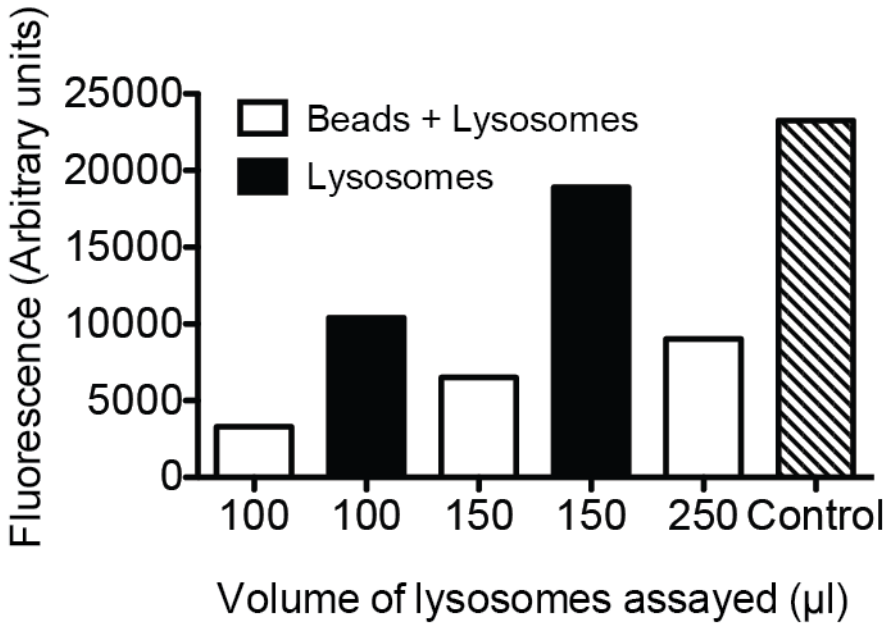

Fig. 3.31. Binding of biotin-HRP from lysosomes to streptavidin beads. Lysosomes were purified from J774.2 cells that were incubated with or without biotin-HRP. 20 µl of streptavidin beads were incubated overnight at 4ºC with 150, 150 or 250 µl of control or HRP-containing lysosomes. The beads were then washed, and assayed for HRP activity using Amplex Red. For clarity, the fluorescence from non-HRP control lysosomes are omitted. 20 µl of beads saturated with biotin-HRP by incubation with 500 ng/ml HRP is shown (control; hatched bar). Data are fluorescence values after 10 min, taken while the fluorescence signal for all samples was still increasing (n=1).

The aim of these experiments was to try and saturate 20 µl of beads with biotin-HRP, in order to have a set of conditions where control beads could be used to determine if the assay was set up optimally. The next experiment was to determine the volume of bead containing-phagosomes necessary to establish the volume of phagosomes saturated with biotin-HRP that gave a signal equal to that of 20 µl of beads saturated with HRP. This would then give a set of conditions under which there would be suitable volumes of both phagosomes and lysosomes, to maximise the potential of seeing a true fusion signal. Phagosomes were isolated using the standard protocol (MOI:3, approximately 14 x 10^6 cells) and resuspended in 100 µl of STM containing 0.1 % (v/v) TX-100. 5, 10, 20, 30, and 35 µl of phagosomes were incubated with a saturating amount of HRP (500 ng/ml) overnight (to maximise binding) and the HRP signal was measured using 150 µl of

Amplex Red (Fig. 3.32). An HRP signal was detected from all of the volumes of phagosomes used, which increased as more phagosomes were used. The fluorescence values (as a percentage of the control) were 1.96 %, 7.32 %, 15.8 %, 23.3 % and 23.7 % (from 5,10,20,40 and 35 µl of phagosomes, respectively). As these phagosomes were unblocked, the total amount of biotin-HRP that could bind to these volumes of phagosomes would drop further when biocytin was used (in the fusion assay). Therefore the volume of phagosomes needed to be increased to maximise the chance of seeing a fusion signal (given that blocked phagosomes would not participate in fusion reactions, and that fusion rates would likely be low). As approximately 100 µl of beads were used for each phagosome preparation (1 6-well plate) around 4 6-well plates worth of phagosomes would have been needed to give a signal equivalent to that of the saturated bead control.

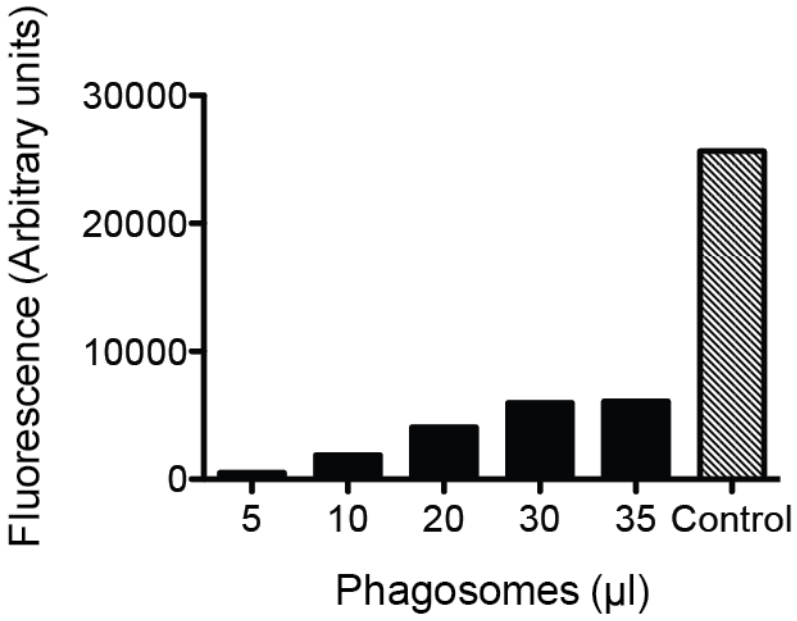

Fig. 3.32. Saturating streptavidin bead-phagosomes with biotin-HRP. Streptavidin bead-containing phagosomes were purified from approximately 14 x 10^6 J774.2 cells as described previously. Phagosomes were isolated and resuspended in 100 µl of STM containing 0.1 % (v/v) TX-100. 5, 10, 20, 30, and 35 µl of phagosomes were incubated with a saturating amount of biotin-HRP (500 ng/ml) overnight (to maximise binding). The beads were washed and the amount of biotin-HRP bound to the beads was determined using Amplex Red. As a control, 20 µl of beads saturated with biotin-HRP were also assayed (control; hatched bar). Data are the fluorescence values of samples after 25 min, at which point the fluorescence signals were still increasing (n=1).

Previous experiments sought to determine the volumes of lysosomes and phagosomes to use in the fusion assay, so that neither component was limiting. Around 100 µl of lysosomes were found to have enough biotin-HRP to produce a strong signal, but only 1/3rd of this was able to bind to beads. However, if this 1/3rd was enough to saturate beads, then the signal would be high enough. Therefore, biotin-HRP lysosomes were then mixed with an increased volume of phagosomes in a mixing assay, to determine how much lysosomal biotin-HRP could be transferred to phagosomes (Fig. 3.33). Phagosomes were purified from 4 x 6-well plates of J774.2 cells (approximately 350 µl of beads). 50 % of the sample was incubated in STM, and the remaining 50 % was incubated in STM containing 500 ng/ml biocytin, to block phagosomes and determine how much of the binding capacity of the phagosomes would drop when used in the fusion assay. The phagosomes were then resuspended in 175 µl of STM containing 0.1 % (v/v) T X-100 (to lyse organelle membranes), and 25 µl, 50 µl and 100 µl of phagosomes were then incubated with biotin-HRP lysosomes (25 µl, 100 µl and 200 µl, respectively), overnight at 4 ºC. The beads were recovered on a magnet, washed three times with RIPA buffer, and assayed with 150 µl of Amplex Red. As a control, 20 µl of HRP saturated beads were also assayed, as were the same volumes of lysosomes used in the mixing assay. 25 µl, 100 µl, and 200 µl of lysosomes gave fluorescence signals that were 8 %, 28 % and 78 % of the control, respectively. This was in agreement with previous experiments. 25 µl of blocked phagosomes gave no fluorescence signal, whereas 25 µl of unblocked phagosomes gave 3 % of the total possible signal (from 25 µl of lysosomes). 100 µl of unblocked phagosomes gave 0.4 % of the signal from 100 µl of lysosomes, whereas blocked phagosomes gave 7.1 %. The fact that blocked phagosomes gave a higher signal indicates that these data are likely to be the result of random variation, and are not actually the result of the transfer of biotin-HRP to the beads. However, 100 µl of blocked phagosomes gave 1.6 % of the signal from 200 µl of lysosomes, which rose to 3.7 % when phagosomes were not blocked, suggesting the latency of this preparation was low (43 %). These results also indicate that the overall capacity of phagosomes to bind biotin-HRP was very low meaning a very large number of beads would be needed for each experiment, which would be prohibitively expensive. One way to improve the binding capacity of a phagosome preparation would be to increase the uptake of beads. As seen previously, this could be achieved by increasing the MOI, but this required yet more beads.

Alternatively, the beads could be opsonised with immunoglobulin, to try and improve the uptake of beads.

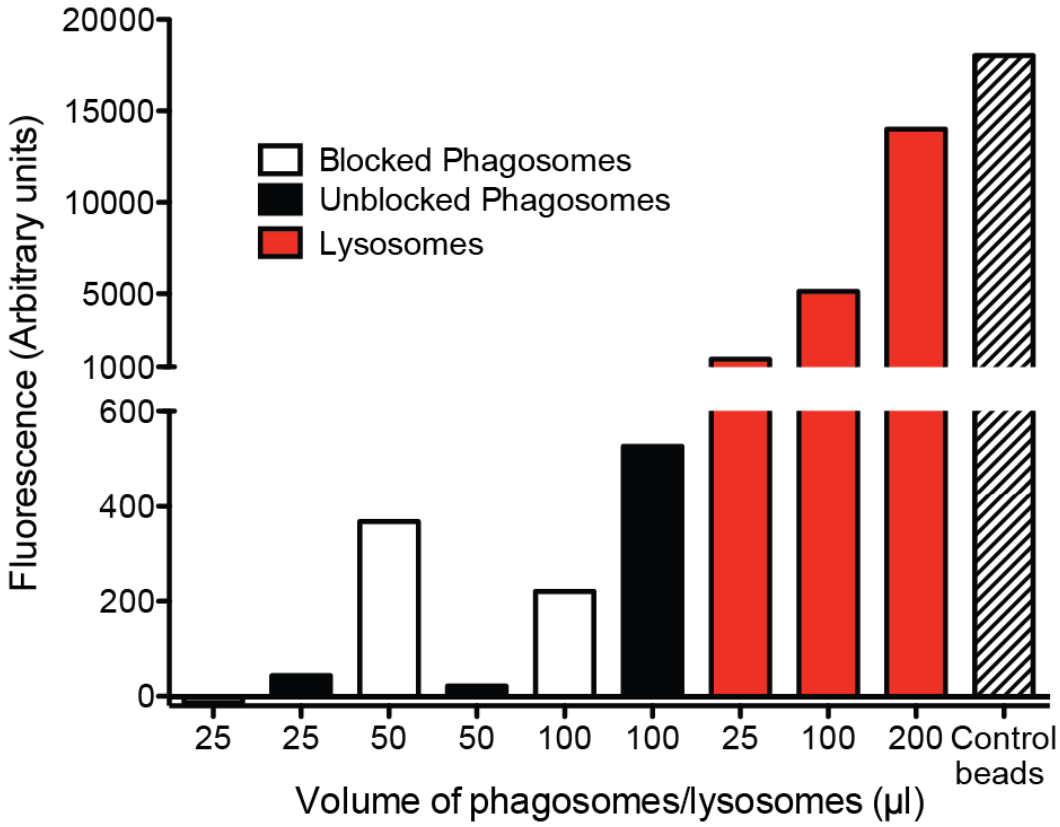

Fig. 3.33. Phagosome-lysosome mixing *in vitro.* Streptavidin bead phagosomes were purified from four 6 well plates of J774.2 cells (MOI of 3 approximately 18 x 10^6 cells per plate). Briefly, beads were centrifuged onto cells at *50 x g* for 5 min followed by a 55 min incubation at 37 ºC to allow bead uptake. Cells were then washed three times to remove unbound beads, and chased for a further 1 h at 37 ºC. Phagosomes were the released from cells by ball-bearing homogenisation and purified (as previously described). One half of the phagosomes were incubated with STM containing 500 ng/ml biocytin (blocked phagosomes) and the other half in STM alone (unblocked phagosomes) for 30 min. Each set of phagosomes were washed once more in STM and resuspended in 175 µl of STM. Biotin-HRP lysosomes were purified from cells as previously described. The lysosomes were eluted into 1 ml of STM, and Triton X-100 added to a final concentration of 0.1 % (v/v). The indicated volumes of phagosomes (25 µl, 50 µl and 100 µl) were then incubated with biotin-HRP lysosomes (25 µl, 100 µl and 200 µl, respectively), overnight at 4 ºC. The beads were recovered, and the captured biotin-HRP assayed using 150 µl of Amplex Red. 25 µl, 100 µl, and 200 µl of HRP-lysosomes were also assayed. 20 µl of beads saturated with HRP were assayed as a control (hatched bar). Data are fluorescence signals after 25 min, at a point where fluorescence values were still increasing (n=1).

To try and increase the uptake of beads and number of phagosomes recovered, beads were opsonised with mouse immunoglobulin before centrifuging onto cells (Fig. 3.34). 100 µl of beads were incubated with 490 µl of mouse IgG in PBS, overnight at 4 ºC to coat the beads in IgG. 100 µl of beads incubated with PBS were used as a control. Secondly, the protocol was altered slightly to try and increase bead uptake further. Bead uptake was performed for 1 h at 37 ºC, and the cells washed three times to remove unbound beads. For this experiment, it was accepted that the resulting phagosomes would be different to those previously characterised in section 3.7. The cells were then cultured for a further hour, and the resulting phagosomes were isolated as previously described. Half of the phagosomes were incubated with 500 ng/ml of biocytin for 30 min at room temperature. The phagosomes were then incubated overnight at 4 º C with 500 ng/ml biotin-HRP in STM containing 0.1 % (v/v) T-X100 to lyse phagosomal membranes, and allow binding of biotin-HRP. The beads were washed and then assayed for bound HRP.

The fluorescence signal after 10 min from phagosomes from non-opsonised beads was approximately 5389 (PBS, - biocytin) and 2481 (PBS, + biocytin) compared to 11,097 AU (IgG, - biocytin) and 4,777 AU (IgG, + biocytin), for opsonised beads. In both cases, blocking the bead-phagosomes with biocytin before incubation with HRP, led to a reduction in fluorescence (46 % for non-opsonised beads, and 43 % for opsonised beads). This indicated that not all the phagosomes were intact. The non-opsonised beads had 13.4 % and 29 % (+/- biocytin respectively) of the fluorescence of the control beads, and which increased to 25.7 % and 59.7 % for opsonised beads. Thus, opsonisation appeared to increase bead internalisation resulting in a 50 % increase in the amount of phagosomes recovered that could participate in the fusion assay. There are many different ligands and receptors involved in phagocytosis (Kwiatkowska and Sobota, 1999), and internalisation of pathogens occurs through a heterogeneous set of mechanisms (Aderem and Underhill, 1999). Thus not all phagosomes are created equally. It should be noted that altering the pulse and chase time of the phagosomes, is likely to result in a change in their composition, especially when using opsonised beads which would become phagocytosed through a different set of molecular mechanisms to particles not internalised via Fc receptors (Vieira et al., 2002). However, for the fusion assay, it was deemed more important to demonstrate that it could work, and

that fusion could be detected. The phagosome protocol could then be further optimised to purify phagosomes at earlier stages, or characterise the phagosomes produced when beads were opsonised and chased for a longer period of time.

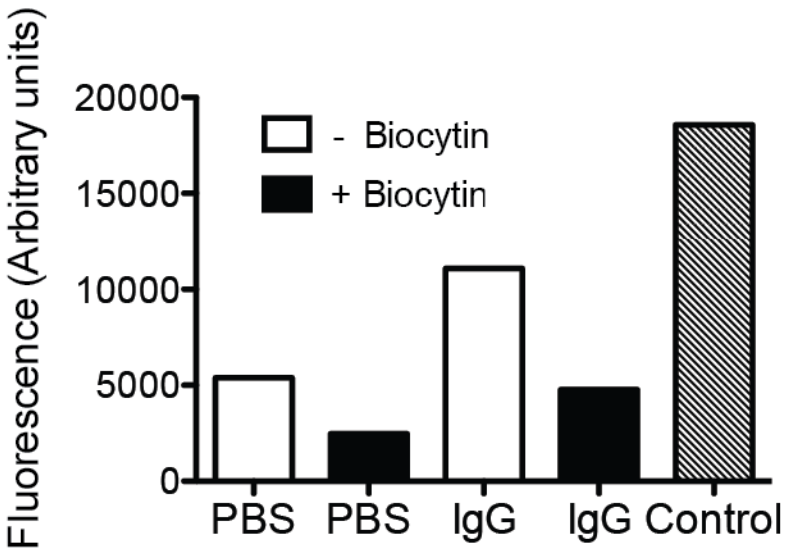

Fig. 3.34. The effect of opsonisation on bead uptake and phagosome recovery. Streptavidin beads were incubated in PBS or 5 mg/ml mouse IgG in PBS overnight at 4 ºC. Beads were then centrifuged onto J774.2 cells to promote uptake, and were cultured for 1 h at 37 ºC to allow bead binding and internalisation. Cells were washed briefly to remove unbound beads, and cultured for a further 1 h. Bead-containing phagosomes were purified from cells as previously described, and incubated in 0.5 ml of STM (- Biocytin) or STM containing 500 ng/ml biocytin (+ Biocytin). Phagosomes were then washed three times with STM, and incubated overnight at 4 ºC in STM containing 0.1 % (v/v) Triton X-100, and 500 ng/ml biotin-HRP. The beads were then recovered, washed, and bound HRP assayed using Amplex Red reagent. 20 µl of beads were saturated with 500 ng/ml biotin-HRP were also assayed as a control (hatched bar). Data are fluorescence signals after 10 min, at a point where fluorescence values were still increasing (n=1).

3.3.3.7 Fusion of lysosomes and phagosomes in vitro

These experiments had been performed to demonstrate that fusion of lysosomes and phagosomes *in* vitro was feasible. Biotin-HRP from lysosomes was detectable using Amplex Red reagent and could bind to phagosomes isolated from cells. The binding of biotin-HRP could be blocked with biocytin and the amount of lysosomes and phagosomes needed to maximise the potential to see a fusion signal was also investigated. The next step was to combine these experiments into a full fusion assay. Previous fusion assays described the requirement of cytosol for fusion to occur (Jahraus et al., 1998, Mullock et al., 1998). Cytosol was isolated from pig brain as described in section 3.12.2. Briefly, 4 g of pig brain (finely minced) was homogenised in a Potter-Elvehjem homogeniser in 3 ml of ice cold STKM (250 mM sucrose, 25 mM KCl, 1 mM $MgCl_2$, 10 mM TES, pH 7.4). The lysate was centrifuged at *104,000 x g* for 15 min at 4 ºC. To demonstrate an energy requirement for the fusion assay, the cytosol was depleted of ATP and GTP by passing the lysate through a PD10 de-salting column. The cytosol was eluted from the column with 4 ml of ice cold STKM and snap frozen in liquid nitrogen, before storage at – 80 ºC. The protein concentration of cytosol used for the fusion assay was 4.25 mg/ml.

Biotin-HRP lysosomes were purified from four 10 cm tissue culture dishes of cells as previously described, but were eluted from the cell column using 1 ml of pig brain cytosol. Phagosomes were isolated as previously described, with some changes. Briefly, 800 µl of beads were opsonised in 5 mg/ml mouse IgG in PBS overnight at 4 ºC. 100 µl of beads was then centrifuged onto cells of a 6 well plate (8 in total) and the cells were then cultured at 37 ºC for 1 h. After washing to remove unbound beads, the cells were cultured for a further hour to allow internalisation and phagosome maturation. The cells were then resuspended in 8 ml of ice cold STM and homogenised using a ball-bearing homogeniser as previously described. Phagosomes were washed three times in STM and resuspended in a final volume of 1 ml of pig brain cytosol. The fusion assay was then set up in duplicate as follows: All reactions were set up in 0.5 ml Eppendorf tubes on ice. 60 µl of phagosomes were added to each tube, followed by either 60 µl of 2000 ng/ml biocytin in STKM (500 ng/ml final concentration) or PBS. 60 µl of biotin-HRP lysosomes were added next, and finally 60 µl of an energy

regenerating system (per 25 µl: 2.5 µl ATP (50mM), 2.5 µl GTP (50 mM), 10 µl of creatine kinase (4 mg/ml in PBS stock), 10 µl of creatine phosphate (261.2 mg/ml in PBS stock). The fusion assay was assembled as per table 3.1, the tubes gently vortexed, and then incubated for 90 min at 37 ºC in a water bath, or on ice. After 90 min, the tubes were placed on ice and 240 µl of 2X RIPA buffer (0.4 % (v/v) NP-40, 2 % (v/v) TX-100, 2 % (w/v) deoxycholate, 300 mM NaCl, 100 mM Tris, pH 7.5, plus protease inhibitors) was added. The tubes were incubated on ice for 15 min, and then washed three times with 1 x RIPA buffer. The beads were then resuspended in 100 µl of RIPA buffer and assayed with 150 µl of Amplex Red (Fig. 3.35). The following controls were also set up: 20 µl of beads and 60 µl of phagosomes were incubated with 0.5 ml of 500 ng/ml biotin-HRP in STM. 60 µl of biotin-HRP lysosomes were also assayed to give the maximum obtainable signal obtainable from the lysosomes. 60 µl of cytosol was also assayed, as it had previously been seen that pig brain cytosol reacts with Amplex Red to give a strong fluorescence signal (data not shown).

4 ºC + Biocytin	37 ºC + Biocytin	37 ºC - Biocytin
1. Phagosomes Lysosomes - ATP	3. Phagosomes Lysosomes - ATP	5. Phagosomes Lysosomes - ATP
2. Phagosomes Lysosomes + ATP	4. Phagosomes Lysosomes + ATP	6. Phagosomes Lysosomes + ATP

Table 3.1. Components of the *in vitro* lysosome-phagosome fusion assay. The fusion assay was assembled on ice as per the table above. 60 µl of phagosomes were added to each tube, followed by 60 µl of 2000 ng/ml biocytin in STKM (500 ng/ml final concentration) or PBS. 60 µl of biotin-HRP lysosomes were added next, and finally 60 µl of an energy regenerating system or PBS, was added where appropriate to give a final volume of 240 µl.

The total obtainable fusion signal was represented by conditions 5 & 6 (37 ºC no biocytin), as without biocytin, there should be maximal binding of biotin-HRP from lysosomes to the streptavidin beads. Moreover, conditions 5 & 6 should have the same levels of HRP activity. This would then be followed by 3 & 4 (37 ºC + biocytin) which would be the signal from fusion of phagosome and lysosomes. Lastly, conditions 1 & 2 (4 ºC + biocytin), would represent the background signal. Thus, 5 & 6 should always be higher than 3 & 4, which should be higher than 1 & 2 if fusion has occurred. In all cases, the fluorescence signal was above the background, but was very low (127 to 418 AU) when compared to the highest obtainable signal (100 % fusion, represented by the phagosomes + HRP control), which was approximately 18,900 AU. The highest to lowest fluorescent signals were as follows; 3,5,1,4,6,2. The low signals and the fact that the control conditions (5 & 6) did not yield a signal suggested that the signals were just background noise and no fusion or HRP binding had occurred. The phagosome + HRP control gave a large fluorescence signal almost equal to that of the 20 µl HRP-saturated control (18,900 AU compared to 23,700 AU). This indicated that the phagosomes used in the assay were still capable of binding biotin-HRP, and that the HRP binding capacity of the phagosomes used in the assay was large. The lysosome signal (with pig brain cytosol signal subtracted as a blank) was much lower than expected, possibly as a result of biotin-HRP degradation in lysosomes. However, there was still a reasonable signal (6,090 AU), and even if the fusion rate was only 10 % (600 AU), then this should still have been observable. These data are confusing, as even in the absence of any fusion signal whatsoever, the lysis of phagosomes and biotin-HRP lysosomes in the absence of any biocytin to block binding (conditions 5 & 6) should have resulted in the binding of HRP to the beads. The lack of any such signal suggested that something in the assay was possibly inhibiting the binding of HRP to the beads. This could have been temperature but previous experiments had demonstrated that biotin-HRP could be transferred to beads at 4 ºC and besides, conditions 5 & 6 were incubated at 37 ºC. The other possibility was that the cytosol used for the fusion assay somehow interfered with the binding of biotin-HRP to the beads. Thus, this was subsequently investigated to see if this was the cause of the problem.

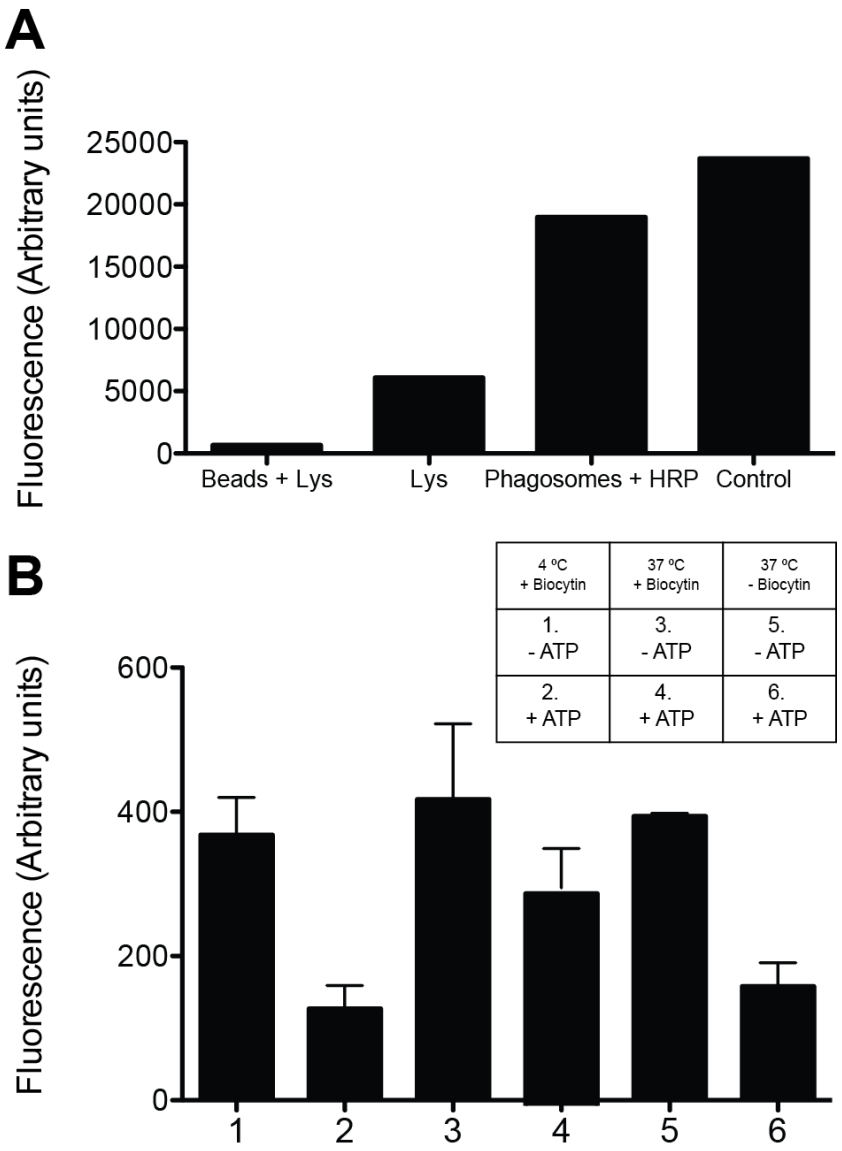

Fig. 3.35. Characterisation of *in vitro* lysosomes-phagosome fusion assay. The transfer of biotin-HRP from lysosomes to streptavidin bead containing-phagosomes was monitored in an *in vitro* lysosome-phagosome fusion assay. The assay was assembled as per table 3.1. Fusion was allowed to proceed on ice or at 37 ºC for 90 min before the tubes were placed on ice. An equal volume of 2X RIPA buffer was added to each tube and samples were incubated on ice for 15 min. The beads were then recovered, washed three times with 1X RIPA buffer and the amount of bound HRP (as a measure of fusion) was determined by Amplex Red assay. The following controls were also included (**A**). 20 µl of beads saturated with biotin-HRP (Control), 60 µl of biotin-HRP lysosomes (Lys) 20 µl of beads incubated with 60 µl of biotin-HRP lysosomes (Beads + Lys) and 60 µl of phagosomes incubated with biotin-HRP (Phagosomes + HRP). **B** shows the fluorescence signals from the different conditions used in the fusion assay. Data are means of duplicates ± the range. Data are fluorescence values after 20 min at a point when the fluorescence of each sample was still increasing (n=1).

3.3.3.8 Pig brain cytosol interferes with biotin-HRP binding to beads

The previous data were puzzling, as in the controls used for the fusion assay, the transfer of biotin-HRP to beads was prevented. A key difference in the fusion assay experiment (Fig. 3.35) compared to the mixing assay (Fig. 3.24), was that it was carried out in the presence of pig brain (PB) cytosol, which may have interfered with binding. This was then investigated. 20 µl of beads were incubated with or without biocytin for 30 min to give blocked and unblocked beads. These beads were then incubated in either STM, J774.2 cytosol, or PB cytosol, for 30 min at room temperature. Both J774.2 and PB cytosol were normalised to protein concentration and were used at the same concentration as in the fusion assay (4.25 mg/ml). The beads were then extensively washed and incubated with 0.5 ml of 500 ng/ml biotin-HRP for 30 min at room temperature. The beads were washed again and the bound HRP assayed using Amplex Red (Fig. 3.36).

The total amount of fluorescence in the saturated bead control after 10 min was 27,266 AU. The total fluorescence seen with 20 µl of (unblocked) beads was 20,020 AU (73 %) of this, most likely representing loss of beads from the multiple washing steps (control beads were only subjected to a single round of washes). Thus, in this case, it is more appropriate to use the (unblocked) beads sample as a control for the total signal possible. When blocked beads were incubated with J774.2 cytosol, or PB cytosol the fluorescence signal was low (1061 AU and 801 AU) and comparable to that of blocked beads (820 AU). This suggests that pre – blocked beads incubated in cytosol do not give an appreciable fluorescence signal. Unblocked beads incubated with J774.2 cytosol and then biotin-HRP gave a fluorescence signal of 21,255 AU (106 % of the unblocked beads sample, or 78 % of the control beads). In contrast, unblocked beads incubated with PB cytosol and then biotin-HRP gave a fluorescence signal of 12,288 AU (61 % of the unblocked beads sample, or 45 % of the control beads). 120 µl of J774.2 and PB cytosol were also assayed, as 120 µl was the volume of cytosol used in the fusion assay. J774.2 cytosol gave a fluorescence signal of 1091, compared to 9582 AU for PB cytosol. The J774.2 cytosol was slightly above that of the background signal (blocked beads 801 AU) but the PB cytosol gave a clear signal. These data suggest that i) a factor in pig brain cytosol (but not in J774.2 cytosol of the same protein concentration) blocks binding of biotin-HRP to beads and ii) pig brain

cytosol reacts with Amplex Red reagent, and J774.2 cytosol does not. Thus, this could explain why no binding of biotin-HRP was seen the in the fusion assay control conditions.

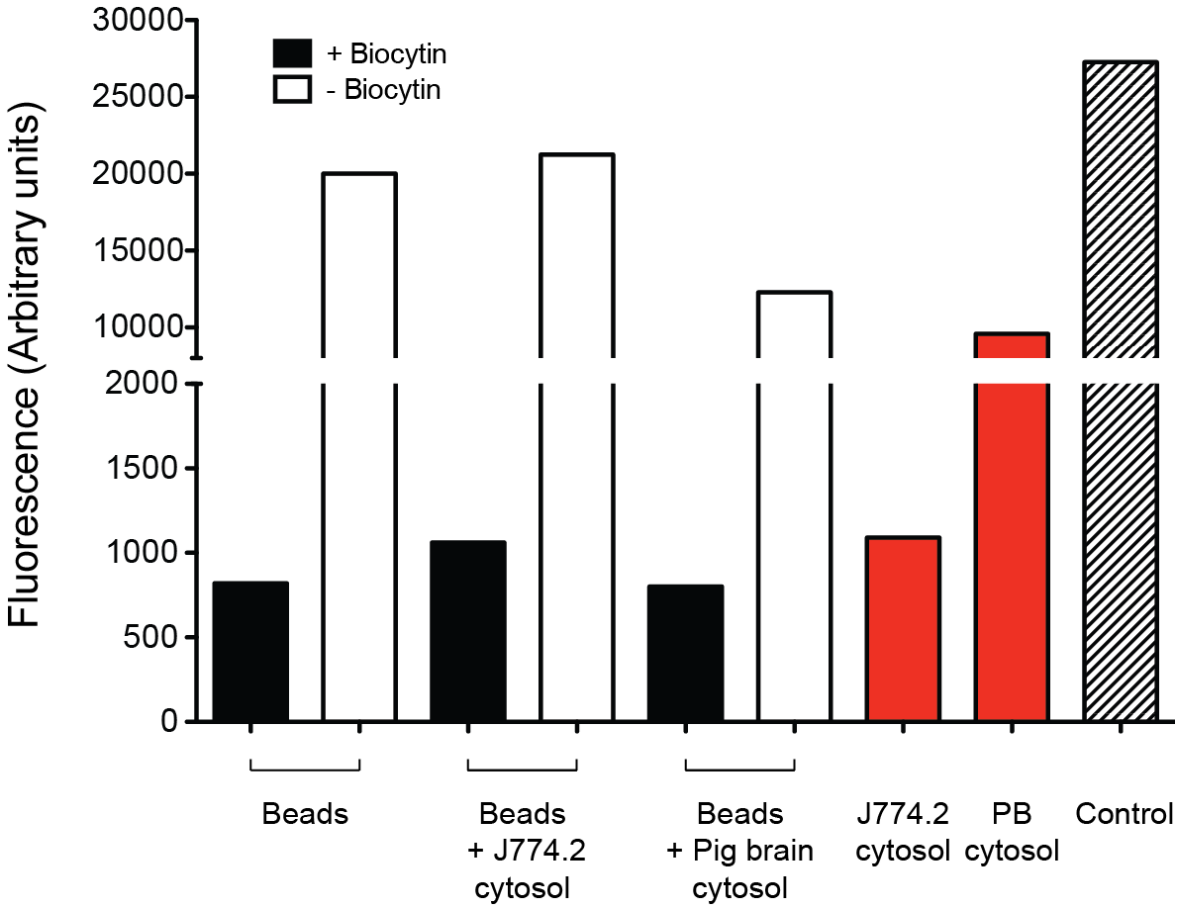

Fig. 3.36. Pig brain cytosol interferes with biotin-HRP binding with streptavidin beads. 20 µl of streptavidin beads were incubated in either 0.5 ml of STM or 0.5 ml of STM containing biocytin at 500 ng/ml. The beads were washed three times with STM and incubated in either 0.5 ml of STM, J774.2 cytosol (4.25 mg/ml) or pig brain (PB) cytosol (4.25 mg/ml) for 30 min at room temperature. The beads were washed three times with STM, and incubated with 0.5 ml of STM containing biotin-HRP at a final concentration of 500 ng/ml, for 30 min at room temperature. The beads were washed three times with RIPA buffer and bound HRP assayed using Amplex Red. 120 µl of J774.2 or PB cytosol were also assayed (red bars). 20 µl of beads saturated with HRP were included as a control (hatched bar). Data are fluorescence values after 10 min at a point when the fluorescence of each sample was still increasing (n=1).

3.3.4 Phagosome-lysosome fusion - Discussion

3.3.4.1 Principle of the fusion assay

For the fusion assay, it was necessary to have a suitable system to report the fusion of phagosomes and lysosomes. The principle of the assay was to measure the transfer of one marker to another, as a quantification of vesicle fusion. Other assays based up confocal microscopy report vesicle fusion as having occurred when separate fluorescent markers present in the two organelles co-localise (Becken et al., 2010). However, this method cannot distinguish between two vesicles that have fused, tethered, or are just within close proximity to one another. This is because the resolution of the light microscope is 200-350 nm, in that range. Alternatively, the colocalisation of the two markers could be monitored by FRET (Förester resonance energy transfer), to measure the transfer of energy from an excited donor fluorophor to another acceptor molecule. This is an attractive method, as the maximum distance over which FRET can occur is approximately 10 nm (Stryer, 1978). This would therefore allow the distinction between real fusion events and vesicle tethering. However, this method requires that the fluorphores remain intact after delivery to the lysosome and phagosomes. It can also be pH sensitive, which could be a potential problem due to the low pH of the lysosome, and the change in pH when vesicles fuse. However, this approach has been successfully used to study retrograde transport of molecules from lysosomes to late endosomes *in vivo* (Kaufmann et al., 2009). This method would also require the use of a confocal microscope, which would increase the cost of the assay. Using a simple enzyme-based assay that can be measured in a plate reader significantly reduces the costs associated with performing multiple experiments.

Horseradish peroxidase is widely used enzyme that uses hydrogen peroxide to oxidise a wide variety of substrates (Veitch, 2004). One potential problem with delivering compounds to the lysosome is that they are exposed to the low pH and hydrolytic enzymes which may degrade them. Horseradish peroxidase (HRP) however, is relatively resistant to lysosomal degradation (Graham and Rickwood, 1997). Moreover, biotin-conjugated HRP binds extremely strongly to streptavidin beads due to the high affinity interaction between these two molecules (biotin-

streptavidin K_d ~ 10^{-14} M, (Dundas et al., 2013), making it a suitable system to report vesicle fusion. Moreover, biotin-avidin binding has been successfully used in other fusion assays (Jahraus et al., 1998, Mullock et al., 1998, Mullock et al., 1994).

The purification of biotin-HRP containing lysosomes using superparamagnetic iron particles was shown to be a viable method of lysosome purification (Fig. 3.23) While it is possible that the toxic effects of iron accumulation could result in lysosomal damage, this method has previously been used to purify lysosomes for use in a fusion assay (Becken et al., 2010). As discussed previously, the choice of system for phagosome purification such as an inert latex bead, or a heat-killed bacterium, would influence the properties of the resulting phagosome. For example, the receptors and pathways used to internalise a large particle (such as a 3 μm magnetic bead) are likely to differ slightly from those used to phagocytose a opsonised bacterium. This may result in different maturation rates, phagosome compositions and differences in the ability to fuse with other endocytic compartments. However, the molecular machinery needed for vesicle fusion would remain the same. For this assay, magnetic beads were chosen due to their ease of purification from a cell lysate. This method requires no centrifugation steps on gradients (as with latex beads), and is very rapid – phagosomes are simply resuspended in a wash buffer multiple times, and can easily be transferred from one buffer to another. These phagosomes were also characterised by western blotting and were shown to have late endocytic and lysosomal markers, as well as increased lysosomal enzyme activity. Therefore, the components of the fusion assay were sufficiently characterised and purified, to begin to assemble the complete assay.

3.3.4.2 Biotin-HRP from lysosomes could be detected using Amplex Red

While lysosomes were easily purified, it was not clear whether biotin-HRP could be detected after passing through lysosomes. Thus, purified lysosomes were tested to determine whether Amplex Red was sensitive enough to detect HRP activity (Fig. 3.23). Indeed, a fluorescence signal was seen when biotin-HRP lysosomes were incubated with Amplex Red, indicating that sufficient biotin-HRP remained non-degraded to give a signal. Control lysosomes did not produce a fluorescence

signal. This indicates that the fluorescence was a direct result of HRP activity, and not endogenous activity from lysosomal enzymes. Additionally, lysosomal material does not autofluoresce at the wavelengths used in the assay. The lowest volume of lysosomes where an increase in fluorescence was seen was 0.2 µl, which was 1/500th of the total volume of lysosomes purified. Thus, Amplex Red could be used to detect very low amounts of HRP activity from purified lysosomes.

3.3.4.3 Biotin-HRP from lysosomes can still bind to beads from phagosomes

Although biotin-HRP activity could be detected in purified lysosomes it was necessary to check biotin-HRP could still bind to streptavidin beads after they had passed through cells. Both the biotin and streptavidin had the potential to be degraded and unable to bind each other. To test this, phagosomes and lysosomes were mixed together in the presence of detergent to lyse lipid membranes and allow biotin-HRP to bind to the beads (Fig. 3.24). HRP activity was detected on phagosome beads after 15 min of mixing. The binding of HRP was also blocked by the addition of biocytin. Approximately 12.5 µl of phagosomes was the lowest volume where the fluorescence signal was sufficient such that if the total vesicle fusion was only 10 % of the maximum possible, a fluorescence signal could still be detected above the background noise. This experiment used 100 µl of beads, but it was not known how this related to the final amount of phagosomes purified (as beads were lost during washes, or were not released from the cells during homogenisation).

3.3.4.4 Binding of biotin-HRP to beads was blocked by biocytin

The fusion assay needed to distinguish between actual fusion of intact organelles, and the mixing of contents from damaged lysosomes and phagosomes. The assay was performed in the presence of saturating amounts of biocytin (biotinylated lysine), which would bind to streptavidin beads and prevent biotin-streptavidin interactions outside of an intact membrane This would reduce the overall possible signal that could be seen, but also reduce the background noise of the assay. Importantly, biocytin is not membrane permeable (due to the presence of a charged lysine group), and should only block the binding of biotin-HRP on phagosomes without an intact membrane. Biocytin was titrated to determine at

what concentration it prevented the binding of biotin-HRP to streptavidin beads. The binding of biotin-HRP to beads was dose dependent, and was determined to be 500 ng/ml (Fig. 3.25).

3.3.4.5 J774.2 cell lysate does not react with Amplex Red

Phagosome beads were released from J774.2 cells from by ball-bearing homogenisation and isolated from the cell lysate on a magnet. Any endogenous material that was non-specifically bound to the beads may have oxidised Amplex Red to give a false fluorescence signal. When a J774.2 cell lysate was incubated with Amplex Red to test this, no fluorescence signal was observed (Fig. 3.26). These data along with the previous experiments suggested that any change in fluorescence was only due to the presence of biotin-HRP alone.

3.3.4.6 Optimising the amount of lysosomes and phagosomes used in the fusion assay

While it was clear that both markers could still bind after passing through cells, the amounts to use in the fusion assay needed to be optimised to ensure that neither was limiting. To help with this, an arbitrary volume of beads (20 µl) were used as a control to determine a set of conditions under which neither biotin-HRP lysosomes nor phagosome beads were limiting. The rationale behind this was as follows: 20 µl of beads were incubated with biotin-HRP (not from lysosomes), until a point was reached where no more HRP could bind, and the availability of Amplex Red reagent was not limiting. This would then be a standard control for all further experiments, to show the maximum fluorescence signal from 20 µl of beads. Next, increasing volumes of biotin-HRP lysosomes were incubated with 20 µl of beads until the beads were saturated with HRP. This would give the conditions necessary to saturate beads with HRP from lysosomes. Next, increasing volumes of phagosomes would be incubated with biotin-HRP lysosomes, to determine the volume of phagosomes that corresponded to 20 µl of beads. This would then result in a set of conditions under which there was sufficient biotin-HRP and phagosomes capable of binding the majority of the HRP, to maximise the chance of seeing phagosome-lysosome fusion.

20 µl of beads were saturated with biotin-HRP when used at 500 ng/ml, and 150 µl of Amplex Red reagent was deemed sufficient to not be a limiting factor. When biotin-HRP lysosomes were used to try and saturate 20 µl of beads only approximately 35 % of the total possible fluorescence signal was obtained from beads (Fig. 3.29-3.31), indicating that a large proportion was unable to bind to the beads, possibly due to partial degradation of biotin-HRP. It remains to be seen whether inhibiting lysosomal enzymes (through the use of inhibitors such as leupeptin) would protect biotin-HRP from degradation and result in higher binding to phagosomes. Overall, around 100-250 µl of purified biotin-HRP lysosomes (from a total of 1 ml) was deemed to be a reasonable balance between sufficient signal, and having enough sample for duplicates over a range of experimental conditions tested.

Next, the volume of phagosomes needed was investigated. Approximately 100 µl of beads were used per 6 well plate of J774.2 cells (MOI:3) to purify phagosomes. While 100 µl of beads would be able to bind a significant amount of biotin-HRP, it was not known how the volume of phagosomes related to this. Unbound beads were lost when cells were washed and some cells likely remained intact. Furthermore, extracellular beads and damaged phagosomes were blocked with biocytin, meaning that amount of intact phagosomes recovered would not be the same as the starting volume of beads. However, the amount of viable phagosomes was extremely low, as the phagosomes purified from 100 µl of beads only bound 1.6 % of the total lysosomal biotin-HRP (Fig. 3.33). To improve upon this, beads were opsonised and the pulse and chase time increased to a total of 2 h (1 h pulse, 1 h chase). Although this would alter the characteristic of the phagosome preparation, it was deemed more important to first establish a working assay. This increased the amount of biotin-HRP that the phagosomes could bind to 25 % of the total (Fig. 3.34). Thus, the biggest limiting factor appeared to be the phagosomes. In an attempt to get a working fusion assay, it was decided to proceed with the fusion assay based upon the results of these experiments.

3.3.4.7 Fusion of lysosomes and phagosomes *in vitro*

The fusion assay was set up using conditions to demonstrate a requirement for physiological temperature and energy. An internal control was included, that had lysosomes, phagosomes, and either an energy regenerating system, or PBS without the addition of biocytin (table 3.1 conditions 5 & 6). This was incubated at either 4 ºC or 37 ºC. The lack of biocytin meant that upon the addition of RIPA buffer, biotin-HRP from lysosomes would have been free to bind to the beads. Therefore the highest fluorescent signal should have been seen with conditions 5 & 6. Even in the absence of any fusion, HRP should have been detected in these samples, and the fluorescence should have been higher than all other samples. As no fluorescence was observed, it suggested that there was a fundamental problem with the assay that prevented any biotin-HRP binding to the phagosome beads, even in the absence of biocytin. This is confirmed by fact that the phagosomes were capable of binding biotin-HRP, and that the HRP-lysosomes yielded a fluorescence signal when assayed. Moreover, the binding capacity of the phagosomes was much greater than in previous experiments. If the phagosomes had a very low latency, or the phagosomes were not released from cells properly, then this could account for the lack of a signal although this is unlikely. Therefore, it is unclear why no fusion signal was seen. Fusion reactions were lysed with RIPA buffer at 4 ºC for 15 min. It is possible that this time was insufficient to see transfer of biotin-HRP to beads in control conditions. However, previous optimisation experiments have showed binding of biotin-HRP at 4 ºC within 30 min, suggesting that at least some biotin-HRP should bind. One change to the protocol was that it was performed in the presence of pig brain cytosol, as cytosol had previously been shown to be necessary for vesicle fusion *in vitro* (Mullock et al., 1989, Becken et al., 2010, Mullock et al., 1998, Ward et al., 1997). When the cytosol was assayed with Amplex Red, it gave a high fluorescent signal (data not shown). However, it was concluded that this should not have been a problem for the fusion assay, as it would be removed with multiple washes after the beads were recovered. Additionally, using cytosol to elute lysosomes from the cell column and resuspend phagosomes after washing, could have conceivably enhanced fusion, by allowing the formation of molecular complexes that are required for vesicle fusion

One possibility to determine whether or not vesicle fusion had occurred and not been reported, would be to examine the ultrastructure of the organelles before and after fusion had occurred. The interactions of endocytic organelles and phagosomes has been previous investigated by electron microscopy (Jahraus et al., 1998, Mayorga et al., 1991, Duclos et al., 2000). As FeDex would be particularly electron dense, it may have been possible to see the transfer of FeDex to phagosomes, which would be readily identifiable. This could be used to confirm whether fusion of phagosomes and lysosomes had occurred but the transfer of biotin-HRP to the beads had not.

Phagosomes and lysosomes were mixed together to allow fusion to proceed for 90 min to maximise the amount of fusion. Previous cell-free assays report fusion of phagosomes and endosomes/lysosomes as early as 10 min (Mayorga et al., 1991), and late endosomes and lysosomes after 10 min (Mullock et al., 1998). Alternatively, fusion reactions were allowed to proceed for up to 80 min (Jahraus et al., 1998) but have also been reported to reach a plateau after 40 min (Becken et al., 2010). Had a reproducible fusion signal been detected, the length of time could have been varied to investigate the rate at which fusion occurred. The minimum time needed to see a fusion signal, and the time at which no further fusion occurred could also be studied.

3.3.4.8 Pig brain cytosol may have interfered with vesicle fusion

One source of error could be the possibility of endogenous biotin present in the brain cytosol. Biotin in rat brain may give false-positive results with streptavidin-biotin assays (McKay et al., 2008) and it is not unreasonable to assume that the same may be true for pig brain cytosol. Biotin in pig brain cytosol would then compete with biotin-HRP for streptavidin binding sites in the control conditions. This could have been a significant problem if biotin crossed the phagosome membrane and bound to the streptavidin beads, but this is unlikely as biotin is actively transported into cells rather than freely diffusing across cellular membranes (Dyer and Said, 1997). Thus, while pig brain cytosol possible reduced the transfer of biotin-HRP to the beads in control conditions, this does not explain why no fusion was seen in the other conditions.

3.3.4.9 Troubleshooting of the fusion assay

There are several ways that the fusion assay could be troubleshooted. Firstly, it was seen that biotin-HRP was slightly degraded after passing through cells. This could be prevented by using inhibitors of lysosomal hydrolases to increase the amount of intact biotin HRP and increase the total available biotin signal. This could also be achieved by using biotin-HRP at a high concentration in the cell culture media (although this would likely prove too costly). Alternatively, more cells could be used to purify biotin-HRP lysosomes, but again this would require the use of more biotin-HRP.

It is likely that a limiting factor in the fusion assay was the amount of intact phagosomes that could fuse with lysosomes. To investigate this, more phagosomes could be purified from cells, or the phagosome protocol could be further optimised to i) remove more unbound beads, giving a better estimation of actual phagosomes purified (rather than extracellular beads), ii) increase phagosome latency further, or iii) investigate how phagosomes could be further separated from unbroken cells containing beads. This has previously been done using Ficoll-Paque centrifugation media and a 30 min centrifugation step (Shapiro et al., 2005). The ability of FeDex/biotin-HRP lysosomes and bead phagosomes to fuse with other endocytic organelles *in vivo* was not known. This could be investigated using fluorescent tracers (such as fluorescent dextrans) to examine the fusion of these organelles in living cells. This would confirm whether or not the these marker-loaded compartments are actually fusogenic. In an *in vitro* setting, a different approach could be used to investigate whether the purified lysosomes or phagosomes were receptive to vesicle fusion. Using previously established fusion assays it maybe possible to substitute in FeDeX purified lysosomes or streptavidin bead phagosomes. This may help to identify if either of these organelles can still participate in fusion. Finally, the first step that should be taken would be to identify conditions in which transfer of the biotin-HRP to beads in control conditions could be detected. This may include lysing the fusion reactions at room temperature, or allowing binding between biotin-HRP and beads to occur for a longer period of time. This should not affect other fusion conditions, as i) the vesicle membranes are lysed preventing further fusion from occurring, and ii) they contain biocytin that would block any further binding between free biotin-HRP and beads.

3.3.4.10 Conclusions

Overall, the development of the fusion assay resulted in the optimisation of both lysosome and phagosome purification. While the fusion assay itself was unsuccessful, the experiments were invaluable for furthering lysosome purification. Firstly, SPION purified lysosomes were successfully purified with high latency (> 75 %) and a reasonable recovery (~ 10 %). The purification of lysosomes by isopycnic centrifugation required the setting up of a gradient the day before purification, a 1 h centrifugation followed by fraction collecting (approximately 1 h). In contrast, magnetic isolation took approximately 1 h in total. Secondly, the lysosomes recovered were characterised by western blotting and shown to be enriched for lysosomal markers. The protocol can also easily be adapted to purify other endocytic compartments, by altering the pulse and chase of SPIONS. Alternatively, FeDex could be used to label pathogens such as *Rhodococcus equi*, (Sydor et al., 2013) and the resulting phagosomes could be purified and biochemically analysed. Such approaches have already been used to isolate *Mycobacterium*-containing phagosomes (Steinhauser et al., 2013, Pethe et al., 2004, Sydor et al., 2013). Crucially, biotin-HRP still function when delivered to lysosomes. Although some was likely degraded, this could be improved using inhibitors of lysosomal proteases. This opens up the possibility of using other markers for different applications. For example, the protocol could easily be adapted to include fluorescent markers in both lysosomes and phagosomes that could be used to examine FRET between organelles, should a microscopy-based assay be required.

Had vesicle fusion been successful, it could have been used to examine the molecular requirements for phagosome-lysosome fusion. Firstly, it is highly likely that there would be a requirement for energy, in the form of ATP. The fact that many different *in vitro* membrane fusion assays require ATP, demonstrates energy is absolutely required for fusion to proceed, or at the very least greatly reduces the overall amount of vesicle fusion when it is omitted (Balch and Rothman, 1985, Mullock et al., 1998, Jahraus et al., 1998, Becken et al., 2010, Mullock et al., 1989, Mayorga et al., 1991, Ward et al., 1997, Happe and Weidman, 1998).

Secondly, the assay could be used to determine the role of Rab proteins. Rab GTPases are key regulators of membrane trafficking and localise to distinct subcellular organelles, and their ability to promote selective tethering between membranes (Zerial and McBride, 2001). A key feature of Rab proteins, are their ability to function as molecular switches, which requires GTP. Rabs cycle between a functional “On” state where they bind GTP, and an inactive “off” state, where GTP is hydrolysed to GDP (Hutagalung and Novick, 2011). Inclusion of the poorly hydrolysable GTP analogue GTPγS in fusion assays, has been shown to enhance vesicle fusion (Jahraus et al., 1998, Mullock et al., 1998), suggesting a requirement for active Rab proteins in this process. Furthermore, Rab7 is found on late endosomal membranes, and is important in the regulation of late endocytic membrane traffic (Press et al., 1998, Vitelli et al., 1997, Bucci et al., 2000) The role of Rab7 in phagosome maturation is not as well characterised, but α-Rab7 antibodies reduced the amount of fusion between lysosomes and *E.coli* containing phagosomes *in vitro* (Becken et al., 2010). The inclusion of mutant Rab7 proteins (such as the dominant-negative Rab7T22N or constitutively active Rab7Q67L or Rab7I41M (Vitelli et al., 1997), to fusion reactions could be used to investigate the requirement for Rab7 in phagosome-lysosome fusion. However, it is likely recombinant Rab7 protein would be unable to enhance fusion, as it requires lipid modification (geranlygeranylation) to associate with membranes (Seabra, 1996). Alternatively, siRNA depletion of cells could be used to generate cytosol depleted of Rab7 (Vanlandingham and Ceresa, 2009) or other fusion machineries such as components of the HOPS complex (Pols et al., 2013) to investigate their role in phagosome-lysosome fusion. Cytosol has been found to either increase, (Becken et al., 2010, Mayorga et al., 1991), or be essential for vesicle fusion (Mullock et al., 1998). Altering the concentration of cytosol also influences the amount of fusion (Jahraus et al., 1998). Thus, the optimal level of cytosol needed for the assay could be determined. The source of the cytosol may also influence the amount of fusion seen. In general, cell-free fusion assays have demonstrated a requirement for NSF (Ward et al., 1997, Wattenberg et al., 1992, Balch and Rothman, 1985, Diaz et al., 1989), and fusion is inhibited by the addition of NEM to fusion reactions (Rodriguez et al., 1994, Robinson et al., 1997). SNARES are essential for membrane fusion, yet the specific SNARES involved in fusion at the phagosome membrane have not been extensively studied. Syntaxin 13 and 7 have been demonstrated to be important for phagosome maturation (Collins et al., 2002) but

the stage at which they are involved is unclear. In an *in vitro* phagosome-lysosome fusion assay, SNARE involvement in membrane fusion was tested by the addition of recombinant cytosolic domains of SNARE proteins into the reaction mixture (Becken et al., 2010). These solSNARES lack the transmembrane domains needed to drive vesicle fusion, and thus compete with wild type SNARES which has the effect of inhibiting vesicle fusion. However, results of such experiments need to be interpreted carefully, due to the promiscuous formation of some SNARE complexes (Wendler and Tooze, 2001). A working fusion assay could also be used to investigate the SNAREs involved in fusion between phagosomes and lysosomes.Inhibitors of lysosomal function may also reveal the mechanisms involved in lysosome-phagosome fusion. Bafilomycin A inhibits the action of the vATPase proton pump resulting in the dissipation of proton gradients (and thus pH) and nigericin (a potassium ionophore) which disrupts membrane potentials, both increase lysosomal pH. Bafilomycin was found not to inhibit membrane fusion (Mullock et al., 1998, Becken et al., 2010) and its absence in knockout mice does not affect phagosome-lysosome fusion (Kissing et al., 2015). Thus, acidification of the phagosome might be required for pathogen-killing, but not for fusion with the lysosome *per se*. Other chemical inhibitors have also been used to investigate the requirements of phagosome-lysosome fusion. The microtubule depolymerising agent nocodazole has been demonstrated to disrupt fusion with the lysosome *in vivo* (Funato et al., 1997, Matteoni and Kreis, 1987, Desjardins et al., 1994b) but microtubules may not be necessary for vesicle fusion in an *in vitro* setting (Becken et al., 2010). Finally, the fusion assay could be used to examine the disruption of phagosome-lysosome fusion by bacterial effector proteins. To date, there are no publications describing the inhibition of phagosome-lysosome membrane fusion by exogenously added bacterial effector proteins. However, cytosol from cells infected with *Mycobacterium smegmatis* or cytosol incubated with bacteria was able to inhibit phagosome-lysosome fusion *in vitro* (Peyron et al., 2001), indicating secreted bacterial factors are involved. In the case of *R. equi*, it may be possible to purify VapA-containing lysosomes and determine if they are still fusogenic. Alternatively, the cytosol of infected macrophages could be used in the assay as a potential source of bacterial effectors.

Chapter 4: Identifying *R. equi* effector proteins

4.1 Introduction

4.1.1 Yeast as a tool to investigate bacterial pathogenicity

Model organisms are extensively used in almost all aspects of research into human biology and disease (reviewed extensively in Hedges, 2002, Aitman *et al.*, 2011 and Spradling, 2006). In particular, the budding yeast *Saccharomyces cerevisiae* (*S. cerevisiae*) is a widely used model (Botstein and Fink, 2011) as it has several advantages over other model organisms. The use of yeast overcomes the ethical and financial restraints of using higher eukaryotes such as primates. Yeast can be used for high-throughput screens such as DNA microarrays (Eisen et al., 1998) yeast-two hybrid screens (Roberts et al., 2012) and plasmid overexpression (Fleming and Gitler, 2011). They have reasonable growth rates and temperature-sensitive mutants can be used to study the effects of mutations that would be lethal in other organisms (Li et al., 2011, Tan et al., 2009). The genetics of yeast are heavily characterised and the genome has been sequenced (Goffeau et al., 1996) allowing it to be compared to the human genome (Adekoya et al., 2001). Due to the conservation of essential cellular processes between eukaryotic species, such as chromosome segregation (Kitagawa and Hieter, 2001), intracellular protein transport through the Golgi (Dunphy et al., 1986) and endocytic membrane trafficking (Conibear, 2010), yeast can be used to understand many aspects of mammalian cell biology.

Intracellular pathogens must disrupt host cell defences if they are to survive intracellularly. This is achieved by the production of virulence factors, which interact with a vast array of different host lipids and proteins to disrupt host defences. For example, the lipid component of the *M. tuberculosis* cell wall (mannose-capped lipoarabinomannan) is thought to arrest phagosome maturation (Fratti et al., 2003), whereas *Legionella penumophilia* is predicted to have over 300 effector proteins that prevent the *Legionella* containing-vacuole (LCV) from fusing with the lysosome (Hubber and Roy, 2010a). Some intracellular pathogens lack suitable animal models that accurately reflect the human disease or are not genetically tractable (Curak et al., 2009). Likewise, many effector proteins lack homology to proteins of known function meaning bioinformatics approaches are challenging. Those proteins that are identified by computational approaches often

have homology to known proteins, meaning many that do not, are overlooked (Zou et al., 2013). One way of understanding bacterial pathogenesis is to determine how bacterial effector proteins interfere with eukaryotic cell processes. This can be achieved by expressing single bacterial proteins in host cells and investigating any phenotype that arises. In yeast, disruption of intracellular trafficking produces easily identifiable phenotypes, such as aberrant protein secretion (Bankaitis et al., 1986) or disrupted trafficking to the yeast vacuole (Bryant and Stevens, 1998). Alternatively, other phenotypes can be examined such as the inhibition of growth (Slagowski et al., 2008). Thus, bacterial genes can be expressed in yeast to determine whether they may be involved in pathogenicity and in particular disruption of membrane trafficking.

4.1.2 Orthologous system to lysosomes

The yeast vacuole is widely considered to be the equivalent of the mammalian lysosome (Matile and Wiemken, 1967) and is a useful tool to study lysosome biology. The biochemical and genetic tractability of the vacuole makes it an attractive model to study mammalian lysosome function. The yeast vacuole has a lipid composition that is distinct from other cellular membranes such as the plasma membrane (Zinser et al., 1991). In particular, the vacuole is rich in lipids essential for membrane fusion such as phosphatidylinositol 3,5-bisphosphate (PtdIns [3,5]P_2) and yeast mutants that cannot produce this lipid have defective vacuoles that cannot undergo fission (Yamamoto et al., 1995). Similarly, in mammalian cells, disruption of PtdIns [3,5]P_2 expression results in the formation of swollen endocytic compartments (Rutherford et al., 2006). However, the yeast vacuole also has additional functions, such as the storage of macromolecules and metabolites and is not just concerned with intracellular degradation (Klionsky et al., 1990). The yeast vacuole is also large and easily seen under the light microscope. Any disruption in trafficking that results in aberrant vacuole morphology can easily be identified and quantified. Lipid-labelling dyes such as FM4-64 also allow visualisation of trafficking from the plasma membrane in live cells, allowing membrane trafficking to be studied in real-time (Vida and Emr, 1995).

4.1.3 Conserved steps in trafficking

Many of the processes involved in trafficking to the lysosome in mammalian cells are conserved in yeast. These include proteins and protein complexes involved in vesicle priming, tethering, docking and fusion. For example, fusion of yeast vacuoles requires priming of vesicles by Sec18p (yeast NSF) and its cofactor sec17p (α-SNAP), to dissociate *cis* SNARE complexes to allow the formation of *trans* SNAREs (Collins and Wickner, 2007). This then allows vesicle docking through the association of the Vam2/6p complex (Price et al., 2000) and tethering through the concerted actions of Ypt7p (Mayer and Wickner, 1997) and the HOPS complex (Stroupe et al., 2006). This brings the membranes of acceptor and donor vesicles in close enough apposition for SNARE pairing and membrane fusion. There are many examples of orthology between mammals and yeast. For example, the human orthologue of Vam2p is *VPS41* (Radisky et al., 1997) and VPS39 is the orthologue of Vam6p (Caplan et al., 2001a, Caplan et al., 2001b). Similarly, Rab7 is the human orthologue of yeast Ypt7p (Gallwitz et al., 1989, Haubruck et al., 1989, Wichmann et al., 1989). In mammalian cells, VPS41 and VPS39 are additional components of the HOPS complex, along with Vps11, 16, 18 and 33 (Seals et al., 2000, Wurmser et al., 2000). Clearly, given the high degree of conservation between yeast and mammalian systems, *S. cerevisiae* is a powerful tool for studying membrane trafficking.

4.1.4 Pathogen effector screening in yeast – PEPSY

Pathogen effector screening in yeast, or PEPSY (Shohdy et al., 2005), takes advantage of the similarity between membrane trafficking in mammalian and yeast cells to identify bacterial genes that disrupt membrane trafficking. In yeast, membrane trafficking to the vacuole is controlled by vacuolar protein sorting (VPS) proteins. Many mammalian trafficking events are controlled by orthologues of yeast VPS proteins. For example, sorting nexin (SNX) 1 and SNX2 are orthologues of Vps5p, a core component of the yeast retromer complex (Haft et al., 2000); hVPS11 and hVPS18 are orthologues of yeast VPS11 and VPS18, components of the homotypic fusion and vacuolar protein sorting (HOPS) complex involved in late endosome/lysosome fusion (Kim et al., 2001). In mammalian cells, soluble proteins destined for the lysosome exit from the endoplasmic reticulum (ER) and are delivered to the Golgi. In the Golgi they may undergo extensive post-translational modifications, including the addition of mannose-6-phosphate (M6P)

residues (Braulke and Bonifacino, 2009). M6P-tagged proteins are recognised by mannose-6-phosphate receptors (M6PR), of which there are two forms, a ~ 46kDa cation-dependent (cdM6PR) form and a ~ 250-300 kDa cation-independent (ciM6PR) form. The transport of M6PRs and their ligands (from the Golgi to late endosomes) is dependent on C-terminal signal sequences in the cytoplasmic tails of both variations of the receptor (Ghosh et al., 2003). The M6PR-cargo complexes exit the trans-Golgi network (TGN) and deliver their cargo to late endosomes, where the low pH causes dissociation between the receptor and its ligand (Fig. 4.0 A). The receptor is then retrieved and returned to the Golgi to pick up more cargo (Ni et al., 2006). A similar pathway exists in yeast. Newly synthesised proteases and other vacuolar enzymes contain signal sequences to target them to the endoplasmic reticulum (Valls et al., 1990) upon which they transit through the Golgi before they are delivered to the vacuole. In yeast, carboxypeptidase-Y (CPY) associates with a sorting receptor, vps10 (Marcusson et al., 1994) that cycles between the Golgi and a pre-vacuolar compartment to perform multiple rounds of CPY delivery (Cooper and Stevens, 1996). In yeast however, disruption of trafficking to the vacuole results in missorting of vacuolar enzymes into secretory vesicles (Fig. 4.0 B), giving rise to a VPS phenotype. Using previously established methodologies (Bankaitis et al., 1986, Robinson et al., 1988) VPS phenotypes can be identified by assaying for the secretion of a hybrid fusion protein. The yeast strain used for PEPSY screening expresses an Invertase (Inv) - Carboxypeptidase Y (CPY) fusion protein. The *SUC2* gene encodes Inv (β-D – fructofuranoside fructohydrolase), which is normally secreted. The *PRC1* gene encodes CPY. The first 50 amino acids of CPY contain a vacuolar sorting signal, which is fused to the last 433 amino acids of Inv. This results in an invertase protein that is sequestered within the vacuole and is not able to hydrolyse sucrose present at the cell surface. If normal trafficking is disrupted by the expression of exogenous genes (or lack of VPS proteins such as Vps10) target vesicles do not reach the vacuole and CPY-Inv is missorted into vesicles destined for the cell surface. This results in CPY-Inv being secreted and this secretion can be measured using a simple qualitative agar overlay assay on single colonies, or by a quantitative assay on liquid cultures (Darsow et al., 2000). PEPSY screening works by expressing a random library of bacterial genes in yeast. If the expressed protein disrupts membrane trafficking to the yeast vacuole then CPY-Inv is secreted. Therefore, entire bacterial genomes can be screened for effector proteins that may disrupt trafficking in mammalian cells.

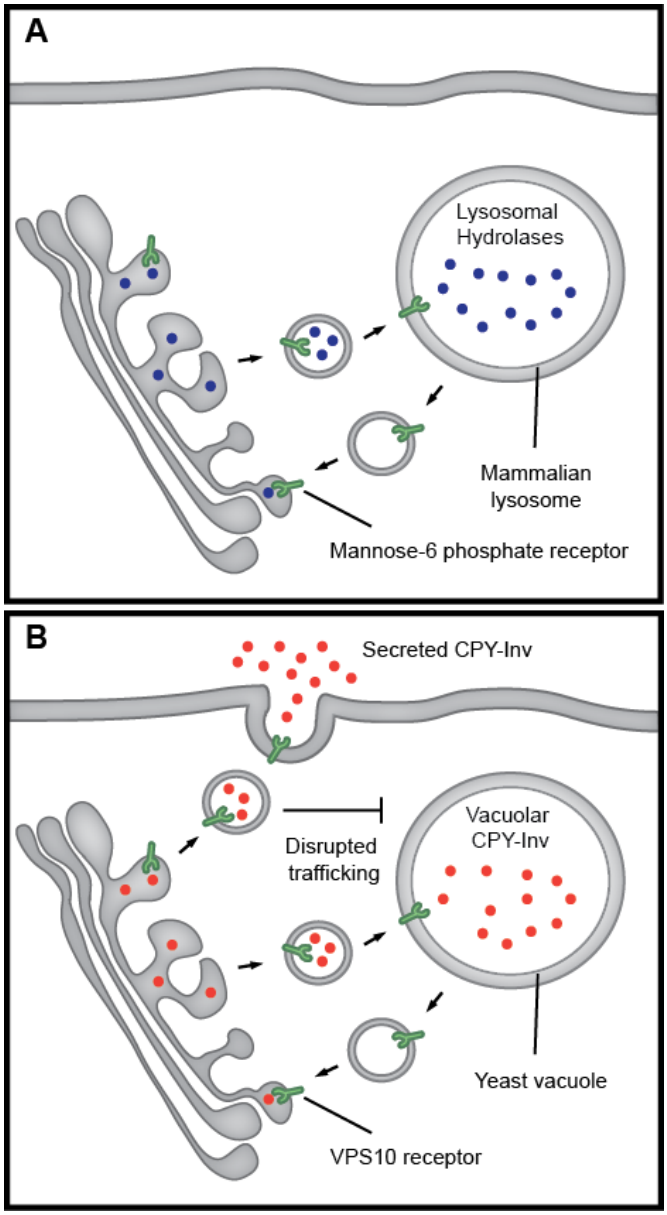

Fig. 4.0. Schematic representation of PEPSY – Pathogen Effector Screening in Yeast. A. Mannose-6-phosphate tagged lysosomal hydrolases associate with mannose-6-phosphate receptors (M6PR) in the Golgi. M6PRs and their cargo are then trafficked to the lysosome, (via late endosomes) where the low pH causes dissociation of the receptor and ligand. The receptor then recycles back to the Golgi to accept more cargo. **B**. In yeast, the vacuole is the equivalent of the mammalian lysosome. In yeast expressing a hybrid Carboxypeptidase-Y (CPY)-Invertase (Inv) fusion protein, CPY-Inv is trafficked to the vacuole by the CPY receptor, VPS10, in a mechanism analogous to M6PR trafficking in mammalian cells. If trafficking in CPY-Inv expressing yeast is disrupted, CPY-Inv becomes missorted into secretory vesicles and is secreted. The secreted invertase can be assayed.

4.1.5 Yeast as a tool to study the virulence of *Rhodococcus equi*

The horse pathogen *Rhodococcus equi* causes granulomatous pneumonia in foal (Yager et al., 1987), which is fatal if left untreated. *R. equi* is also becoming increasingly isolated from human patients, particularly from immunocompromised hosts (Kedlaya et al., 2001, Topino et al., 2010). *R. equi* can also be mistaken as *M. tuberculosis* (Mistry et al., 2006) due to the similarities between these two pathogens. *R. equi* is an intracellular pathogen that resides inside alveolar macrophages (Hondalus, 1997), but how it circumvents host defences is not clear. As such, elucidating the mechanisms by which *R. equi* manipulates the host cell may give insights into bacterial pathogenesis, but also host cell function.

To date, yeast have not been used to study *R. equi* virulence, nor have *Rhodococcus* genes been expressed in yeast. Yeast have however, been used to express *Mycobacterium* genes (Gurvitz et al., 2009). In this study, a *Rhodococcus equi* genomic and plasmid gene library was created for PEPSY screening to identify bacterial genes that resulted in a VPS phenotype. The optimisation of gene library generation and screening of the *R. equi* genome is discussed below. A schematic diagram depicting this methodology is show in figure 4.1.

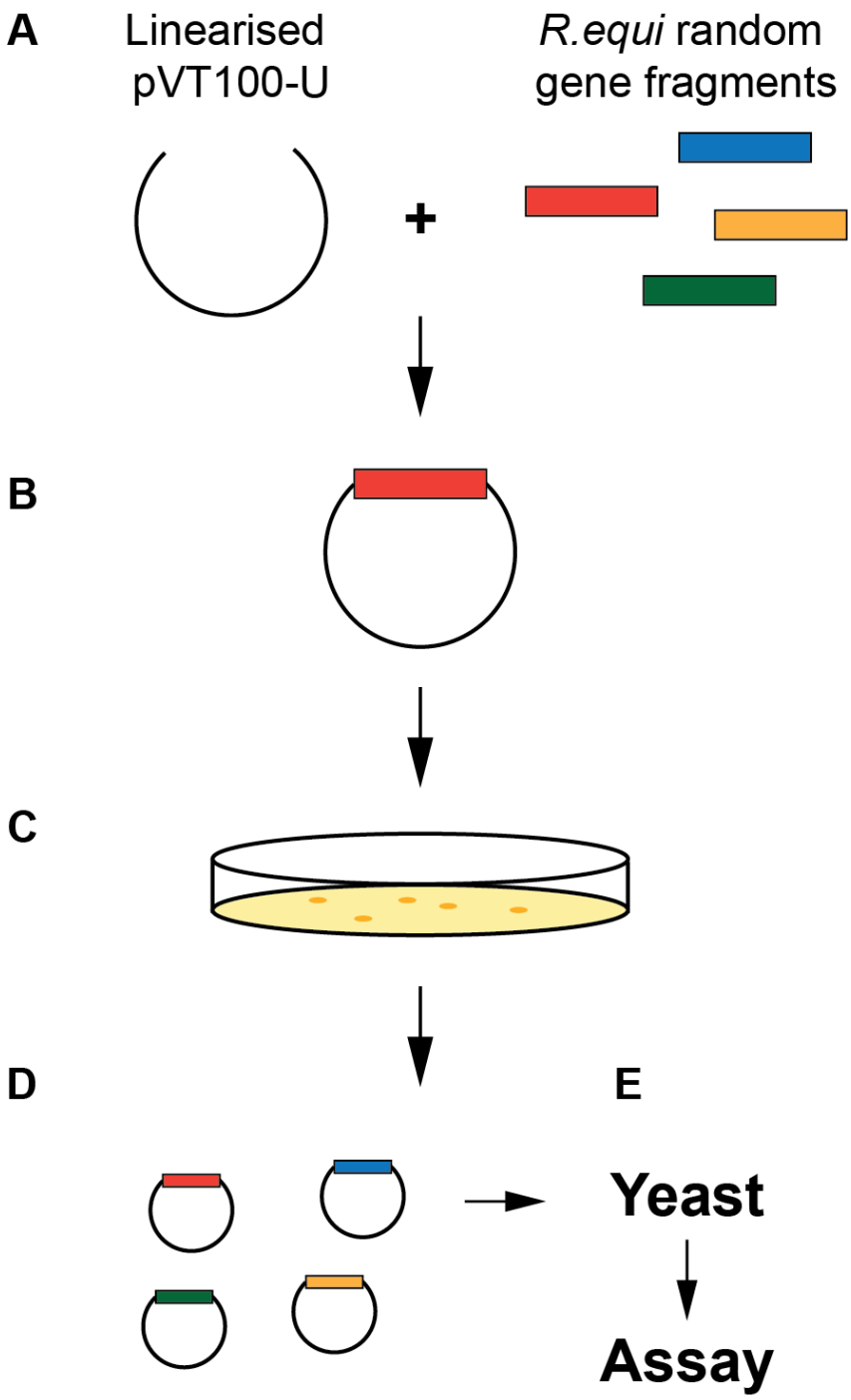

Fig. 4.1. Schematic representation of *R. equi* library generation for the PEPSY screen. A. The yeast expression vector is linearised by *BamHI* and *R. equi* DNA digested with *Sau3AI* to produce random fragments. **B.** The gene fragments are ligated into pVT100-U **C**. Ligated plasmid are transformed into *E.coli* for plasmid propagation. **D.** Plasmids are extracted from *E.coli* by Midiprep and pooled to give a complete *R. equi* gene library. **E.** Plasmids are then transformed into yeast, which are assayed for a VPS phenotype using the CPY overlay assay previously described.

4.2 PEPSY screen-specific methods

4.2.1 Yeast strains

The following table contains the genotype and source of *Saccharomyces cerevisiae* strains used in this study.

Strain	Genotype	Source/Reference
SEY6210	*MATα leu2-3,112 ura3-52 his3-Δ200 trp1-Δ901 lys2-801 suc2-Δ9*	(Horazdovsky et al., 1994)
SEY6211	*MAT**a** leu2-3,112 ura3-52 his3-Δ200 trp1-Δ901 ade2-101 suc2-Δ9*	(Horazdovsky et al., 1994)
BHY10	SEY6210 *leu2-3*,112::pBHY11 (CPY-Inv *LEU2*)	(Horazdovsky et al., 1994)
BHY11	SEY6211 *leu2-3*,112::pBHY11 (CPY-Inv *LEU2*)	(Horazdovsky et al., 1994)
BHY12	*MATα/MAT**a** leu2-3*,112::pBHY11 (CPY-Inv *LEU2*)/ *leu2-3*,112::pBHY11 (CPY-Inv *LEU2*) *ura3-52/ ura3-52 his3-Δ200/ his3-Δ200 trp1-Δ901/ trp1-Δ901 suc2-Δ9/ suc2-Δ9 ADE2/ ade2-101 lys2-801/LYS2*	(Horazdovsky et al., 1994)
BHY10 pVT100-U	BHY10 [pVT100-U *URA3*]	This study
BHY10 ΔVPS10	BHY10:: ΔVPS10:TRP [pVT100-U *URA3*]	This study

Table 4.0 Yeast strains used in this study

4.2.2 Yeast transformation

A single colony of BHY12 yeast were grown overnight in 10 ml YEP fructose at 30^{o}C with shaking. 0.5 ml aliquots of yeast were pelleted at *3,300 x g* for 1 min in a microcentrifuge and the supernatant discarded. Cells were resuspended by vortexing with 20 µl single stranded carrier DNA (2 mg/ml salmon sperm DNA heated to 95^{o}C for 5 min and rapidly cooled to 4^{o}C) and 2.4 µg plasmid DNA and incubated at room temperature for 15 min. 250 µl of sterile filtered PLATE solution (10 mM Tris, pH 7.4, 1mM EDTA, 100 mM lithium acetate, 40 % (w/v) PEG4000) was added , mixed thoroughly and incubated at 30^{o}C overnight. Cells were heat shocked for 15 min at 42 ^{o}C in a water bath. Cells were then gently resuspended in 400 µl YEP fructose and incubated at 30 ^{o}C for 1-2 h. Cells were then resuspended in 100 µl sterile ddH_2O and 80 µl spread onto the appropriate selective agar.

4.2.3 Preparation of yeast protein extracts.

5-10 ml of selective media was inoculated with a single yeast colony and grown overnight at 30 ºC with shaking. The next day, 1.0 OD_{600} was pelleted at *3,300 x g* for 1 min in a bench top centrifuge, washed once with ddH_2O and cell pellets resuspended in 100 µl TWIRL buffer (50 mM Tris-HCl, pH. 6.8, 5 % (w/v) SDS, 8 M urea, 10 % (v/v) glycerol, 0.2 % (w/v) bromophenol blue and 10 % (v/v) β – mercaptoethanol). Samples were heated at 65 ºC for 10 min, vortexed briefly and stored at -20 ºC until needed. For western blot analysis, 75 µl was loaded per lane of an SDS polyacrylamide minigel. Alternatively, 7.5 OD_{600} was washed once in ddH_2O and cell pellets snap frozen in liquid nitrogen. The pellets were resuspended in 100 µl of TWIRL buffer (without β – mercaptoethanol), with approximately 80 µl of glass beads (acid washed, Sigma) and heated to 70 ºC for 10 min. Cells were vortexed vigorously for 1 min and centrifuged at *16,000 x g* for 10 min. The supernatants were collected and placed on ice. β – mercaptoethanol was added to 10 % (v/v) and samples heated to 95 ºC for 5 min then frozen at -20 ºC until further use. For western blot analysis, 75 µl was loaded per lane of an SDS polyacrylamide minigel.

4.2.4 Extraction of *R. equi* genomic and plasmid DNA

50 ml of BHI medium was inoculated with a single *R. equi* colony and incubated overnight at 30 ^{o}C with shaking. The cell pellet was resuspended in 2 ml TE buffer (10 mM Tris, 1 mM EDTA pH 8.0) and split equally between 5 aliquots. 0.5g of acid washed glass beads were added and the suspension was vortexed for 5 minutes. The supernatants were transferred to a fresh tubes and lysozyme added to a final concentration of 5 mg/ml. This was incubated at 55 ^{o}C for 2 h. 30 µl of 10% (w/v) SDS and 3 µl proteinase K (20mg/ml) were added and incubated at 37 ^{o}C for 1 h. 100 µl of 5 M NaCl was added and mixed thoroughly and 80 µl of CTAB (10 % w/v Cetyl trimethylammonium bromidide dissolved in 0.7M NaCl) warmed to 65^{o}C was added. This was mixed gently and incubated at 65 ^{o}C for 10 min. 750 µl of chloroform:isoamyl alcohol (24:1) was added, mixed well and the samples were centrifuged at *16,100 x g* in a bench top centrifuge for 10 min. The upper aqueous phase was transferred to a fresh tube and an equal volume of phenol:chloroform:isoamyl alcohol (25:24:1) was added and mixed gently. This was centrifuged at *16,100 x g* for 10 min. The upper aqueous phase was transferred once more to a fresh tube and DNA (genomic and plasmid) was precipitated by the addition of 0.6 volumes of isopropanol. The tubes were gently inverted with a flicking motion to aggregate the DNA. The DNA pellet was removed from the tube using a sterile glass Pasteur pipette where the end had been melted to form a small hook. The DNA was dunked into 70 % (v/v) ethanol twice. The pellet was then dissolved in 100 µl TE by leaving the Pasteur pipette in TE at 37 ºC until the pellet was no longer visible.

4.2.5. R. equi random gene library generation

10 µg of *Rhodococcus equi* 103S genomic and plasmid DNA was digested with Sau3AI for 64 min at 37 ^{o}C. The restriction enzyme was heat inactivated at 70 ^{o}C for 20 min. 1.5 ml of buffer PB (Qiagen miniprep kit) was added and the DNA bound to a Qiagen gel extraction column, washed and eluted into 30 µl buffer EB. The digested DNA was run on a 0.8 % (w/v) agarose gel and fragments between 1.5-5 Kb were excised with a sterile scalpel blade. The DNA was purified using a Qiagen gel extraction kit as per the manufacturers' instructions. The DNA fragments were then ligated into the yeast expression vector pVT100-U, which had

been linearised with BamHI. *E.coli* were then transformed with plasmids as follows: XL1-blue electrocompetent cells (Agilent Technologies, UK) were defrosted on ice and mixed with 1 µl of the ligation reaction and then transferred to an ice cold electroporation cuvette with a 0.1 cm gap (Biorad). Cells were then electroporated using a Biorad Micropulser with a field strength of 17 kV/cm. The cells were then rapidly transferred to 960 µl of prewarmed to 37^{o}C SOC medium and incubated with shaking at 37^{o}C for 1 hr. 500 µl of cells were spread (using glass plating beads) onto a 15 cm plates of LB agar + ampicillin and incubated at 37^{o}C overnight or until colonies were visible but not overgrown. Ampicillin resistant colonies from 116 plates (~ 427,000) were then scraped into LB and processed using 9 Midiprep columns (Qiagen) as per the manufacturer's instructions. Approximately 5 ml of DNA was collected at 138.1 ng/µl and stored at -80^{o}C.

4.2.6 PEPSY screen

20 ml of YEP supplemented with 2 % (v/v) fructose as the sole carbon source was inoculated with a single BHY12 yeast colony and grown overnight at 30 ºC with shaking. The next day, 0.5 ml aliquots of the yeast culture were centrifuged and resuspended in 0.5 ml of sterile ddH_2O. The yeast were centrifuged again and the ddH_2O removed. The cell pellets were resuspended by vortexing with 20 µl of sterile salmon sperm DNA (2 mg/ml heated to 95 ºC for 5 min and rapidly cooled to 4 ºC to generate single stranded DNA) and 2 µg of the *R. equi* library (per transformation). Yeast were then incubated at room temperature for 15 min. 250 µl of sterile PLATE solution (10 mM Tris-HCl, pH 8.0, 1 mM EDTA, 100 mM Lithium acetate, 40 % (v/v) PEG 4000) was then added to the yeast and the yeast were vortexed once more beforing incubating at 30 ºC overnight. The next day, cells were heat shocked at 42 ºC for 15 min, pelleted at *3,300 x g* for 1 min and resuspended in 400 µl YEP fructose. Cells were allowed to recovered at 30 ºC for 1-2 h, pelleted and resuspended in 400 µl sterile ddH_2O. Approximately 80 µl was spread onto selective agar plates (synthetic depleted -ura), which were incubated at 30 ºC until colonies appeared. Approximately 100 plates were screened, with 750,000 colonies assayed for CPY secretion by the overlay assay. Colonies that showed a CPY secretion phenotype and turned brown were picked with a sterile toothpick and streaked onto a fresh agar plate for retesting. In order to determine if CPY secretion was plasmid dependent, colonies were streaked onto SD-ura 5-FOA plates to cure yeast of their plasmids. Plasmids were extracted from yeast that lost secretion when grown on 5-FOA and were used to transform *E.coli.*

Plasmids were then used to re-transform BHY12 yeast and the CPY assay repeated. Plasmids that caused secretion were then sent off for DNA sequence analysis.

4.2.7 Assays of CPY fusion protein secretion

The assessment of a VPS phenotype was performed using previously described qualitative or quantitative methodologies (Darsow et al., 2000). A rapid qualitative overlay assay was performed to screen large numbers of yeast colonies for CPY secretion. Briefly, yeast were assayed by overlaying agar containing glucostat reagent directly onto yeast colonies. 100 ml of overlay solution was prepared as follows: 4.3 g of ultrapure sucrose (Fluka) was dissolved in 60 ml of ddH_2O taking care not to introduce excess oxygen. Once the sucrose was dissolved, 10 ml of 1 M sodium acetate, pH 5.5, 2 ml of 20 mM *N*-ethylmaleimide (NEM), 1 ml of Horseradish peroxidase (Type IV, 1 mg/ml), 0.8 ml of glucose oxidase (1000U/ml), 6 ml of *O*-diansidine (10 mg/ml) and 20 ml of 3 % (w/v) Agar solution (heated to 55^{o}C) were added in that order. The solution was gently mixed and immediately poured onto yeast colonies, taking care not to wash yeast across the plate. Colour changes indicating invertase secretion were observed after approximately 30 min. Yeast positive for CPY secretion turned brown, whereas non-secreting yeast remained white.

Alternatively, CPY secretion was quantitatively assayed by liquid CPY assay. Yeast expressing *R. equi* genes were grown in SD-ura selective media to stationary phase. 1 ml of yeast culture was taken and pelleted at *3,300 x g* for 1 min in a bench top centrifuge. Yeast were washed once with ddH_2O and resuspended in 1 ml of ddH_2O. 25 µl of yeast were then added to 775 µl (1 in 32 dilution) of acetate buffer (0.1 M Sodium acetate, pH 4.9). 200 µl of this was taken (and kept on ice until required) to assay exogenous invertase activity (Secretion sample). 40 µl of the 1 in 32 dilution (or as a blank, 40 µl of acetate buffer) was added to 360 µl of acetate buffer and 10 µl of 20 % (v/v) Triton X-100 was added. Yeast were vortexed and freeze-thawed for 3 cycles by snap freezing in liquid nitrogen and thawing in a 30 ºC water bath. 200 µl of these yeast were taken to assay total invertase activity. At regular timed intervals, 50 µl of sucrose (0.5 M, sterile filtered) was added to the bottom of the tube containing the yeast samples using a positive displacement pipette. Tubes were placed in a 30 ºC shaking water bath for precisely 30 min to allow CPY-Inv to hydrolyse the sucrose. The reaction

was stopped by adding 0.3 ml of K_2HPO_4 (0.2 M, pH 10) and placing the tubes in a 95 ºC water bath for 3 min. The tubes were placed on ice to cool and 2 ml of glucostat reagent (containing 39 ml 0.1 M K_2HPO_4, pH 7, 80 µl glucose oxidase (1000U/ml in PBS), 100 µl Horseradish peroxidase (Type VI 1 mg/ml in PBS), 200 µl 20 mM NEM and 600 µl 10 mg/ml *O*-diansidine) was added at regular intervals to each tube. Tubes were then placed in a 30 ºC shaking water bath for precisely 30 min. The reaction was stopped by the addition of 2 ml of 6 M HCl. 1 ml of the reaction was transferred to a cuvette and the absorbance was then read at 540 nm using a spectrophotometer. The percentage of CPY secretion was calculated as: [Extracellular OD_{540} /(Total OD_{540} X 10)] X 100 %. Yeast lacking the Vps10 receptor (ΔVPS10) were used as a positive control for CPY mislocalisation. BHY12 yeast harbouring an empty pVT100-U plasmid were used as a negative control.

4.2.8 Extraction of plasmids from yeast

Yeast were grown overnight in 10 ml of selective media at 30 ºC. The cells were pelleted and washed once with 500 µl of water. The cells were then resuspended in 200 µl of lysis buffer (2 % (v/v) Triton X-100, 1 % (v/v) SDS, 100 mM NaCl, 10 mM Tris, pH 8, 1 mM EDTA). 200 µl of phenol-chloroform-isoamyl alcohol (25:24:1) and 0.3 g of acid washed glass beads, were added to each sample. Cells were vortexed vigorously for 4 min and then 200 µl of TE (10 mM Tris, pH 8, 1 mM EDTA) was added. The sample was vortexed briefly and centrifuged at *13,200 x g* for 5 min. The upper aqueous phase was carefully transferred to a fresh microcentrifuge tube and 1 ml of 100 % ethanol (prechilled to - 20 ºC) was added. The sample was mixed gently by inverting the tube and then incubated at -20 ºC for 30 min. Precipitated DNA was then pelleted by centrifugation at *13,200 x g* for 5 min at 4 ºC. The supernatant was discarded and the pellet washed with 200 µl of 70 % (v/v) ethanol. The pellet was vortexed and centrifuged again. The ethanol wash was discarded and the pellet left to air dry. If transformation of *E.coli* was required, the pellet was resuspended in 40 µl of sterile water. For further purification, the DNA pellet was resuspended in 400 µl of TE and processed as follows. 30 µg of RNAse A, or 1 µg of RNAse 1 was added and incubated at 37 ºC for 10 min.10 µl of 4M Ammonium acetate and 1 ml of 100 % ethanol were added and mixed by inversion. The DNA was precipitated at -20 ºC for 10 min and pelleted by centrifugation at *13,200 x g* for 5 min. The pellet was washed with 200 µl of 70 % (v/v) ethanol and centrifuged once more for 2 min. The supernatant was

discarded and the DNA pellet dried at 37 ºC. The pellet was then resuspended in 100 µl of TE and stored at – 20 ºC.

4.2.7 Scoring of yeast vacuoles

Yeast cultures were grown overnight in selective media and diluted so that the cultures had the same OD_{600}. 1 µl of the diluted culture was placed onto a glass slide and covered with a glass coverslip. 3 separate images of each yeast strain, containing approximately 300 cells per image, were blindly scored for as having either single or multiple vacuoles, as judged by the expression of GFP-ALP or GFP-ALP myc-VapA. Counts were repeated a minimum of 3 times.

4.3 Results

4.3.1 Construction of the R. equi gene library

In order to identify *R. equi* genes that induced a VPS phenotype when expressed in yeast a random *R. equi* gene library was required. When generating a library there are several considerations. Firstly, the DNA must be isolated and digested sufficiently to produce suitable fragment sizes and be representative of the entire genome. Secondly, it should not be skewed towards large or small fragments. Third, it must be relatively free of non-transformants to increase the likely hood of finding positive clones and finally it must cover the entire bacterial genome to increase the probability of each gene being represented.

As the *R. equi* virulence factor VapA is the only known virulence factor that is essential for growth of *R. equi* inside macrophages (Jain et al., 2003, Giguere et al., 1999), yet it is not sufficient to enable plasmid-cured strains to survive intracellularly (Giguere et al., 1999), it was hypothesised that there must be additional virulence genes that may be present on the chromosome. Therefore, it was decided to try and purify chromosomal DNA rather than the plasmid, to identify these unknown factors. Secondly, to prevent the potential skewing of the library towards plasmid-encoded virulence factors, it was necessary to separate the plasmid and chromosomal DNA. To this end, different DNA extraction methods were used to purify genomic and plasmid DNA and then separate them using a caesium chloride gradient. The plasmid DNA could also be used to create a plasmid only library to screen for plasmid-encoded genes.

To generate a random gene library it was necessary to purify *Rhodoccocus* DNA in sufficient quantity to perform the appropriate optimisation experiments. *R. equi* DNA (genomic and plasmid) has previously been purified using a variety of methods including alkaline lysis (Birnboim and Doly, 1979, Miranda-Casoluengo et al., 2005, Byrne et al., 2007, Makrai et al., 2002), phenol-chloroform/CTAB extraction (Rahman et al., 2003, Pei et al., 2007, Rodriguez-Lazaro et al., 2006) or caesium chloride density centrifugation (Tkachuk-Saad and Prescott, 1991, Takai et al., 1991). Figure 4.2 depicts the workflow used to optimise the purification of *R. equi* DNA. The purification of the 90 Kb plasmid DNA was attempted using a commercially available plasmid extraction kit (Qiagen Large construct kit). Despite several attempts, purification of *R. equi* DNA using this method proved

unsuccessful, possibly due to the copious amounts of mycolic acids produced by *R. equi*, which makes cell lysis difficult (Brennan and Nikaido, 1995). Next, a Qiagen Midiprep kit was used to try and purify *R. equi* DNA. Although some DNA was purified, it appeared to be a mixture of chromosomal and plasmid DNA and the yield was low (72ng/µl, data not shown). Next, a standard CTAB/phenol protocol was used to try and isolate DNA. This method also proved unsuccessful, until an extended 2 h digest with proteinase K at 37 ºC was included. This modified protocol yielded 31.4 µg of total chromosomal and plasmid DNA. Finally, the CTAB protocol was modified a final time. *R. equi* cell pellets were vortexed with glass beads for 5 min, to mechanically disrupt the cells before digestion with proteinase K. Additionally, bacteria were digested for 2 h at 55 ºC with lysozyme added to a final concentration of 5 mg/ml. These modifications were incorporated to produce a final method for the purification of total *R. equi* DNA, which is described in section 4.2.4. This method gave a total of 73 µg of DNA from 50 ml of *R. equi* culture.

The genomic and plasmid *R. equi* DNA was applied to a caesium chloride gradient, to separate plasmid and genomic DNA. However, all attempts at this protocol were unsuccessful. The rationale for this step, was to separate out plasmid and genomic genes, to prevent skewing of the *R. equi* DNA library with plasmid virulence genes, which may have masked any chromosomally-encoded genes from appearing in the PEPSY screen. As an alternative approach, *R. equi* was sub-cultured continuously for over 20 passages at 37 ºC to cure the strain of the virulence plasmid (Takai et al., 1994). Colonies were periodically tested for the presence of the plasmid by PCR of the traA and VapA genes. Despite these efforts, bacteria were not cured of the virulence plasmid and a library was generated using total *R. equi* DNA. Due to the difficulty in separating out the DNA elements and inducing plasmid loss, it was decided to proceed with the creation of the library using both genomic and plasmid DNA. It was hypothesised that as only ~25 genes of the plasmid were part of the pathogenicity island (the rest being concerned with plasmid propagation and partitioning), that skewing of the library may not have been a concern.

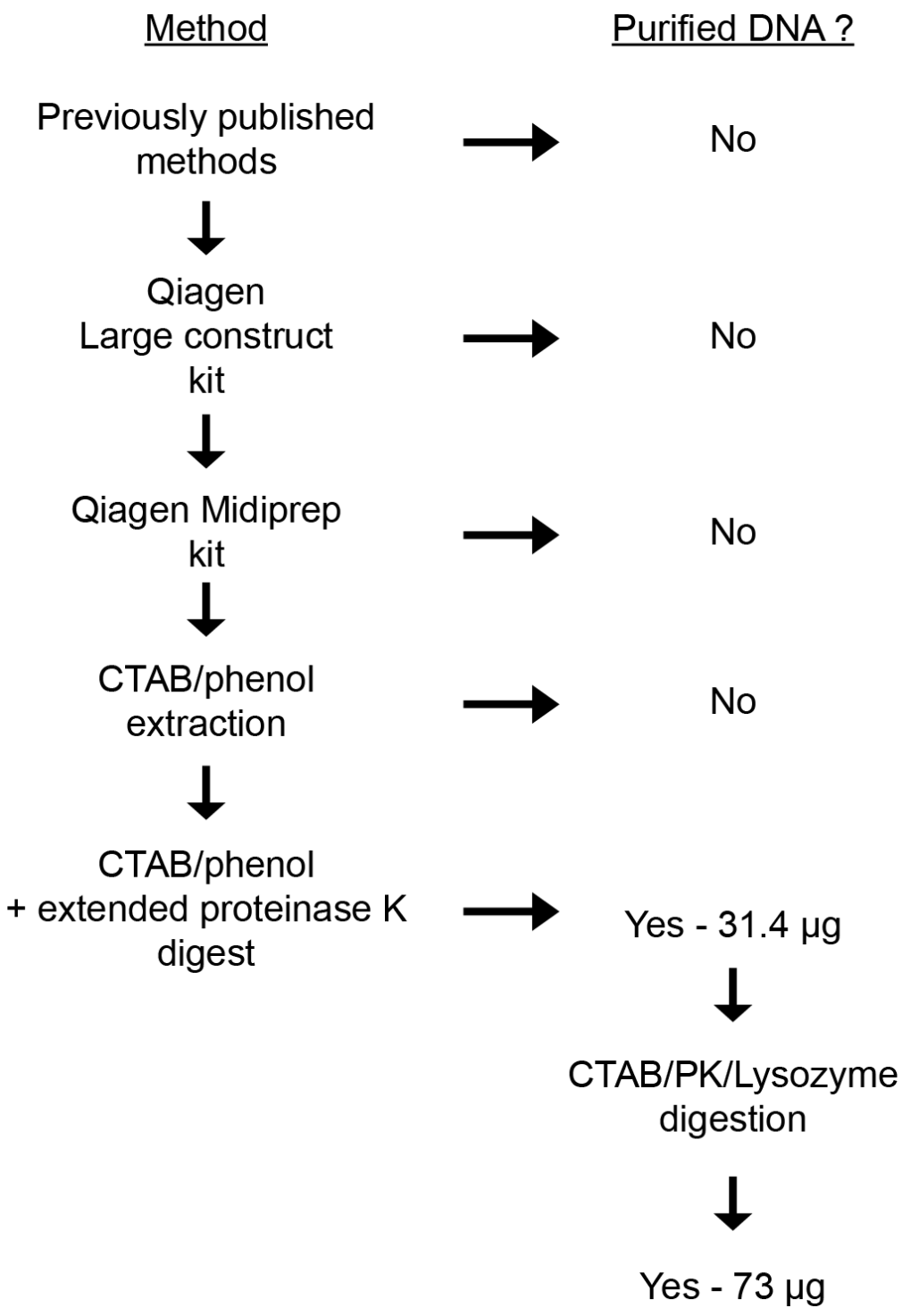

Fig. 4.2. Work flow of *R. equi* DNA extraction. Schematic representation of different strategies used to purify *Rhodococcus* DNA. The final CTAB protocol used is described in section 4.2.4

To generate the library, the extent and time of digestion with *Sau3AI* was determined in order to produce fragments of 1.5 – 5 Kb. This fragment size was chosen to maximise the chance of including entire ORFs within each digested fragment, as the average size of a bacterial protein (300 amino acids, (Brocchieri and Karlin, 2005) which equates to approximately 1 Kb of DNA (Casjens, 1998). The optimal ratio of enzyme: DNA and time of DNA digestion, were determined by small scale digests of *R. equi* DNA (Fig. 4.3 A&B). 0.9 µg of *R. equi* DNA was incubated with 1 to $3.9x10^{-3}$ units of the restriction enzyme *Sau3AI* for 1 h at 37 ºC. The digested DNA was then electrophoresed. The optimal ratio of DNA: enzyme (that gave fragments between 0.5 and 5.0 Kbp) was determined to be $3.125x10^{-2}$ units per 0.9 µg of DNA (Fig. 4.3 A). Next, the optimal time of digestion was determined. 10 µg of DNA was digested with 1.04 units of *Sau3AI* at 37 ºC. Every 8 min, $1/10^{th}$ of the reaction was heat inactivated at 70 ºC for 20 min. Digested DNA was analysed by gel electrophoresis (Fig. 4.3 B). The optimal time of digestion was determined to be 64 min. These parameters were then used to scale up the digest of 10 µg of *R. equi* DNA (Fig. 4.4 A). *R. equi* DNA fragments ranging from 1.5 Kbp – 5.0 Kbp were then ligated into the *BamHI* site of the $URA3^{+}$ 2µ yeast expression vector pVT100-U (Vernet et al., 1987) where expression of gene inserts is under control of the constitutive yeast ADH3 promoter.

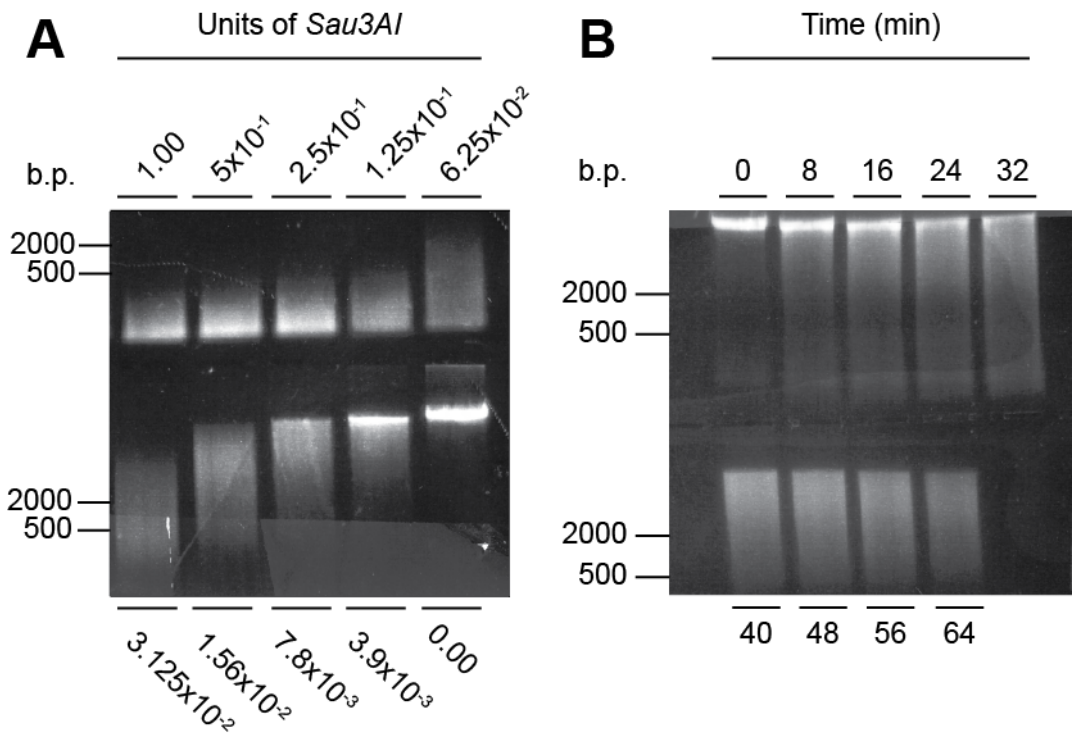

Fig. 4.3. Generation of a *R. equi* gene library. **A**. 0.9 µg of *R. equi* genomic and plasmid DNA was digested with the indicated units of *Sau3AI* for 1h at 37 º C. DNA was then electrophoresed on a 0.6 % (w/v) agarose gel **B.** 10 µg of *R. equi* DNA (27.4 µl) was added to 239.6 µl of 10 mM Tris, pH 8.0, containing 3 µl of BSA (10 mg/ml), 30 µl of 10X enzyme buffer and 1 µl (1.04 units). The reaction mixture was incubated at 37 ºC. 30 µl was taken at 8 minute intervals and heat inactivated at 70 ºC for 20 min. The digested DNA was then electrophoresed on a 0.6 % (w/v) agarose gel.

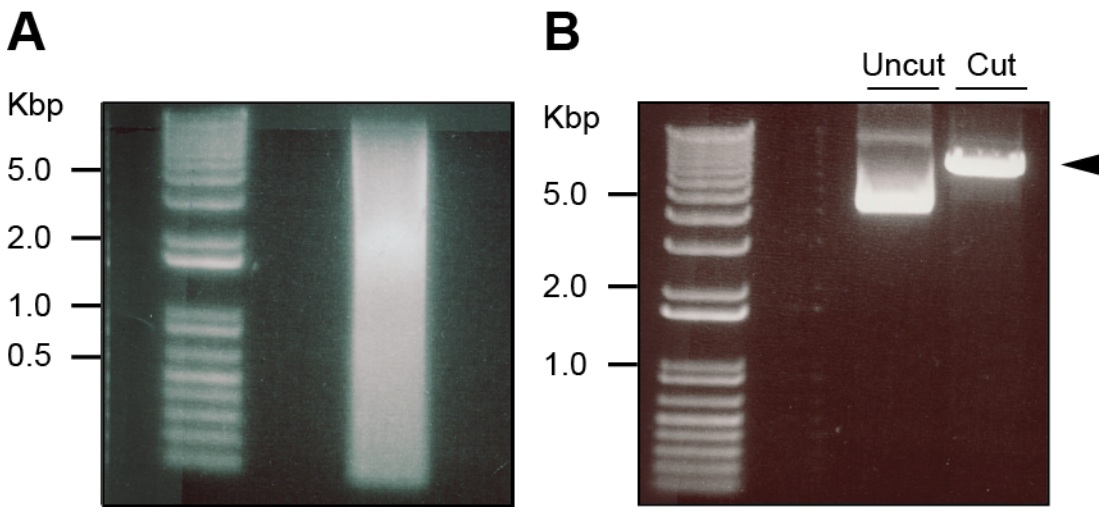

Fig. 4.4. Restriction digestion of *R. equi* DNA and yeast expression vector pVT100-U. A. 10 µg of *R. equi* genomic and plasmid DNA was digested for 64 min at 37 ºC with 1.04 units of *Sau3AI*. Digested DNA fragments between 0.5 and 5.0 Kbp were excised from the gel with a sterile scalpel and gel purified using a Qiagen gel purification kit as per the manufacturers' instructions. **B.** 1 µg of the yeast expression vector pVT100-U was digested with *BamHI* overnight at 37 ºC. The linearised vector (arrowhead) was cut from the gel and purified as described in A.

The manufacturer's recommendations for the ligase suggested using an Insert:Vector ratio of 3:1 (3-30 fmol of vector ends and 9-90 fmol of insert ends), with a total DNA amount of 0.01-0.1 µg and 0.1 units of T4 ligase. For optimal transformation, it was also suggested to dilute the ligation reaction at least 5-fold before transforming it into competent cells. Therefore, small-scale ligations and transformations were performed to determine the optimal ligation conditions to produce the highest possible number of transformants. Ligation reactions were set up using different vector and insert ratios and the number of transformed colonies counted. A vector only control was included to estimate the number of background colonies transformed with non-linearised vector (Table 4.1. & 4.2). The optimal ratio of vector : insert was determined to be 27 fmol of vector and 81 fmol of insert, as this gave the highest number of colonies. Next, the volume of the reaction used to transform a single aliquot of competent cells was investigated (Table 4.1) .The recommended protocol was to dilute the reaction at least 5-fold before transforming into competent cells. The reaction mixture was undiluted and 1 µl used to transform cells. Alternatively, a tandem reaction was set up and diluted 5-fold to 100 µl and 10 µl was used to transform cells. The total number of

obtainable colonies from the total volume of ligation reaction these transformations was determined to be 1.406 x 10^5 (undiluted) and 6.72 x 10^4 (diluted).

DNA (fmol)		Ratio (I:V)	Total DNA (µg)	Number of colonies per ligation
Vector (V)	Insert (I)			
9	81	9	0.0789	$1.1x10^5$
27	81	3	0.1392	$1.94x10^5$
9	108	12	0.1254	$6.2x10^4$

Table 4.0 Ratios of vector : insert used to optimise ligation reactions. The ligation of *R. equi* random gene fragments and pVT100-U yeast expression vector was optimised using the ratios of vector:insert shown. Each ligation reaction (20 µl) was made up to 100 µl and 1 µl was used to transform one aliquot of competent cells. Cells were recovered in 1 ml of S.O.C. medium and 100 µl of cells were plated out. Thus, the number of colonies obtained from the entire transformation reaction (100 µl) was calculated by multiplying the number of colonies from 100 µl of cells by 1000

Volume of ligation	Volume used to transform 1 aliquot of cells	No. of colonies from 10 % of transformants	No. of colonies obtainable from 1 ligation reaction
20 µl (undiluted)	1 µl	703	$1.406x10^5$
100 µl (5-fold dilution)	10 µl	672	$6.72x10^4$

Table 4.1. Volume of ligation reactions used to transform competent cells. Ligation reactions were set up in tandem (27 fmol Vector : 81 fmol Insert) and 1 µl of the undiluted or 10 µl of the diluted reaction used to transform competent *E.coli*. 10 % of the ligation reaction was transformed into *E.coli* and the total number of transformants was determined.

One potential problem with generating a random gene library is that bacteria harbouring plasmids containing small plasmids would grow faster than those with larger plasmid, heavily skewing the library with a large proportion of partial or smaller reading frames. To analyse the size of inserts, plasmids from 10 individual colonies were extracted by DNA miniprep. A diagnostic digest was then performed using *DraI* to determine the average insert size (Fig. 4.5). When digested with DraI, the empty pVT100-U plasmid gives fragments of 3809 bp, 1381 bp, 955 bp and 692 bp (with an additional 2 x 18 bp fragments). By estimating the size of the shift of the 1381 bp fragment, it was possible to estimate the average insert size in the library. This was determined to be around 2.7 Kbp. This was also important to know, as the average size of the inserts determines how many times a genome must be covered in order to find one particular clone. As the average insert was a reasonable size, the ligation reactions were scaled up using the data obtained from the previous optimisations. Thus, 4 ligations reactions were performed, using 27 fmol of vector and 81 fmol of insert DNA. Competent *E.coli* cells were electroporated with 1 µl of the undiluted ligation reaction and plated onto 116 15 cm LB agar plates and incubated for 16 h. Approximately 426,000 colonies were obtained. The colonies were scraped from the plates, pooled and the DNA plasmids extracted by midiprep. Approximately 5 ml of DNA library was recovered, at a concentration of 138 ng/µl.

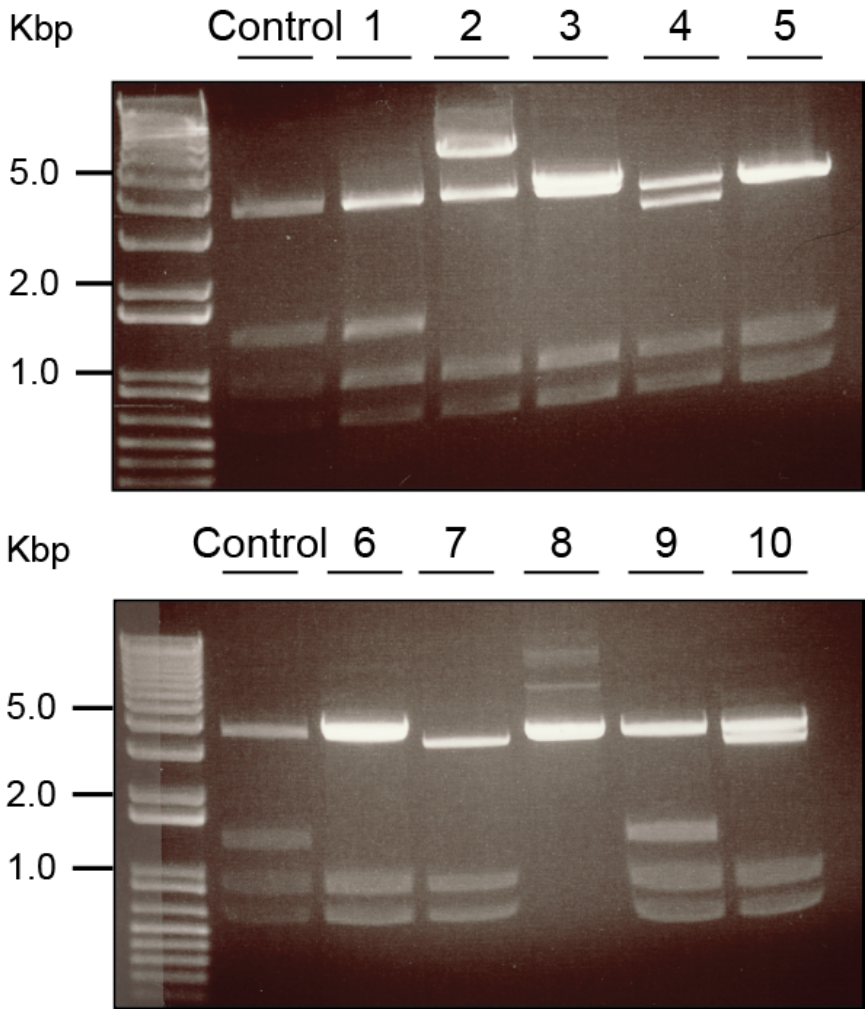

Fig. 4.5. Restriction digest analysis of a *R. equi* gene library. Plasmids from 10 *E.coli* colonies (1-10) containing *R. equi* random gene fragments were digested with *DraI*. Control – pVT100-U control plasmid containing no *R. equi* insert.

The Clarke-Carbon equation was used to determine the size of the *E.coli* library needed to cover 99 % of the *R. equi* genome (Clarke and Carbon, 1976). It was calculated that 8696 *E.coli* colonies were needed to find any one *R. equi* gene once. As 426,000 *E.coli* colonies were obtained, each *R. equi* gene should have been represented 48.9 times (Fig. 4.6).

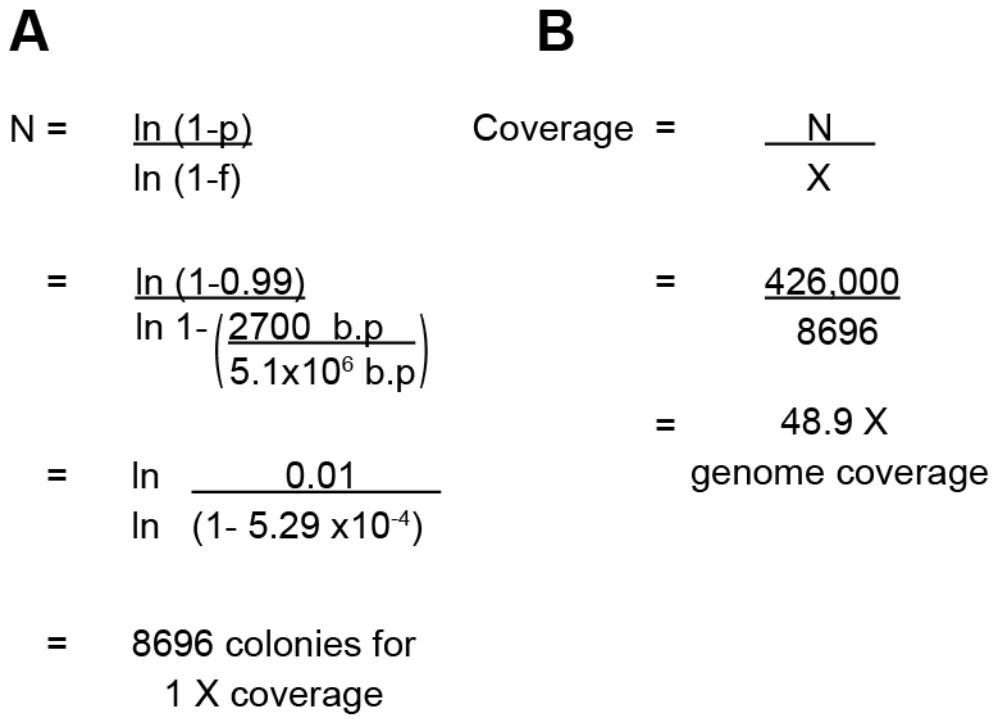

Fig. 4.6. Size of *R. equi* library needed for exhaustive screening of the genome. A. Carbon-Clark equation for determining number of colonies required to find any one particular gene. P – the desired probability of finding any one clone. f – fraction of insert to genome size. Average insert size 2700 bp, *R. equi* genome, $5.1x10^6$ Mb. **B.** Library coverage of *R. equi* genome, where N is the number of colonies obtained and X is the number of colonies needed to be screened to find one particular gene. Calculations based upon the Clark-Carbon equation (Clarke and Carbon, 1976)

4.3.2 Screening of the R. equi genome

The plasmid library was transformed into the URA3$^-$ diploid yeast strain BHY12, containing two copies of the intergrated CPY-Inv gene. Yeast transformants were plated onto selective plates containing fructose as the carbon source (SD-Ura F). Approximately 746,000 yeast colonies were obtained, giving ~ 87 X coverage of the *R. equi* genome. Yeast were screened for a VPS phenotype using the overlay assay, as previously described in section 4.2.7. Briefly, agar containing glucostat reagent is poured over yeast colonies. Exogenous CPY invertase is able to hydrolyse sucrose to glucose and fructose. Glucose oxidase then oxidises the glucose, producing H_2O_2, which is then in turn used by horseradish peroxidase (HRP) to oxidise *O*-diansidine, which results in a dark brown colour change (Fig. 4.7)

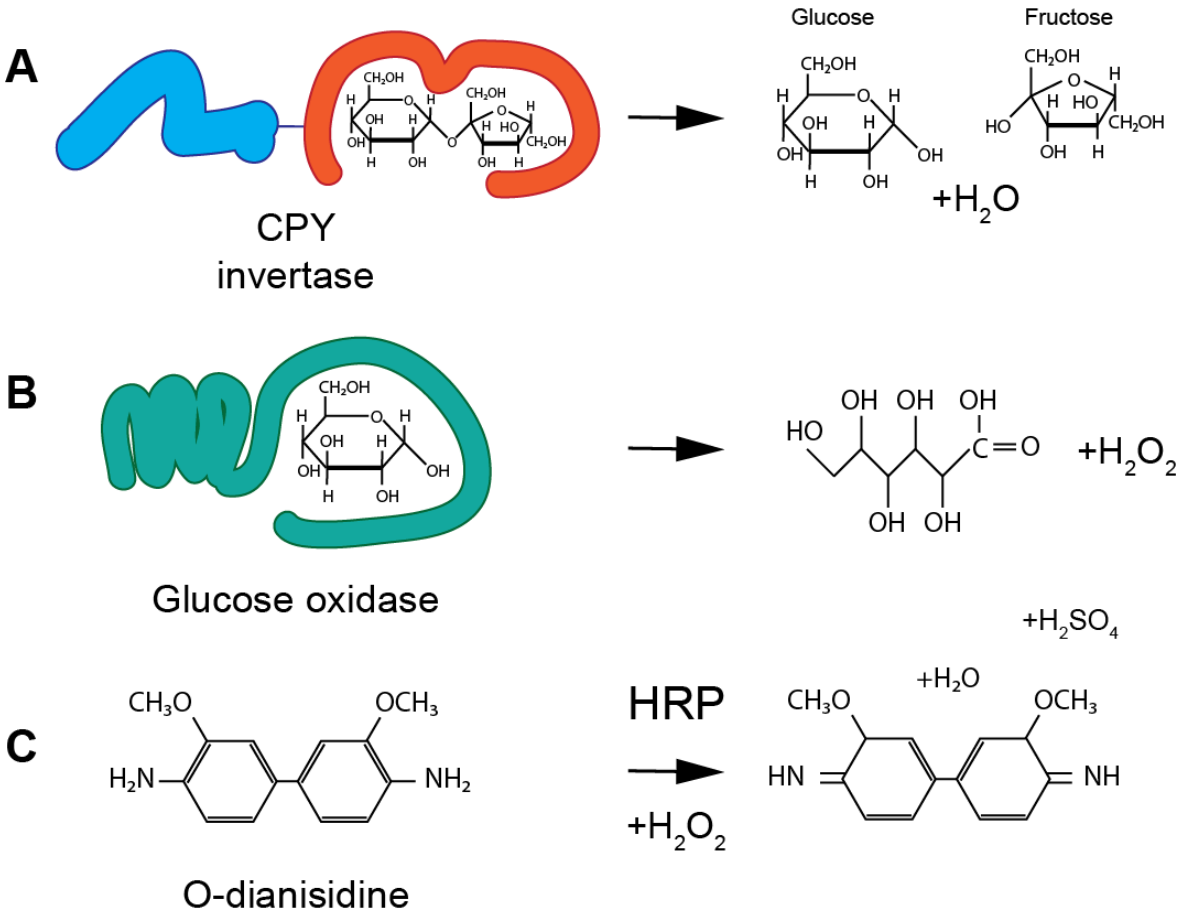

Fig. 4.7. Schematic representation of CPY-invertase assay. A. Exogenous CPY invertase hydrolyses sucrose to glucose and fructose. **B.** Glucose oxidase then oxidises the glucose, producing H_2O_2. **C.** Horseradish peroxidase (HRP) utilises H_2O_2 to oxidise *O*-diansidine, which results in a dark brown colour change

Thus, yeast that turn brown when assayed potentially have a trafficking defect. These yeast colonies were picked, restreaked and retested. Those that remained positive for secretion were selected for validation, to ensure that the secretion of CPY was due to the expression of an *R. equi* effector protein and not a random mutation introduced through the transformation procedure. The screen was repeated 3 times in total. The first round of screening yielded 3 clones which displayed a VPS-like phenotype (Fig. 4.8 A&B). When restreaked and retested only one remained positive for CPY secretion (Fig. 4.8 C). To ensure the VPS phenotype was plasmid dependent, the clone was grown on media containing 5-fluoroorotic acid (5-FOA). Yeast harbouring the *URA3* gene (the selectable marker in pVT100-U) produces a toxic metabolite when grown on 5-FOA. In wild type yeast, 5-FOA is converted to 5-fluoro-orotidine monophosphate by conjugation to phosphoribosyl pyrophosphate (PRPP). PRPP is then decarboxylated to form 5-fluoro-uridine monophosphate (FUMP). These steps are catalysed by the *URA5* and *URA3* genes, respectively (Amberg et al., 2005, Boeke et al., 1984). Fluorodeoxyuridine is formed downstream and is a strong inhibitor of thymidylate synthetase (Sklower et al., 1986) preventing DNA replication. Therefore, yeast expressing with the URA3 gene are not viable and the plasmid is not maintained. Yeast grown on 5-FOA were then assayed along side secreting yeast. However, as 5-FOA-cured yeast can no longer grow on selective media they must be grown on non-selective media along side the secreting clone for a direct comparison (Fig. 4.8 D). The positive clone lost secretion when grown on 5-FOA but secreted on selective media, indicating secretion was plasmid dependent.

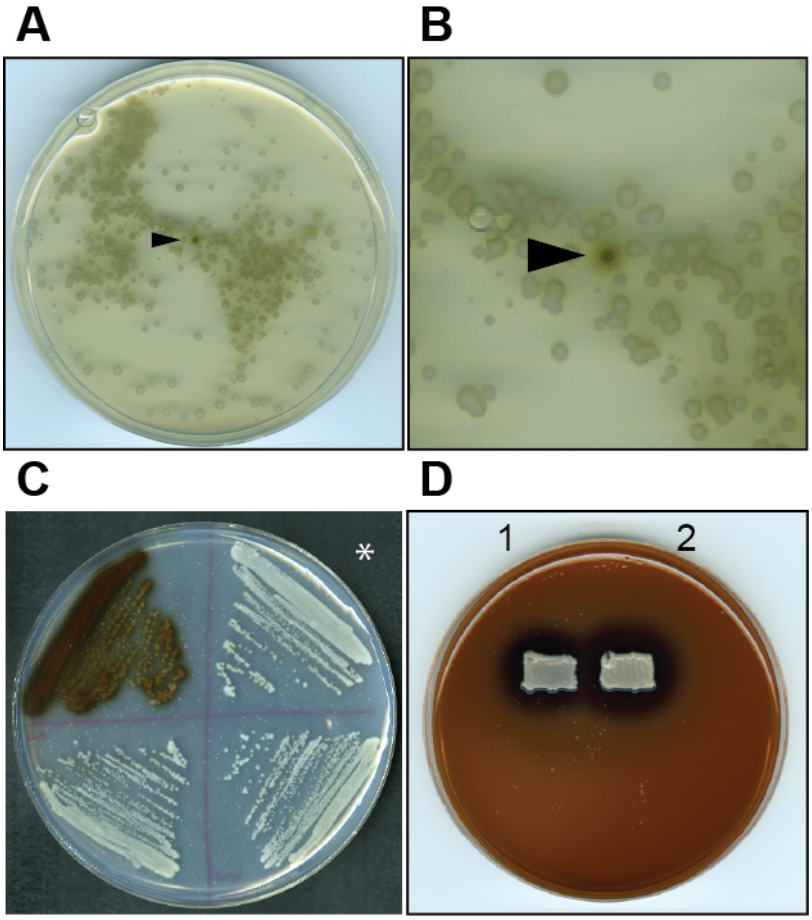

Fig. 4.8. CPY overlay assay of yeast expressing a *R. equi* gene library. BHY12 yeast were transformed with an *R. equi* random gene library and assessed for a VPS phenotype by assaying for the activity of secreted CPY-invertase. **A.** Arrowhead shows a yeast colony positive for CPY secretion. **B.** Enlarged image of **A. C.**3 positive clones were picked, restreaked and re-assayed. Asterisk indicates a negative control which remains white. **D.** CPY secreting clone from C. was grown on non-selective (1) and 5-FOA (2) media and then streaked onto non-selective media and re-assayed.

Plasmid DNA was then extracted from the yeast and used to transform into *E.coli*. Plasmids were then extracted from *E.coli* and sequenced. Unexpectedly, sequencing revealed the insert to be a 160 bp fragment of an *E.coli* phage protein and not a *Rhodococcus* gene. However, for completeness, this plasmid was retransformed back into yeast back into BHY12 yeast. The clone was retested for secretion but no VPS phenotype was observed. Due to the variable nature of the overlay assay, we hypothesised that secreting yeast may have harboured more than one plasmid. To try and prevent this, yeast were sub cultured for more than 24 h to ensure proper plasmid segregation (Scanlon et al., 2009). Although unlikely, *E.coli* transformed with DNA extracted from yeast may have harboured more than one plasmid. However PCR analysis of yeast and *E.coli* DNA showed

that this was not the case. The PCR results showed that the plasmids had an insert of approximately 150 bp (+ 154 bp of the cloning site), consistent with the sequencing data (Fig. 4.9). Furthermore, PCR analysis showed that yeast grown on 5-FOA did indeed lose plasmids (Fig. 4.10).

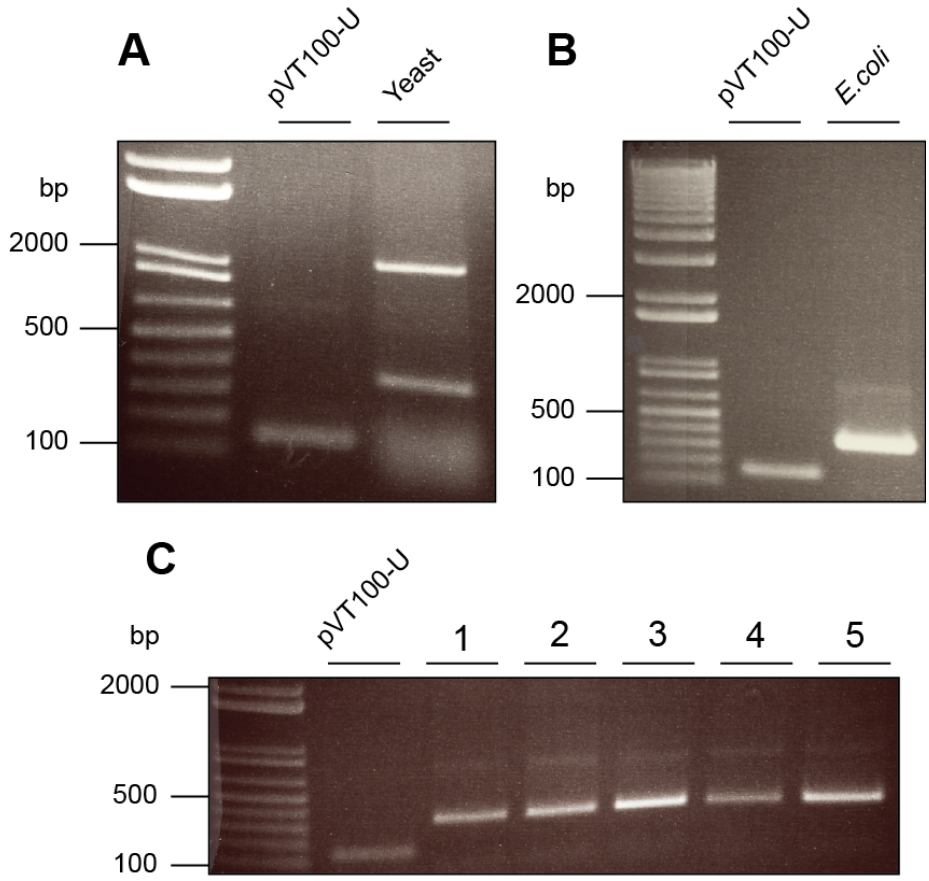

Fig. 4.9. PCR analysis of plasmid DNA extracted from yeast displaying a VPS phenotype. Yeast transformed with an *R. equi* gene library were screened for a VPS phenotype. Plasmids were extracted from positive clones for PCR analysis. **A.** PCR of pVT100-U plasmid extracted from a yeast clone (expressing an *R. equi* gene),identified as displaying a VPS phenotype. **B.** Colony PCR of *E.coli* transformed with plasmid DNA extracted from yeast in A. **C.** PCR on plasmids extracted from multiple colonies of *E.coli* transformed with DNA extracted from yeast in A. The pVT100-U empty vector control gives a product of 154 bp. Strong band of approximately 1500 bp in A. is a non-specific product produced when pVT100-U primers are used for yeast colony PCR.

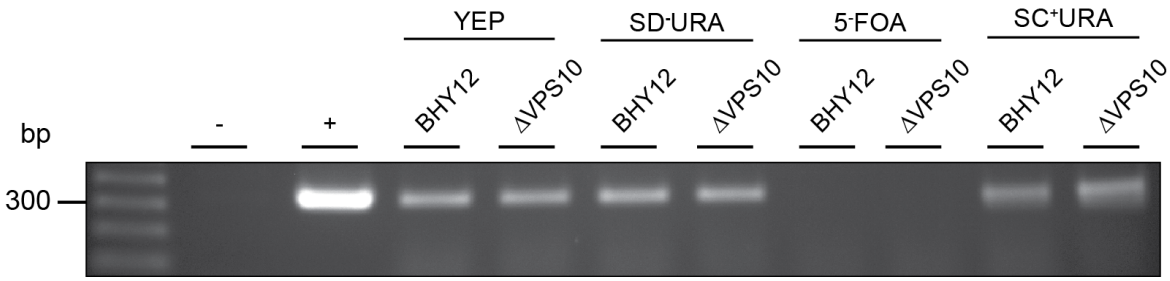

Fig. 4.10. PCR analysis of yeast grown on media with or without 5-FOA. BHY12 and BHY10 ΔVPS10 yeast strains (auxotrophic for uracil) were both transformed with pVT100-U (a yeast expression vector with the URA3 gene as a selectable marker). Yeast were grown on different media supplemented with or without 5-flouroorotic acid. The presence of the pVT100-U plasmid was determined by yeast colony PCR using primers for the 351 bp multiple cloning site of pVT100-U. +, positive control (pVT100-U plasmid DNA).

The screen was repeated for a second time and yielded a total of 269 colonies displaying varying levels of secretion. Due to the large number of clones, yeast were retested and validated in batches (Fig. 4.11). Positive clones were selected for retesting (Fig. 4.11 A). Those that still displayed a secretion phenotype were grown on 5-FOA to cure them of plasmids and they were retested. Yeast grown on selective media were then streaked out side by side (onto non selective media), next to yeast that were cured of their plasmids by 5-FOA selection, to compare secretion between them. If a yeast colony did not secrete after growth on 5-FOA, the secretion phenotype was deemed to be plasmid dependent (Fig. 4.11 B). Additionally, yeast were subjectively grouped according to the level of secretion (Fig. 4.11 B, coloured boxes). 13 clones were identified that appeared to displayed plasmid-dependent secretion. The plasmids from two of these clones were sequenced were in order to confirm that the plasmids contained *R. equi* genes and found to contain *R. equi* genes. Indeed, these two clones were found to have *R. equi* inserts of 3.8 Kbp and at least 1.7 Kbp (additional sequencing was required to determine the full size of this insert, which was not performed). However, when the plasmids from these 13 clones were retransformed back into BHY12 yeast, no secretion was observed (Fig. 4.12).

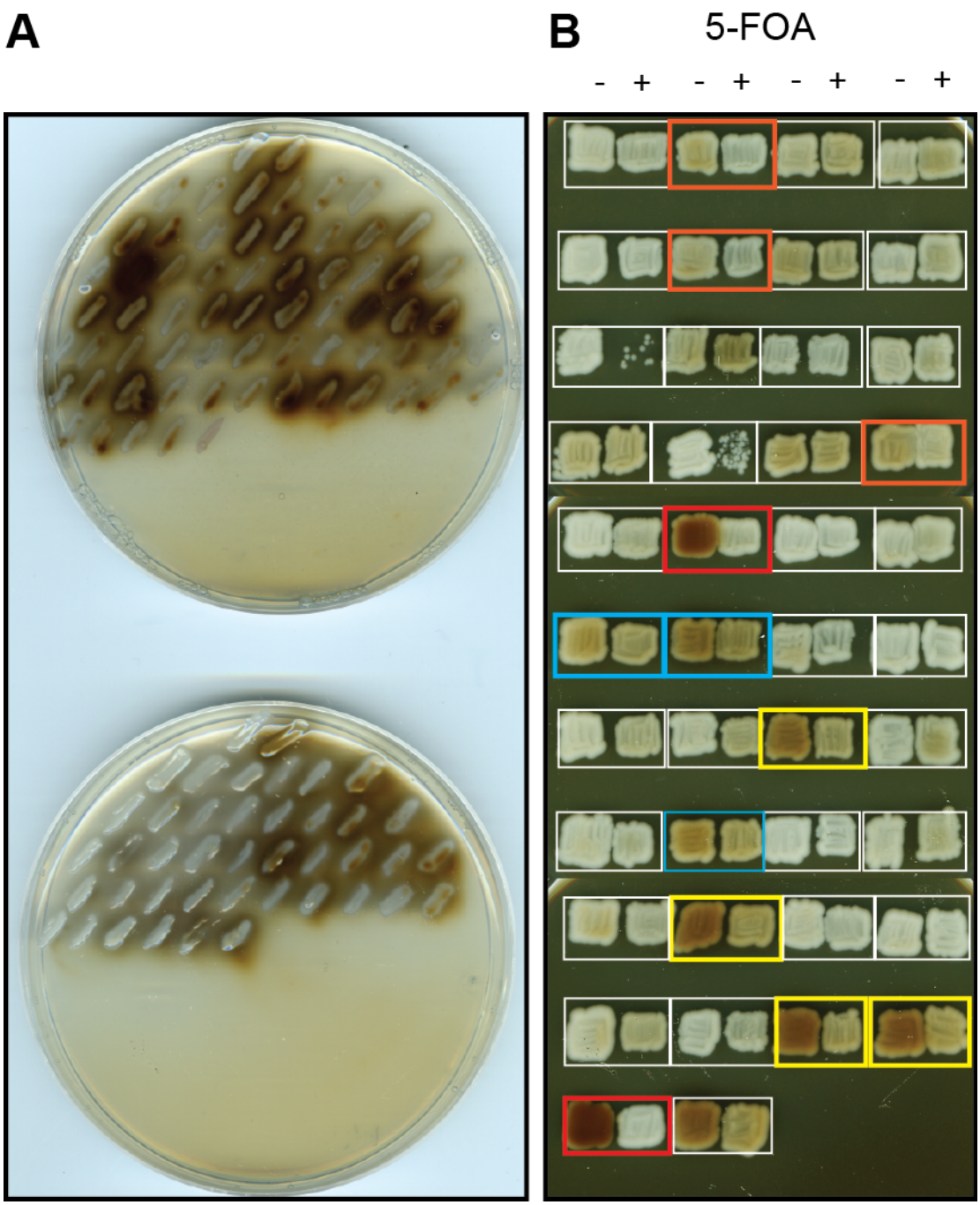

Fig. 4.11. Validation of yeast clones displaying a vacuolar trafficking defect when expressing *R. equi* genes. Yeast transformed with an *R. equi* random gene library were tested for a trafficking defect by overlay assay (yeast with a VPS phenotype turn brown). **A.** Retesting of positive clones 1-42 (top) and 43-107 (bottom). **B.** Positive clones from **A.** were grown on selective media and media containing 5-FOA, before being assayed side by side on non-selective media (left and right patches respectively). Clones were classed as displaying strong secretion (red boxes), moderate secretion (yellow box), weak secretion (blue box), very weak secretion (orange box), or no secretion/plasmid independent secretion (white boxes).

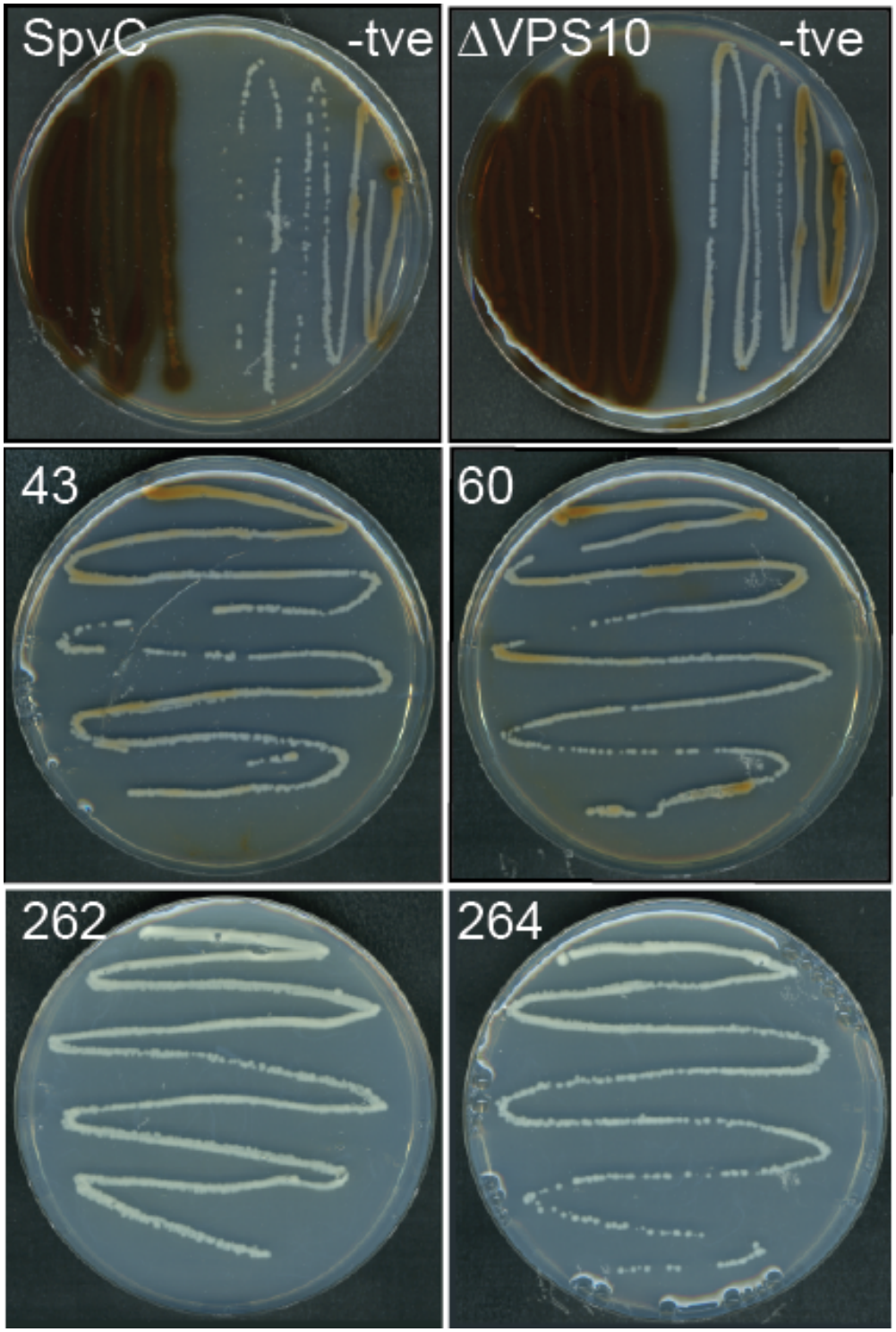

Fig. 4.12. Validation of yeast screen hits. Yeast displaying a trafficking defect when expressing *R. equi* genes were retested to ensure a plasmid dependent effect. Plasmids were extracted from positive clones and used to re-transform yeast. Yeast were once more retested for a secretion phenotype using an agar overlay assay (yeast with a trafficking defect secrete CPY-Inv and turn brown when overlaid with Glucostat reagent, whereas WT yeast remain white). ΔVPS10, SpvC (yeast expressing *Salmonella* effector protein SpvC), positive controls. –tve , BHY12 yeast negative control. Yeast clones 43,60,262 and 264 were tested.

As the invertase overlay assay was qualitative and not quantitative, it was inconsistent in the results that it would give and it was not always clear if a yeast colony was secreting CPY. There are several possibilities for this. Firstly, there may have been incomplete plasmid segregation in transformed yeast, which could have resulted in yeast that stopped secreting when the trafficking defect causing plasmid was lost. Secondly, the transformed yeast (and negative control yeast) all secrete a basal level of CPY (Valls et al., 1987). As the assay is qualitative, it was not always easy to distinguish between secreting and negative control yeast if the assay had a high level of background. Additionally, the age of the yeast and the amount of yeast also likely affected the results of the overlay assay. In hindsight, it may have been better to allow yeast to grow for a set period of time to more easily compare yeast of the same age. This may have avoided any potential cell death and cell lysis, which would have released vacuolar CPY and given the impression that a yeast colony was secreting. Similarly, it may have been better to inoculate agar plates so that they had approximately the same amount of yeast each time. Inoculating with too much yeast would result in large colonies that would turn brown due to the shear amount of CPY present. Thirdly, as CPY-Inv was secreted into the agar, it was possible that the movement of the overlay-agar solution across the plate had the effect of washing CPY-Inv over yeast colonies that were not secreting, resulting in what appeared to be a high level of background secretion. To try and prevent this, overlay solution was poured onto a region of the plate absent of yeast and the agar solution was allowed to slowly settle across the plate, rather than rocking the plate to cover all of the yeast. Finally, there were some inconsistencies with the overlay assay solution. On occasion, the glucostat reagent would immediately develop with the addition of o-diansidine, possibly indicating the presence of a contaminating oxidising agent in the glassware. To try and prevent this, the glucostat reagent was made up using disposable plastics.

However, in order to be thorough, the screen for a third and final time, taking into account some of these considerations. After the first round of screening, 23 clones were picked that displayed a VPS phenotype (Fig. 4.13).

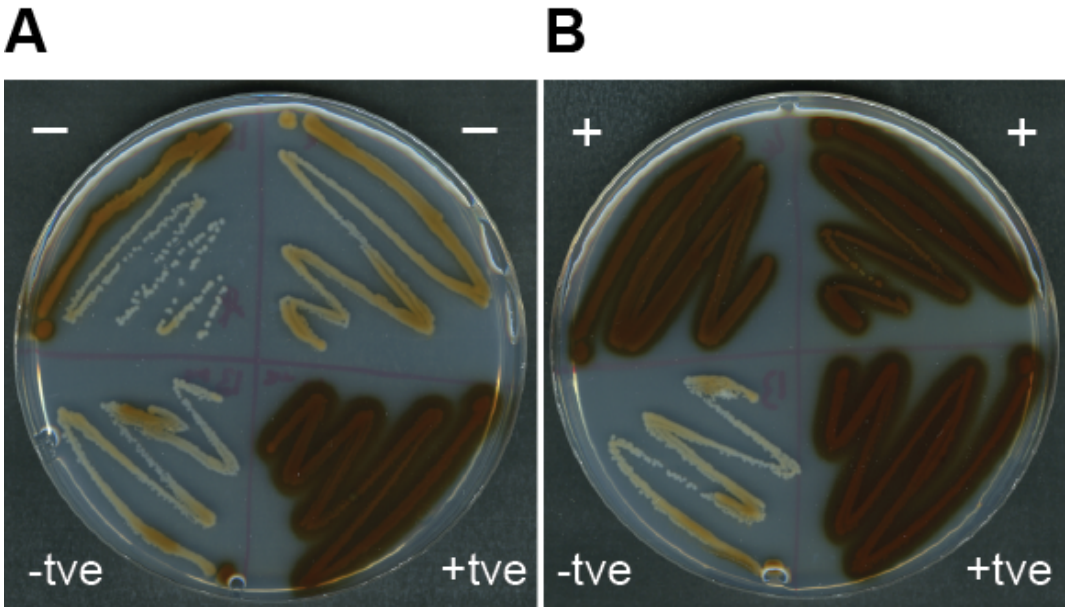

Fig. 4.13. Qualitative CPY overlay assay of yeast expressing *R. equi* genes. Yeast expressing *Rhodococcus* genes were assayed for secretion of CPY-Invertase using an agar overlay assay (yeast displaying a VPS phenotype turn brown, those that do not remain white). –tve, negative control +tve , ΔVPS10 positive control. **A.** shows examples of two negative clones, while **B.** shows two examples of secreting clones.

These clones were restreaked onto selective media and retested once more using the overlay assay. 15 of the 23 colonies remained positive for CPY secretion and were then validated by plasmid curing on 5-FOA media as previously described (data not shown). Due to the inconsistency seen with this assay previously, the 5-FOA plasmid curing was repeated a second time to ensure the result was reliable (Fig. 4.14). When retested a second time, only clones 2, 5 and 8 appeared to stop secreting, indicating that only these clones had plasmid-dependent CPY secretion.

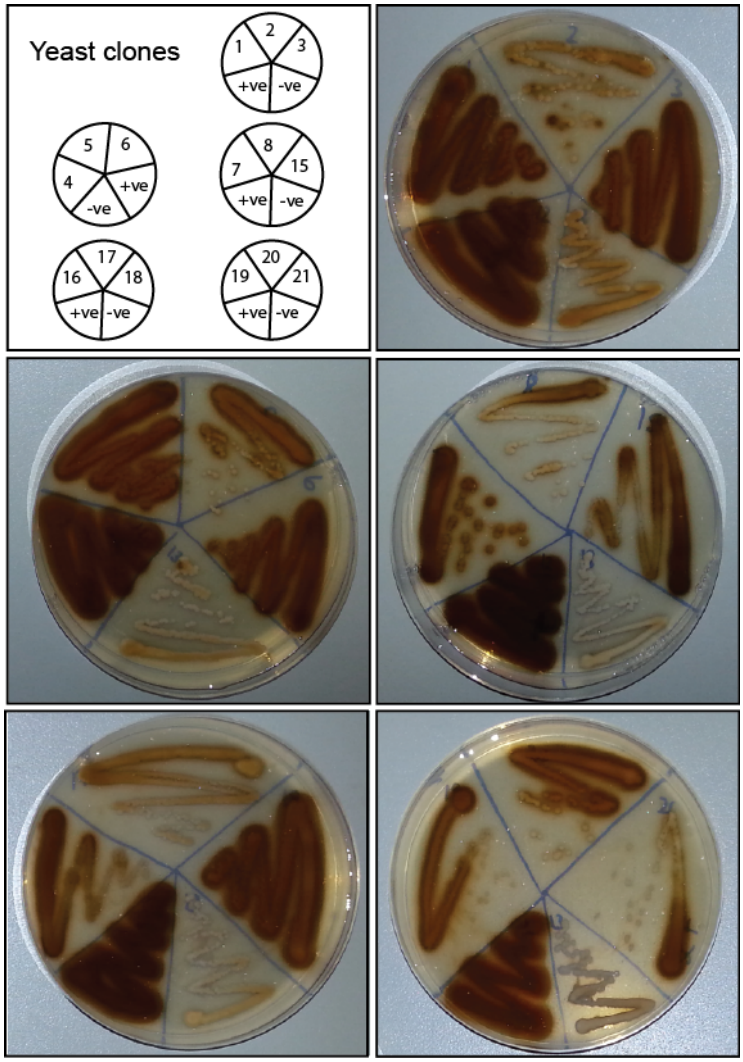

Fig. 4.14. Validation of yeast clones displaying a vacuolar trafficking defect using 5-FOA plasmid curing. Yeast transformed with plasmids containing *R. equi* genes were assayed for the secretion of CPY invertase as an indication of a trafficking defect. Yeast were then grown on media containing 5-fluoroorotic acid to cure them of the plasmids and assayed again for CPY secretion. Secretion was deemed to be plasmid dependent if yeast clones did not secrete CPY when assayed after growth on 5-FOA. –tve, negative control +tve , ΔVPS10 positive control.

Despite thoroughly investigating the cause of inconsistency the overlay assay was still not reproducible. Therefore performed a quantitative assay of CPY secretion on liquid cultures of clones picked from all three screens. Unfortunately, none of the clones displayed any significant secretion of CPY-Inv (Fig. 4.15).

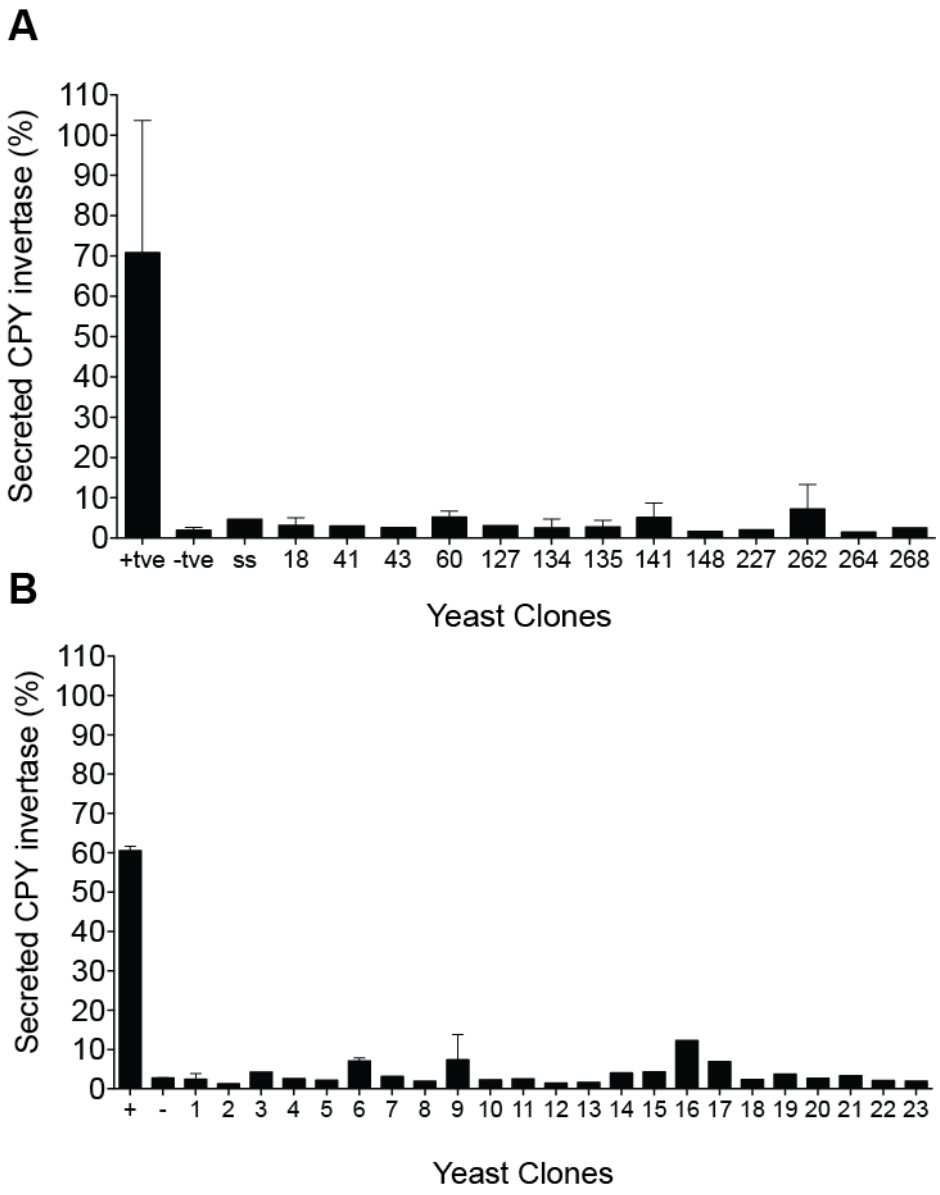

Fig. 4.15. Quantitative assessment of CPY secretion by yeast expressing *R. equi* genes. Yeast were transformed with a random *R. equi* gene library. *R. equi* genes that interfere with trafficking to the yeast vacuole cause yeast to secrete CPY-Inv. Yeast clones from three rounds of screening were assessed for CPY secretion using a quantitative assay of liquid cultures as described in section 2.3.7. **A.** Clones from screens 1 & 2 (SS-strong secretor, screen one, all other clones, screen two) **B.** Clones 1-23 from third round of screening. +/+tve – positive control (ΔVPS10, constitutive CPY secretor), -/-tve – negative control. Data are means ± the range (n=2).

4.3.3 Expression of VapA in Yeast

Despite the extensive screening of the *R. equi* genome, no genes were found that could perturb yeast membrane trafficking. Three caveats to this approach were that i) it was not clear if yeast could express *R. equi* proteins correctly, ii) the screen relied on *R. equi* proteins having their targets in the cytoplasm of the host cell and iii) that there was sufficient homology between the mammalian target of VapA and its yeast counterpart. To address the first caveat, the *R. equi* virulence factor VapA was cloned into the yeast expression vector pVT100-U, with a myc epitope on the N-terminus (myc-VapA). Western blotting of yeast lysates with anti-myc antibodies revealed the presence of a 25 kDa protein. This was slightly larger than the predicted molecular weight of myc-VapA (20 kDa), but was consistent with the expression of myc-tagged VapA as it was not present in the untransformed control yeast (Fig. 4.16 A). Secondly, as VapA was an essential *R. equi* virulence factor, it was asked whether myc-VapA could disrupt membrane trafficking in yeast. Liquid cultures of VapA-expressing yeast were quantitatively assayed for secretion of CPY-Inv, as a measure of disrupted trafficking. Yeast clones expressing myc-VapA did not display significant levels of CPY secretion above that of the untransformed negative control (Fig. 4.16 B, p=0.993).

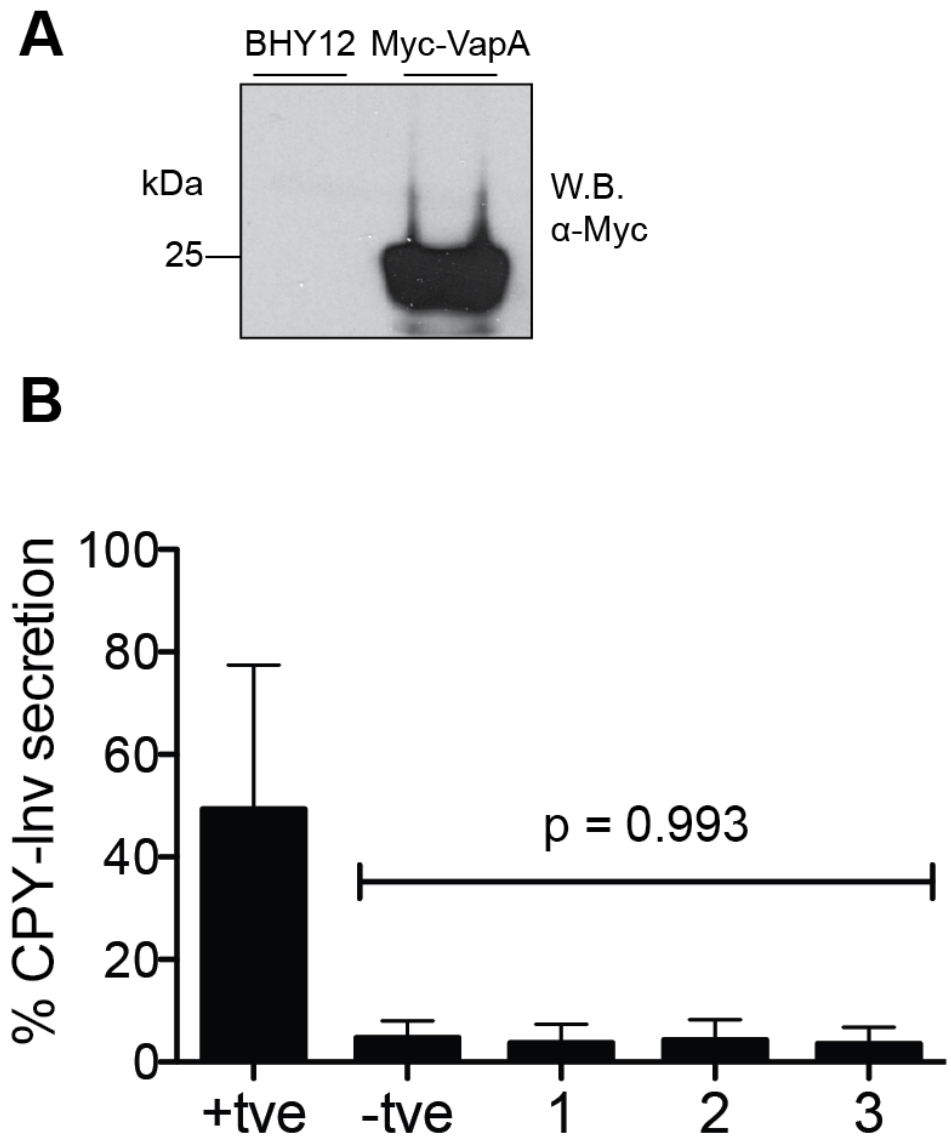

Fig. 4.16. Expression of myc-VapA in yeast. A. BHY12 yeast (BHY12) or BHY12 yeast expressing myc-VapA (myc-VapA) were western blotted for myc. Equal OD_{600} units were loaded per lane. Western blots are representative of at least two separate experiments. **B.** Three separate yeast clones expressing myc-VapA (1-3) were subjected to a quantitive assay of CPY-Inv secretion. Positive control (+tve, BHY12 ΔVPS10 yeast), negative control (-tve, BHY12 yeast). Data are means ± SEM. Statistical analysis was performed using one-way ANOVA between the negative control and clones 1-3 (n=2).

As VapA did not cause a trafficking defect when expressed in the yeast cytoplasm (but is the only described essential virulence factor) it was hypothesised that this may be because VapA has its cellular target inside the host vacuole. This hypothesis was further supported by the fact that *R. equi* has no known secretion system that can span host cellular membranes. Therefore an alternative methodology was used to target VapA to the yeast vacuole. Alkaline phosphatase (ALP) is a yeast vacuolar enzyme synthesised in an immature form that is proteolytically processed in the vacuole by cleavage of a small portion of its C-terminus (Klionsky and Emr, 1989). Fluorescently tagged ALP has been used in numerous studies to visualise the yeast vacuole (Cowles et al., 1997, Berger et al., 2007, Coonrod et al., 2013). Myc-tagged VapA was cloned onto the C-terminal end of GFP-ALP in order to target it to the vacuole (Fig. 4.17) The vacuole morphology of yeast expressing GFP-ALP or GFP-ALP myc-VapA (GAMV) was then assessed by confocal microscopy (Fig. 4.18). No clear differences in yeast vacuole morphology were observed in yeast expressing GAMV compared to the GFP-ALP control. The numbers of vacuoles in these yeast strains was also counted. GA or GAMV expressing yeast were scored as having single or multiple vacuoles. There were no significant differences between the different yeast strains ($p = 0.211$, Fig. 4.18 B). It was noted that expression of GFP-ALP and GAMV was inconsistent and highly variable. This was most likely due to the fact that the expression vector was a 2-micron (2 μm) plasmid. 2 μm plasmids are stably maintained at a high copy number (60-100), but it is probable that individual yeast had varying copies of the plasmid, resulting in uneven protein expression (Caunt et al., 1988).

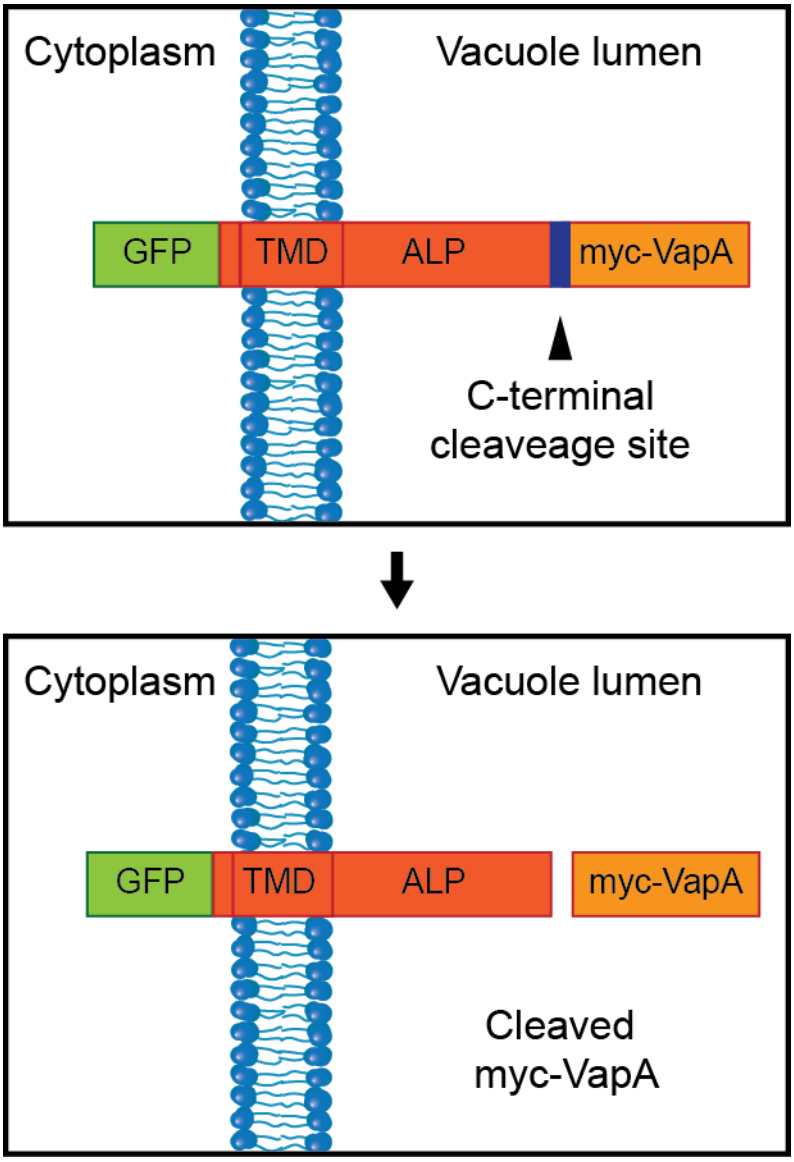

Fig. 4.17. Targeting VapA to the yeast vacuole. Schematic representation of the strategy used to target VapA to the yeast vacuole. GFP was fused to the yeast vacuolar enzyme, alkaline phosphatase (ALP) The GFP remains cytoplasmic and marks the vacuole membrane, while cleavage of a small C-terminal portion of ALP, (by endogenous vacuolar proteases) produces a mature enzyme. Myc-tagged VapA was added to the C-terminus of GFP-ALP (GAMV). Thus, upon cleavage of ALP, myc-VapA is liberated.

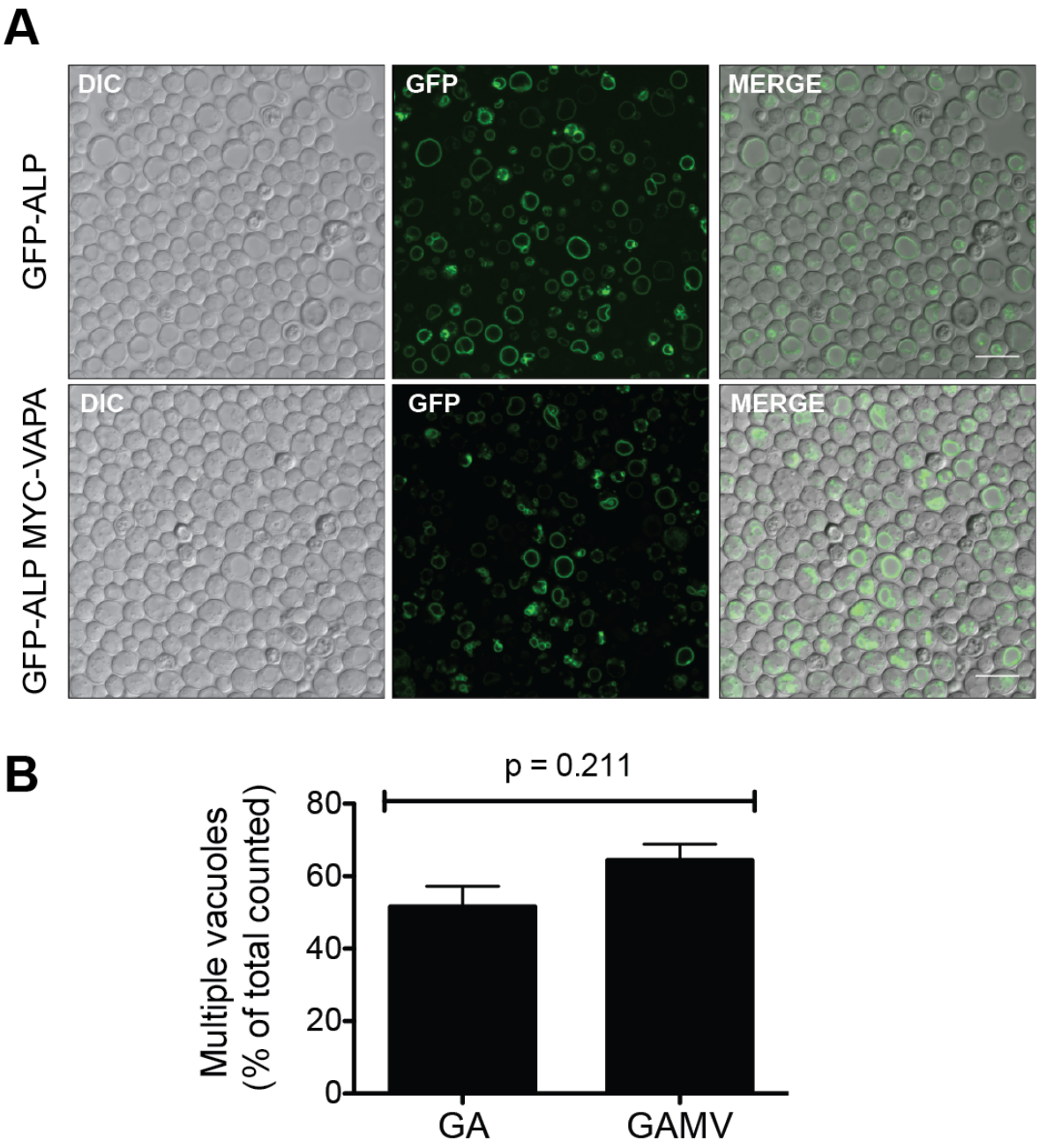

Fig. 4.18. Confocal analysis of yeast vacuole morphology and number. A. Differential interface contrast (DIC) and confocal images of yeast expressing either GFP-ALP (GA) or GFP-ALP myc-VapA (GAMV). Scale bars 10 μm. **B.** Quantification of yeast vacuole size in A. Yeast expressing GA or GAMV were scored as having single or multiple vacuoles. Yeast from at least 9 individual fields of view were counted (approximately 1000 individual cells scored per construct per experiment). Data are means ± SEM. The % of yeast cells with multiple vacuoles was statistically analysed by t-test (n=2).

As no change in vacuole morphology could be seen between yeast expressing GFP-ALP or GFP-ALP myc-VapA, it was reasoned that this could be due to low levels of exogenous protein expression. Yeast expressing either construct were western blotted with α- ALP antibodies to analyse protein expression (Fig. 4.19 A). Endogenous ALP is found as immature pro-ALP (pALP ~72 kDa) and mature ALP (mALP ~66-68 kDa). Two proteins bands were seen in the BHY12 control between 50 kDa and 75 kDa and were found in all lysates. These bands ran slightly differently to the predicted sizes of pALP and mALP but were consistent with the processing of ALP. A further band of ~100 kDa was found in yeast expressing GFP-ALP (closed arrowhead) and GAMV, indicating expression of GFP-ALP (predicted size 91 kDa) and probable processing of GAMV to form GFP-ALP. An additional band at a higher molecular weight (~110-120 kDa, open arrowhead) was found only in GAMV lysates (GAMV predicted size 110 kDa). This band was most likely full length GAMV. The same yeast lysates were then probed with α-myc antibodies (Fig. 4.19 B) which revealed the expression of a protein of ~120 kDa, specific to yeast expressing GAMV but not GFP-ALP (closed arrowhead). A stronger band of 100 kDa detected by the myc antibody could be due to the degradation of VapA from the C-terminal end of the fusion protein. However, cleaved myc-VapA could not be detected. Next, myc-VapA, GA and GAMV yeast lysates were probed with α-VapA antibodies (Fig. 4.19 C). A band of ~25 kDa was detected in myc-VapA expressing yeast (closed arrowhead), along with bands at ~20 kDa and 15 kDa indicating possible degradation of myc-VapA. In GAMV yeast, a doublet band was detected at ~120 kDa (open arrowhead), along with a single band at ~15 kDa (Fig. 4.19 *). This is consistent with expression of GAMV and cleavage of the C-terminal signal sequence to yield myc-VapA. No protein bands were seen in GFP-ALP yeast demonstrating that the bands seen were specific to yeast expressing myc-VapA and GAMV. In all these cases, the detected bands ran slightly higher than the predicted molecular weights of the proteins. The laddering pattern seen in both GFP-ALP and GAMV lysates (Fig. 4.19 A & B) was probably due to degradation of the expressed fusion proteins. Taken together these data are consistent with the expression of GFP-ALP and GAMV. Next, GFP-ALP and GAMV expressing yeast were assessed for secretion of CPY (Fig. 4.19 D). Yeast expressing GFP-ALP or GAMV secreted levels of CPY-Inv above that of the negative control (2.35 % & 1.65 % compared to 0.86 %, respectively) but this was not significant ($p = 0.367$). The degradation of VapA may have masked any potential effects of VapA on CPY secretion.

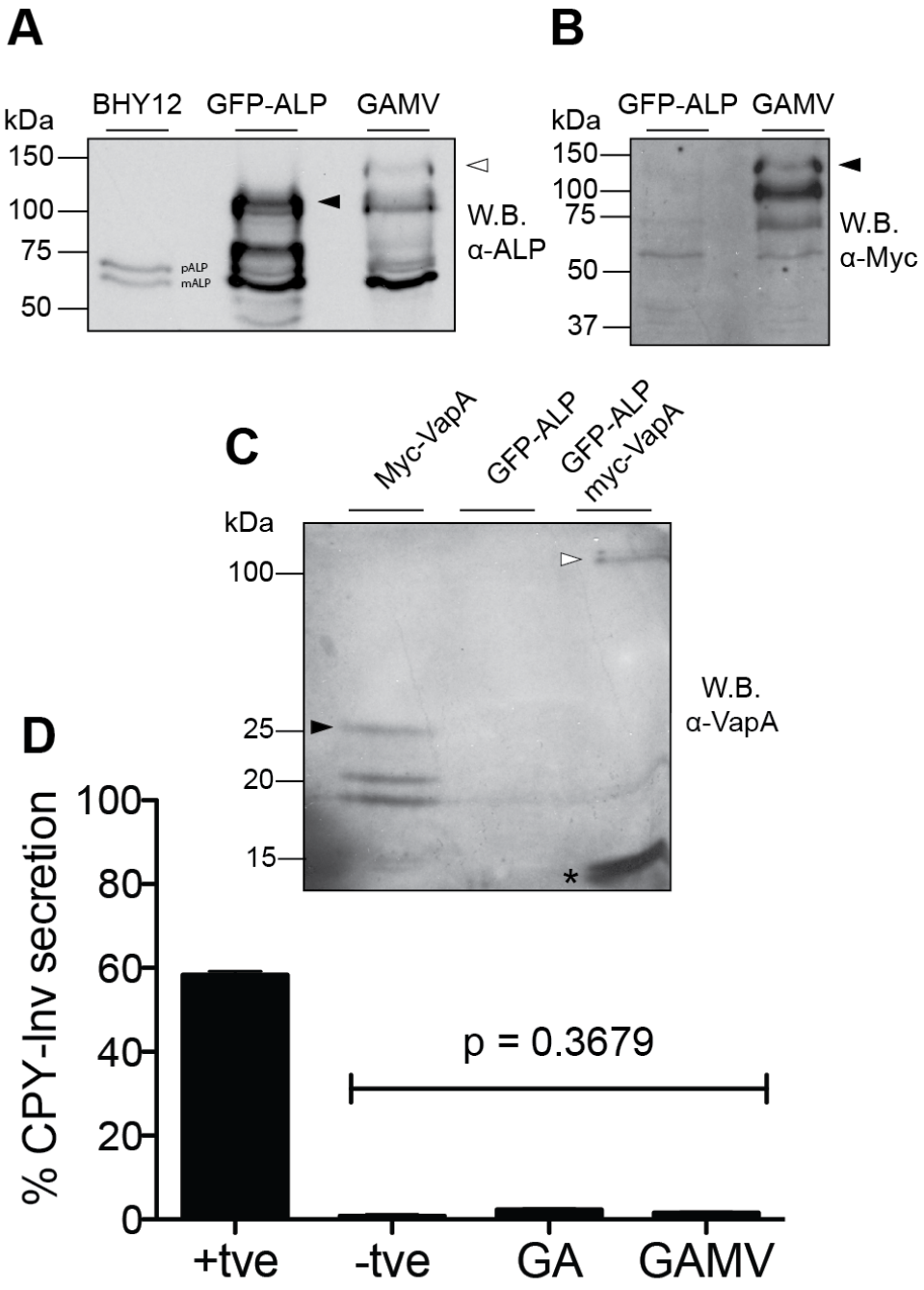

Fig. 4.19. Expression of VapA in the yeast vacuole. A. BHY12 yeast (BHY12) or BHY12 yeast expressing GFP-ALP or GFP-ALP myc-VapA (GAMV) were subjected to western blotting (W.B.) using α-ALP antibodies. Endogenous ALP appears as a doublet in pro (pALP) and mature (mALP) forms. **B**. Yeast lysates in A were probed with α-myc antibodies **C.** BHY12 yeast expressing myc-VapA, GFP-ALP, or GAMV were subjected to western blotting with α-VapA antibodies. Equal OD_{600} units of yeast were loaded per lane for all western blots. **D.** Quantitative assay of CPY-Inv secretion by yeast expressing GFP-ALP (GA) or GAMV. Positive control (+tve, BHY12 ΔVPS10 yeast), negative control (-tve, BHY12 yeast). Data are means ± SEM and were analysed by one-way ANOVA and significance compare to the –tve control determined (n=2). Western blots are representative of at least two separate experiments except for C (n=1).

4.3.4 Expression of VapA in mammalian cells

Since no effect on vacuolar trafficking was observed when VapA was expressed in yeast, it was hypothesised that the yeast orthologue of the mammalian target of VapA may not have sufficient homology for VapA to interact. As mammals are a natural host of *R. equi*, expressing *Rhodococcus* proteins in mammalian cells may be more representative of an *in vivo* infection. An inducible HeLa cell line stably expressing myc-tagged VapA was generated (Fig. 4.20). Expression of myc-VapA was induced with 1 µg/ml doxycycline for 24 h (Fig. 4.20 A) and the cellular localisation of VapA was examined by immunofluorescence. VapA appeared to be evenly distributed throughout the cell cytoplasm and not associated with any specific organelles. HeLa cell morphology also appeared normal, as did lysosome distribution and morphology. As it was hypothesised that *R. equi* prevents delivery to the lysosome by interfering with membrane trafficking, the colocalisation of myc-VapA with early endosomes, late endosomes and lysosomes, was examined. Expression was induced for 24 h and cells were treated with cytosol extraction buffer (CEB) before fixation, in order to remove any myc-VapA that was not associated with cellular organelles. Myc-VapA did not co-localise with EAA1 (early endosomes), ciM6PR (late endosomes) or LAMP1 (lysosomes, Fig. 4.21). As previously discussed, VapA may need to be on the lumenal side of an endocytic organelle in order to have a functional effect. Therefore, it was decided to produce recombinant proteins in order to feed to cells and test this hypothesis.

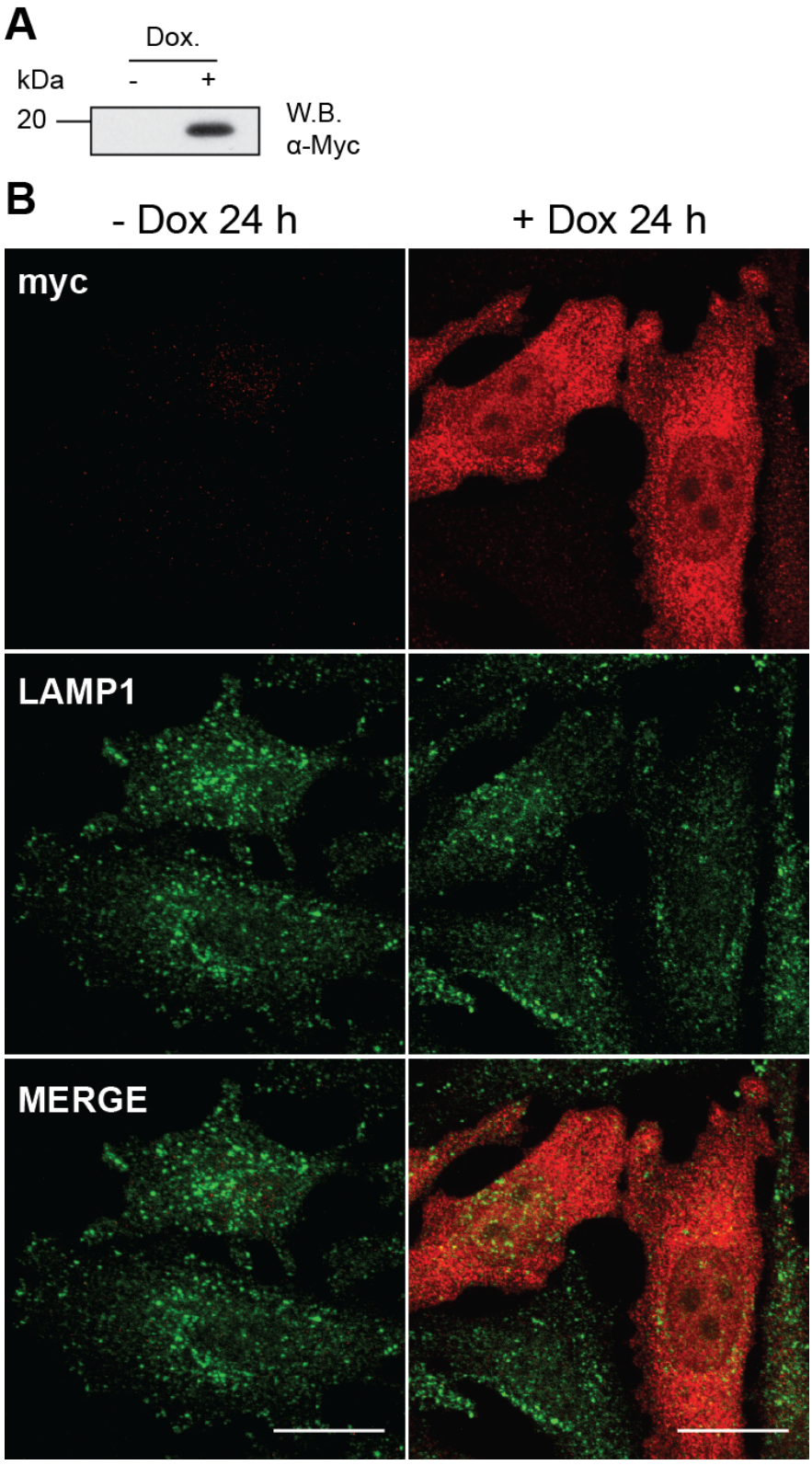

Fig. 4.20. Expression of myc-VapA in HeLa cells. A. myc-VapA expression was induced with doxycycline for 24 h. Protein lysates were probed by western blotting with α-myc antibodies. 20 µg of protein per lane. **B.** VapA expressing HeLa cells were double labelled with α-myc and α-LAMP1 antibodies followed by fluorescently labelled secondary-antibodies (Alexa fluor 555; red and Alexa fluor 488; green, respectively). All images are confocal maximum-intensity z-projections. Scale bars 20 µm.

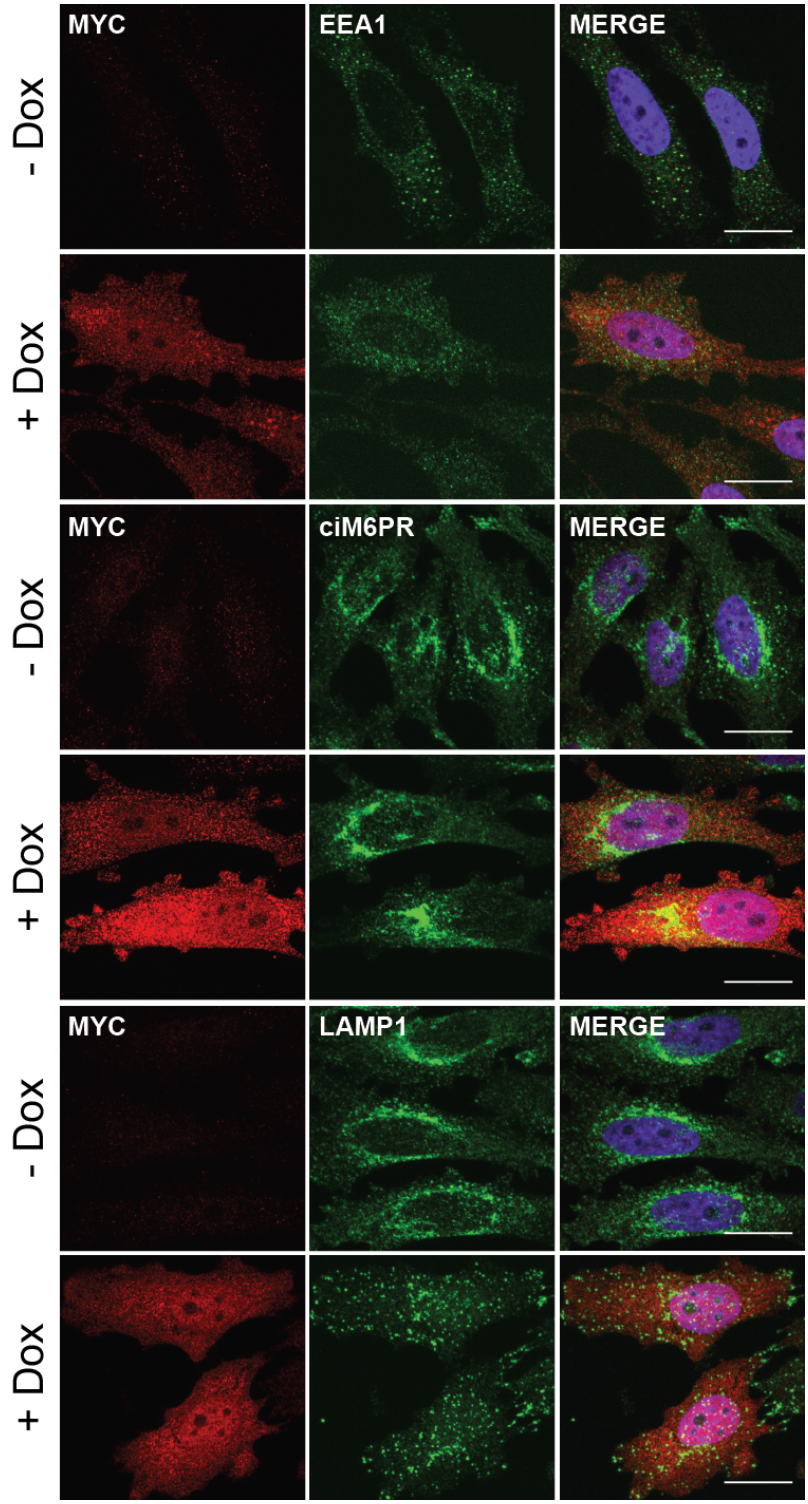

Fig. 4.21. myc-tagged VapA does not co-localise with endocytic markers when expressed in the cell cytoplasm. Doxycycline was added to HeLa cells to induce the expression of myc-VapA for 24 h. Cells were then fixed and double labelled with α-myc and α-EEA1 (early endosomes), α-ciM6PR (late endosomes), or α-LAMP1 (lysosomes) followed by fluorescently labelled secondary-antibodies. Myc labelling is shown in red, organelle labelling is shown in green and nuclei were stained with DAPI (blue). All images are confocal maximum-intensity z-projections. Scale bar 20 μm.

4.3.5 Production of recombinant VapA

In order to target VapA to the lumen of the mammalian lysosome, recombinant VapA was produced to feed to cells. VapA was cloned into the *E.coli* expression vector pGEX 3-PLX, with a myc tag on either the N or C terminus of VapA (Fig. 4.22). A small scale test expression was performed to assess the solubility of each fusion protein. Two individual clones were chosen for each construct. For both fusion proteins, a large band of approximately 46 kDa was observed upon the addition of IPTG, but not in the pre-induction sample. A band at the same molecular weight was also observed in the soluble and insoluble fractions, consistent with the expression of myc-tagged (N or C) GST-VapA. The addition of the myc tag to the C-terminus of VapA appeared to decrease its solubility. Therefore, GST-myc-VapA was chosen for large-scale purification (Fig. 4.22 B). Recombinant VapA was purified from a 1 L culture using affinity chromatography and 1 ml fractions of the eluate were analysed by SDS PAGE. A single band at 46 kDa was found in the eluates, along with a strong band at 26 kDa, likely to be free GST. Fractions 1-5 were then pooled and dialysed into PBS for further use. Approximately 1 mg of fusion protein was recovered from a 1 L culture. In addition to the production of GST-myc-VapA, myc-VapA with a C-terminal His tag was also produced, as the yield of GST fusion protein was relatively low compared to the higher yield of the His-tagged protein. Moreover, a large proportion of the purified protein was likely to be free GST, which would further reduce the actual amount of active VapA protein. Recombinant VapA-His_6 was produced by cloning VapA into the expression vector pMW172. Small scale test expressions were carried out as previously described (Fig. 4.23 A). Two clones were tested for the expression of the fusion protein by western blotting using α-myc antibodies, which revealed the expression of a protein between 20 kDa and 25 kDa present in the induced, soluble and insoluble samples, but to a much lesser extent in the pre-induction sample. This clone was then selected for large scale production of myc-VapA-His. The supernatant from a 1 L culture was incubated with nickel sepharose for 2 h at 4 ºC. The sepharose was washed extensively and the fusion protein eluted from the column using an elution buffer containing 250 mM imidazole. 1 ml fractions were collected an analysed by SDS PAGE (Fig. 4.23 B). Fractions 1-5 were pooled and extensively dialysed into PBS. The yield was approximately 1 mg from a 1 L culture.

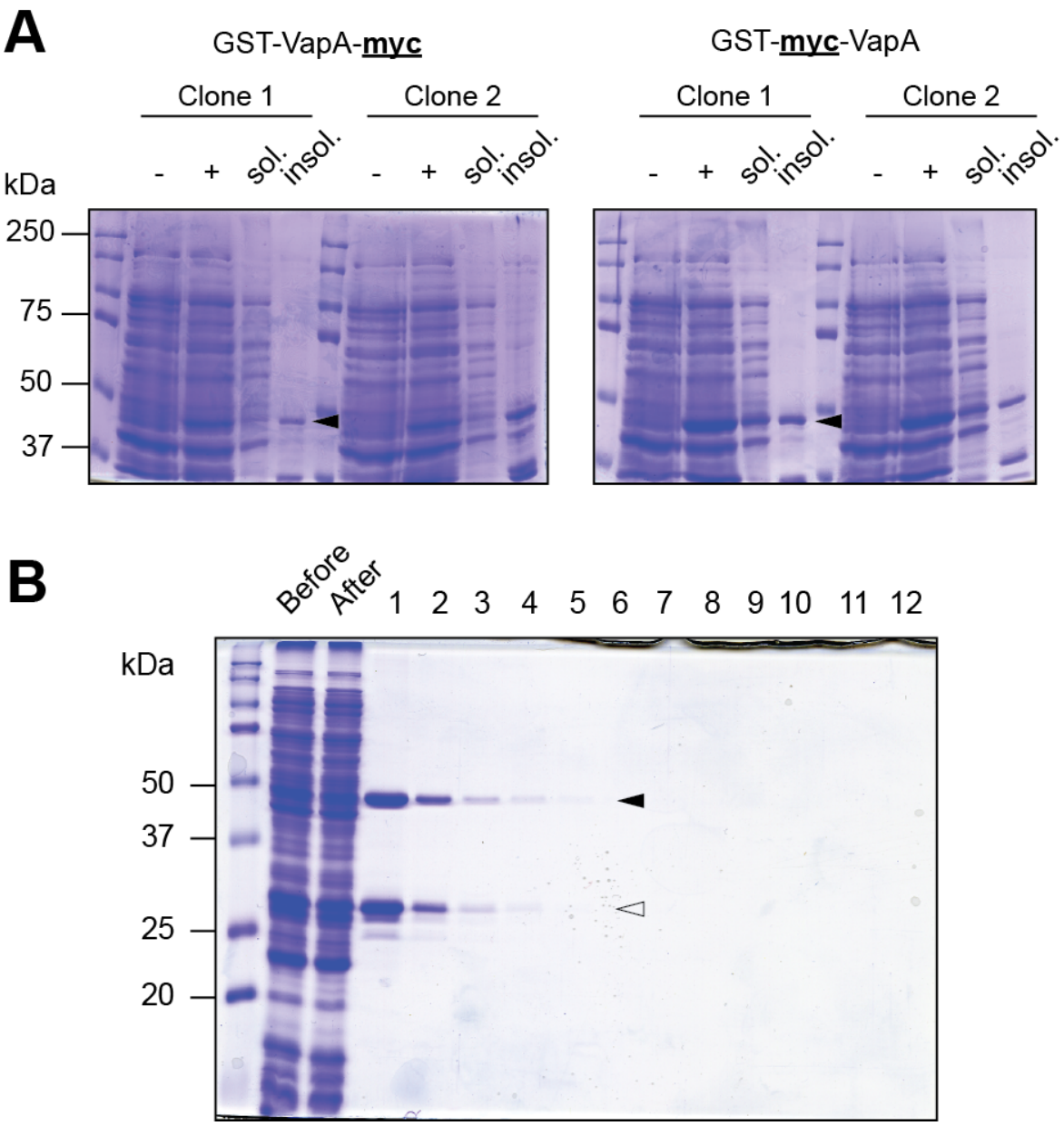

Fig. 4.22. Purification of recombinant VapA. A. GST-tagged VapA was expressed in *E.coli* with a myc epitope on the N or C terminus of VapA. Expression of VapA was induced with 0.2 mM IPTG. Pre-induction (-), post-induction (+), soluble (sol.) and insoluble (insol.) fractions were analysed for expression of GST-VapA. Closed arrowheads indicate GST-VapA-myc/GST-myc-VapA at approximately 46 kDa. **B.** *E.coli* expressing GST-myc-VapA were grown to an OD_{600} of 1.0-2.0. Protein expression was induced with the addition of IPTG to 0.2 mM for 4 hours. The cell pellet was lysed and the soluble fraction applied to a GST-sepharose column. Samples of the lysate were collected before and after the column for analysis. The column was washed extensively and 1 ml fractions were eluted from the column and analysed by SDS PAGE. Closed arrowhead indicates GST-myc-VapA, open arrowhead indicates soluble GST/degradation products.

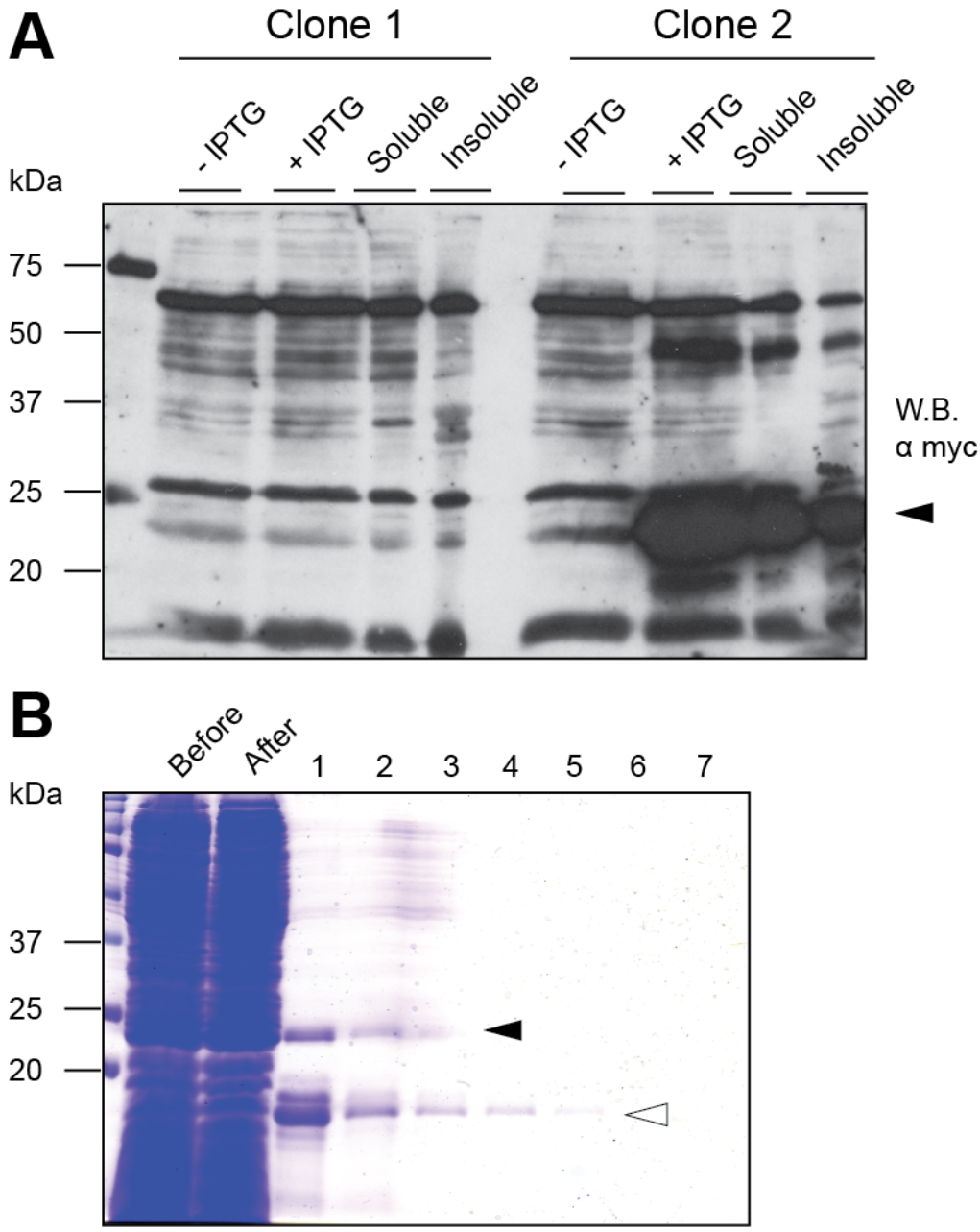

Fig. 4.23. Production of myc-VapA-His. A. Small scale test expression of Myc-VapA-his. Two *E.coli* clones were grown to an OD_{600} of 1.0-2.0 and protein expression was induced for 4 h by the addition of IPTG to 0.2 mM. Cell pellets were lysed and soluble and insoluble fractions analysed by western blot using anti-myc antibodies. Closed arrowhead indicates induction of VapA expression in clone 2. **B.** Large scale expression of myc-VapA-his. The cell pellet from a 1 l culture was lysed and the soluble fraction applied to a Ni-affinity sepharose column. Samples of the lysate were collected before and after the column for analysis. The column was washed extensively and 1 ml fractions of recombinant protein were eluted from the column and analysed by SDS PAGE. The closed arrowhead indicates myc-VapA-His, the open arrowhead indicates degradation products. The predicted molecular weight of myc-VapA-His is 21 kDa.

4.3.6 Recombinant VapA causes swelling of lysosomes in mammalian cells.

As VapA did not cause a phenotype when expressed in the mammalian cell cytoplasm, it was targeted to the lysosome lumen. By culturing cells in the presence of recombinant protein, VapA would be internalised through fluid-phase endocytosis and trafficked to the lysosome for degradation. Thus, if the target of VapA is on the lumenal side of the lysosomal membrane then this methodology should reveal if VapA is able to disrupt lysosome function. To investigate whether VapA had any effect on mammalian intracellular trafficking, J774.2 mouse macrophages were incubated with either GST or GST-myc-VapA at 100 µg/ml for 24 h and the effect on lysosomes examined by confocal microscopy (Fig. 4.24). A potential caveat to this method is that any effect on the cells could be due to contaminating proteins or endotoxin from the bacterial expression strain. To control for this cells were also incubated with GST alone at the same concentration.

Lysosome size and distribution in J774.2 cells incubated with GST did not appear be different from control cells. However, cells incubated with GST-myc-VapA appeared to have larger and swollen lysosomes compared to control cells and cells incubated with GST alone. Therefore, it was decided to further characterise the effect of VapA on lysosomes and identify the underlying mechanisms behind this. Although macrophages are the normal host cell for *R. equi*, the available cell line (J774.2) was not ideal for confocal analysis of lysosome morphology. This was because J774.2 cells have a small cytoplasmic volume and their lysosomes do not form discrete puncta (see control cells). Moreover, there is not a clear perinuclear distribution of lysosomes and larger puncta can sometimes be observed in control cells. The magnification needed to view these cells also makes it difficult to resolve the morphology of the lysosomes. An alternative cell line, Normal Rat Kidney (NRK) cells, were available to confirm the observation that recombinant VapA induces lysosome swelling. In NRK cells, the lysosomes are primarily distributed around the perinuclear region and take the form of discrete puncta (Fig. 4. 26). To see if NRK cells could be used as an alternative cell line for these experiments, cells were incubated with GST or GST-Myc-VapA at 10 µg/ml or 100 µg/ml for 24 h. Cells were then imaged using confocal microscopy to assess the lysosome phenotype. When incubated with GST at either 10 µg/ml or 100 µg/ml, the lysosomes remained perinuclear and punctate (Fig. 4.25). When the cells were

incubated with GST-myc-VapA at 10 μg/ml and 100 μg/ml, lysosomes in both the perinuclear region and cell periphery showed a swollen morphology. Moreover, to demonstrate that this was an effect of the VapA protein and not contaminating endotoxin, cells were incubated with VapA that had been heated to 95 ºC for 15 min (Fig. 4.26). This would denature the secondary protein structure of VapA, abolishing its activity, but would not destroy LPS. Thus, any effects seen after the protein was heated would not be attributable to VapA. Lysosomes in cells incubated with heated VapA were indistinguishable from control cells. These data confirmed the previous observations in J774.2 macrophages. Therefore, NRK cells were used for further experiments to more easily examine the effect of VapA and the other Vap proteins on lysosome morphology, since the effects of VapA were more readily visualised in this cell line. Lysosomal swelling in cells treated with VapA-His appeared to be exaggerated compared to cells incubated with GST-myc-VapA. This may have been due to a higher purity his-tagged protein compared to the GST fusion protein, which also contained soluble GST. Therefore, his-tagged VapA was used for further experiments.

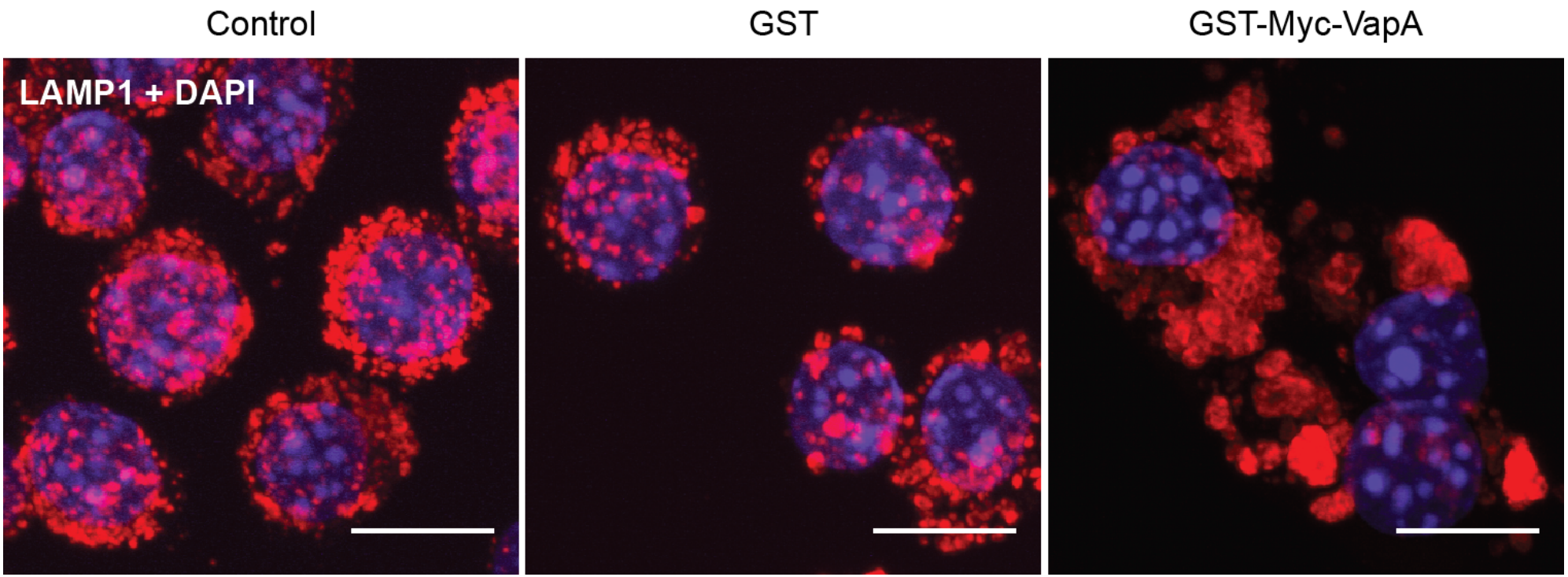

Fig. 4.24. The effect of recombinant GST-VapA on lysosome morphology. J774.2 mouse macrophages were incubated with no protein (control), GST or GST-myc-VapA at 100 µg/ml for 24 h. Cells were washed in PBS and then fixed by incubation in methanol at – 20 ºC for 5 min. Cells were then labelled with α-LAMP1 antibodies followed by a fluorescently secondary antibody (Alexa fluor 555; red) and nuclei stained with DAPI (blue). Scale bar 10 µm. Confocal images are maximum-intensity z-projections. Images are representative of two independent experiments.

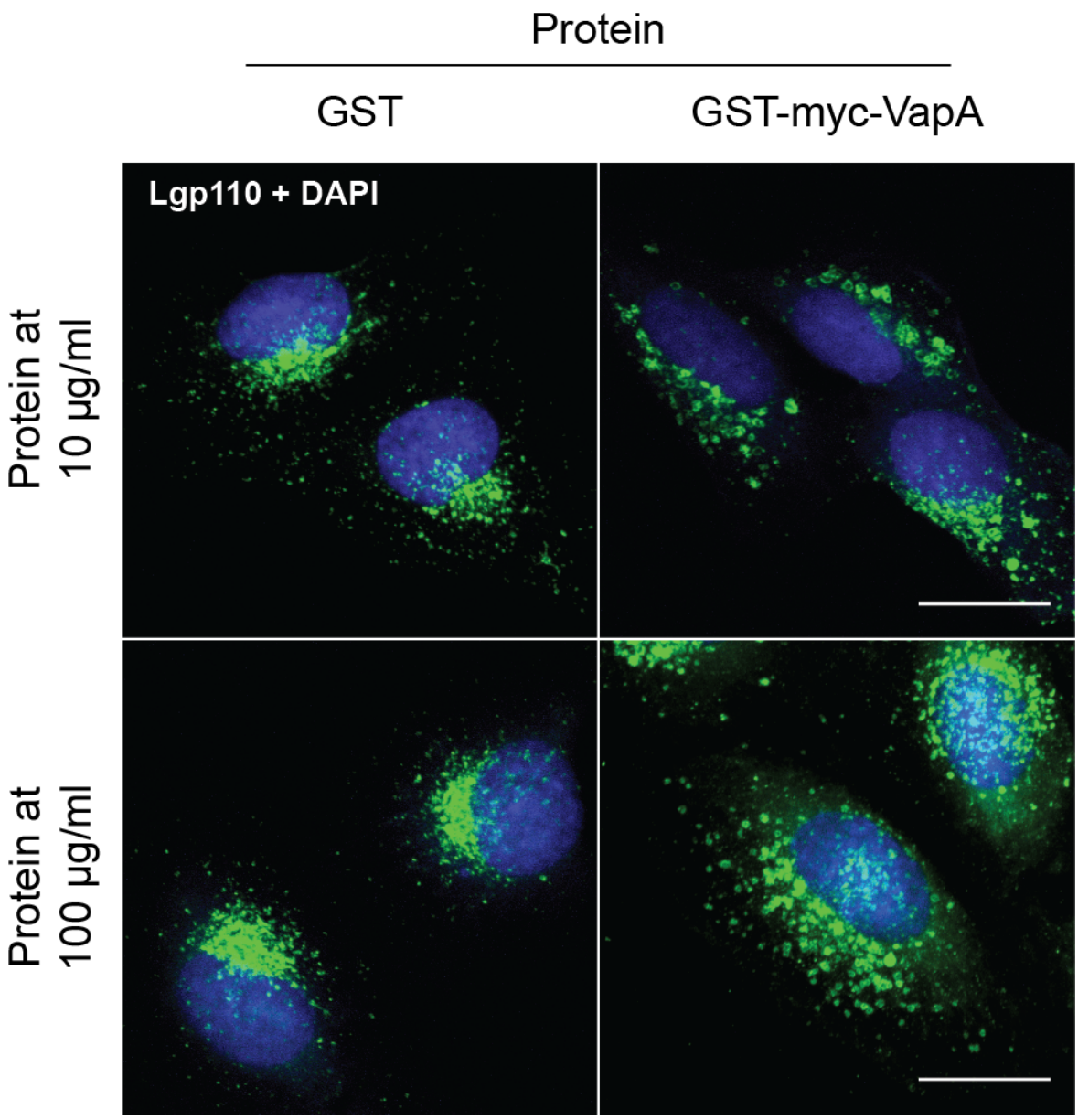

Fig. 4.25. The effect of recombinant VapA on lysosome morphology. Normal Rat Kidney (NRK) cells were incubated with GST or GST-myc-VapA or at 10 µg/ml or 100 µg/ml for 24 h. Cells were washed three times with PBS and fixed in 4 % formaldehyde in PBS. Cells were then permeabilised and labelled with α-Lysosomal glycoprotein 110 (Lgp110) antibodies followed by fluorescent secondary antibodies (Alex Fluor 488; green). Nuclei were stained with DAPI (blue). Scale bar 20 µm. Confocal images are maximum-intensity z-projections and images are representative of two independent experiments.

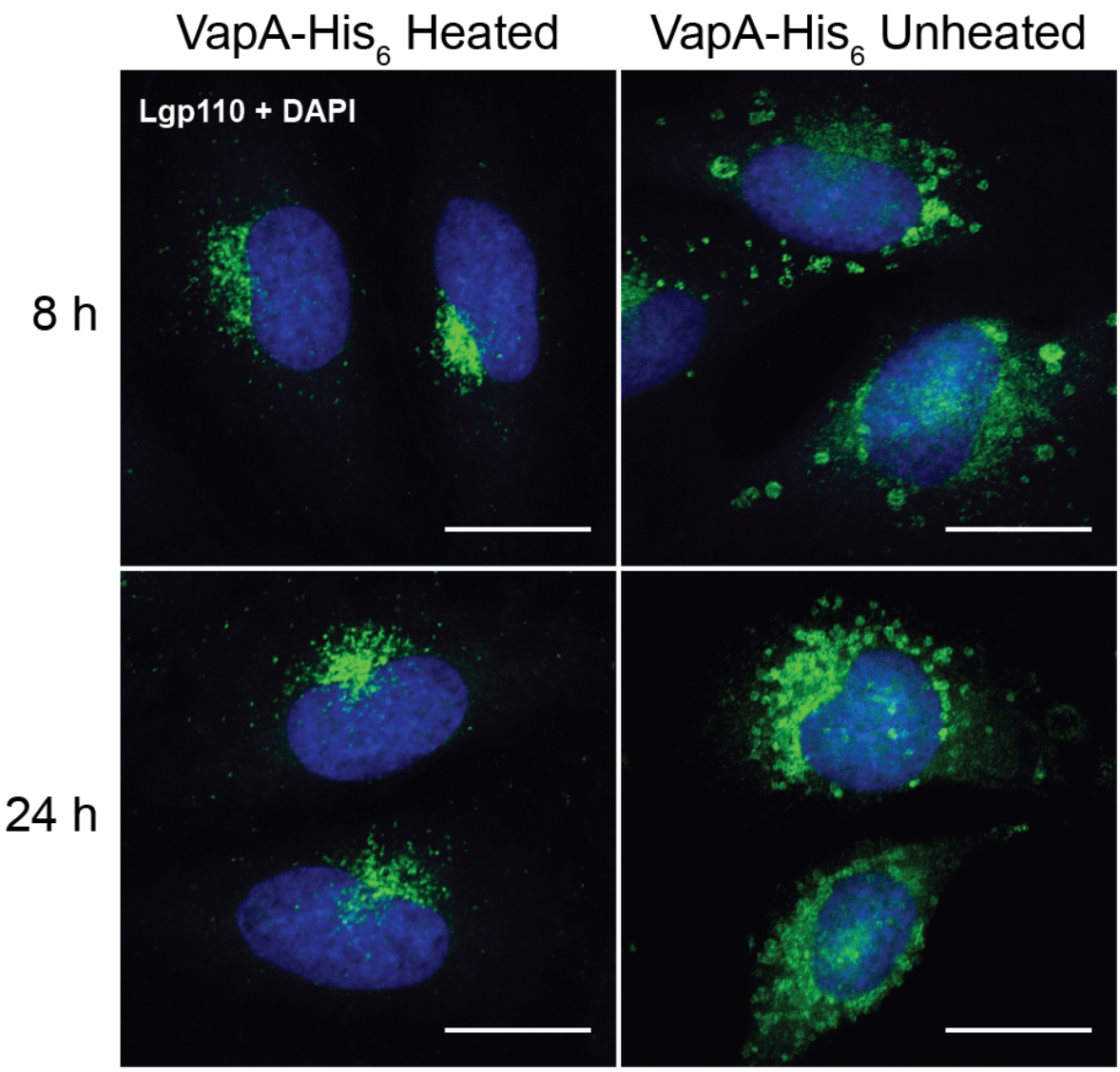

Fig. 4.26. Heat denatured recombinant VapA does not induce lysosomal swelling. NRK cells were incubated with recombinant VapA-His_6 (for 8h or 24 h), where the protein had either been heated or not to 95 ºC for 15 min,. Cells were rinsed with PBS and fixed with 4 % formaldehyde in PBS. Cells were permeabilised and labelled with α-Lgp110 antibodies followed by fluorescent secondary antibodies (Alex Fluor 488; green). Nuclei were stained with DAPI (blue). Scale bar 20 µm. Confocal images are maximum-intensity z-projections (n=1).

4.4 Discussion

4.4.1 Generation of an *R. equi* gene library

The purification of sufficient quantities of *R. equi* DNA was challenging. At the time of this work, there were no published instance of the creation of a *R. equi* gene library. Previously described methods were inefficient and did not yield enough DNA. This is most likely due to difficulty in releasing DNA from the cells. In another mycobacterial species, *Mycobacterium tubercuolosis*, DNA purification using commercial kits is difficult unless additional digestion/chemical lysis steps are added to weaken the bacterial cell wall (Thakur et al., 2011), which is particularly resistant to degradation due to its thickness and large amount of polysaccharides (Brennan and Nikaido, 1995). Despite this, a modified CTAB/Phenol:chloroform method was successful at purifying large amounts of *R. equi* for generating the library. The separation of plasmid and chromosomal DNA using caesium chloride centrifugation was unfortunately unsuccessful. This may have been because more DNA was needed to clearly see the separation of DNA at different parts of the gradient, since the virulence plasmid is at a low copy number. However, the inclusion of the plasmid DNA in the library was deemed to be acceptable due to the low number of putative virulence genes (~ 25). Thus, a library was made that covered the *R. equi* genome sufficiently and required the screening of 8,700 colonies to cover each gene once.

4.4.2 Screening of the R. equi genome

As ~8,700 colonies were needed to find one particular clone and 746,000 yeast colonies were screened, this gave an average of 87 yeast colonies for any one *R. equi* gene. As the screen was repeated 3 times this represents a substantial screening of the *R. equi* genome. The fact that the PEPSY screen did not yield any positive clones, despite the significant coverage of the *R. equi* genome and high number of clones may indicate that this particular methodology was not suitable for *Rhodococcus.* The PEPSY screen is a proven methodology that has been used successfully for, *Legionella* (Shohdy et al., 2005), *Salmonella* and *Yersinia* (Tabuchi et al., 2009). These pathogens are all gram negative and posses type three secretion systems (T3SS), or in the case of *Legionella*, type four secretion systems (T4SS). These are multi-subunit protein translocation

apparatus, related to the flagellum (Gophna et al., 2003), that are used by bacteria to deliver effector proteins across host cell membranes (Cornelis, 2006). For intracellular pathogens, a T3SS/T4SS may be used to deliver factors across the phagosome membrane into the host cell cytosol. In the case of *Salmonella* and *Legionella*, these virulence proteins may act to prevent the fusion of the pathogen containing phagosome with the lysosome (Ramos-Morales, 2012, Hubber and Roy, 2010b). The host cell targets of these proteins are therefore cytoplasmic. This is in stark contrast to *R. equi* which does not have a T3SS. *R. equi* has a type seven secretion system (T7SS) which is unable to span host cellular membranes (Letek et al., 2010). It must be assumed that *R. equi* can only secrete factors into its immediate surroundings and cannot actively translocate proteins into the host cell cytoplasm. As such, the host cell targets of any *R. equi* virulence factors that prevent its delivery to the lysosome are likely to be on the lumenal side of the phagosome membrane. Expressing these proteins in the yeast cytoplasm may not result in a VPS phenotype, as their targets are inaccessible. Similarly, *M. tuberculosis* does not have a T3SS but does have multiple T7SSs (Abdallah et al., 2007). Interestingly, *M. tuberculosis* has several virulence factors which act upon cytoplasmic host cell proteins (Chopra et al., 2004, Sun et al., 2013, Wong et al., 2011) including a type seven secretion substrate (Mehra et al., 2013). Despite the current ambiguity as surrounding the mechanisms by which *M. tuberculosis* factors enter the cytoplasm, clearly there are some proteins that do indeed escape the phagosome and exert their effects cytoplasmically. Furthermore, PEPSY screening has also been used to identify a novel *M. tuberculosis* effector that disrupts phagosome maturation (Thi et al., 2013). Given this fact and the similarities between *R. equi* and *M. tuberculosis*, it was not unreasonable to assume that this methodology may have been suitable for *Rhodococcus.*

Yeast has been used extensively to study the effects of over expressing bacterial proteins on yeast cellular functions. Aleman *et al.*, (2009), screened two separate *Salmonella* gene libraries and identified 68 ORFs that induced a growth inhibition phenotype when over expressed in yeast, including two previously unidentified effector proteins, SteC and SseF. A similar methodology was employed by Slagowski *et al.*, (2008), who developed a high throughput screen which analysed the growth kinetics of yeast expressing *Shigella* or *Francisella* proteins. The authors demonstrated that growth inhibition phenotypes in yeast expressing

pathogen effector proteins, is specific and sensitive. The expression of 19 T3SS substrates resulted in half of them causing growth inhibition, whereas expression of 20 non-translocated proteins did not. The expression of >1000 *Francisella* genes resulted in only three that induced minimal growth inhibition. Many of these genes had previously been assigned a putative housekeeping function, indicating that the over expression of proteins that do not have eukaryotic targets rarely causes a negative phenotype. *Francisella* prevents phagosome acidification and ultimately escapes into the host cell cytoplasm (Steiner et al., 2014). Interestingly it does not have a known (identified) secretion system that is capable of translocating proteins into the host cell cytoplasm (Forsberg and Guina, 2007). Similarly, *Rhodococcus* effector proteins may be secreted within the phagosome lumen and have no effect when expressed in the yeast cytoplasm. Yeast have been used to express a variety of different bacterial effector proteins from both gram negative and gram positive bacteria, including Salmonella (Vinh et al., 2010) *Legionella* (Shohdy et al., 2005*)* and *Mycobacterium* (Thi et al., 2013). Lesser and Miller (2001), found that both *Salmonella* and *Yersinia* effector proteins localised to the same subcellular locations in yeast as in mammalian cells. This shows firstly, that yeast can be used as a system to study bacterial virulence factors, providing that the targets of those effector proteins are evolutionarily conserved between higher and lower eukaryotes. Secondly, it demonstrates that the mode of delivery is not important when studying these proteins in yeast, (i.e. delivery through a bacterial secretion system, or *de novo* synthesis). The relative easy at genetically manipulating yeast also makes them a good system for studying bacterial pathogenesis.

4.4.3 Expression of VapA in yeast

As the PEPSY screen failed to identify any *R. equi* genes able to disrupt intracellular trafficking, it was decided to take a more targeted approach to unravelling the intracellular survival of *R. equi.* The genome analysis of *R. equi* revealed several potential genes that shared homology to known or putative virulence factors in other pathogenic species of bacteria (Letek et al., 2010). Given that *R. equi* strains lacking the virulence plasmid are non-pathogenic it was possible that genes present on the virulence plasmid were most likely responsible in part for its virulence. As such, genes from the plasmid pathogenicity island,

(specifically the Vap genes) were good candidates to express in yeast and mammalian cells to determine if they had any functional effects. One of the Vap genes, VapA, was an obvious target, having been shown to be the only known essential gene for *R. equi* virulence (Giguere et al., 1999, Jain et al., 2003).

The PEPSY screen relied upon yeast being able to effectively express *R. equi* proteins with correct protein folding. The expression of proteins could not be tested on yeast clones transformed with the gene library, as the pVT100-U expression vector did not include an epitope tag. Myc-tagged VapA was expressed using the same expression plasmid as the PEPSY screen, to determine i) if *R. equi* genes could be expressed properly in yeast and ii), if VapA had a functional effect. Western blotting of yeast lysates using α-myc antibodies revealed the presence of a 20-25 kDa band in myc-VapA expressing yeast, but not in control yeast, indicating that VapA could be expressed. To date, this is the first instance of *R. equi* genes being expressed in yeast. Western blotting using α-VapA antibodies showed a similar band of 25 kDa was detected, along with two smaller bands < 20 kDa, indicating possible degradation of the over-expressed protein. To determine whether myc-VapA disrupted trafficking in yeast, clones over-expressing the protein were assessed for secretion of CPY-invertase, using a qualitative assay. None of the clones exhibited a VPS phenotype. The variable expression of myc-VapA may have masked any phenotype, or yeast expressing enough myc-VapA to cause a trafficking defect may not have been viable.

While expression of VapA could be detected, no phenotype was observed when analysing endocytic trafficking (by CPY assay). Given that *R. equi* has no known means of translocating proteins from the *Rhodococcus*-containing vacuole into the cytoplasm, VapA would never see the cell cytoplasm in an infection *in vivo*. If VapA plays a role in pathogenesis from within the vacuole, it may be unsurprising that no phenotype is observed when VapA is expressed in the cell cytoplasm. To address this issue, VapA was targetted to the yeast vacuole by expressing it as a GFP-ALP fusion protein. When analysed by western blotting, a ~100 kDa band was found in strains expressing GFP-ALP, but not in the control parental strain. GAMV strains were found to express a band of the same molecular weight, but also one of ~120 kDa. This most likely corresponded to the expression of full length GAMV, but also with the expression of the cleaved protein. However,

cleaved VapA could not be detected using α-myc antibodies. Protein bands of 120 kDa and 15 kDa were detected when GAMV yeast were blotted using α-VapA antibodies. This was consistent with the cleavage of VapA from GFP-ALP, but the result of this single experiment should be viewed with caution. These data may explain the lack of CPY secretion, as rapid degradation of cleaved VapA by resident vacuole proteases would prevent VapA from disrupting vacuolar trafficking. Secondly, the epitope tag used to detect expression by western blotting may have hindered the ability of VapA to disrupt trafficking. To determine if this was the case, these experiments were repeated with the myc tag added to the C-terminus of VapA. However, this did not result in a change in CPY secretion, suggesting that the epitope tag had no effect (data not shown). The most likely explanation for the lack of a phenotype in yeast expressing VapA, is that the mammalian target of VapA may not have an orthologue in yeast, or the yeast equivalent may not have a high enough degree of homology to interact with VapA. As with myc-VapA, the heterogeneous expression of exogenous proteins driven off of 2 μm plasmids may have also masked any potential effects of GAMV. Alternatively, yeast expressing enough GAMV to cause a trafficking defect may not have been viable.

4.4.4 Expression of VapA in mammalian cells

As the natural host of *R. equi* is equine alveolar macrophages, expressing VapA in mammalian cells would be more representative of *Rhodococcus* infection. Myc-VapA was expressed in HeLa cells to examine the effects of VapA. Myc-VapA was detectable in HeLa cell lysates, but immunofluorescence microscopy revealed that only 10-20 % of cells expressed VapA strongly. To determine if VapA had an effect on endocytic trafficking, it was asked whether VapA co-localised with markers of the endocytic pathway. Expression of VapA was induced for 16 h and cells were labelled with antibodies for early endosomes (EEA1), late endosomes (ciM6PR) and lysosomes (LAMP1). Surprisingly, VapA did not co-localise with any of these markers and the appearance of these organelles was indistinguishable from control cells.

As with the yeast, it was hypothesised that VapA had to be on the lumenal side of the lysosome in order to exert any effect. To target VapA to the mammalian lysosome, recombinant fusion proteins were made. A myc tag was added to the N or C terminus of VapA, as it was not clear whether the epitope tag would interfere with VapA function when added to either end of the protein. This was so VapA could be visualised by immunofluorescence using α-myc antibodies should the GST affinity tag be removed. The GST-VapA-myc proved less soluble than GST-myc-VapA, which was then taken forward for large scale production. The yield of protein was low (1 mg from a 1 L culture), but sufficient for feeding experiments. As the GST-tag may have inhibited VapA function, His_6-tagged VapA was also produced, as the smaller his tag (1 kDa c.f. 26 kDa) would be much less likely to disrupt VapA function. The presence of GST did not prevent VapA from functioning, as indicated by the feeding experiments. However, the presence of soluble GST/GST-VapA degradation products in the purified protein reduced the actual amount of full-length VapA present in the sample. Therefore, VapA-His was used for further experiments.

Recombinant VapA was able to induce swelling of lysosomes when taken up J774.2 cells. These cells were used initially as macrophages are the natural host of *R. equi*. However, their small size and general lack of small/discrete lysosomal puncta made it hard to perform any quantification on lysosomal size, as multiple coalescing lysosomes would be scored as a single lysosome when using image analysis software. NRK cells are much larger and have an easily identifiable perinuclear distribution of small lysosomes. When VapA was fed to NRK cells, the effect of VapA was more readily observable. Heating of VapA before adding to cells abolished the lysosomal swelling phenotype. This indicated the effect was protein-dependent and not due any contaminants or co-purified endotoxins. These results may indicate that VapA may affect mammalian cells regardless of cell type. The functional effects of VapA seen when in the mammalian cell lysosome but not in the yeast vacuole, indicates that yeast may not be a suitable system to study *R. equi* pathogenicity. These data also suggest that VapA is not active in the host cell cytoplasm, as recombinant VapA only caused lysosomal swelling when introduced to the lysosome lumen by fluid phase endocytosis. Thus, this effect of VapA was further characterised to determine how it may facilitate the intracellular survival of *R. equi*.

Chapter 5: The role of VapA in the intracellular survival of *R. equi*

5.1 Introduction

5.1.1 *Rhodococcus equi*

Rhodococcus equi (R. equi), is a Gram-positive facultative intracellular pathogen with similarities to *Mycobacterium tuberculosis (*Vazquez-Boland et al., 2013). It infects a wide variety of animals, but has increasingly been isolated from patients with a significant mortality rate (Khan et al., 2013, Nath et al., 2013, Topino et al., 2010, Hayes et al., 2011). *R. equi* survives and replicates in a vacuolar compartment within the host cell (Hondalus and Mosser, 1994), but it is unclear whether *R. equi* prevents its delivery to the lysosome (Fernandez-Mora et al., 2005) or alters the degradative capacity of the lysosome itself (Toyooka et al., 2005).

5.1.2 *R. equi* virulence plasmid

The 90 Kb virulence plasmid of *R. equi* plays a crucial role in intracellular survival. Loss of the virulence plasmid renders the bacteria unable to replicate inside macrophages *in vitro* (Hondalus and Mosser, 1994, Giguere et al., 1999). Avirulent strains are cleared significantly faster in a mouse lung infection model than those strains harbouring the extrachromosomal element (Gonzalez-Iglesias et al., 2014). The virulence plasmid has 73 coding sequences including 8 pseudogenes (Letek et al., 2010). Within the virulence plasmid is an approximately 27 Kb pathogenicity island (PI) characterised by the presence of insertion elements (ORF61 and ORF22) at either end of a block of genes (Takai et al., 2000). A striking feature of the PI is the presence of seven virulence-associated protein (Vap) genes (VapC-H), which were found due to their similarity to VapA (Takai et al., 2000). VapA, C and D are located in close proximity to each other. VapE and VapF are adjacent genes. VapG and VapH are present as separate genes, with VapH as the only Vap gene found on the negative strand. Vaps A,C,D,E,G,H are found as full length genes, whereas VapF, I and X are found as pseudogenes (Letek et al., 2008, Polidori and Haas, 2006, Takai et al., 2000). Figure 5.0 shows a schematic representation of the plasmid pathogenicity island and protein alignment of the different Vaps.

A

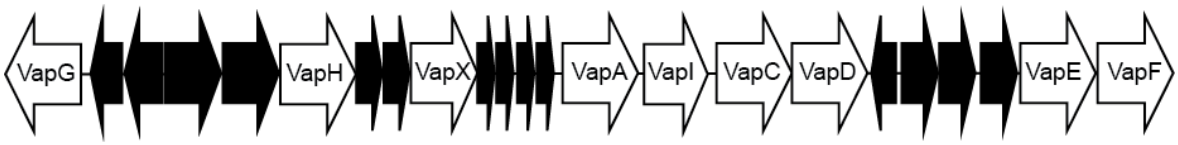
~18.8 Kbp
VapG
VapH
VapX
VapA
VapI
VapC
VapD
VapE
VapF

B

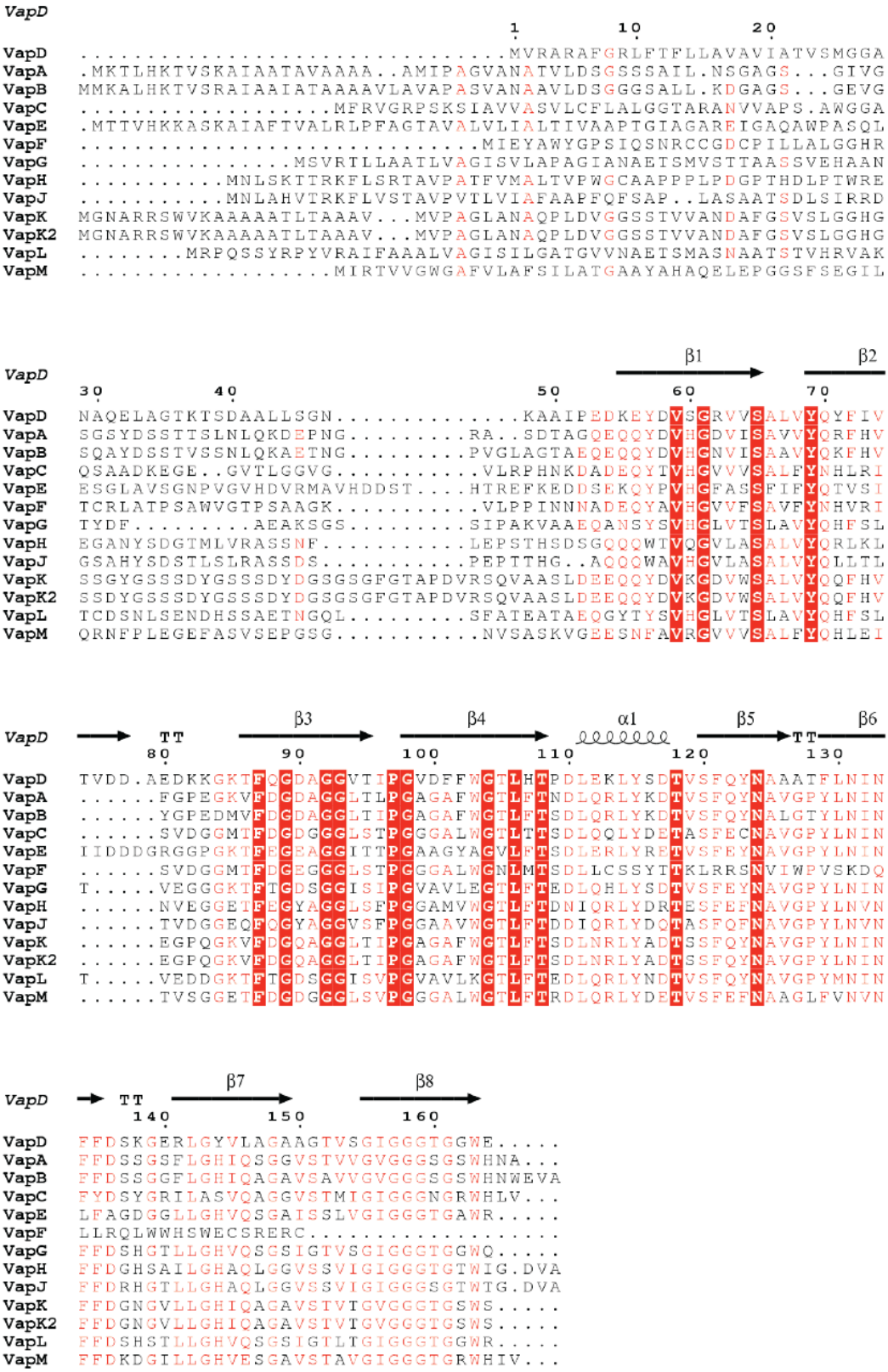
VapD
VapD
VapA
VapB
VapC
VapE
VapF
VapG
VapH
VapJ
VapK
VapK2
VapL
VapM
β1
β2
β3
β4
α1
β5
β6
β7
β8

Non-equine isolates of *R. equi* also possess a virulence plasmid, but these strains produce VapB instead of VapA. VapB is a slightly larger surface protein that shares a high degree of sequence similarity to VapA (81% nucleotide sequence identity). Consistent with a role in virulence, plasmids containing the VapB gene harbour 5 genes with similarity to the Vap containing region of VapA plasmids. VapA and VapB are allelic variants of a single ancestral gene (Letek et al., 2008). Both VapG and VapL are on the negative strand and are likely to be derived from a common gene. Similarly, VapK is the counterpart to VapD and VapM to that of VapX. VapB plasmids also contain two additional genes, VapK1 and VapK2, which likely arose from a duplication event of the ancestral AB gene (Fig. 5.1, Letek *et al*., 2008). The conservation of Vap genes between strains isolated from different hosts may indicate their role in virulence. Isolates obtained from foals are exclusively VapA+ strains with isolates obtained from non-equine sources (including humans) harbouring plasmids with VapA, VapB or no plasmid at all (Makrai et al., 2002). Interestingly, VapB+ strains only display intermediate virulence in a mouse infection model (Takai et al., 1995). These differences in plasmid architecture and Vap genes may indicate that they play a key role in host tropism.

Fig. 5.0. Organisation of VapA-plasmid pathogenicity island and Vap protein alignment. A. Schematic representation demonstrating the gene order and orientation of the *R. equi* VapA-type virulence plasmid pVAPA1037 (Genbank accession no. AM947677.1). Vap genes are shown in white. **B.** Multiple amino acid alignment of the family of Vap genes (including signal peptides) encoded by the plasmids pVAPA1037 (Takai et al., 2000) and pVAPB1593 (Letek et al., 2008). Protein alignment was performed using ESPript (http://espript.ibcp.fr (Robert and Gouet, 2014). The secondary structure of VapD is shown above the alignment. Identical residues are shown in red.

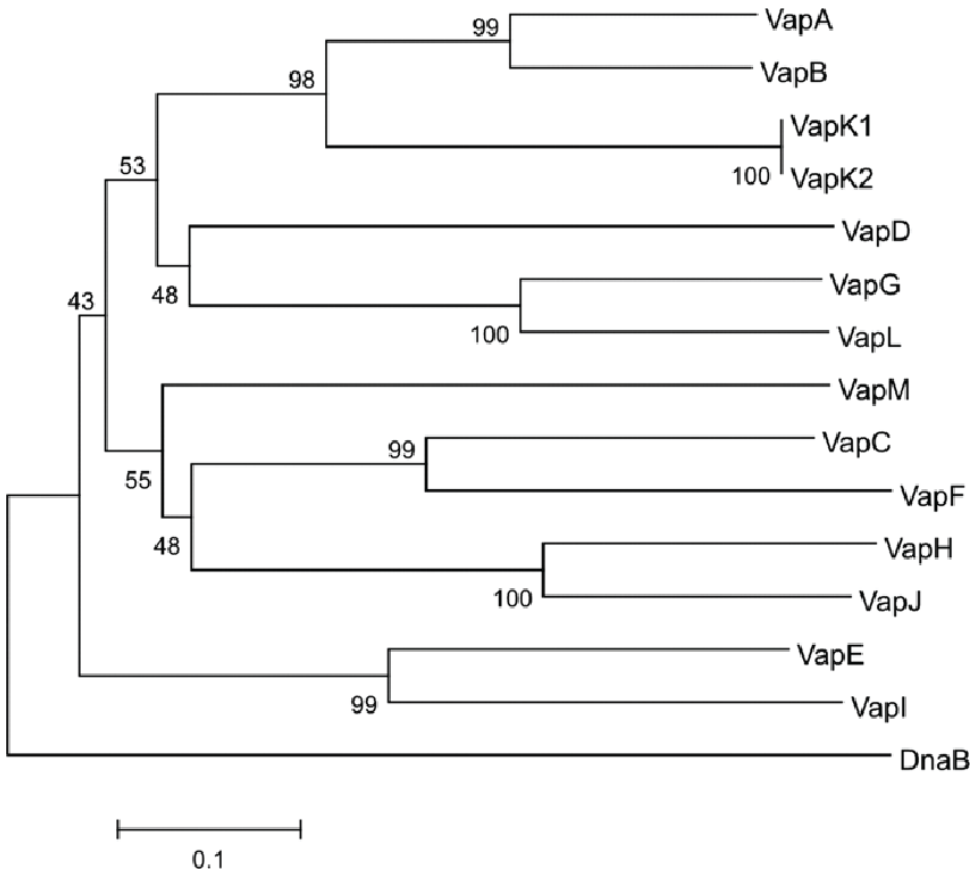

Fig. 5.1. Phylogenetic tree of the Vap genes of *R. equi*. Neighbour-joining unrooted phylogenetic tree of the Vap multigene family constructed from a ClustalW alignment of the mature Vap proteins encoded by pVAPB1593 and pVAPA1037. For the analyses, a full-length VapF protein was reconstructed by correcting the two frameshift mutations in the 3′ region of the gene. Bootstrap values (10,000 replicates) are indicated at the nodes. Outgroup, putative DnaB protein from pVAPB1593 (pVAPB_0390). The bar indicates genetic distance. Figure and figure legend reproduced, with permission, from Letek *et al*., 2008.

5.1.3 VapA is essential but not sufficient for virulence

The presence of the plasmid is widely accepted as a prerequisite for intracellular survival and replication inside eukaryotic cells, although plasmid free strains may also persist inside non-phagocytic cell types (Ramos-Vivas et al., 2011). The expression of VapA in particular has been associated with virulence *in vivo* in both mice and foals (Takai et al., 1991, Giguere et al., 1999). VapA has also been shown to be necessary but not sufficient for virulence, since VapA alone can restore virulence to a VapC-F mutant, (Jain et al., 2003) but cannot restore virulence to plasmid-cured *R. equi* strains (Giguere et al., 1999).

Recently, it has been shown that the expression of VapA along with two other genes *VirR* and *VirS* are the minimum genes required for intracellular growth of *R. equi* (Coulson et al., 2015). VirR is a LysR-type transcriptional regulator (Russell et al., 2004) and VirS is an OmpR/PhoB response regulator (Kakuda et al., 2014), both of which required for proper VapA gene expression (Ren and Prescott, 2004). When VirR, VirS and VapA were added back to plasmid cured *R. equi* (under control of their native promoters), virulence was restored to near wild-type levels (Coulson et al., 2015). This may explain why VapA alone cannot restore virulence. Additionally, the presence of *VirR* and *VirS* was shown to induce changes in gene transcription in 18 % of the *R. equi* genome (Coulson et al., 2015). This suggests that the presence of the plasmid is needed to regulate chromosomal genes that may be required for intracellular growth. It is also interesting to note that another gene *Icga*, actually lowers the intracellular replication of *R. equi* resulting in prolonged infection of macrophages (Wang et al., 2014).

5.1.4 Induction of Vap gene expression

The expression of the Vap proteins has been shown to be regulated by several different factors. Growth at 37 ºC but not 30 ºC results in production of the Vap proteins (Byrne et al., 2001). Similarly, growth at 38 ºC induces VapA expression, but not unless the pH is below 8 (Takai et al., 1996). Exposure of *R. equi* to low pH (5.0) has also been shown to increase the expression of VapA (Benoit et al., 2001) and expression of plasmid genes in low concentrations of iron, calcium and magnesium, mimics that of protein expression *in vivo* (Ren and Prescott, 2003). These are conditions encountered inside the macrophage phagosome and these data are consistent with the Vap proteins having a role in pathogenicity (Byrne et al., 2001). Interestingly, VapA appears to be the only Vap that is not secreted and that is anchored to the bacterial surface (Tan et al., 1995).

5.1.5 The structure of VapA

The structures of VapB, (Geerds et al., 2014) VapD, (Whittingham et al., 2014) and VapG (Okoko et al., 2015) have been solved. While the N-terminus of the Vaps varies and is presumed to be disordered, the C-terminal core is remarkable conserved between the different Vaps (Fig. 5.0 & 5.2). While there are some differences the core of the Vap proteins is very similar. The core of VapD consists of a compact, closed β-barrel (Whittingham et al., 2014). One end of the barrel has

a smooth apolar surface, whilst the more complex end of the barrel is made of polar and charged residues. However, the structure of the Vap proteins lacks an obvious ligand-binding site or an enzyme active site and gives no clues as to its function (Whittingham et al., 2014).

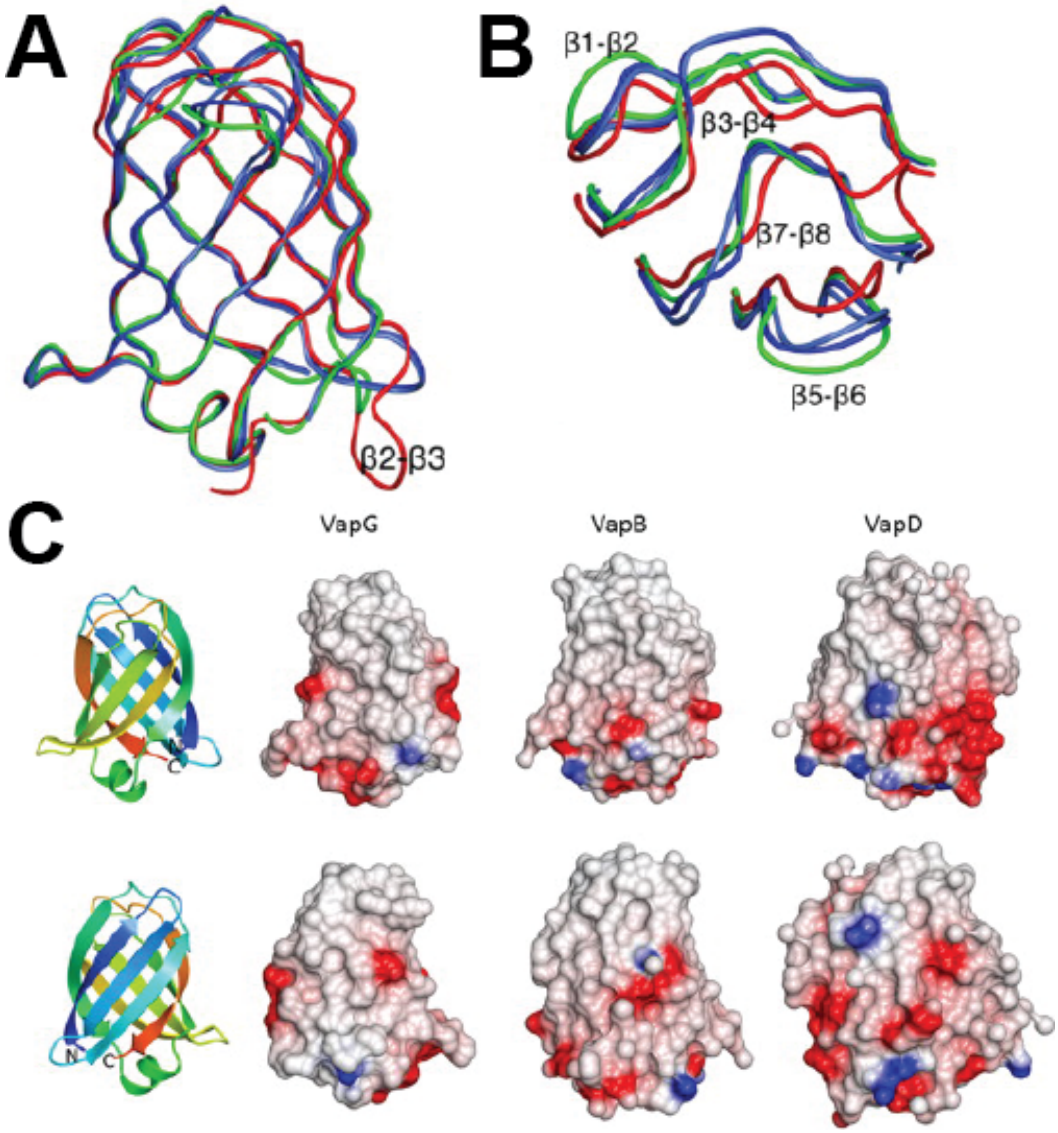

Fig 5.2. The crystal structures of VapB, VapG and VapD. **A&B.** The structures of VapG (blue), VapD (red) and VapB (green) polypeptide backbones displayed as worm tracings. The superposed protein chains are viewed from the side illustrating the whole molecules (A) and from above parallel to the long axis of the barrel with the molecule clipped for clarity (B). **C**. Electrostatic surface renderings of VapB, VapD and VapG with positive electrostatic potential in blue and negative electrostatic potential in red. The three molecules are viewed in two orientations which are illustrated by the ribbon tracing for VapG at the left. The extended apolar surface previously noted for VapD and VapB is evident. Figure and figure legend reproduced with permission from Okoko *et al.,* (2015).

5.2 Materials and methods

5.2.1 Recombinant VapA feeding

J774.2 mouse macrophages were seeded in 6 well-plates containing glass coverslips at a density of $1x10^5$ cells per well and cultured in DMEM for 24 h. Alternatively, Normal Rat Kidney (NRK) cells were plated onto glass coverslips at a density of $1x10^4$ cells per well of a 24 well plate and cultured in DMEM for 24 h. The media was then replaced with 1 ml of DMEM containing recombinantly produced GST (100 µg/ml) or DMEM containing recombinant GST-myc-VapA or VapA-His_6 (100 µg/ml) and cells cultured for the different lengths of time. Where protease inhibitors were used, leupeptin was added to all cells at the beginning of the time course to a final concentration of 21 µM. Coverslips were rinsed three times with Dulbecco's modified phosphate buffered saline (Sigma) and fixed using methanol, or alternatively, 4 % formaldehyde in PBS, followed by immunolabelling using appropriate antibodies, as previously described in section 2.16.

5.2.2 Infection assays

J774.2 cells were seeded at 5 x 10^5 cells per well of a 6-well plate and cultured overnight in antibiotic-free DMEM supplemented with 10 % (v/v) FBS (heat inactivated to 56 ºC for 30 min) and 2 mM glutamine. *R. equi* was cultured overnight in BHI media with shaking at 30 ºC followed by a 1 h incubation at 37 ºC to induce the production of Vaps (virulence associated proteins) and other virulence factors. Bacteria were pelleted at *3000 x g* for 10 min in a microcentrifuge and washed twice in PBS. Cell number was determined by measuring the OD_{600} and comparing the value to a standard curve of bacterial OD_{600} vs colony forming units (cfu). An OD_{600} of 1.0 was approximately $1x10^8$ bacteria per ml. Bacteria were resuspended in PBS and an appropriate number of cells taken to infect mammalian cells at an MOI (multiplicity of infection) of 10. Bacteria were centrifuged onto cells at *80 x g* for 5 min and incubated for 1 h at 37 ºC to allow phagocytosis of bacteria. Monolayers were rinsed 3 times with DMEM to remove unbound bacteria and the media replaced with DMEM containing 150 µg/ml gentamycin to kill extracellular bacteria. The cells were cultured for a further hour and washed again with PBS. The media was then replaced with DMEM containing 10 µg/ml gentamycin and cells cultured for different lengths of time, upon which the cells were fixed with 4 % formaldehyde in PBS for 20 min at room

temperature, or by incubation at -20 ºC in 1 ml of methanol that had been cooled to -20ºC, for 5 min. Cells were then labelled using the appropriate primary and fluorescently labelled secondary antibodies, as described in section 2.16. Colony PCR of *R. equi* for VapA and traA (both plasmid encoded genes) were performed to check for plasmid loss, as previously described in section 2.9.4.

5.2.3 Affinity capture of biotinylated proteins in the cytoplasm

Flp In HeLa cells transfected with either myc-BirA* or VapA-myc-BirA* were grown to confluency (4 x 75 cm^2 flasks per condition) and expression of myc-BirA* or myc-BirA*-VapA was induced with 1 µg/ml doxycycline, in DMEM supplemented with biotin (to a final concentration of 50 µM) for 24 h. The cells were then rinsed three times with PBS and detergent soluble lysates generated as follows: cells were lysed at room temperature (approximately 25 ºC) with 1 ml of lysis buffer (50 mM Tris, pH 7.4, 500 mM NaCl, 0.4 % (w/v) SDS, 5 mM EDTA, 1 mM DTT with protease inhibitors) per flask. Lysates were sonicated in 15 ml tubes for 10 s on ice. Triton X-100 was added to a final concentration of 2 % (v/v) and lysates were sonicated once more for 10 s. An equal volume of 4 ºC 50 mM Tris, (pH 7.4) was added before a final sonication was performed. Lysates were then centrifuged at *16,000 x g* for 15 min at 4 ºC. Detergent soluble supernatants were collected and their protein concentration determined by BCA assay. Lysates were normalised to protein concentration and were then incubated with 600 µl of Dynabeads (MyOne Streptavidin C1, Invitrogen) overnight at 4 ºC with gentle rotation to capture biotinylated proteins (20 µg of each lysate was taken before and after incubation with the beads to determine the efficiency of the experiment by western blotting with a streptavidin-HRP conjugate). The beads were collected on a magnet and resuspended in 1 ml of 2 % (w/v) SDS in ddH_2O for 8 min. The beads were collected on the magnet and the supernatant was discarded. The beads were washed once more in 2 % SDS for 8 min. This was repeated once with the second wash buffer (0.1 % (w/v) sodium deoxycholate, 1 % (v/v) Triton X-100, 500 mM NaCl, 1 mM EDTA, 50 mM HEPES, pH 7.5), once with the third wash buffer (250 mM LiCl, 0.5 % (v/v) NP-40, 0.5 % (w/v) sodium deoxycholate, 1 mM EDTA, 10 mM Tris, pH 8.1) and twice with the fourth wash buffer (50 mM Tris, pH 7.4, 50 mM NaCl). The beads were resuspended in 600 µl of the final wash buffer and 10 % (60 µl) taken for western blot analysis. The remainder of the beads to be analysed by (mass spectrometry) were washed twice (1 ml each wash for 8 min) with 50 mM NH_4HCO_3.

5.2.4 Affinity capture of biotinylated proteins in the lysosome

For capture of biotinylated proteins from the lysosome lumen, Flp In HeLa cells were grown to confluency in T75 flasks (2 flasks for myc-BirA* control, 2 flasks for myc-VapA-BirA*). The cells were then incubated with DMEM containing 100 µg/ml myc-BirA*-His or VapA-myc-BirA*-His for 16 hours. The media was then replaced with fresh DMEM and the cells cultured for a further 4 h. The media was then supplemented with 0.55 ml of PBS saturated with biotin (900 µM) to give a final biotin concentration of 50 µM. Cells were then cultured for a further 24 h. Cells were rinsed 3 times with PBS and the generation of lysates and capture of biotinylated proteins performed as described in section 5.2.3. 20 µg of each lysate before and after incubation with the beads and 10 % of eluted proteins were kept to determine the efficiency of the experiment by western blotting with a streptavidin-HRP conjugate.

5.3 Results

Previously, a yeast-based screen was carried out to identify *R. equi* genes that caused a VPS$^-$ phenotype. The screen did not identify any *R. equi* genes and a target approach was taken to study *R. equi* virulence. The only known essential virulence factor, VapA, was expressed in the yeast cytoplasm and vacuole, but no phenotype was observed. When VapA was expressed in the mammalian cell cytoplasm, no effect on endocytic trafficking was observed. In stark contrast to these results, when VapA was target to the mammalian lysosome lumen (by way of feeding cells recombinant VapA protein), the lysosomes swelled up. This swelling phenotype was further characterised and attempts made to dissect the mechanism behind it.

5.3.1 Lysosomal swelling increases over time

The lysosomes of NRK cells were previously shown to swell up when incubated with recombinant VapA for 8 h or 24 h. Next, NRK cells were incubated with GST or GST-VapA at 100 µg/ml for 2 h, 4 h, 8 h, 16 h, or 24 h (Fig. 5.3) Cells incubated with GST showed lysosomes of normal size and distribution at all time points. The effect of VapA on lysosomes was observable as soon as 2 h, with large lysosomal puncta observable in the perinuclear and peripheral regions of the cell. The number of larger puncta increased over time. At later time points (16 h and 24 h) the vast majority of lysosomes were affected. The overall area of lysosomal staining within the cell appeared to have increased. However, it was not clear whether this was due to increased numbers of lysosomes or an increase in the size of the lysosomes.

.

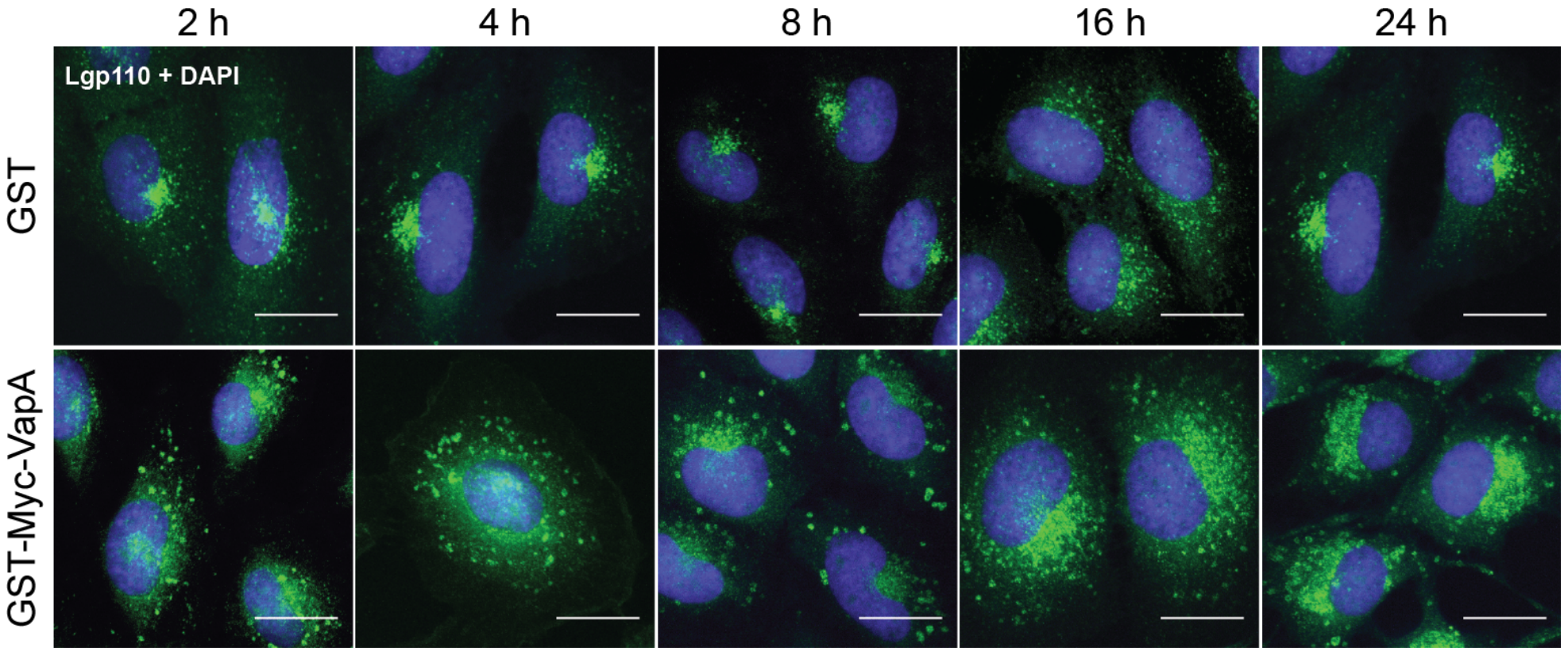

Fig. 5.3. VapA induced lysosomal swelling increases over time. NRK cells were incubated with GST or GST-myc-VapA at 100 µg/ml for the times indicated. Cells were rinsed three times with PBS and fixed with 4 % formaldehyde in PBS before processing for immunofluorescence microscopy. Cells were labelled with α-Lgp110 antibodies followed by fluorescently labelled secondary antibodies (Alexa Fluor 488; green). Nuclei were stained with DAPI (blue). Scale bar 20 µm. Images are maximum-intensity z-projections (n=1).

5.3.2 VapA affects late endocytic compartments

Although the effect of VapA on lysosomal compartments in NRK cells was clear, it was not known if this was specific to lysosomes, or whether early and late endocytic compartments were also affected. To test this, NRK cells were incubated with VapA-His at 100 µg/ml for 8 h, 24 h, or 48 h and processed for immunofluorescence using α-EEA1 and α-Lgp120 antibodies, followed by fluorescent secondary antibodies to visualise early endosomes and late endosomes/lysosomes respectively (Fig. 5.4). In control cells, EEA1 is both cytoplasmic and membrane associated, giving a weak cytoplasmic staining pattern, with some small puncta. After 8 h incubation with VapA, the majority of cells were indistinguishable from control cells. In ~ 1 % of cells however, the distribution of EEA1 altered slightly, with some staining concentrating around the perinuclear region. Some larger EEA1 positive puncta were also observable in these cells. This was also seen at 24 and 48 h. These vesicles were often in close proximity to lysosomes, but there was little colocalisation between the two and the compartments remained distinct. As expected, Lgp120 staining showed that the lysosomes continued to swell and coalesce from 8 h to 48 h.

As there was not a pronounced effect on early endosomes, the effect of VapA on late endosomes/ciM6PR positive vesicles was investigated. NRK cells were incubated with 100 µg/ml VapA for 24 h and the morphology of late endosomes and lysosomes was examined (Fig. 5.5) In contrast to early endosomes, ciM6PR compartments formed large swollen puncta after 24 h of incubation with VapA. Co-staining for ciM6PR and LAMP proteins was performed to distinguish between late endosomes (ciM6PR +, Lgp120 -), lysosomes (ciM6PR -, Lgp120 +) and endolysosomes (ciM6PR +, Lgp120 +). All three of these compartments displayed a swollen morphology after incubation with VapA. Interestingly, some of the ciM6PR staining appeared to be surrounded by Lgp120 staining, but these structures were difficult to resolve. These data indicate that VapA selectively effects late endocytic compartments and does not appear to directly affect early endosomes.

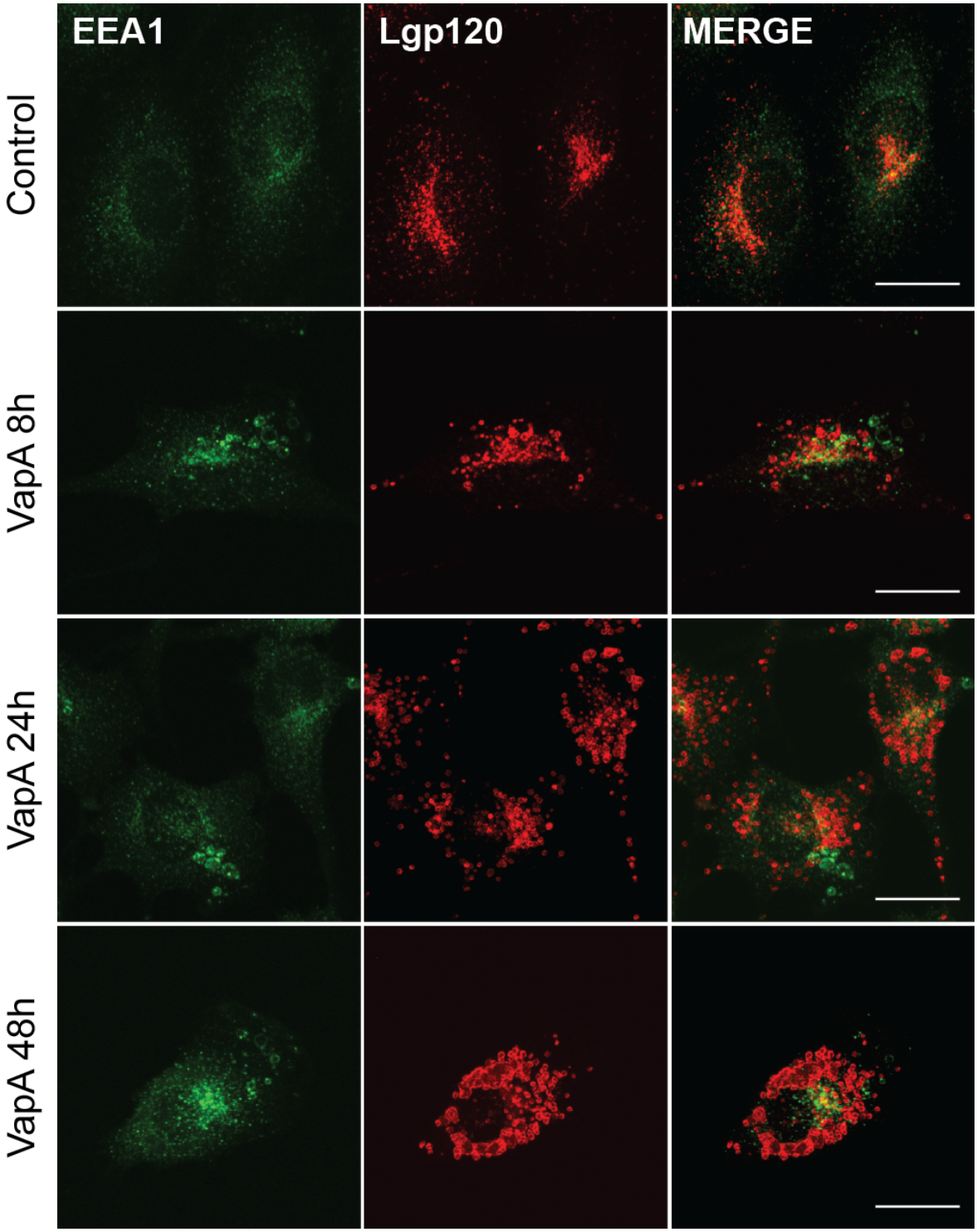

Fig. 5.4. VapA does not affect EEA1$^+$ endocytic compartments. NRK cells were incubated with recombinant VapA-His_6 at 100 µg/ml for the times indicated. Cells were rinsed three times with PBS and fixed with 4 % formaldehyde in PBS before processing for immunofluorescence microscopy. Cells were double labelled with α-EEA1 antibodies and α-Lgp120 antibodies, followed by fluorescently secondary antibodies (Alexa fluor 488; green and Alexa fluor 555; red, respectively). Scale bars 20 µm. Images are maximum-intensity z-projections. Images shown are representative of three separate experiments.

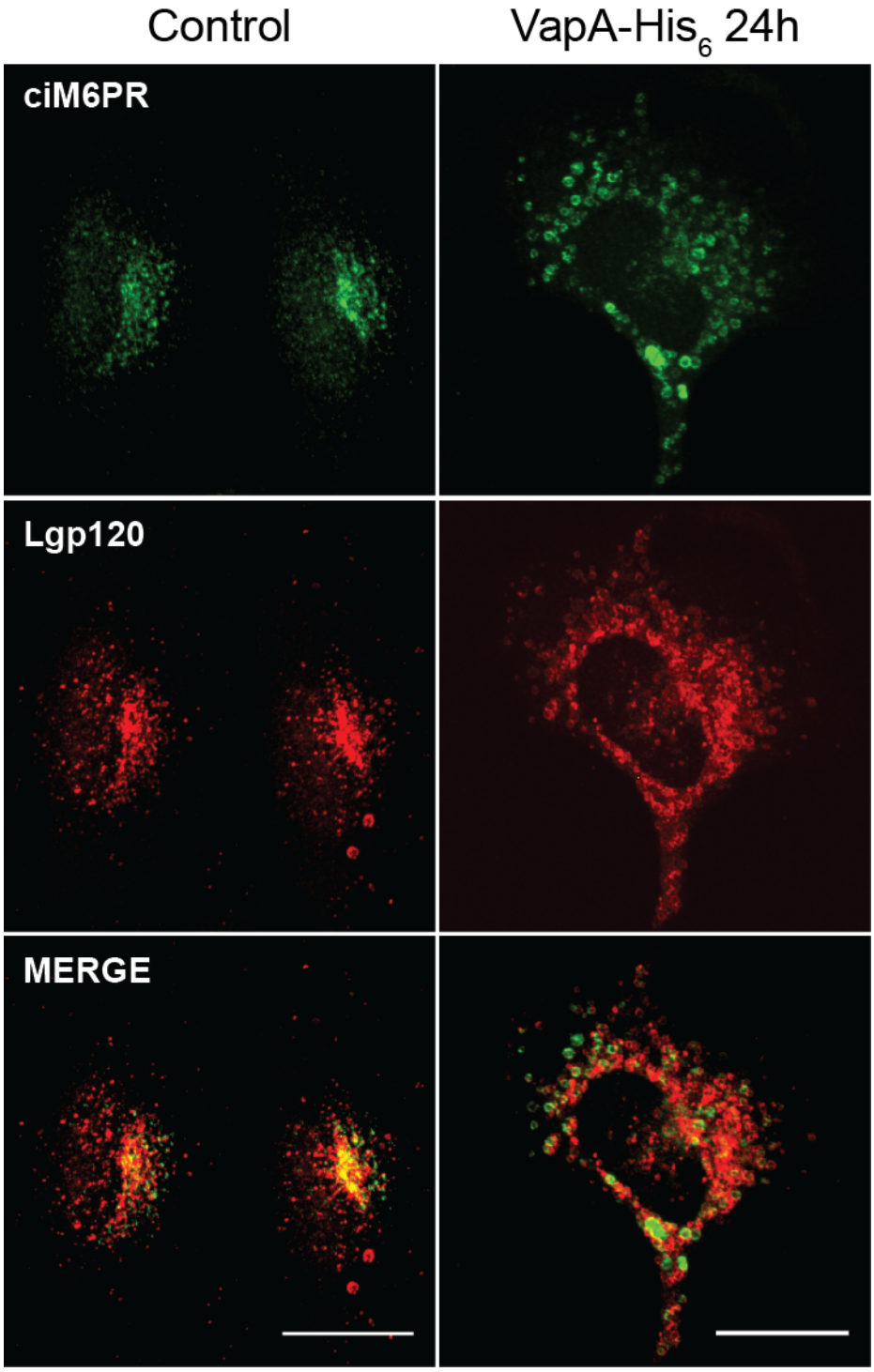

Fig. 5.5. VapA causes swelling of ciM6PR$^+$ compartments. NRK cells were incubated with recombinant VapA-His_6 at 100 µg/ml for 24 h. Cells were rinsed three times with PBS and fixed with 4 % formaldehyde in PBS before processing for immunofluorescence microscopy. Cells were double labelled with α-ciM6PR antibodies and α-Lgp120 antibodies, followed by fluorescently secondary antibodies (Alexa fluor 488; green and Alexa fluor 555; red, respectively). Scales bar 20 µm. Images are maximum-intensity z-projections. Images shown are representative of three separate experiments.

The size of VapA affected lysosomes was quantified over a longer time course. NRK cells were incubated with VapA for 24 h, 48 h and 72 h. Cells were labelled with α-Lgp120 antibodies followed by fluorescently labelled secondary antibodies and lysosome size analysed (Fig. 5.6). The swollen lysosome phenotype was observed when cells were incubated with VapA for 24 h (Fig. 5.6 A). By 48 h, the size of lysosomal aggregates had increased greatly, with large, singular structures clearly observable. However, by 72 h the larger lysosomes appeared to have collapsed, with many smaller puncta filling the majority of the cell. The size of these lysosomes was analysed using ImageJ analysis software (Fig. 5.6 B). The average area of individual control cell lysosomes was 0.25 μm^2, which is consistent with the area of a lysosome with a diameter of 500 nm (0.20 μm^2). This increased to 0.51 μm^2 after 24 h of incubation with VapA. Lysosome area dropped to 0.33 μm^2 and 0.31 μm^2 after 48 h and 72 h respectively, but remained higher larger than that of control cells. Larger puncta and regions where lysosomes in close apposition were counted as one large particle, were omitted from the analysis by disregarding any particle with an area greater than 50 μm^2. This was performed to prevent large regions of unresolvable puncta from being scored as a single large puncta. While this may have underestimated the size of the lysosomes at 48 h and 72 h, the lysosomes at all time points were significantly larger than those of control cells ($p = < 0.001$).

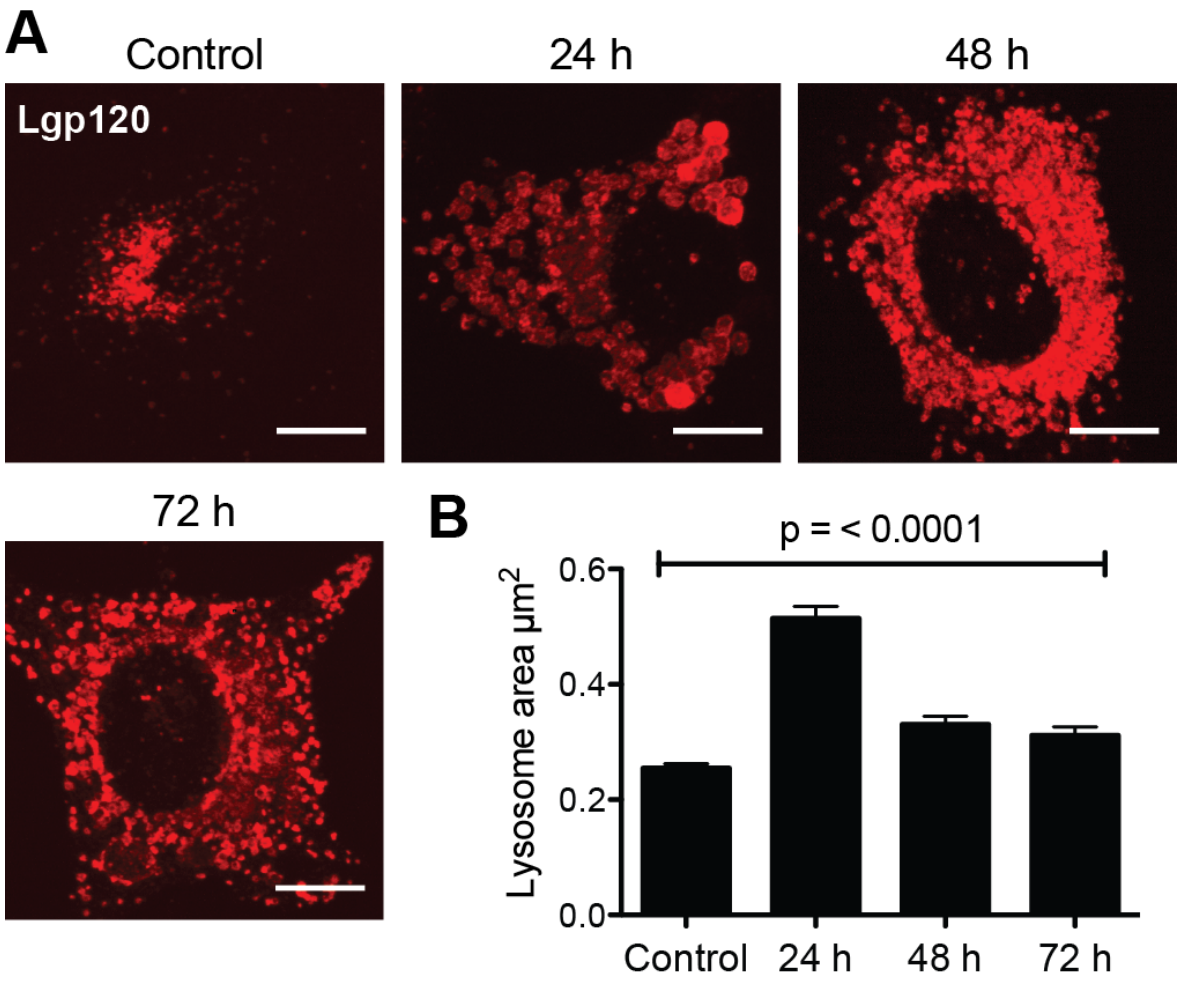

Fig. 5.6. Quantification of lysosome size in cells incubated with VapA. A. NRK cells were fed recombinant VapA-His_6 at 100 µg/ml for the times indicated. Cells were then rinsed three times with PBS and fixed with 4 % formaldehyde in PBS. Cells were labelled with α-Lgp120 antibodies, followed by fluorescently secondary antibodies (Alexa fluor 555; red). Scale bars 10 µm. Images are maximum-intensity z-projections (n=1). **B.** Quantification of lysosome size from images in A. Lysosome size was quantified using ImageJ software. Images were converted to binary images and puncta area was measured. To prevent the perinuclear and other unresolvable regions of each cell being counted as single lysosome, particles with an area greater than 50 μm^2 were excluded from the analysis. A minimum of 5 separate images were counted for each time point, with approximately 5 separate cells per image and 1000 individual particles counted per image. Data are means ± SEM and were analysed using One-way ANOVA (n=1).

5.3.3 VapA alone causes lysosomal swelling

VapA has previously been shown to be the only *Rhodococcus* Vap protein necessary for virulence. A *R. equi* mutant lacking Vap proteins A,C,D,E & F was found to be attenuated for virulence in mice, a phenotype that could be rescued by complementation with VapA, but not VapD (Jain et al., 2003). Expression of VapG is highly upregulated in macrophages, yet VapG mutants remain fully virulent (Coulson et al., 2010). To determine whether these other Vap proteins were able to cause swelling of lysosomes, cells were incubated with recombinant VapD or VapG for 8 h and 24 h at 100 µg/ml (Fig. 5.7). Neither VapD nor VapG induced any changes in lysosome morphology or distribution at any of the time points analysed.

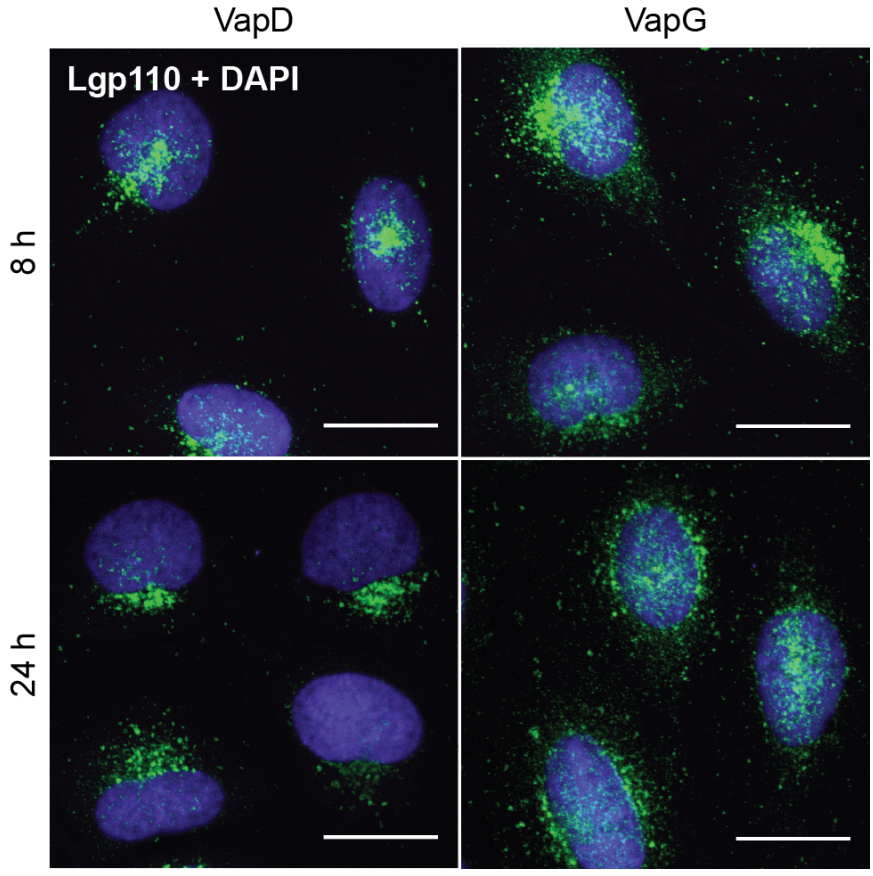

Fig. 5.7. Recombinant VapD and VapG do not effect lysosome morphology or distribution. NRK cells were incubated with 100 µg/ml of recombinant VapD or VapG for the times indicated. Cells were then rinsed three times with PBS and fixed with 4 % formaldehyde in PBS. Cells were labelled with α-Lgp120 antibodies, followed by fluorescently secondary antibodies (Alexa fluor 488; green). Cell nuclei were stained with DAPI (blue). Scale bar 20 µm. All images are maximum-intensity z-projections (n=2).

The Vap proteins have a conserved core structure, with a variable N-terminus (Okoko et al., 2015). As VapA appeared to be the only Vap capable of inducing lysosomal dysfunction, it was asked whether the N-terminus was responsible and/or necessary for this activity, given the similarity between the core of the other Vaps yet their inability to disrupt lysosomes. To test this, NRK cells were incubated with either a VapA N-terminus - VapD-core chimeric protein (VapA/D), or VapA core lacking the N-terminus (residues 22-136) for 8 h and 24 h. The Vap D/A chimeric protein did not induce an observable change in lysosomal morphology or distribution in the cells at either 8 h or 24 h (Fig. 5.8) Unexpectedly, at both 8 h and 24 h the VapA-core induced lysosomal swelling. Thus, taken together, these data indicate that the ability of VapA to cause lysosomal disruption is conferred by the core barrel of the protein and the N-terminus is not responsible for the observed phenotype. This hypothesis is further supported by the fact that neither VapD and VapG, which have different N-termini, have the same effect on lysosomes as VapA.

As lysosomal swelling was induced by the core of VapA, but not VapD or VapG, it was hypothesised that the N-terminus of the other Vap proteins could potentially be inhibitory to any function that the core region of the protein may posses. This was tested by incubating cells with a VapD/A chimeric protein. Residues 1-20 of the mature VapD protein, were fused to the C-terminal core of VapA (starting at residue 22 of the mature VapA protein). NRK cells were then incubated with recombinant protein at 100 µg/ml for 8 h, 24 h and 48 h and the morphology of early endosomes and lysosomes was examined (Fig. 5.9). At all time points, the majority of EEA1 positive puncta appeared normal. Interestingly, at 24 h and 48 h, there were examples of larger EEA1 puncta, although this was only seen in around 1 % of cells, suggesting that they were not directly affected as seen previously (Fig. 5.4). At 48 h, some early endosomes appeared to be in close apposition to lysosomes and displayed a more perinuclear distribution compared to earlier time points (8 h). After 8 h of incubation with VapD/A, large, swollen Lgp120 positive puncta were observable in cells incubated with VapD-A. The lysosomes continued to coalesce and/or enlarge at both 24 h and 48 h. At 48 h several large vacuoles were observable in the cells. This data indicates that the N-terminus of VapD is not inhibitory, suggesting that the core of VapA alone induces lysosomal swelling and early endosomes remain largely unaffected.

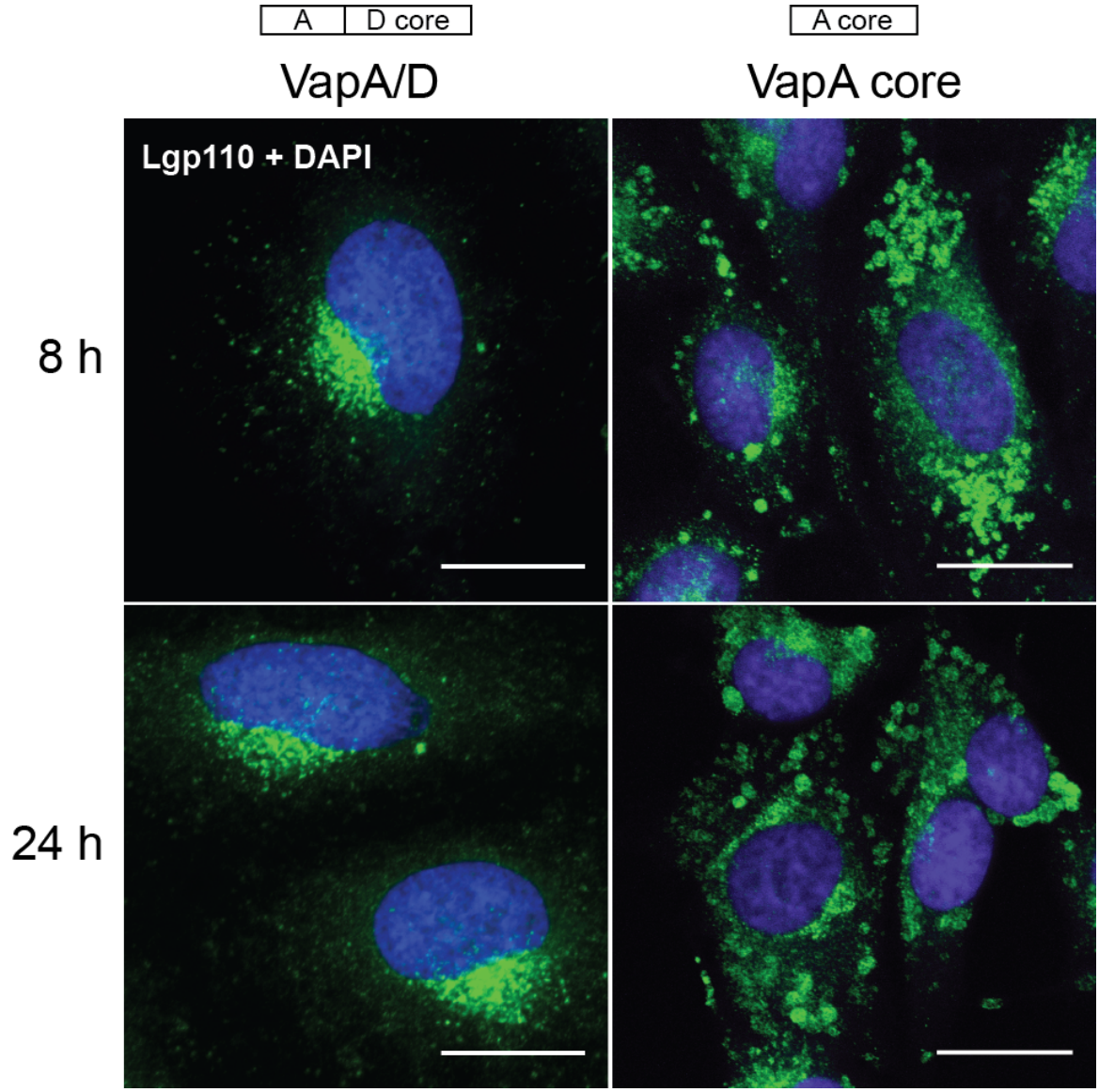

Fig. 5.8. The C-terminal core of VapA is sufficient to cause lysosomal dysfunction. NRK cells were incubated with a VapA N terminus/VapD core chimeric protein, or VapA core, (residues 22-136 as per the numbering of (Whittingham et al., 2014)). Cells were rinsed three times with PBS and fixed with 4 % formaldehyde in PBS before cells were labelled with α-Lgp110 antibodies followed by fluorescently secondary antibodies (Alexa fluor 488; green). Nuclei were stained with DAPI (blue). Scale bars 20 μm. Images are maximum-intensity z-projections (n =1).

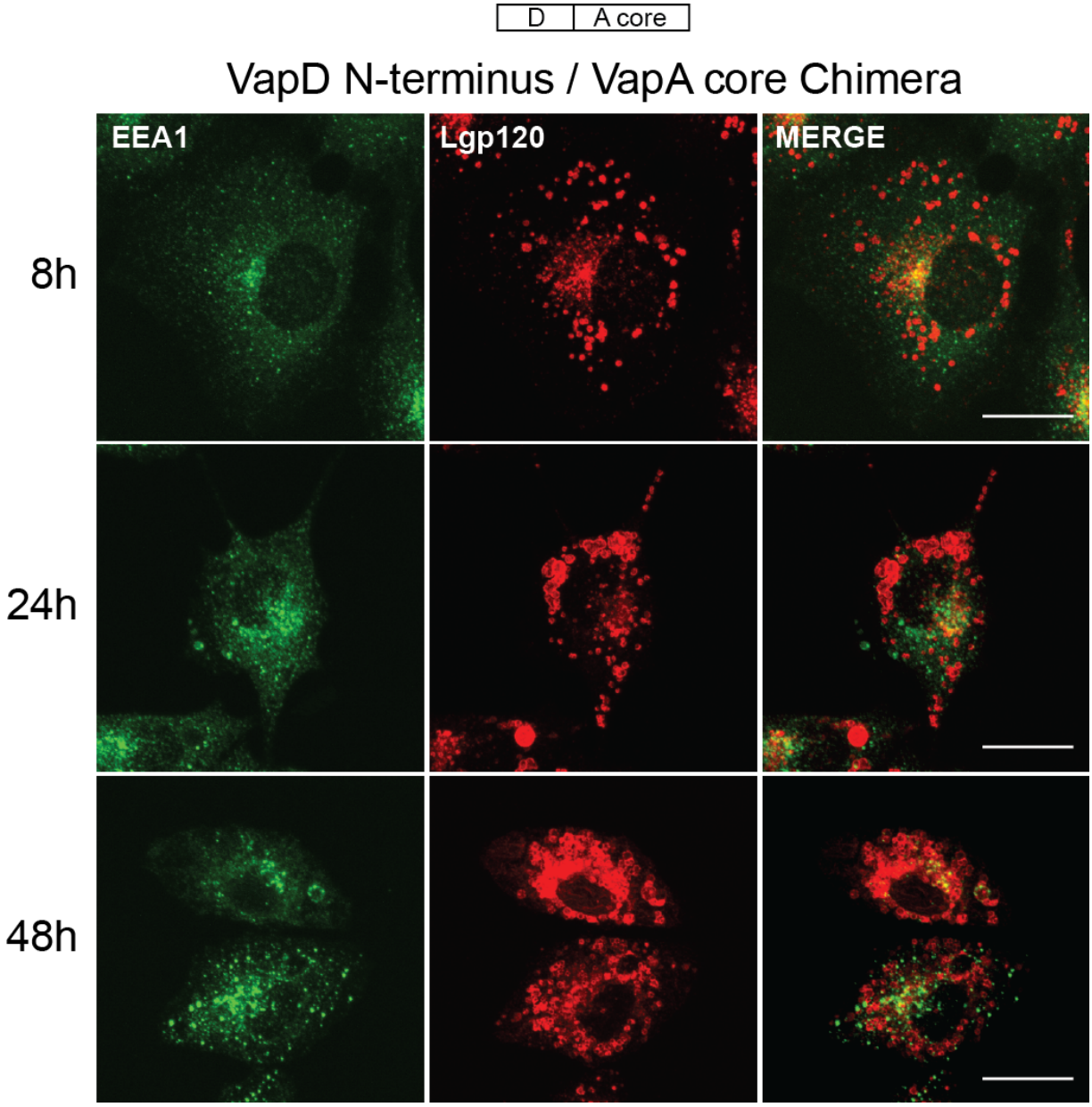

Fig. 5.9. VapD-A chimera induces lysosomal swelling. NRK cells were incubated with recombinant VapD-A chimeric protein at 100 µg/ml for the times indicated. Cells were fixed in 4 % formaldehyde in PBS. The cells were then double labelled with α-EEA1 antibodies and α-Lgp120 antibodies followed by fluorescently labelled secondary antibodies (Alexa fluor 488; green and Alexa fluor 555; red, respectively). Scale bars 20 µm. Images are maximum-intensity z-projections (n=1).

5.3.4 VapA fed cells still contain acidic endocytic compartments

As VapA induced swelling of lysosomes and late endocytic compartments was reminiscent of the phenotype of some lysosomal storage disorders, it was hypothesised that like LSDs, these aberrant organelles may no longer be functional. To test this, VapA-fed cells were incubated with Magic Red (MR) cathepsin B substrate. MR is a non-cytotoxic, membrane permeable, cresyl violet flurophore, with two cathepsin cleavage sites added to it, rendering it non-fluorescent. Upon cleavage by cathepsin B, the MR becomes fluorescent. Therefore, fluorescent MR accumulates in compartments containing active proteases. MR was added to NRK cells and imaged using spinning disk confocal microscopy (Fig. 5.10). In control cells, the MR flurophore was observed in small puncta in the perinuclear region and in the periphery of the cell. Unexpectedly, VapA-fed cells also contained fluorescently labelled, large, swollen puncta, consistent with the lysosome/late endocytic staining obtained in previous experiments. This indicated that VapA-fed cells still possessed proteolytically active vesicles. However, it was not possible to determine the identity of these compartments in this experiment.

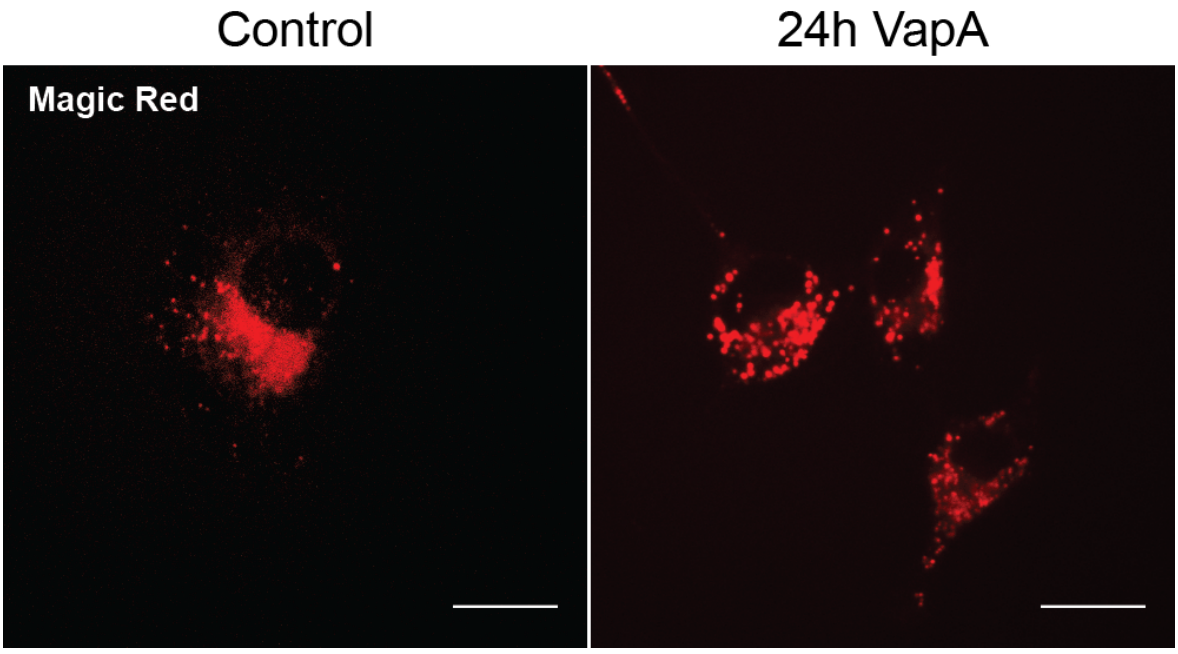

Fig. 5.10. Cathepsin B is still active in VapA-fed NRK cells. NRK cells were cultured for 48 h on glass bottomed dishes and then incubated with or without VapA at 100 µg/ml for 24 h. Cells were then incubated with Magic Red (MR) cathepsin B substrate for 5 minutes before live-cell images were acquired. Scale bars 20 µm (n=2).

The experiment was then repeated using NRK cells transiently transfected with LAMP1-GFP, in order to specifically label the lysosomes (Fig. 5.11). In control cells, LAMP1-GFP was found to label discrete puncta in the perinuclear region and throughout the cell. Some of these puncta colocalised with MR positive vesicles, but MR puncta that did not co-localise with LAMP1-GFP were also seen. In cells incubated with VapA for 24 h, larger, swollen vacuoles were visible, which colocalised with LAMP1-GFP positive vesicles confirming these vesicles were late endocytic/lysosomal in origin. However, there were many puncta that did not co-localise with MR. As cathepsin B has a long half-life (14 h, Katunuma, 2010) any disruption of trafficking to the lysosome (preventing delivery of newly synthesised lysosomal proteins) would not been seen within the time frame of the experiment. Despite this, it can be concluded that VapA-affected compartments retain their low pH.

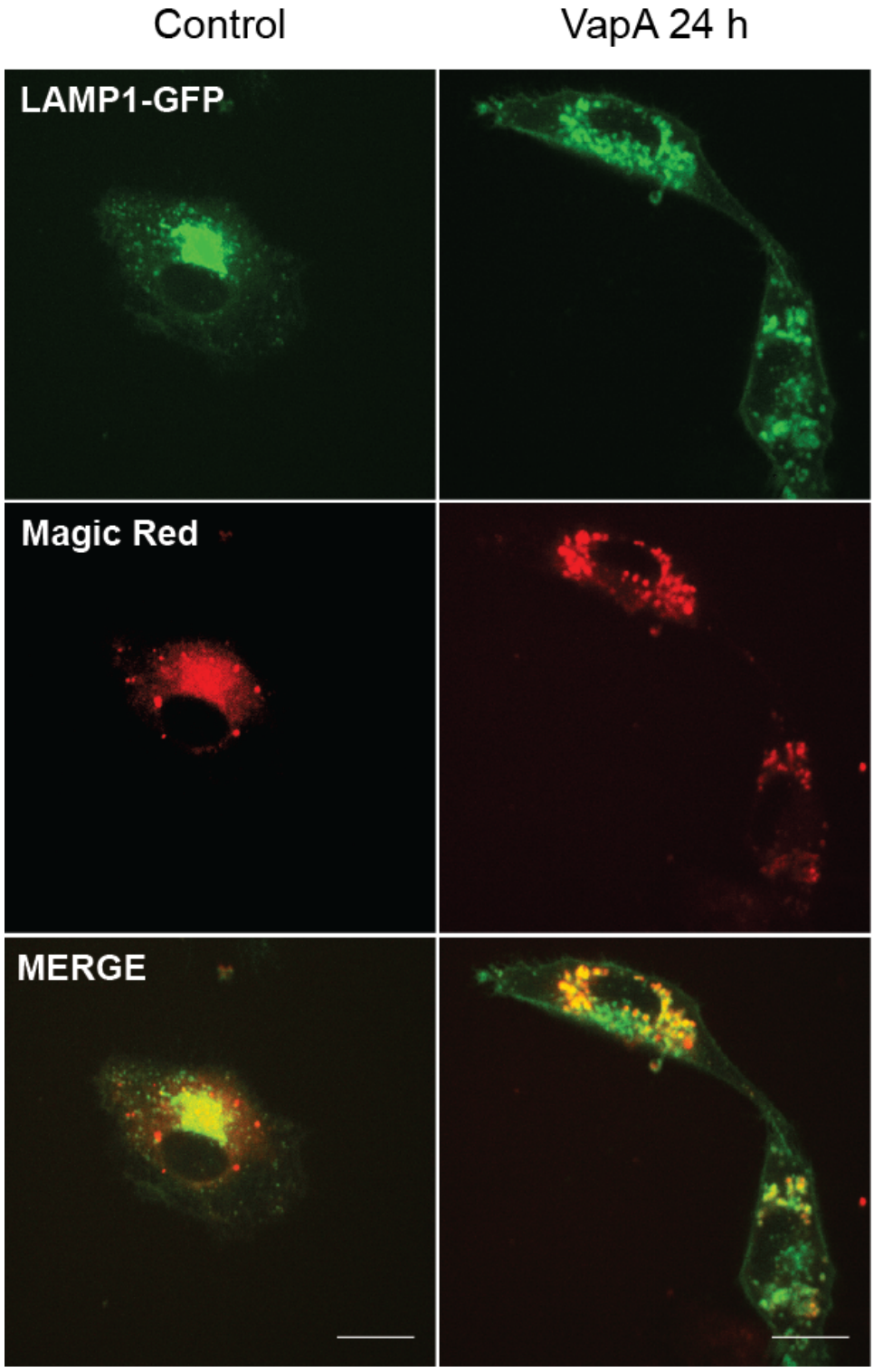

Fig. 5.11. Lysosomes retain protease activity in VapA-fed NRK cells. A. NRK cells were transiently transfected with LAMP1 GFP for 24 h to visualise lysosomes. Cells were then incubated in DMEM or DMEM containing 100 µg/ml VapA, for 24 h. Magic Red (MR) cathepsin B substrate was added to the cells for 5 minutes before live cell images were acquired. Scale bars 20 µm (n=2).

5.3.5 Both virulent and plasmid-cured R. equi reside in LAMP1 positive compartments.

R. equi has previously been reported to arrest phagosome maturation after the early endosomal/phagosomal stage (Fernandez-Mora et al., 2005). *Rhodococcus* containing vacuoles (RCVs), do not fuse with pre-labelled lysosomes and are devoid of classical markers of late endocytic vesicles, such as the vATPase and cathepsin D. After 48 h of intracellular growth inside bone marrow-derived macrophages (BMDMs), virulence plasmid associated strains maintain a non-acidified compartment (Fernandez-Mora et al., 2005). Secondly, a caveat to the VapA feeding experiments was that it was unknown at what level, if at all, VapA is secreted during infection of cells with *R. equi*. 100 µg/ml of recombinant protein was chosen as an arbitrary level, as this was sufficient to elucidate whether a Vap or chimeric protein was able to disrupt lysosome function. During an infection, the physiological amount of VapA produced by *R. equi* is unknown. To confirm some of this data, J774.2 cells were infected with virulent ($103s^+$) and avirulent ($103s^-$) strains of *R. equi* at an MOI of 10 and the intracellular location of the bacteria after 16 h was determined (Fig. 5.12).

Small numbers of *R. equi* lacking the virulence plasmid ($103s^-$) were found surrounded by LAMP1 positive membrane after 16 h (Fig. 5.11 A). Consistent with the lack of Vap proteins in avirulent strains, $103s^-$ *R. equi* did not stain with α-VapA antibodies and only weak levels of background staining were detected with this antibody. In contrast, J774.2 cells were found to be heavily infected with 103^+ *R. equi* 16 h post-infection, indicating intracellular replication of bacteria (Fig. 5.12 B). The majority of these bacteria were also found to be surrounded by a LAMP1 positive membrane, although some intracellular bacteria were not associated with LAMP1 staining. Interestingly, VapA appeared to colocalise to a high degree with LAMP1 positive membranes, as well a large proportion of bacteria. Those bacteria that colocalised with VapA, were either in LAMP1 compartments (large arrowheads), or not associated with LAMP1 staining (small arrowheads). Some bacteria were found to be devoid of LAMP1 and VapA staining.

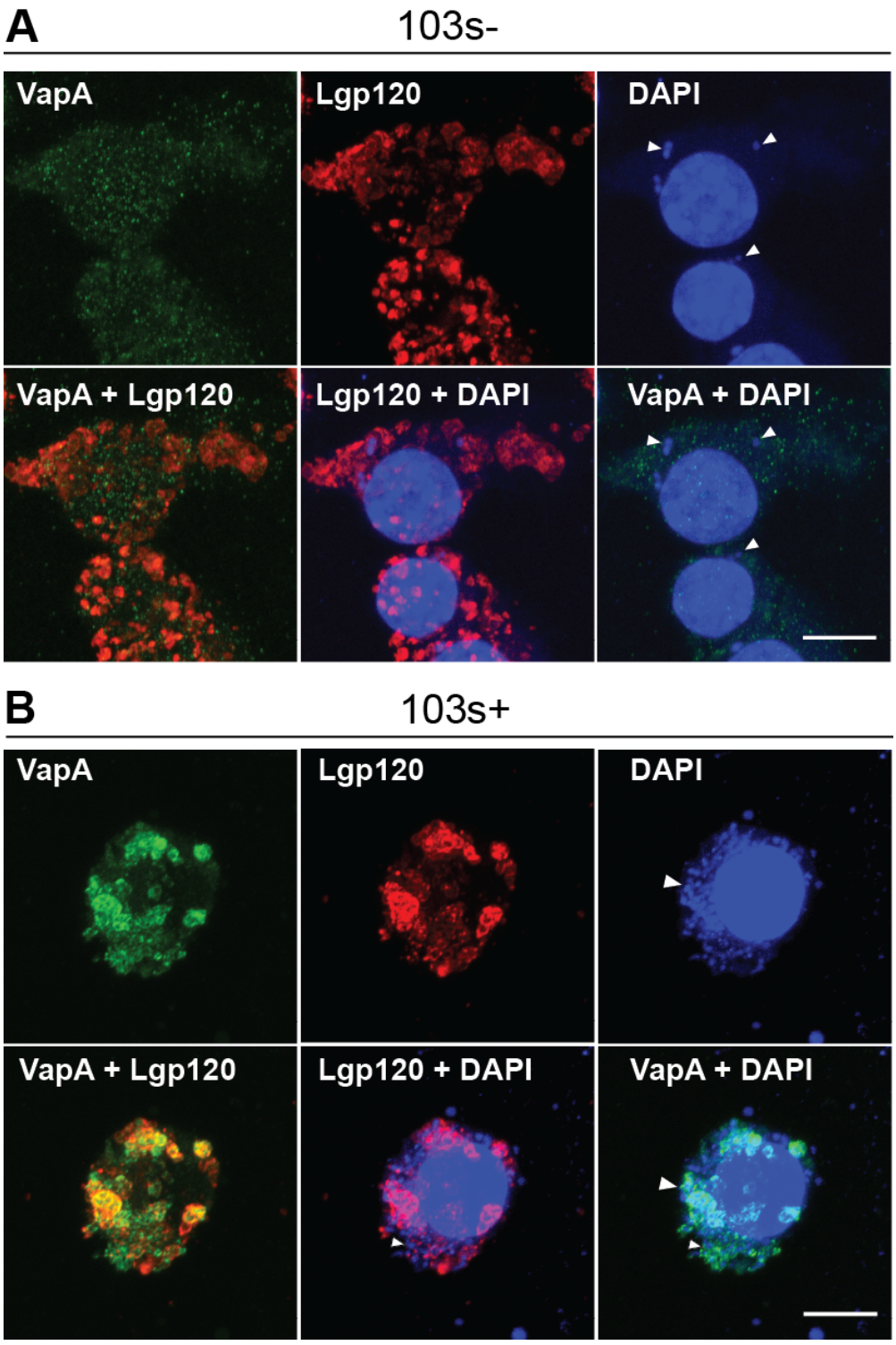

Fig. 5.12. Infection of J774.2 macrophages with *Rhodococcus equi*. J774.2 cells were infected with avirulent ($103s^-$, **A**) or virulent (103^+, **B**) *R. equi*, at an MOI of 10. At 16 h post infection, cells were rinsed 5 times with PBS and fixed in 4 % formaldehyde in PBS. Cells were then double labelled with α-Lgp120 antibodies and α-VapA antibodies, followed by fluorescently labelled secondary antibodies (Alexa fluor 555; red and Alexa fluor 488; green, respectively). Large arrowheads show bacteria surrounded by a LAMP1+ membrane, small arrowheads shown bacteria with no LAMP1 staining. Bacteria and cell nuclei were stained with DAPI (blue). Scale bar 10 µm. Images are maximum-intensity z-projections (n=2).

5.3.6 Incubation with VapA causes changes in levels of LAMP1

Lysosome biogenesis is upregulated in response to lysosome dysfunction (Sardiello et al., 2009). At later time points in previous experiments (48 h-72 h), the number of lysosome puncta observed in Vap-fed cells appeared to increase. However, it was not clear if this was due to collapse of swollen vacuoles, lysosomes aggregating, or a genuine upregulation of lysosome biogenesis. To try and answer this, the levels of LAMP1 in control and Vap fed cells were analysed by western blotting (Fig. 5.13 A&B). J774.2 or NRK cells were incubated with recombinant VapA, VapD, or VapG at 100 μg/ml for 8 h, 24 h, 48 h, or 72 h. Cell lysates probed with α-LAMP1 (J774.2 cells), or α-Lgp120 and cation-independent mannose-6-phosphate receptor (ciM6PR) antibodies (NRK cells). In J774.2 cells incubated with VapA, levels of LAMP1 increased from 24 h to 72 h, with the highest levels seen at 48 h. In contrast, cells incubated with VapD or VapG did not show an increase in LAMP1 levels. Similarly, in NRK cells, the levels of Lgp120 (LAMP1) increased after cells were incubated with VapA, but not with VapD or VapG. Levels of Lgp120 increased from 8 h and were at their highest at 72 h. The levels of ciM6PR in NRK cells were also probed. Between 8 and 72 h there was no significant change in the levels of ciM6PR in NRK lysates of cells incubated with any of the Vap proteins tested. It was observed that J774.2 macrophages began to die after 24 h of incubation with VapA, whereas NRK cells could be cultured for up to 72 h (data not shown). In most cases, the amount of α-tubulin loading control was roughly equivalent, with levels of α-tubulin decreasing at 72 h in VapA fed J774.2 cell lysates. The activity of the lysosomal enzyme β-hexosaminidase in cells incubated with the different Vap proteins was also measured. In both J774.2 (Fig. 5.13 C) and NRK (Fig. 5.13 D) cells, the activity of β-hexosaminidase (as a fold change of the control cells at 72 h) did not significantly alter when cells were incubated with any of the Vaps tested ($p = 0.510$ J774.2 cells, $p = 0.258$ NRK cells).

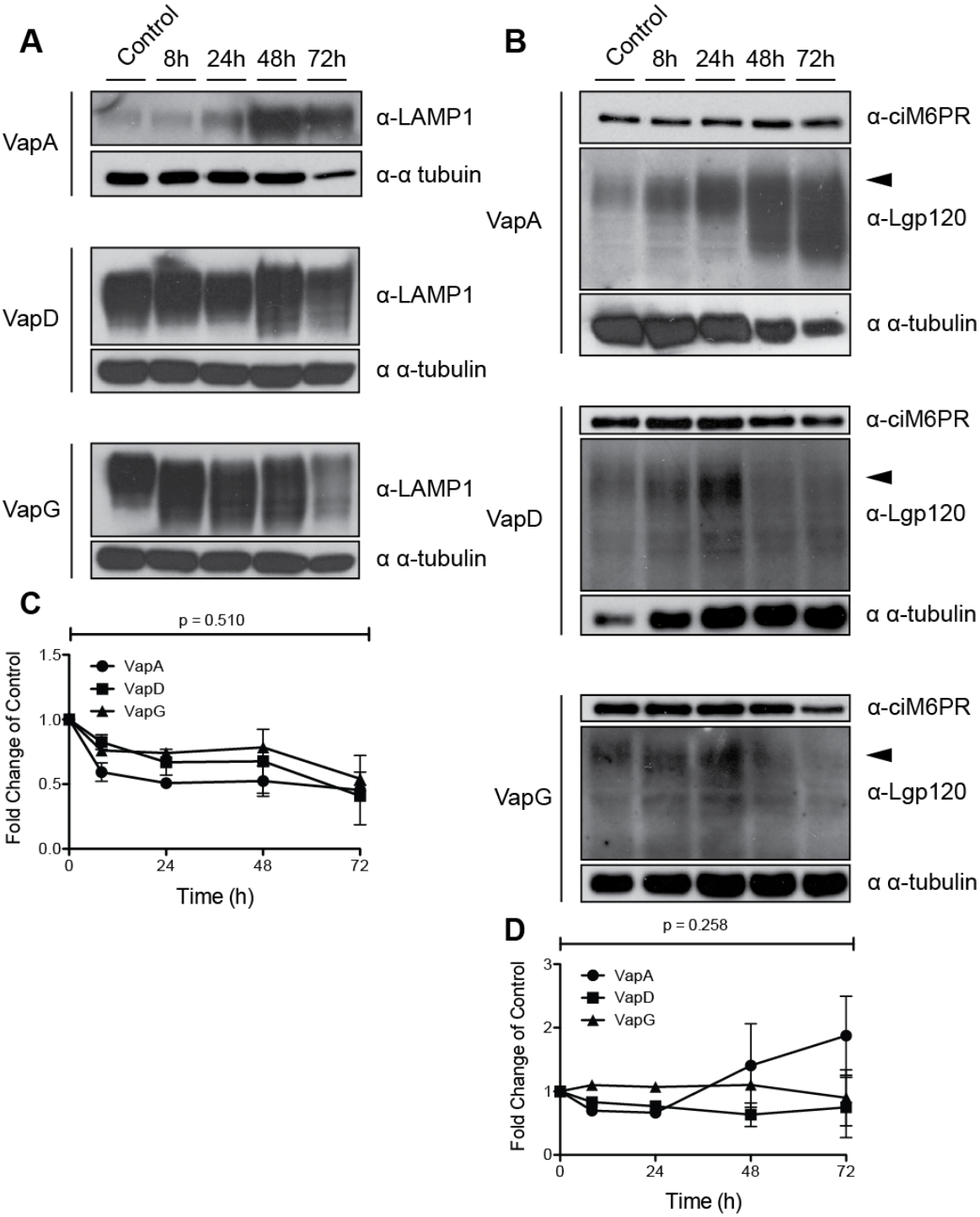

Fig. 5.13. Upregulation of lysosome biogenesis in cells incubated with VapA. J774.2 macrophages (**A**) or NRK cells (**B**) were incubated with recombinant VapA, VapD or VapG at 100 μg/ml for the times indicated. Cell lysates were then probed using α-Lgp120/α-LAMP1, α-α tubulin and α-ciM6PR antibodies. The levels of the lysosomal enzyme β-hexosaminidase were also measured at the indicated time points in VapA-fed J774.2 and NRK lysates (**C&D**). Data are represented as arbitrary units of β-hexosaminidase enzyme activity per μg of protein, as a fold change of the control sample. Western blots are representative of at least two independent experiments. Graphs show mean + the range and data were analysed by two-way ANOVA (n=2).

5.3.7 Identifying the binding partner of VapA

The data accumulated thus far demonstrates that VapA, (but not VapD or VapG), is able to induce a swollen lysosomal phenotype. While these observations are important to understand how VapA promotes intracellular survival, they do not provide any evidence of a mechanism by which VapA acts. To try dissect the molecular mechanism by which VapA allows *Rhodoccocus* survive inside macrophages, immunoprecipitation experiments were performed to identify what host protein(s) VapA interacts with. Immunoprecipitation experiments were performed on lysates generated from myc-VapA expressing HeLa cells (Fig. 5.14 A). Initially, the IP protocol was optimised to maximise the chance of finding an interacting partner. 10 µg of α-myc antibody was covalently coupled to sepharose and incubated with 0.75 mg, 1.0 mg, 1.5 mg, or 2.0 mg of lysate for 2 h. The sepharose was washed and proteins eluted from the sepharose using a low pH elution buffer. Equal volumes of all samples were subjected to western blotting using α-myc antibodies. There was less myc-VapA detected in 0.75 mg and 1.0 mg samples compared to the 1.5 mg and 2.0 mg samples. However, 1.5 mg of lysate appeared to reach the binding capacity of 10 µg antibody, as no more was pulled out when the sepharose was incubated with 2.0 mg of lysate. Therefore, 1.5 mg and 10 µg of antibody was chosen as the optimal ratio for further experiments.

In all cases, there was a significant amount of myc-VapA remaining after incubation with α-myc sepharose. To improve the efficiency of the IP, 1.5 mg of lysate was incubated with α-myc sepharose for 1 h or overnight at 4 ºC (Fig. 5.14 B). Western blotting of the eluted proteins showed that the efficiency of the IP was increased when incubating the lysates overnight. Therefore, this was continued for further experiments. As the lysates still had significant amounts of myc-VapA after incubation with the sepharose, the amount of sepharose was increased to try and leave no more than 10 % of myc-VapA in the lysate after incubation with the α-myc sepharose (Fig. 5.14 C). 1.5 mg of lysate was incubated with 10, 20, 30, or 40 µg of coupled antibody overnight. Protein eluates were then subjected to western blotting. 40 µg of antibody was sufficient to pull out the majority of myc-VapA from 1.5 mg of HeLa cell lysate. Therefore, further experiments were performed overnight using a ratio of 1.5 mg of lysate to 40 µg of covalently coupled antibody.

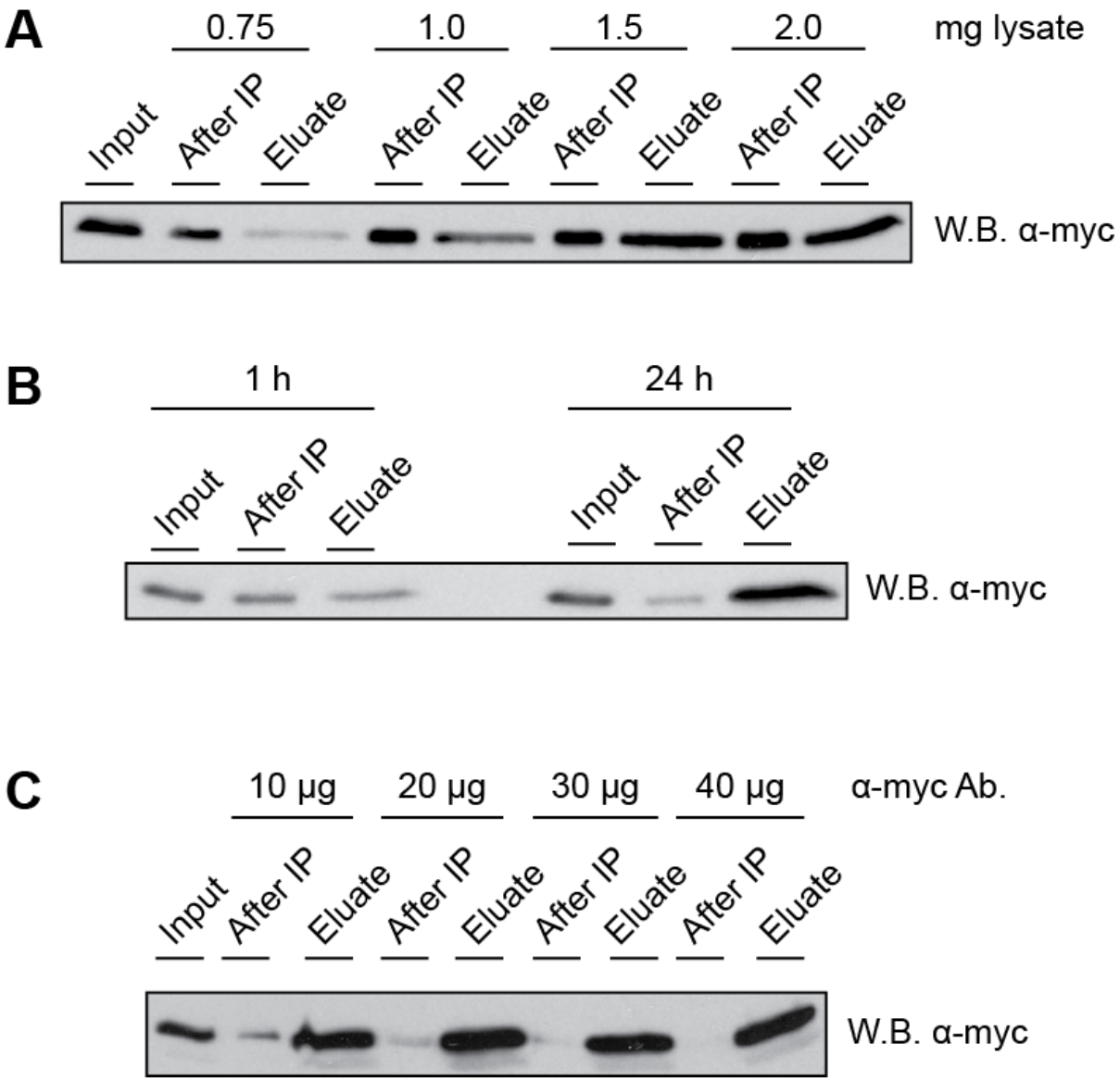

Fig. 5.14. Optimisation of myc-tagged VapA Immunoprecipitation. A. 10 µg of α-myc antibody was covalently coupled to sepharose and incubated with the indicated amounts of lysates of myc-VapA expressing HeLa cells. After 2 h, the sepharose was washed and bound proteins eluted. Equal volumes of the input and lysate after the IP were loaded. Lysates and eluted proteins were then probed by western blotting (W.B.) with α-myc antibodies. **B.** 1.5 mg of myc-VapA expressing HeLa cell lysate was incubated with α-myc sepharose for 1 h or overnight at 4 ºC. The input, lysate after IP and eluates were probed with α-myc antibodies **C.** 1.5 mg of myc-VapA expressing HeLa cell lysate was incubated with the indicated amounts of α-myc antibody covalently coupled to sepharose, for 2 h at 4 ºC. The input, lysate after IP and eluate were probed with α-myc antibodies.

Next, the IP was scaled up using the determined ratio of antibody and lysate until immunoprecipitated proteins were visible by silver staining on an SDS PAGE gel (Fig. 5.15 A & B). 1.5 mg, 3 mg, 6 mg and 12 mg of myc-VapA or control lysate was incubated with α-myc sepharose overnight at 4 ºC. Eluates were resolved on a 8-15 % SDS PAGE gel and visualised by coomassie stain. As protein bands were only just visible by coomassie stain, the gel was then silver stained. No clear band of the approximate molecular weight corresponding to over-expressed myc-VapA (~ 25 kDa) was visible by silver staining.

While immunoprecipitated myc-VapA was detectable by western blotting (Fig. 5.14), it was not visible on larger scale IPs. As it was possible that the myc-VapA was not being efficiently eluted from the sepharose, different elution conditions were compared to improve the efficiency of the IP (Fig. 5.15 C). 5 different elution buffers were used to elute immunoprecipitated proteins from 20 µl of sepharose. The sepharose was then resuspended in 50 µl of SDS PAGE sample buffer and remaining proteins eluted by boiling at 95 ºC for 5 min. Samples were then resolved by SDS PAGE and subjected to western blotting using α-myc antibodies. In all cases, elution of protein from the sepharose was inefficient, with the majority remaining bound to the beads (eluates c.f. beads, Fig. 5.15 C). Heavy and light immunoglobulin chains were also eluted with immunoprecipitated proteins with all elution buffers. However, this was much less for the low pH IgG and glycine elution buffer compared to the others. 1 % SDS and 100 mM triethylamine were the most efficient at eluting immunoprecipitated proteins, but also had the highest amounts of heavy and light Ig chains. 3.5 M $MgCl_2$ did not elute any protein from the sepharose. As none of the elution buffers were significantly better at eluting the protein from the sepharose, low pH IgG buffer continued to be used. In all cases, the amount of myc-VapA that was immunoprecipitated was very low (arrowheads) and myc-VapA was not detected in the input sample by western blotting. Therefore the expression of myc-VapA was optimised to improve the efficiency of the IP.

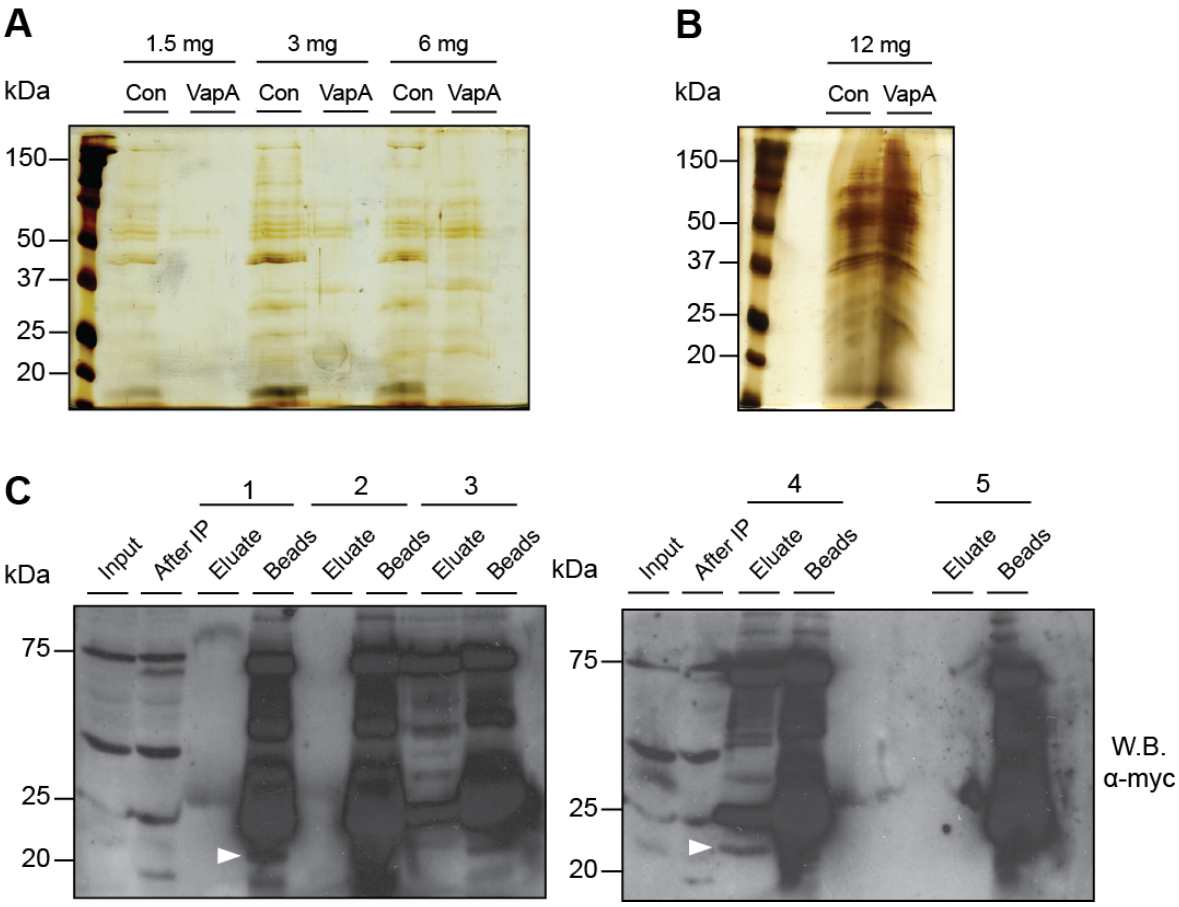

Fig. 5.15. Scaling up of myc-VapA IP. A. Increasing concentrations of HeLa (Con) or myc-VapA expressing HeLa (VapA) cell lysates were incubated with α-myc Sepharose (40 µg of α-myc antibody per 1.5 mg of lysate) overnight at 4ºC. Sepharose was extensively washed and bound proteins eluted with 300 µl of low pH IgG elution buffer. Eluates were neutralised with 1 M Tris (pH 8.0) and were resolved on an 8-15 % SDS PAGE gel. Proteins were visualised by silver staining. **B.** As in A, but with 12 mg of lysate. **C.** Comparison of efficiencies of different elution buffers. 20 µg of α-myc antibody covalently coupled to sepharose was incubated with 0.75 mg of myc-VapA HeLa lysate overnight at 4 ºC. Immunoprecipitated proteins were eluted from the sepharose by the addition of a pre elution buffer (10 mM phosphate, pH 8.0), followed by 50 µl of elution buffer (1- low pH IgG elution buffer, 2 – Glycine, pH 2.5, 3 - 100 mM Triethylamine, pH 11.5, 4 - 1 % (w/v) SDS, 5 - 3.5 M $MgCl_2$, pH 7.0). The sepharose beads were then boiled in 50 µl of Laemmli sample buffer at 95 ºC for 5 min. The equal volumes of before and after samples, eluates and proteins liberated from the beads were western blotting for myc. Arrowheads indicate immunoprecipitated myc-VapA. W.B.-western blot.

To improve IP efficiency, low passage (P2) and high passage (P10) myc-VapA expressing HeLa cells were compared for over-expression of myc-VapA. (Fig. 5.16 A). Cells were induced to express myc-VapA with 1 µg of doxycycline for 16 h and protein lysates subjected to western blotting for myc. Lower passage cells expressed more myc-VapA than higher passage cells, indicating that protein expression was being lost as the passage number of the cells increased. This was puzzling, as the Flp In system should result in the selection of an isogenic cell line and protein expression should be consistent. It is possible that expression of myc-VapA was detrimental to the cells, or reduced their growth rate, resulting in selection of cells which expressed lower amounts of myc-VapA. This was unlikely, as expression of myc-VapA did not appear to result in a phenotype and ii) exogenous protein express was inducible and not constitutive. One possibility is that trace amounts of tetracycline (a doxycycline analogue) found in fetal calf serum could induce low levels of protein expression, that may have resulted in the selection of low-expressing clones. Nethertheless, lower passage clones were used for further experiments. Previous IP experiments had shown that elution of proteins from α-myc sepharose was inefficient. As such, the number of elutions was increased to determine if this resulted in improved protein elution (Fig. 5.16 B). A small-scale IP experiment was performed using 1 mg of lysate. After the first elution, 5 further elutions (of equal volume) were performed. Western blotting of these eluates revealed that not all of the myc-VapA had been eluted from the sepharose. Therefore, the volume of elution buffer used in further IPs was increased from 5 x the sepharose volume to approximately 10 x. The amount of doxycycline used to induce the cells and the length of induction, was also investigated (Fig. 5.16 C). Cells were induced for 16 h, 24 h and 48 h, with 0.1 µg/ml, 1.0 µg/ml, or 10 µg/ml doxycycline. Expression of myc-VapA was strongest at 16 h when cells were induced with 1.0 µg/ml doxycycline, whereas expression of myc-VapA was poorest when cells were induced with 10 µg/ml. The levels of myc-VapA also appeared to slightly decrease from 16 h to 48 h. For further experiments, protein over-expression was performed for no longer than 16 h. These optimisations were incorporated into the IP protocol and a large scale IP was performed with 40 mg of protein lysate (Fig. 5.16 D). Despite the improvements in protocol efficiency, no obvious band corresponding to immunoprecipitated myc-VapA was identifiable. The IP was then repeated a final time, using lysate that had been precleared with control resin before the IP (Fig. 5.16 E).

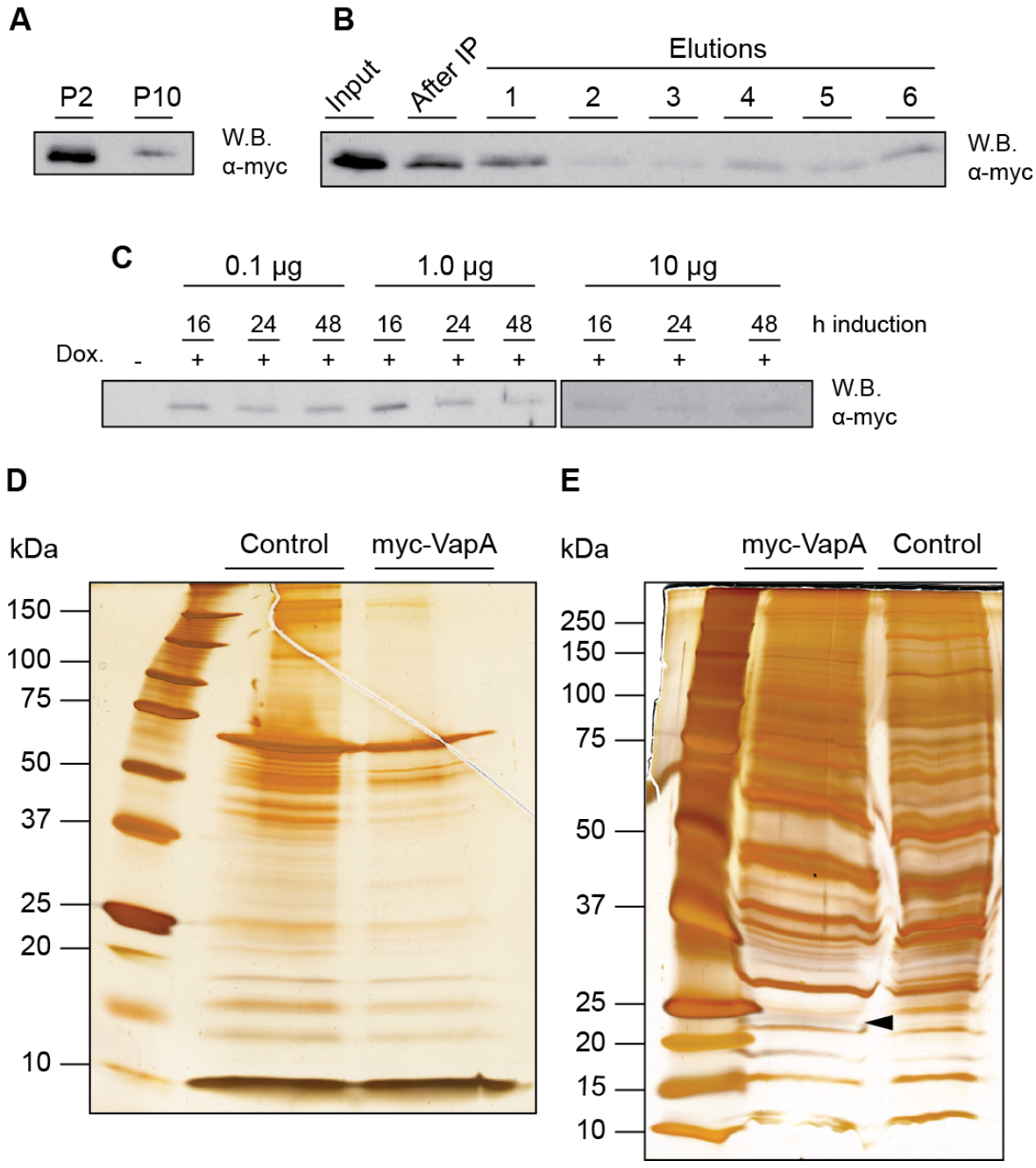

Fig. 5.16. Large scale myc-VapA co-IP.A. Expression levels of low and high passage myc-VapA expressing HeLa cells.20 µg of protein per lane **B.** Small scale myc-VapA co-IP. Immunoprecipitated proteins were eluted with 50 µl of low pH IgG elution buffer. 5 further elutions (50 µl each) were collected and eluates subjected to western blotting using α-myc antibodies. **C.** HeLa cells were induced to over express myc-VapA with 0.1, 1.0 or 10 µg/ml doxycycline for 16 h, 24 h, or 48 h. 20 µg of protein per lane **D & E.** Large scale myc-VapA co-IP. 40 mg of HeLa or myc-VapA HeLa lysate was incubated with α-myc sepharose overnight at 4 ºC. Immunoprecipitated proteins were concentrated using Slide-A-Lyzer cassettes (3.5 kDa cut-off) and then resolved on a 8-15 % SDS PAGE gel and visualised by silver staining. Arrowhead indicates immunoprecipitated myc-VapA.

Despite preclearing the lysate by incubating it with control resin for 2 h, the background was particularly high. A band of approximately 22 kDa was present in the myc-VapA sample, which may have been immunoprecipitated VapA (arrowhead). However, the efficiency of the IP was still particularly poor. Moreover, there were no obvious bands present in the myc-VapA sample compared to the control. The background was also particularly high, with many protein bands stained in both samples. Therefore, an alternative methodology was used to try and identify the interacting partner of VapA.

5.3.8 BirA-VapA biotin-ligase pull down*

Due to the problems encounter with the IP, an alternate methodology to identify the mammalian target(s) of VapA was used. A recent publication by Roux *et al.* (Roux et al., 2012), described proximity-dependent biotin-labelling of proteins (BioID). This system utilises a promiscuous prokaryotic biotin ligase (BirA*) that is fused to a protein of interest. The chimera is then expressed in mammalian cells where the BirA* biotinylates proteins in its immediate vicinity when the tissue culture media is supplemented with biotin. Biotinylated proteins can then be isolated from a cell lysate using streptavidin beads and proteins identified by mass spectrometry. A BirA*-VapA expressing HeLa cell line was generated to identify VapA interactors using this approach (Fig. 5.17 A). Firstly, protein expression was induced in HeLa cells expressing myc-BirA*-VapA for 16 h and the subcellular localisation of the protein examined (Fig. 5.17 B). Myc staining revealed that myc-BirA*-VapA was expressed throughout the cell cytoplasm and was not associated with any one organelle. No staining was visible in uninduced control cells. Next, a pulldown experiment was performed. Protein expression was induced in myc-BirA*-VapA cells with doxycycline for 24 h, in tissue culture media supplemented with 50 µM biotin. A control BirA* expressing parental HeLa cell line was used as a control Cells were subsequently lysed and the lysate incubated overnight with 600 µl of magnetic streptavidin beads (Dynabeads MyOne Streptavidin C1, Thermo, catalogue # 65001). The beads were subjected to several washes and biotinylated proteins eluted by boiling the beads at 95 ºC for 5 min in SDS PAGE sample buffer saturated with biotin. 10 % of the eluted proteins were then analysed by western blotting, using a streptavidin-HRP conjugate (Fig. 5.17 C). Western blotting revealed single obvious band at ~40 kDa, which was most likely self-biotinylated myc-BirA*. Correspondingly, a larger band running at >50 kDa was seen in the BirA*-VapA sample. Additional biotinylated proteins were seen in the BirA*-VapA

sample, but not in the BirA* control, suggesting that BirA* does not biotinylate non-specific proteins.

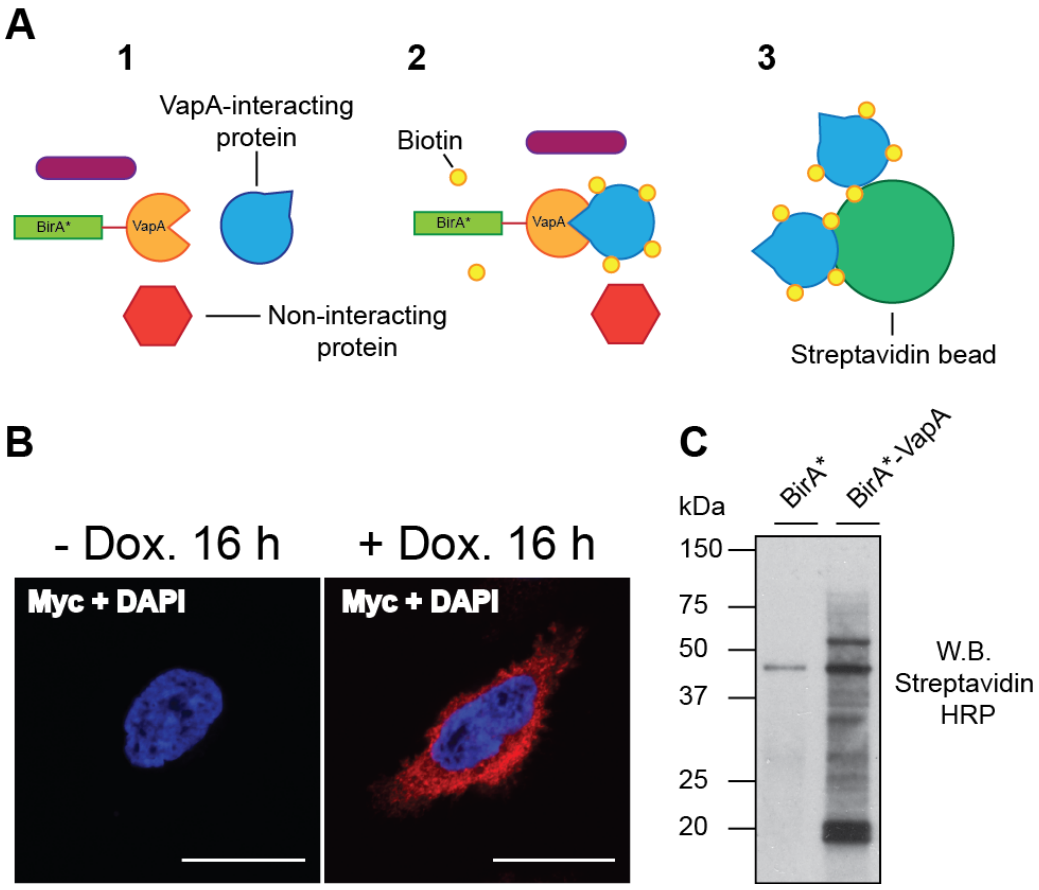

Fig. 5.17. Proximity-dependent promiscuous biotinylation by BirA*-VapA. A. Schematic of representation of proximity dependent biotinylation.1. BirA*-VapA fusion protein is expressed inducibly in HeLa cells. 2. Expression of BirA* VapA is induced for 24 h. Tissue culture media is supplemented with biotin and VapA interacting and proximal proteins become biotinylated. Non-proximal proteins that do not interact with VapA do not become biotinylated. 3. After cell lysis and protein denaturation, biotinylated proteins are captured on streptavidin beads. Biotinylated proteins are then eluted from the beads and identified by mass spectrometry. **B.** Confocal analysis of myc-BirA-VapA expression. Protein over-expression was induced in HeLa cells expressing BirA*-VapA for 16 h. Cells were then fixed with 4 % formaldehyde in PBS and cells labelled with α-myc antibodies followed by fluorescently labelled secondary antibodies (Alexa fluor 555; red). Cell nuclei were stained with DAPI (blue). Scale bar 20 μm. Image is a maximum-intensity z-projection **C.** Protein over-expression was induced in HeLa cells expressing BirA*-VapA or BirA* (control) for 24 h in the presence of excess biotin. Cells were lysed and biotinylated proteins recovered on streptavidin beads. The beads were boiled in SDS PAGE sample buffer saturated with biotin for 5 min at 95 ºC. 5 % of the total eluate was analysed by western blotting using a streptavidin-HRP conjugate (1:40,000).

Biotinylated proteins were analysed by 1D LC-MS. Proteins unique to the BirA*-VapA pull-down were classed as possible VapA-interactors (Table 5.0, full list appendix 1.1). The mass spectrometry data did reveal many proteins unique to the VapA sample. Three of these proteins were highlighted due to their roles in membrane trafficking and lysosome function. These included Annexin A1, found on endosomal membranes (Seemann et al., 1996), Exocyst component 6B, involved in vesicle exocytosis (Heider and Munson, 2012) and Cathepsin D, a lysosomal protease (Benes et al., 2008).

Protein Identity	Mascot Score	Spectra matches	Maximum Peptide Sequences	Molar %
Annexin A 1	51	3	3	0.38
Exocyst complex component 6B	17	1	1	0.04
Cathepsin D	15	1	1	0.10

Table 5.0. BirA*-VapA interacting proteins. A proximity-dependent biotin ligation experiment was performed in HeLa cells expressing myc-BirA*-VapA to identify proteins that interacted with VapA, as described in section 5.2.3. Biotinylated proteins were analysed by 1D LC-MS. Hits unique to myc-BirA*-VapA were classed as potential VapA-interacting proteins.

5.3.9 Production of recombinant BirA-His$_6$ and VapA- BirA*-His$_6$*

While the BirA*-VapA pulldown identified some possible VapA-interacting proteins, a caveat to this experiment was that VapA exerts its effects upon late endocytic and lysosomal compartments from within those vesicles. As such, VapA would most likely interact with proteins on the lumenal side of these compartments. BirA*-VapA was expressed in the cell cytoplasm and so would not have access to any potential interacting proteins on the lumenal side of the lysosome membrane. Therefore, similar to the VapA feeding experiments, a BirA*-VapA fusion protein would need to be introduced to the lysosome lumen by fluid phase endocytosis. To this end, C-terminal His$_6$-tagged BirA* and BirA*-VapA recombinant proteins were produced to feed to cells.

BirA*-His was purified to use as a control for BioID experiments. Small scale test expression of BirA*-His was assessed by western blotting (Fig. 5.18 A). There was a clear induction of the expression of a < 37 kDa protein upon addition of IPTG (predicted molecular weight of BirA*-His 36 kDa). Similar to VapA-BirA* expression, his-tagged protein was detected in the insoluble fraction, as well as in soluble eluates (1-3). The western blot also revealed that not all of the his-tagged protein was removed after incubation with the affinity resin. The yield of BirA*-his was also very low, with around 60 µg obtained from a 1 L culture. When the purification was repeated and the volume of nickel affinity resin used was increased to 1 ml, the yield was greatly improved (Fig. 5.18 B). Analysis of samples before and after incubation with the resin indicated that there was a large amount of protein that was not pulled out of the lysate. Despite this, a < 37 kDa band was detected in eluted fractions (arrowhead). However, some degradation was also visible. Fractions 1-4 were pooled and dialysed into PBS. The protein concentration was 1.68 mg/ml.

Expression of VapA-BirA*-His was analysed by small scale test expression of two bacterial clones (Fig. 5.18 C). A small level of basal level of expression was detected. However, there was a large induction of protein expression upon addition of IPTG. His-tagged protein was detected in both the insoluble and soluble fractions. Degradation products were also detected in the soluble fraction. BirA*-VapA was then purified from a 1 L culture (arrowhead, Fig. 5.18 D). A bacterial supernatant was generated and incubated with nickel affinity resin overnight at 4 ºC. Equal volumes of the supernatant were taken before and after

for SDS PAGE analysis, as were 4 µl samples of each eluted fraction. A ~50 kDa protein was detected in almost all of the 12 eluted fractions analysed (estimated molecular weight of VapA-BirA*-His, 53 kDa). Fractions 1-5 were pooled and dialysed into PBS. The protein concentration of the purified VapA-BirA* was determined to be 1.3 mg/ml.

To ensure VapA remained functional with the addition of BirA* to its C-terminus, NRK cells were incubated with BirA*-VapA at 100 µg/ml for 24 h and then fixed with 4% formaldehyde in PBS. Lysosome morphology was then assessed by confocal microscopy (Fig. 5.18 E). Lysosomes were found to be swollen in NRK cells incubated with BirA*-VapA, indicating that the BirA* protein did not interfere with the ability of VapA to disrupt lysosomal morphology.

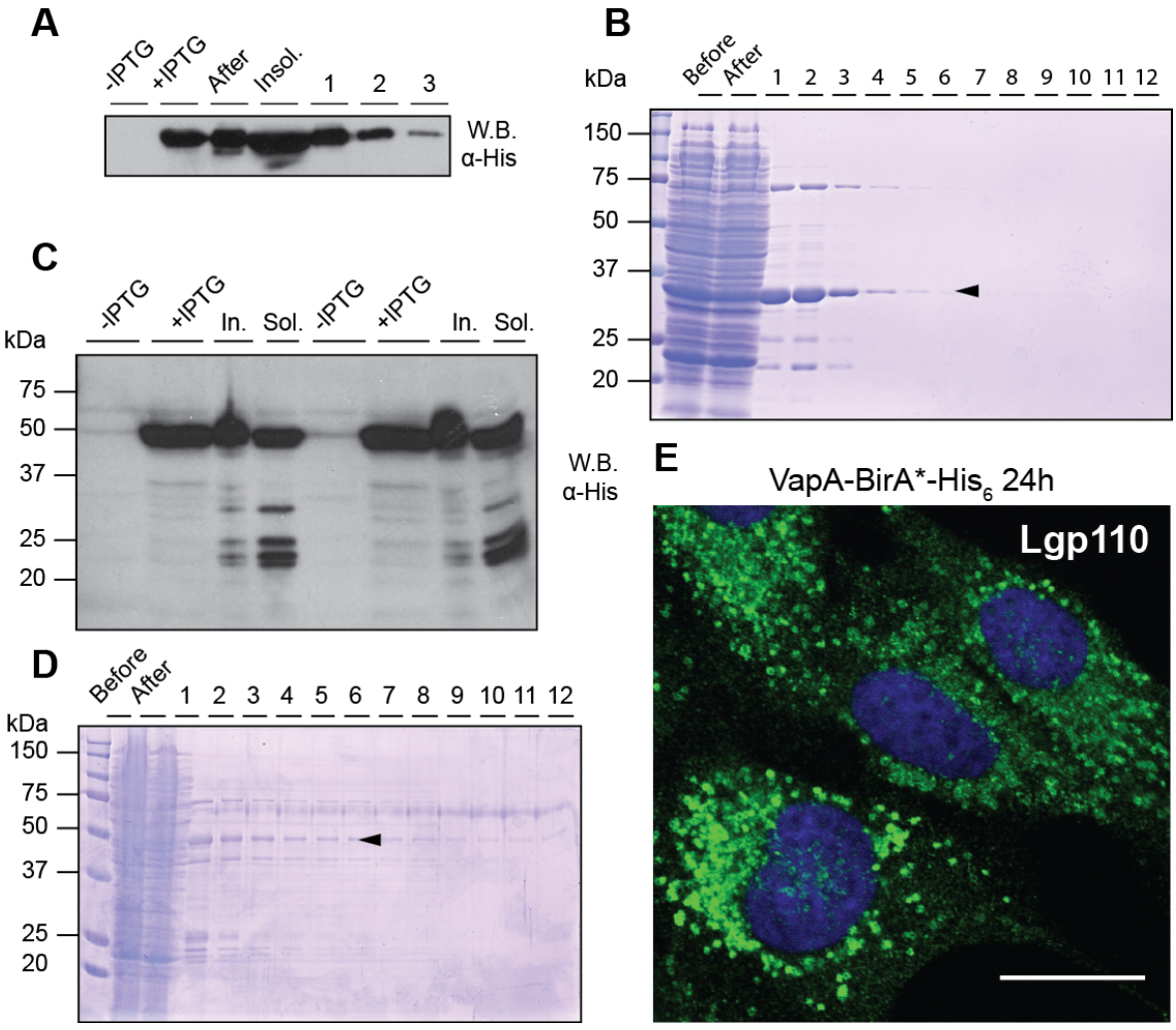

Fig. 5.18. Purification of BirA*-His$_6$ and VapA-BirA*-His$_6$. A. Small scale test expression of BirA*-His. Uninduced (-IPTG), induced (+ITPG), insoluble (In.) soluble (sol.) and 3 eluted fractions were probed with α-His antibodies. **B.** Large scale purification of BirA*-His. A Bacterial supernatant from a 1l culture was incubated with Ni affinity resin overnight at 4 ºC. The resin was washed thoroughly and 1 ml fractions eluted. 20 µl samples were taken before and after incubation with the resin. 4 µl of each eluted fraction was analysed by SDS PAGE. Arrowhead indicates ~35 kDa BirA*-His **C.** Western blot analysis of VapA-BirA*-his expression. Two clones expressing VapA-BirA* were analysed for protein expression. Fractions were probed with α-His antibodies. **D**. Large scale expression of VapA-BirA*-His. The bacterial supernatant from a 1l culture was incubated with Ni affinity resin overnight at 4 ºC. The resin was washed thoroughly and 1 ml fractions eluted. 20 µl samples were taken before and after incubation with the resin. 4 µl of each eluted fraction was analysed by SDS PAGE. Arrowhead indicates ~ 50 kDa VapA-BirA*-His **E.** NRK cells were incubated with recombinant BirA*-VapA at 100 µg/ml for 24 h and then fixed in 4 % formaldehyde in PBS. Cells were labelled with α-Lgp110 antibodies followed by fluorescently labelled secondary antibodies (Alexa fluor 488; green). Cell nuclei were stained with DAPI (blue). Image is a maximum-intensity z-projection. Scale bar 20 µm.

5.3.10 Affinity capture of biotinylated proteins using recombinant VapA-BirA-His$_6$*

As expression of BirA*-VapA in HeLa cells was on the cytoplasmic side of the lysosome membrane and VapA was hypothesised to function when in the lumen of the lysosome, BirA*-His and VapA-BirA*-His were made recombinantly to feed to NRK cells. Cells were pulsed with these proteins at 100 µg/m for a 16 h chase, followed by a 4 hour protein-free incubation to chase BirA* and VapA-BirA*-His to the lysosome. The cells were then cultured in the presence of biotin, to allow biotinylation of VapA-interacting proteins. Detergent-soluble lysates were then made and incubated with streptavidin beads to capture biotylated proteins. After a stringent washing protocol, biotinylated proteins were eluted from the beads by boiling at 95 ºC with Laemmli sample buffer saturated with biotin. 90 % of the sample was analysed by 1D liquid chromatography – mass spectrometry (LC-MS) and 10 % was subjected to western blotting using a streptavidin-HRP conjugate (Fig. 5.19). Equal volumes of the input lysates before and after incubation with the beads were also blotted to analyse the efficiency of the pulldown. No biotinylated proteins could be detected in either of these samples for both BirA* and BirA*-VapA. A strong band was detected at ~ 37 kDA in BirA*-His eluate and similarly, a ~ 50 kDA in VapA-BirA*-His eluate. These were probably biotinylated BirA* and BirA*-VapA, which become-self biotinylated. In both samples, a few protein bands were detected just under each of these strong bands. Proteins of < 25 kDa and > 25 kDa were also seen in BirA* and VapA-BirA* eluates respectively, which may be degradation products of the recombinant proteins. However, there were no obvious differences between samples detected by western blotting.

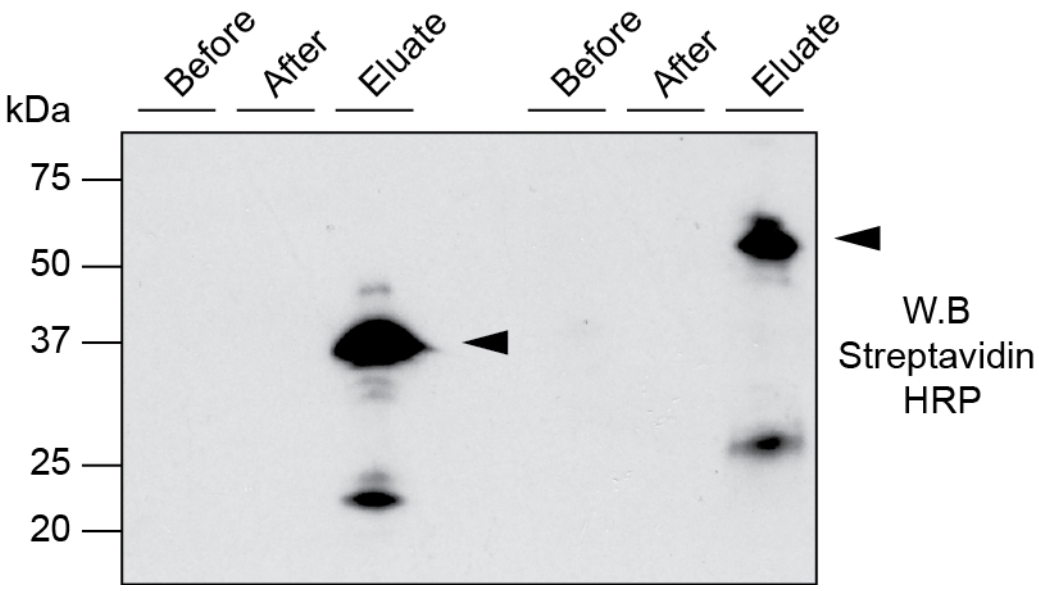

Fig. 5.19. Western blot analysis of VapA-BirA biotin ligase-pulldown. NRK cells were pulsed with recombinant BirA*-His or VapA-BirA*-His at 100 µg/ml for 16 h. The cells were rinsed once with PBS and the media replaced with DMEM for a further 4 h chase period. The cells were then cultured for a further 24 h in DMEM supplemented with biotin to a final concentration of 50 µM. The cells were rinsed with PBS and detergent-soluble lysates generated. Lysates were normalised to protein and incubated overnight at 4 ºC with 600 µl of streptavidin beads to capture biotinylated proteins. The beads were washed thoroughly and biotinylated proteins eluted by boiling in Laemmli sample buffer saturated in biotin. 10 % of the sample was retained for western blotting (W.B.) with a streptavidin-HRP conjugate. Equal volumes of the lysates before and after incubation with the beads were loaded. Arrowheads indicate 37 kDa BirA*-His and 50 kDa VapA-BirA*-His.

Biotinylated proteins were identified by 1D LC-MS. Proteins unique to the VapA-BirA* pulldown were deemed to be possible-VapA interactors. The pulldown experiment yielded more possible VapA interacting proteins than the previous methodology, but as before, the confidence in these hits was not high due to the low number of matched peptides. Regardless, several of these hits were associated with membrane trafficking and endocytosis. These included positively charged multivesicluar body protein 4B-like protein 1 (CHMP4BP1), AP-5, AP-4, Rab10, Rab21 and VPS35 (Table 5.1). The full list of identified proteins is shown in appendix 1.2.

Protein Identity	Mascot Score	Spectra matches	Maximum Peptide Sequences	Molar %
Charged multivesicular body protein 4B-like protein CHMP4BP1	56	1	1	0.09
AP-5 complex subunit zeta-1	53	3	1	0.04
Ras-related protein Rab-10	32	1	1	0.08
Ras-related protein Rab-21	28	1	1	0.07
AP-4 complex subunit epsilon-1	17	1	1	0.01
Vacuolar protein sorting-associated protein 35	16	1	1	0.02
Rho guanine nucleotide exchange factor 12	14	1	1	0.01
Dynein heavy chain 17	14	1	1	0.01

Table 5.1. VapA-BirA* interacting proteins A proximity-dependent biotin ligation experiment was performed in HeLa cells fed recombinant VapA-BirA*-His to identify proteins that interacted with VapA, as described in section 5.2.4. Biotinylated proteins were analysed by 1D LC-MS. Hits unique to VapA-BirA*-His were classed as potential VapA-interacting proteins.

5.4 Discussion

5.4.1 Characterisation of VapA-induced lysosomal swelling

The effect of VapA on lysosomes could be observed as early as 2 h and the number of larger lysosomal puncta steadily increased over a 24 h period. At 24 h, the majority of the lysosomes seen in NRK cells were enlarged. It was not clear if this phenotype was unique to lysosomes, or whether other endocytic organelles were affected. It was found that early endosomes were not effected by VapA, but a small proportion of cells had an altered EEA1 distribution, with staining concentrating around the perinuclear region. Occasionally, larger EEA1 puncta were seen, but not to the extent or size of affected lysosomes. This may indicate an indirect effect on early endosomal trafficking events, as a result of disrupted lysosome function. In some lysosomal storage disorders, the accumulation of macromolecules can result in off-target inhibition of other lysosomal enzymes (Walkley and Vanier, 2009). This can result in a disruption of not just lysosome, but the endolysosomal system as a whole. Similarly, if VapA disrupts lysosomal function, then other components of the endocytic system may be affected. ciM6PR^{+} late endosomes also swelled up when cells were incubated with VapA. To ascertain whether endolysosomes were also effected, cells were co-stained for ciM6PR and LAMP1. It was found that lysosomal, late endocytic and ciM6PR^{+}/LAMP1^{+} endolysosomes also swelled up. This suggested that VapA effects late endocytic compartments. One explanation for this result is that VapA may not accumulate in early endosomes to the same extent as in late endosome/lysosomes. This may be difficult to test, as delaying the maturation of early endosomes (EEs) to examine whether VapA disrupts EE morphology, is itself likely to result in the swelling of EEs. One key difference between early endosomes and late endosomes/lysosomes, is the decrease in pH between these compartments. As VapA only appeared to affect late endocytic organelles, it is possible that VapA is only active at a pH lower than that of early endosomes. Given that VapA has no obvious ligand binding sites and its barrel does not seem to form a pore, it is not inconceivable that a pH-induced conformational change is needed for VapA activity. This could be tested using inhibitors such as Bafilomycin A1 or chloroquine, which increase lysosomal pH and might abolish the activity of VapA. Alternatively, VapA may be interacting with protein(s) such as LAMPs, that present in both late endosomes and lysosomes, but not present in early endosomes.

From 0 h – 48 h, lysosomes continued to aggregate and swell, forming very large structures. Interestingly, at 72 h, these appeared to collapse and the cell cytoplasm was filled with many smaller puncta, similar to 8 h time points seen previously. This may be due to collapse of the large lysosomes into multiple smaller vesicles. This could also be due to upregulation of lysosomal biogenesis as a result in the dysfunction of the lysosomes. Western blotting of LAMP1 levels of VapA fed cells supported this idea, as LAMP1 was shown to increase over time in both NRK and J774.2 cells. Cells incubated with VapD or VapG showed no increase in LAMP levels. The localisation of the transcription factor TFEB, could be monitored by confocal microscopy to investigate whether VapA-induced lysosome swelling causes translocation of TFEB from the cytosol to the nucleus. It was observed that J774.2 cells were particularly susceptible to VapA, which killed cells some when between 24 h and 48 h. NRK cells may be more resilient, or VapA may affect macrophages more strongly than other cell types.

The swelling of lysosomes induced by VapA may be indicative of lysosomal dysfunction. In some lysosomal storage disorders, (such as Fabry disease (Masson et al., 2004) non-functional enzymes fail to metabolise substrate macromolecules, resulting in their accumulation within the lysosome. Alternatively, lysosomes may become swollen due to decrease in lysosomal fission/reformation, such as in Chediak- Higashi syndrome (Durchfort et al., 2012) or Niemann-Pick disease (Platt et al., 2012). It is not clear however, if the lysosomal swelling seen in VapA treated cells is due to an accumulation of non-degraded macro molecules, or is due to an actual disruption to lysosomal fission/fusion. The Magic Red data indicates that lysosomal pH is unaffected by VapA. Some intracellular pathogens also disrupt membrane trafficking, giving rise to a phenotype reminiscent of an LSD. *Coxiella burnetii,* the causative agent of Q fever, resides in a large, cholesterol-rich swollen vacuole (Howe and Heinzen, 2006). Similarly, *Mycobacterium tuberculosis* promotes a “foamy macrophage” phenotype, in which Infected macrophages accumulate lipid droplets that the bacterium uses as nutrient source (Singh et al., 2012).

5.4.2 VapA is the only Vap capable of inducing lysosomal swelling

The large degree of homology in the Vaps in both sequence and structure, suggested that other Vap proteins may be able to induce the same effects as VapA. When both VapD and VapG were incubated with NRK cells, no changes to

lysosome morphology were seen and lysosomal staining was indistinguishable from that of control cells. It may have been possible that the other Vap proteins act synergistically, or some how modified or regulated the activity of VapA. However, when incubated in combination, VapD and VapG had no effect on lysosomes. Additionally, lysosomal swelling was still observed when VapD or VapG were incubated along with VapA, indicating that they do not inhibit the activity of VapA (data not shown). It is therefore unclear what the function of these additional Vaps is, considering that the expression of these proteins is induced during intracellular growth (Ren and Prescott, 2003), or conditions encountered in the macrophage phagosome, such as low pH (Benoit et al., 2001) or an increase in temperature (Byrne et al., 2001).

5.4.3 The activity of VapA is confined to its C-terminal core

While it was clear that VapA exerted an effect on lysosomes, it was not known what regions of VapA were responsible for this activity. The Vap proteins share significant homology in their C-terminal core structure, with variability in the N-terminal regions. Given that VapA had previously been identified as the only Vap essential for virulence, it was hypothesised that the activity of VapA may lie in this N-terminal peptide. Surprisingly, it was found that the core of VapA alone was sufficient to induce lysosomal swelling. This was confirmed by the fact that a VapA N-terminus/ VapD core chimeric protein had no effect on lysosome morphology. These data strongly suggest that the activity of VapA can be attributed to the core barrel structure.

It is striking that only the core of VapA is able to cause swelling of lysosomes, given the large degree of homology between the Vap proteins. However, this may not be so surprising, given that the N-terminal region of the Vap proteins is predicted to be natively unstructured and as such may have no function in virulence (Whittingham et al., 2014). The novel structure of the core of VapD has similarities to other β-barrel proteins, including OmpX from *E.coli* (Vogt and Schulz, 1999) and PliC from *S. typhimurium* (Leysen et al., 2011). OmpX is an outer membrane-spanning barrel, that has a high unusual protruding “flag waving” β-sheet formed by loops 2 and 3 of the barrel. This may be important in virulence by facilitating attachment and invasion of host cells and by acting as a binding partner for host complement proteins. The Vap structure does not have this feature, nor does it have any obvious ligand binding sites or grooves. The barrel of

OmpX is highly unlikely to form a pore. Similarly, the core Vap structure is a closed barrel, which has no obvious passage for small molecules. Unlike OmpX, some of the Vap proteins are secreted (namely VapG and VapD). VapA is thought to be be cell surface anchored (Takai et al., 2000) but it remains to be seen whether VapA interacts with the lysosome while it is bound to the bacterial surface, but the immunofluorescence data suggested that this is the case. The interaction of VapD with octyl-β-d-glucoside (used in its crystallisation solution) suggests it may transiently interact with the cell wall mycolic acids (Whittingham et al., 2014). This may also be true for VapA. It is particularly interesting that in infected macrophages, VapA was found to colocalise not only with lysosomes but also bacteria. However, this does not rule out the possibility that VapA may be released from the bacterial cell surface.

Given that the N-terminus of the Vap proteins is not required to swell lysosomes and its activity lies within the core barrel structure, any differences in the core between VapA and the other Vaps may hint at which regions are important. One such region lies between the 2nd and 3rd β-sheet (see Fig. 5.0 & 5.2). The generation of chimeric Vap-fusion proteins would be a useful tool in understanding which regions of the protein are essential for virulence. For example, this region of VapA could be used to replace the same region in VapD and vice versa. This might reveal whether the key activity is conferred by a particular part of the protein. Alternatively, individual residues could be mutated to unravel those that are necessary for the function of the protein. However, it should be noted that given the structural similarity between the Vaps and the striking difference in their function, it cannot be concluded that the remaining untested Vaps do no not have any role in virulence.

5.4.4 VapA-affected compartments are still acidic

Upon discovering VapA was able to induce the swelling of lysosomes, it was hypothesised that (like in an LSD) the lysosomes were non-functional. It was possible that the Vaps may render host endosome/lysosome-associated enzymes inactive. To test this, VapA-fed cells were incubated with the fluorescent cathepsin B substrate, Magic Red (MR). Unexpectedly, VapA-fed cells had large, swollen, MR positive vesicles. The half-life of cathepsin B is particularly long, meaning any VapA effects would take some time to manifest. However, NRK cells still had Magic Red puncta after 72 h of incubation with VapA (data not shown), suggesting

this was unlikely. Two things can be inferred from this result. Firstly, VapA does not inhibit the activity of cathepsins and secondly, the swelling phenotype does not (at 24h) affect the pH of these compartments. Moreover, it was observed that in control cells, MR and LAMP1-GFP did not completely colocalise, demonstrating a distinction between MR positive endolysosomes and lysosomes (MR negative). Interestingly, in VapA-fed cells, few MR puncta were found that did not colocalise with LAMP1-GFP. It is tempting to speculate that the reformation of lysosomes from MR positive endolysosomes had been perturbed, although this remains to be tested or quantified. An alternate hypothesis may be that these VapA affected lysosomes are non-fusogenic and therefore unable to deliver their bactericidal enzymes to the *R. equi* containing vacuole. The question then remains, how VapA is able to spread from affected organelles to other lysosomes, to prevent them from fusing with the RCV?

5.4.5 Infection of cells with *R. equi*

R. equi has previously been reported to arrest phagosome maturation at an early phagosome/endosome stage RCVs of both virulent and avirulent strains were found to acquire LAMP1. Phagosomes of virulent strains did not acquire the vATPase, nor did they acidify to the same extent as plasmid-cured bacteria (Fernandez-Mora et al., 2005). The acidification of RCVs in this study was not investigated. In agreement with this data, both plasmid-cured and virulent *R. equi* were surrounded by LAMP1 staining. Some plasmid-positive bacteria were not associated with LAMP1. VapA colocalised with both bacteria and LAMP1 staining, which is not unexpected given that it may remain associated with the cell surface and disrupts lysosome morphology. Purified RCVs (virulent and avirulent) were found to be devoid of Cathepsin B and had low levels β-galactosidase activity, suggesting that RCVs do not acquire these enzymes (Fernandez-Mora et al., 2005). Although compartments affected by VapA retain their acidity and have active cathepsin B, it is not known if this is the case in an *in vivo* infection. Thus data presented here, in part, supports previous observations.

5.4.6 Induction of lysosome biogenesis in cells treated with VapA

The biogenesis of lysosomes is highly regulated and under the control of the TFEB transcription factor (Sardiello et al., 2009). Expression levels of lysosomal genes are upregulated in a response to accumulation of substrates in lysosomes in both

sucrose-induced vacuolation models (Karageorgos et al., 1997, Helip-Wooley and Thoene, 2004) and fibroblasts derived from LSD patients (Song et al., 2013). To determine whether VapA-induced swelling of lysosomes resulted in their dysfunction, levels of a common lysosomal protein, LAMP1, were analysed by western blotting. In both NRK and J774.2 cells, it was found that LAMP1 levels increased over the course of the experiment. Moreover, when the levels of the lysosomal enzyme β-hexosaminidase in NRK cell lysates were measured, it was found that the level of enzyme activity increased over the time course, although not significantly. In J774.2 cells, the levels remained constant, which is most likely explained by the fact that the cells begin to die after 24h incubation with VapA. In addition, where cells were not adhered to the tissue culture dishes, the cells were pelleted and resuspended in cell lysis buffer. The loss of lysosomal and plasma membrane integrity in J774.2 cells would result in the leaking of lysosomal enzymes into the cell culture media, which was discarded when the cells were pelleted, thus underestimating the amount of β-hexosaminidase at later time points.

Levels of LAMP1 and other lysosomal enzymes have also been observed to increase during intracellular infection of macrophages with *Salmonella.* In infected cells, levels of LAMP1 and acid phosphatase were elevated compared to uninfected cells. This increase could have been a cellular response to target more lysosomes to *Salmonella*-containing vacuoles *(Eswarappa et al., 2010).* Interestingly, LAMP1 is also the target of bacterial enzymes. The type 2 IgA1 protease produced by species of *Neisseria* actively cleaves LAMP1 to promote intracellular survival (Lin et al., 1997). It is unclear if lysosome biogenesis is upregulated in response to a loss of lysosomal integrity in these studies. Other components of the endocytic pathway have also shown to be upregulated in response to pathogen manipulation of intracellular compartments. The LYST (Lysosomal trafficking regulator protein) gene is and is upregulated during infection of bone marrow derived macrophages by *Leishmania amazonensis* to limit the expansion of the parasitophorous vacuole (Wilson et al., 2008). LYST is mutated in Chediak-Higashi syndrome (CHS) (Barbosa et al., 1996). One hallmark of this disease is enlarged lysosomes and lysosome-related organelles. LYST has has previously been shown to regulate lysosome size (Holland et al., 2014), but although lysosomes are enlarged in CHS cells, they remain acidic and trafficking, autophagy and endocytosis is not affected in these cells. Parallels can be drawn to

lysosomes of cells treated with VapA, which also remain acidic despite being swollen. It could be speculated therefore, that similar to many LSDs, lysosomes of VapA treated cells have disrupted fission/fusion.

Taken together, these data indicate that VapA –induced swelling of lysosomes may lead to increased lysosome biogenesis as a response to lysosomal dysfunction. However, the Magic Red experiments showed that VapA-swollen lysosomes were still acidic and contained active proteases. Therefore, this dysfunction may be separate to the degradative function of the lysosome. This is further supported by the observation that LAMP1 and Magic Red signals overlapped in VapA treated cells, but remained largely separate in control cells. This hints at the possibility that VapA swollen lysosomes may be endolysosomal compartments from which lysosomes are unable to reform. In this manner, *R. equi* may be able to deplete the available pool of lysosomes that can fuse with the RCV.

5.4.7 Identifying the mammalian target of VapA

Identification of the target of VapA is critical in understanding how it effects eukaryotic cells and contributes to the intracellular survival of *R. equi.* There are two main approaches that could have been used. Firstly, yeast two-hybrid (Y2H) systems use transcription factor domains to drive reporter gene expression as a measure of protein interactions. The second approach is utilisation of pull-downs or co-immunoprecipitation, whereby a protein of interest is expressed with an epitope tag and interacting proteins are identified by mass spectrometry. Each of these techniques has its own particular advantages and drawbacks. Y2H systems rely upon the correct folding of both “bait” and “prey” proteins when they are expressed as a fusion protein with a transcription factor domain. This assumes that the proteins are still able to interact when expressed as a hybrid protein, without their usual chaperones and post-translational modifications and often outside of their normal cellular localisation. This may result in false-positive interactions between proteins that would never normally be expressed in the same location, e.g DNA binding proteins being expressed in the cytoplasm. This is particular problematic for integral membrane proteins (although split-ubiquitin Y2H systems can be used in this case). An advantage of the Y2H approach is that as it is based on a cDNA library screen, it can identify interactions between proteins that are of particularly low abundance, or that have a weak or transient interaction.

The immunoprecipitation approach has been used extensively to identify protein-protein interactions. One limitation to this approach is the availability of a protein of interest. In some instances, it may not be practical to express or purify enough starting material to be able to detect an interacting protein. This becomes extremely difficult if the interactions are weak or transient. Secondly, this approach is only viable if the protein of interest remains soluble under the conditions used to generate a cell lysate. Moreover, it depends upon protein-protein interactions still taking place under these conditions.

5.4.8 VapA immunoprecipitation

To understand how VapA disrupts lysosomes, immunoprecipitation experiments were performed to try and identify the mammalian target of VapA. The IP protocol was heavily optimised to increase the chance of finding any low abundance proteins, or weak interactions. Firstly, the optimal ratio of α-myc antibody and protein lysate needed to immunoprecipitate detectable amounts of myc-VapA was determined. It was found that 10 µg of antibody was saturated when incubated with 1.5 mg of myc-VapA lysate. However, the IP was still inefficient, as the majority of the myc-VapA remained in the lysate. This was improved when lysates were incubated with the antibody overnight compared to 1 h. The amount of antibody necessary to remove > 90 % of myc-VapA from 1.5 mg of lysate was found to be 40 µg. With these optimisations, the IP was scaled up using 1.5, 3, 6 and 12 mg of lysate. These amounts were visible on SDS PAGE gels by coomassie staining. However, no band corresponding to immunoprecipitated myc-VapA was visible. Gels were then silver stained, but no protein of the expected molecular weight was identified. This may have been due to inefficient elution of proteins from the α-myc sepharose. To address this, a small scale IP was carried out with several elution conditions. 1 % SDS and 100 mM Triethylamine were found to be the most effective at eluting proteins from the sepharose. However, these buffers were also the two that resulted in the elution of large amounts of heavy and light IgG chains from the sepharose. Eluates using low pH IgG and glycine elutions buffers were relatively free of IgG chains. 3.5 M $MgCl_2$ salt elution buffer did not elute any proteins or IgG chains. In all cases, a large amount of protein remained bound to the sepharose. The inefficiency of elution of proteins from the sepharose was confirmed when additional elutions were found to still contain myc-VapA. Therefore, the volume of elution buffer used was doubled for remaining experiments. The amount of myc-VapA that was immunoprecipitated

was low in these optimisation experiments. The loss of protein expression most likely contributed to this problem, but it was not clear why this happened as the expressing of myc-VapA was inducible and not constitutive. Low passage cells were subsequently used for the large scale IPs to try and increase the amount of expressed protein. Protein expression was also optimised by changing the levels of doxycycline and time of expression. Despite these changes, two IPs using 40 mg of lysate did not immunoprecipitate sufficient amounts of myc-VapA to detect any interacting proteins.

There are several possible reasons why the immunoprecipitation experiments did not work effectively. Firstly, it was clear that some myc-VapA could be immunoprecipitated, but the IP was inefficient. While it was detectable by western blot, insufficient protein may have been immunoprecipitated for detection by silver staining. This would have been further complicated by the inconsistent expression of exogenous protein seen in the myc-VapA cell line. Secondly, the myc-tag was on the N-terminus of VapA. Any cleavage of the N-terminus from the main core of the VapA protein would have resulted in immunoprecipitation of the non-functional N-terminus, leaving behind the C-terminal core. It is possible that immunoprecipitated myc-VapA remained bound to the α-myc sepharose and was not efficiently eluted. Thirdly, the myc-VapA was expressed in the cytoplasm of HeLa cells, but it was demonstrated that VapA needed to be on the lumenal side vesicle membranes to have any function. This suggested its target is in the lysosome lumen, which would not have been accessible until a cell lysate was generated. This also relied upon the interaction between VapA and its partner being stable in the lysis conditions. Finally, it is possible that VapA interacts with a lipid specific to late endosomes/lysosomes (such as lysobisphosphatidic acid, LBPA). If this is the case, other approaches are needed to identify what VapA interacts with. These could include vesicle cosedimentation/cofloatation assays, to asses the affinity and specificity of lipid binding, diphenylhexatriene (DPH) anisotropy, to measure membrane fluidics up protein binding and fluorometric based assays, using fluorescent probes such as boron-dipyrromethene (BODIPY), to measure fluorescence quenching when proteins bind to lipid layers (Zhao and Lappalainen, 2012).

5.4.9 Proximity-dependent biotin identification - BioID

Due to the technical difficulty of identifying the binding partner of VapA through a traditional immunoprecipitation approach, an alternative method was used that circumvented these issues. BioID utilises a prokaryotic biotin-ligase, BirA, to attach biotin molecules to primary amines, in a proximity dependent manner. This approach has been used to successfully identify proteins that are interacting partners, or in close proximity to Lamin-A, an intermediate filament of the nuclear lamina (Roux et al., 2012).

The immunoprecipitation of VapA most likely proved difficult due to low expression of myc-tagged VapA, but may have also been due to the disruption of protein-protein interactions under the denaturing conditions used to generate a cell lysate. A key advantage of BioID in this respect, is that biotinylation of interacting proteins occurs before the generation of a cell lysate. Therefore, weak or transient interactions can be detected and protein-protein interactions do to not need to remain intact for biotinylated proteins to be immunoprecipitated and identified. The abundance of biotinylated material does not indicate the strength of an interaction, more the abundance of primary amines within an identified protein. Therefore, this approach should be used a screen to identify candidate proteins, which should be validated using other biochemical analyses.

This method was dependent upon the ability of VapA to function properly when expressed as a chimera with BirA*. The addition of BirA* did not effect the localisation of VapA in HeLa cells. However, as discussed previously, the expression of BirA*-VapA in the cytoplasm was most likely not optimal given that VapA has no effect unless on the lumenal side of endocytic membranes. This was confirmed when VapA-BirA* was expressed as a his-tagged protein and fed to cells, as these cells showed the same swelling phenotype as cells incubated with VapA-his. Furthermore, producing VapA-BirA* in *E.coli*, rather than expressing it *in vivo* meant that low expression of VapA was not an issue and ensured that VapA reached the lumen of the lysosome/late endosome, where it carries out its function.

Despite the limitations of expressing BirA-VapA* in the cytoplasm, some proteins unique to BirA*-VapA included Annexin 1a, Exocyst complex component 6b (Sec15/EXOC6) and cathepsin D (Table 5.0). Annexin 1a is a calcium-dependent

phospholipid binding protein that is found on the plasma membrane and early endosomes (Rescher et al., 2000) and has also been found on phagosomal membranes (Diakonova et al., 1997). It is also thought to be important in *M. tuberculosis* infections, as mice deficient in Annexin 1 were more susceptible to infections and were less able to mount a T-Cell response to the bacteria (Tzelepis et al., 2015). Overall, relatively little is known about the precise functions of annexins in the endocytic pathway.

The exocyst is a multisubunit tethering complex made up of 8 subunits (Sec3, Sec5, Sec6, Sec8, Sec10, Sec15, Exo70 and Exo84), that is involved in exocytosis of secretory vesicles at the plasma membrane (Yu et al., 2011). As such, it is localised to the inner leaflet of the plasma membrane. The exocyst complex also mediates many of the membrane trafficking functions of the GTPase Rab11, such as the trafficking of the Toll-Like receptor TLR4 to phagosomes and the exocytosis of pore-forming toxins from the cell surface (Guichard et al., 2014). Sec15 interacts with Rab11 and may be important for endosomal recycling (Zhang et al., 2004). Some pathogens hijack Rab11/exocyst function to promote intracellular survival. A component of the *Salmonella* type three secretion system, SipC, interacts with the exocyst subunit Exo70, to recruit the exocyst complex to the plasma membrane and promote invasion of the host cell (Nichols and Casanova, 2010).

Cathepsin D is a aspartic endopeptidase that is synthesised as a preprocathepsin D (Benes et al., 2008). After the removal of a signal peptide, procathepsin D is then targeted to lysosomes (Hasilik and Neufeld, 1980). Cathepsin D is a glycoprotein, that is glycosylated by the addition of mannose-6-phosphate residues at asparagine 70 and 199, which is essential for its correct targeting to the lysosome (Fortenberry et al., 1995). Genetic deficiency of cathepsin D in mice is not lethal, but results in abnormalities in later life (Saftig et al., 1995, Koike et al., 2000). In humans, cathepsin D deficiency is associated with lysosomal accumulation of lipofusin, resulting in neuronal ceriod lipofusinosis (Siintola et al., 2006, Steinfeld et al., 2006). Cathepsin D is also important for macrophage apoptosis in the mouse lung, to help clear *Streptococcus pneumoniae* infections (Bewley et al., 2011). Cathepsins L and B are inhibited by a cysteine-protease inhibitor expressed on the surface of *Plesiomonas shigellodies*, a possible mechanism of bacterial protection against host defences (Pavlova et al., 2006).

Whether VapA interacts with these proteins has yet to be validated. It is interesting that these proteins are involved in different aspects of the endocytic pathway and are found on endosomes and in the case of cathepsin D, in the lumen of the lysosome. However, from the immunofluorescence data it appears that expressed myc-VapA does not colocalise with the plasma membrane in HeLa cells. Thus, its possible association with Annexin 1a and Exo6B is not supported by this. Secondly, it is hard to see how myc-VapA would associate with cathepsin D when expressed in the cell cytoplasm, suggesting this is not likely to be a real interaction. This is idea is also supported by the fact that VapA-BirA* was not found to interact with cathepsin D.

The experiment was repeated with recombinant VapA-BirA* to target VapA to the lysosome lumen. This identified several biotinylated proteins unique to the VapA sample, some of which are involved in membrane trafficking. Charged multivesicluar body protein pseudogene 1 (CHMP4BP1), was classed as a possible VapA interactor. CHMP4BP1 has > 95 % sequence similarity to CHMP4B. CHMP4B is part of the endosomal sorting complexes required for protein transport (ESCRT) machinery. In particular, CHMP4B (Snf7) forms the core of the ESCRT III complex, along with CHMP6 (Vps20), CHMP2 (Vps2) and CHMP3 (Vps24). These four subunits are joined by three accessory proteins, CHMP1 (Did2), CHMP5 (Vps60) and Ist1 (Schmidt and Teis, 2012). Unlike the other ESCRT complexes (0, I and II), which form stable cytoplasmic complexes, ESCRT III polymerises from cytoplasmic monomers and transiently associates with endosomes (Henne et al., 2011), where it is required for the sorting of cell surface receptors into intraluminal vesicles for degradation (Babst et al., 2002). CHMP4B is the most important component of the ESCRT III machinery (Wollert et al., 2009). It is present in the highest concentrations in the cytoplasm and the other subunits of the complex act to polymerise CHMP4 (Teis et al., 2008). However, little is known about CHMP4BP1, with regards to its localisation, expression, or its function.

Adapter proteins (AP) are heterotetramic protein complexes that facilitate the sorting of membrane proteins in the endocytic and exocytic pathways (Nakatsu and Ohno, 2003). APs are essential for clathrin-coated vesicle formation, as they act as a bridge between clathrin coats and lipid membranes (Young, 2007). Currently, 5 different adaptor protein complexes are known to exist. While the roles of AP-1, AP-2 and AP-3 are known, the role of AP-4 and AP-5 in protein

sorting are poorly understood (Hirst et al., 2013). AP-1 and AP-2 knockouts are lethal, (Zizioli et al., 1999, Mitsunari et al., 2005), whereas mutations in AP-3 causes Hermansky-Pudlack syndrome (Dell'Angelica et al., 1999). Mutations in AP-4 and AP-5 cause human neurological disorders (Abou Jamra et al., 2011, Slabicki et al., 2010). Unlike the other adaptor complexes, AP-4 and AP-5 do not appear to interact with clathrin. AP-4 may function as an exporter of specific proteins from the *Trans* Golgi network (TGN), but the function of AP-5 is not known (Hirst et al., 2013).

Rab10 has a role in protein trafficking to the plasma membrane and associates with the exocyst complex (Babbey et al., 2010). Rab10 also regulates the translocation of GLUT4 storage vesicles to the adipocyte plasma membrane (Sano et al., 2007) and is involved in the regulation of ER dynamics (English and Voeltz, 2013). Rab10 has also been found in phagosome proteomic studies (Rogers and Foster, 2007, Garin et al., 2001). Rab10 has been shown to be required for recycling of proteins from the phagosome back to the plasma membrane and over expression of Rab10 accelerates the maturation of *M. tuberculosis* containing phagosomes (Cardoso et al., 2010).

Rab21 regulates endosomal traffic (Pellinen et al., 2006, Simpson et al., 2004) as well as the formation of macropinosomes (Egami and Araki, 2009). In *Dictyostelium*, Rab21 regulates phagocytosis, along with two novel LIM domain proteins, LimF and ChLim (Khurana et al., 2005). Rab21 has been found in proteomic studies of *M.bovis* Bacille Calmette-Guérin (BCG) phagosomes (Lee et al., 2010). The *Legionella* effector protein Lpg0393 has recently been shown to be a guanine-nucleotide exchange factor (GEF) for Rabs 5, 21 and 22, raising the possibility that modulating the activity of these GTPases promotes bacterial intracellular survival (Sohn et al., 2015).

VPS35 (vacuolar protein sorting associated-protein 35), is a key component of retromer, a complex of proteins required retrograde transport of hydrolase receptors from endosomes to the Golgi (Seaman, 2012). Retromer is a pentameric subunit complex, consisting of a sorting nexin (SNX) dimer, which binds to phosphatidylinositol 3-phosphate (PI(3)P) and a cargo recognition complex heterotrimer, consisting of Vps26, Vps35 and Vps29 (Bonifacino and Hurley, 2008). Cells lacking Vps26 fail to retrieve ciM6PR from late endosomes, resulting in its degradation or mislocalisation to the plasma membrane (Seaman, 2004) and

a mutation in VPS35 causes a rare form of Parkinson's disease (Zavodszky et al., 2014) with a similar phenotype seen in a VPS35 knockdown in *Drosophila* (Miura et al., 2014). Thus, retromer function is crucial to normal cell function. Proper retromer function is also important in bacterial pathogenesis, as siRNA knockdown of the Vps26-Vps35-Vps29 complex prevented intracellular replication of *Coxiella* (McDonough et al., 2013), suggesting this pathway is important for bacterial replication.

In contrast to cytoplasmic expression of BirA*-VapA, VapA-BirA*-His was on the correct side of the lysosome lumen. It is therefore unclear how VapA could interact with these proteins considering they function in the cytoplasm. One possibility is that VapA may have caused lysosome lysis, upon which VapA would then have access to the cytoplasm. The hazy LAMP1 staining sometimes seen in immunofluorescence of VapA-fed cells may support this idea. These data should also be viewed with caution considering that for many of them, only single peptides were found. Nethertheless, it is interesting that components of membrane trafficking complexes were identified using this approach.

A potential caveat to the feeding of VapA-BirA* to cells, is that it is not known whether VapA-affected compartments remain fusogenic. If they do, the biotin taken up by fluid phase endocytosis should reach lysosomes that contain VapA-BirA*-His and biotinylation should occur. If these lysosomes are not fusogenic, then it is not clear how biotin would gain access to the lysosome lumen, as there was a 4 h chase period before biotin was added to the tissue culture media. Future experiments should aim to determine if these swollen lysosomes can still accept material from the endocytic pathway, which would also confirm the practicality of this methodology. Should they be repeated, producing BirA*-His and VapA-BirA*-His to a higher quality would be advantageous. This would also allow the optimisation of the protocol. For example, both proteins were used at 100 µg/ml, but it was not known how much of this was actually taken up by cells and whether it was sufficient to biotinylate enough target protein for detection by LC-MS. BirA* combines biotin with ATP to form biotinoyl-5' AMP (bioAMP), which reacts with primary amines of interacting proteins, resulting in their biotinylation. The bioAMP molecule is thought to only diffuse 20-30 nm from the BirA* enzyme before reacting with a protein (Roux et al., 2012). Thus, the active radius of VapA-BirA* is unknown and is likely to limit the volume of the lysosome that could potentially be biotinylated. If VapA-BirA* inserts into lysosomal membranes, (which may be a

possibility given that the immunofluorescence data showed VapA colocalising with LAMP1), then BirA* can only biotinylate proteins within 20-30 nm of the limiting membrane. However, this may not be a problem given that VapA-BirA* can still cause swelling of lysosomes, indicating that if it is interacting with a protein, it is able to do so while fused to BirA*. Thus, the limitation of this approach is likely to be the volume of material required to identify proteins, which can easily be optimised and scaled up accordingly.

5.4.10 Conclusions

The data presented here demonstrates that recombinant VapA induces swelling of late endosomes and lysosomes, but not early endosomes. This activity is dependent upon delivery of VapA to the lysosome lumen and is not seen when VapA is expressed in the cell cytoplasm. The ability of VapA to induce swelling is conferred wholly by the C-terminal core of the VapA protein and the N-terminus of VapA is dispensable for this activity. Other Vap proteins (VapD and VapG), that have a similar structure, are not able to induce lysosomal disruption. Lysosome biogenesis may have been upregulated in response to lysosomal disruption by VapA, as levels of LAMP1 increased in VapA-fed J774.2 and NRK cells. The swollen-lysosome phenotype was also seen in J774.2 cells infected with virulent *R. equi*, but not avirulent strains that do not posses VapA. Both virulent and non-virulent *R. equi* were shown to reside within a LAMP1 positive compartment, although avirulent plasmid-cured strains did not replicate. Moreover, VapA was found to colocalise with both bacteria and lysosomes. Thus, VapA induced lysosome disruption may be a mechanism used by *R. equi* to survive inside cells. Two biochemical approaches were taken to identify the binding partner of VapA, but these were inconclusive.

These data give rise to some key research questions that should be addressed in the future. Firstly, what are the protein domains or residues responsible for the activity of VapA? Secondly, given the similarity in their structure and the fact that they are upregulated in macrophages, what are the functions of the other Vap proteins? Finally, what is the target of VapA and how does VapA interfere with its function to induce lysosomal disruption and promote bacterial survival?

Chapter 6: General Discussion

The purification of subcellular organelles has been instrumental in studying their function and composition. Decades of research has led to the development of a variety of different methods to achieve this aim. These methods are not without their caveats, but in general relatively pure fractions of most organelles can be isolated. The purification of lysosomes can be tricky. Isolating them on centrifugation gradients is not trivial and lysosomal fractions will be contaminated with organelles of the same density unless specific centrifugation media is used or the density of the lysosome is altered. Endocytic vesicles present themselves nicely for purification using endocytosed substrates which only label vesicles that have taken up the substrate used to aid in their purification. Such techniques have been developed extensively and are becoming the method of choice for purifying endocytic vesicles (Walker and Lloyd-Evans, 2015). The purification of phagosomes presents similar challenges but is often simpler. Most phagosome purification protocols involve the use of latex beads or other synthetic particles that are chosen as their properties allow easier purification. For example, latex beads will float to the top of a sucrose gradient and magnetic bead phagosomes can easily be removed from a cell lysate using a strong magnet. The isolation of phagosomes has been used extensively in proteomic analysis of phagosome maturation (Desjardins and Griffiths, 2003, Garin et al., 2001, Buschow et al., 2012, Guo et al., 2015).

The development of *in vitro* assays to study vesicle fusion have been influential in unravelling the molecular basis behind the fusion of membranes. Such techniques require the development of protocols to purify both acceptor and donor compartments and have a method of reporting membrane fusion. They must also include appropriate controls to ensure that the results seen are due to *bona fide* membrane fusion and not the mixing of membrane fragments or damaged organelles. The endocytic pathway is a key part of our innate immunity and is critical for the destruction of phagocytosed microbes. Given that phagosome-lysosome fusion is so important, it is surprising that only one current *in vitro* assay of phagosome-lysosome fusion has been published (Becken et al., 2010).

Intracellular pathogens manipulate membrane trafficking events in the endocytic pathway to prevent their delivery to the lysosome. One such pathogen, *Rhodococcus equi*, arrests phagosome maturation at an early endosomal-like stage. The mechanisms behind this are unclear, but are likely to involve the key virulence associated proteins (Vaps) produced by *R. equi*. This thesis describes the optimisation of techniques for the purification of lysosomes and phagosomes for use in an *in vitro* phagosome-lysosome fusion assay. Secondly, it details the characterisation of Vap-induced lysosome dysfunction and builds upon our understanding of the survival mechanisms of *Rhodococcus.*

6.1 Purification of lysosomes

The purification of lysosomes from J774.2 mouse macrophages using superparamagnetic iron oxide nanoparticles (SPIONS) was an established method in the laboratory and was based upon a previously established method (Rodriguez-Paris et al., 1993). This method was chosen as it was quicker and simpler than purifying lysosomes by isopycnic centrifugation and could be performed on smaller numbers of cells. However, this method had not been optimised to purify lysosomes for use in a phagosome-lysosome *in vitro* fusion assay. To purify lysosomes for such a use, a protocol was needed that had two main requirements; i) that purified lysosomes were intact and largely free from contamination of other organelles and ii) that the lysosomes contained a marker that could be used to detect the fusion of lysosomes and phagosomes. Therefore, optimisations were performed to achieve these aims.

Initial experiments began with the comparison of two methods to break open cells and release lysosomes. These were ball-bearing homogenisation and nitrogen cavitation. It was found that these methods yielded similar results with regards to the latency and recovery of lysosomes. Both of these methods have previously been used to release lysosomes from cells (Graves et al., 2008, Ward et al., 1997). It was decided to continue using nitrogen cavitation as the method of choice as it could more easily accommodate larger sample volumes and changes in the protocol than the use of the ball-bearing homogeniser. Further experiments were performed to optimise lysosome purification. These included varying cell number, the pressure used to disrupt cells, and the use of different

homogenisation buffers. In general, these variables did not significantly influence the intactness or recovery of purified lysosomes. When the time of the SPION pulse and chase periods was altered it was found that these had a large influence on lysosome latency and recovery suggesting that these were the most important variables when using this method. Biochemical analysis of purified lysosome fractions showed that they were enriched with LAMP-1 and Rab5 and Rab7, but had lesser amounts of EEA1. This is in agreement with previous analysis of purified lysosomes (Becken et al., 2010). Overall, it is difficult to know what variables may influence lysosome purification as published protocols do not give details on the development of the method, only the final outcome. Despite this, lysosomes were purified from cells with a latency of ~80 % latency and ~7 % recovery.

6.2 Purification of phagosomes

Phagosomes were purified from J774.2 cells using magnetic streptavidin beads. This method was chosen as it was rapid and avoided the use of density centrifugation. After lysate generation, streptavidin-bead phagosomes were isolated on a magnet and washed (approximately 10-15 min). In contrast, the centrifugation steps used in latex bead phagosome purification alone can take between 1 and 4 hours (Gotthardt et al., 2006, Desjardins et al., 1994).

The uptake of beads was shown to be dependent upon the number of beads per cell used (multiplicity of infection; MOI). At a low MOI centrifuging beads onto cells helped to promote uptake but at a higher MOI centrifugation did not increase uptake. This suggests that promoting cell and bead contact is important when using low numbers of particles but not at higher particle:cell ratios. It is possible that higher ratios of particle uptake may influence the maturation of phagosomes. Although the phagosome isolation protocol aimed to synchronise bead uptake, it is likely that this can only go so far to try and yield phagosomes of the same composition. Within individual cells the composition of phagosomes will differ (Griffiths, 2004). When using a low number of particles, it is likely that a cell could take up several particles at once. With a high number of particles, a cell may need to divert extra membrane to the cell surface which could result in a delay in particle

internalisation. The end result would be a more heterogeneous population of organelles compared to lower ratios.

Initial optimisation experiments suggested that nitrogen cavitation was not suitable to release phagosomes from cells as the majority of phagosomes were not intact when using this method. One possibility of this is that as the pressure within the nitrogen bomb was increased the phagosome membrane would have been forced tightly against the streptavidin bead. Any rough edges on the beads could have created weakness in the phagosomal membranes causes them to rupture. Ball-bearing homogenisation was investigated and found to be a suitable method for releasing phagosomes from cells. This may have been because the release of phagosomes from cells involved mechanical disruption rather than gas expansion and the pressures involved would have been much lower.

When phagosomes were analysed by western blotting markers of the early and late endocytic pathway could be seen. Phagosomes were generally enriched with LAMP1 and levels of LAMP1 increased the longer the phagosomes were given to mature. EEA1 was also found on phagosomes, as well as Rab5, Rab7 and α-tubulin. This was not surprising given the fact that phagosomes are heterogeneous (Griffiths, 2004). Other studies have also found these proteins on isolated phagosomes (Garin et al., 2001, Becken et al., 2010) and it is not surprising given their roles in phagosome maturation (Vieira et al., 2002). Similarly, it was seen that levels of the lysosomal enzyme β-hexosaminidase increased as phagosomes were allowed to mature for increasing lengths of time, suggesting some were reaching lysosomes. This is also in agreement with previous data (Becken et al., 2010). The final outcome was the purification of phagosomes that were approximately 75 % intact. The overall recovery of phagosomes was not determined. This study builds upon previous methods and presents an alternative and rapid method of isolating phagosomes from cells that can be optimised to produce phagosomes of different ages.

6.3 Fusion assay

One aim of the thesis was to establish an *in vitro* phagosome-lysosome fusion assay. To this end, two protocols were successfully developed to purify both phagosomes and lysosomes from cells that were intact and biochemically characterised. To analyse phagosome-lysosome fusion it was necessary to analyse the transfer of a marker between the two compartments. This assay aimed to analyse the transfer of biotin-HRP from purified lysosomes to streptavidin bead-phagosomes. The assessment of transfer of biotin-HRP was performed using a highly sensitive substrate, Amplex Red. Control experiments showed that biotin-HRP fed to cells and isolated from lysosomes were still able to bind to streptavidin-phagosomes isolated from cells. Only around 30 % of the biotin-HRP from lysosomes was able to bind to beads suggesting that some was degraded. Moreover, the biotin-HRP binding capacity of phagosomes was often lower than that of a similar number of beads that had not passed through cells suggesting some degradation of the surface streptavidin. Despite this, the amount of biotin-HRP that could be detected yielded a strong fluorescent signal when assayed using Amplex Red.

Fusion of lysosomes and phagosomes was then attempted *in vitro*. Unfortunately, no fusion signal could be seen. The reasons for this were unclear, as biotin-HRP from lysosomes was able to give a fluorescent signal when incubated with Amplex Red, and likewise, phagosomes were able to bind biotin-HRP. One possibility was that the pig brain cytosol used to support vesicle fusion contained endogenous biotin and other factors which may have interfered with vesicle fusion when using biotin-HRP as a marker of fusion. Despite these challenges, the purification of phagosomes and lysosomes was successful and this thesis presents the framework on which to determine the conditions needed to see a fusion signal.

It was demonstrated that biotin-HRP binding to beads that had been incubated in pig brain cytosol was reduced (Fig. 3.36). The next experiment that it would be important to perform would be an *in vitro* mixing assay between HRP-lysosomes and streptavidin-phagosomes in the presence of pig brain cytosol. These components could be mixed and vesicle membranes lysed with detergents to allow mixing of contents. Although this was in essence the control for the *in vitro*

fusion assay (conditions 5&6 Fig 3.35) it was performed at 4 ºC for 15 min which may not have been long enough to see transfer of biotin-HRP to streptavidin beads. Thus, performing this experiment at room temperature or overnight at 4 ºC may demonstrate if pig brain cytosol was responsible for a lack of a fusion signal. For the final fusion assay beads were opsonised with IgG before use. As previously discussed, this was done in an attempt to increase bead uptake and get a working fusion assay. This would undoubtedly change the kinetics of phagosome maturation. Thus, it would also be important to characterise the composition of these phagosomes.

6.4 PEPSY screen

The mechanisms by which *Rhodococcus equi* manipulates host cell membrane trafficking are not clear, but it is suggested that the *R. equi* phagosome is arrested at an early endosomal stage (Fernandez-Mora et al., 2005). The bacterial effector proteins that facilitate this are not known. To identify putative virulence factors, the *R. equi* genome was screened for proteins that disrupted membrane traffic in yeast. This was performed using pathogen effector screening in yeast (PEPSY), a previously established methodology in which a bacterial gene library is expressed in yeast and yeast are then screened for a VPS phenotype (Shohdy et al., 2005). This thesis is the first example of the generation of an *R. equi* gene library and expression of *R. equi* genes in yeast. Unfortunately, the screen failed to determine any virulence factors that altered membrane trafficking in yeast. This may have been due to a lack of similarity between the human targets of *R. equi* effector proteins and their yeast orthologues. Alternatively, *R. equi* effector proteins may have needed to be on the vacuolar side of the yeast lumen to see an effect on membrane trafficking. To test these hypotheses (and to take a targeted approach to investigating *R. equi* virulence) the essential *R. equi* virulence factor, VapA, was expressed in the yeast cytoplasm and also targeted to the yeast vacuole. When expressed in the yeast cytoplasm and targeted to the vacuole, VapA did not produce an observable membrane trafficking defect as no secretion of CPY was seen. However, VapA has been determined to be an essential virulence factor for *R. equi* intracellular survival (Jain et al., 2003). So, for completion, VapA was expressed in the cytoplasm of mammalian cells. VapA had no effect on membrane trafficking when expressed in the mammalian cell cytoplasm. Strikingly, when

VapA was recombinantly produced and introduced to the mammalian lysosome lumen (via fluid-phase endocytosis), it resulted in the swelling of lysosomes. This effect was then further characterised.

6.5 The role of VapA in the intracellular survival of *Rhodococcus equi*

Recombinantly produced VapA caused swelling of lysosomes. This effect was time and dose dependent and was abrogated when VapA was heat denatured before feeding to cells. VapA selectively affected late endocytic (ciM6PR$^+$) and lysosomal (LAMP1$^+$) compartments and may have had an indirect effect on early endosomal compartments (but this was not clear). Given the similarity between the C-terminal core structure of the Vap proteins of *R. equi*, it was hypothesised that VapD and VapG may also induce lysosomal dysfunction but they had no observable effect. As the variability in the protein sequence of the Vaps is in their N-terminal regions, it was thought that this may be responsible for the activity of VapA. Experiments involving chimeric proteins of the VapD N terminus and VapA core or the core of VapA alone showed that the core of VapA is sufficient to cause lysosomal swelling and that the N-terminal region is not important. Moreover, the N-terminal regions of the other Vaps were not inhibitory to any potential activity that they possessed, as the addition of VapD N-terminal region to the VapA core did not prevent lysosomal swelling. As the swelling of the lysosomes by VapA was indicative of lysosomal dysfunction it hypothesised that VapA-affected compartments may have had reduced proteolytic activity or a disrupted pH. Using the fluorescent cathepsin B substrate, Magic Red, it was seen that this was not the case and that VapA-affected compartments contained active cathepsins (and were by proxy determined to still be acidic).

The swelling of lysosomes was also seen in infection of J774.2 macrophage with *R. equi.* Both plasmid cured avirulent and plasmid positive strains of *R. equi* were found to reside in a LAMP1 positive compartment in agreement with previous data (Fernandez-Mora et al., 2005, Toyooka et al., 2005). This compartment was also found to colocalise with VapA produced by the bacterium. Additionally, VapA fed cells showed an upregulation of LAMP1 but VapD or VapG cells did not. This was suggestive of lysosome dysfunction and therefore lysosome biogenesis was increased, but this needs to be investigated further.

This study demonstrates that it is important to consider the subcellular localisation of a bacterial virulence factor, especially if it is not clear whether the bacterial effector is actively translocated into the host cell cytoplasm. This methodology could be used along with cytoplasmic expression of bacterial proteins to more thoroughly investigate their function.

To understand the mechanism behind Vap-induced lysosomal swelling it was necessary to identify the mammalian target of VapA. This was attempted using two biochemical approaches; i) immunoprecipitation and ii) proximity-dependent biotinylation. Small amounts of myc-tagged VapA were immunoprecipitated but large scale experiments were unsuccessful. This may have also been due to the cytoplasmic expression of VapA or a lack of enough immunoprecipitated protein. The second approach was more successful and some potential VapA-interacting proteins (of endocytic origin) were identified. However, these experiments needed to be repeated and the protein hits validated.

6.6 Conclusions

In summary, the purification protocols presented within this thesis offer an alternative method of lysosome and phagosome purification, which could be used for further studies of phagosome and lysosome function. While the aim was to detect fusion of these organelles *in vitro* this was not seen. However, these protocols provide a basis of future work to achieve this aim. The second aim of the thesis was to investigate the pathogenesis of *R. equi*. This thesis presents the first characterisation of the effect of the *R. equi* virulence protein, VapA, on the mammalian endocytic system. VapA-induced disruption of lysosome function may be a mechanism by which *R. equi* prevents its delivery to the lysosome and survives intracellularly. This work also builds upon our knowledge of the function of the Vap proteins and has identified the region of the protein that is essential for its function.

6.7 Future Perspectives

Further studies could aim to build upon this work in several ways. Firstly, the protocols described in this study could be adapted for different cell types and purposes. For example, this protocol could be used to purify pathogen-containing compartments for use in proteomic studies. Secondly, a working fusion assay would be a powerful tool to study the requirements of phagosome-lysosome fusion. While it is likely that these will be similar to the requirements of late endosome-lysosome fusion, such studies may discover novel proteins that are involved in this process. Should future work be successful in establishing *in vitro* fusion, the assay could be used to study the effect of bacterial effector proteins on phagosome-lysosome fusion. This raises the exciting prospect of using VapA-containing lysosomes to determine if VapA disrupts phagosome-lysosome fusion.

This study demonstrated a key role for VapA in the pathogenesis of *R. equi.* Future studies should also aim to identify the mammalian target of VapA in order to elucidate its function. Key to understanding the function of VapA will be the generation of mutated VapA proteins to uncover key residues that are necessary for its activity. The lysosomal swelling assay described in this thesis could be used for this purpose. This study has shown that despite their similarity in structure the Vap proteins appear to differ in their functions. Thus, structure is not a good indicator as to whether or not any of the remaining Vaps can disrupt lysosome function. Recombinantly producing the remaining Vap proteins and testing them will be key to understanding their functions.

The fact that VapA alone is not sufficient to restore virulence to plasmid-cured strains suggests that *R. equi* may have other virulence factors that are used in conjunction with VapA to disrupt membrane trafficking. It has recently been shown that the presence of the virulence plasmid alters the transcription of 18 % of chromosomal genes, suggesting that *R. equi* may have the ability to grow intracellularly but this requires a large overhaul of its physiology (Coulson et al., 2015). It would be interesting to know if any of these genes themselves are effector proteins that disrupt membrane trafficking. The role of lipids and the bacterial surface chemistry in the pathogenicity of *R. equi* has not been heavily investigated, but it has been shown that the length of mycolic acid changes is

important in preventing delivery of *R. equi* to the lysosome (Sydor et al., 2013). Conversely, an *R. equi* mutant lacking a polysaccharide capsule was not attenuated for virulence in a macrophage cell line or mouse model (Sydor et al., 2008). It remains to be seen if any other lipids or surface molecules produced by *Rhodococcus* are involved in virulence. Finally, it may be interesting to discover the basis behind host tropism between VapA and VapB expressing strains of *R. equi* and determine if any of the untested Vap proteins have a similar effect to VapA.

Appendix 1.0

BirA*-VapA LC MS raw data. Table shows the number of peptide matches and quantified relative abundance (molar %) of identified proteins (calculated by dividing the number of observed peptides by the number of observable peptides). Green boxes indicate proteins unique to the control sample; red boxes indicate proteins unique to BirA*-VapA.

Protein	BirA* Matches	BirA*-VapA Matches	BirA* Molar %	BirA*-VapA Molar %	BirA*/BirA*-VapA Ratio
P35527-Keratin, type I cytoskeletal 9 OS=Homo sapiens GN=KRT9 PE=1 SV=3	82	73	4.46	2.59	1.72
P04264-Keratin, type II cytoskeletal 1 OS=Homo sapiens GN=KRT1 PE=1 SV=6	70	109	5.46	4.05	1.35
P35908-Keratin, type II cytoskeletal 2 epidermal OS=Homo sapiens GN=KRT2 PE=1 SV=2	69	63	3.19	2.21	1.44
P0CW18-Serine protease 56 OS=Homo sapiens GN=PRSS56 PE=1 SV=1	27		2.18		Bir A Only
P62829-60S ribosomal protein L23 OS=Homo sapiens GN=RPL23 PE=1 SV=1	27	60	17.56	38.28	-2.18
Q14244-Ensconsin OS=Homo sapiens GN=MAP7 PE=1 SV=1	26	12	2.10	0.49	4.31
P13645-Keratin, type I cytoskeletal 10 OS=Homo sapiens GN=KRT10 PE=1 SV=6	21	54	2.48	3.05	-1.23
P37802-Transgelin-2 OS=Homo sapiens GN=TAGLN2 PE=1 SV=3	17		7.97		Bir A Only
P13647-Keratin, type II cytoskeletal 5 OS=Homo sapiens GN=KRT5 PE=1 SV=3	15	24	1.18	1.28	-1.09
P08779-Keratin, type I cytoskeletal 16 OS=Homo sapiens GN=KRT16 PE=1 SV=4	13	12	1.74	1.16	1.50
P02538-Keratin, type II cytoskeletal 6A OS=Homo sapiens GN=KRT6A PE=1 SV=3	12	25	1.24	1.34	-1.08
Q8IVT5-Kinase suppressor of Ras 1 OS=Homo sapiens GN=KSR1 PE=1 SV=2	10	3	0.56	0.13	4.23
Q6P1L8-39S ribosomal protein L14, mitochondrial OS=Homo sapiens GN=MRPL14 PE=1 SV=1	10	11	4.31	3.71	1.16
P04259-Keratin, type II cytoskeletal 6B OS=Homo sapiens GN=KRT6B PE=1 SV=5	10	28	1.03	1.34	-1.30
P02533-Keratin, type I cytoskeletal 14 OS=Homo sapiens GN=KRT14 PE=1 SV=4	9	13	1.24	1.00	1.24
A6NCM1-Putative IQ and AAA domain-containing protein 1-like OS=Homo sapiens GN=IQCA1P1 PE=5 SV=2	8	10	0.00	0.00	2.00

Q9Y618-Nuclear receptor corepressor 2 OS=Homo sapiens GN=NCOR2 PE=1 SV=2	7	2	0.21	0.03	7.01
P15924-Desmoplakin OS=Homo sapiens GN=DSP PE=1 SV=3	6	2	0.15	0.03	5.01
P08729-Keratin, type II cytoskeletal 7 OS=Homo sapiens GN=KRT7 PE=1 SV=5	5	7	0.56	0.28	2.00
Q5TFE4-5'-nucleotidase domain-containing protein 1 OS=Homo sapiens GN=NT5DC1 PE=1 SV=1	5	4	0.18	0.09	2.00
P63173-60S ribosomal protein L38 OS=Homo sapiens GN=RPL38 PE=1 SV=2	5	13	2.83	4.18	-1.48
Q5VTE0-Putative elongation factor 1-alpha-like 3 OS=Homo sapiens GN=EEF1A1P5 PE=5 SV=1	4	2	0.80	0.19	4.16
P60709-Actin, cytoplasmic 1 OS=Homo sapiens GN=ACTB PE=1 SV=1	4	1	0.71	0.10	6.87
Q14247-Src substrate cortactin OS=Homo sapiens GN=CTTN PE=1 SV=2	4		0.47		Bir A Only
P62633-Cellular nucleic acid-binding protein OS=Homo sapiens GN=CNBP PE=1 SV=1	4	3	0.44	0.22	2.00
Q6KB66-Keratin, type II cytoskeletal 80 OS=Homo sapiens GN=KRT80 PE=1 SV=2	4	6	0.35	0.18	2.00
P62263-40S ribosomal protein S14 OS=Homo sapiens GN=RPS14 PE=1 SV=3	4	4	2.07	1.52	1.36
P62899-60S ribosomal protein L31 OS=Homo sapiens GN=RPL31 PE=1 SV=1	4	5	1.45	1.81	-1.25
P04792-Heat shock protein beta-1 OS=Homo sapiens GN=HSPB1 PE=1 SV=2	3	1	0.86	0.21	4.15
Q15365-Poly(rC)-binding protein 1 OS=Homo sapiens GN=PCBP1 PE=1 SV=2	3		0.80		Bir A Only
A6NMY6-Putative annexin A2-like protein OS=Homo sapiens GN=ANXA2P2 PE=5 SV=2	3		0.77		Bir A Only
P08670-Vimentin OS=Homo sapiens GN=VIM PE=1 SV=4	3	1	0.53	0.09	6.01
Q9NQ39-Putative 40S ribosomal protein S10-like OS=Homo sapiens GN=RPS10P5 PE=5 SV=1	3	1	0.47	0.24	2.00
Q15797-Mothers against decapentaplegic homolog 1 OS=Homo sapiens GN=SMAD1 PE=1 SV=1	3	3	0.35	0.18	2.00
Q02413-Desmoglein-1 OS=Homo sapiens GN=DSG1 PE=1 SV=2	3	2	0.24	0.07	3.21
Q7Z2W4-Zinc finger CCCH-type antiviral protein 1 OS=Homo sapiens GN=ZC3HAV1 PE=1 SV=3	3	1	0.18	0.04	4.01
P21333-Filamin-A OS=Homo sapiens GN=FLNA PE=1 SV=4	3		0.09		Bir A Only
O75122-CLIP-associating protein 2 OS=Homo sapiens GN=CLASP2 PE=1 SV=2	3	3	0.06	0.03	2.00
P25685-DnaJ homolog subfamily B member 1 OS=Homo sapiens GN=DNAJB1 PE=1 SV=4	3	3	0.50	0.38	1.31
P62805-Histone H4 OS=Homo sapiens GN=HIST1H4A PE=1 SV=2	2	3	1.95	0.97	2.00
O15235-28S ribosomal protein S12, mitochondrial OS=Homo sapiens GN=MRPS12 PE=1 SV=1	2	1	1.33	0.31	N/A
Q86WX3-Active regulator of SIRT1 OS=Homo sapiens GN=RPS19BP1 PE=1 SV=1	2	1	1.33	0.31	N/A

Q9Y5V0-Zinc finger protein 706 OS=Homo sapiens GN=ZNF706 PE=1 SV=1	2	3	1.12	1.34	-1.19
P62701-40S ribosomal protein S4, X isoform OS=Homo sapiens GN=RPS4X PE=1 SV=2	2	5	0.65	0.52	1.26
O60783-28S ribosomal protein S14, mitochondrial OS=Homo sapiens GN=MRPS14 PE=1 SV=1	2	1	0.62	0.31	N/A
P04406-Glyceraldehyde-3-phosphate dehydrogenase OS=Homo sapiens GN=GAPDH PE=1 SV=3	2		0.53		N/A
P62750-60S ribosomal protein L23a OS=Homo sapiens GN=RPL23A PE=1 SV=1	2	4	0.53	0.57	-1.08
Q14919-Dr1-associated corepressor OS=Homo sapiens GN=DRAP1 PE=1 SV=3	2	1	0.41	0.21	N/A
Q9BY77-Polymerase delta-interacting protein 3 OS=Homo sapiens GN=POLDIP3 PE=1 SV=2	2	4	0.41	0.31	1.34
P13646-Keratin, type I cytoskeletal 13 OS=Homo sapiens GN=KRT13 PE=1 SV=4	2	4	0.38	0.40	-1.04
Q96DF8-Protein DGCR14 OS=Homo sapiens GN=DGCR14 PE=1 SV=1	2	2	0.35	0.18	N/A
Q96HC4-PDZ and LIM domain protein 5 OS=Homo sapiens GN=PDLIM5 PE=1 SV=5	2		0.30		N/A
Q96EK4-THAP domain-containing protein 11 OS=Homo sapiens GN=THAP11 PE=1 SV=2	2	1	0.27	0.13	N/A
P11498-Pyruvate carboxylase, mitochondrial OS=Homo sapiens GN=PC PE=1 SV=2	2		0.15		N/A
P27816-Microtubule-associated protein 4 OS=Homo sapiens GN=MAP4 PE=1 SV=3	2	2	0.15	0.07	N/A
P27448-MAP/microtubule affinity-regulating kinase 3 OS=Homo sapiens GN=MARK3 PE=1 SV=4	2	3	0.12	0.10	1.15
P49790-Nuclear pore complex protein Nup153 OS=Homo sapiens GN=NUP153 PE=1 SV=2	2	4	0.12	0.09	1.34
Q9HCD6-Protein TANC2 OS=Homo sapiens GN=TANC2 PE=1 SV=3	2	1	0.09	0.01	N/A
Q5SW79-Centrosomal protein of 170 kDa OS=Homo sapiens GN=CEP170 PE=1 SV=1	2	3	0.06	0.06	1.00
Q8WWI1-LIM domain only protein 7 OS=Homo sapiens GN=LMO7 PE=1 SV=3	2	1	0.06	0.03	N/A
Q14980-Nuclear mitotic apparatus protein 1 OS=Homo sapiens GN=NUMA1 PE=1 SV=2	2	2	0.03	0.04	N/A
Q5VTU8-ATP synthase subunit epsilon-like protein, mitochondrial OS=Homo sapiens GN=ATP5EP2 PE=3 SV=1	1	2	1.74	2.22	N/A
Q71UM5-40S ribosomal protein S27-like OS=Homo sapiens GN=RPS27L PE=1 SV=3	1		1.00		N/A
Q9GZT3-SRA stem-loop-interacting RNA-binding protein, mitochondrial OS=Homo sapiens GN=SLIRP PE=1 SV=1	1	1	0.77	0.38	N/A
O43920-NADH dehydrogenase [ubiquinone] iron-sulfur protein 5 OS=Homo sapiens GN=NDUFS5 PE=1 SV=3	1	1	0.74	0.37	N/A
P62318-Small nuclear ribonucleoprotein Sm D3 OS=Homo sapiens GN=SNRPD3 PE=1 SV=1	1	2	0.68	0.34	N/A
P62851-40S ribosomal protein S25 OS=Homo sapiens GN=RPS25 PE=1 SV=1	1	2	0.68	0.34	N/A

Q5QNW6-Histone H2B type 2-F OS=Homo sapiens GN=HIST2H2BF PE=1 SV=3	1	2	0.68	0.77	N/A
P37108-Signal recognition particle 14 kDa protein OS=Homo sapiens GN=SRP14 PE=1 SV=2	1		0.65		N/A
P62249-40S ribosomal protein S16 OS=Homo sapiens GN=RPS16 PE=1 SV=2	1	1	0.56	0.28	N/A
P62979-Ubiquitin-40S ribosomal protein S27a OS=Homo sapiens GN=RPS27A PE=1 SV=2	1	2	0.50	0.25	N/A
Q14011-Cold-inducible RNA-binding protein OS=Homo sapiens GN=CIRBP PE=1 SV=1	1		0.50		N/A
P0DI83-Ras-related protein Rab-34, isoform NARR OS=Homo sapiens GN=RAB34 PE=1 SV=1	1	2	0.44	0.47	N/A
P61081-NEDD8-conjugating enzyme Ubc12 OS=Homo sapiens GN=UBE2M PE=1 SV=1	1		0.44		N/A
P46782-40S ribosomal protein S5 OS=Homo sapiens GN=RPS5 PE=1 SV=4	1		0.41		N/A
Q06830-Peroxiredoxin-1 OS=Homo sapiens GN=PRDX1 PE=1 SV=1	1	2	0.41	0.21	N/A
P23284-Peptidyl-prolyl cis-trans isomerase B OS=Homo sapiens GN=PPIB PE=1 SV=2	1		0.38		N/A
P23396-40S ribosomal protein S3 OS=Homo sapiens GN=RPS3 PE=1 SV=2	1		0.35		N/A
Q9BS40-Latexin OS=Homo sapiens GN=LXN PE=1 SV=2	1		0.35		N/A
Q9NSI2-Protein FAM207A OS=Homo sapiens GN=FAM207A PE=1 SV=2	1	2	0.35	0.38	N/A
A6NLX3-Speedy protein E4 OS=Homo sapiens GN=SPDYE4 PE=2 SV=2	1		0.32		N/A
Q99943-1-acyl-sn-glycerol-3-phosphate acyltransferase alpha OS=Homo sapiens GN=AGPAT1 PE=1 SV=2	1	1	0.30	0.15	N/A
P05089-Arginase-1 OS=Homo sapiens GN=ARG1 PE=1 SV=2	1	1	0.27	0.13	N/A
P09486-SPARC OS=Homo sapiens GN=SPARC PE=1 SV=1	1		0.27		N/A
Q8NG68-Tubulin--tyrosine ligase OS=Homo sapiens GN=TTL PE=1 SV=2	1		0.21		N/A
P31930-Cytochrome b-c1 complex subunit 1, mitochondrial OS=Homo sapiens GN=UQCRC1 PE=1 SV=3	1		0.18		N/A
P55010-Eukaryotic translation initiation factor 5 OS=Homo sapiens GN=EIF5 PE=1 SV=2	1		0.18		N/A
Q8ND56-Protein LSM14 homolog A OS=Homo sapiens GN=LSM14A PE=1 SV=3	1		0.18		N/A
Q9BR76-Coronin-1B OS=Homo sapiens GN=CORO1B PE=1 SV=1	1	1	0.18	0.09	N/A
Q9BXS6-Nucleolar and spindle-associated protein 1 OS=Homo sapiens GN=NUSAP1 PE=1 SV=1	1	1	0.18	0.09	N/A
P10809-60 kDa heat shock protein, mitochondrial OS=Homo sapiens GN=HSPD1 PE=1 SV=2	1		0.15		N/A
P29353-SHC-transforming protein 1 OS=Homo sapiens GN=SHC1 PE=1 SV=4	1		0.15		N/A
Q8N1N4-Keratin, type II cytoskeletal 78 OS=Homo sapiens GN=KRT78 PE=2 SV=2	1	1	0.15	0.07	N/A

Q9HCS2-Cytochrome P450 4F12 OS=Homo sapiens GN=CYP4F12 PE=1 SV=2	1		0.15		N/A
Q9NY93-Probable ATP-dependent RNA helicase DDX56 OS=Homo sapiens GN=DDX56 PE=1 SV=1	1		0.15		N/A
Q9UQ13-Leucine-rich repeat protein SHOC-2 OS=Homo sapiens GN=SHOC2 PE=1 SV=2	1	1	0.15	0.07	N/A
O00571-ATP-dependent RNA helicase DDX3X OS=Homo sapiens GN=DDX3X PE=1 SV=3	1	1	0.12	0.06	N/A
P08107-Heat shock 70 kDa protein 1A/1B OS=Homo sapiens GN=HSPA1A PE=1 SV=5	1		0.12		N/A
P08238-Heat shock protein HSP 90-beta OS=Homo sapiens GN=HSP90AB1 PE=1 SV=4	1		0.12		N/A
P14923-Junction plakoglobin OS=Homo sapiens GN=JUP PE=1 SV=3	1	1	0.12	0.06	N/A
Q14684-Ribosomal RNA processing protein 1 homolog B OS=Homo sapiens GN=RRP1B PE=1 SV=3	1		0.12		N/A
Q7Z353-Highly divergent homeobox OS=Homo sapiens GN=HDX PE=1 SV=1	1		0.12		N/A
Q96N16-Janus kinase and microtubule-interacting protein 1 OS=Homo sapiens GN=JAKMIP1 PE=1 SV=1	1		0.12		N/A
Q9NZQ3-NCK-interacting protein with SH3 domain OS=Homo sapiens GN=NCKIPSD PE=1 SV=1	1		0.12		N/A
Q6PJF5-Inactive rhomboid protein 2 OS=Homo sapiens GN=RHBDF2 PE=1 SV=2	1		0.09		N/A
Q7KZI7-Serine/threonine-protein kinase MARK2 OS=Homo sapiens GN=MARK2 PE=1 SV=2	1	3	0.09	0.10	-1.16
Q8IWC1-MAP7 domain-containing protein 3 OS=Homo sapiens GN=MAP7D3 PE=1 SV=2	1	1	0.09	0.04	N/A
Q8N163-Cell cycle and apoptosis regulator protein 2 OS=Homo sapiens GN=CCAR2 PE=1 SV=2	1	3	0.09	0.13	-1.50
Q9H0D6-5'-3' exoribonuclease 2 OS=Homo sapiens GN=XRN2 PE=1 SV=1	1	2	0.09	0.04	N/A
Q9NRA8-Eukaryotic translation initiation factor 4E transporter OS=Homo sapiens GN=EIF4ENIF1 PE=1 SV=2	1	1	0.09	0.04	N/A
Q9Y2X9-Zinc finger protein 281 OS=Homo sapiens GN=ZNF281 PE=1 SV=1	1		0.09		N/A
A2RUR9-Coiled-coil domain-containing protein 144A OS=Homo sapiens GN=CCDC144A PE=1 SV=1	1		0.06		N/A
O75339-Cartilage intermediate layer protein 1 OS=Homo sapiens GN=CILP PE=1 SV=4	1		0.06		N/A
Q14432-cGMP-inhibited 3',5'-cyclic phosphodiesterase A OS=Homo sapiens GN=PDE3A PE=1 SV=3	1	1	0.06	0.03	N/A
Q7Z2Y5-Nik-related protein kinase OS=Homo sapiens GN=NRK PE=1 SV=2	1		0.06		N/A
Q86UR5-Regulating synaptic membrane exocytosis protein 1 OS=Homo sapiens GN=RIMS1 PE=1 SV=1	1	1	0.06	0.03	N/A
Q86UU1-Pleckstrin homology-like domain family B member 1 OS=Homo sapiens GN=PHLDB1 PE=1 SV=1	1		0.06		N/A
Q92878-DNA repair protein RAD50 OS=Homo sapiens GN=RAD50 PE=1 SV=1	1		0.06		N/A
Q96EV2-RNA-binding protein 33 OS=Homo sapiens GN=RBM33 PE=1 SV=3	1	1	0.06	0.03	N/A

Q96RT1-Protein LAP2 OS=Homo sapiens GN=ERBB2IP PE=1 SV=2	1	1	0.06	0.03	N/A
Q9H2P0-Activity-dependent neuroprotector homeobox protein OS=Homo sapiens GN=ADNP PE=1 SV=1	1	2	0.06	0.03	N/A
Q9HAU0-Pleckstrin homology domain-containing family A member 5 OS=Homo sapiens GN=PLEKHA5 PE=1 SV=1	1		0.06		N/A
Q9P2J5-Leucine--tRNA ligase, cytoplasmic OS=Homo sapiens GN=LARS PE=1 SV=2	1		0.06		N/A
Q9UPQ0-LIM and calponin homology domains-containing protein 1 OS=Homo sapiens GN=LIMCH1 PE=1 SV=4	1		0.06		N/A
P20930-Filaggrin OS=Homo sapiens GN=FLG PE=1 SV=3	1		0.03		N/A
Q15652-Probable JmjC domain-containing histone demethylation protein 2C OS=Homo sapiens GN=JMJD1C PE=1 SV=2	1		0.03		N/A
Q86YA3-Uncharacterized protein C4orf21 OS=Homo sapiens GN=C4orf21 PE=2 SV=3	1		0.03		N/A
Q86YZ3-Hornerin OS=Homo sapiens GN=HRNR PE=1 SV=2	1	2	0.03	0.03	N/A
Q8IZT6-Abnormal spindle-like microcephaly-associated protein OS=Homo sapiens GN=ASPM PE=1 SV=2	1		0.03		N/A
Q9UPY3-Endoribonuclease Dicer OS=Homo sapiens GN=DICER1 PE=1 SV=3	1		0.03		N/A
P04083-Annexin A1 OS=Homo sapiens GN=ANXA1 PE=1 SV=2		3		0.38	BiravepA Only
P0C0S5-Histone H2A.Z OS=Homo sapiens GN=H2AFZ PE=1 SV=2		4		1.99	BiravepA Only
P19013-Keratin, type II cytoskeletal 4 OS=Homo sapiens GN=KRT4 PE=1 SV=4		10		0.34	BiravepA Only
P42677-40S ribosomal protein S27 OS=Homo sapiens GN=RPS27 PE=1 SV=3		11		4.82	BiravepA Only
P48681-Nestin OS=Homo sapiens GN=NES PE=1 SV=2		4		0.03	BiravepA Only
O75179-Ankyrin repeat domain-containing protein 17 OS=Homo sapiens GN=ANKRD17 PE=1 SV=3		1		0.01	N/A
O75385-Serine/threonine-protein kinase ULK1 OS=Homo sapiens GN=ULK1 PE=1 SV=2		1		0.04	N/A
O95168-NADH dehydrogenase [ubiquinone] 1 beta subcomplex subunit 4 OS=Homo sapiens GN=NDUFB4 PE=1 SV=3		1		0.31	N/A
P07339-Cathepsin D OS=Homo sapiens GN=CTSD PE=1 SV=1		1		0.10	N/A
P09669-Cytochrome c oxidase subunit 6C OS=Homo sapiens GN=COX6C PE=1 SV=2		1		0.56	N/A
P11021-78 kDa glucose-regulated protein OS=Homo sapiens GN=HSPA5 PE=1 SV=2		1		0.06	N/A
P29372-DNA-3-methyladenine glycosylase OS=Homo sapiens GN=MPG PE=1 SV=3		1		0.13	N/A

P39019-40S ribosomal protein S19 OS=Homo sapiens GN=RPS19 PE=1 SV=2		2		0.65	N/A
P41223-Protein BUD31 homolog OS=Homo sapiens GN=BUD31 PE=1 SV=2		1		0.27	N/A
P48634-Protein PRRC2A OS=Homo sapiens GN=PRRC2A PE=1 SV=3		1		0.01	N/A
P50454-Serpin H1 OS=Homo sapiens GN=SERPINH1 PE=1 SV=2		1		0.10	N/A
P55042-GTP-binding protein RAD OS=Homo sapiens GN=RRAD PE=1 SV=2		1		0.13	N/A
P62244-40S ribosomal protein S15a OS=Homo sapiens GN=RPS15A PE=1 SV=2		1		0.31	N/A
P62269-40S ribosomal protein S18 OS=Homo sapiens GN=RPS18 PE=1 SV=3		1		0.27	N/A
P62280-40S ribosomal protein S11 OS=Homo sapiens GN=RPS11 PE=1 SV=3		1		0.25	N/A
P62847-40S ribosomal protein S24 OS=Homo sapiens GN=RPS24 PE=1 SV=1		1		0.31	N/A
P62917-60S ribosomal protein L8 OS=Homo sapiens GN=RPL8 PE=1 SV=2		2		0.34	N/A
P82979-SAP domain-containing ribonucleoprotein OS=Homo sapiens GN=SARNP PE=1 SV=3		1		0.19	N/A
Q12947-Forkhead box protein F2 OS=Homo sapiens GN=FOXF2 PE=1 SV=2		1		0.10	N/A
Q13464-Rho-associated protein kinase 1 OS=Homo sapiens GN=ROCK1 PE=1 SV=1		1		0.03	N/A
Q13573-SNW domain-containing protein 1 OS=Homo sapiens GN=SNW1 PE=1 SV=1		1		0.07	N/A
Q14978-Nucleolar and coiled-body phosphoprotein 1 OS=Homo sapiens GN=NOLC1 PE=1 SV=2		2		0.13	N/A
Q15032-R3H domain-containing protein 1 OS=Homo sapiens GN=R3HDM1 PE=1 SV=3		1		0.04	N/A
Q15054-DNA polymerase delta subunit 3 OS=Homo sapiens GN=POLD3 PE=1 SV=2		1		0.09	N/A
Q15517-Corneodesmosin OS=Homo sapiens GN=CDSN PE=1 SV=3		1		0.09	N/A
Q16527-Cysteine and glycine-rich protein 2 OS=Homo sapiens GN=CSRP2 PE=1 SV=3		1		0.21	N/A
Q5JPF3-Ankyrin repeat domain-containing protein 36C OS=Homo sapiens GN=ANKRD36C PE=2 SV=3		1		0.03	N/A
Q5M775-Cytospin-B OS=Homo sapiens GN=SPECC1 PE=1 SV=1		1		0.04	N/A
Q5VWN6-Protein FAM208B OS=Homo sapiens GN=FAM208B PE=1 SV=1		1		0.01	N/A
Q69YL0-Uncharacterized protein DKFZp762I1415 OS=Homo sapiens PE=4 SV=1		2		0.44	N/A
Q6MZP7-Protein lin-54 homolog OS=Homo sapiens GN=LIN54 PE=1 SV=3		1		0.06	N/A
Q6P0Q8-Microtubule-associated serine/threonine-protein kinase 2 OS=Homo sapiens GN=MAST2 PE=1 SV=2		2		0.04	N/A
Q6PJT7-Zinc finger CCCH domain-containing protein 14 OS=Homo sapiens GN=ZC3H14 PE=1 SV=1		1		0.06	N/A

Q6UUV7-CREB-regulated transcription coactivator 3 OS=Homo sapiens GN=CRTC3 PE=1 SV=2		1		0.07	N/A
Q7RTV0-PHD finger-like domain-containing protein 5A OS=Homo sapiens GN=PHF5A PE=1 SV=1		1		0.37	N/A
Q8IY67-Ribonucleoprotein PTB-binding 1 OS=Homo sapiens GN=RAVER1 PE=1 SV=1		1		0.07	N/A
Q8TAE8-Growth arrest and DNA damage-inducible proteins-interacting protein 1 OS=Homo sapiens GN=GADD45GIP1 PE=1 SV=1		1		0.18	N/A
Q8TEQ8-GPI ethanolamine phosphate transferase 3 OS=Homo sapiens GN=PIGO PE=1 SV=3		1		0.04	N/A
Q96BP2-Coiled-coil-helix-coiled-coil-helix domain-containing protein 1 OS=Homo sapiens GN=CHCHD1 PE=1 SV=1		1		0.35	N/A
Q96DZ1-Endoplasmic reticulum lectin 1 OS=Homo sapiens GN=ERLEC1 PE=1 SV=1		1		0.09	N/A
Q96GD4-Aurora kinase B OS=Homo sapiens GN=AURKB PE=1 SV=3		1		0.12	N/A
Q96NU1-Sterile alpha motif domain-containing protein 11 OS=Homo sapiens GN=SAMD11 PE=2 SV=3		1		0.06	N/A
Q96PK6-RNA-binding protein 14 OS=Homo sapiens GN=RBM14 PE=1 SV=2		1		0.06	N/A
Q99741-Cell division control protein 6 homolog OS=Homo sapiens GN=CDC6 PE=1 SV=1		1		0.07	N/A
Q9BQ48-39S ribosomal protein L34, mitochondrial OS=Homo sapiens GN=MRPL34 PE=1 SV=1		1		0.47	N/A
Q9H496-Torsin-1A-interacting protein 2, isoform IFRG15 OS=Homo sapiens GN=TOR1AIP2 PE=2 SV=1		2		0.29	N/A
Q9NX20-39S ribosomal protein L16, mitochondrial OS=Homo sapiens GN=MRPL16 PE=1 SV=1		1		0.16	N/A
Q9P2N5-RNA-binding protein 27 OS=Homo sapiens GN=RBM27 PE=1 SV=2		1		0.04	N/A
Q9UBV7-Beta-1,4-galactosyltransferase 7 OS=Homo sapiens GN=B4GALT7 PE=1 SV=1		1		0.12	N/A
Q9UBZ4-DNA-(apurinic or apyrimidinic site) lyase 2 OS=Homo sapiens GN=APEX2 PE=1 SV=1		1		0.07	N/A
Q9ULD9-Zinc finger protein 608 OS=Homo sapiens GN=ZNF608 PE=1 SV=4		1		0.03	N/A
Q9ULE3-DENN domain-containing protein 2A OS=Homo sapiens GN=DENND2A PE=2 SV=4		1		0.04	N/A
Q9UNX3-60S ribosomal protein L26-like 1 OS=Homo sapiens GN=RPL26L1 PE=1 SV=1		1		0.28	N/A
Q9Y2D4-Exocyst complex component 6B OS=Homo sapiens GN=EXOC6B PE=1 SV=3		1		0.04	N/A
Q9Y2H8-Zinc finger protein 510 OS=Homo sapiens GN=ZNF510 PE=2 SV=1		1		0.06	N/A
Q9Y2R2-Tyrosine-protein phosphatase non-receptor type 22 OS=Homo sapiens GN=PTPN22 PE=1 SV=2		1		0.04	N/A
Q9Y5Q5-Atrial natriuretic peptide-converting enzyme OS=Homo sapiens GN=CORIN PE=1 SV=2		1		0.04	N/A

Appendix 1.1

VapA-BirA*-His LC MS raw data Table shows the number of peptide matches and quantified relative abundance (molar %) of identified proteins (calculated by dividing the number of observed peptides by the number of observable peptides). Red boxes indicate proteins unique to the control sample; green boxes indicate proteins unique to VapA-BirA*-His.

Protein	BirA* Matches	VapA-BirA* Matches	BirA* Molar %	VapA-BirA* Molar %	BirA*/VapA-BirA* Ratio
Pyruvate carboxylase, mitochondrial OS=Homo sapiens GN=PC PE=1 SV=2 - P11498	84	85	11.24	11.46	1.02
Acetyl-CoA carboxylase 1 OS=Homo sapiens GN=ACACA PE=1 SV=2 - Q13085	74	78	0.87	0.92	1.06
Protein SON OS=Homo sapiens GN=SON PE=1 SV=4 - P18583	53	61	0.63	0.66	1.04
Propionyl-CoA carboxylase alpha chain, mitochondrial OS=Homo sapiens GN=PCCA PE=1 SV=4 - P05165	55	55	11.33	8.85	-1.28
Keratin, type II cytoskeletal 2 epidermal OS=Homo sapiens GN=KRT2 PE=1 SV=2 - P35908	46	46	5.51	5.37	-1.03
Guanine nucleotide-binding protein-like 3 OS=Homo sapiens GN=GNL3 PE=1 SV=2 - Q9BVP2	35	42	4.80	5.82	1.21
Keratin, type II cytoskeletal 1 OS=Homo sapiens GN=KRT1 PE=1 SV=6 - P04264	39	40	5.15	4.31	-1.20
Keratin, type I cytoskeletal 10 OS=Homo sapiens GN=KRT10 PE=1 SV=6 - P13645	36	36	7.71	6.79	-1.14
Keratin, type I cytoskeletal 9 OS=Homo sapiens GN=KRT9 PE=1 SV=3 - P35527	25	27	3.67	3.41	-1.07
Keratin, type II cytoskeletal 5 OS=Homo sapiens GN=KRT5 PE=1 SV=3 - P13647	25	19	1.76	0.95	-1.84
Arginine and glutamate-rich protein 1 OS=Homo sapiens GN=ARGLU1 PE=1 SV=1 - Q9NWB6	20	23	3.85	5.62	1.46
Transcription termination factor 1 OS=Homo sapiens GN=TTF1 PE=1 SV=3 - Q15361	20	22	0.49	0.52	1.07
Methylcrotonoyl-CoA carboxylase subunit alpha, mitochondrial OS=Homo sapiens GN=MCCC1 PE=1 SV=3 - Q96RQ3	20	22	0.84	0.79	-1.07
Keratin, type II cytoskeletal 6C OS=Homo sapiens GN=KRT6C PE=1 SV=3 - P48668	21	17	1.33	0.93	-1.43
Keratin, type II cytoskeletal 6A OS=Homo sapiens GN=KRT6A PE=1 SV=3 - P02538	20		1.24		BirA only

Histone H1.5 OS=Homo sapiens GN=HIST1H1B PE=1 SV=3 - P16401	15	18	7.88	9.18	1.16
E3 ubiquitin-protein ligase RBBP6 OS=Homo sapiens GN=RBBP6 PE=1 SV=1 - Q7Z6E9	11	17	0.12	0.17	1.36
Treacle protein OS=Homo sapiens GN=TCOF1 PE=1 SV=3 - Q13428	12	16	0.17	0.22	1.30
Histone H1.4 OS=Homo sapiens GN=HIST1H1E PE=1 SV=2 - P10412	12	13	4.06	4.85	1.19
60S ribosomal protein L6 OS=Homo sapiens GN=RPL6 PE=1 SV=3 - Q02878	7	12	0.79	1.23	1.57
Histone H1.2 OS=Homo sapiens GN=HIST1H1C PE=1 SV=2 - P16403	11	12	3.67	4.43	1.21
Round spermatid basic protein 1-like protein OS=Homo sapiens GN=RSBN1L PE=1 SV=2 - Q6PCB5	10	12	0.29	0.25	-1.14
Hornerin OS=Homo sapiens GN=HRNR PE=1 SV=2 - Q86YZ3	11	11	0.11	0.09	-1.21
Keratin, type II cytoskeletal 79 OS=Homo sapiens GN=KRT79 PE=1 SV=2 - Q5XKE5	11	9	0.48	0.32	-1.48
Heterogeneous nuclear ribonucleoprotein U OS=Homo sapiens GN=HNRNPU PE=1 SV=6 - Q00839	3	10	0.06	0.21	3.43
Keratin, type I cytoskeletal 14 OS=Homo sapiens GN=KRT14 PE=1 SV=4 - P02533	9	10	0.55	0.61	1.11
Ribosomal RNA processing protein 1 homolog B OS=Homo sapiens GN=RRP1B PE=1 SV=3 - Q14684	10	9	0.27	0.21	-1.29
Chromodomain-helicase-DNA-binding protein 4 OS=Homo sapiens GN=CHD4 PE=1 SV=2 - Q14839	10	8	0.09	0.07	-1.42
Multiple myeloma tumor-associated protein 2 OS=Homo sapiens GN=MMTAG2 PE=1 SV=1 - Q9BU76	10	8	1.25	0.80	-1.55
Nuclease-sensitive element-binding protein 1 OS=Homo sapiens GN=YBX1 PE=1 SV=3 - P67809	10	5	0.81	0.28	-2.84
Cell growth-regulating nucleolar protein OS=Homo sapiens GN=LYAR PE=1 SV=2 - Q9NX58	9	8	0.60	0.46	-1.31
Keratin, type II cytoskeletal 1b OS=Homo sapiens GN=KRT77 PE=2 SV=3 - Q7Z794	6	8	0.25	0.30	1.21
Lysine-rich nucleolar protein 1 OS=Homo sapiens GN=KNOP1 PE=1 SV=1 - Q1ED39	7	8	0.31	0.32	1.04
Acetyl-CoA carboxylase 2 OS=Homo sapiens GN=ACACB PE=1 SV=3 - O00763	8	7	0.06	0.05	-1.02
Keratin, type I cytoskeletal 16 OS=Homo sapiens GN=KRT16 PE=1 SV=4 - P08779	8	8	0.49	0.43	-1.14
Keratin, type II cytoskeletal 7 OS=Homo sapiens GN=KRT7 PE=1 SV=5 - P08729		7		0.28	VapA only
Vimentin OS=Homo sapiens GN=VIM PE=1 SV=4 - P08670	5	7	0.20	0.26	1.32
Actin, cytoplasmic 1 OS=Homo sapiens GN=ACTB PE=1 SV=1 - P60709	6	7	0.33	0.42	1.28
40S ribosomal protein S8 OS=Homo sapiens GN=RPS8 PE=1 SV=2 - P62241	3	6	0.27	0.73	2.66
Probable ATP-dependent RNA helicase DDX46 OS=Homo sapiens GN=DDX46 PE=1 SV=2 - Q7L014	4	6	0.07	0.09	1.36
DNA topoisomerase 1 OS=Homo sapiens GN=TOP1 PE=1 SV=2 - P11387	6	5	0.14	0.10	-1.39

Serine/threonine-protein kinase PRP4 homolog OS=Homo sapiens GN=PRPF4B PE=1 SV=3 - Q13523	6	4	0.11	0.06	-1.76
Keratin, type I cytoskeletal 13 OS=Homo sapiens GN=KRT13 PE=1 SV=4 - P13646	5		0.38		BirA only
60S ribosomal protein L23a OS=Homo sapiens GN=RPL23A PE=1 SV=1 - P62750	3	5	0.40	0.70	1.77
Tubulin alpha-1C chain OS=Homo sapiens GN=TUBA1C PE=1 SV=1 - Q9BQE3	3	5	0.12	0.19	1.54
Ribosomal L1 domain-containing protein 1 OS=Homo sapiens GN=RSL1D1 PE=1 SV=3 - O76021	3	5	0.11	0.17	1.52
Ubiquitin carboxyl-terminal hydrolase 42 OS=Homo sapiens GN=USP42 PE=1 SV=3 - Q9H9J4	4	5	0.06	0.06	1.08
AP-3 complex subunit delta-1 OS=Homo sapiens GN=AP3D1 PE=1 SV=1 - O14617	5	5	0.07	0.07	-1.14
Probable rRNA-processing protein EBP2 OS=Homo sapiens GN=EBNA1BP2 PE=1 SV=2 - Q99848	5	3	0.33	0.16	-2.08
Nucleolar protein 56 OS=Homo sapiens GN=NOP56 PE=1 SV=4 - O00567	5	2	0.19	0.05	-3.52
Heat shock protein HSP 90-beta OS=Homo sapiens GN=HSP90AB1 PE=1 SV=4 - P08238		4		0.09	VapA only
Putative elongation factor 1-alpha-like 3 OS=Homo sapiens GN=EEF1A1P5 PE=5 SV=1 - Q5VTE0		4		0.15	VapA only
40S ribosomal protein S6 OS=Homo sapiens GN=RPS6 PE=1 SV=1 - P62753	1	4	0.07	0.28	4.08
Alpha-enolase OS=Homo sapiens GN=ENO1 PE=1 SV=2 - P06733	2	4	0.08	0.16	1.96
Pyruvate kinase PKM OS=Homo sapiens GN=PKM PE=1 SV=4 - P14618	2	4	0.07	0.13	1.84
Carbamoyl-phosphate synthase [ammonia], mitochondrial OS=Homo sapiens GN=CPS1 PE=1 SV=2 - P31327	2	4	0.02	0.04	1.76
40S ribosomal protein S30 OS=Homo sapiens GN=FAU PE=1 SV=1 - P62861	3	4	1.52	2.29	1.51
Elongation factor 1-alpha 2 OS=Homo sapiens GN=EEF1A2 PE=1 SV=1 - Q05639	3	4	0.12	0.15	1.25
Nucleolar RNA helicase 2 OS=Homo sapiens GN=DDX21 PE=1 SV=5 - Q9NR30	3	4	0.07	0.08	1.20
Peptidyl-prolyl cis-trans isomerase G OS=Homo sapiens GN=PPIG PE=1 SV=2 - Q13427	3	4	0.07	0.08	1.20
A-kinase anchor protein 17A OS=Homo sapiens GN=AKAP17A PE=1 SV=2 - Q02040	3	4	0.07	0.09	1.17
Glyceraldehyde-3-phosphate dehydrogenase OS=Homo sapiens GN=GAPDH PE=1 SV=3 - P04406	4	4	0.24	0.21	-1.14
Heat shock cognate 71 kDa protein OS=Homo sapiens GN=HSPA8 PE=1 SV=1 - P11142	4	4	0.12	0.10	-1.14
Chromodomain-helicase-DNA-binding protein 3 OS=Homo sapiens GN=CHD3 PE=1 SV=3 - Q12873	4	4	0.03	0.03	-1.14
Serine/arginine repetitive matrix protein 2 OS=Homo sapiens GN=SRRM2 PE=1 SV=2 - Q9UQ35	4	3	0.02	0.02	-1.52
Nucleolar protein of 40 kDa OS=Homo sapiens GN=ZCCHC17 PE=1 SV=1 - Q9NP64	4	3	0.33	0.21	-1.58
ADP-ribosylation factor-like protein 6-interacting protein 4 OS=Homo sapiens GN=ARL6IP4 PE=1 SV=1 - Q66PJ3	4	2	0.22	0.09	-2.41

G patch domain-containing protein 4 OS=Homo sapiens GN=GPATCH4 PE=1 SV=2 - Q5T3I0	4	1	0.17	0.03	-5.11
Desmoplakin OS=Homo sapiens GN=DSP PE=1 SV=3 - P15924	4	1	0.03	0.01	-5.68
L-lactate dehydrogenase A chain OS=Homo sapiens GN=LDHA PE=1 SV=2 - P00338		3		0.15	VapA only
Probable ATP-dependent RNA helicase DDX5 OS=Homo sapiens GN=DDX5 PE=1 SV=1 - P17844		3		0.08	VapA only
Tubulin beta-2B chain OS=Homo sapiens GN=TUBB2B PE=1 SV=1 - Q9BVA1		3		0.11	VapA only
Elongation factor 1-alpha 1 OS=Homo sapiens GN=EEF1A1 PE=1 SV=1 - P68104	3		0.12		BirA only
Keratin, type II cytoskeletal 78 OS=Homo sapiens GN=KRT78 PE=2 SV=2 - Q8N1N4	3		0.11		BirA only
Ubiquitin carboxyl-terminal hydrolase 36 OS=Homo sapiens GN=USP36 PE=1 SV=3 - Q9P275	1	3	0.01	0.04	3.52
Filaggrin-2 OS=Homo sapiens GN=FLG2 PE=1 SV=1 - Q5D862	2	3	0.01	0.02	1.76
Histone H4 OS=Homo sapiens GN=HIST1H4A PE=1 SV=2 - P62805	2	3	0.41	0.62	1.51
Hemoglobin subunit alpha OS=Homo sapiens GN=HBA1 PE=1 SV=2 - P69905	2	3	0.29	0.42	1.47
Histone H2B type 2-F OS=Homo sapiens GN=HIST2H2BF PE=1 SV=3 - Q5QNW6	2	3	0.32	0.47	1.47
40S ribosomal protein S23 OS=Homo sapiens GN=RPS23 PE=1 SV=3 - P62266	2	3	0.27	0.40	1.46
Heterogeneous nuclear ribonucleoproteins C1/C2 OS=Homo sapiens GN=HNRNPC PE=1 SV=4 - P07910	2	3	0.12	0.16	1.39
Heat shock 70 kDa protein 1A/1B OS=Homo sapiens GN=HSPA1A PE=1 SV=5 - P08107	2	3	0.06	0.08	1.37
Transcription initiation factor TFIID subunit 3 OS=Homo sapiens GN=TAF3 PE=1 SV=1 - Q5VWG9	2	3	0.04	0.05	1.32
Serine/arginine-rich splicing factor 11 OS=Homo sapiens GN=SRSF11 PE=1 SV=1 - Q05519	3	3	0.11	0.10	-1.14
Heat shock protein HSP 90-alpha OS=Homo sapiens GN=HSP90AA1 PE=1 SV=5 - P07900	3	3	0.07	0.06	-1.14
Splicing factor, arginine/serine-rich 19 OS=Homo sapiens GN=SCAF1 PE=1 SV=3 - Q9H7N4	3	3	0.04	0.04	-1.14
60S ribosomal protein L29 OS=Homo sapiens GN=RPL29 PE=1 SV=2 - P47914	3	3	0.58	0.35	-1.65
Serum albumin OS=Homo sapiens GN=ALB PE=1 SV=2 - P02768	3	2	0.09	0.05	-1.77
40S ribosomal protein S2 OS=Homo sapiens GN=RPS2 PE=1 SV=2 - P15880	3	2	0.20	0.11	-1.79
Elongation factor 2 OS=Homo sapiens GN=EEF2 PE=1 SV=4 - P13639	3	2	0.06	0.03	-1.89
Dermcidin OS=Homo sapiens GN=DCD PE=1 SV=2 - P81605	3	2	0.69	0.35	-1.96
60S ribosomal protein L13 OS=Homo sapiens GN=RPL13 PE=1 SV=4 - P26373		2		0.15	VapA only
60S ribosomal protein L7a OS=Homo sapiens GN=RPL7A PE=1 SV=2 - P62424		2		0.12	VapA only

A-kinase anchor protein 9 OS=Homo sapiens GN=AKAP9 PE=1 SV=3 - Q99996		2		0.01	VapA only
Dolichyl-diphosphooligosaccharide--protein glycosyltransferase subunit 1 OS=Homo sapiens GN=RPN1 PE=1 SV=1 - P04843		2		0.05	VapA only
Filamin-A OS=Homo sapiens GN=FLNA PE=1 SV=4 - P21333		2		0.01	VapA only
Golgin subfamily B member 1 OS=Homo sapiens GN=GOLGB1 PE=1 SV=2 - Q14789		2		0.01	VapA only
Histone-lysine N-methyltransferase NSD2 OS=Homo sapiens GN=WHSC1 PE=1 SV=1 - O96028		2		0.02	VapA only
Peptidyl-prolyl cis-trans isomerase A OS=Homo sapiens GN=PPIA PE=1 SV=2 - P62937		2		0.21	VapA only
Titin OS=Homo sapiens GN=TTN PE=1 SV=4 - Q8WZ42	2	1	0.00	0.00	VapA only
Tubulin beta chain OS=Homo sapiens GN=TUBB PE=1 SV=2 - P07437	2		0.08		BirA only
Tubulin beta-4A chain OS=Homo sapiens GN=TUBB4A PE=1 SV=2 - P04350	2		0.08		BirA only
Nuclear mitotic apparatus protein 1 OS=Homo sapiens GN=NUMA1 PE=1 SV=2 - Q14980	1	2	0.01	0.02	2.64
ATP-dependent RNA helicase DDX3X OS=Homo sapiens GN=DDX3X PE=1 SV=3 - O00571	1	2	0.02	0.05	1.98
Macrophage migration inhibitory factor OS=Homo sapiens GN=MIF PE=1 SV=4 - P14174	1	2	0.16	0.32	1.96
60S ribosomal protein L4 OS=Homo sapiens GN=RPL4 PE=1 SV=5 - P36578	1	2	0.04	0.07	1.91
60S ribosomal protein L5 OS=Homo sapiens GN=RPL5 PE=1 SV=3 - P46777	1	2	0.06	0.10	1.86
Triosephosphate isomerase OS=Homo sapiens GN=TPI1 PE=1 SV=3 - P60174	1	2	0.06	0.11	1.85
Eukaryotic translation initiation factor 5B OS=Homo sapiens GN=EIF5B PE=1 SV=4 - O60841	1	2	0.01	0.02	1.76
Nucleophosmin OS=Homo sapiens GN=NPM1 PE=1 SV=2 - P06748	1	2	0.06	0.11	1.76
60S ribosomal protein L36a-like OS=Homo sapiens GN=RPL36AL PE=1 SV=3 - Q969Q0	2	2	0.35	0.31	-1.14
ATP-binding cassette sub-family F member 1 OS=Homo sapiens GN=ABCF1 PE=1 SV=2 - Q8NE71	2	2	0.04	0.03	-1.14
Core histone macro-H2A.1 OS=Homo sapiens GN=H2AFY PE=1 SV=4 - O75367	2	2	0.10	0.09	-1.14
Filaggrin OS=Homo sapiens GN=FLG PE=1 SV=3 - P20930	1	2	0.01	0.01	-1.14
Heterogeneous nuclear ribonucleoprotein A1 OS=Homo sapiens GN=HNRNPA1 PE=1 SV=5 - P09651	2	2	0.11	0.09	-1.14
Heterogeneous nuclear ribonucleoprotein Q OS=Homo sapiens GN=SYNCRIP PE=1 SV=2 - O60506	2	2	0.06	0.05	-1.14
Histone H2A type 1 OS=Homo sapiens GN=HIST1H2AG PE=1 SV=2 - P0C0S8	2	2	0.32	0.28	-1.14
HMG box transcription factor BBX OS=Homo sapiens GN=BBX PE=1 SV=1 - Q8WY36	2	2	0.04	0.03	-1.14

Nucleolin OS=Homo sapiens GN=NCL PE=1 SV=3 - P19338	2	2	0.05	0.04	-1.14
Parathymosin OS=Homo sapiens GN=PTMS PE=1 SV=2 - P20962	2	2	0.40	0.35	-1.14
Sp110 nuclear body protein OS=Homo sapiens GN=SP110 PE=1 SV=5 - Q9HB58	2	2	0.05	0.04	-1.14
Argininosuccinate synthase OS=Homo sapiens GN=ASS1 PE=1 SV=2 - P00966	2	2	0.09	0.08	-1.14
Desmoglein-1 OS=Homo sapiens GN=DSG1 PE=1 SV=2 - Q02413	2	2	0.03	0.03	-1.14
Eukaryotic initiation factor 4A-I OS=Homo sapiens GN=EIF4A1 PE=1 SV=1 - P60842	2	2	0.09	0.08	-1.14
Protein SREK1IP1 OS=Homo sapiens GN=SREK1IP1 PE=1 SV=1 - Q8N9Q2	2	2	0.23	0.20	-1.14
RNA-binding protein 39 OS=Homo sapiens GN=RBM39 PE=1 SV=2 - Q14498	2	2	0.07	0.06	-1.14
U2 snRNP-associated SURP motif-containing protein OS=Homo sapiens GN=U2SURP PE=1 SV=2 - O15042	2	2	0.03	0.03	-1.14
Antigen KI-67 OS=Homo sapiens GN=MKI67 PE=1 SV=2 - P46013	2	1	0.01	0.01	-2.27
Pre-mRNA-processing factor 40 homolog A OS=Homo sapiens GN=PRPF40A PE=1 SV=2 - O75400	2	1	0.04	0.02	-2.27
pre-rRNA processing protein FTSJ3 OS=Homo sapiens GN=FTSJ3 PE=1 SV=2 - Q8IY81	2	1	0.04	0.02	-2.27
NF-kappa-B-activating protein OS=Homo sapiens GN=NKAP PE=1 SV=1 - Q8N5F7	2	1	0.09	0.04	-2.27
Propionyl-CoA carboxylase beta chain, mitochondrial OS=Homo sapiens GN=PCCB PE=1 SV=3 - P05166	2	1	0.07	0.03	-2.50
40S ribosomal protein S16 OS=Homo sapiens GN=RPS16 PE=1 SV=2 - P62249		1		0.10	VapA only
40S ribosomal protein S3a OS=Homo sapiens GN=RPS3A PE=1 SV=2 - P61247		1		0.05	VapA only
40S ribosomal protein S7 OS=Homo sapiens GN=RPS7 PE=1 SV=1 - P62081		1		0.08	VapA only
60 kDa heat shock protein, mitochondrial OS=Homo sapiens GN=HSPD1 PE=1 SV=2 - P10809		1		0.03	VapA only
60S ribosomal protein L15 OS=Homo sapiens GN=RPL15 PE=1 SV=2 - P61313		1		0.07	VapA only
60S ribosomal protein L35a OS=Homo sapiens GN=RPL35A PE=1 SV=2 - P18077		1		0.14	VapA only
78 kDa glucose-regulated protein OS=Homo sapiens GN=HSPA5 PE=1 SV=2 - P11021		1		0.02	VapA only
ADP/ATP translocase 4 OS=Homo sapiens GN=SLC25A31 PE=2 SV=1 - Q9H0C2		1		0.05	VapA only
AP-4 complex subunit epsilon-1 OS=Homo sapiens GN=AP4E1 PE=1 SV=2 - Q9UPM8		1		0.01	VapA only
AP-5 complex subunit zeta-1 OS=Homo sapiens GN=AP5Z1 PE=1 SV=2 - O43299		1		0.04	VapA only
Arginase-1 OS=Homo sapiens GN=ARG1 PE=1 SV=2 - P05089		1		0.05	VapA only
ATP synthase subunit beta, mitochondrial OS=Homo sapiens GN=ATP5B PE=1 SV=3 - P06576		1		0.03	VapA only

ATPase family AAA domain-containing protein 3B OS=Homo sapiens GN=ATAD3B PE=1 SV=1 - Q5T9A4		1		0.02	VapA only
ATP-dependent RNA helicase DDX24 OS=Homo sapiens GN=DDX24 PE=1 SV=1 - Q9GZR7		1		0.02	VapA only
Bcl-2-associated transcription factor 1 OS=Homo sapiens GN=BCLAF1 PE=1 SV=2 - Q9NYF8		1		0.02	VapA only
Calcium-binding mitochondrial carrier protein SCaMC-3 OS=Homo sapiens GN=SLC25A23 PE=1 SV=2 - Q9BV35		1		0.03	VapA only
Calcium-independent phospholipase A2-gamma OS=Homo sapiens GN=PNPLA8 PE=1 SV=1 - Q9NP80		1		0.02	VapA only
Cyclin-dependent kinase 11A OS=Homo sapiens GN=CDK11A PE=1 SV=4 - Q9UQ88		1		0.02	VapA only
DNA topoisomerase 2-alpha OS=Homo sapiens GN=TOP2A PE=1 SV=3 - P11388		1		0.01	VapA only
Dynein heavy chain 17, axonemal OS=Homo sapiens GN=DNAH17 PE=1 SV=2 - Q9UFH2		1		0.01	VapA only
E3 ubiquitin-protein ligase ARIH1 OS=Homo sapiens GN=ARIH1 PE=1 SV=2 - Q9Y4X5		1		0.03	VapA only
Echinoderm microtubule-associated protein-like 6 OS=Homo sapiens GN=EML6 PE=2 SV=2 - Q6ZMW3		1		0.01	VapA only
Envoplakin OS=Homo sapiens GN=EVPL PE=1 SV=3 - Q92817		1		0.01	VapA only
Fascin OS=Homo sapiens GN=FSCN1 PE=1 SV=3 - Q16658		1		0.03	VapA only
Heat shock protein beta-1 OS=Homo sapiens GN=HSPB1 PE=1 SV=2 - P04792		1		0.08	VapA only
Histone H1x OS=Homo sapiens GN=H1FX PE=1 SV=1 - Q92522		1		0.08	VapA only
Homeobox protein NOBOX OS=Homo sapiens GN=NOBOX PE=1 SV=4 - O60393		1		0.02	VapA only
HRAS-like suppressor 2 OS=Homo sapiens GN=HRASLS2 PE=1 SV=1 - Q9NWW9		1		0.10	VapA only
Kinesin-like protein KIF22 OS=Homo sapiens GN=KIF22 PE=1 SV=5 - Q14807		1		0.02	VapA only
Mediator of RNA polymerase II transcription subunit 25 OS=Homo sapiens GN=MED25 PE=1 SV=2 - Q71SY5		1		0.02	VapA only
Moesin OS=Homo sapiens GN=MSN PE=1 SV=3 - P26038		1		0.03	VapA only
Nestin OS=Homo sapiens GN=NES PE=1 SV=2 - P48681		1		0.01	VapA only
Neuroblast differentiation-associated protein AHNAK OS=Homo sapiens GN=AHNAK PE=1 SV=2 - Q09666		1		0.00	VapA only
Neuroepithelial cell-transforming gene 1 protein OS=Homo sapiens GN=NET1 PE=1 SV=1 - Q7Z628		1		0.03	VapA only
NHS-like protein 1 OS=Homo sapiens GN=NHSL1 PE=1 SV=2 - Q5SYE7		1		0.01	VapA only
Non-POU domain-containing octamer-binding protein OS=Homo sapiens GN=NONO PE=1 SV=4 - Q15233		1		0.03	VapA only
Nuclear receptor coactivator 3 OS=Homo sapiens GN=NCOA3 PE=1 SV=1 - Q9Y6Q9		1		0.01	VapA only
Olfactory receptor 2V1 OS=Homo sapiens GN=OR2V1 PE=3 SV=2 - Q8NHB1		1		0.05	VapA only

Peroxiredoxin-1 OS=Homo sapiens GN=PRDX1 PE=1 SV=1 - Q06830		1		0.08	VapA only
Plasminogen activator inhibitor 1 RNA-binding protein OS=Homo sapiens GN=SERBP1 PE=1 SV=2 - Q8NC51		1		0.08	VapA only
Pogo transposable element with ZNF domain OS=Homo sapiens GN=POGZ PE=1 SV=2 - Q7Z3K3		1		0.01	VapA only
Poly [ADP-ribose] polymerase 1 OS=Homo sapiens GN=PARP1 PE=1 SV=4 - P09874		1		0.02	VapA only
Polypyrimidine tract-binding protein 1 OS=Homo sapiens GN=PTBP1 PE=1 SV=1 - P26599		1		0.03	VapA only
Potassium channel subfamily K member 4 OS=Homo sapiens GN=KCNK4 PE=1 SV=2 - Q9NYG8		1		0.04	VapA only
Potassium channel subfamily K member 9 OS=Homo sapiens GN=KCNK9 PE=1 SV=1 - Q9NPC2		1		0.04	VapA only
Probable phosphoglycerate mutase 4 OS=Homo sapiens GN=PGAM4 PE=2 SV=1 - Q8N0Y7		1		0.06	VapA only
Protein kinase C theta type OS=Homo sapiens GN=PRKCQ PE=1 SV=3 - Q04759		1		0.02	VapA only
Protein S100-A9 OS=Homo sapiens GN=S100A9 PE=1 SV=1 - P06702		1		0.13	VapA only
Putative charged multivesicular body protein 4B-like protein CHMP4BP1 OS=Homo sapiens GN=CHMP4BP1 PE=5 SV=1 - P59074		1		0.09	VapA only
Putative pre-mRNA-splicing factor ATP-dependent RNA helicase DHX15 OS=Homo sapiens GN=DHX15 PE=1 SV=2 - O43143		1		0.02	VapA only
Putative RNA-binding protein Luc7-like 2 OS=Homo sapiens GN=LUC7L2 PE=1 SV=2 - Q9Y383		1		0.04	VapA only
Putative uncharacterized protein C11orf40 OS=Homo sapiens GN=C11orf40 PE=2 SV=1 - Q8WZ69		1		0.07	VapA only
Rap guanine nucleotide exchange factor-like 1 OS=Homo sapiens GN=RAPGEFL1 PE=1 SV=2 - Q9UHV5		1		0.02	VapA only
Ras-related protein Rab-10 OS=Homo sapiens GN=RAB10 PE=1 SV=1 - P61026		1		0.08	VapA only
Ras-related protein Rab-21 OS=Homo sapiens GN=RAB21 PE=1 SV=3 - Q9UL25		1		0.07	VapA only
Receptor-transporting protein 4 OS=Homo sapiens GN=RTP4 PE=2 SV=3 - Q96DX8		1		0.06	VapA only
Rho guanine nucleotide exchange factor 12 OS=Homo sapiens GN=ARHGEF12 PE=1 SV=1 - Q9NZN5		1		0.01	VapA only
Ribosome biogenesis protein BRX1 homolog OS=Homo sapiens GN=BRIX1 PE=1 SV=2 - Q8TDN6		1		0.04	VapA only
RNA-binding motif protein, X-linked 2 OS=Homo sapiens GN=RBMX2 PE=1 SV=2 - Q9Y388		1		0.04	VapA only
RNA-binding protein 26 OS=Homo sapiens GN=RBM26 PE=1 SV=3 - Q5T8P6		1		0.02	VapA only
Serpin B12 OS=Homo sapiens GN=SERPINB12 PE=1 SV=1 - Q96P63		1		0.04	VapA only
Sodium channel protein type 5 subunit alpha OS=Homo sapiens GN=SCN5A PE=1 SV=2 - Q14524		1		0.01	VapA only
Stromal interaction molecule 2 OS=Homo sapiens GN=STIM2 PE=1 SV=2 - Q9P246		1		0.02	VapA only

Suprabasin OS=Homo sapiens GN=SBSN PE=2 SV=2 - Q6UWP8		1		0.03	VapA only
Sushi, nidogen and EGF-like domain-containing protein 1 OS=Homo sapiens GN=SNED1 PE=2 SV=2 - Q8TER0		1		0.01	VapA only
THO complex subunit 4 OS=Homo sapiens GN=ALYREF PE=1 SV=3 - Q86V81		1		0.07	VapA only
Transketolase OS=Homo sapiens GN=TKT PE=1 SV=3 - P29401		1		0.02	VapA only
Vacuolar protein sorting-associated protein 35 OS=Homo sapiens GN=VPS35 PE=1 SV=2 - Q96QK1		1		0.02	VapA only
Zinc finger CCCH-type with G patch domain-containing protein OS=Homo sapiens GN=ZGPAT PE=1 SV=3 - Q8N5A5		1		0.03	VapA only
Zinc finger protein 483 OS=Homo sapiens GN=ZNF483 PE=1 SV=3 - Q8TF39		1		0.02	VapA only
26S proteasome non-ATPase regulatory subunit 14 OS=Homo sapiens GN=PSMD14 PE=1 SV=1 - O00487	1		0.06		BirA only
40S ribosomal protein S4, X isoform OS=Homo sapiens GN=RPS4X PE=1 SV=2 - P62701	1		0.06		BirA only
60S ribosomal protein L18 OS=Homo sapiens GN=RPL18 PE=1 SV=2 - Q07020	1		0.09		BirA only
60S ribosomal protein L26 OS=Homo sapiens GN=RPL26 PE=1 SV=1 - P61254	1		0.12		BirA only
Annexin A1 OS=Homo sapiens GN=ANXA1 PE=1 SV=2 - P04083	1		0.05		BirA only
APC membrane recruitment protein 1 OS=Homo sapiens GN=AMER1 PE=1 SV=2 - Q5JTC6	1		0.01		BirA only
Apoptosis-inducing factor 3 OS=Homo sapiens GN=AIFM3 PE=1 SV=1 - Q96NN9	1		0.03		BirA only
ATP-dependent RNA helicase DDX25 OS=Homo sapiens GN=DDX25 PE=1 SV=2 - Q9UHL0	1		0.04		BirA only
Basal body-orientation factor 1 OS=Homo sapiens GN=CCDC176 PE=2 SV=3 - Q8ND07	1		0.03		BirA only
Branched-chain-amino-acid aminotransferase, cytosolic OS=Homo sapiens GN=BCAT1 PE=1 SV=3 - P54687	1		0.04		BirA only
Bromodomain adjacent to zinc finger domain protein 2A OS=Homo sapiens GN=BAZ2A PE=1 SV=4 - Q9UIF9	1		0.01		BirA only
Calponin-2 OS=Homo sapiens GN=CNN2 PE=1 SV=4 - Q99439	1		0.06		BirA only
CAP-Gly domain-containing linker protein 2 OS=Homo sapiens GN=CLIP2 PE=1 SV=1 - Q9UDT6	1		0.02		BirA only
Cathepsin D OS=Homo sapiens GN=CTSD PE=1 SV=1 - P07339	1		0.04		BirA only
Collagen alpha-1(XXV) chain OS=Homo sapiens GN=COL25A1 PE=1 SV=2 - Q9BXS0	1		0.03		BirA only
Decapping and exoribonuclease protein OS=Homo sapiens GN=DXO PE=2 SV=2 - O77932	1		0.04		BirA only
Diacylglycerol kinase alpha OS=Homo sapiens GN=DGKA PE=1 SV=3 - P23743	1		0.02		BirA only
DNA polymerase theta OS=Homo sapiens GN=POLQ PE=1 SV=2 - O75417	1		0.01		BirA only

DNA-directed RNA polymerase III subunit RPC4 OS=Homo sapiens GN=POLR3D PE=1 SV=2 - P05423	1		0.04		BirA only
EMILIN-2 OS=Homo sapiens GN=EMILIN2 PE=1 SV=3 - Q9BXX0	1		0.02		BirA only
Ensconsin OS=Homo sapiens GN=MAP7 PE=1 SV=1 - Q14244	1		0.02		BirA only
Eukaryotic translation initiation factor 3 subunit A OS=Homo sapiens GN=EIF3A PE=1 SV=1 - Q14152	1		0.01		BirA only
Fer-1-like protein 6 OS=Homo sapiens GN=FER1L6 PE=2 SV=2 - Q2WGJ9	1		0.01		BirA only
Fez family zinc finger protein 1 OS=Homo sapiens GN=FEZF1 PE=2 SV=1 - A0PJY2	1		0.04		BirA only
GTP-binding nuclear protein Ran OS=Homo sapiens GN=RAN PE=1 SV=3 - P62826	1		0.08		BirA only
Heterogeneous nuclear ribonucleoprotein M OS=Homo sapiens GN=HNRNPM PE=1 SV=3 - P52272	1		0.02		BirA only
Heterogeneous nuclear ribonucleoprotein U-like protein 2 OS=Homo sapiens GN=HNRNPUL2 PE=1 SV=1 - Q1KMD3	1		0.02		BirA only
Heterogeneous nuclear ribonucleoproteins A2/B1 OS=Homo sapiens GN=HNRNPA2B1 PE=1 SV=2 - P22626	1		0.05		BirA only
Histone deacetylase 9 OS=Homo sapiens GN=HDAC9 PE=1 SV=2 - Q9UKV0	1		0.02		BirA only
Junction plakoglobin OS=Homo sapiens GN=JUP PE=1 SV=3 - P14923	1		0.02		BirA only
Kinesin-like protein KIF21A OS=Homo sapiens GN=KIF21A PE=1 SV=2 - Q7Z4S6	1		0.01		BirA only
Luc7-like protein 3 OS=Homo sapiens GN=LUC7L3 PE=1 SV=2 - O95232	1		0.04		BirA only
Lysine-specific demethylase 3A OS=Homo sapiens GN=KDM3A PE=1 SV=4 - Q9Y4C1	1		0.01		BirA only
Lysine-specific demethylase PHF2 OS=Homo sapiens GN=PHF2 PE=1 SV=4 - O75151	1		0.02		BirA only
Monocarboxylate transporter 7 OS=Homo sapiens GN=SLC16A6 PE=1 SV=2 - O15403	1		0.03		BirA only
Mortality factor 4-like protein 1 OS=Homo sapiens GN=MORF4L1 PE=1 SV=2 - Q9UBU8	1		0.04		BirA only
Mucin-19 OS=Homo sapiens GN=MUC19 PE=1 SV=2 - Q7Z5P9	1		0.01		BirA only
Myb-binding protein 1A OS=Homo sapiens GN=MYBBP1A PE=1 SV=2 - Q9BQG0	1		0.01		BirA only
Neurogenic locus notch homolog protein 2 OS=Homo sapiens GN=NOTCH2 PE=1 SV=3 - Q04721	1		0.01		BirA only
Neutral alpha-glucosidase AB OS=Homo sapiens GN=GANAB PE=1 SV=3 - Q14697	1		0.02		BirA only
Nucleolar protein 58 OS=Homo sapiens GN=NOP58 PE=1 SV=1 - Q9Y2X3	1		0.03		BirA only
Oxidoreductase NAD-binding domain-containing protein 1 OS=Homo sapiens GN=OXNAD1 PE=1 SV=1 - Q96HP4	1		0.06		BirA only
Peroxiredoxin-2 OS=Homo sapiens GN=PRDX2 PE=1 SV=5 - P32119	1		0.09		BirA only

Peroxiredoxin-4 OS=Homo sapiens GN=PRDX4 PE=1 SV=1 - Q13162	1		0.06		BirA only
PHD and RING finger domain-containing protein 1 OS=Homo sapiens GN=PHRF1 PE=1 SV=3 - Q9P1Y6	1		0.01		BirA only
Plexin-B2 OS=Homo sapiens GN=PLXNB2 PE=1 SV=3 - O15031	1		0.01		BirA only
Prelamin-A/C OS=Homo sapiens GN=LMNA PE=1 SV=1 - P02545	1		0.02		BirA only
Protein FAM9A OS=Homo sapiens GN=FAM9A PE=1 SV=1 - Q8IZU1	1		0.05		BirA only
Protein Smaug homolog 1 OS=Homo sapiens GN=SAMD4A PE=1 SV=3 - Q9UPU9	1		0.02		BirA only
Protein unc-45 homolog A OS=Homo sapiens GN=UNC45A PE=1 SV=1 - Q9H3U1	1		0.02		BirA only
Putative 60S ribosomal protein L37a-like OS=Homo sapiens GN=RPL37L PE=5 SV=2 - A6NKH3	1		0.19		BirA only
Putative ATP-dependent RNA helicase DHX30 OS=Homo sapiens GN=DHX30 PE=1 SV=1 - Q7L2E3	1		0.01		BirA only
Putative uncharacterized protein encoded by LINC00478 OS=Homo sapiens GN=LINC00478 PE=5 SV=1 - A1L4M7	1		0.17		BirA only
RAD52 motif-containing protein 1 OS=Homo sapiens GN=RDM1 PE=1 SV=1 - Q8NG50	1		0.06		BirA only
Ras GTPase-activating protein 2 OS=Homo sapiens GN=RASA2 PE=1 SV=3 - Q15283	1		0.02		BirA only
RNA-binding protein 34 OS=Homo sapiens GN=RBM34 PE=1 SV=2 - P42696	1		0.04		BirA only
rRNA 2'-O-methyltransferase fibrillarin OS=Homo sapiens GN=FBL PE=1 SV=2 - P22087	1		0.06		BirA only
Serine/threonine-protein kinase ULK1 OS=Homo sapiens GN=ULK1 PE=1 SV=2 - O75385	1		0.02		BirA only
Serine/threonine-protein phosphatase 4 regulatory subunit 4 OS=Homo sapiens GN=PPP4R4 PE=1 SV=1 - Q6NUP7	1		0.02		BirA only
Short transient receptor potential channel 5 OS=Homo sapiens GN=TRPC5 PE=1 SV=1 - Q9UL62	1		0.04		BirA only
Spermatogenesis-associated protein 4 OS=Homo sapiens GN=SPATA4 PE=2 SV=1 - Q8NEY3	1		0.06		BirA only
Spermatogenesis-associated protein 7 OS=Homo sapiens GN=SPATA7 PE=2 SV=3 - Q9P0W8	1		0.03		BirA only
Thioredoxin OS=Homo sapiens GN=TXN PE=1 SV=3 - P10599	1		0.17		BirA only
Thyroid hormone receptor-associated protein 3 OS=Homo sapiens GN=THRAP3 PE=1 SV=2 - Q9Y2W1	1		0.02		BirA only
Transmembrane protein 2 OS=Homo sapiens GN=TMEM2 PE=1 SV=1 - Q9UHN6	1		0.01		BirA only
Tripartite motif-containing protein 77 OS=Homo sapiens GN=TRIM77 PE=2 SV=2 - I1YAP6	1		0.04		BirA only
Tyrosine-protein kinase ABL1 OS=Homo sapiens GN=ABL1 PE=1 SV=4 - P00519	1		0.01		BirA only
Uncharacterized protein CXorf23 OS=Homo sapiens GN=CXorf23 PE=1 SV=1 - A2AJT9	1		0.02		BirA only

Unconventional myosin-Ih OS=Homo sapiens GN=MYO1H PE=2 SV=2 - Q8N1T3	1		0.02		BirA only
Versican core protein OS=Homo sapiens GN=VCAN PE=1 SV=3 - P13611	1		0.01		BirA only
Xaa-Pro aminopeptidase 2 OS=Homo sapiens GN=XPNPEP2 PE=1 SV=3 - O43895	1		0.00		BirA only
Zinc finger protein 232 OS=Homo sapiens GN=ZNF232 PE=2 SV=1 - Q9UNY5	1		0.04		BirA only
U4/U6.U5 tri-snRNP-associated protein 1 OS=Homo sapiens GN=SART1 PE=1 SV=1 - O43290	1	1	0.02	0.04	2.05
Trypsin-1 OS=Homo sapiens GN=PRSS1 PE=1 SV=1 - P07477	1	1	0.07	0.13	1.76
40S ribosomal protein S15a OS=Homo sapiens GN=RPS15A PE=1 SV=2 - P62244	1	1	0.13	0.11	-1.14
60S ribosomal protein L11 OS=Homo sapiens GN=RPL11 PE=1 SV=2 - P62913	1	1	0.09	0.08	-1.14
60S ribosomal protein L19 OS=Homo sapiens GN=RPL19 PE=1 SV=1 - P84098	1	1	0.08	0.07	-1.14
Arginine/serine-rich protein PNISR OS=Homo sapiens GN=PNISR PE=1 SV=2 - Q8TF01	1	1	0.02	0.02	-1.14
ATP-dependent RNA helicase DDX18 OS=Homo sapiens GN=DDX18 PE=1 SV=2 - Q9NVP1	1	1	0.02	0.02	-1.14
Caspase recruitment domain-containing protein 14 OS=Homo sapiens GN=CARD14 PE=1 SV=2 - Q9BXL6	1	1	0.02	0.02	-1.14
Chromodomain-helicase-DNA-binding protein 1 OS=Homo sapiens GN=CHD1 PE=1 SV=2 - O14646	1	1	0.01	0.01	-1.14
Elongation factor 1-gamma OS=Homo sapiens GN=EEF1G PE=1 SV=3 - P26641	1	1	0.04	0.03	-1.14
Fatty acid synthase OS=Homo sapiens GN=FASN PE=1 SV=3 - P49327	1	1	0.01	0.01	-1.14
Fructose-bisphosphate aldolase A OS=Homo sapiens GN=ALDOA PE=1 SV=2 - P04075	1	1	0.05	0.04	-1.14
INO80 complex subunit B OS=Homo sapiens GN=INO80B PE=1 SV=2 - Q9C086	1	1	0.05	0.04	-1.14
Interleukin enhancer-binding factor 3 OS=Homo sapiens GN=ILF3 PE=1 SV=3 - Q12906	1	1	0.02	0.02	-1.14
Lipoprotein lipase OS=Homo sapiens GN=LPL PE=1 SV=1 - P06858	1	1	0.04	0.03	-1.14
Mannosyl-oligosaccharide 1,2-alpha-mannosidase IA OS=Homo sapiens GN=MAN1A1 PE=1 SV=3 - P33908	1	1	0.02	0.02	-1.14
Mitochondrial uncoupling protein 3 OS=Homo sapiens GN=UCP3 PE=1 SV=1 - P55916	1	1	0.06	0.05	-1.14
M-phase inducer phosphatase 3 OS=Homo sapiens GN=CDC25C PE=1 SV=2 - P30307	1	1	0.04	0.03	-1.14
Paladin OS=Homo sapiens GN=PALD1 PE=1 SV=3 - Q9ULE6	1	1	0.02	0.02	-1.14
PHD finger protein 14 OS=Homo sapiens GN=PHF14 PE=1 SV=2 - O94880	1	1	0.02	0.02	-1.14
Polyhomeotic-like protein 2 OS=Homo sapiens GN=PHC2 PE=1 SV=1 - Q8IXK0	1	1	0.02	0.02	-1.14
Protein LLP homolog OS=Homo sapiens GN=LLPH PE=2 SV=1 - Q9BRT6	1	1	0.13	0.11	-1.14

Putative IQ and AAA domain-containing protein 1-like OS=Homo sapiens GN=IQCA1P1 PE=5 SV=2 - A6NCM1	1	1	0.02	0.02	-1.14
Retinitis pigmentosa 9 protein OS=Homo sapiens GN=RP9 PE=1 SV=2 - Q8TA86	1	1	0.07	0.07	-1.14
Serine/Arginine-related protein 53 OS=Homo sapiens GN=RSRC1 PE=1 SV=1 - Q96IZ7	1	1	0.05	0.04	-1.14
StAR-related lipid transfer protein 6 OS=Homo sapiens GN=STARD6 PE=2 SV=1 - P59095	1	1	0.07	0.07	-1.14
Transcription elongation factor SPT6 OS=Homo sapiens GN=SUPT6H PE=1 SV=2 - Q7KZ85	1	1	0.01	0.01	-1.14
Transcriptional adapter 2-beta OS=Homo sapiens GN=TADA2B PE=1 SV=2 - Q86TJ2	1	1	0.04	0.03	-1.14
Ubiquitin-40S ribosomal protein S27a OS=Homo sapiens GN=RPS27A PE=1 SV=2 - P62979	1	1	0.11	0.09	-1.14
Uncharacterized protein C11orf57 OS=Homo sapiens GN=C11orf57 PE=1 SV=2 - Q6ZUT1	1	1	0.06	0.05	-1.14
Voltage-dependent L-type calcium channel subunit alpha-1S OS=Homo sapiens GN=CACNA1S PE=1 SV=4 - Q13698	1	1	0.01	0.01	-1.14
ATP synthase subunit alpha, mitochondrial OS=Homo sapiens GN=ATP5A1 PE=1 SV=1 - P25705	1	1	0.03	0.03	-1.14
Calcium/calmodulin-dependent 3',5'-cyclic nucleotide phosphodiesterase 1A OS=Homo sapiens GN=PDE1A PE=2 SV=2 - P54750	1	1	0.06	0.05	-1.14
Caspase-14 OS=Homo sapiens GN=CASP14 PE=1 SV=2 - P31944	1	1	0.07	0.06	-1.14
Cyclic GMP-AMP synthase OS=Homo sapiens GN=MB21D1 PE=1 SV=2 - Q8N884	1	1	0.03	0.03	-1.14
Heterogeneous nuclear ribonucleoprotein L OS=Homo sapiens GN=HNRNPL PE=1 SV=2 - P14866	1	1	0.03	0.03	-1.14
Keratinocyte proline-rich protein OS=Homo sapiens GN=KPRP PE=1 SV=1 - Q5T749	1	1	0.03	0.03	-1.14
Membrane-spanning 4-domains subfamily A member 10 OS=Homo sapiens GN=MS4A10 PE=2 SV=3 - Q96PG2	1	1	0.06	0.05	-1.14
N(G),N(G)-dimethylarginine dimethylaminohydrolase 1 OS=Homo sapiens GN=DDAH1 PE=1 SV=3 - O94760	1	1	0.06	0.05	-1.14
Pre-mRNA-splicing factor 38B OS=Homo sapiens GN=PRPF38B PE=1 SV=1 - Q5VTL8	1	1	0.03	0.03	-1.14
Proliferation-associated protein 2G4 OS=Homo sapiens GN=PA2G4 PE=1 SV=3 - Q9UQ80	1	1	0.04	0.04	-1.14
Protein RIC-3 OS=Homo sapiens GN=RIC3 PE=1 SV=1 - Q7Z5B4	1	1	0.04	0.04	-1.14
Splicing regulatory glutamine/lysine-rich protein 1 OS=Homo sapiens GN=SREK1 PE=1 SV=1 - Q8WXA9	1	1	0.03	0.03	-1.14
Surfeit locus protein 6 OS=Homo sapiens GN=SURF6 PE=1 SV=3 - O75683	1	1	0.04	0.04	-1.14
Voltage-dependent anion-selective channel protein 2 OS=Homo sapiens GN=VDAC2 PE=1 SV=2 - P45880	1	1	0.06	0.05	-1.14
Zinc finger protein 503 OS=Homo sapiens GN=ZNF503 PE=1 SV=1 - Q96F45	1	1	0.03	0.03	-1.14

List of definitions

ADP	Adenosine diphosphate
ALP	Alkaline phosphatase
ATP	Adenosine triphosphate
BCA	Bicinchoninic acid
β-Hex	β-Hexosaminidase
bp	Base pairs
cdM6PR	cation-dependent mannose 6-phosphate receptor
ciM6PR	cation-independent mannose 6-phosphate receptor
CLEAR	Coordinated lysosomal expression and regulation
CMA	Chaperone-mediated autophagy
co-IP	co-immunoprecipitation
CPY	Carboxypeptidase Y
CPY-Inv	Carboxypeptidase Y- Invertase
DAPI	4',6-diamidino 2-phenylindole
DMSO	Dimethylsulfoxide
DNA	Deoxyribonucleic acid
EDTA	Ethylenediaminetetraacetic acid
EE	Early endosome
EEA1	Early endosome antigen 1

ERC	Endocytic recycling compartment
ESCRT	Endosomal sorting complex required for transport
FCS	Foetal calf serum
GDP	Guanosine diphosphate
GFP	Green fluorescent protein
GTP	Guanosine triphosphate
HeLa	Henrietta Lacks' cancer cell line
HOPS	Homotypic fusion and protein sorting complex
IgG	Immunoglobulin G
ILV	Intraluminal vesicle
kbp	Kilobase pairs
kDa	Kilodaltons
L	Litre
LAMP1	Lysosomal-associated membrane protein 1
LBPA	Lysobisphosphatidic acid
LCV	*Legionella* containing vacuole
LE	Late endosome
LIMP	Lysosome integral membrane protein
LPS	Lipopolysaccharide
LSD	Lysosomal storage disorder

M	Molar
mg	Milligram
mL	Millilitre
mM	Millimolar
mRNA	Messenger ribonucleic acid
MVB	Multivesicular body
ng	Nanomolar
nm	Nanometre
nM	Nanomolar
n.s.	Non-significant
NSF	*N*-ethylmaleimide-sensitive factor
PAMP	Pathogen-associated molecular pattern
PBS	Phosphate buffered saline
PCR	Polymerase Chain Reaction
PEPSY	Pathogen effector protein screening in yeast
PRR	Pattern recognition receptor
PtdIns[3]P	Phosphatidylinositol 3-phosphate
PtdIns[3,5]P_2	Phosphatidylinositol 3,5-bisphosphate
PtdIns[4,5]P_2	Phosphatidylinositol 4,5-bisphosphate
RCV	*Rhodococcus* containing vacuole

RILP	Rab-interacting lysosomal protein
RNA	Ribonucleic acid
RPM	Revolutions per minute
SCV	*Salmonella* containing vacuole
SDS	Sodium dodecyl sulfate
SNARE	Soluble-NSF attachment protein receptor
TES	2-[[1,3-dihydroxy-2-(hydroxymethyl)propan-2-yl]amino]ethanesulfonic acid
TFEB	Transcription factor EB
TGN	*trans* Golgi network
Tris	Trisaminomethane
µg	Microgram
µl	Microlitre
µm	Micrometer
µM	Micromolar
Vap	Virulence associated protein
vATPase	Vacuolar ATPase
VPS	Vacuole protein sorting
W.B.	Western blot

References

ABDALLAH, A. M., GEY VAN PITTIUS, N. C., CHAMPION, P. A., COX, J., LUIRINK, J., VANDENBROUCKE-GRAULS, C. M., APPELMELK, B. J. & BITTER, W. 2007. Type VII secretion--mycobacteria show the way. *Nature reviews. Microbiology,* 5**,** 883-91.

ABOU JAMRA, R., PHILIPPE, O., RAAS-ROTHSCHILD, A., ECK, S. H., GRAF, E., BUCHERT, R., BORCK, G., EKICI, A., BROCKSCHMIDT, F. F., NOTHEN, M. M., MUNNICH, A., STROM, T. M., REIS, A. & COLLEAUX, L. 2011. Adaptor protein complex 4 deficiency causes severe autosomal-recessive intellectual disability, progressive spastic paraplegia, shy character, and short stature. *American journal of human genetics,* 88**,** 788-95.

ABRAHAMS, G. L., MULLER, P. & HENSEL, M. 2006. Functional dissection of SseF, a type III effector protein involved in positioning the salmonella-containing vacuole. *Traffic,* 7**,** 950-65.

ADEKOYA, E., AIT-ZAHRA, M., ALLEN, N., ANDERSON, M., ANDERSON, S., ANUFRIEV, F., AMBRUSTER, J., AYELE, K., BAKER, J., BALDWIN, J., BARNA, N., BASTIEN, V., BATZOGLOU, S., BECKERLY, R., BEDA, F., BERNARD, J., BIRREN, B., BLUMENSTEIL, B., BOGUSLAVSKY, L., BOUKGHALTER, B., BROWN, A., BURKETT, G., CAMARATA, J., CAMPOPIANO, A., CARNEIRO, H., CHEN, Z., CHOEPHAL, Y., COLANGELO, M., COLLINS, S., COLLYMORE, A., COOKE, P., DAVIS, C., DAWOE, T., DEARELLANO, K., DEVON, K., DEWAR, K., DIAZ, J. S., DODGE, S., DONELAN, E., DORJEE, K., DOYLE, M., DUBE, A., DUPES, A., ENDRIZZI, M., FARINA, A., FARO, S., FERGUSON, D., FERRIERA, P., FISCHER, H., FITZHUGH, W., FLAHERTY, K., FOLEY, K., FUNKE, R., GAGE, D., GALAGAN, J., GARDYNA, S., GILBERT, D., GINDE, S., GOMES, A., GOYETTE, M., GRAHAM, J., GRAHAM, L., GRANDBOIS, E., GRAND-PIERRE, N., GRANT, G., GREGOIRE, D., GUERRERO, R., HAGOS, B., HARRIS, K., HART, D., HATCHER, B., HEAFORD, A., HORTON, L., HOSAGE-NORMAN, C., HOWLAND, J., HULME, B., ILIEV, I., JOHNSON, R., JONES, C., JOSEPH, M., JUDD, M., KANN, L., KARATAS, A., KELLEY, D., KELLY, M., LAMA, D., LAMAZARES, J., LANDER, E. S., LANDERS, T., LANE, A., LAROCQUE, K., LEBLANC, H., LEGER, J. P., LEHOCZKY, J., LEVINE, R., LEWIS, D., LEWIS, T., LIEU, C., LINTON, L., LIU, G., et al. 2001. Initial sequencing and analysis of the human genome. *Nature,* 409**,** 860-921.

ADELL, M. A., VOGEL, G. F., PAKDEL, M., MULLER, M., LINDNER, H., HESS, M. W. & TEIS, D. 2014. Coordinated binding of Vps4 to ESCRT-III drives membrane neck constriction during MVB vesicle formation. *The Journal of cell biology,* 205**,** 33-49.

ADEREM, A. & UNDERHILL, D. M. 1999. Mechanisms of phagocytosis in macrophages. *Annual review of immunology,* 17**,** 593-623.

AMBERG, D. C., BURKE, D., STRATHERN, J. N. & COLD SPRING HARBOR LABORATORY. 2005. *Methods in yeast genetics : a Cold Spring Harbor Laboratory course manual,* Cold Spring Harbor, N.Y., Cold Spring Harbor Laboratory Press.

ANAND, R. J., DAI, S., GRIBAR, S. C., RICHARDSON, W., KOHLER, J. W., HOFFMAN, R. A., BRANCA, M. F., LI, J., SHI, X. H., SODHI, C. P. & HACKAM, D. J. 2008. A role for connexin43 in macrophage phagocytosis and host survival after bacterial peritoneal infection. *Journal of immunology,* 181**,** 8534-43.

ARIGHI, C. N., HARTNELL, L. M., AGUILAR, R. C., HAFT, C. R. & BONIFACINO, J. S. 2004. Role of the mammalian retromer in sorting of the cation-independent mannose 6-phosphate receptor. *The Journal of cell biology,* 165**,** 123-33.

ARORA, P. D., MANOLSON, M. F., DOWNEY, G. P., SODEK, J. & MCCULLOCH, C. A. 2000. A novel model system for characterization of phagosomal maturation, acidification, and intracellular collagen degradation in fibroblasts. *The Journal of biological chemistry,* 275**,** 35432-41.

AZMI, I., DAVIES, B., DIMAANO, C., PAYNE, J., ECKERT, D., BABST, M. & KATZMANN, D. J. 2006. Recycling of ESCRTs by the AAA-ATPase Vps4 is regulated by a conserved VSL region in Vta 1. *Journal of Cell Biology,* 172**,** 705-717.

BAARS, T. L., PETRI, S., PETERS, C. & MAYER, A. 2007. Role of the V-ATPase in regulation of the vacuolar fission-fusion equilibrium. *Molecular biology of the cell,* 18**,** 3873-82.

BABBEY, C. M., BACALLAO, R. L. & DUNN, K. W. 2010. Rab10 associates with primary cilia and the exocyst complex in renal epithelial cells. *American journal of physiology. Renal physiology,* 299**,** F495-506.

BABST, M., KATZMANN, D. J., ESTEPA-SABAL, E. J., MEERLOO, T. & EMR, S. D. 2002a. ESCRT-III: An endosome-associated heterooligomeric protein complex required for MVB sorting. *Developmental cell,* 3**,** 271-282.

BABST, M., KATZMANN, D. J., SNYDER, W. B., WENDLAND, B. & EMR, S. D. 2002b. Endosome-associated complex, ESCRT-II, recruits transport machinery for protein sorting at the multivesicular body. *Developmental cell,* 3**,** 283-289.

BACH, H., PAPAVINASASUNDARAM, K. G., WONG, D., HMAMA, Z. & AV-GAY, Y. 2008. Mycobacterium tuberculosis virulence is mediated by PtpA dephosphorylation of human vacuolar protein sorting 33B. *Cell host & microbe,* 3**,** 316-22.

BALCH, W. E. & ROTHMAN, J. E. 1985. Characterization of protein transport between successive compartments of the Golgi apparatus: asymmetric properties of donor and acceptor activities in a cell-free system. *Archives of biochemistry and biophysics,* 240**,** 413-25.

BALCH, W. E., WAGNER, K. R. & KELLER, D. S. 1987. Reconstitution of transport of vesicular stomatitis virus G protein from the endoplasmic reticulum to the Golgi complex using a cell-free system. *The Journal of cell biology,* 104**,** 749-60.

BALDERHAAR, H. J., LACHMANN, J., YAVAVLI, E., BROCKER, C., LURICK, A. & UNGERMANN, C. 2013. The CORVET complex promotes tethering and fusion of Rab5/Vps21-positive membranes. *Proceedings of the National Academy of Sciences of the United States of America,* 110**,** 3823-8.

BALDERHAAR, H. J. & UNGERMANN, C. 2013. CORVET and HOPS tethering complexes - coordinators of endosome and lysosome fusion. *Journal of cell science,* 126**,** 1307-16.

BALLABIO, A. & GIESELMANN, V. 2009. Lysosomal disorders: from storage to cellular damage. *Biochimica et biophysica acta,* 1793**,** 684-96.

BANANIS, E., NATH, S., GORDON, K., SATIR, P., STOCKERT, R. J., MURRAY, J. W. & WOLKOFF, A. W. 2004. Microtubule-dependent movement of late endocytic vesicles in vitro: requirements for Dynein and Kinesin. *Molecular biology of the cell,* 15**,** 3688-97.

BANKAITIS, V. A., JOHNSON, L. M. & EMR, S. D. 1986. Isolation of yeast mutants defective in protein targeting to the vacuole. *Proceedings of the National Academy of Sciences of the United States of America,* 83**,** 9075-9.

BARBOSA, M. D., NGUYEN, Q. A., TCHERNEV, V. T., ASHLEY, J. A., DETTER, J. C., BLAYDES, S. M., BRANDT, S. J., CHOTAI, D., HODGMAN, C., SOLARI, R. C., LOVETT, M. & KINGSMORE, S. F. 1996. Identification of the homologous beige and Chediak-Higashi syndrome genes. *Nature,* 382**,** 262-5.

BARLOWE, C. 1997. Coupled ER to Golgi transport reconstituted with purified cytosolic proteins. *The Journal of cell biology,* 139**,** 1097-108.

BAUCKMAN, K. A., OWUSU-BOAITEY, N. & MYSOREKAR, I. U. 2015. Selective autophagy: xenophagy. *Methods,* 75**,** 120-7.

BEAUFAY, H. 1969. *Methods for the isolation of lysosomes,* Amsterdam, North Holland Publishing Co.

BECICH, M. J. & BAENZIGER, J. U. 1991. Ligand-specific isolation of endosomes and lysosomes using superparamagnetic colloidal iron dextran glycoconjugates and high

gradient magnetic affinity chromatography. *European journal of cell biology,* 55**,** 71-82.
BECKEN, U., JESCHKE, A., VELTMAN, K. & HAAS, A. 2010. Cell-free fusion of bacteria-containing phagosomes with endocytic compartments. *Proceedings of the National Academy of Sciences of the United States of America,* 107**,** 20726-31.
BEGLEY, M. J. & DIXON, J. E. 2005. The structure and regulation of myotubularin phosphatases. *Current opinion in structural biology,* 15**,** 614-20.
BENES, P., VETVICKA, V. & FUSEK, M. 2008. Cathepsin D--many functions of one aspartic protease. *Critical reviews in oncology/hematology,* 68**,** 12-28.
BENOIT, S., BENACHOUR, A., TAOUJI, S., AUFFRAY, Y. & HARTKE, A. 2001. Induction of vap genes encoded by the virulence plasmid of Rhodococcus equi during acid tolerance response. *Research in microbiology,* 152**,** 439-49.
BENOIT, S., BENACHOUR, A., TAOUJI, S., AUFFRAY, Y. & HARTKE, A. 2002. H(2)O(2), which causes macrophage-related stress, triggers induction of expression of virulence-associated plasmid determinants in Rhodococcus equi. *Infection and immunity,* 70**,** 3768-76.
BERDYYEVA, T. K., WOODWORTH, C. D. & SOKOLOV, I. 2005. Human epithelial cells increase their rigidity with ageing in vitro: direct measurements. *Physics in medicine and biology,* 50**,** 81-92.
BERGER, A. C., SALAZAR, G., STYERS, M. L., NEWELL-LITWA, K. A., WERNER, E., MAUE, R. A., CORBETT, A. H. & FAUNDEZ, V. 2007. The subcellular localization of the Niemann-Pick Type C proteins depends on the adaptor complex AP-3. *Journal of cell science,* 120**,** 3640-52.
BERGHAUS, L. J., GIGUERE, S. & GULDBECH, K. 2013. Mutant prevention concentration and mutant selection window for 10 antimicrobial agents against Rhodococcus equi. *Veterinary microbiology,* 166**,** 670-5.
BEWLEY, M. A., MARRIOTT, H. M., TULONE, C., FRANCIS, S. E., MITCHELL, T. J., READ, R. C., CHAIN, B., KROEMER, G., WHYTE, M. K. & DOCKRELL, D. H. 2011. A cardinal role for cathepsin d in co-ordinating the host-mediated apoptosis of macrophages and killing of pneumococci. *PLoS pathogens,* 7**,** e1001262.
BILODEAU, P. S., URBANOWSKI, J. L., WINISTORFER, S. C. & PIPER, R. C. 2002. The Vps27p-Hse1p complex binds ubiquitin and mediates endosomal protein sorting. *Nature Cell Biology,* 4**,** 534-539.
BIRNBOIM, H. C. & DOLY, J. 1979. A rapid alkaline extraction procedure for screening recombinant plasmid DNA. *Nucleic acids research,* 7**,** 1513-23.
BLOCKER, A., GRIFFITHS, G., OLIVO, J. C., HYMAN, A. A. & SEVERIN, F. F. 1998. A role for microtubule dynamics in phagosome movement. *Journal of cell science,* 111 (Pt 3)**,** 303-12.
BLOCKER, A., SEVERIN, F. F., BURKHARDT, J. K., BINGHAM, J. B., YU, H., OLIVO, J. C., SCHROER, T. A., HYMAN, A. A. & GRIFFITHS, G. 1997. Molecular requirements for bi-directional movement of phagosomes along microtubules. *The Journal of cell biology,* 137**,** 113-29.
BLOCKER, A., SEVERIN, F. F., HABERMANN, A., HYMAN, A. A., GRIFFITHS, G. & BURKHARDT, J. K. 1996. Microtubule-associated protein-dependent binding of phagosomes to microtubules. *The Journal of biological chemistry,* 271**,** 3803-11.
BOEKE, J. D., LACROUTE, F. & FINK, G. R. 1984. A Positive Selection for Mutants Lacking Orotidine-5'-Phosphate Decarboxylase Activity in Yeast - 5-Fluoro-Orotic Acid Resistance. *Molecular & General Genetics,* 197**,** 345-346.
BONIFACINO, J. S. & HURLEY, J. H. 2008. Retromer. *Current opinion in cell biology,* 20**,** 427-36.
BOTSTEIN, D. & FINK, G. R. 2011. Yeast: an experimental organism for 21st Century biology. *Genetics,* 189**,** 695-704.

BOUVIER, G., BENOLIEL, A. M., FOA, C. & BONGRAND, P. 1994. Relationship between phagosome acidification, phagosome-lysosome fusion, and mechanism of particle ingestion. *Journal of leukocyte biology,* 55**,** 729-34.
BOYA, P., REGGIORI, F. & CODOGNO, P. 2013. Emerging regulation and functions of autophagy. *Nature Cell Biology,* 15**,** 713-20.
BRAULKE, T. & BONIFACINO, J. S. 2009. Sorting of lysosomal proteins. *Biochimica Et Biophysica Acta-Molecular Cell Research,* 1793**,** 605-614.
BRENNAN, P. J. & NIKAIDO, H. 1995. The envelope of mycobacteria. *Annual review of biochemistry,* 64**,** 29-63.
BRIGHT, N. A., REAVES, B. J., MULLOCK, B. M. & LUZIO, J. P. 1997. Dense core lysosomes can fuse with late endosomes and are re-formed from the resultant hybrid organelles. *Journal of cell science,* 110 (Pt 17)**,** 2027-40.
BROCCHIERI, L. & KARLIN, S. 2005. Protein length in eukaryotic and prokaryotic proteomes. *Nucleic acids research,* 33**,** 3390-400.
BROCKER, C., KUHLEE, A., GATSOGIANNIS, C., BALDERHAAR, H. J., HONSCHER, C., ENGELBRECHT-VANDRE, S., UNGERMANN, C. & RAUNSER, S. 2012. Molecular architecture of the multisubunit homotypic fusion and vacuole protein sorting (HOPS) tethering complex. *Proceedings of the National Academy of Sciences of the United States of America,* 109**,** 1991-6.
BRYANT, N. J. & STEVENS, T. H. 1998. Vacuole biogenesis in Saccharomyces cerevisiae: Protein transport pathways to the yeast vacuole. *Microbiology and Molecular Biology Reviews,* 62**,** 230-+.
BUCCI, C., THOMSEN, P., NICOZIANI, P., MCCARTHY, J. & VAN DEURS, B. 2000. Rab7: a key to lysosome biogenesis. *Molecular biology of the cell,* 11**,** 467-80.
BULINA, M. E., CHUDAKOV, D. M., BRITANOVA, O. V., YANUSHEVICH, Y. G., STAROVEROV, D. B., CHEPURNYKH, T. V., MERZLYAK, E. M., SHKROB, M. A., LUKYANOV, S. & LUKYANOV, K. A. 2006. A genetically encoded photosensitizer. *Nature biotechnology,* 24**,** 95-9.
BULLOUGH, P. A., HUGHSON, F. M., SKEHEL, J. J. & WILEY, D. C. 1994. Structure of influenza haemagglutinin at the pH of membrane fusion. *Nature,* 371**,** 37-43.
BURKHARDT, J. K., ECHEVERRI, C. J., NILSSON, T. & VALLEE, R. B. 1997. Overexpression of the dynamitin (p50) subunit of the dynactin complex disrupts dynein-dependent maintenance of membrane organelle distribution. *The Journal of cell biology,* 139**,** 469-84.
BUSCHOW, S. I., LASONDER, E., SZKLARCZYK, R., OUD, M. M., DE VRIES, I. J. & FIGDOR, C. G. 2012. Unraveling the human dendritic cell phagosome proteome by organellar enrichment ranking. *Journal of proteomics,* 75**,** 1547-62.
BYRNE, B. A., PRESCOTT, J. F., PALMER, G. H., TAKAI, S., NICHOLSON, V. M., ALPERIN, D. C. & HINES, S. A. 2001. Virulence plasmid of Rhodococcus equi contains inducible gene family encoding secreted proteins. *Infection and immunity,* 69**,** 650-6.
BYRNE, G. A., RUSSELL, D. A., CHEN, X. & MEIJER, W. G. 2007. Transcriptional regulation of the virR operon of the intracellular pathogen Rhodococcus equi. *Journal of bacteriology,* 189**,** 5082-9.
CALLAGHAN, J., NIXON, S., BUCCI, C., TOH, B. H. & STENMARK, H. 1999a. Direct interaction of EEA1 with Rab5b. *European journal of biochemistry / FEBS,* 265**,** 361-6.
CALLAGHAN, J., SIMONSEN, A., GAULLIER, J. M., TOH, B. H. & STENMARK, H. 1999b. The endosome fusion regulator early-endosomal autoantigen 1 (EEA1) is a dimer. *The Biochemical journal,* 338 (Pt 2)**,** 539-43.
CANTALUPO, G., ALIFANO, P., ROBERTI, V., BRUNI, C. B. & BUCCI, C. 2001. Rab-interacting lysosomal protein (RILP): the Rab7 effector required for transport to lysosomes. *The EMBO journal,* 20**,** 683-93.

CAPLAN, S., HARTNELL, L. M., AGUILAR, R. C., NASLAVSKY, N. & BONIFACINO, J. S. 2001a. Human Vam6p promotes lysosome clustering and fusion in vivo. *Journal of Cell Biology,* 154**,** 109-121.
CAPLAN, S., HARTNELL, L. M., NASLAVSKY, N., PATTERSON, G. H., LODGE, R. & BONIFACINO, J. S. 2001b. Molecular cloning and characterization of human Vam6p/Vps39p: a novel protein involved in lysosome biogenesis. *Faseb Journal,* 15**,** A1175-A1175.
CARDOSO, C. M., GROTH-PEDERSEN, L., HOYER-HANSEN, M., KIRKEGAARD, T., CORCELLE, E., ANDERSEN, J. S., JAATTELA, M. & NYLANDSTED, J. 2009. Depletion of kinesin 5B affects lysosomal distribution and stability and induces peri-nuclear accumulation of autophagosomes in cancer cells. *PloS one,* 4**,** e4424.
CARDOSO, C. M., JORDAO, L. & VIEIRA, O. V. 2010. Rab10 regulates phagosome maturation and its overexpression rescues Mycobacterium-containing phagosomes maturation. *Traffic,* 11**,** 221-35.
CARLTON, J., BUJNY, M., PETER, B. J., OORSCHOT, V. M., RUTHERFORD, A., MELLOR, H., KLUMPERMAN, J., MCMAHON, H. T. & CULLEN, P. J. 2004. Sorting nexin-1 mediates tubular endosome-to-TGN transport through coincidence sensing of high-curvature membranes and 3-phosphoinositides. *Current biology : CB,* 14**,** 1791-800.
CASJENS, S. 1998. The diverse and dynamic structure of bacterial genomes. *Annual review of genetics,* 32**,** 339-77.
CASTANEDA, J. A., LIM, M. J., COOPER, J. D. & PEARCE, D. A. 2008. Immune system irregularities in lysosomal storage disorders. *Acta neuropathologica,* 115**,** 159-74.
CASTELLO, P. R., DRECHSEL, D. A. & PATEL, M. 2007. Mitochondria are a major source of paraquat-induced reactive oxygen species production in the brain. *The Journal of biological chemistry,* 282**,** 14186-93.
CASTLE, J. D. 2004. Overview of cell fractionation. *Current protocols in protein science / editorial board, John E. Coligan ... [et al.],* Chapter 4**,** Unit 4 1.
CAUNT, P., IMPOOLSUP, A. & GREENFIELD, P. F. 1988. Stability of Recombinant Plasmids in Yeast. *Journal of biotechnology,* 8**,** 173-192.
CHAMPION, J. A., WALKER, A. & MITRAGOTRI, S. 2008. Role of particle size in phagocytosis of polymeric microspheres. *Pharmaceutical research,* 25**,** 1815-21.
CHAVRIER, P., PARTON, R. G., HAURI, H. P., SIMONS, K. & ZERIAL, M. 1990. Localization of low molecular weight GTP binding proteins to exocytic and endocytic compartments. *Cell,* 62**,** 317-29.
CHEN, Y. A. & SCHELLER, R. H. 2001. SNARE-mediated membrane fusion. *Nature reviews. Molecular cell biology,* 2**,** 98-106.
CHOPRA, P., KODURI, H., SINGH, R., KOUL, A., GHILDIYAL, M., SHARMA, K., TYAGI, A. K. & SINGH, Y. 2004. Nucleoside diphosphate kinase of Mycobacterium tuberculosis acts as GTPase-activating protein for Rho-GTPases. *FEBS letters,* 571**,** 212-6.
CHRISTOFORIDIS, S., MCBRIDE, H. M., BURGOYNE, R. D. & ZERIAL, M. 1999a. The Rab5 effector EEA1 is a core component of endosome docking. *Nature,* 397**,** 621-5.
CHRISTOFORIDIS, S., MIACZYNSKA, M., ASHMAN, K., WILM, M., ZHAO, L., YIP, S. C., WATERFIELD, M. D., BACKER, J. M. & ZERIAL, M. 1999b. Phosphatidylinositol-3-OH kinases are Rab5 effectors. *Nature Cell Biology,* 1**,** 249-52.
CISEK, A. A., RZEWUSKA, M., WITKOWSKI, L. & BINEK, M. 2014. Antimicrobial resistance in Rhodococcus equi. *Acta biochimica Polonica,* 61**,** 633-8.
CLARKE, L. & CARBON, J. 1976. A colony bank containing synthetic Col El hybrid plasmids representative of the entire E. coli genome. *Cell,* 9**,** 91-9.
CLARKE, M., KOHLER, J., ARANA, Q., LIU, T., HEUSER, J. & GERISCH, G. 2002. Dynamics of the vacuolar H(+)-ATPase in the contractile vacuole complex and the endosomal pathway of Dictyostelium cells. *Journal of cell science,* 115**,** 2893-905.
CLARKE, M., MADDERA, L., ENGEL, U. & GERISCH, G. 2010. Retrieval of the vacuolar H-ATPase from phagosomes revealed by live cell imaging. *PloS one,* 5**,** e8585.

CLEMENS, D. L., LEE, B. Y. & HORWITZ, M. A. 2000. Deviant expression of Rab5 on phagosomes containing the intracellular pathogens Mycobacterium tuberculosis and Legionella pneumophila is associated with altered phagosomal fate. *Infection and immunity,* 68**,** 2671-84.
COBURN, B., GRASSL, G. A. & FINLAY, B. B. 2007. Salmonella, the host and disease: a brief review. *Immunology and cell biology,* 85**,** 112-8.
COLLINS, K. M. & WICKNER, W. T. 2007. trans-SNARE complex assembly and yeast vacuole membrane fusion. *Proceedings of the National Academy of Sciences of the United States of America,* 104**,** 8755-8760.
COLLINS, R. F., SCHREIBER, A. D., GRINSTEIN, S. & TRIMBLE, W. S. 2002. Syntaxins 13 and 7 function at distinct steps during phagocytosis. *Journal of immunology,* 169**,** 3250-6.
CONIBEAR, E. 2010. Converging views of endocytosis in yeast and mammals. *Current opinion in cell biology,* 22**,** 513-518.
COONROD, E. M., GRAHAM, L. A., CARPP, L. N., CARR, T. M., STIRRAT, L., BOWERS, K., BRYANT, N. J. & STEVENS, T. H. 2013. Homotypic vacuole fusion in yeast requires organelle acidification and not the V-ATPase membrane domain. *Developmental cell,* 27**,** 462-8.
COOPER, A. A. & STEVENS, T. H. 1996. Vps10p cycles between the late-Golgi and prevacuolar compartments in its function as the sorting receptor for multiple yeast vacuolar hydrolases. *The Journal of cell biology,* 133**,** 529-41.
CORDONNIER, M. N., DAUZONNE, D., LOUVARD, D. & COUDRIER, E. 2001. Actin filaments and myosin I alpha cooperate with microtubules for the movement of lysosomes. *Molecular biology of the cell,* 12**,** 4013-29.
CORNELIS, G. R. 2006. The type III secretion injectisome. *Nature reviews. Microbiology,* 4**,** 811-25.
COSTA, T. R., FELISBERTO-RODRIGUES, C., MEIR, A., PREVOST, M. S., REDZEJ, A., TROKTER, M. & WAKSMAN, G. 2015. Secretion systems in Gram-negative bacteria: structural and mechanistic insights. *Nature reviews. Microbiology,* 13**,** 343-59.
COULSON, G. B., AGARWAL, S. & HONDALUS, M. K. 2010. Characterization of the role of the pathogenicity island and vapG in the virulence of the intracellular actinomycete pathogen Rhodococcus equi. *Infection and immunity,* 78**,** 3323-34.
COULSON, G. B., MIRANDA-CASOLUENGO, A. A., MIRANDA-CASOLUENGO, R., WANG, X., OLIVER, J., WILLINGHAM-LANE, J. M., MEIJER, W. G. & HONDALUS, M. K. 2015. Transcriptome reprogramming by plasmid-encoded transcriptional regulators is required for host niche adaption of a macrophage pathogen. *Infection and immunity,* 83**,** 3137-45.
COWLES, C. R., ODORIZZI, G., PAYNE, G. S. & EMR, S. D. 1997. The AP-3 adaptor complex is essential for cargo-selective transport to the yeast vacuole. *Cell,* 91**,** 109-18.
CUI, Y., ZHAO, Q., GAO, C., DING, Y., ZENG, Y., UEDA, T., NAKANO, A. & JIANG, L. 2014. Activation of the Rab7 GTPase by the MON1-CCZ1 Complex Is Essential for PVC-to-Vacuole Trafficking and Plant Growth in Arabidopsis. *The Plant cell,* 26**,** 2080-2097.
CURAK, J., ROHDE, J. & STAGLJAR, I. 2009. Yeast as a tool to study bacterial effectors. *Current opinion in microbiology,* 12**,** 18-23.
DAMIANI, M. T., PAVAROTTI, M., LEIVA, N., LINDSAY, A. J., MCCAFFREY, M. W. & COLOMBO, M. I. 2004. Rab coupling protein associates with phagosomes and regulates recycling from the phagosomal compartment. *Traffic,* 5**,** 785-97.
DARSOW, T., ODORIZZI, G. & EMR, S. D. 2000. Invertase fusion proteins for analysis of protein trafficking in yeast. *Methods in enzymology,* 327**,** 95-106.
DAVE, S. R. & GAO, X. 2009. Monodisperse magnetic nanoparticles for biodetection, imaging, and drug delivery: a versatile and evolving technology. *Wiley interdisciplinary reviews. Nanomedicine and nanobiotechnology,* 1**,** 583-609.

DE DUVE, C., PRESSMAN, B. C., GIANETTO, R., WATTIAUX, R. & APPELMANS, F. 1955. Tissue fractionation studies. 6. Intracellular distribution patterns of enzymes in rat-liver tissue. *The Biochemical journal,* 60**,** 604-17.

DE LARTIGUE, J., POLSON, H., FELDMAN, M., SHOKAT, K., TOOZE, S. A., URBE, S. & CLAGUE, M. J. 2009. PIKfyve regulation of endosome-linked pathways. *Traffic,* 10**,** 883-93.

DE MATTEIS, M. A. & GODI, A. 2004. PI-loting membrane traffic. *Nature Cell Biology,* 6**,** 487-92.

DE NARDI, P., STRATTA, G., FUMAGALLI, L., FERRETTI, F., ALBARELLO, L. & STAUDACHER, C. 2011. Rhodococcus equi colonic lesion mimicking colon cancer. *Colorectal disease : the official journal of the Association of Coloproctology of Great Britain and Ireland,* 13**,** e353-4.

DEL CONTE-ZERIAL, P., BRUSCH, L., RINK, J. C., COLLINET, C., KALAIDZIDIS, Y., ZERIAL, M. & DEUTSCH, A. 2008. Membrane identity and GTPase cascades regulated by toggle and cut-out switches. *Molecular systems biology,* 4.

DELL'ANGELICA, E. C., SHOTELERSUK, V., AGUILAR, R. C., GAHL, W. A. & BONIFACINO, J. S. 1999. Altered trafficking of lysosomal proteins in Hermansky-Pudlak syndrome due to mutations in the beta 3A subunit of the AP-3 adaptor. *Molecular cell,* 3**,** 11-21.

DESJARDINS, M., CELIS, J. E., VAN MEER, G., DIEPLINGER, H., JAHRAUS, A., GRIFFITHS, G. & HUBER, L. A. 1994a. Molecular characterization of phagosomes. *The Journal of biological chemistry,* 269**,** 32194-200.

DESJARDINS, M. & GRIFFITHS, G. 2003. Phagocytosis: latex leads the way. *Current opinion in cell biology,* 15**,** 498-503.

DESJARDINS, M., HUBER, L. A., PARTON, R. G. & GRIFFITHS, G. 1994b. Biogenesis of phagolysosomes proceeds through a sequential series of interactions with the endocytic apparatus. *The Journal of cell biology,* 124**,** 677-88.

DESJARDINS, M., NZALA, N. N., CORSINI, R. & RONDEAU, C. 1997. Maturation of phagosomes is accompanied by changes in their fusion properties and size-selective acquisition of solute materials from endosomes. *Journal of cell science,* 110 (Pt 18)**,** 2303-14.

DI PAOLO, G. & DE CAMILLI, P. 2006. Phosphoinositides in cell regulation and membrane dynamics. *Nature,* 443**,** 651-7.

DIACOVICH, L., DUMONT, A., LAFITTE, D., SOPRANO, E., GUILHON, A. A., BIGNON, C., GORVEL, J. P., BOURNE, Y. & MERESSE, S. 2009. Interaction between the SifA virulence factor and its host target SKIP is essential for Salmonella pathogenesis. *The Journal of biological chemistry,* 284**,** 33151-60.

DIAKONOVA, M., GERKE, V., ERNST, J., LIAUTARD, J. P., VAN DER VUSSE, G. & GRIFFITHS, G. 1997. Localization of five annexins in J774 macrophages and on isolated phagosomes. *Journal of cell science,* 110 (Pt 10)**,** 1199-213.

DIAZ, E. & PFEFFER, S. R. 1998. TIP47: a cargo selection device for mannose 6-phosphate receptor trafficking. *Cell,* 93**,** 433-43.

DIAZ, R., MAYORGA, L. S., WEIDMAN, P. J., ROTHMAN, J. E. & STAHL, P. D. 1989. Vesicle fusion following receptor-mediated endocytosis requires a protein active in Golgi transport. *Nature,* 339**,** 398-400.

DIETTRICH, O., MILLS, K., JOHNSON, A. W., HASILIK, A. & WINCHESTER, B. G. 1998. Application of magnetic chromatography to the isolation of lysosomes from fibroblasts of patients with lysosomal storage disorders. *FEBS letters,* 441**,** 369-72.

DIMITRIOU, E., KAIRIS, M., SARAFIDOU, J. & MICHELAKAKIS, H. 2000. Iron overload and kidney lysosomes. *Biochimica et biophysica acta,* 1501**,** 138-48.

DOBROWOLSKI, R. & DE ROBERTIS, E. M. 2012. Endocytic control of growth factor signalling: multivesicular bodies as signalling organelles. *Nature reviews. Molecular cell biology,* 13**,** 53-60.

DOHERTY, G. J. & MCMAHON, H. T. 2009. Mechanisms of endocytosis. *Annual review of biochemistry,* 78**,** 857-902.
DONG, X. P., SHEN, D., WANG, X., DAWSON, T., LI, X., ZHANG, Q., CHENG, X., ZHANG, Y., WEISMAN, L. S., DELLING, M. & XU, H. 2010. PI(3,5)P(2) controls membrane trafficking by direct activation of mucolipin Ca(2+) release channels in the endolysosome. *Nature communications,* 1**,** 38.
DOWBEN, R. M., GAFFEY, A. & LYNCH, P. M. 1968. Isolation of liver and muscle polyribosomes in high yield after cell disruption by nitrogen cavitation. *FEBS letters,* 2**,** 1-3.
DUCLOS, S., DIEZ, R., GARIN, J., PAPADOPOULOU, B., DESCOTEAUX, A., STENMARK, H. & DESJARDINS, M. 2000. Rab5 regulates the kiss and run fusion between phagosomes and endosomes and the acquisition of phagosome leishmanicidal properties in RAW 264.7 macrophages. *Journal of cell science,* 113 Pt 19**,** 3531-41.
DUNDAS, C. M., DEMONTE, D. & PARK, S. 2013. Streptavidin-biotin technology: improvements and innovations in chemical and biological applications. *Applied microbiology and biotechnology,* 97**,** 9343-53.
DUNPHY, W. G., PFEFFER, S. R., CLARY, D. O., WATTENBERG, B. W., GLICK, B. S. & ROTHMAN, J. E. 1986. Yeast and Mammals Utilize Similar Cytosolic Components to Drive Protein-Transport through the Golgi-Complex. *Proceedings of the National Academy of Sciences of the United States of America,* 83**,** 1622-1626.
DURCHFORT, N., VERHOEF, S., VAUGHN, M. B., SHRESTHA, R., ADAM, D., KAPLAN, J. & WARD, D. M. 2012. The enlarged lysosomes in beige j cells result from decreased lysosome fission and not increased lysosome fusion. *Traffic,* 13**,** 108-19.
DURRER, P., GALLI, C., HOENKE, S., CORTI, C., GLUCK, R., VORHERR, T. & BRUNNER, J. 1996. H+-induced membrane insertion of influenza virus hemagglutinin involves the HA2 amino-terminal fusion peptide but not the coiled coil region. *The Journal of biological chemistry,* 271**,** 13417-21.
DUVVURI, M., GONG, Y., CHATTERJI, D. & KRISE, J. P. 2004. Weak base permeability characteristics influence the intracellular sequestration site in the multidrug-resistant human leukemic cell line HL-60. *The Journal of biological chemistry,* 279**,** 32367-72.
DYER, D. L. & SAID, H. M. 1997. Biotin uptake in cultured cell lines. *Methods in enzymology,* 279**,** 393-405.
EGAMI, Y. & ARAKI, N. 2009. Dynamic changes in the spatiotemporal localization of Rab21 in live RAW264 cells during macropinocytosis. *PloS one,* 4**,** e6689.
EISEN, M. B., SPELLMAN, P. T., BROWN, P. O. & BOTSTEIN, D. 1998. Cluster analysis and display of genome-wide expression patterns. *Proceedings of the National Academy of Sciences of the United States of America,* 95**,** 14863-8.
ENGLISH, A. R. & VOELTZ, G. K. 2013. Rab10 GTPase regulates ER dynamics and morphology. *Nature Cell Biology,* 15**,** 169-78.
ESKELINEN, E. L., TANAKA, Y. & SAFTIG, P. 2003. At the acidic edge: emerging functions for lysosomal membrane proteins. *Trends in cell biology,* 13**,** 137-45.
ESWARAPPA, S. M., NEGI, V. D., CHAKRABORTY, S., CHANDRASEKHAR SAGAR, B. K. & CHAKRAVORTTY, D. 2010. Division of the Salmonella-containing vacuole and depletion of acidic lysosomes in Salmonella-infected host cells are novel strategies of Salmonella enterica to avoid lysosomes. *Infection and immunity,* 78**,** 68-79.
EZEKOWITZ, R. A., SASTRY, K., BAILLY, P. & WARNER, A. 1990. Molecular characterization of the human macrophage mannose receptor: demonstration of multiple carbohydrate recognition-like domains and phagocytosis of yeasts in Cos-1 cells. *The Journal of experimental medicine,* 172**,** 1785-94.
FASSHAUER, D. 2003. Structural insights into the SNARE mechanism. *Biochimica et biophysica acta,* 1641**,** 87-97.

FASSHAUER, D., ELIASON, W. K., BRUNGER, A. T. & JAHN, R. 1998a. Identification of a minimal core of the synaptic SNARE complex sufficient for reversible assembly and disassembly. *Biochemistry,* 37**,** 10354-62.
FASSHAUER, D., SUTTON, R. B., BRUNGER, A. T. & JAHN, R. 1998b. Conserved structural features of the synaptic fusion complex: SNARE proteins reclassified as Q- and R-SNAREs. *Proceedings of the National Academy of Sciences of the United States of America,* 95**,** 15781-6.
FELTCHER, M. E., SULLIVAN, J. T. & BRAUNSTEIN, M. 2010. Protein export systems of Mycobacterium tuberculosis: novel targets for drug development? *Future microbiology,* 5**,** 1581-97.
FERNANDEZ-MORA, E., POLIDORI, M., LUHRMANN, A., SCHAIBLE, U. E. & HAAS, A. 2005. Maturation of Rhodococcus equi-containing vacuoles is arrested after completion of the early endosome stage. *Traffic,* 6**,** 635-53.
FIDZIANSKA, A., WALCZAK, E. & WALSKI, M. 2007. Abnormal chaperone-mediated autophagy (CMA) in cardiomyocytes of a boy with Danon disease. *Folia neuropathologica / Association of Polish Neuropathologists and Medical Research Centre, Polish Academy of Sciences,* 45**,** 133-9.
FLEMING, M. S. & GITLER, A. D. 2011. High-throughput yeast plasmid overexpression screen. *Journal of visualized experiments : JoVE*.
FORGAC, M. 2007. Vacuolar ATPases: rotary proton pumps in physiology and pathophysiology. *Nature reviews. Molecular cell biology,* 8**,** 917-29.
FORSBERG, A. & GUINA, T. 2007. Type II secretion and type IV pili of Francisella. *Annals of the New York Academy of Sciences,* 1105**,** 187-201.
FORTENBERRY, S. C., SCHOREY, J. S. & CHIRGWIN, J. M. 1995. Role of glycosylation in the expression of human procathepsin D. *Journal of cell science,* 108 (Pt 5)**,** 2001-6.
FRALDI, A., ANNUNZIATA, F., LOMBARDI, A., KAISER, H. J., MEDINA, D. L., SPAMPANATO, C., FEDELE, A. O., POLISHCHUK, R., SORRENTINO, N. C., SIMONS, K. & BALLABIO, A. 2010. Lysosomal fusion and SNARE function are impaired by cholesterol accumulation in lysosomal storage disorders. *The EMBO journal,* 29**,** 3607-20.
FRANCHI, L., WARNER, N., VIANI, K. & NUNEZ, G. 2009. Function of Nod-like receptors in microbial recognition and host defense. *Immunological reviews,* 227**,** 106-28.
FRANCO, I. S., SHOHDY, N. & SHUMAN, H. A. 2012. The Legionella pneumophila effector VipA is an actin nucleator that alters host cell organelle trafficking. *PLoS pathogens,* 8**,** e1002546.
FRATTI, R. A., BACKER, J. M., GRUENBERG, J., CORVERA, S. & DERETIC, V. 2001. Role of phosphatidylinositol 3-kinase and Rab5 effectors in phagosomal biogenesis and mycobacterial phagosome maturation arrest. *The Journal of cell biology,* 154**,** 631-44.
FRATTI, R. A., CHUA, J., VERGNE, I. & DERETIC, V. 2003. Mycobacterium tuberculosis glycosylated phosphatidylinositol causes phagosome maturation arrest. *Proceedings of the National Academy of Sciences of the United States of America,* 100**,** 5437-42.
FREEMAN, S. A. & GRINSTEIN, S. 2014. Phagocytosis: receptors, signal integration, and the cytoskeleton. *Immunological reviews,* 262**,** 193-215.
FROLOV, V. A. & ZIMMERBERG, J. 2010. Cooperative elastic stresses, the hydrophobic effect, and lipid tilt in membrane remodeling. *FEBS letters,* 584**,** 1824-9.
FULLER, M., MEIKLE, P. J. & HOPWOOD, J. J. 2006. Epidemiology of lysosomal storage diseases: an overview. *In:* MEHTA, A., BECK, M. & SUNDER-PLASSMANN, G. (eds.) *Fabry Disease: Perspectives from 5 Years of FOS.* Oxford.
FUNATO, K., BERON, W., YANG, C. Z., MUKHOPADHYAY, A. & STAHL, P. D. 1997. Reconstitution of phagosome-lysosome fusion in streptolysin O-permeabilized cells. *The Journal of biological chemistry,* 272**,** 16147-51.
FUNDERBURK, S. F., WANG, Q. J. & YUE, Z. 2010. The Beclin 1-VPS34 complex--at the crossroads of autophagy and beyond. *Trends in cell biology,* 20**,** 355-62.

GABEL, C. A., GOLDBERG, D. E. & KORNFELD, S. 1983. Identification and characterization of cells deficient in the mannose 6-phosphate receptor: evidence for an alternate pathway for lysosomal enzyme targeting. *Proceedings of the National Academy of Sciences of the United States of America,* 80**,** 775-9.

GABRIELS, P., JOOSEN, H., PUT, E., VERHAEGEN, J., MAGERMAN, K. & CARTUYVELS, R. 2006. Recurrent Rhodococcus equi infection with fatal outcome in an immunocompetent patient. *European journal of clinical microbiology & infectious diseases : official publication of the European Society of Clinical Microbiology,* 25**,** 46-8.

GALLWITZ, D., HAUBRUCK, H., MOLENAAR, C., PRANGE, R., PUZICHA, M., SCHMITT, H. D., VORGIAS, C. & WAGNER, P. 1989. Structural and Functional-Analysis of Ypt Proteins, a Family of Ras-Related Nucleotide-Binding Proteins in Eukaryotic Cells. *Guanine-Nucleotide Binding Proteins,* 165**,** 257-264.

GANLEY, I. G., CARROLL, K., BITTOVA, L. & PFEFFER, S. 2004. Rab9 GTPase regulates late endosome size and requires effector interaction for its stability. *Molecular biology of the cell,* 15**,** 5420-30.

GARCIA-DEL PORTILLO, F. & FINLAY, B. B. 1995. Targeting of Salmonella typhimurium to vesicles containing lysosomal membrane glycoproteins bypasses compartments with mannose 6-phosphate receptors. *The Journal of cell biology,* 129**,** 81-97.

GARIN, J., DIEZ, R., KIEFFER, S., DERMINE, J. F., DUCLOS, S., GAGNON, E., SADOUL, R., RONDEAU, C. & DESJARDINS, M. 2001. The phagosome proteome: insight into phagosome functions. *The Journal of cell biology,* 152**,** 165-80.

GEERDS, C., WOHLMANN, J., HAAS, A. & NIEMANN, H. H. 2014. Structure of Rhodococcus equi virulence-associated protein B (VapB) reveals an eight-stranded antiparallel beta-barrel consisting of two Greek-key motifs. *Acta crystallographica. Section F, Structural biology communications,* 70**,** 866-71.

GERONDOPOULOS, A., LANGEMEYER, L., LIANG, J. R., LINFORD, A. & BARR, F. A. 2012. BLOC-3 mutated in Hermansky-Pudlak syndrome is a Rab32/38 guanine nucleotide exchange factor. *Current biology : CB,* 22**,** 2135-9.

GEUZE, H. J., SLOT, J. W., STROUS, G. J., HASILIK, A. & VON FIGURA, K. 1985. Possible pathways for lysosomal enzyme delivery. *The Journal of cell biology,* 101**,** 2253-62.

GHISLAT, G., AGUADO, C. & KNECHT, E. 2012. Annexin A5 stimulates autophagy and inhibits endocytosis. *Journal of cell science,* 125**,** 92-107.

GHOSH, P., DAHMS, N. M. & KORNFELD, S. 2003. Mannose 6-phosphate receptors: New twists in the tale. *Nature Reviews Molecular Cell Biology,* 4**,** 202-212.

GIGUERE, S., HONDALUS, M. K., YAGER, J. A., DARRAH, P., MOSSER, D. M. & PRESCOTT, J. F. 1999. Role of the 85-kilobase plasmid and plasmid-encoded virulence-associated protein A in intracellular survival and virulence of Rhodococcus equi. *Infection and immunity,* 67**,** 3548-57.

GILL, D. J., TEO, H., SUN, J., PERISIC, O., VEPRINTSEV, D. B., EMR, S. D. & WILLIAMS, R. L. 2007. Structural insight into the ESCRT-I/-II link and its role in MVB trafficking. *Embo Journal,* 26**,** 600-612.

GLAUMANN, H., JANSSON, H., ARBORGH, B. & ERICSSON, J. L. 1975. Isolation of liver lysosomes by iron loading. Ultrastructural characterization. *The Journal of cell biology,* 67**,** 887-94.

GOFFEAU, A., BARRELL, B. G., BUSSEY, H., DAVIS, R. W., DUJON, B., FELDMANN, H., GALIBERT, F., HOHEISEL, J. D., JACQ, C., JOHNSTON, M., LOUIS, E. J., MEWES, H. W., MURAKAMI, Y., PHILIPPSEN, P., TETTELIN, H. & OLIVER, S. G. 1996. Life with 6000 genes. *Science,* 274**,** 546, 563-7.

GOLUB, B., FALK, G. & SPINK, W. W. 1967. Lung abscess due to Corynebacterium equi. Report of first human infection. *Annals of internal medicine,* 66**,** 1174-7.

GONZALEZ-IGLESIAS, P., SCORTTI, M., MACARTHUR, I., HAPESHI, A., RODRIGUEZ, H., PRESCOTT, J. F. & VAZQUEZ-BOLAND, J. A. 2014. Mouse lung infection model to

assess Rhodococcus equi virulence and vaccine protection. *Veterinary microbiology,* 172**,** 256-64.
GOODFELLOW, M. & ALDERSON, G. 1977. The actinomycete-genus Rhodococcus: a home for the "rhodochrous" complex. *Journal of general microbiology,* 100**,** 99-122.
GOODFELLOW, M., SANGAL, V., JONES, A. L. & SUTCLIFFE, I. C. 2015. Charting stormy waters: A commentary on the nomenclature of the equine pathogen variously named Prescottella equi, Rhodococcus equi and Rhodococcus hoagii. *Equine veterinary journal,* 47**,** 508-9.
GOPHNA, U., RON, E. Z. & GRAUR, D. 2003. Bacterial type III secretion systems are ancient and evolved by multiple horizontal-transfer events. *Gene,* 312**,** 151-63.
GORVEL, J. P., CHAVRIER, P., ZERIAL, M. & GRUENBERG, J. 1991. rab5 controls early endosome fusion in vitro. *Cell,* 64**,** 915-25.
GOTTHARDT, D., DIECKMANN, R., BLANCHETEAU, V., KISTLER, C., REICHARDT, F. & SOLDATI, T. 2006. Preparation of intact, highly purified phagosomes from Dictyostelium. *Methods in molecular biology,* 346**,** 439-48.
GOTTHARDT, D., WARNATZ, H. J., HENSCHEL, O., BRUCKERT, F., SCHLEICHER, M. & SOLDATI, T. 2002. High-resolution dissection of phagosome maturation reveals distinct membrane trafficking phases. *Molecular biology of the cell,* 13**,** 3508-20.
GOTTLIEB, R. A. & ADACHI, S. 2000. Nitrogen cavitation for cell disruption to obtain mitochondria from cultured cells. *Methods in enzymology,* 322**,** 213-21.
GRAHAM, J. M. 2001. *Isolation of Peroxisomes from Tissues and Cells by Differential and Density Gradient Centrifugation*, John Wiley & Sons, Inc.
GRAHAM, J. M. & RICKWOOD, D. 1997. *Subcellular fractionation : a practical approach,* Oxford ; New York, IRL Press at Oxford University Press.
GRANT, B. D. & DONALDSON, J. G. 2009. Pathways and mechanisms of endocytic recycling. *Nature reviews. Molecular cell biology,* 10**,** 597-608.
GRAVES, A. R., CURRAN, P. K., SMITH, C. L. & MINDELL, J. A. 2008. The Cl-/H+ antiporter ClC-7 is the primary chloride permeation pathway in lysosomes. *Nature,* 453**,** 788-92.
GRIFFITHS, G. 2004. On phagosome individuality and membrane signalling networks. *Trends in cell biology,* 14**,** 343-51.
GRUENBERG, J. & VAN DER GOOT, F. G. 2006. Mechanisms of pathogen entry through the endosomal compartments. *Nature reviews. Molecular cell biology,* 7**,** 495-504.
GUERRERO, R., BHARGAVA, A. & NAHLEH, Z. 2011. Rhodococcus equi venous catheter infection: a case report and review of the literature. *Journal of medical case reports,* 5**,** 358.
GUICHARD, A., NIZET, V. & BIER, E. 2014. RAB11-mediated trafficking in host-pathogen interactions. *Nature reviews. Microbiology,* 12**,** 624-34.
GUO, M., HARTLOVA, A., DILL, B. D., PRESCOTT, A. R., GIERLINSKI, M. & TROST, M. 2014. High-resolution quantitative proteome analysis reveals substantial differences between phagosomes of RAW 264.7 and bone marrow-derived macrophages. *Proteomics*.
GUO, M., HARTLOVA, A., DILL, B. D., PRESCOTT, A. R., GIERLINSKI, M. & TROST, M. 2015. High-resolution quantitative proteome analysis reveals substantial differences between phagosomes of RAW 264.7 and bone marrow derived macrophages. *Proteomics,* 15**,** 3169-74.
GURVITZ, A., HILTUNEN, J. K. & KASTANIOTIS, A. J. 2009. Heterologous expression of mycobacterial proteins in Saccharomyces cerevisiae reveals two physiologically functional 3-hydroxyacyl-thioester dehydratases, HtdX and HtdY, in addition to HadABC and HtdZ. *Journal of bacteriology,* 191**,** 2683-90.
GUTIERREZ, M. G. 2013. Functional role(s) of phagosomal Rab GTPases. *Small GTPases,* 4**,** 148-58.
HACKAM, D. J., ROTSTEIN, O. D., BENNETT, M. K., KLIP, A., GRINSTEIN, S. & MANOLSON, M. F. 1996. Characterization and subcellular localization of target

membrane soluble NSF attachment protein receptors (t-SNAREs) in macrophages. Syntaxins 2, 3, and 4 are present on phagosomal membranes. *Journal of immunology,* 156**,** 4377-83.
HAFT, C. R., DE LA LUZ SIERRA, M., BAFFORD, R., LESNIAK, M. A., BARR, V. A. & TAYLOR, S. I. 2000. Human orthologs of yeast vacuolar protein sorting proteins Vps26, 29, and 35: assembly into multimeric complexes. *Molecular biology of the cell,* 11**,** 4105-16.
HAM, H., SREELATHA, A. & ORTH, K. 2011. Manipulation of host membranes by bacterial effectors. *Nature reviews. Microbiology,* 9**,** 635-46.
HANSON, P. I., ROTH, R., LIN, Y. & HEUSER, J. E. 2008. Plasma membrane deformation by circular arrays of ESCRT-III protein filaments. *The Journal of cell biology,* 180**,** 389-402.
HAPPE, S. & WEIDMAN, P. 1998. Cell-free transport to distinct Golgi cisternae is compartment specific and ARF independent. *The Journal of cell biology,* 140**,** 511-23.
HARAGA, A. & MILLER, S. I. 2003. A Salmonella enterica serovar typhimurium translocated leucine-rich repeat effector protein inhibits NF-kappa B-dependent gene expression. *Infection and immunity,* 71**,** 4052-8.
HARRISON, R. E., BUCCI, C., VIEIRA, O. V., SCHROER, T. A. & GRINSTEIN, S. 2003. Phagosomes fuse with late endosomes and/or lysosomes by extension of membrane protrusions along microtubules: role of Rab7 and RILP. *Molecular and cellular biology,* 23**,** 6494-506.
HASILIK, A. & NEUFELD, E. F. 1980. Biosynthesis of lysosomal enzymes in fibroblasts. Synthesis as precursors of higher molecular weight. *The Journal of biological chemistry,* 255**,** 4937-45.
HAUBRUCK, H., PRANGE, R., VORGIAS, C. & GALLWITZ, D. 1989. The Ras-Related Mouse Ypt1 Protein Can Functionally Replace the Ypt1 Gene-Product in Yeast. *Embo Journal,* 8**,** 1427-1432.
HAY, J. C. 2007. Calcium: a fundamental regulator of intracellular membrane fusion? *EMBO reports,* 8**,** 236-40.
HAYES, D., JR., DIAZ-GUZMAN, E. & HOOPES, C. W. 2011. Rhodococcus equi infection after lung transplantation. *Respiratory care,* 56**,** 1605-7.
HEIDER, M. R. & MUNSON, M. 2012. Exorcising the exocyst complex. *Traffic,* 13**,** 898-907.
HELIP-WOOLEY, A. & THOENE, J. G. 2004. Sucrose-induced vacuolation results in increased expression of cholesterol biosynthesis and lysosomal genes. *Experimental cell research,* 292**,** 89-100.
HENNE, W. M., BUCHKOVICH, N. J. & EMR, S. D. 2011. The ESCRT pathway. *Developmental cell,* 21**,** 77-91.
HENNING, R. & PLATTNER, H. 1974. Isolation of rat liver lysosomes by loading with colloidal gold. *Biochimica et biophysica acta,* 354**,** 114-20.
HERNANDEZ, L. D., HUEFFER, K., WENK, M. R. & GALAN, J. E. 2004. Salmonella modulates vesicular traffic by altering phosphoinositide metabolism. *Science,* 304**,** 1805-7.
HIERRO, A., SUN, J., RUSNAK, A. S., KIM, J., PRAG, G., EMR, S. D. & HURLEY, J. H. 2004. Structure of the ESCRT-II endosomal trafficking complex. *Nature,* 431**,** 221-225.
HIROTA, Y., KURONITA, T., FUJITA, H. & TANAKA, Y. 2007. A role for Rab5 activity in the biogenesis of endosomal and lysosomal compartments. *Biochemical and biophysical research communications,* 364**,** 40-47.
HIRST, J., FUTTER, C. E. & HOPKINS, C. R. 1998. The kinetics of mannose 6-phosphate receptor trafficking in the endocytic pathway in HEp-2 cells: the receptor enters and rapidly leaves multivesicular endosomes without accumulating in a prelysosomal compartment. *Molecular biology of the cell,* 9**,** 809-16.

HIRST, J., IRVING, C. & BORNER, G. H. 2013. Adaptor protein complexes AP-4 and AP-5: new players in endosomal trafficking and progressive spastic paraplegia. *Traffic,* 14**,** 153-64.
HO, C. Y., CHOY, C. H., WATTSON, C. A., JOHNSON, D. E. & BOTELHO, R. J. 2015. The Fab1/PIKfyve phosphoinositide phosphate kinase is not necessary to maintain the pH of lysosomes and of the yeast vacuole. *The Journal of biological chemistry,* 290**,** 9919-28.
HOLLAND, P., TORGERSEN, M. L., SANDVIG, K. & SIMONSEN, A. 2014. LYST affects lysosome size and quantity, but not trafficking or degradation through autophagy or endocytosis. *Traffic,* 15**,** 1390-405.
HOLM, A., TEJLE, K., MAGNUSSON, K. E., DESCOTEAUX, A. & RASMUSSON, B. 2001. Leishmania donovani lipophosphoglycan causes periphagosomal actin accumulation: correlation with impaired translocation of PKCalpha and defective phagosome maturation. *Cellular microbiology,* 3**,** 439-47.
HONDALUS, M. K. 1997. Pathogenesis and virulence of Rhodococcus equi. *Veterinary microbiology,* 56**,** 257-68.
HONDALUS, M. K. & MOSSER, D. M. 1994. Survival and replication of Rhodococcus equi in macrophages. *Infection and immunity,* 62**,** 4167-75.
HORAZDOVSKY, B. F., BUSCH, G. R. & EMR, S. D. 1994. VPS21 encodes a rab5-like GTP binding protein that is required for the sorting of yeast vacuolar proteins. *The EMBO journal,* 13**,** 1297-309.
HORIUCHI, H., LIPPE, R., MCBRIDE, H. M., RUBINO, M., WOODMAN, P., STENMARK, H., RYBIN, V., WILM, M., ASHMAN, K., MANN, M. & ZERIAL, M. 1997. A novel Rab5 GDP/GTP exchange factor complexed to Rabaptin-5 links nucleotide exchange to effector recruitment and function. *Cell,* 90**,** 1149-59.
HOWE, D. & HEINZEN, R. A. 2006. Coxiella burnetii inhabits a cholesterol-rich vacuole and influences cellular cholesterol metabolism. *Cellular microbiology,* 8**,** 496-507.
HUBBER, A. & ROY, C. R. 2010. Modulation of Host Cell Function by Legionella pneumophila Type IV Effectors. *Annual Review of Cell and Developmental Biology, Vol 26,* 26**,** 261-283.
HUECK, C. J. 1998. Type III protein secretion systems in bacterial pathogens of animals and plants. *Microbiology and molecular biology reviews : MMBR,* 62**,** 379-433.
HUMPHRIES, W. H. T., SZYMANSKI, C. J. & PAYNE, C. K. 2011. Endo-lysosomal vesicles positive for Rab7 and LAMP1 are terminal vesicles for the transport of dextran. *PloS one,* 6**,** e26626.
HUNT, S. D., TOWNLEY, A. K., DANSON, C. M., CULLEN, P. J. & STEPHENS, D. J. 2013. Microtubule motors mediate endosomal sorting by maintaining functional domain organization. *Journal of cell science,* 126**,** 2493-501.
HUTAGALUNG, A. H. & NOVICK, P. J. 2011. Role of Rab GTPases in membrane traffic and cell physiology. *Physiological reviews,* 91**,** 119-49.
HUYNH, K. K., ESKELINEN, E. L., SCOTT, C. C., MALEVANETS, A., SAFTIG, P. & GRINSTEIN, S. 2007. LAMP proteins are required for fusion of lysosomes with phagosomes. *The EMBO journal,* 26**,** 313-24.
HUYNH, K. K., GERSHENZON, E. & GRINSTEIN, S. 2008. Cholesterol accumulation by macrophages impairs phagosome maturation. *The Journal of biological chemistry,* 283**,** 35745-55.
IKONOMOV, O. C., SBRISSA, D., DELVECCHIO, K., XIE, Y., JIN, J. P., RAPPOLEE, D. & SHISHEVA, A. 2011. The phosphoinositide kinase PIKfyve is vital in early embryonic development: preimplantation lethality of PIKfyve-/- embryos but normality of PIKfyve+/- mice. *The Journal of biological chemistry,* 286**,** 13404-13.
ITAKURA, E., KISHI, C., INOUE, K. & MIZUSHIMA, N. 2008. Beclin 1 forms two distinct phosphatidylinositol 3-kinase complexes with mammalian Atg14 and UVRAG. *Molecular biology of the cell,* 19**,** 5360-72.

JABER, N., DOU, Z., CHEN, J. S., CATANZARO, J., JIANG, Y. P., BALLOU, L. M., SELINGER, E., OUYANG, X., LIN, R. Z., ZHANG, J. & ZONG, W. X. 2012. Class III PI3K Vps34 plays an essential role in autophagy and in heart and liver function. *Proceedings of the National Academy of Sciences of the United States of America,* 109**,** 2003-8.

JAHN, R. & SCHELLER, R. H. 2006. SNAREs--engines for membrane fusion. *Nature reviews. Molecular cell biology,* 7**,** 631-43.

JAHRAUS, A., TJELLE, T. E., BERG, T., HABERMANN, A., STORRIE, B., ULLRICH, O. & GRIFFITHS, G. 1998. In vitro fusion of phagosomes with different endocytic organelles from J774 macrophages. *The Journal of biological chemistry,* 273**,** 30379-90.

JAIN, S., BLOOM, B. R. & HONDALUS, M. K. 2003. Deletion of vapA encoding Virulence Associated Protein A attenuates the intracellular actinomycete Rhodococcus equi. *Molecular microbiology,* 50**,** 115-28.

JANEWAY, C. A., JR. 1992. The immune system evolved to discriminate infectious nonself from noninfectious self. *Immunology today,* 13**,** 11-6.

JONES, A. L., SUTCLIFFE, I. C. & GOODFELLOW, M. 2013. Proposal to replace the illegitimate genus name Prescottia Jones et al. 2013 with the genus name Prescottella gen. nov. and to replace the illegitimate combination Prescottia equi Jones et al. 2013 with Prescottella equi comb. nov. *Antonie van Leeuwenhoek,* 103**,** 1405-7.

KAKUDA, T., HIROTA, T., TAKEUCHI, T., HAGIUDA, H., MIYAZAKI, S. & TAKAI, S. 2014. VirS, an OmpR/PhoB subfamily response regulator, is required for activation of vapA gene expression in Rhodococcus equi. *BMC microbiology,* 14**,** 243.

KARAGEORGOS, L. E., ISAAC, E. L., BROOKS, D. A., RAVENSCROFT, E. M., DAVEY, R., HOPWOOD, J. J. & MEIKLE, P. J. 1997. Lysosomal biogenesis in lysosomal storage disorders. *Experimental cell research,* 234**,** 85-97.

KARUNAKARAN, S. & FRATTI, R. A. 2013. The lipid composition and physical properties of the yeast vacuole affect the hemifusion-fusion transition. *Traffic,* 14**,** 650-62.

KATO, S., ESPINOZA, N., LANGE, S., VILLALON, M., CUELLO, M. & OWEN, G. I. 2008. Characterization and phenotypic variation with passage number of cultured human endometrial adenocarcinoma cells. *Tissue & cell,* 40**,** 95-102.

KATZMANN, D. J., BABST, M. & EMR, S. D. 2001. Ubiquitin-dependent sorting into the multivesicular body pathway requires the function of a conserved endosomal protein sorting complex, ESCRT-I. *Cell,* 106**,** 145-155.

KAUFMAN, M., LETO, T. & LEVY, R. 1996. Translocation of annexin I to plasma membranes and phagosomes in human neutrophils upon stimulation with opsonized zymosan: possible role in phagosome function. *The Biochemical journal,* 316 (Pt 1)**,** 35-42.

KAUFMANN, A. M., GOLDMAN, S. D. & KRISE, J. P. 2009. A fluorescence resonance energy transfer-based approach for investigating late endosome-lysosome retrograde fusion events. *Analytical biochemistry,* 386**,** 91-7.

KAUSHIK, S. & CUERVO, A. M. 2008. Chaperone-mediated autophagy. *Methods in molecular biology,* 445**,** 227-44.

KAUSHIK, S. & CUERVO, A. M. 2009. Methods to monitor chaperone-mediated autophagy. *Methods in enzymology,* 452**,** 297-324.

KAWASAKI-NISHI, S., NISHI, T. & FORGAC, M. 2001. Yeast V-ATPase complexes containing different isoforms of the 100-kDa a-subunit differ in coupling efficiency and in vivo dissociation. *The Journal of biological chemistry,* 276**,** 17941-8.

KEDLAYA, I., ING, M. B. & WONG, S. S. 2001. Rhodococcus equi infections in immunocompetent hosts: case report and review. *Clinical infectious diseases : an official publication of the Infectious Diseases Society of America,* 32**,** E39-46.

KELLY, B. M., YU, C. Z. & CHANG, P. L. 1989. Presence of a lysosomal enzyme, arylsulfatase-A, in the prelysosome-endosome compartments of human cultured fibroblasts. *European journal of cell biology,* 48**,** 71-8.

KHAN, M. Y., ALI, S. & BAQI, S. 2013. Rhodococcus equi pneumonia in a live related renal transplant recipient. *JPMA. The Journal of the Pakistan Medical Association,* 63**,** 635-8.
KHURANA, T., BRZOSTOWSKI, J. A. & KIMMEL, A. R. 2005. A Rab21/LIM-only/CH-LIM complex regulates phagocytosis via both activating and inhibitory mechanisms. *The EMBO journal,* 24**,** 2254-64.
KIM, B. Y., KRAMER, H., YAMAMOTO, A., KOMINAMI, E., KOHSAKA, S. & AKAZAWA, C. 2001. Molecular characterization of mammalian homologues of class C Vps proteins that interact with syntaxin-7. *The Journal of biological chemistry,* 276**,** 29393-402.
KIM, G. H., DAYAM, R. M., PRASHAR, A., TEREBIZNIK, M. & BOTELHO, R. J. 2014. PIKfyve inhibition interferes with phagosome and endosome maturation in macrophages. *Traffic,* 15**,** 1143-63.
KINCHEN, J. M., DOUKOUMETZIDIS, K., ALMENDINGER, J., STERGIOU, L., TOSELLO-TRAMPONT, A., SIFRI, C. D., HENGARTNER, M. O. & RAVICHANDRAN, K. S. 2008. A pathway for phagosome maturation during engulfment of apoptotic cells. *Nature Cell Biology,* 10**,** 556-66.
KINCHEN, J. M. & RAVICHANDRAN, K. S. 2008. Phagosome maturation: going through the acid test. *Nature reviews. Molecular cell biology,* 9**,** 781-95.
KINCHEN, J. M. & RAVICHANDRAN, K. S. 2010. Identification of two evolutionarily conserved genes regulating processing of engulfed apoptotic cells. *Nature,* 464**,** 778-82.
KISSING, S., HERMSEN, C., REPNIK, U., NESSET, C. K., VON BARGEN, K., GRIFFITHS, G., ICHIHARA, A., LEE, B. S., SCHWAKE, M., DE BRABANDER, J., HAAS, A. & SAFTIG, P. 2015. Vacuolar ATPase in phagosome-lysosome fusion. *The Journal of biological chemistry,* 290**,** 14166-80.
KITAGAWA, K. & HIETER, P. 2001. Evolutionary conservation between budding yeast and human kinetochores. *Nature Reviews Molecular Cell Biology,* 2**,** 678-687.
KLEMPNER, M. S., MIKKELSEN, R. B., CORFMAN, D. H. & ANDRE-SCHWARTZ, J. 1980. Neutrophil plasma membranes. I. High-yield purification of human neutrophil plasma membrane vesicles by nitrogen cavitation and differential centrifugation. *The Journal of cell biology,* 86**,** 21-8.
KLIONSKY, D. J. & EMR, S. D. 1989. Membrane protein sorting: biosynthesis, transport and processing of yeast vacuolar alkaline phosphatase. *The EMBO journal,* 8**,** 2241-50.
KLIONSKY, D. J., HERMAN, P. K. & EMR, S. D. 1990. The Fungal Vacuole - Composition, Function, and Biogenesis. *Microbiological Reviews,* 54**,** 266-292.
KNODLER, L. A. & STEELE-MORTIMER, O. 2003. Taking possession: biogenesis of the Salmonella-containing vacuole. *Traffic,* 4**,** 587-99.
KOBAYASHI, T., BEUCHAT, M. H., LINDSAY, M., FRIAS, S., PALMITER, R. D., SAKURABA, H., PARTON, R. G. & GRUENBERG, J. 1999. Late endosomal membranes rich in lysobisphosphatidic acid regulate cholesterol transport. *Nature Cell Biology,* 1**,** 113-8.
KOBAYASHI, T., STANG, E., FANG, K. S., DE MOERLOOSE, P., PARTON, R. G. & GRUENBERG, J. 1998. A lipid associated with the antiphospholipid syndrome regulates endosome structure and function. *Nature,* 392**,** 193-7.
KOEHLER, T. M. & COLLIER, R. J. 1991. Anthrax toxin protective antigen: low-pH-induced hydrophobicity and channel formation in liposomes. *Molecular microbiology,* 5**,** 1501-6.
KOGA, H., MARTINEZ-VICENTE, M., ARIAS, E., KAUSHIK, S., SULZER, D. & CUERVO, A. M. 2011. Constitutive upregulation of chaperone-mediated autophagy in Huntington's disease. *The Journal of neuroscience : the official journal of the Society for Neuroscience,* 31**,** 18492-505.
KOIKE, M., NAKANISHI, H., SAFTIG, P., EZAKI, J., ISAHARA, K., OHSAWA, Y., SCHULZ-SCHAEFFER, W., WATANABE, T., WAGURI, S., KAMETAKA, S., SHIBATA, M.,

YAMAMOTO, K., KOMINAMI, E., PETERS, C., VON FIGURA, K. & UCHIYAMA, Y. 2000. Cathepsin D deficiency induces lysosomal storage with ceroid lipofuscin in mouse CNS neurons. *The Journal of neuroscience : the official journal of the Society for Neuroscience,* 20**,** 6898-906.

KOPITZ, J., ARNOLD, A., MEISSNER, T. & CANTZ, M. 1993. Protein catabolism in fibroblasts cultured from patients with mucolipidosis II and other lysosomal disorders. *The Biochemical journal,* 295 (Pt 2)**,** 577-80.

KOSTELANSKY, M. S., SCHLUTER, C., TAM, Y. Y. C., LEE, S., GHIRLANDO, R., BEACH, B., CONIBEAR, E. & HURLEY, J. H. 2007. Molecular architecture and functional model of the complete yeast ESCRT-I heterotetramer. *Cell,* 129**,** 485-498.

KOTSIAS, F., HOFFMANN, E., AMIGORENA, S. & SAVINA, A. 2013. Reactive oxygen species production in the phagosome: impact on antigen presentation in dendritic cells. *Antioxidants & redox signaling,* 18**,** 714-29.

KUBORI, T. & GALAN, J. E. 2003. Temporal regulation of salmonella virulence effector function by proteasome-dependent protein degradation. *Cell,* 115**,** 333-42.

KÜHNEL, M., ANES, E. & GRIFFITHS, G. 2006. Chapter 8 - Isolation of Latex Bead-and Mycobacteria-Containing Phagosomes. *In:* CELIS, J. E. (ed.) *Cell Biology (Third Edition).* Burlington: Academic Press.

KUMAR, Y. & VALDIVIA, R. H. 2009. Leading a sheltered life: intracellular pathogens and maintenance of vacuolar compartments. *Cell host & microbe,* 5**,** 593-601.

KURZ, T., EATON, J. W. & BRUNK, U. T. 2011. The role of lysosomes in iron metabolism and recycling. *The international journal of biochemistry & cell biology,* 43**,** 1686-97.

KWIATKOWSKA, K. & SOBOTA, A. 1999. Signaling pathways in phagocytosis. *BioEssays : news and reviews in molecular, cellular and developmental biology,* 21**,** 422-31.

LAFOURCADE, C., SOBO, K., KIEFFER-JAQUINOD, S., GARIN, J. & VAN DER GOOT, F. G. 2008. Regulation of the V-ATPase along the endocytic pathway occurs through reversible subunit association and membrane localization. *PloS one,* 3**,** e2758.

LAM, J., HERANT, M., DEMBO, M. & HEINRICH, V. 2009. Baseline mechanical characterization of J774 macrophages. *Biophysical journal,* 96**,** 248-54.

LAMB, F. S., HOOK, J. S., HILKIN, B. M., HUBER, J. N., VOLK, A. P. & MORELAND, J. G. 2012. Endotoxin priming of neutrophils requires endocytosis and NADPH oxidase-dependent endosomal reactive oxygen species. *The Journal of biological chemistry,* 287**,** 12395-404.

LARKIN, M. J., KULAKOV, L. A. & ALLEN, C. C. 2005. Biodegradation and Rhodococcus--masters of catabolic versatility. *Current opinion in biotechnology,* 16**,** 282-90.

LATZ, E., XIAO, T. S. & STUTZ, A. 2013. Activation and regulation of the inflammasomes. *Nature reviews. Immunology,* 13**,** 397-411.

LAWE, D. C., PATKI, V., HELLER-HARRISON, R., LAMBRIGHT, D. & CORVERA, S. 2000. The FYVE domain of early endosome antigen 1 is required for both phosphatidylinositol 3-phosphate and Rab5 binding. Critical role of this dual interaction for endosomal localization. *The Journal of biological chemistry,* 275**,** 3699-705.

LEE, B. Y., JETHWANEY, D., SCHILLING, B., CLEMENS, D. L., GIBSON, B. W. & HORWITZ, M. A. 2010. The Mycobacterium bovis bacille Calmette-Guerin phagosome proteome. *Molecular & cellular proteomics : MCP,* 9**,** 32-53.

LETEK, M., GONZALEZ, P., MACARTHUR, I., RODRIGUEZ, H., FREEMAN, T. C., VALERO-RELLO, A., BLANCO, M., BUCKLEY, T., CHEREVACH, I., FAHEY, R., HAPESHI, A., HOLDSTOCK, J., LEADON, D., NAVAS, J., OCAMPO, A., QUAIL, M. A., SANDERS, M., SCORTTI, M. M., PRESCOTT, J. F., FOGARTY, U., MEIJER, W. G., PARKHILL, J., BENTLEY, S. D. & VAZQUEZ-BOLAND, J. A. 2010. The genome of a pathogenic rhodococcus: cooptive virulence underpinned by key gene acquisitions. *PLoS genetics,* 6**,** e1001145.

LETEK, M., OCAMPO-SOSA, A. A., SANDERS, M., FOGARTY, U., BUCKLEY, T., LEADON, D. P., GONZALEZ, P., SCORTTI, M., MEIJER, W. G., PARKHILL, J., BENTLEY, S. & VAZQUEZ-BOLAND, J. A. 2008. Evolution of the Rhodococcus equi vap pathogenicity island seen through comparison of host-associated vapA and vapB virulence plasmids. *Journal of bacteriology,* 190**,** 5797-805.

LEYSEN, S., VAN HERREWEGHE, J. M., CALLEWAERT, L., HEIRBAUT, M., BUNTINX, P., MICHIELS, C. W. & STRELKOV, S. V. 2011. Molecular basis of bacterial defense against host lysozymes: X-ray structures of periplasmic lysozyme inhibitors PliI and PliC. *Journal of molecular biology,* 405**,** 1233-45.

LI, K., YANG, L., ZHANG, C., NIU, Y., LI, W. & LIU, J. J. 2014. HPS6 interacts with dynactin p150Glued to mediate retrograde trafficking and maturation of lysosomes. *Journal of cell science,* 127**,** 4574-88.

LI, X., GARRITY, A. G. & XU, H. 2013. Regulation of membrane trafficking by signalling on endosomal and lysosomal membranes. *The Journal of physiology,* 591**,** 4389-401.

LI, Z., VIZEACOUMAR, F. J., BAHR, S., LI, J., WARRINGER, J., VIZEACOUMAR, F. S., MIN, R., VANDERSLUIS, B., BELLAY, J., DEVIT, M., FLEMING, J. A., STEPHENS, A., HAASE, J., LIN, Z. Y., BARYSHNIKOVA, A., LU, H., YAN, Z., JIN, K., BARKER, S., DATTI, A., GIAEVER, G., NISLOW, C., BULAWA, C., MYERS, C. L., COSTANZO, M., GINGRAS, A. C., ZHANG, Z., BLOMBERG, A., BLOOM, K., ANDREWS, B. & BOONE, C. 2011. Systematic exploration of essential yeast gene function with temperature-sensitive mutants. *Nature biotechnology,* 29**,** 361-7.

LIANG, C., FENG, P., KU, B., DOTAN, I., CANAANI, D., OH, B. H. & JUNG, J. U. 2006. Autophagic and tumour suppressor activity of a novel Beclin1-binding protein UVRAG. *Nature Cell Biology,* 8**,** 688-99.

LIN, L., AYALA, P., LARSON, J., MULKS, M., FUKUDA, M., CARLSSON, S. R., ENNS, C. & SO, M. 1997. The Neisseria type 2 IgA1 protease cleaves LAMP1 and promotes survival of bacteria within epithelial cells. *Molecular microbiology,* 24**,** 1083-94.

LIPPE, R., MIACZYNSKA, M., RYBIN, V., RUNGE, A. & ZERIAL, M. 2001. Functional synergy between Rab5 effector Rabaptin-5 and exchange factor Rabex-5 when physically associated in a complex. *Molecular biology of the cell,* 12**,** 2219-28.

LOBINGIER, B. T. & MERZ, A. J. 2012. Sec1/Munc18 protein Vps33 binds to SNARE domains and the quaternary SNARE complex. *Molecular biology of the cell,* 23**,** 4611-22.

LOMBARDI, D., SOLDATI, T., RIEDERER, M. A., GODA, Y., ZERIAL, M. & PFEFFER, S. R. 1993. Rab9 functions in transport between late endosomes and the trans Golgi network. *The EMBO journal,* 12**,** 677-82.

LONNBRO, P., NORDENFELT, P. & TAPPER, H. 2008. Isolation of bacteria-containing phagosomes by magnetic selection. *BMC cell biology,* 9**,** 35.

LOO, Y. M. & GALE, M., JR. 2011. Immune signaling by RIG-I-like receptors. *Immunity,* 34**,** 680-92.

LOUBERY, S., WILHELM, C., HURBAIN, I., NEVEU, S., LOUVARD, D. & COUDRIER, E. 2008. Different microtubule motors move early and late endocytic compartments. *Traffic,* 9**,** 492-509.

LUHRMANN, A. & HAAS, A. 2000. A method to purify bacteria-containing phagosomes from infected macrophages. *Methods in cell science : an official journal of the Society for In Vitro Biology,* 22**,** 329-41.

LUZIO, J. P., POUPON, V., LINDSAY, M. R., MULLOCK, B. M., PIPER, R. C. & PRYOR, P. R. 2003. Membrane dynamics and the biogenesis of lysosomes. *Molecular membrane biology,* 20**,** 141-54.

MAK, I. T. & WEGLICKI, W. B. 1985. Characterization of iron-mediated peroxidative injury in isolated hepatic lysosomes. *The Journal of clinical investigation,* 75**,** 58-63.

MAKRAI, L., TAKAI, S., TAMURA, M., TSUKAMOTO, A., SEKIMOTO, R., SASAKI, Y., KAKUDA, T., TSUBAKI, S., VARGA, J., FODOR, L., SOLYMOSI, N. & MAJOR, A.

2002. Characterization of virulence plasmid types in Rhodococcus equi isolates from foals, pigs, humans and soil in Hungary. *Veterinary microbiology,* 88**,** 377-84.
MALLO, G. V., ESPINA, M., SMITH, A. C., TEREBIZNIK, M. R., ALEMAN, A., FINLAY, B. B., RAMEH, L. E., GRINSTEIN, S. & BRUMELL, J. H. 2008. SopB promotes phosphatidylinositol 3-phosphate formation on Salmonella vacuoles by recruiting Rab5 and Vps34. *The Journal of cell biology,* 182**,** 741-52.
MANOURY, B. 2013. Isolation of Phagosomes from Dentritic Cells by Using Magnetic Beads. *Bio-protocol,* 3**,** e820.
MARCUSSON, E. G., HORAZDOVSKY, B. F., CEREGHINO, J. L., GHARAKHANIAN, E. & EMR, S. D. 1994. The Sorting Receptor for Yeast Vacuolar Carboxypeptidase-Y Is Encoded by the Vps10 Gene. *Cell,* 77**,** 579-586.
MARODI, L., KAPOSZTA, R., TOTH, J. & LASZLO, A. 1995. Impaired microbicidal capacity of mononuclear phagocytes from patients with type I Gaucher disease: partial correction by enzyme replacement therapy. *Blood,* 86**,** 4645-9.
MASSON, C., CISSE, I., SIMON, V., INSALACO, P. & AUDRAN, M. 2004. Fabry disease: a review. *Joint, bone, spine : revue du rhumatisme,* 71**,** 381-3.
MATILE, P. & WIEMKEN, A. 1967. Vacuole as Lysosome of Yeast Cell. *Archiv Fur Mikrobiologie,* 56**,** 148-&.
MATSUO, H., CHEVALLIER, J., MAYRAN, N., LE BLANC, I., FERGUSON, C., FAURE, J., BLANC, N. S., MATILE, S., DUBOCHET, J., SADOUL, R., PARTON, R. G., VILBOIS, F. & GRUENBERG, J. 2004. Role of LBPA and Alix in multivesicular liposome formation and endosome organization. *Science,* 303**,** 531-4.
MATTEONI, R. & KREIS, T. E. 1987. Translocation and clustering of endosomes and lysosomes depends on microtubules. *The Journal of cell biology,* 105**,** 1253-65.
MAXFIELD, F. R. 2014. Role of endosomes and lysosomes in human disease. *Cold Spring Harbor perspectives in biology,* 6**,** a016931.
MAXFIELD, F. R. & MCGRAW, T. E. 2004. Endocytic recycling. *Nature reviews. Molecular cell biology,* 5**,** 121-32.
MAXFIELD, F. R. & YAMASHIRO, D. J. 1987. Endosome acidification and the pathways of receptor-mediated endocytosis. *Advances in experimental medicine and biology,* 225**,** 189-98.
MAY, A. P., WHITEHEART, S. W. & WEIS, W. I. 2001. Unraveling the mechanism of the vesicle transport ATPase NSF, the N-ethylmaleimide-sensitive factor. *The Journal of biological chemistry,* 276**,** 21991-4.
MAYER, A. & WICKNER, W. 1997. Docking of yeast vacuoles is catalyzed by the Ras-like GTPase Ypt7p after symmetric priming by Sec18p (NSF). *Journal of Cell Biology,* 136**,** 307-317.
MAYOR, S. & PAGANO, R. E. 2007. Pathways of clathrin-independent endocytosis. *Nature reviews. Molecular cell biology,* 8**,** 603-12.
MAYORGA, L. S., BERTINI, F. & STAHL, P. D. 1991. Fusion of newly formed phagosomes with endosomes in intact cells and in a cell-free system. *The Journal of biological chemistry,* 266**,** 6511-7.
MAZZOCCOLI, G., MAZZA, T., VINCIGUERRA, M., CASTELLANA, S. & SCARPA, M. 2015. The biological clock and the molecular basis of lysosomal storage diseases. *JIMD reports,* 18**,** 93-105.
MCBRIDE, H. M., RYBIN, V., MURPHY, C., GINER, A., TEASDALE, R. & ZERIAL, M. 1999. Oligomeric complexes link Rab5 effectors with NSF and drive membrane fusion via interactions between EEA1 and syntaxin 13. *Cell,* 98**,** 377-86.
MCCLELLAND, M., HANISH, J., NELSON, M. & PATEL, Y. 1988. KGB: a single buffer for all restriction endonucleases. *Nucleic acids research,* 16**,** 364.
MCDONOUGH, J. A., NEWTON, H. J., KLUM, S., SWISS, R., AGAISSE, H. & ROY, C. R. 2013. Host pathways important for Coxiella burnetii infection revealed by genome-wide RNA interference screening. *mBio,* 4**,** e00606-12.

MCKAY, B. E., MOLINEUX, M. L. & TURNER, R. W. 2008. Endogenous biotin in rat brain: implications for false-positive results with avidin-biotin and streptavidin-biotin techniques. *Methods in molecular biology,* 418**,** 111-28.
MEENA, L. S. & RAJNI 2010. Survival mechanisms of pathogenic Mycobacterium tuberculosis H37Rv. *The FEBS journal,* 277**,** 2416-27.
MEHRA, A., ZAHRA, A., THOMPSON, V., SIRISAENGTAKSIN, N., WELLS, A., PORTO, M., KOSTER, S., PENBERTHY, K., KUBOTA, Y., DRICOT, A., ROGAN, D., VIDAL, M., HILL, D. E., BEAN, A. J. & PHILIPS, J. A. 2013. Mycobacterium tuberculosis type VII secreted effector EsxH targets host ESCRT to impair trafficking. *PLoS pathogens,* 9**,** e1003734.
MELLMAN, I., FUCHS, R. & HELENIUS, A. 1986. Acidification of the endocytic and exocytic pathways. *Annual review of biochemistry,* 55**,** 663-700.
MERCER, J., SCHELHAAS, M. & HELENIUS, A. 2010. Virus entry by endocytosis. *Annual review of biochemistry,* 79**,** 803-33.
MILLS, I. G., JONES, A. T. & CLAGUE, M. J. 1998. Involvement of the endosomal autoantigen EEA1 in homotypic fusion of early endosomes. *Current biology : CB,* 8**,** 881-4.
MIRANDA-CASOLUENGO, R., DUFFY, P. S., O'CONNELL, E. P., GRAHAM, B. J., MANGAN, M. W., PRESCOTT, J. F. & MEIJER, W. G. 2005. The iron-regulated iupABC operon is required for saprophytic growth of the intracellular pathogen Rhodococcus equi at low iron concentrations. *Journal of bacteriology,* 187**,** 3438-44.
MISTRY, N. F., DHOLAKIA, Y., D'SOUZA, D. T., TAYLOR, M., HOFFNER, S. & BIRDI, T. J. 2006. Rhodococcus and Mycobacterium Tuberculosis: masquerade or mixed infection. *The international journal of tuberculosis and lung disease : the official journal of the International Union against Tuberculosis and Lung Disease,* 10**,** 351-3.
MITSUNARI, T., NAKATSU, F., SHIODA, N., LOVE, P. E., GRINBERG, A., BONIFACINO, J. S. & OHNO, H. 2005. Clathrin adaptor AP-2 is essential for early embryonal development. *Molecular and cellular biology,* 25**,** 9318-23.
MIURA, E., HASEGAWA, T., KONNO, M., SUZUKI, M., SUGENO, N., FUJIKAKE, N., GEISLER, S., TABUCHI, M., OSHIMA, R., KIKUCHI, A., BABA, T., WADA, K., NAGAI, Y., TAKEDA, A. & AOKI, M. 2014. VPS35 dysfunction impairs lysosomal degradation of alpha-synuclein and exacerbates neurotoxicity in a Drosophila model of Parkinson's disease. *Neurobiology of disease,* 71**,** 1-13.
MOGENSEN, T. H. 2009. Pathogen recognition and inflammatory signaling in innate immune defenses. *Clinical microbiology reviews,* 22**,** 240-73, Table of Contents.
MORITA, E., SANDRIN, V., ALAM, S. L., ECKERT, D. M., GYGI, S. P. & SUNDQUIST, W. I. 2007. Identification of human MVB12 proteins as ESCRT-I subunits that function in HIV budding. *Cell host & microbe,* 2**,** 41-53.
MOTTOLA, G., BOUCHERIT, N., TROUPLIN, V., OURY BARRY, A., SOUBEYRAN, P., MEGE, J. L. & GHIGO, E. 2014. Tropheryma whipplei, the agent of Whipple's disease, affects the early to late phagosome transition and survives in a Rab5- and Rab7-positive compartment. *PloS one,* 9**,** e89367.
MUKHERJEE, S., GHOSH, R. N. & MAXFIELD, F. R. 1997. Endocytosis. *Physiological reviews,* 77**,** 759-803.
MULLOCK, B. M., BRANCH, W. J., VAN SCHAIK, M., GILBERT, L. K. & LUZIO, J. P. 1989. Reconstitution of an endosome-lysosome interaction in a cell-free system. *The Journal of cell biology,* 108**,** 2093-9.
MULLOCK, B. M., BRIGHT, N. A., FEARON, C. W., GRAY, S. R. & LUZIO, J. P. 1998. Fusion of lysosomes with late endosomes produces a hybrid organelle of intermediate density and is NSF dependent. *The Journal of cell biology,* 140**,** 591-601.
MULLOCK, B. M., PEREZ, J. H., KUWANA, T., GRAY, S. R. & LUZIO, J. P. 1994. Lysosomes can fuse with a late endosomal compartment in a cell-free system from rat liver. *The Journal of cell biology,* 126**,** 1173-82.

MULLOCK, B. M., SMITH, C. W., IHRKE, G., BRIGHT, N. A., LINDSAY, M., PARKINSON, E. J., BROOKS, D. A., PARTON, R. G., JAMES, D. E., LUZIO, J. P. & PIPER, R. C. 2000. Syntaxin 7 is localized to late endosome compartments, associates with Vamp 8, and Is required for late endosome-lysosome fusion. *Molecular biology of the cell,* 11**,** 3137-53.

MUNOZ, P., PALOMO, J., GUINEA, J., YANEZ, J., GIANNELLA, M. & BOUZA, E. 2008. Relapsing Rhodococcus equi infection in a heart transplant recipient successfully treated with long-term linezolid. *Diagnostic microbiology and infectious disease,* 60**,** 197-9.

MURRAY, J. T., PANARETOU, C., STENMARK, H., MIACZYNSKA, M. & BACKER, J. M. 2002. Role of Rab5 in the recruitment of hVps34/p150 to the early endosome. *Traffic,* 3**,** 416-27.

MURRAY, M. Y., BIRKLAND, T. P., HOWE, J. D., ROWAN, A. D., FIDOCK, M., PARKS, W. C. & GAVRILOVIC, J. 2013. Macrophage migration and invasion is regulated by MMP10 expression. *PloS one,* 8**,** e63555.

MUSCATELLO, G., ANDERSON, G. A., GILKERSON, J. R. & BROWNING, G. F. 2006. Associations between the ecology of virulent Rhodococcus equi and the epidemiology of R. equi pneumonia on Australian thoroughbred farms. *Applied and environmental microbiology,* 72**,** 6152-60.

MYERS, B. M., PRENDERGAST, F. G., HOLMAN, R., KUNTZ, S. M. & LARUSSO, N. F. 1991. Alterations in the structure, physicochemical properties, and pH of hepatocyte lysosomes in experimental iron overload. *The Journal of clinical investigation,* 88**,** 1207-15.

NAKANAGA, T., NADEL, J. A., UEKI, I. F., KOFF, J. L. & SHAO, M. X. 2007. Regulation of interleukin-8 via an airway epithelial signaling cascade. *American journal of physiology. Lung cellular and molecular physiology,* 292**,** L1289-96.

NAKANISHI-MATSUI, M., YANO, S., MATSUMOTO, N. & FUTAI, M. 2012. Lipopolysaccharide induces multinuclear cell from RAW264.7 line with increased phagocytosis activity. *Biochemical and biophysical research communications,* 425**,** 144-9.

NAKATSU, F. & OHNO, H. 2003. Adaptor protein complexes as the key regulators of protein sorting in the post-Golgi network. *Cell structure and function,* 28**,** 419-29.

NATH, S. R., MATHEW, A. P., MOHAN, A. & ANILA, K. R. 2013. Rhodococcus equi granulomatous mastitis in an immunocompetent patient. *Journal of medical microbiology,* 62**,** 1253-5.

NAZARIAN, R., FALCON-PEREZ, J. M. & DELL'ANGELICA, E. C. 2003. Biogenesis of lysosome-related organelles complex 3 (BLOC-3): a complex containing the Hermansky-Pudlak syndrome (HPS) proteins HPS1 and HPS4. *Proceedings of the National Academy of Sciences of the United States of America,* 100**,** 8770-5.

NI, X., CANUEL, M. & MORALES, C. R. 2006. The sorting and trafficking of lysosomal proteins. *Histology and Histopathology,* 21**,** 899-913.

NICHOLS, C. D. & CASANOVA, J. E. 2010. Salmonella-directed recruitment of new membrane to invasion foci via the host exocyst complex. *Current biology : CB,* 20**,** 1316-20.

NICKERSON, D. P., WEST, M. & ODORIZZI, G. 2006. Did2 coordinates Vps4-mediated dissociation of ESCRT-III from endosomes. *Journal of Cell Biology,* 175.

NORDMANN, M., CABRERA, M., PERZ, A., BROCKER, C., OSTROWICZ, C., ENGELBRECHT-VANDRE, S. & UNGERMANN, C. 2010. The Mon1-Ccz1 complex is the GEF of the late endosomal Rab7 homolog Ypt7. *Current biology : CB,* 20**,** 1654-9.

NORDMANN, P., CHAVANET, P., CAILLON, J., DUEZ, J. M. & PORTIER, H. 1992. Recurrent pneumonia due to rifampicin-resistant Rhodococcus equi in a patient infected with HIV. *The Journal of infection,* 24**,** 104-7.

NOVIKOFF, A. B., BEAUFAY, H. & DE DUVE, C. 1956. Electron microscopy of lysosomerich fractions from rat liver. *The Journal of biophysical and biochemical cytology,* 2**,** 179-84.
ODORIZZI, G. 2006. The multiple personalities of Alix. *Journal of cell science,* 119**,** 3025-32.
ODORIZZI, G. 2015. Membrane manipulations by the ESCRT machinery. *F1000Research,* 4**,** 516.
OGAWA, M., YOSHIMORI, T., SUZUKI, T., SAGARA, H., MIZUSHIMA, N. & SASAKAWA, C. 2005. Escape of intracellular Shigella from autophagy. *Science,* 307**,** 727-31.
OH, Y. K. & SWANSON, J. A. 1996. Different fates of phagocytosed particles after delivery into macrophage lysosomes. *The Journal of cell biology,* 132**,** 585-93.
OKOKO, T., BLAGOVA, E. V., WHITTINGHAM, J. L., DOVER, L. G. & WILKINSON, A. J. 2015. Structural characterisation of the virulence-associated protein VapG from the horse pathogen Rhodococcus equi. *Veterinary microbiology*.
PALMIERI, M., IMPEY, S., KANG, H., DI RONZA, A., PELZ, C., SARDIELLO, M. & BALLABIO, A. 2011. Characterization of the CLEAR network reveals an integrated control of cellular clearance pathways. *Human molecular genetics,* 20**,** 3852-66.
PAUL, D., ACHOURI, S., YOON, Y. Z., HERRE, J., BRYANT, C. E. & CICUTA, P. 2013. Phagocytosis dynamics depends on target shape. *Biophysical journal,* 105**,** 1143-50.
PAVLOVA, A., KROVACEK, K., CIZNAR, I. & GONZALEZ-REY, C. 2006. Inhibition of mammalian cathepsins by Plesiomonas shigelloides. *Folia microbiologica,* 51**,** 393-400.
PEI, Y., DUPONT, C., SYDOR, T., HAAS, A. & PRESCOTT, J. F. 2006. Cholesterol oxidase (ChoE) is not important in the virulence of Rhodococcus equi. *Veterinary microbiology,* 118**,** 240-6.
PEI, Y., PARREIRA, V., NICHOLSON, V. M. & PRESCOTT, J. F. 2007. Mutation and virulence assessment of chromosomal genes of Rhodococcus equi 103. *Canadian journal of veterinary research = Revue canadienne de recherche veterinaire,* 71**,** 1-7.
PELLINEN, T., ARJONEN, A., VUORILUOTO, K., KALLIO, K., FRANSEN, J. A. & IVASKA, J. 2006. Small GTPase Rab21 regulates cell adhesion and controls endosomal traffic of beta1-integrins. *The Journal of cell biology,* 173**,** 767-80.
PERTOFT, H., WARMEGARD, B. & HOOK, M. 1978. Heterogeneity of lysosomes originating from rat liver parenchymal cells. Metabolic relationship of subpopulations separated by density-gradient centrifugation. *The Biochemical journal,* 174**,** 309-17.
PETERS, C. & MAYER, A. 1998. Ca2+/calmodulin signals the completion of docking and triggers a late step of vacuole fusion. *Nature,* 396**,** 575-80.
PETERS, T. J. & SEYMOUR, C. A. 1976. Acid hydrolase activities and lysosomal integrity in liver biopsies from patients with iron overload. *Clinical science and molecular medicine,* 50**,** 75-8.
PETHE, K., SWENSON, D. L., ALONSO, S., ANDERSON, J., WANG, C. & RUSSELL, D. G. 2004. Isolation of Mycobacterium tuberculosis mutants defective in the arrest of phagosome maturation. *Proceedings of the National Academy of Sciences of the United States of America,* 101**,** 13642-7.
PEYRON, P., MARIDONNEAU-PARINI, I. & STEGMANN, T. 2001. Fusion of human neutrophil phagosomes with lysosomes in vitro: involvement of tyrosine kinases of the Src family and inhibition by mycobacteria. *The Journal of biological chemistry,* 276**,** 35512-7.
PIPER, R. C. & KATZMANN, D. J. 2007. Biogenesis and function of multivesicular bodies. *Annual review of cell and developmental biology,* 23**,** 519-47.
PITT, A., MAYORGA, L. S., STAHL, P. D. & SCHWARTZ, A. L. 1992. Alterations in the protein composition of maturing phagosomes. *The Journal of clinical investigation,* 90**,** 1978-83.

PLATT, F. M., BOLAND, B. & VAN DER SPOEL, A. C. 2012. The cell biology of disease: lysosomal storage disorders: the cellular impact of lysosomal dysfunction. *The Journal of cell biology,* 199**,** 723-34.
PLATTNER, H., HENNING, R. & BRAUSER, B. 1975. Formation of triton WR 1339-filled rat liver lysosomes. II. Involvement of autophagy and of pre-existing lysosomes. *Experimental cell research,* 94**,** 377-91.
POLIDORI, M. & HAAS, A. 2006. VapI, a new member of the Rhodococcus equi Vap family. *Antonie van Leeuwenhoek,* 90**,** 299-304.
POLS, M. S., TEN BRINK, C., GOSAVI, P., OORSCHOT, V. & KLUMPERMAN, J. 2013. The HOPS proteins hVps41 and hVps39 are required for homotypic and heterotypic late endosome fusion. *Traffic,* 14**,** 219-32.
POTERYAEV, D., DATTA, S., ACKEMA, K., ZERIAL, M. & SPANG, A. 2010. Identification of the switch in early-to-late endosome transition. *Cell,* 141**,** 497-508.
PRESCOTT, J. F. 1991. Rhodococcus equi: an animal and human pathogen. *Clinical microbiology reviews,* 4**,** 20-34.
PRESS, B., FENG, Y., HOFLACK, B. & WANDINGER-NESS, A. 1998. Mutant Rab7 causes the accumulation of cathepsin D and cation-independent mannose 6-phosphate receptor in an early endocytic compartment. *The Journal of cell biology,* 140**,** 1075-89.
PRICE, A., SEALS, D., WICKNER, W. & UNGERMANN, C. 2000. The docking stage of yeast vacuole fusion requires the transfer of proteins from a cis-SNARE complex to a Rab/Ypt protein. *Journal of Cell Biology,* 148**,** 1231-1238.
PROGIDA, C., MALEROD, L., STUFFERS, S., BRECH, A., BUCCI, C. & STENMARK, H. 2007. RILP is required for the proper morphology and function of late endosomes. *Journal of cell science,* 120**,** 3729-37.
PRYOR, P. R., MULLOCK, B. M., BRIGHT, N. A., GRAY, S. R. & LUZIO, J. P. 2000. The role of intraorganellar Ca(2+) in late endosome-lysosome heterotypic fusion and in the reformation of lysosomes from hybrid organelles. *The Journal of cell biology,* 149**,** 1053-62.
PRYOR, P. R., MULLOCK, B. M., BRIGHT, N. A., LINDSAY, M. R., GRAY, S. R., RICHARDSON, S. C., STEWART, A., JAMES, D. E., PIPER, R. C. & LUZIO, J. P. 2004. Combinatorial SNARE complexes with VAMP7 or VAMP8 define different late endocytic fusion events. *EMBO reports,* 5**,** 590-5.
RAAS-ROTHSCHILD, A., CORMIER-DAIRE, V., BAO, M., GENIN, E., SALOMON, R., BREWER, K., ZEIGLER, M., MANDEL, H., TOTH, S., ROE, B., MUNNICH, A. & CANFIELD, W. M. 2000. Molecular basis of variant pseudo-hurler polydystrophy (mucolipidosis IIIC). *The Journal of clinical investigation,* 105**,** 673-81.
RABINOVITCH, M. 1995. Professional and non-professional phagocytes: an introduction. *Trends in cell biology,* 5**,** 85-7.
RABINOWITZ, S., HORSTMANN, H., GORDON, S. & GRIFFITHS, G. 1992. Immunocytochemical characterization of the endocytic and phagolysosomal compartments in peritoneal macrophages. *The Journal of cell biology,* 116**,** 95-112.
RADHAKRISHNAN, G. K. & SPLITTER, G. A. 2012. Modulation of host microtubule dynamics by pathogenic bacteria. *Biomolecular concepts,* 3**,** 571-580.
RADISKY, D. C., SNYDER, W. B., EMR, S. D. & KAPLAN, J. 1997. Characterization of VPS41, a gene required for vacuolar trafficking and high-affinity iron transport in yeast. *Proceedings of the National Academy of Sciences of the United States of America,* 94**,** 5662-5666.
RAHMAN, M. T., HERRON, L. L., KAPUR, V., MEIJER, W. G., BYRNE, B. A., REN, J., NICHOLSON, V. M. & PRESCOTT, J. F. 2003. Partial genome sequencing of Rhodococcus equi ATCC 33701. *Veterinary microbiology,* 94**,** 143-58.
RAHMAN, M. T., PARREIRA, V. & PRESCOTT, J. F. 2005. In vitro and intra-macrophage gene expression by Rhodococcus equi strain 103. *Veterinary microbiology,* 110**,** 131-40.

RAMACHANDRA, L. & HARDING, C. V. 2000. Phagosomes acquire nascent and recycling class II MHC molecules but primarily use nascent molecules in phagocytic antigen processing. *Journal of immunology,* 164**,** 5103-12.
RAMOS-MORALES, F. 2012. Impact of Salmonella enterica Type III Secretion System Effectors on the Eukaryotic Host Cell. *ISRN Cell Biology,* 2012**,** 36.
RAMOS-VIVAS, J., PILARES-ORTEGA, L., REMUZGO-MARTINEZ, S., PADILLA, D., GUTIERREZ-DIAZ, J. L. & NAVAS-MENDEZ, J. 2011. Rhodococcus equi human clinical isolates enter and survive within human alveolar epithelial cells. *Microbes and infection / Institut Pasteur,* 13**,** 438-46.
RATHMAN, M., SJAASTAD, M. D. & FALKOW, S. 1996. Acidification of phagosomes containing Salmonella typhimurium in murine macrophages. *Infection and immunity,* 64**,** 2765-73.
REINER, N. E. 2009. Methods in molecular biology. Macrophages and dendritic cells. Methods and protocols. Preface. *Methods in molecular biology,* 531**,** v-vi.
REN, J. & PRESCOTT, J. F. 2003. Analysis of virulence plasmid gene expression of intra-macrophage and in vitro grown Rhodococcus equi ATCC 33701. *Veterinary microbiology,* 94**,** 167-82.
REN, J. & PRESCOTT, J. F. 2004. The effect of mutation on Rhodococcus equi virulence plasmid gene expression and mouse virulence. *Veterinary microbiology,* 103**,** 219-30.
REN, X. F. & HURLEY, J. H. 2011. Structural basis for endosomal recruitment of ESCRT-I by ESCRT-0 in yeast. *Embo Journal,* 30**,** 2130-2139.
RESCHER, U., ZOBIACK, N. & GERKE, V. 2000. Intact Ca(2+)-binding sites are required for targeting of annexin 1 to endosomal membranes in living HeLa cells. *Journal of cell science,* 113 (Pt 22)**,** 3931-8.
RHOADES, E. R. & ULLRICH, H. J. 2000. How to establish a lasting relationship with your host: lessons learned from Mycobacterium spp. *Immunology and cell biology,* 78**,** 301-10.
RINK, J., GHIGO, E., KALAIDZIDIS, Y. & ZERIAL, M. 2005. Rab conversion as a mechanism of progression from early to late endosomes. *Cell,* 122**,** 735-749.
ROBERT, X. & GOUET, P. 2014. Deciphering key features in protein structures with the new ENDscript server. *Nucleic acids research,* 42**,** W320-4.
ROBERTS, E. A., CHUA, J., KYEI, G. B. & DERETIC, V. 2006. Higher order Rab programming in phagolysosome biogenesis. *The Journal of cell biology,* 174**,** 923-9.
ROBERTS, G. G., 3RD, PARRISH, J. R., MANGIOLA, B. A. & FINLEY, R. L., JR. 2012. High-throughput yeast two-hybrid screening. *Methods in molecular biology,* 812**,** 39-61.
ROBINSON, F. L. & DIXON, J. E. 2006. Myotubularin phosphatases: policing 3-phosphoinositides. *Trends in cell biology,* 16**,** 403-12.
ROBINSON, J. S., KLIONSKY, D. J., BANTA, L. M. & EMR, S. D. 1988. Protein sorting in Saccharomyces cerevisiae: isolation of mutants defective in the delivery and processing of multiple vacuolar hydrolases. *Molecular and cellular biology,* 8**,** 4936-48.
ROBINSON, L. J., ANIENTO, F. & GRUENBERG, J. 1997. NSF is required for transport from early to late endosomes. *Journal of cell science,* 110 (Pt 17)**,** 2079-87.
ROCHE, P. A. & FURUTA, K. 2015. The ins and outs of MHC class II-mediated antigen processing and presentation. *Nature reviews. Immunology,* 15**,** 203-16.
RODRIGUEZ, L., STIRLING, C. J. & WOODMAN, P. G. 1994. Multiple N-ethylmaleimide-sensitive components are required for endosomal vesicle fusion. *Molecular biology of the cell,* 5**,** 773-83.
RODRIGUEZ-LAZARO, D., LEWIS, D. A., OCAMPO-SOSA, A. A., FOGARTY, U., MAKRAI, L., NAVAS, J., SCORTTI, M., HERNANDEZ, M. & VAZQUEZ-BOLAND, J. A. 2006. Internally controlled real-time PCR method for quantitative species-specific detection and vapA genotyping of Rhodococcus equi. *Applied and environmental microbiology,* 72**,** 4256-63.

RODRIGUEZ-PARIS, J. M., NOLTA, K. V. & STECK, T. L. 1993. Characterization of lysosomes isolated from Dictyostelium discoideum by magnetic fractionation. *The Journal of biological chemistry,* 268**,** 9110-6.
ROGERS, L. D. & FOSTER, L. J. 2007. The dynamic phagosomal proteome and the contribution of the endoplasmic reticulum. *Proceedings of the National Academy of Sciences of the United States of America,* 104**,** 18520-5.
ROSENFELD, J. L., MOORE, R. H., ZIMMER, K. P., ALPIZAR-FOSTER, E., DAI, W. P., ZARKA, M. N. & KNOLL, B. J. 2001. Lysosome proteins are redistributed during expression of a GTP-hydrolysis-defective rab5a. *Journal of cell science,* 114**,** 4499-4508.
ROTHMAN, J. E. 1987. Transport of the vesicular stomatitis glycoprotein to trans Golgi membranes in a cell-free system. *The Journal of biological chemistry,* 262**,** 12502-10.
ROUX, K. J., KIM, D. I., RAIDA, M. & BURKE, B. 2012. A promiscuous biotin ligase fusion protein identifies proximal and interacting proteins in mammalian cells. *The Journal of cell biology,* 196**,** 801-10.
RUPPER, A., GROVE, B. & CARDELLI, J. 2001. Rab7 regulates phagosome maturation in Dictyostelium. *Journal of cell science,* 114**,** 2449-60.
RUSSELL, D. A., BYRNE, G. A., O'CONNELL, E. P., BOLAND, C. A. & MEIJER, W. G. 2004. The LysR-type transcriptional regulator VirR is required for expression of the virulence gene vapA of Rhodococcus equi ATCC 33701. *Journal of bacteriology,* 186**,** 5576-84.
RUTHERFORD, A. C., TRAER, C., WASSMER, T., PATTNI, K., BUJNY, M. V., CARLTON, J. G., STENMARK, H. & CULLEN, P. J. 2006. The mammalian phosphatidylinositol 3-phosphate 5-kinase (PIKfyve) regulates endosome-to-TGN retrograde transport. *Journal of cell science,* 119**,** 3944-3957.
SAFTIG, P., HETMAN, M., SCHMAHL, W., WEBER, K., HEINE, L., MOSSMANN, H., KOSTER, A., HESS, B., EVERS, M., VON FIGURA, K. & ET AL. 1995. Mice deficient for the lysosomal proteinase cathepsin D exhibit progressive atrophy of the intestinal mucosa and profound destruction of lymphoid cells. *The EMBO journal,* 14**,** 3599-608.
SAFTIG, P., SCHRODER, B. & BLANZ, J. 2010. Lysosomal membrane proteins: life between acid and neutral conditions. *Biochemical Society transactions,* 38**,** 1420-3.
SAKSENA, S., WAHLMAN, J., TEIS, D., JOHNSON, A. E. & EMR, S. D. 2009. Functional reconstitution of ESCRT-III assembly and disassembly. *Cell,* 136**,** 97-109.
SAKURAI, C., HASHIMOTO, H., NAKANISHI, H., ARAI, S., WADA, Y., SUN-WADA, G. H., WADA, I. & HATSUZAWA, K. 2012. SNAP-23 regulates phagosome formation and maturation in macrophages. *Molecular biology of the cell,* 23**,** 4849-63.
SAMIES, J. H., HATHAWAY, B. N., ECHOLS, R. M., VEAZEY, J. M., JR. & PILON, V. A. 1986. Lung abscess due to Corynebacterium equi. Report of the first case in a patient with acquired immune deficiency syndrome. *The American journal of medicine,* 80**,** 685-8.
SANO, H., EGUEZ, L., TERUEL, M. N., FUKUDA, M., CHUANG, T. D., CHAVEZ, J. A., LIENHARD, G. E. & MCGRAW, T. E. 2007. Rab10, a target of the AS160 Rab GAP, is required for insulin-stimulated translocation of GLUT4 to the adipocyte plasma membrane. *Cell Metabolism,* 5**,** 293-303.
SARDIELLO, M., PALMIERI, M., DI RONZA, A., MEDINA, D. L., VALENZA, M., GENNARINO, V. A., DI MALTA, C., DONAUDY, F., EMBRIONE, V., POLISHCHUK, R. S., BANFI, S., PARENTI, G., CATTANEO, E. & BALLABIO, A. 2009. A gene network regulating lysosomal biogenesis and function. *Science,* 325**,** 473-7.
SATORI, C. P., KOSTAL, V. & ARRIAGA, E. A. 2011. Individual organelle pH determinations of magnetically enriched endocytic organelles via laser-induced fluorescence detection. *Analytical chemistry,* 83**,** 7331-9.
SBRISSA, D., IKONOMOV, O. C. & SHISHEVA, A. 1999. PIKfyve, a mammalian ortholog of yeast Fab1p lipid kinase, synthesizes 5-phosphoinositides. Effect of insulin. *The Journal of biological chemistry,* 274**,** 21589-97.

SCANLON, T. C., GRAY, E. C. & GRISWOLD, K. E. 2009. Quantifying and resolving multiple vector transformants in S. cerevisiae plasmid libraries. *BMC biotechnology,* 9**,** 95.
SCHEKMAN, R. 1998. Membrane fusion. Ready...aim...fire! *Nature,* 396**,** 514-5.
SCHIFF, D. E., KLINE, L., SOLDAU, K., LEE, J. D., PUGIN, J., TOBIAS, P. S. & ULEVITCH, R. J. 1997. Phagocytosis of gram-negative bacteria by a unique CD14-dependent mechanism. *Journal of leukocyte biology,* 62**,** 786-94.
SCHMIDT, O. & TEIS, D. 2012. The ESCRT machinery. *Current Biology,* 22**,** R116-R120.
SCHNEIDER, C. A., RASBAND, W. S. & ELICEIRI, K. W. 2012. NIH Image to ImageJ: 25 years of image analysis. *Nature methods,* 9**,** 671-5.
SCHRODER, B. A., WROCKLAGE, C., HASILIK, A. & SAFTIG, P. 2010. The proteome of lysosomes. *Proteomics,* 10**,** 4053-76.
SCHUETTE, C. G., HATSUZAWA, K., MARGITTAI, M., STEIN, A., RIEDEL, D., KUSTER, P., KONIG, M., SEIDEL, C. & JAHN, R. 2004. Determinants of liposome fusion mediated by synaptic SNARE proteins. *Proceedings of the National Academy of Sciences of the United States of America,* 101**,** 2858-63.
SCHUH, A. L. & AUDHYA, A. 2014. The ESCRT machinery: from the plasma membrane to endosomes and back again. *Critical Reviews in Biochemistry and Molecular Biology,* 49**,** 242-61.
SCHWAKE, M., SCHRODER, B. & SAFTIG, P. 2013. Lysosomal membrane proteins and their central role in physiology. *Traffic,* 14**,** 739-48.
SCOTT, C. C., VACCA, F. & GRUENBERG, J. 2014. Endosome maturation, transport and functions. *Seminars in cell & developmental biology,* 31**,** 2-10.
SEABRA, M. C. 1996. Nucleotide dependence of Rab geranylgeranylation. Rab escort protein interacts preferentially with GDP-bound Rab. *The Journal of biological chemistry,* 271**,** 14398-404.
SEALS, D. F., EITZEN, G., MARGOLIS, N., WICKNER, W. T. & PRICE, A. 2000. A Ypt/Rab effector complex containing the Sec1 homolog Vps33p is required for homotypic vacuole fusion. *Proceedings of the National Academy of Sciences of the United States of America,* 97**,** 9402-9407.
SEAMAN, M. N. 2004. Cargo-selective endosomal sorting for retrieval to the Golgi requires retromer. *The Journal of cell biology,* 165**,** 111-22.
SEAMAN, M. N. 2012. The retromer complex - endosomal protein recycling and beyond. *Journal of cell science,* 125**,** 4693-702.
SEAMAN, M. N., MARCUSSON, E. G., CEREGHINO, J. L. & EMR, S. D. 1997. Endosome to Golgi retrieval of the vacuolar protein sorting receptor, Vps10p, requires the function of the VPS29, VPS30, and VPS35 gene products. *The Journal of cell biology,* 137**,** 79-92.
SEEMANN, J., WEBER, K., OSBORN, M., PARTON, R. G. & GERKE, V. 1996. The association of annexin I with early endosomes is regulated by Ca2+ and requires an intact N-terminal domain. *Molecular biology of the cell,* 7**,** 1359-74.
SEGAL, G. 2013. The Legionella pneumophila two-component regulatory systems that participate in the regulation of Icm/Dot effectors. *Current topics in microbiology and immunology,* 376**,** 35-52.
SELDEN, C., OWEN, M., HOPKINS, J. M. & PETERS, T. J. 1980. Studies on the concentration and intracellular localization of iron proteins in liver biopsy specimens from patients with iron overload with special reference to their role in lysosomal disruption. *British journal of haematology,* 44**,** 593-603.
SETTEMBRE, C., DI MALTA, C., POLITO, V. A., GARCIA ARENCIBIA, M., VETRINI, F., ERDIN, S., ERDIN, S. U., HUYNH, T., MEDINA, D., COLELLA, P., SARDIELLO, M., RUBINSZTEIN, D. C. & BALLABIO, A. 2011. TFEB links autophagy to lysosomal biogenesis. *Science,* 332**,** 1429-33.
SHAPIRO, E. M., SKRTIC, S. & KORETSKY, A. P. 2005. Sizing it up: cellular MRI using micron-sized iron oxide particles. *Magnetic resonance in medicine,* 53**,** 329-38.

SHIN, M. S., COOPER, J. A., JR. & HO, K. J. 1999. Pulmonary malacoplakia associated with Rhodococcus equi infection in a patient with AIDS. *Chest,* 115**,** 889-92.
SHOHDY, N., EFE, J. A., EMR, S. D. & SHUMAN, H. A. 2005. Pathogen effector protein screening in yeast identifies Legionella factors that interfere with membrane trafficking. *Proceedings of the National Academy of Sciences of the United States of America,* 102**,** 4866-71.
SHORT, C. R., MAINES, M. D. & DAVIS, L. E. 1972. Preparation of hepatic microsomal fraction for drug metabolism studies by rapid decompression homogenization. *Proceedings of the Society for Experimental Biology and Medicine. Society for Experimental Biology and Medicine,* 140**,** 58-65.
SIINTOLA, E., PARTANEN, S., STROMME, P., HAAPANEN, A., HALTIA, M., MAEHLEN, J., LEHESJOKI, A. E. & TYYNELA, J. 2006. Cathepsin D deficiency underlies congenital human neuronal ceroid-lipofuscinosis. *Brain : a journal of neurology,* 129**,** 1438-45.
SIMONSEN, A., GAULLIER, J. M., D'ARRIGO, A. & STENMARK, H. 1999. The Rab5 effector EEA1 interacts directly with syntaxin-6. *The Journal of biological chemistry,* 274**,** 28857-60.
SIMONSEN, A., LIPPE, R., CHRISTOFORIDIS, S., GAULLIER, J. M., BRECH, A., CALLAGHAN, J., TOH, B. H., MURPHY, C., ZERIAL, M. & STENMARK, H. 1998. EEA1 links PI(3)K function to Rab5 regulation of endosome fusion. *Nature,* 394**,** 494-8.
SIMPSON, J. C., GRIFFITHS, G., WESSLING-RESNICK, M., FRANSEN, J. A., BENNETT, H. & JONES, A. T. 2004. A role for the small GTPase Rab21 in the early endocytic pathway. *Journal of cell science,* 117**,** 6297-311.
SIMPSON, R. J. 2010. Disruption of cultured cells by nitrogen cavitation. *Cold Spring Harbor protocols,* 2010**,** pdb prot5513.
SINGH, V., JAMWAL, S., JAIN, R., VERMA, P., GOKHALE, R. & RAO, K. V. 2012. Mycobacterium tuberculosis-driven targeted recalibration of macrophage lipid homeostasis promotes the foamy phenotype. *Cell host & microbe,* 12**,** 669-81.
SKLOWER, S. L., JENKINS, E. C., ANDERSON, M. L., CHAN, C. B. & BROWN, W. T. 1986. Variability of Thymidylate Synthase Activity in Whole-Blood Cultures Treated with Fudr. *American Journal of Medical Genetics,* 23**,** 483-490.
SLABICKI, M., THEIS, M., KRASTEV, D. B., SAMSONOV, S., MUNDWILLER, E., JUNQUEIRA, M., PASZKOWSKI-ROGACZ, M., TEYRA, J., HENINGER, A. K., POSER, I., PRIEUR, F., TRUCHETTO, J., CONFAVREUX, C., MARELLI, C., DURR, A., CAMDESSANCHE, J. P., BRICE, A., SHEVCHENKO, A., PISABARRO, M. T., STEVANIN, G. & BUCHHOLZ, F. 2010. A genome-scale DNA repair RNAi screen identifies SPG48 as a novel gene associated with hereditary spastic paraplegia. *PLoS biology,* 8**,** e1000408.
SLAGOWSKI, N. L., KRAMER, R. W., MORRISON, M. F., LABAER, J. & LESSER, C. F. 2008. A functional genomic yeast screen to identify pathogenic bacterial proteins. *PLoS pathogens,* 4**,** e9.
SLAGSVOLD, T., AASLAND, R., HIRANO, S., BACHE, K. G., RAIBORG, C., TRAMBAIOLO, D., WAKATSUKI, S. & STENMARK, H. 2005. Eap45 in mammalian ESCRT-II binds ubiquitin via a phosphoinositide-interacting GLUE domain. *Journal of Biological Chemistry,* 280**,** 19600-19606.
SOHN, Y. S., SHIN, H. C., PARK, W. S., GE, J., KIM, C. H., LEE, B. L., HEO, W. D., JUNG, J. U., RIGDEN, D. J. & OH, B. H. 2015. Lpg0393 of Legionella pneumophila is a guanine-nucleotide exchange factor for Rab5, Rab21 and Rab22. *PloS one,* 10**,** e0118683.
SOLINGER, J. A. & SPANG, A. 2013. Tethering complexes in the endocytic pathway: CORVET and HOPS. *The FEBS journal,* 280**,** 2743-57.

SOLLNER, T., WHITEHEART, S. W., BRUNNER, M., ERDJUMENT-BROMAGE, H., GEROMANOS, S., TEMPST, P. & ROTHMAN, J. E. 1993. SNAP receptors implicated in vesicle targeting and fusion. *Nature,* 362**,** 318-24.
SONG, W., WANG, F., SAVINI, M., AKE, A., DI RONZA, A., SARDIELLO, M. & SEGATORI, L. 2013. TFEB regulates lysosomal proteostasis. *Human molecular genetics,* 22**,** 1994-2009.
SPARROW, J. R., KIM, S. R., CUERVO, A. M. & BANDHYOPADHYAYAND, U. 2008. A2E, a pigment of RPE lipofuscin, is generated from the precursor, A2PE by a lysosomal enzyme activity. *Advances in experimental medicine and biology,* 613**,** 393-8.
SRIKANTH, C. V., MERCADO-LUBO, R., HALLSTROM, K. & MCCORMICK, B. A. 2011. Salmonella effector proteins and host-cell responses. *Cellular and molecular life sciences : CMLS,* 68**,** 3687-97.
STARAI, V. J., HICKEY, C. M. & WICKNER, W. 2008. HOPS proofreads the trans-SNARE complex for yeast vacuole fusion. *Molecular biology of the cell,* 19**,** 2500-8.
STEELE-MORTIMER, O., MERESSE, S., GORVEL, J. P., TOH, B. H. & FINLAY, B. B. 1999. Biogenesis of Salmonella typhimurium-containing vacuoles in epithelial cells involves interactions with the early endocytic pathway. *Cellular microbiology,* 1**,** 33-49.
STEIN, M. P., FENG, Y., COOPER, K. L., WELFORD, A. M. & WANDINGER-NESS, A. 2003. Human VPS34 and p150 are Rab7 interacting partners. *Traffic,* 4**,** 754-71.
STEINER, D. J., FURUYA, Y. & METZGER, D. W. 2014. Host-pathogen interactions and immune evasion strategies in Francisella tularensis pathogenicity. *Infection and drug resistance,* 7**,** 239-51.
STEINFELD, R., REINHARDT, K., SCHREIBER, K., HILLEBRAND, M., KRAETZNER, R., BRUCK, W., SAFTIG, P. & GARTNER, J. 2006. Cathepsin D deficiency is associated with a human neurodegenerative disorder. *American journal of human genetics,* 78**,** 988-98.
STEINGRIMSSON, E., COPELAND, N. G. & JENKINS, N. A. 2004. Melanocytes and the microphthalmia transcription factor network. *Annual review of genetics,* 38**,** 365-411.
STEINHAUSER, C., HEIGL, U., TCHIKOV, V., SCHWARZ, J., GUTSMANN, T., SEEGER, K., BRANDENBURG, J., FRITSCH, J., SCHROEDER, J., WIESMULLER, K. H., ROSENKRANDS, I., WALTHER, P., POTT, J., KRAUSE, E., EHLERS, S., SCHNEIDER-BRACHERT, W., SCHUTZE, S. & REILING, N. 2013. Lipid-labeling facilitates a novel magnetic isolation procedure to characterize pathogen-containing phagosomes. *Traffic,* 14**,** 321-36.
STEINMAN, R. M., BRODIE, S. E. & COHN, Z. A. 1976. Membrane flow during pinocytosis. A stereologic analysis. *The Journal of cell biology,* 68**,** 665-87.
STEINMAN, R. M., MELLMAN, I. S., MULLER, W. A. & COHN, Z. A. 1983. Endocytosis and the recycling of plasma membrane. *The Journal of cell biology,* 96**,** 1-27.
STENMARK, H., AASLAND, R., TOH, B. H. & D'ARRIGO, A. 1996. Endosomal localization of the autoantigen EEA1 is mediated by a zinc-binding FYVE finger. *The Journal of biological chemistry,* 271**,** 24048-54.
STENMARK, H., VITALE, G., ULLRICH, O. & ZERIAL, M. 1995. Rabaptin-5 is a direct effector of the small GTPase Rab5 in endocytic membrane fusion. *Cell,* 83**,** 423-32.
STORRIE, B. & DESJARDINS, M. 1996. The biogenesis of lysosomes: is it a kiss and run, continuous fusion and fission process? *BioEssays : news and reviews in molecular, cellular and developmental biology,* 18**,** 895-903.
STRASSER, B., IWASZKIEWICZ, J., MICHIELIN, O. & MAYER, A. 2011. The V-ATPase proteolipid cylinder promotes the lipid-mixing stage of SNARE-dependent fusion of yeast vacuoles. *The EMBO journal,* 30**,** 4126-41.
STROUPE, C., COLLINS, K. M., FRATTI, R. A. & WICKNER, W. 2006. Purification of active HOPS complex reveals its affinities for phosphoinositides and the SNARE Vam7p. *The EMBO journal,* 25**,** 1579-89.

STRYER, L. 1978. Fluorescence energy transfer as a spectroscopic ruler. *Annual review of biochemistry,* 47**,** 819-46.
SUN, J., SINGH, V., LAU, A., STOKES, R. W., OBREGON-HENAO, A., ORME, I. M., WONG, D., AV-GAY, Y. & HMAMA, Z. 2013. Mycobacterium tuberculosis nucleoside diphosphate kinase inactivates small GTPases leading to evasion of innate immunity. *PLoS pathogens,* 9**,** e1003499.
SUN, Q., WESTPHAL, W., WONG, K. N., TAN, I. & ZHONG, Q. 2010. Rubicon controls endosome maturation as a Rab7 effector. *Proceedings of the National Academy of Sciences of the United States of America,* 107**,** 19338-43.
SUPEK, F., SUPEKOVA, L., MANDIYAN, S., PAN, Y. C., NELSON, H. & NELSON, N. 1994. A novel accessory subunit for vacuolar H(+)-ATPase from chromaffin granules. *The Journal of biological chemistry,* 269**,** 24102-6.
SUTCLIFFE, I. C. 1998. Cell envelope composition and organisation in the genus Rhodococcus. *Antonie van Leeuwenhoek,* 74**,** 49-58.
SUTTON, R. B., FASSHAUER, D., JAHN, R. & BRUNGER, A. T. 1998. Crystal structure of a SNARE complex involved in synaptic exocytosis at 2.4 A resolution. *Nature,* 395**,** 347-53.
SWANSON, J., BUSHNELL, A. & SILVERSTEIN, S. C. 1987. Tubular lysosome morphology and distribution within macrophages depend on the integrity of cytoplasmic microtubules. *Proceedings of the National Academy of Sciences of the United States of America,* 84**,** 1921-5.
SYDOR, T., VON BARGEN, K., BECKEN, U., SPUERCK, S., NICHOLSON, V. M., PRESCOTT, J. F. & HAAS, A. 2008. A mycolyl transferase mutant of Rhodococcus equi lacking capsule integrity is fully virulent. *Veterinary microbiology,* 128**,** 327-41.
SYDOR, T., VON BARGEN, K., HSU, F. F., HUTH, G., HOLST, O., WOHLMANN, J., BECKEN, U., DYKSTRA, T., SOHL, K., LINDNER, B., PRESCOTT, J. F., SCHAIBLE, U. E., UTERMOHLEN, O. & HAAS, A. 2013. Diversion of phagosome trafficking by pathogenic Rhodococcus equi depends on mycolic acid chain length. *Cellular microbiology,* 15**,** 458-73.
TABUCHI, M., KAWAI, Y., NISHIE-FUJITA, M., AKADA, R., IZUMI, T., YANATORI, I., MIYASHITA, N., OUCHI, K. & KISHI, F. 2009. Development of a novel functional high-throughput screening system for pathogen effectors in the yeast Saccharomyces cerevisiae. *Bioscience, biotechnology, and biochemistry,* 73**,** 2261-7.
TAKAI, S., FUKUNAGA, N., KAMISAWA, K., IMAI, Y., SASAKI, Y. & TSUBAKI, S. 1996a. Expression of virulence-associated antigens of Rhodococcus equi is regulated by temperature and pH. *Microbiology and immunology,* 40**,** 591-4.
TAKAI, S., FUKUNAGA, N., OCHIAI, S., IMAI, Y., SASAKI, Y., TSUBAKI, S. & SEKIZAKI, T. 1996b. Identification of intermediately virulent Rhodococcus equi isolates from pigs. *Journal of clinical microbiology,* 34**,** 1034-7.
TAKAI, S., HINES, S. A., SEKIZAKI, T., NICHOLSON, V. M., ALPERIN, D. A., OSAKI, M., TAKAMATSU, D., NAKAMURA, M., SUZUKI, K., OGINO, N., KAKUDA, T., DAN, H. & PRESCOTT, J. F. 2000. DNA sequence and comparison of virulence plasmids from Rhodococcus equi ATCC 33701 and 103. *Infection and immunity,* 68**,** 6840-7.
TAKAI, S., IKEDA, T., SASAKI, Y., WATANABE, Y., OZAWA, T., TSUBAKI, S. & SEKIZAKI, T. 1995. Identification of virulent Rhodococcus equi by amplification of gene coding for 15- to 17-kilodalton antigens. *Journal of clinical microbiology,* 33**,** 1624-7.
TAKAI, S., SEKIZAKI, T., OZAWA, T., SUGAWARA, T., WATANABE, Y. & TSUBAKI, S. 1991. Association between a large plasmid and 15- to 17-kilodalton antigens in virulent Rhodococcus equi. *Infection and immunity,* 59**,** 4056-60.
TAKAI, S., SUGAWARA, T., WATANABE, Y., SASAKI, Y., TSUBAKI, S. & SEKIZAKI, T. 1994. Effect of growth temperature on maintenance of virulent Rhodococcus equi. *Veterinary microbiology,* 39**,** 187-92.

TAKIKITA, S., MYEROWITZ, R., SCHREINER, C., BAUM, R., RABEN, N. & PLOTZ, P. H. 2009. The values and limits of an in vitro model of Pompe disease: the best laid schemes o' mice an' men. *Autophagy,* 5**,** 729-31.

TAN, C., PRESCOTT, J. F., PATTERSON, M. C. & NICHOLSON, V. M. 1995. Molecular characterization of a lipid-modified virulence-associated protein of Rhodococcus equi and its potential in protective immunity. *Canadian journal of veterinary research = Revue canadienne de recherche veterinaire,* 59**,** 51-9.

TAN, G., CHEN, M., FOOTE, C. & TAN, C. 2009. Temperature-sensitive mutations made easy: generating conditional mutations by using temperature-sensitive inteins that function within different temperature ranges. *Genetics,* 183**,** 13-22.

TEIS, D., SAKSENA, S. & EMR, S. D. 2008. Ordered assembly of the ESCRT-III complex on endosomes is required to sequester cargo during MVB formation. *Developmental cell,* 15**,** 578-89.

TEIS, D., SAKSENA, S., JUDSON, B. L. & EMR, S. D. 2010. ESCRT-II coordinates the assembly of ESCRT-III filaments for cargo sorting and multivesicular body vesicle formation. *Embo Journal,* 29**,** 871-883.

TEREBIZNIK, M. R., VIEIRA, O. V., MARCUS, S. L., SLADE, A., YIP, C. M., TRIMBLE, W. S., MEYER, T., FINLAY, B. B. & GRINSTEIN, S. 2002. Elimination of host cell PtdIns(4,5)P(2) by bacterial SigD promotes membrane fission during invasion by Salmonella. *Nature Cell Biology,* 4**,** 766-73.

THAKUR, R., SARMA, S. & GOYAL, R. 2011. Comparison of DNA Extraction Protocols for Mycobacterium Tuberculosis in Diagnosis of Tuberculous Meningitis by Real-time Polymerase Chain Reaction. *Journal of global infectious diseases,* 3**,** 353-6.

THI, E. P., HONG, C. J., SANGHERA, G. & REINER, N. E. 2013. Identification of the Mycobacterium tuberculosis protein PE-PGRS62 as a novel effector that functions to block phagosome maturation and inhibit iNOS expression. *Cellular microbiology,* 15**,** 795-808.

THI, E. P., LAMBERTZ, U. & REINER, N. E. 2012. Class IA phosphatidylinositol 3-kinase p110alpha regulates phagosome maturation. *PloS one,* 7**,** e43668.

THIELE, L., MERKLE, H. P. & WALTER, E. 2003. Phagocytosis and phagosomal fate of surface-modified microparticles in dendritic cells and macrophages. *Pharmaceutical research,* 20**,** 221-8.

THOENE, J. G. 1992. *Pathophysiology of lysosomal transport,* Boca Raton, CRC Press.

THOMAS, C. A., LI, Y., KODAMA, T., SUZUKI, H., SILVERSTEIN, S. C. & EL KHOURY, J. 2000. Protection from lethal gram-positive infection by macrophage scavenger receptor-dependent phagocytosis. *The Journal of experimental medicine,* 191**,** 147-56.

THORESEN, S. B., PEDERSEN, N. M., LIESTOL, K. & STENMARK, H. 2010. A phosphatidylinositol 3-kinase class III sub-complex containing VPS15, VPS34, Beclin 1, UVRAG and BIF-1 regulates cytokinesis and degradative endocytic traffic. *Experimental cell research,* 316**,** 3368-78.

TINDALL, B. J. 2014. The correct name of the taxon that contains the type strain of Rhodococcus equi. *International journal of systematic and evolutionary microbiology,* 64**,** 302-8.

TJELLE, T. E., BRECH, A., JUVET, L. K., GRIFFITHS, G. & BERG, T. 1996. Isolation and characterization of early endosomes, late endosomes and terminal lysosomes: their role in protein degradation. *Journal of cell science,* 109 (Pt 12)**,** 2905-14.

TKACHUK-SAAD, O. & PRESCOTT, J. 1991. Rhodococcus equi plasmids: isolation and partial characterization. *Journal of clinical microbiology,* 29**,** 2696-700.

TOPINO, S., GALATI, V., GRILLI, E. & PETROSILLO, N. 2010. Rhodococcus equi infection in HIV-infected individuals: case reports and review of the literature. *AIDS patient care and STDs,* 24**,** 211-22.

TOYOOKA, K., TAKAI, S. & KIRIKAE, T. 2005. Rhodococcus equi can survive a phagolysosomal environment in macrophages by suppressing acidification of the phagolysosome. *Journal of medical microbiology,* 54**,** 1007-15.
TSUJITA, K., ITOH, T., IJUIN, T., YAMAMOTO, A., SHISHEVA, A., LAPORTE, J. & TAKENAWA, T. 2004. Myotubularin regulates the function of the late endosome through the gram domain-phosphatidylinositol 3,5-bisphosphate interaction. *The Journal of biological chemistry,* 279**,** 13817-24.
TZELEPIS, F., VERWAY, M., DAOUD, J., GILLARD, J., HASSANI-ARDAKANI, K., DUNN, J., DOWNEY, J., GENTILE, M. E., JAWORSKA, J., SANCHEZ, A. M., NEDELEC, Y., VALI, H., TABRIZIAN, M., KRISTOF, A. S., KING, I. L., BARREIRO, L. B. & DIVANGAHI, M. 2015. Annexin1 regulates DC efferocytosis and cross-presentation during Mycobacterium tuberculosis infection. *The Journal of clinical investigation,* 125**,** 752-68.
UNGERMANN, C., SATO, K. & WICKNER, W. 1998. Defining the functions of trans-SNARE pairs. *Nature,* 396**,** 543-8.
UNGERMANN, C., WICKNER, W. & XU, Z. 1999. Vacuole acidification is required for trans-SNARE pairing, LMA1 release, and homotypic fusion. *Proceedings of the National Academy of Sciences of the United States of America,* 96**,** 11194-9.
URBE, S., MILLS, I. G., STENMARK, H., KITAMURA, N. & CLAGUE, M. J. 2000. Endosomal localization and receptor dynamics determine tyrosine phosphorylation of hepatocyte growth factor-regulated tyrosine kinase substrate. *Molecular and cellular biology,* 20**,** 7685-7692.
VACCARI, T., DUCHI, S., CORTESE, K., TACCHETTI, C. & BILDER, D. 2010. The vacuolar ATPase is required for physiological as well as pathological activation of the Notch receptor. *Development,* 137**,** 1825-32.
VALLS, L. A., HUNTER, C. P., ROTHMAN, J. H. & STEVENS, T. H. 1987. Protein sorting in yeast: the localization determinant of yeast vacuolar carboxypeptidase Y resides in the propeptide. *Cell,* 48**,** 887-97.
VALLS, L. A., WINTHER, J. R. & STEVENS, T. H. 1990. Yeast Carboxypeptidase-Y Vacuolar Targeting Signal Is Defined by 4 Propeptide Amino-Acids. *Journal of Cell Biology,* 111**,** 361-368.
VAN DER KANT, R., FISH, A., JANSSEN, L., JANSSEN, H., KROM, S., HO, N., BRUMMELKAMP, T., CARETTE, J., ROCHA, N. & NEEFJES, J. 2013. Late endosomal transport and tethering are coupled processes controlled by RILP and the cholesterol sensor ORP1L. *Journal of cell science,* 126**,** 3462-74.
VANLANDINGHAM, P. A. & CERESA, B. P. 2009. Rab7 regulates late endocytic trafficking downstream of multivesicular body biogenesis and cargo sequestration. *The Journal of biological chemistry,* 284**,** 12110-24.
VAZQUEZ-BOLAND, J. A., GIGUERE, S., HAPESHI, A., MACARTHUR, I., ANASTASI, E. & VALERO-RELLO, A. 2013. Rhodococcus equi: The many facets of a pathogenic actinomycete. *Veterinary microbiology*.
VEITCH, N. C. 2004. Horseradish peroxidase: a modern view of a classic enzyme. *Phytochemistry,* 65**,** 249-59.
VENUGOPAL, B., MESIRES, N. T., KENNEDY, J. C., CURCIO-MORELLI, C., LAPLANTE, J. M., DICE, J. F. & SLAUGENHAUPT, S. A. 2009. Chaperone-mediated autophagy is defective in mucolipidosis type IV. *Journal of cellular physiology,* 219**,** 344-53.
VERGNE, I., CHUA, J. & DERETIC, V. 2003. Tuberculosis toxin blocking phagosome maturation inhibits a novel Ca2+/calmodulin-PI3K hVPS34 cascade. *The Journal of experimental medicine,* 198**,** 653-9.
VERGNE, I., CHUA, J., LEE, H. H., LUCAS, M., BELISLE, J. & DERETIC, V. 2005. Mechanism of phagolysosome biogenesis block by viable Mycobacterium tuberculosis. *Proceedings of the National Academy of Sciences of the United States of America,* 102**,** 4033-8.

VERNET, T., DIGNARD, D. & THOMAS, D. Y. 1987. A family of yeast expression vectors containing the phage f1 intergenic region. *Gene,* 52**,** 225-33.
VIDA, T. A. & EMR, S. D. 1995. A New Vital Stain for Visualizing Vacuolar Membrane Dynamics and Endocytosis in Yeast. *Journal of Cell Biology,* 128**,** 779-792.
VIEIRA, O. V., BOTELHO, R. J. & GRINSTEIN, S. 2002. Phagosome maturation: aging gracefully. *The Biochemical journal,* 366**,** 689-704.
VIEIRA, O. V., BOTELHO, R. J., RAMEH, L., BRACHMANN, S. M., MATSUO, T., DAVIDSON, H. W., SCHREIBER, A., BACKER, J. M., CANTLEY, L. C. & GRINSTEIN, S. 2001. Distinct roles of class I and class III phosphatidylinositol 3-kinases in phagosome formation and maturation. *The Journal of cell biology,* 155**,** 19-25.
VIEIRA, O. V., BUCCI, C., HARRISON, R. E., TRIMBLE, W. S., LANZETTI, L., GRUENBERG, J., SCHREIBER, A. D., STAHL, P. D. & GRINSTEIN, S. 2003. Modulation of Rab5 and Rab7 recruitment to phagosomes by phosphatidylinositol 3-kinase. *Molecular and cellular biology,* 23**,** 2501-14.
VINH, D. B., KO, D. C., RACHUBINSKI, R. A., AITCHISON, J. D. & MILLER, S. I. 2010. Expression of the Salmonella spp. virulence factor SifA in yeast alters Rho1 activity on peroxisomes. *Molecular biology of the cell,* 21**,** 3567-77.
VITELLI, R., SANTILLO, M., LATTERO, D., CHIARIELLO, M., BIFULCO, M., BRUNI, C. B. & BUCCI, C. 1997. Role of the small GTPase Rab7 in the late endocytic pathway. *The Journal of biological chemistry,* 272**,** 4391-7.
VOGT, J. & SCHULZ, G. E. 1999. The structure of the outer membrane protein OmpX from Escherichia coli reveals possible mechanisms of virulence. *Structure,* 7**,** 1301-9.
VON BARGEN, K. & HAAS, A. 2009. Molecular and infection biology of the horse pathogen Rhodococcus equi. *FEMS microbiology reviews,* 33**,** 870-91.
WAHAJUDDIN & ARORA, S. 2012. Superparamagnetic iron oxide nanoparticles: magnetic nanoplatforms as drug carriers. *International journal of nanomedicine,* 7**,** 3445-71.
WALKER, M. W. & LLOYD-EVANS, E. 2015. A rapid method for the preparation of ultrapure, functional lysosomes using functionalized superparamagnetic iron oxide nanoparticles. *Methods in cell biology,* 126**,** 21-43.
WALKLEY, S. U. & VANIER, M. T. 2009. Secondary lipid accumulation in lysosomal disease. *Biochimica et biophysica acta,* 1793**,** 726-36.
WANG, X., COULSON, G. B., MIRANDA-CASOLUENGO, A. A., MIRANDA-CASOLUENGO, R., HONDALUS, M. K. & MEIJER, W. G. 2014. IcgA is a virulence factor of Rhodococcus equi that modulates intracellular growth. *Infection and immunity,* 82**,** 1793-800.
WARD, D. M., LESLIE, J. D. & KAPLAN, J. 1997. Homotypic lysosome fusion in macrophages: analysis using an in vitro assay. *The Journal of cell biology,* 139**,** 665-73.
WATTENBERG, B. W., RAUB, T. J., HIEBSCH, R. R. & WEIDMAN, P. J. 1992. The activity of Golgi transport vesicles depends on the presence of the N-ethylmaleimide-sensitive factor (NSF) and a soluble NSF attachment protein (alpha SNAP) during vesicle formation. *The Journal of cell biology,* 118**,** 1321-32.
WATTIAUX, R., WATTIAUX-DE CONINCK, S., RONVEAUX-DUPAL, M. F. & DUBOIS, F. 1978. Isolation of rat liver lysosomes by isopycnic centrifugation in a metrizamide gradient. *The Journal of cell biology,* 78**,** 349-68.
WATTIAUX, R., WIBO, M. & BAUDHUIN, P. 1963. [Effect of the injection of Triton WR 1339 on the hepatic lysosomes of the rat]. *Archives internationales de physiologie et de biochimie,* 71**,** 140-2.
WAYMOUTH, C. 1970. Osmolality of mammalian blood and of media for culture of mammalian cells. *In vitro,* 6**,** 109-27.

WEBER, T., ZEMELMAN, B. V., MCNEW, J. A., WESTERMANN, B., GMACHL, M., PARLATI, F., SOLLNER, T. H. & ROTHMAN, J. E. 1998. SNAREpins: minimal machinery for membrane fusion. *Cell,* 92**,** 759-72.

WEGLICKI, W. B., RUTH, R. C. & OWENS, K. 1973. Changes in lipid composition of tritosomes during lysis. *Biochemical and biophysical research communications,* 51**,** 1077-82.

WEGNER, C. S., MALEROD, L., PEDERSEN, N. M., PROGIDA, C., BAKKE, O., STENMARK, H. & BRECH, A. 2010. Ultrastructural characterization of giant endosomes induced by GTPase-deficient Rab5. *Histochemistry and cell biology,* 133**,** 41-55.

WEINSTOCK, D. M. & BROWN, A. E. 2002. Rhodococcus equi: an emerging pathogen. *Clinical infectious diseases : an official publication of the Infectious Diseases Society of America,* 34**,** 1379-85.

WEISMAN, R. A. & KORN, E. D. 1967. Phagocytosis of latex beads by Acanthamoeba. I. Biochemical properties. *Biochemistry,* 6**,** 485-97.

WENDLER, F. & TOOZE, S. 2001. Syntaxin 6: the promiscuous behaviour of a SNARE protein. *Traffic,* 2**,** 606-11.

WHITLEY, P., REAVES, B. J., HASHIMOTO, M., RILEY, A. M., POTTER, B. V. & HOLMAN, G. D. 2003. Identification of mammalian Vps24p as an effector of phosphatidylinositol 3,5-bisphosphate-dependent endosome compartmentalization. *The Journal of biological chemistry,* 278**,** 38786-95.

WHITTINGHAM, J. L., BLAGOVA, E. V., FINN, C. E., LUO, H., MIRANDA-CASOLUENGO, R., TURKENBURG, J. P., LEECH, A. P., WALTON, P. H., MURZIN, A. G., MEIJER, W. G. & WILKINSON, A. J. 2014. Structure of the virulence-associated protein VapD from the intracellular pathogen Rhodococcus equi. *Acta crystallographica. Section D, Biological crystallography,* 70**,** 2139-51.

WICHMANN, H., DISELA, C., HAUBRUCK, H. & GALLWITZ, D. 1989. Nucleotide-Sequence of the Mouse Yptl Gene Encoding a Ras-Related Gtp-Binding Protein. *Nucleic acids research,* 17**,** 6737-6738.

WILCKE, M., JOHANNES, L., GALLI, T., MAYAU, V., GOUD, B. & SALAMERO, J. 2000. Rab11 regulates the compartmentalization of early endosomes required for efficient transport from early endosomes to the trans-golgi network. *The Journal of cell biology,* 151**,** 1207-20.

WILSON, J., HUYNH, C., KENNEDY, K. A., WARD, D. M., KAPLAN, J., ADEREM, A. & ANDREWS, N. W. 2008. Control of parasitophorous vacuole expansion by LYST/Beige restricts the intracellular growth of Leishmania amazonensis. *PLoS pathogens,* 4**,** e1000179.

WOLLERT, T., WUNDER, C., LIPPINCOTT-SCHWARTZ, J. & HURLEY, J. H. 2009. Membrane scission by the ESCRT-III complex. *Nature,* 458**,** 172-7.

WONG, D., BACH, H., SUN, J., HMAMA, Z. & AV-GAY, Y. 2011. Mycobacterium tuberculosis protein tyrosine phosphatase (PtpA) excludes host vacuolar-H+-ATPase to inhibit phagosome acidification. *Proceedings of the National Academy of Sciences of the United States of America,* 108**,** 19371-6.

WONG, D., CHAO, J. D. & AV-GAY, Y. 2013. Mycobacterium tuberculosis-secreted phosphatases: from pathogenesis to targets for TB drug development. *Trends in microbiology,* 21**,** 100-9.

WRIGHT, S. D., REDDY, P. A., JONG, M. T. & ERICKSON, B. W. 1987. C3bi receptor (complement receptor type 3) recognizes a region of complement protein C3 containing the sequence Arg-Gly-Asp. *Proceedings of the National Academy of Sciences of the United States of America,* 84**,** 1965-8.

WU, Y., TIBREWAL, N. & BIRGE, R. B. 2006. Phosphatidylserine recognition by phagocytes: a view to a kill. *Trends in cell biology,* 16**,** 189-97.

WUBBOLTS, R., FERNANDEZ-BORJA, M., JORDENS, I., REITS, E., DUSSELJEE, S., ECHEVERRI, C., VALLEE, R. B. & NEEFJES, J. 1999. Opposing motor activities of dynein and kinesin determine retention and transport of MHC class II-containing compartments. *Journal of cell science,* 112 (Pt 6)**,** 785-95.

WURMSER, A. E., SATO, T. K. & EMR, S. D. 2000. New component of the vacuolar class C-Vps complex couples nucleotide exchange on the Ypt7 GTPase to SNARE-dependent docking and fusion. *Journal of Cell Biology,* 151**,** 551-562.

YAGER, J. A., DUDER, C. K., PRESCOTT, J. F. & ZINK, M. C. 1987. The interaction of Rhodococcus equi and foal neutrophils in vitro. *Veterinary microbiology,* 14**,** 287-94.

YAGER, J. A., PRESCOTT, C. A., KRAMAR, D. P., HANNAH, H., BALSON, G. A. & CROY, B. A. 1991. The effect of experimental infection with Rhodococcus equi on immunodeficient mice. *Veterinary microbiology,* 28**,** 363-76.

YAMAMOTO, A., DEWALD, D. B., BORONENKOV, I. V., ANDERSON, R. A., EMR, S. D. & KOSHLAND, D. 1995. Novel Pi(4)P 5-Kinase Homolog, Fab1p, Essential for Normal Vacuole Function and Morphology in Yeast. *Molecular biology of the cell,* 6**,** 525-539.

YAMASHIRO, D. J., TYCKO, B., FLUSS, S. R. & MAXFIELD, F. R. 1984. Segregation of transferrin to a mildly acidic (pH 6.5) para-Golgi compartment in the recycling pathway. *Cell,* 37**,** 789-800.

YAMSHCHIKOV, A. V., SCHUETZ, A. & LYON, G. M. 2010. Rhodococcus equi infection. *The Lancet. Infectious diseases,* 10**,** 350-9.

YOUNG, A. 2007. Structural insights into the clathrin coat. *Seminars in cell & developmental biology,* 18**,** 448-58.

YU, G., KUSHWAHA, A., LEE, J. K., SHAQFEH, E. S. & BAO, Z. 2011. The shear flow processing of controlled DNA tethering and stretching for organic molecular electronics. *ACS nano,* 5**,** 275-82.

YU, H., RATHORE, S. S., LOPEZ, J. A., DAVIS, E. M., JAMES, D. E., MARTIN, J. L. & SHEN, J. 2013. Comparative studies of Munc18c and Munc18-1 reveal conserved and divergent mechanisms of Sec1/Munc18 proteins. *Proceedings of the National Academy of Sciences of the United States of America,* 110**,** E3271-80.

ZAVODSZKY, E., SEAMAN, M. N., MOREAU, K., JIMENEZ-SANCHEZ, M., BREUSEGEM, S. Y., HARBOUR, M. E. & RUBINSZTEIN, D. C. 2014. Mutation in VPS35 associated with Parkinson's disease impairs WASH complex association and inhibits autophagy. *Nature communications,* 5**,** 3828.